VOL.29 NO.7
JULY
2026

AJSTR
of Scientific and Technological Reports

ASEAN JOURNAL

of Scientific and Technological Report



ISSN 2773-8752 (online)



ASEAN
Journal of Scientific and Technological Reports
Online ISSN:2773-8752

ASEAN Journal of Scientific and Technological Reports (AJSTR)

Name ASEAN Journal of Scientific and Technological Reports (AJSTR)

Owner Thaksin University

Advisory Board Assoc. Prof. Dr. Nathapong Chitniratna
(President of Thaksin University, Thailand)
Assoc. Prof. Dr. Samak Kaewsuksaeng
(Vice President for Reserach and Innovation, Thaksin University, Thailand)
Assoc. Prof. Dr. Samak Kaewsuksaeng
(Acting Director of Reserach and Innovation, Thaksin University, Thailand)

Editor-in-Chief Assoc. Prof. Dr. Sompong O-Thong, Mahidol University, Thailand

Associate Editor

1. Prof. Dr. Jompob Waewsak, Thaksin University, Thailand
2. Assoc. Prof. Dr. Samak Kaewsuksaeng, Thaksin University, Thailand

Session Editors

1. Prof. Dr. Rattana Jariyaboon, Prince of Songkla University, Thailand
2. Assoc. Prof. Dr. Jakkree Boonlakhorn, Thaksin University, Thailand
3. Assoc. Prof. Dr. Supawadee Thawaro, Nakhon Si Thammarat Rajabhat University, Thailand
4. Assoc. Prof. Dr. Surapon Boonlue, King Mongkut's University of Technology Thonburi, Thailand
5. Assoc. Prof. Dr. Warangkana Jutidamrongphan, Prince of Songkla University, Thailand
6. Asst. Prof. Dr. Aungkana Jattamart, Rajamangala University of Technology Rattanakosin, Thailand
7. Asst. Prof. Dr. Suphada Kiriratnikom, Thaksin University, Thailand
8. Dr. Pawadee Hamtanon, Thaksin University, Thailand

Editor Board

1. Amir Sada Khan, American University of Sharjah, United Arab Emirates
2. Chart Chiemchaisri, Kasetsart University,Thailand
3. Chen-Yeon Chu, Feng Chia University, Taiwan
4. Dariusz Jakobczak, National University, Pakistan
5. Ganjar Samudro, Universitas Diponegoro, Indonesia
6. Ghulam Murtaza, Government College University Lahore, Pakistan
7. Hidenari Yasui, University of Kitakyushu, Japan
8. Jatuporn Kaew-On, Thaksin University, Thailand
9. José Antonio Álvarez-Bermejo, University of Almeria, Spain
10. Jutamas Kumchai, Chiang Mai University, Thailand
11. Karun Thongprajukaew, Prince of Songkla University, Thailand
12. Marchee T. Picardal, Cebu Normal University, Philippines
13. Nares Chimres, Thaksin University, Thailand
14. Nasser Ahmed, Kyushu University, Japan
15. Noppamas Pukkhem, Thaksin University, Thailand
16. Peer Mohamed Abdul, Universiti Kebangsaan Malaysia, Malaysia
17. Prasong Kessaratikoon, Thaksin University, Thailand
18. Prawit Kongjan, Prince of Songkla University, Thailand
19. Sappasith Klomklao, Thaksin University, Thailand
20. Shahrul Isamail, Universiti Malaysia Terengganu, Malaysia
21. Supawadee Theerathammakorn, Sukhothai Thammatirat Open University, Thailand
22. Tharith Sriv, Royal University of Phnom Penh, Cambodia
23. Tjokorda Gde Tirta Nindhia, Udayana University in Bali, Indonesia
24. Tsuyoshi Imai, Yamaguchi University, Japan
25. Visit Boonchom, Thaksin University, Thailand
26. Win Win Myo, University of Information Technology, Myanmar
27. Yves Gagnon, University of Moncton, Canada
28. Zairi Ismael Rizman, Universiti Teknologi MARA, Malaysia

Staff: Journal Management Division

Miss Kanyanat Liadrak, Thaksin University, Thailand

Contact Us Institute of Research and Innovation, Thaksin University
222 M. 2 Ban-Prao sub-district, Pa-Pra-Yom district, Phaᵒhalung province, Thailand
Tel. 0 7460 9600 # 7258, 09 1070 0916, 08 1540 7304, E-mail: aseanjstr@tsu.ac.th

List of Contents

Comparative Assessment of Biofungicide Formulations: Strategies Towards Stable Biocontrol Products **e261766**
Karl Christian T. Caracas, May V. Tampus, and Francis Dave C. Siacor

Energy, Protein and Fiber Digestibility of Arrowroot Plant (*Maranta arundinacea* L.) as Feed for Native Pigs **e261767**
Roger Y. Ibañez Jr., Sheilo L. Mark Vasquez, Ulysses A. Cagasan, Julius V. Abela, Ginas Aurea A. Villagonzalo, and Manuel D. Gacutan, Jr.

Development and Evaluation of a Web-Based GIS-Enabled Demographic Profiling System for Data-Driven Local Government Policy Making **e262067**
Anna Monica Paculaba

Dietary Lecithin Modulates Growth, Selected Hematoimmunological Indices, and Glutathione Peroxidase Activity of Hoven's Carp (*Leptobarbus hoevenii*) **e262095**
Poosana Keawkong, Nutt Nuntapong, and Naraid Suanyuk

Comparative Analysis of Forecasting Models for Hourly Solar Irradiance in Southern Thailand **e262134**
Mojtaba Safari, Suttipan Aksornniem, Tanawat Srirugsa, Wiwat Su-hren and Supachai Kaewpoung

Enhancing Oil Palm (*Elaeis guineensis* Jacq.) Growth Using Microbial Consortia: Roles of Phosphate Solubilization and Nitrogen Fixation **e262347**
Korakot Nakkanong, Thanyakorn Rongsawat, Charassri Nualsri, Palakrit Jiwanit, Nurainee Salaemae, and Natthakorn Woraathasin

Development of High-performance Activated Carbon Derived from Longan Peel for Caffeine Removal in Ion-rich Hospital Wastewater **e262381**
Chetnipat Kunawong, Napaphat Datpratoom, Panupong Uprajong, Jidapa Pimthong, and Sakdinun Nuntang

A Contextual Framework for Agricultural IoT Adoption: Integrating TAM, Innovation–Decision Process, and Governmental Support in Smart Farming Contexts **e262844**
Sompoch Tongnamtiang, Manirath Wongsim, and Natarpha Satchawatee

Genetic Relationship Assessment of Micropropagated *Nymphaea colorata* Peter Seedlings using HAT-RAPD **e262883**
Itsaraphong Khaenthong, Theerachai Thanananta, and Narumol Thanananta

Development of a Sustainable Wood Treatment Process for Palmyra Palm Fronds toward Furniture Production **e263161**
Palachai Khaonuan, Noppadon Podkumnerd, Kosin Teeparuksapun, Jirapat Phookwantong, Supranee Wunsri, Nuntachai Chusilp, and Mahamasuhaimi Masae

FlexIoU: Modularity and Flexibility IoU for Bounding Box Regression in Agricultural Disease Detection **e263179**
Naphat Keawpibal, Ajaree Naco, Kanida Sinmai, and Noppamas Pukkhem

Carbon Footprint Assessment and GHG Reduction Guidelines for the Rubberwood Processing Industry in Yala Province **e263215**
Jutamas Kaewmanee, and Adulsman Sukkaew

***Trichoderma asperelloides* TSUxPT3.5 Exhibits Antifungal Activity Against Plant Pathogenic Fungi and Enhances the Growth of Mini Cos Lettuce (*Lactuca sativa* L.)** **e264555**
Wankuson Chanasit, Prisana Wonglom, Nakarin Suwannarach, Jaturong Kumla, Anurag Sunpapao, Kamonthip Jiadkong , Monthon Lertworapreecha , Nugul Intrasungkha , Panadda Promjun , Chaisit Niyasom , and Pumin Nutaratat

List of Contents

Phytochemical Characterization, Curcuminoid Quantification by HPLC, and Biological Activities of Ethanolic and Aqueous Extracts of *Zingiber cassumunar* and *Curcuma longa* Prepared by Ultrasonic-Assisted Extraction **e264707**
Aurawan Boonyataeng, Ratchaneekorn Reudhabibadh, Lukman Sueree, Khanittha Yottrai, Nattakan Nin-On, and Thanawat Pitakpornpreecha

Numerical Solutions of Fractional Integro-Differential Equations with Weakly Singular Kernel by Using a Hybrid of Block-Pulse Functions and Taylor Polynomials **e264757**
Weerachai Thadee, Onuma Ruksachol, Walisa Intarapak, Rattiya Rittichuai, and Nattinee Khongnual

Facial Emotion Recognition – A Comprehensive Review of Deep Learning and Traditional Learning Approaches with Emerging Challenges **e262457**
Sushilkumar Salve, Shubham Kumar, Irfan Shaikh, Pranay Gawade, Sujit Ramesh Borey, and Puja Padiya

Baseline Assessment of Dairy Cow Welfare Using Animal and Resource-based Indicators in Camarines Sur, Philippines **e260555**
Angelo Francis F. Atole

Study of Surface Water Quality Using Biological Indicators Inside the Ruean Thai Pond Area, Nakhon Si Thammarat Rajabhat University **e264369**
Wilasinee Nongnueang, and Wattananarong Markphan

Participatory Extension Approaches for Good Manufacturing Practices (GMP) Adoption in Rural Fish Processing: Evidence from Southern Thailand **e262437**
Amonrat Thanonkaew, Pornpimon Mayachiew, Thanidchaya Luanunkarb, Pimchana Hoktha, Suphada Kiriratnikom, and Vilailak Klompong

Analysis of Electromagnetic Shielding Effectiveness of Multilayer to Protect Against Lightning Strike Effect on Aerospace Applications **e260760**
Siva Chakra Avinash Bikkina, G. Suneetha, and Kakarla Gopi Sri Koushiki



ASEAN
Journal of Scientific and Technological Reports
Online ISSN:2773-8752

ASEAN
Journal of Scientific and Technological Reports
Online ISSN:2773-8752

Research article

Comparative Assessment of Biofungicide Formulations: Strategies Towards Stable Biocontrol Products

Karl Christian T. Caracas[1], May V. Tampus[1], and Francis Dave C. Siacor[1*]

[1] Department of Chemical Engineering, University of San Carlos, Cebu City, Cebu, 6000, Philippines
* Correspondence: fcsiacor@usc.edu.ph

Citation:
Caracas, K.C.T.; Tampus, M.V.; Siacor, F.D.C. Comparative assessment of biofungicide formulations: strategies towards stable biocontrol products. *ASEAN J. Sci. Tech. Report.* **2026**, *29*(7), e261766. https://doi.org/10.55164/ajstr.v29i7.261766

Article history:
Received: October 7, 2025
Revised: April 14, 2026
Accepted: May 13, 2026
Available online: June 14, 2026

Publisher's Note:
This article is published and distributed under the terms of the Thaksin University.

Abstract: The growing demand for sustainable disease management in agriculture has driven continuous development in biofungicide formulation. Despite advances in microbial discovery and screening, the formulation stage remains a bottleneck for commercialization due to limited shelf life, low field efficacy, and scalability. This review critically examines the performance, suitability, and scalability of biofungicide formulations, encompassing conventional (dry and liquid) and alternative forms (cell-free supernatants, microbial metabolites, and encapsulated systems). Dry formulations provide stability and ease of handling, while liquid formulations enable rapid microbial deployment but require protective additives. Alternative approaches, including the use of purified metabolites and encapsulated microbes, address issues of microbial viability and delivery but face challenges in formulation standardization and large-scale production. This paper also highlights formulation improvement strategies that revolve in the use of sugars as co-solutes in encapsulated formulations and the use of spore-based agents to enhance field survival and efficacy. Future research should focus on linking formulation design with microbial physiology and ecological performance to develop scalable, stable, and high-performing biofungicides.

Keywords: Biocontrol; biofungicides; formulation; stability; efficacy

1. Introduction

Improving agricultural productivity has become a critical priority in response to increasing global food demand and the need to ensure food security. One of the major constraints in crop production is the prevalence of phytopathogens, which are responsible for an estimated 20% to 40% loss in global yield annually [1, 2]. These plant disease causing phytopathogens include *Erwinia amylovora*, the causative agent of fire blight in apples and pears [3], *Colletotrichum gloeosporioides,* which causes anthracnose in mangoes [4], and *Lasiodiplodia theobromae,* responsible for stem-end rot in several tropical fruit crops [5].

Conventional control strategies rely heavily on agrochemicals, which, despite their effectiveness, pose significant environmental and health risks. These include contamination of soil and water systems, disruption of ecological balance, the emergence of resistant pathogen strains, and health-related concerns due to their ability to disrupt normal cell cycle regulation in humans [6-10].

Such concerns have accelerated the development of sustainable alternatives, particularly biological fungicides or biofungicides, which utilize either beneficial microorganisms or their bioactive metabolites to suppress phytopathogens in the field. Beneficial microorganisms effectively inhibit these fungal pathogens through two main mechanisms: antibiosis and competitive exclusion [11-15]. These mechanisms include induced systemic resistance (ISR) in host plants, siderophore production that limits pathogen access to essential nutrients such as iron, and the secretion of lytic enzymes that degrade fungal cell walls. Their consistent use can bring long-term disease suppression in the field, promotion of plant and root growth through nutrient solubilization, and compatibility with other sustainable practices, such as the use of biofertilizers [16, 17].

Despite their potential, the practical application of biofungicides remains limited by inconsistent field performance, short shelf life, and challenges in maintaining microbial viability during storage and application [18]. These limitations are not solely due to the biological agent itself, but are strongly influenced by formulation design, which governs stability, delivery efficiency, and interaction with environmental conditions. As a result, formulation has emerged as a critical bottleneck in the development and commercialization of biofungicide products.

To address these challenges, various formulation strategies have been developed, including conventional approaches such as liquid and dry formulations, as well as alternative strategies involving purified microbial metabolites, cell-free supernatants, and encapsulated systems. Each formulation type presents distinct advantages and limitations depending on the intended application, target pathogen, and environmental conditions. However, existing literature largely focuses on describing the different types and processes involved in biofungicide formulation [19-21], the composition and function of additives used [22, 23], mechanisms of biocontrol and a framework for development [24], or identification of key components in biofungicide development [25], with limited emphasis on systematic comparison across key performance criteria.

This review aims to provide a comparative assessment of biofungicide formulation strategies based on four critical parameters. First, stability, which refers to the shelf life and resistance to environmental stress. Second is efficacy, which is defined as the consistency and strength of biocontrol performance. Third is its scalability, which considers the feasibility of large-scale production. Lastly, the field applicability encompasses the delivery efficiency and compatibility of the biofungicide with current agricultural practices. By applying this framework, the review evaluates both conventional and emerging formulation approaches, identifies key trade-offs, and highlights areas requiring further research. Ultimately, this work seeks to bridge the gap between microbial potential and practical application by linking formulation design with performance outcomes, thereby contributing to the development of stable, scalable, and high-performing biofungicide products.

2. Formulation Types

Biofungicide field performance is inherently tied to formulation design, which dictates the product's physicochemical stability, delivery efficiency, and interaction with the environment. This design encompasses both the primary physical state of the product and the strategic incorporation of functional additives. These additives, such as surfactants, UV protectants, and anti-freezing agents, are essential for mitigating environmental stressors and optimizing application parameters in the field [25-27].

A robust formulation consists of three fundamental components: (1) the active ingredient (AI), which may include viable microbial antagonists (cells or spores) or their bioactive metabolites (purified compounds or cell-free supernatants); (2) the carrier, which facilitates the transport of the active ingredient to the target site; and (3) additives, which stabilize the system and maintain viability during storage [28]. In this context, the "additives" serve as an umbrella term for various functional subsets; specifically, co-solutes are additives used to improve microbial survival through osmotic or thermal regulation, while nutrient carriers are subsets that provide immediate metabolic support to the microbes during field establishment.

Biofungicide form can be categorized through a dual-axis matrix, as summarized in Figure 1 [29]. This approach distinguishes formulations based on their active-ingredient type (viable microbes vs non-

viable metabolites) and their physical form (liquid vs solid/dry). Within this framework, encapsulation and capsule suspensions serve as bridging technologies; they act as sophisticated delivery systems that stabilize both microbes and metabolites in either liquid or solid forms to enhance persistence and controlled release [30-33].

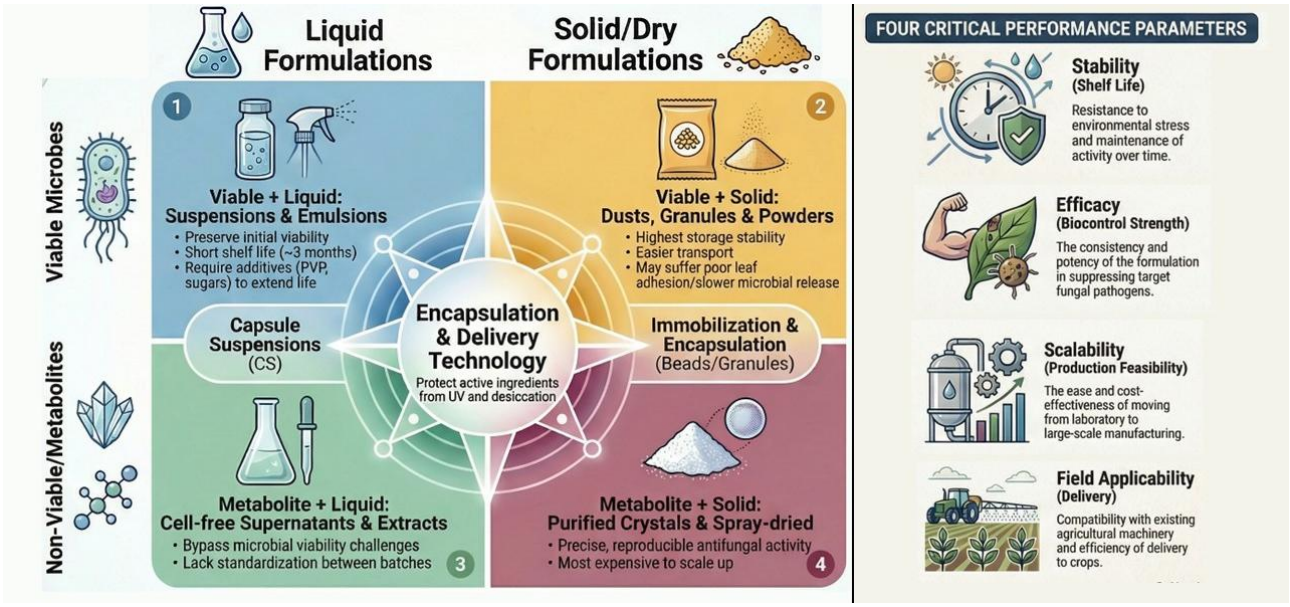


Figure 1. Overview of biofungicide formulation strategies, application modes, and performance considerations

2.1 Active Ingredient Selection: Viable Cells vs Non-Viable Metabolites

The first axis considers that the type of AI is the primary determinant of a product's biological mechanism and long-term reliability.

2.1.1 Viable Cells

The selection of the AI is a fundamental design decision in biofunicide formulation, as it directly influences stability, efficacy, and performance consistency. Broadly, biofungicide formulations utilize either viable microbial cells or non-viable bioactive metabolites.

Formulations based on viable cells rely on the microorganisms' ability to colonize the target environment, compete for nutrients and space while providing sustained biocontrol activity through the continuous production of lytic enzymes, biosurfactants, and siderophores, as well as the induction of systemic resistance (ISR) in host plants [34].

The advantage of this approach is demonstrated in the semi-commercial postharvest trials, where *Bacillus velezensis* TS3B-45 bacterial suspensions managed to control anthracnose in mango fruits [35]. However, the reliance on living systems introduces significant performance variability, as microbial survival and activity are strictly governed by their shelf life and high sensitivity to physicochemical stressors such as fluctuating temperatures, UV exposure, and moisture levels [36,37]. Consequently, maintaining viability during storage and after application remains a primary bottleneck for cell-based formulations, often necessitating the use of specialized protective additives or nutrient supplements to ensure long-term stability [38, 39].

2.1.2 Non-Viable Metabolites

Alternatively, non-viable microbial metabolites, which are bioactive compounds secreted during the fermentation process. To bypass the persistent challenge of preserving microbial viability during storage and application, these agents are employed either as purified molecules or cell-free supernatants (CFS). While this approach eliminates the viability bottleneck, it introduces new challenges regarding field persistence and production costs.

a. Purified Microbial Metabolites

Purified microbial metabolites have demonstrated potent antifungal activity through defined modes of action. Lipopeptides from *Bacillus* spp., such as iturin, surfactin, and fengycin, disrupt fungal membranes and inhibit spore germination [40-43]. These compounds have confirmed efficacy against various phytopathogens, including *Venturia inaequalis* (apple scab) [44], *Alternaria linariae* (early blight) [45], and *Fusarium oxysporum* f. sp. *iridacearum* (wilting and root rot) [46]. Similar results are achieved with purified lytic enzymes, specifically, such as β-1,3-glucanase, chitinase, and protease, which specifically degrade fungal structural components [13,47,48].

However, a critical limitation of purified metabolites is that fungal pathogens are not passive targets; some pathogens are capable of deploying counter-strategies such as chitin deacetylation, glucan masking, or the production of chitin-binding proteins to shield their cell walls from enzymatic access [49, 50]. Furthermore, fungal sensitivity to lipopeptides is heavily dictated by physicochemical determinants in the cell wall, such as ergosterol levels [51]. This indicates that reliance on a single purified metabolite may limit the spectrum of efficacy across diverse phytopathogens.

From a commercialization perspective, the long-term reliability of purified metabolites is undermined by high scalability hurdles. Production is often cost-prohibitive because active compounds accumulate in low quantities during standard fermentation. For example, optimization of iturin A from *B. subtilis* ZK-H2 yields only 0.85 g/L over 60 hours [52]. While higher yields of 6.8 g/L are achievable, they require specialized biofilm reactors, which increase the complexity and capital expenditure of large-scale production, often making purified forms less economically feasible than whole-cell formulations [53, 54].

b. Cell-free Supernatants

An alternative to purified microbial metabolites is the use of cell-free supernatants (CFS), obtained through centrifugation or filtration to remove microbial cells while retaining the extracellular metabolites. CFS is a strategically attractive biocontrol platform because it bypasses the viability bottleneck and leverages the synergistic cocktail of bioactive compounds secreted during growth, which is often harder for pathogens to resist than a single purified metabolite [55]. For example, 5% CFS from *B. subtilis* BS-1 inhibited *Botryosphaeria dothidea* (kiwi rot) by inducing oxidative damage and hyphal rupture [56]. Similarly, a 1% CFS from *Paenibacillus polymyxa* YF, *B. velezensis* BQ, and *B. amyloliquefaciens* HT significantly suppressed *F. oxysporum* [57].

However, a critical assessment reveals that CFS faces unique scalability and standardization hurdles [58,59]. A primary constraint is the requirement for low-temperature storage to maintain the structural integrity and biological activity of bioactive compounds; such as cold-chain requirements significantly increase commercialization costs and complicate large-scale logistics. While CFS offers a more practical and cost-effective production route than purified metabolites, it lacks the precision and reproducibility of purified molecules due to inherent variability in metabolite diversity and abundance across different fermentation batches [60]. Furthermore, compared with microbial cell-based formulations, CFS provides rapid initial antifungal action but lacks the field persistence afforded by living antagonists, which can colonize the host and continuously secrete bioactive compounds. Consequently, the efficacy of CFS is highly susceptible to environmental degradation from UV exposure and wash-off, often necessitating frequent re-application to maintain suppressive levels. This underscores a fundamental limitation; while CFS eliminates the challenges of maintaining microbial viability, its long-term reliability in the field requires integration into encapsulation systems to provide a physicochemical shield against environmental degradation.

Between purified microbial metabolite and CFS use, there is a trade-off between precision and practicality, as presented in Table 1. Purified metabolites provide precise and reproducible antifungal activity but are constrained by low yields and the high costs of scaling up. In contrast, CFS is easier to produce and scale, yet its application is hindered by variability in metabolite composition and difficulties in standardizing dosage across different phytopathogens. This duality underscores a fundamental limitation of metabolite-based biofungicides, as their long-term reliability often depends on the presence of viable microbes to ensure consistent activity.

Table 1. Microbial Metabolites Formulation [20, 59-61]

Property	Purified Microbial Metabolite	Cell-free Supernatant
Efficacy	Defined mode of action with reproducible antifungal activity. However, pathogen adaptability can limit effectiveness.	Rapid antifungal action due to the synergistic effects between metabolites. However, the optimal concentration to achieve the needed effects is highly variable.
Persistence in the Field	No to limited persistence in the field; requires doses due to metabolite degradation.	Also lacks viable microbes, but the metabolite concoction may prolong functional activity. Still subject to metabolite degradation.
Scalability	Expensive for large-scale production due to low yields per liter.	More scalable since only cell removal is required, but it suffers from a cold-chain requirement.
Applicability	Stable and easy to dose precisely; best suited for targeted, high-value applications.	Simple preparation and direct application; difficult to standardize dosage and frequency.

2.2 Physical States and Delivery Platforms

While the selection of the active ingredient defines the biological mechanism of the biofungicide, the physical state and delivery platform determine how that ingredient is protected, transported, and deployed in the field. This second axis of formulation design categorizes products into liquid or dry systems, each presenting distinct trade-offs between immediate bioactivity, storage stability, and economic scalability.

a. Liquid Formulations

Liquid formulations, also referred to as flowable or aqueous suspensions, consist of biomass suspended in water, oil, or emulsions [62]. Liquid systems represent a primary physical form of delivery that can accommodate both viable cells and non-viable metabolites. These formulations enable direct delivery of the active ingredient without exposure to dehydration or thermal stress during the process, thereby preserving high initial microbial viability and metabolic activity [63, 64]. Their biocontrol performance depends on the type and concentration of the active ingredient, stability, spray volume, water dilution, and droplet size, all of which influence the biofungicide's retention, coverage, and overall efficacy in the field [65, 66].

However, beyond the challenges of microbial viability, liquid formulations are inherently prone to gas build-up, especially if the microbe is active and is present at high concentration. While some reported that there is no clumping and sedimentation of biomass, it is still important to observe the formulation's physical properties [67]. Other properties to consider are the influence of storage temperature and the effect of the formulation's variable pH, as it can affect their pre or post-microbial application [68].

From a production standpoint, liquid formulations require the manipulation of high volumes of liquid with minimal protection from contamination [28]. Coupled with strict temperature requirements, this raises inconvenience for practical use, as having a short commercial life significantly increases the cost of storage [39]. Overall, liquid formulations provide clear advantages in terms of delivery efficiency and immediate bioactivity, particularly for foliar applications. However, these benefits are counterbalanced by challenges in maintaining long-term stability and consistent performance during storage. Compared to solid formulations, liquid systems prioritize ease of application and rapid efficacy but are limited by shorter shelf life, highlighting a fundamental trade-off between field performance and storage stability.

b. Dry Formulations

Dried formulations, on the other hand, involve combining a biologically active ingredient with a solid carrier to ensure delivery to the target site on the crop. A wide range of carriers has been explored in the literature, including charcoal, coal-bentonite mixture, talc, lignite, soybean meal, composts, corn meal, polyacrylamide gel, alginate, and perlite [69]. This makes them a more feasible alternative to liquid formulations, as they are reported to have low production costs and are easy to store and transport [28].

Several forms of dry formulations are commercially recognized, such as dust, granules, wettable powders, and water-soluble packets [65, 70]. These types differ in their physical properties and mode of application but share the advantages of relative stability in storage and ease of bulk transport, as summarized in Table 2.

Table 2. Evaluation of Dry Bioformulations [65, 70, 71]

Dry Formulation Type	Description	Advantages	Disadvantages
Dusts	Finely ground mineral powder (e.g., talc, clay) carrying an active ingredient.	Simple, low-cost, and easy to apply.	Low adhesion to target surfaces; inhalation and abrasion hazards.
Granules	Larger and heavier particles (100 to 1000 microns) with active and inert carriers.	Easy handling; reduced dust hazard; slow release	Limited foliar coverage
Wettable powders	Finely ground powders mixed with dispersants and surfactants.	Long storage stability; good miscibility with water, which allows foliar use.	Prone to clumping; inhalation risks; requires mixing with additives.
Water-dispersible granules	Compressed particles disintegrate in water to form a suspension.	Dust-free; uniform spray distribution	Requires constant agitation and specialized mixing equipment.
Water-soluble packet	Pre-measured doses in soluble film packets.	Safe handling; accurate dosing; reduces farmer exposure.	Higher production cost; limited adoption in resource-poor settings.

Regardless of the specific delivery format, solid-based formulations provide a protective and nutritive platform that enhances microbial survival compared to simple liquid suspensions [72]. However, when evaluated collectively, these types illustrate a distinct trade-off between scalability, stability, and field applicability. The simple options, such as dusts and granules, are highly scalable and inexpensive to produce; yet, their poor foliar adhesion and slow microbial release make them more suitable for soil-borne pathogens than foliar diseases. Conversely, advanced systems like water-dispersible granules (WDG) and soluble packets address critical needs for dosing accuracy and foliar delivery. However, these benefits are countered by higher production costs and physical requirements, such as the constant need for agitation to prevent sedimentation, which may limit their adoption outside of high-value cropping systems. These differences underscore that the success of a dry formulation depends not only on preserving microbial viability but on the physicochemical alignment of product design with the target pathogens and the economic realities of diverse farming systems.

2.3 The Encapsulation Bridge: Advanced Delivery Systems

Encapsulation serves as a technically sophisticated bridge between liquid and dry platforms, utilizing polymeric substances to immobilize and protect active ingredients (both the viable cells and metabolites) from environmental stressors. This can be achieved via encapsulation and capsule suspension formulation.

a. *Encapsulation and Immobilization*

Encapsulation serves as a technically sophisticated bridge between liquid and dry platforms, utilizing polymeric substances to immobilize and protect active ingredients (both viable cells and metabolites) from environmental stressors [54,72]. By using materials such as pectin-starch blends [73] or alginate-gelatin matrices [74], these systems create a physicochemical shield against various stressors, such as desiccation, UV radiation, and temperature fluctuations, while enabling the controlled release of the antagonist in the field [21,72]. This mechanism directly addresses the "viability bottleneck" identified in

liquid suspensions by maintaining high microbial fitness under fluctuating field conditions. Furthermore, the co-encapsulation of *B. velezensis* VRU1 in an alginate-gelatin matrix supplemented with nanoparticles significantly enhanced the inhibition of *Rhizoctonia solani* in beans [74]. These additive-enriched systems highlight the potential of encapsulation not only to protect the microbe but also to provide a localized, nutrient-rich microenvironment that promotes initial establishment in the host.

The commercial scalability of encapsulation is heavily dictated by the processing technique used, which ranges from extrusion-casting to fluidized-bed and spray drying [75]. A critical trade-off exists between microbial fitness and production efficiency. For example, *B. amyloliquefaciens* CPA-8 encapsulated via fluidized-bed spray drying demonstrated greater stability and shelf life than freeze-drying, yet the thermal and osmotic stresses of the drying process often necessitate the use of protective additives [76]. Protective additives such as skimmed milk and $MgSO_4$ have been shown to stabilize *B. subtilis* CPA-8 during spray drying to minimize heat and dehydration stress [77].

b. Capsule Suspensions

Capsule suspensions (CS) represent a technically sophisticated liquid delivery platform that bridges the field applicability of liquid sprays with the superior stability of encapsulated systems. In this format, the active ingredient is sequestered within microscopic polymeric shells suspended in an aqueous medium, creating a physicochemical shield against environmental stressors such as UV radiation and desiccation [78].

The primary advantage of CS is its ability to prolong field persistence through the controlled release of the antagonist to the target area. For instance, microcapsules of *B. megaterium* in calcium alginate beads have been shown to maintain high viability and colonization ability following foliar application, performing at levels comparable to non-encapsulated cells while gaining protection from the polymeric matrix [79]. The type of biopolymers used in the microencapsulation can be reinforced with other types of biopolymers, such as nanocellulose and chitosan [80]. This can lead to potential improvement in the physical characteristics of the microencapsulated material and an increase in antagonism properties due to the presence of chitosan.

Despite these performance benefits, the transition of CS from laboratory success to large-scale commercialization faces significant scalability and production costs hurdles. The complexity of the encapsulation process and the requirement for post-encapsulation stabilization remain primary bottlenecks. Consequently, while CS offers a promising high-stability and high efficacy solution for sustainable disease management, its adoption is currently most feasible for high-value cropping systems where economic returns justify the increased formulation costs.

To summarize the fundamental trade-offs inherent in the delivery platforms discussed, Table 3 provides a comparative synthesis based on the four performance criteria established in this review. This overview highlights how selecting an appropriate format requires balancing the physicochemical stability of the product with the economic and practical realities of diverse farming systems.

3. Formulation Improvement Strategies

Despite progress in developing various biofungicide formulations, field-level inconsistency remains a key barrier to adoption. Recent studies offer various strategies to improve current formulation types. This is either done using dormant or stress-tolerant propagules or by integration of multi-purpose additives to enhance field performance.

3.1 Use of Dormant or Stress-Tolerant Propagules

To address the viability issue in biofungicide particularly, its short shelf life of liquid suspensions and the metabolic exhaustion of vegetative cells, formulation design can shift toward the use of dormant or stress-tolerant propagules. While the active ingredient in a bioformulation can exist in a vegetative state, dormant spores offer superior physicochemical resilience against desiccation, temperature fluctuations, and UV radiation that typically limit the commercial viability of microbial products [29, 81, 82].

The transition from vegetative cells to spore-based agents provides a unique opportunity for mechanistic redundancy in the field. Unlike isolated metabolites, viable spores that successfully germinate and colonize the target area offer a sustained biocontrol effect through continuous antibiosis, competitive

exclusion, and the induction of systemic resistance (ISR). Biofungicides that use spore-forming bacteria, particularly from the *Bacillus* genus, are widely recognized for their strong antifungal capacity against pathogens such as *Phytophthora capsici* [16], various *Colletotrichum* spp. [83], and *Botrytis cinerea* [84].

Table 3. Comparative Synthesis of Major Biofungicide Formulation Platforms

Formulation Platform	Stability (Shelf Life)	Scalability and Cost	Field Efficacy	Practical Application
Liquid Suspensions	Prone to gas build-up; generally short shelf life	Straightforward to prepare; low production cost, but high logistic/cold-chain costs	Enables rapid microbial deployment and excellent foliar coverage.	Foliar protection requires immediate colonization and bioactivity.
Dry Formulations	Solid carriers provide a protective platform, easy to transport and store.	Simple dusts are cheap; advanced WDGs have higher technical complexity.	Dependent on moisture for activation, simple forms have poor foliar adhesion.	Soil-borne pathogens or large-scale broadcast applications.
Microbial Metabolites	Bypass viability bottlenecks but sensitive to UV and environmental degradation.	Purified forms are cost-prohibitive due to low fermentation yields.	Provides immediate antifungal action via defined modes of action.	High-value, targeted use or post-harvest disease management.
Encapsulation	Physicochemical shield protects cells/metabolites from UV and desiccation.	High technical complexity and carrier costs are primary bottlenecks.	Controlled release mechanisms prolong field persistence.	High-value cropping systems where long-term protection justifies cost.

a. Upstream Customization of Spore Properties

The sporulation process itself serves as a critical upstream determinant of formulation performance, where the physical properties of the "living" active ingredient are engineered during fermentation. As illustrated in Figure 2, process conditions such as pH and temperature during sporulation directly dictate the resulting spore surface hydrophobicity, adhesion, and UV resistance [85-87]. This can significantly dictate how the agent can adhere to the waxy cuticle of a leaf following foliar application and its survival on the surface of the leaves. Despite the potential for this physiological engineering, there is still a significant lack of empirical data linking specific upstream process conditions to downstream field germination or colonization behavior. This represents an underexplored frontier in biofungicide.

b. Scalability and Reduced Additive Dependency

The primary commercial advantage of spore-based formulations lies in their scalability and potential for process-based customization. In industrial settings, sporulation can be strategically induced at the end of vegetative growth, allowing for efficient scale-up in conventional fermenters before triggering the maturation of these durable units.

By optimizing the microbial physiology during production to yield robust, application-fit spores, developers can minimize the dependency on stabilizing additives, such as specialized co-solutes or UV protectants that are otherwise required to maintain the shelf life of sensitive vegetative cells [38,88]. Integrating spore physiology control into the production design thus offers a path toward consistent, stable, and high-performing biofungicide products that are better suited for the economic reality of large-scale agriculture.

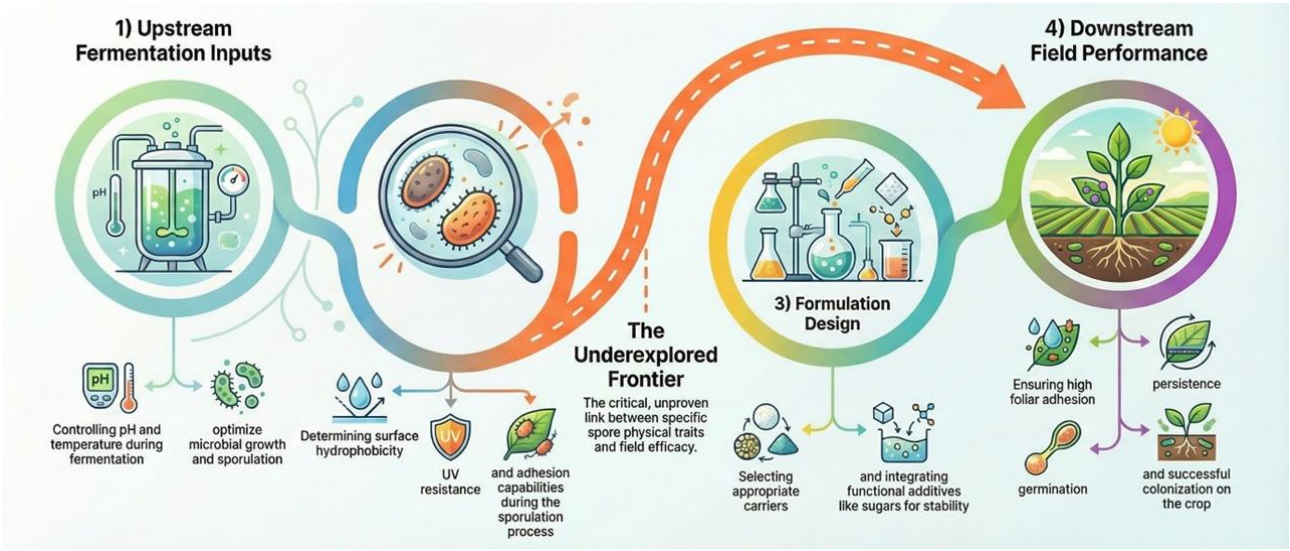


Figure 2. Conceptual framework illustrating how fermentation and sporulation conditions influence spore properties relevant to biofungicide formulation.

3.2 Sugars as co-solutes in encapsulation

To overcome the environmental stress tolerance and inconsistent field performance noted in liquid and dry platforms, recent strategies emphasize the integration of multifunctional additives that serve structural, protective, and nutritional roles. In encapsulation matrices, such as pectin or alginate, incorporating sugars as co-solutes, a functional subset of additives, that can significantly enhance gel firmness [89]. Furthermore, utilizing sugar-rich agro-industrial by-products like sugarcane molasses offers a highly scalable and low-cost substitute that improves the mechanical properties of gels such as pectin while simultaneously enriching the nutritional environment for encapsulated microbes [90]. This leads to a reduction in the concentrations of biopolymers and cross-linking for encapsulation [91].

Similar multifunctionality is observed with protein-based additives like skimmed milk, which can also act as both cryoprotectants and nutrient carriers during the dehydration and storage of agents like *B. subtilis* CPA-8 [76, 77]. These compounds form protective physicochemical shields around microbial cells, mitigating the desiccation and thermal shocks associated with production and application. While these additives promote rapid recovery upon rehydration, limited studies have linked gel entrapment with sugar nutrients to actual antagonistic effects in the field. This presents a vital research priority to determine how these integrated systems can optimize microbial survival and shelf life while maintaining the cost-effectiveness required for commercial adoption.

4. Conclusion

The formulation is the critical bridge that translates laboratory-scale microbial discovery into practical, field-level performance by determining the product's stability, delivery efficiency, and biocontrol efficacy. This review has demonstrated that each formulation platform presents inherent trade-offs. While liquid suspensions offer a rapid microbial deployment and ease of use, they suffer from a significant stability bottleneck and short shelf life. Conversely, dry formulations provide superior storage stability, yet advanced forms like water-dispersible granules often require specialized equipment that may limit adoption among resource-poor growers.

The most promising strategies for the next generation of biofungicides involve the integration of microbial physiology with formulation chemistry to overcome these limitations. Specifically, future work should prioritize the process-level customization of spore-based agents by utilizing upstream fermentation parameters to tune the resulting spores for enhanced physicochemical resilience and foliar adhesion. Alternatively, the rational use of multifunctional additives, such as sugars as co-solutes, can create protective matrices that enhance both the mechanical stability of encapsulation systems and the nutritional fitness of

the microbial antagonist. Lastly, there is the pilot-scale validation of these high-performing platforms (e.g., capsule suspensions) to ensure they remain cost-effective and scalable for commercial production.

Ultimately, achieving a "field-ready" biofungicide requires a holistic design approach that aligns product characteristics with the economic realities of farming systems. By shifting the focus from simple descriptive formulations to engineered systems that leverage the inherent durability of dormant propagules and the protective capacity of additive-enriched matrices, the industry can overcome the current commercialization bottlenecks and provide long-term, sustainable disease management solutions.

5. Acknowledgements

The authors would like to thank the valuable insights and recommendations that helped improve this manuscript. Gratitude is also extended to colleagues and laboratory members for their assistance and encouragement throughout the study.

Author Contributions: Conceptualization, M. V. Tampus; Writing, K. C. T. Caracas; Review, K. C. T. Caracas and F. D. C. Siacor; Visualization, K. C. T. Caracas; Supervision, M. V. Tampus. All authors have read and agreed to the published version of the manuscript.

Funding: This research was funded by the Department of Science and Technology (DOST) through the scholarship of Mr. Caracas, under the Engineering Research and Development for Technology (ERDT) program.

Conflicts of Interest: The authors declare no conflict of interest.

References

[1] Syed Ab Rahman, S. F.; Singh, E.; Pieterse, C. M. J.; Schenk, P. M. Emerging Microbial Biocontrol Strategies for Plant Pathogens. *Plant Sci.* **2018**, *267*(October 2017), 102–111. https://doi.org/10.1016/j.plantsci.2017.11.012

[2] Savary, S.; Ficke, A.; Aubertot, J. N.; Hollier, C. Crop Losses Due to Diseases and Their Implications for Global Food Production Losses and Food Security. *Food Secur.* **2012**, *4*(4), 519–537. https://doi.org/10.1007/s12571-012-0200-5

[3] Zhao, Y.; Tian, Y.; Wang, L.; Geng, G.; Zhao, W.; Hu, B.; Zhao, Y. Fire Blight Disease, a Fast-Approaching Threat to Apple and Pear Production in China. *J. Integr. Agric.* **2019**, *18*(4), 815–820. https://doi.org/10.1016/S2095-3119(18)62033-7

[4] Gautam, A. K. *Colletotrichum Gloeosporioides*: Biology, Pathogenicity and Management in India. *J. Plant Physiol. Pathol.* **2014**, *02*(02). https://doi.org/10.4172/2329-955x.1000125

[5] Karunanayake, K. O. L. C.; Adikaram, N. K. B. Stem-End Rot in Major Tropical and Sub-Tropical Fruit Species. *Ceylon J. Sci.* **2020**, *49*(5), 327. https://doi.org/10.4038/cjs.v49i5.7800

[6] Dighton, J. *Fungi in Ecosystem Processes*; CRC Press, 2018. https://doi.org/10.1201/9781315371528

[7] Grossart, H.-P.; Van den Wyngaert, S.; Kagami, M.; Wurzbacher, C.; Cunliffe, M.; Rojas-Jimenez, K. Fungi in Aquatic Ecosystems. *Nat. Rev. Microbiol.* **2019**, *17*(6), 339–354. https://doi.org/10.1038/s41579-019-0175-8

[8] Usman, H. M.; Tan, Q.; Karim, M. M.; Adnan, M.; Yin, W.-X.; Zhu, F.-X.; Luo, C.-X. Sensitivity of *Colletotrichum Fructicola* and *Colletotrichum Siamense* of Peach in China to Multiple Classes of Fungicides and Characterization of Pyraclostrobin-Resistant Isolates. *Plant Dis.* **2021**, *105*(11), 3459–3465. https://doi.org/10.1094/PDIS-04-21-0693-RE

[9] Yilmaz, N. Management of Postharvest Diseases and Maintaining of Fruit Quality With Antagonistic Microorganisms. In *Advances Plant Research*; 2023; pp 171–187.

[10] Tao, H.; Bao, Z.; Jin, C.; Miao, W.; Fu, Z.; Jin, Y. Toxic Effects and Mechanisms of Three Commonly Used Fungicides on the Human Colon Adenocarcinoma Cell Line Caco-2. *Environ. Pollut.* **2020**, *263*, 114660. https://doi.org/10.1016/j.envpol.2020.114660

[11] Ayaz, M.; Li, C. H.; Ali, Q.; Zhao, W.; Chi, Y. K.; Shafiq, M.; Ali, F.; Yu, X. Y.; Yu, Q.; Zhao, J. T.; Yu, J. W.; Qi, R. De; Huang, W. K. Bacterial and Fungal Biocontrol Agents for Plant Disease Protection:

Journey from Lab to Field, Current Status, Challenges, and Global Perspectives. *Molecules* **2023**, *28*(18). https://doi.org/10.3390/molecules28186735

[12] Ray, R. C.; Swain, M. R.; Panda, S. H.; Lata. Microbial Control of Postharvest Diseases of Fruits, Vegetables, Roots, and Tubers. In *Bioaugmentation, Biostimulation, and Biocontrol*; Singh, A., Parmar, N., Kuhad, R. C., Eds.; 2011; pp 311–355. https://doi.org/10.1007/978-3-642-19769-7_13

[13] Kim, Y. S.; Balaraju, K.; Jeon, Y. Biological Control of Apple Anthracnose by *Paenibacillus Polymyxa* APEC128, an Antagonistic Rhizobacterium. *Plant Pathol. J.* **2016**, *32*(3), 251–259. https://doi.org/10.5423/PPJ.OA.01.2016.0015

[14] Guillén-Navarro, K.; López-Gutiérrez, T.; García-Fajardo, V.; Sergio, G.-C.; Zarza, E.; De la Rosa-García, S.; Chan-Bacab, M. Broad-Spectrum Antifungal, Biosurfactants and Bioemulsifier Activity of *Bacillus Subtilis* subsp. *Spizizenii* —A Potential Biocontrol and Bioremediation Agent in Agriculture. *Plants* **2023**, *12*, 1–20. https://doi.org/10.3390/plants12061374

[15] Kumar, P.; Pandhi, S.; Mahato, D. K.; Kamle, M.; Mishra, A. *Bacillus*-Based Nano-Bioformulations for Phytopathogens and Insect–Pest Management. *Egypt. J. Biol. Pest Control* **2021**, *31*(1). https://doi.org/10.1186/s41938-021-00475-6

[16] Eyegheleme, P. Evaluation of Growth Media and Cost-Effective Formulations for Selected Biological Control Agents; M.S. Thesis, Tennessee State University, Nashville, TN, USA, 2023.

[17] He, D.; Zhan, J.; Xie, L. Problems, Challenges and Future of Plant Disease Management: From an Ecological Point of View. *J. Integr. Agric.* **2016**, *15*(4), 705–715. https://doi.org/10.1016/S2095-3119(15)61300-4

[18] Cray, J. A.; Connor, M. C.; Stevenson, A.; Houghton, J. D. R.; Rangel, D. E. N.; Cooke, L. R.; Hallsworth, J. E. Biocontrol Agents Promote Growth of Potato Pathogens, Depending on Environmental Conditions. *Microb. Biotechnol.* **2016**, *9*(3), 330–354. https://doi.org/10.1111/1751-7915.12349

[19] Rojas-Sánchez, B.; Guzmán-Guzmán, P.; Morales-Cedeño, L. R.; Orozco-Mosqueda, M. del C.; Saucedo-Martínez, B. C.; Sánchez-Yáñez, J. M.; Fadiji, A. E.; Babalola, O. O.; Glick, B. R.; Santoyo, G. Bioencapsulation of Microbial Inoculants: Mechanisms, Formulation Types and Application Techniques. *Appl. Biosci.* **2022**, *1*(2), 198–220. https://doi.org/10.3390/applbiosci1020013

[20] Fadiji, A. E.; Xiong, C.; Egidi, E.; Singh, B. K. Formulation Challenges Associated with Microbial Biofertilizers in Sustainable Agriculture and Paths Forward. *J. Sustain. Agric. Environ.* **2024**, *3*(3). https://doi.org/10.1002/sae2.70006

[21] Saberi Riseh, R.; Hassanisaadi, M.; Vatankhah, M.; Kennedy, J. F. Encapsulating Biocontrol Bacteria with Starch as a Safe and Edible Biopolymer to Alleviate Plant Diseases: A Review. *Carbohydr. Polym.* **2023**, *302* (October 2022), 120384. https://doi.org/10.1016/j.carbpol.2022.120384

[22] Singh, V.; Kumar, B. A Review of Agricultural Microbial Inoculants and Their Carriers in Bioformulation. *Rhizosphere* **2024**, *29*(September 2023), 100843. https://doi.org/10.1016/j.rhisph.2023.100843

[23] Vassilev, N.; Vassileva, M.; Martos, V.; Garcia del Moral, L. F.; Kowalska, J.; Tylkowski, B.; Malusá, E. Formulation of Microbial Inoculants by Encapsulation in Natural Polysaccharides: Focus on Beneficial Properties of Carrier Additives and Derivatives. *Front. Plant Sci.* **2020**, *11*(March), 1–9. https://doi.org/10.3389/fpls.2020.00270

[24] Palmieri, D.; Ianiri, G.; Del Grosso, C.; Barone, G.; De Curtis, F.; Castoria, R.; Lima, G. Advances and Perspectives in the Use of Biocontrol Agents against Fungal Plant Diseases. *Horticulturae* **2022**, *8*(7). https://doi.org/10.3390/horticulturae8070577

[25] Leggett, M.; Leland, J.; Kellar, K.; Epp, B. Formulation of Microbial Biocontrol Agents – an Industrial Perspective. *Can. J. Plant Pathol.* **2011**, *33*(2), 101–107. https://doi.org/10.1080/07060661.2011.563050.

[26] Yi, Y.; Luan, P.; Liu, S.; Shan, Y.; Hou, Z.; Zhao, S.; Jia, S.; Li, R. Efficacy of *Bacillus Subtilis* XZ18-3 as a Biocontrol Agent against *Rhizoctonia Cerealis* on Wheat. *Agric.* **2022**, *12*(2). https://doi.org/10.3390/agriculture12020258

[27] Chaudhary, R.; Nawaz, A.; Khattak, Z.; Butt, M. A.; Fouillaud, M.; Dufossé, L.; Munir, M.; Haq, I. ul; Mukhtar, H. Microbial Bio-Control Agents: A Comprehensive Analysis on Sustainable Pest Management in Agriculture. *J. Agric. Food Res.* **2024**, *18*(April), 101421. https://doi.org/10.1016/j.jafr.2024.101421

[28] Teixidó, N.; Usall, J.; Torres, R. Insight into a Successful Development of Biocontrol Agents: Production, Formulation, Packaging, and Shelf Life as Key Aspects. *Horticulturae* **2022**, *8*(4). https://doi.org/10.3390/horticulturae8040305

[29] Mishra, J.; Arora, N. K. Bioformulations for Plant Growth Promotion and Combating Phytopathogens: A Sustainable Approach. In *Bioformulations: for Sustainable Agriculture*; Springer India: New Delhi, 2016; pp 3–33. https://doi.org/10.1007/978-81-322-2779-3_1

[30] Zabot, G. L.; Schaefer Rodrigues, F.; Polano Ody, L.; Vinícius Tres, M.; Herrera, E.; Palacin, H.; Córdova-Ramos, J. S.; Best, I.; Olivera-Montenegro, L. Encapsulation of Bioactive Compounds for Food and Agricultural Applications. *Polymers (Basel).* **2022**, *14*(19). https://doi.org/10.3390/polym14194194

[31] Bhai, R. S. Preservation and Long-Term Storage of *Trichoderma* Spp. by Sodium Alginate Encapsulation. *J. Plant. Crop.* **2020**, *48*(1), 36–44. https://doi.org/10.25081/jpc.2020.v48.i1.6215

[32] Luft, L.; Mazutti, M. A. Freeze and Spray Drying Technologies to Produce Solid Microbial Formulations for Sustainable Agriculture. *Processes* **2025**, *13*(7). https://doi.org/10.3390/pr13072188

[33] Mondéjar-López, M.; García-Simarro, M. P.; Santiago-González, A.; Martínez-Fajardo, C.; Moreno-Giménez, E.; López-Jiménez, A.; Ahrazem, O.; Gómez-Gómez, L.; Niza, E. Chitosan Nanoparticles Loaded with *Sideritis Serrata* Lag. Extract: A New Eco-Friendly Antifungal Agent for Sustainable Agriculture. *Plants* **2025**, *14*(24), 1–16. https://doi.org/10.3390/plants14243757

[34] Nguyen, H.-T.; Pham, T.-T.; Nguyen, P.-T.; Dinh, N.-C.-G.; Le, M.-T.; Nguyen, T.-D.; Nguyen, T.-T.; Nguyen, V.-B. Microbial Biocontrol in Agriculture: From Mechanistic Understanding to Field Application. *Discov. Plants* **2025**, *2*(1). https://doi.org/10.1007/s44372-025-00421-y

[35] Reyes-Estebanez, M.; Sanmartín, P.; Camacho-Chab, J. C.; De la Rosa-García, S. C.; Chan-Bacab, M. J.; Águila-Ramírez, R. N.; Carrillo-Villanueva, F.; De la Rosa-Escalante, E.; Arteaga-Garma, J. L.; Serrano, M.; Ortega-Morales, B. O. Characterization of a Native *Bacillus Velezensis*-like Strain for the Potential Biocontrol of Tropical Fruit Pathogens. *Biol. Control* **2020**, *141*, 104127. https://doi.org/10.1016/j.biocontrol.2019.104127

[36] Azeem, S.; Agha, S. I.; Jamil, N.; Tabassum, B.; Ahmed, S.; Raheem, A.; Jahan, N.; Ali, N.; Khan, A. Characterization and Survival of Broad-Spectrum Biocontrol Agents against Phytopathogenic Fungi. *Rev. Argent. Microbiol.* **2022**, *54*(3), 233–242. https://doi.org/10.1016/j.ram.2021.10.005

[37] Nguyen, J.; Lara-Gutiérrez, J.; Stocker, R. Environmental Fluctuations and Their Effects on Microbial Communities, Populations and Individuals. *FEMS Microbiol. Rev.* **2021**, *45*(4), 1–16. https://doi.org/10.1093/femsre/fuaa068

[38] Abuhena, M.; Al-Rashid, J.; Azim, M. F.; Khan, M. N. M.; Kabir, M. G.; Barman, N. C.; Rasul, N. M.; Akter, S.; Huq, M. A. Optimization of Industrial (3000 L) Production of *Bacillus Subtilis* CW-S and Its Novel Application for Minituber and Industrial-Grade Potato Cultivation. *Sci. Rep.* **2022**, *12*(1), 1–19. https://doi.org/10.1038/s41598-022-15366-5

[39] Melin, P.; Hakansson, S.; Eberhard, T. H.; Schnurer, J. Survival of the Biocontrol Yeast *Pichia Anomala* after Long-Term Storage in Liquid Formulations at Different Temperatures, Assessed by Flow Cytometry. *J. Appl. Microbiol.* **2006**, *100*(2), 264–271. https://doi.org/10.1111/j.1365-2672.2005.02778.x

[40] Choudhary, M.; Kumar, V.; Naik, B.; Verma, A.; Saris, P. E. J.; Kumar, V.; Gupta, S. Antifungal Metabolites, Their Novel Sources, and Targets to Combat Drug Resistance. *Front. Microbiol.* **2022**, *13*(December). https://doi.org/10.3389/fmicb.2022.1061603

[41] Hirozawa, M. T.; Ono, M. A.; de Souza Suguiura, I. M.; Bordini, J. G.; Ono, E. Y. S. Lactic Acid Bacteria and *Bacillus* Spp. as Fungal Biological Control Agents. *J. Appl. Microbiol.* **2023**, *134*(2), 1–13. https://doi.org/10.1093/jambio/lxac083

[42] Ano, T.; Jin, G. Y.; Mizumoto, S.; Rahman, M. S.; Okuno, K.; Shoda, M. Solid State Fermentation of Lipopeptide Antibiotic Iturin A by Using a Novel Solid State Fermentation Reactor System. *J. Environ. Sci.* **2009**, *21*(SUPPL. 1), 162–165. https://doi.org/10.1016/S1001-0742(09)60064-4

[43] Romano, A.; Vitullo, D.; Senatore, M.; Lima, G.; Lanzotti, V. Antifungal Cyclic Lipopeptides from *Bacillus Amyloliquefaciens* Strain BO5A. *J. Nat. Prod.* **2013**, *76*(11), 2019–2025. https://doi.org/10.1021/np400119n

[44] Leconte, A.; Tournant, L.; Muchembled, J.; Paucellier, J.; Héquet, A.; Deracinois, B.; Deweer, C.; Krier,

F.; Deleu, M.; Oste, S.; Jacques, P.; Coutte, F. Assessment of Lipopeptide Mixtures Produced by *Bacillus Subtilis* as Biocontrol Products against Apple Scab (*Venturia Inaequalis*). *Microorganisms* **2022**, *10*(9), 1810. https://doi.org/10.3390/microorganisms10091810

[45] da Silva Junior, A. L.; Borges, Á. V.; da Silva, H. A. O.; Leite, I. C. H. L.; Alves, K. S.; de Medeiros, L. S.; Abreu, L. M. d. Lipopeptide-Enriched Extracts of *Bacillus Velezensis* B157 for Controlling Tomato Early Blight. *Crop Prot.* **2023**, *172*(April), 106317. https://doi.org/10.1016/j.cropro.2023.106317

[46] Mihalache, G.; Balaes, T.; Gostin, I.; Stefan, M.; Coutte, F.; Krier, F. Lipopeptides Produced by *Bacillus Subtilis* as New Biocontrol Products against Fusariosis in Ornamental Plants. *Environ. Sci. Pollut. Res.* **2018**, *25*(30), 29784–29793. https://doi.org/10.1007/s11356-017-9162-7

[47] Confortin, T. C.; Spannemberg, S. S.; Todero, I.; Luft, L.; Brun, T.; Alves, E. A.; Kuhn, R. C.; Mazutti, M. A. Microbial Enzymes as Control Agents of Diseases and Pests in Organic Agriculture. *New Futur. Dev. Microb. Biotechnol. Bioeng. Microb. Second. Metab. Biochem. Appl.* **2019**, 321–332. https://doi.org/10.1016/B978-0-444-63504-4.00021-9

[48] Chatterton, S.; Punja, Z. K.; Chatterton, S. Chitinase and β-1,3-Glucanase Enzyme Production by the Mycoparasite *Clonostachys Rosea f. Catenulata* against Fungal Plant Pathogens. *Can. J. Microbiol.* **2009**, *55* (4), 356–367. https://doi.org/10.1139/W08-156

[49] Student, M.; Hellmann, M. J.; Cord-Landwehr, S.; Moerschbacher, B. M. Chitins and Chitosans–A Tale of Discovery and Disguise, of Attachment and Attainment. *Curr. Opin. Plant Biol.* **2024**, *82*, 102661. https://doi.org/10.1016/j.pbi.2024.102661

[50] Mapuranga, J.; Chang, J.; Li, H.; Zhang, Y.; Li, R.; Song, L.; Zhang, N.; Yang, W. The Molecular Structure, Biological Roles, and Inhibition of Plant Pathogenic Fungal Chitin Deacetylases. *Front. Plant Sci.* **2024**, *14*. https://doi.org/10.3389/fpls.2023.1335646

[51] Bakker, C.; Graham, H. R.; Popescu, I.; Li, M.; McMullin, D. R.; Avis, T. J. Fungal Membrane Determinants Affecting Sensitivity to Antifungal Cyclic Lipopeptides from *Bacillus* Spp. *Fungal Biol.* **2024**, *128*(7), 2080–2088. https://doi.org/10.1016/j.funbio.2024.08.006

[52] Yue, H.; Zhong, J.; Li, Z.; Zhou, J.; Yang, J.; Wei, H.; Shu, D.; Luo, D.; Tan, H. Optimization of Iturin A Production from *Bacillus Subtilis* ZK-H2 in Submerge Fermentation by Response Surface Methodology. *3 Biotech* **2021**, *11*(2), 36. https://doi.org/10.1007/s13205-020-02540-7

[53] Tang, Z.; Zhang, H.; Xiong, J.; Li, Y.; Luo, W. Enhanced Iturin a Production in a Two-Compartment Biofilm Reactor by *Bacillus Velezensis* ND. *Front. Bioeng. Biotechnol.* **2023**, *11*. https://doi.org/10.3389/fbioe.2023.1102786

[54] Chaudhary, T.; Dixit, M.; Gera, R.; Shukla, A. K.; Prakash, A.; Gupta, G.; Shukla, P. Techniques for Improving Formulations of Bioinoculants. *3 Biotech* **2020**, *10*(5), 199. https://doi.org/10.1007/s13205-020-02182-9

[55] Holguín-Sterling, L. C.; Páez, A. R.; Patiño, A. D.; Gómez-León, J.; Blandón, L. M. Biosurfactants from Marine Bacteria to Control Anthracnose in Mango Fruits. January 3, 2023, pp 1–16. https://doi.org/10.21203/rs.3.rs-2419275/v1

[56] Fan, Y.; Liu, K.; Lu, R.; Gao, J.; Song, W.; Zhu, H.; Tang, X.; Liu, Y.; Miao, M. Cell-Free Supernatant of *Bacillus Subtilis* Reduces Kiwifruit Rot Caused by *Botryosphaeria Dothidea* through Inducing Oxidative Stress in the Pathogen. *J. Fungi* **2023**, *9*(1). https://doi.org/10.3390/jof9010127

[57] Liu, Y.; Zhang, W.; Zhang, Z.; Kou, Z.; Wang, X.; Wang, Y.; Su, X.; Zhang, J.; Liu, L.; Yan, F.; Tian, Y. Biocontrol Effects of Three Antagonistic Bacteria Strains against *Codonopsis Pilosula* Wilt Disease Caused by *Fusarium Oxysporum*. *Biol. Control* **2024**, *190*(January). https://doi.org/10.1016/j.biocontrol.2024.105446

[58] Pellegrini, M.; Pagnani, G.; Bernardi, M.; Mattedi, A.; Spera, D. M.; Gallo, M. Del. Cell-Free Supernatants of Plant Growth-Promoting Bacteria: A Review of Their Use as Biostimulant and Microbial Biocontrol Agents in Sustainable Agriculture. *Sustainability* **2020**, *12*(23), 9917. https://doi.org/10.3390/su12239917

[59] Alori, E. T.; Onaolapo, A. O.; Ibaba, A. L. Cell Free Supernatant for Sustainable Crop Production. *Front. Sustain. Food Syst.* **2025**, *9*(March), 1–15. https://doi.org/10.3389/fsufs.2025.1549048

[60] Köhl, J.; Kolnaar, R.; Ravensberg, W. J. Mode of Action of Microbial Biological Control Agents against

Plant Diseases: Relevance beyond Efficacy. *Front. Plant Sci.* **2019**, *10*(July), 1–19. https://doi.org/10.3389/fpls.2019.00845

[61] Di Rico, F.; Vuolo, F.; Puglisi, E. Evaluating the Role of Viable Cells, Heat-Killed Cells or Cell-Free Supernatants in Bacterial Biocontrol of Fungi: A Comparison Between Lactic Acid Bacteria and *Pseudomonas*. *Microorganisms* **2025**, *13*(1), 1–10. https://doi.org/10.3390/microorganisms13010105

[62] Schisler, D. A.; Slininger, P. J.; Behle, R. W.; Jackson, M. A. Formulation of *Bacillus* Spp. for Biological Control of Plant Diseases. *Phytopathology* **2004**, *94*(11), 1267–1271. https://doi.org/10.1094/PHYTO.2004.94.11.1267

[63] Melin, P.; Schnürer, J.; Håkansson, S. Formulation and Stabilisation of the Biocontrol Yeast *Pichia Anomala*. *Antonie van Leeuwenhoek, Int. J. Gen. Mol. Microbiol.* **2011**, *99*(1), 107–112. https://doi.org/10.1007/s10482-010-9522-5

[64] Kariyanna, B.; Ratnala, S.; Panda, S.; Sainath, G. Formulations of Biopesticides: Techniques, Applications, Challenges and Future Prospects. *Hexapoda* **2024**, *13*, 97–113. https://doi.org/10.55446/hexa.2024.51

[65] Oliver, R. P.; Beckerman, J. L. Formulations. In *Fungicides in Practice*; 2022; pp 107–118. https://doi.org/10.1079.9781789246926.0007

[66] Gossen, B. D.; Peng, G.; Wolf, T. M.; McDonald, M. R. Improving Spray Retention to Enhance the Efficacy of Foliar-Applied Disease- and Pest-Management Products in Field and Row Crops. *Can. J. Plant Pathol.* **2008**, *30*(4), 505–516. https://doi.org/10.1080/07060660809507550

[67] Rai, S.; Mago, Y.; Aggarwal, G.; Yadav, A.; Tewari, S. Liquid Bioformulation : A Trending Approach Towards Achieving Sustainable Agriculture. *Mol. Biotechnol.* **2023**, No. 0123456789. https://doi.org/10.1007/s12033-023-00901-0

[68] Pindi, P.; Satyanarayana, S. D. V. Liquid Microbial Consortium- A Potential Tool for Sustainable Soil Health. **2012**, *3* (4). https://doi.org/10.4172/2155-6202.1000124

[69] Zayed, M. S. Advances in Formulation Development Technologies. In *Microbial Inoculants in Sustainable Agricultural Productivity*; Springer India: New Delhi, 2016; pp 219–237. https://doi.org/10.1007/978-81-322-2644-4_14

[70] Gasic, S.; Tanovic, B. Biopesticide Formulations, Possibility of Application and Future Trends. *Pestic. i fitomedicina* **2013**, *28*(2), 97–102. https://doi.org/10.2298/PIF1302097G

[71] Jones, K. A.; Burges, H. D. Technology of Formulation and Application. In *Beneficial microorganisms, nematodes, and seed treatments*; Springer Dordrecht, 1998

[72] Khan, A.; Singh, A. V.; Gautam, S. S.; Agarwal, A.; Punetha, A.; Upadhayay, V. K.; Kukreti, B.; Bundela, V.; Jugran, A. K.; Goel, R. Microbial Bioformulation: A Microbial Assisted Biostimulating Fertilization Technique for Sustainable Agriculture. *Front. Plant Sci.* **2023**, *14*(December), 1–22. https://doi.org/10.3389/fpls.2023.1270039

[73] Lopes, M. M.; Oliveira-Paiva, C. A. de; Farinas, C. S. Modification of Pectin/Starch-Based Beads with Additives to Improve *Bacillus Subtilis* Encapsulation for Agricultural Applications. *Int. J. Biol. Macromol.* **2023**, *246*(April), 125646. https://doi.org/10.1016/j.ijbiomac.2023.125646

[74] Moradi-Pour, M.; Saberi-Riseh, R.; Esmaeilzadeh-Salestani, K.; Mohammadinejad, R.; Loit, E. Evaluation of *Bacillus Velezensis* for Biological Control of *Rhizoctonia Solani* in Bean by Alginate/Gelatin Encapsulation Supplemented with Nanoparticles. *J. Microbiol. Biotechnol.* **2021**, *31*(10), 1373–1382. https://doi.org/10.4014/jmb.2105.05001

[75] Borges, D. F.; Lopes, E. A.; Fialho Moraes, A. R.; Soares, M. S.; Visôtto, L. E.; Oliveira, C. R.; Moreira Valente, V. M. Formulation of Botanicals for the Control of Plant-Pathogens: A Review. *Crop Prot.* **2018**, *110*(January), 135–140. https://doi.org/10.1016/j.cropro.2018.04.003

[76] Gotor-Vila, A.; Usall, J.; Torres, R.; Abadias, M.; Teixidó, N. Formulation of the Biocontrol Agent *Bacillus Amyloliquefaciens* CPA-8 Using Different Approaches: Liquid, Freeze-Drying and Fluid-Bed Spray-Drying. *BioControl* **2017**, *62*(4), 545–555. https://doi.org/10.1007/s10526-017-9802-3

[77] Yánez-Mendizábal, V.; Viñas, I.; Usall, J.; Torres, R.; Solsona, C.; Abadias, M.; Teixidó, N. Formulation Development of the Biocontrol Agent *Bacillus Subtilis* Strain CPA-8 by Spray-Drying. *J. Appl. Microbiol.* **2012**, *112*(5), 954–965. https://doi.org/10.1111/j.1365-2672.2012.05258.x

[78] Wu, Z.; Zhao, Y.; Kaleem, I.; Li, C. Preparation of Calcium-Alginate Microcapsuled Microbial Fertilizer Coating *Klebsiella Oxytoca* Rs-5 and Its Performance under Salinity Stress. *Eur. J. Soil Biol.* **2011**, *47*(2), 152–159. https://doi.org/10.1016/j.ejsobi.2010.11.008

[79] Wiwattanapatapee, R.; Chumthong, A.; Pengnoo, A.; Kanjanamaneesathian, M. Preparation and Evaluation of *Bacillus Megaterium*-Alginate Microcapsules for Control of Rice Sheath Blight Disease. *World J. Microbiol. Biotechnol.* **2013**, *29*(8), 1487–1497. https://doi.org/10.1007/s11274-013-1314-4

[80] Arias-Chavarría, L. D.; Batista-Menezes, D.; Orozco-Cayasso, S.; Vargas-Martínez, A.; Vega-Baudrit, J. R.; Montes de Oca-Vásquez, G. Evaluation of the Viability of Microencapsulated *Trichoderma Longibrachiatum* Conidia as a Strategy to Prolong the Shelf Life of the Fungus as a Biological Control Agent. *Front. Chem.* **2024**, *12* (January), 1–16. https://doi.org/10.3389/fchem.2024.1473217

[81] Brar, S. K.; Sarma, S. J.; Chaabouni, E. Shelf-Life of Biofertilizers: An Accord between Formulations and Genetics. *J. Biofertilizers Biopestic.* **2012**, *03*(05). https://doi.org/10.4172/2155-6202.1000e109

[82] Raimi, A.; Roopnarain, A.; Adeleke, R. Biofertilizer Production in Africa: Current Status, Factors Impeding Adoption and Strategies for Success. *Sci. African* **2021**, *11*, e00694. https://doi.org /10.1016/j.sciaf.2021.e00694

[83] Cao, H.; Chen, Z.; Li, X.; Song, G.; Wu, Y.; Jin, J.; Cui, F.; Yuan, J.; Qi, H.; Wang, J.; Chen, J. Optimization of Fermentation Conditions for *Bacillus Velezensis* TCS001 and Evaluation of Its Growth Promotion and Disease Prevention Effects on Strawberries. *Biol. Control* **2024**, *198*, 105632. https://doi.org/10.1016/j.biocontrol.2024.105632

[84] Russi, A.; Granada, C. E.; Schwambach, J. Optimization of *Bacillus Velezensis* S26 Sporulation for Enhanced Biocontrol of Gray Mold and Anthracnose in Postharvest Strawberries. *Postharvest Biol. Technol.* **2024**, *210*, 112737. https://doi.org/10.1016/j.postharvbio.2023.112737

[85] Melly, E.; Genest, P. C.; Gilmore, M. E.; Little, S.; Popham, D. L.; Driks, A.; Setlow, P. Analysis of the Properties of Spores of *Bacillus Subtilis* Prepared at Different Temperatures. *J. Appl. Microbiol.* **2002**, *92*(6), 1105–1115. https://doi.org/10.1046/j.1365-2672.2002.01644.x

[86] Eschlbeck, E.; Bauer, S. A. W.; Kulozik, U. Effect of Cultivation PH on the Surface Hydrophobicity of *Bacillus Subtilis* Spores. *AMB Express* **2017**, *7*(1), 157. https://doi.org/10.1186/s13568-017-0458-2

[87] Hamiot, A.; Lemy, C.; Krzewinski, F.; Faille, C.; Dubois, T. Sporulation Conditions Influence the Surface and Adhesion Properties of *Bacillus Subtilis* Spores. *Front. Microbiol.* **2023**, *14* (September), 1–15. https://doi.org/10.3389/fmicb.2023.1219581

[88] Ahmad, A.-G. M.; Attia, A.-Z. G.; Mohamed, M. S.; Elsayed, H. E. Fermentation, Formulation and Evaluation of PGPR *Bacillus Subtilis* Isolate as a Bioagent for Reducing Occurrence of Peanut Soil-Borne Diseases. *J. Integr. Agric.* **2019**, *18*(9), 2080–2092. https://doi.org/10.1016/S2095-3119(19)62578-5

[89] Wu, C.; Liao, J.; Wang, J.; Qi, J. Gelation Behavior and Mechanism of Low Methoxyl Pectin in the Presence of Erythritol and Sucrose: The Role of Co-Solutes. *Int. J. Biol. Macromol.* **2024**, *271*(P1), 132261. https://doi.org/10.1016/j.ijbiomac.2024.132261

[90] Guo, X.; Chen, H.; Wang, Z.; Chen, Z.; Yu, S. Sugarcane Molasses-Induced Gelation of Low-Methoxy Pectin. *Ind. Crops Prod.* **2023**, *205* (September), 117509. https://doi.org/10.1016/j.indcrop.2023.117509

[91] Lara-Espinoza, C.; Carvajal-Millán, E.; Balandrán-Quintana, R.; López-Franco, Y.; Rascón-Chu, A. Pectin and Pectin-Based Composite Materials: Beyond Food Texture. *Molecules* **2018**, *23*(4), 942. https://doi.org/10.3390/molecules23040942

ASEAN
Journal of Scientific and Technological Reports
Online ISSN:2773-8752

Research article

Energy, Protein and Fiber Digestibility of Arrowroot Plant (*Maranta arundinacea* L.) as Feed for Native Pigs

Roger Y. Ibañez Jr.[1, 2*], Sheilo L. Mark Vasquez[2], Ulysses A. Cagasan[3], Julius V. Abela[2], Ginas Aurea A. Villagonzalo[2], and Manuel D. Gacutan, Jr.[2]

[1] Cawayan Campus, Dr. Emilio B. Espinosa Sr. Memorial State College of Agriculture and Technology, 5405, Philippines
[2] Department of Animal Science, Visayas State University, 6521, Philippines
[3] Department of Agronomy, Visayas State University, 6521, Philippines
* Correspondence: ryibanez@debesmscat.edu.ph

Citation:
Ibañez Jr., R.; Vasquez, S.M.; Cagasan, U.; Abela, J.; Villagonzalo, G.A.A.; Gacutan Jr., M. Energy and protein metabolizability of arrowroot plant (*Maranta arundinacea* L.) as feed for native pigs. *ASEAN J. Sci. Tech. Report.* **2026**, *29*(7), e261767. https://doi.org/10.55164/ajstr.v29i7.261767

Article history:
Received: October 7, 2025
Revised: April 14, 2026
Accepted: May 5, 2026
Available online: June 14, 2026

Publisher's Note:
This article is published and distributed under the terms of the Thaksin University.

Abstract: Arrowroot is an underutilized tuber crop with high starch content and potential as an alternative feed ingredient for swine. This study evaluated the energy, protein, and fiber metabolizability of arrowroot-based feedstuffs in native pigs. Fifteen native pigs representing three age groups (2, 4, and 7 months) were assigned to five treatments in a randomized complete block design: fasted pigs for endogenous loss determination (control), commercial feed, ensiled arrowroot whole plant, arrowroot tuber meal, and fresh arrowroot whole plant. Commercial feed recorded the highest true COD_{energy} (92.54%), followed by fresh arrowroot whole plant (90.42%), arrowroot tuber meal (89.51%), and ensiled arrowroot whole plant (86.94%), although differences were not significant ($p=0.1779$). True $COD_{protein}$ differed significantly ($p=0.0034$), with commercial feed (93.61%) and fresh arrowroot whole plant (88.27%) showing higher values compared with arrowroot tuber meal (72.50%) and ensiled arrowroot whole plant (68.27%). Fiber digestibility was generally high, with fresh arrowroot whole plant exhibiting the highest neutral detergent fiber (94.69%) and acid detergent fiber (96.07%) utilization. Voluntary feed intake was significantly higher in pigs fed commercial feed (304.17 g/day) compared with arrowroot-based diets, although fresh whole plant (232.08 g/day) and tuber meal (202.08 g/day) showed acceptable intake levels. These findings suggest that arrowroot, particularly in its fresh whole-plant form, has potential as an alternative energy and fiber source for native pigs under controlled digestibility conditions. However, since this study focused only on coefficient of digestibility (energy, protein, fiber), further research is needed to evaluate growth performance, feed efficiency, carcass characteristics, and economic feasibility.

Keywords: Arrowroot; native pigs; true metabolizable energy; true metabolizable protein

1. Introduction

Arrowroot (*Maranta arundinacea* L.) is an underutilized tuber crop with high potential as a feed ingredient due to its nutrient composition. In many regions, it remains neglected compared to other root crops, despite its carbohydrate-rich profile. Previous studies have shown that arrowroot contains more than 85% starch on a dry-weight basis [1] and up to 98.10% on a wet-weight basis [2], making it a highly digestible energy source [3]. Digestibility

trials conducted by Kumari et al. [4] revealed that arrowroot exhibits an in vitro digestibility of 30.07% and an in vivo digestibility of 95.7%. Erdman and Erdman [5] found that ensiled arrowroot aerial biomass and processing residues have digestibility values ranging from 38.5% to 60.03% of dry matter, with crude protein (CP) contents ranging from 10.8% to 21.1%, ether extract (EE) contents between 11.2% and 30.2%, and ash levels of 3.8% to 17.0%. These findings underscore arrowroot's potential as a nutrient-rich and digestible feed resource. Although arrowroot is primarily valued for its carbohydrate content, it also contains moderate levels of crude protein (2.9–5.3% CP on a dry weight basis) [6] and small amounts of crude fat (2.2–8.5% in aerial parts) [7]. When its aerial parts are preserved through ensiling, arrowroot contains about 12.1% crude protein (CP), 1.99% ether extract (EE), 16.19% ash, and 66.54% neutral detergent fiber (NDF), with a gross energy value of roughly 3,723 calories per gram [7]. It's also packed with essential amino acids, including lysine, methionine, leucine, and valine, as well as minerals such as calcium, magnesium, potassium, and phosphorus [6]. These nutrients support protein synthesis, metabolic processes, and overall animal health, suggesting that arrowroot is a viable supplementary protein and mineral source for livestock.

Despite its nutritional potential, arrowroot also contains antinutritional factors (ANFs), such as alkaloids, glycosides, saponins, phenols, tannins, and flavonoids, that may hinder nutrient availability for animal absorption and utilization [8,9]. However, several studies have shown that fermentation and ensiling can significantly reduce ANFs in feedstuffs [10-12], thereby improving the nutritional value of alternative feed ingredients, including arrowroot. Using alternative feed resources is crucial in swine production, where feed costs can reach up to 70% of total production expenses. Native pigs are important for smallholder and backyard farming systems in the Philippines because they adapt well to tropical climates, thrive on low-quality feeds, and support rural livelihoods [13-15]. Due to their natural eating behavior, these pigs can tolerate high-fiber diets, making them ideal for testing unconventional feed resources like arrowroot. In previous years, arrowroot has been studied as a feed for ruminants and rabbits, but its use in swine diets remains limited, particularly regarding its nutrient digestibility. To assess its potential as feed for native pigs, evaluating its energy and protein contributions, along with its digestibility, is crucial. Therefore, this study aims to evaluate the nutrient digestibility of arrowroot as a feed for native pigs with emphasis on its crude protein, energy value, and digestibility. The findings of this study could support smallholder farmers and reduce reliance on costly commercial feeds.

2. Methodology

2.1 Ethical Considerations in the Use of Pigs in the Study

The ethical treatment of pigs in this study was guaranteed by following established animal welfare protocols and securing authorization from the Institutional Animal Care and Use Committee (IACUC) of the Matias H. Aznar Memorial College of Medicine, Inc. Every procedure focused on the animals' welfare, aiming to reduce any pain or stress throughout the study. Appropriate care, handling, and humane euthanasia techniques were employed in line with ethical guidelines to ensure that the animals' welfare was prioritized at all times.

2.2 Silage Preparation

Arrowroot whole plants were harvested and chopped using a forage chopper into 1–2 cm lengths, following the method described by Hang et al. [16]. The chopped materials were then sun-dried to achieve a target moisture content of approximately 60–70%, as recommended by Lan et al. [17]. This moisture level is considered optimal before ensiling to minimize nutrient losses from effluent seepage and support proper fermentation. The prepared materials were packed into 25-kg polypropylene bags (approximately 61 cm × 74 cm). Air was removed using a vacuum machine to create anaerobic conditions and reduce the risk of undesirable microbial growth during fermentation. The bags were then tightly sealed using rubber bands, weighed, and properly labeled. The sealed silage bags were stored in a room maintained at 20–30°C, consistent with recommended silage fermentation conditions reported by Bai et al. [18]. The materials were allowed to ferment for 21 days before use in the feeding trial. After the 21-day fermentation period, the silage achieved a final pH of 4.96, indicating successful fermentation and good preservation quality suitable for feeding.

2.3 Metabolism Trial

The metabolism trial was conducted to determine the true coefficient of energy digestibility (COD_{energy}), and true coefficient of protein digestibility ($COD_{protein}$) of native pigs, following the protocol of Moughan et al. [19]. A total of 15 native pigs were used, representing three age groups: 2, 4, and 7 months. At the start of the trial, each pig was weighed to record its initial body weight, which served as the basis for calculating the feed allowance. The pigs were given a seven-day adaptation period to acclimate them to the test diets. On the eighth day, they fasted to ensure their digestive tracts were free of residual feed that could affect the digestibility results. On the ninth day, the pigs were fed with a ration equivalent to 4% of their body weight, as recommended by Dong et al. [20]. The ration was divided into two equal meals, administered at 8:00 AM and 4:00 PM. Clean drinking water was provided ad libitum through nipple drinkers throughout the trial. Total fecal collection commenced on the tenth day of the trial and continued for 4 days. Each grab sample of feces collected in the morning and afternoon was weighed, placed in 250 mL plastic containers, and placed in a solar dryer. Both diet and excreta samples were oven-dried for 48 hours at 60–70°C and subsequently weighed. The samples were analyzed for gross energy using bomb calorimetry, as well as for crude protein, ash, NDF, and ADF, following the procedures of the Association of Official Analytical Chemists [21]. Urine was collected in the morning and afternoon during the 4-day collection period. To prevent nitrogen volatilization in urine, 1 mL of sulfuric acid was added per liter of urine [22]. Cotton was soaked in the acidified urine solution and oven-dried at 60–70°C for 24 hours to prepare it for energy and nitrogen analyses.

2.4 Research Design

The study was laid out as a one-factor experiment using a Randomized Complete Block Design (RCBD). The experiment consisted of five treatments: control for endogenous loss, commercial feed, ensiled whole plant, tuber meal, and fresh whole plant. Each treatment was blocked by native pig age. The pigs were housed in uniform metabolism pens equipped with separate sections for feces and urine collection to facilitate accurate sample gathering. Pigs were sourced from reliable native swine raisers in Baybay City. The pens were placed under consistent temperature and humidity conditions to minimize stress-induced variability. Water was provided ad libitum to prevent any potential effects of feed deprivation or dehydration. Health status was monitored daily, and the same personnel handled the pigs throughout the study to minimize variations in handling techniques that could influence behavior and metabolism.

2.5 Data Collection

The data obtained were true coefficient of energy digestibility (COD_{energy}), true coefficient of protein digestibility ($COD_{protein}$), true coefficient of fiber digestibility (COD_{fiber}). The COD_{energy} was determined by quantifying gross energy intake (GEi) and subtracting the energy losses through feces (GEf), urine (GEu), and endogenous sources (GEend). The resulting value was then divided by GEi and multiplied by 100 to obtain COD_{energy} as a percentage:

$$COD_{energy}\ (\%) = \frac{GEi - (GEf + GEu - GEend)}{GEi} \times 100 \quad (1)$$

True Coefficient of protein Digestibility ($COD_{protein}$). The $COD_{protein}$ was calculated by measuring total protein intake (Pi) and subtracting protein losses in feces (Pf), urine (Pu), and endogenous sources (Pend). The value was divided by Pi and expressed as a percentage:

$$COD_{protein}\ (\%) = \frac{Pi - (Pf + Pu - Pend)}{Pi} \times 100 \quad (2)$$

True Coefficient of fiber Digestibility (COD_{fiber}). Fiber digestibility was computed by measuring neutral detergent fiber (NDFi) or acid detergent fiber (ADFi) intake and subtracting the undigested fiber excreted in feces (NDFf or ADFf). The digestibility was expressed as a percentage of intake:

$$COD_{fiber}\ (\%) = \frac{NDFi \text{ or } ADFi - NDFf \text{ or } ADFf}{NDFi \text{ or } ADFi} \times 100 \quad (3)$$

2.6 Data Analysis

Data were analyzed using analysis of variance (ANOVA) in a one-factor Randomized Complete Block Design. Statistical analyses were performed using the Proc General Linear Model in SAS Version 9.4.

Significant differences among treatment means were tested using Tukey's Honest Significant Difference (HSD) test and declared significant at $\alpha = 0.05$.

3. Results and Discussion

3.1 Nutrient composition of feedstuffs

The proximate composition of the experimental diets is presented in Table 1. Commercial feed exhibited the highest crude protein (CP, 16.0%) and gross energy (3,234 cal/g), reflecting its formulated balance of protein and energy sources. In contrast, arrowroot-based feedstuffs contained considerably lower CP levels, ranging from 3.34% in tuber meal to 4.60% in fresh whole plant, consistent with earlier reports that arrowroot is primarily an energy crop with limited protein content [6]. Ether extract (EE) was markedly higher in fresh whole plant (9.82%) compared with both ensiled (0.51%) and tuber meal (6.66%). This indicates that the aerial portion contributes lipid fractions, which may enhance energy density but can also be susceptible to oxidative rancidity if not properly processed [7]. Fiber fractions differed substantially among diets. Ensiled arrowroot whole plant showed the highest neutral detergent fiber (NDF, 42.91%) and acid detergent fiber (ADF, 30.39%), reflecting the structural polysaccharides of mature foliage. Conversely, tuber meal had very low ADF (4.13%), aligning with its starchy nature. Such variation is critical because high fiber generally reduces nutrient availability in monogastrics [21]. Interestingly, commercial feed contained the lowest fiber content (NDF, 10.70%; ADF, 2.67%), highlighting the deliberate formulation to optimize nutrient digestibility. The high ash content in ensiled material (10.91%) compared to tuber meal (0.89%) suggests that foliage contributes greater mineral fractions, supporting the role of arrowroot aerial biomass as a mineral source. Similar findings were reported by Heuzé et al. [6], who documented higher mineral content in arrowroot aerial parts compared with tubers. Likewise, Tarique et al. [7] reported that arrowroot foliage contains appreciable ash and mineral components, reinforcing its potential as a mineral-rich feed resource.

Table 1. Nutrient composition of arrowroot-based feedstuffs and commercial diet fed to native pig (DM basis).

Diets	DM (%)	OM (%)	GE (cal/g)	CP (%)	EE (%)	NDF (%)	ADF (%)	HC (%)	Ash (%)
Ensilaged arrowroot whole plant	70.55	89.09	2906	4.33	0.51	42.91	30.39	9.19	10.91
Arrowroot tuber meal	28.0	99.11	3298	3.34	6.66	15.74	4.13	11.62	0.89
Fresh arrowroot whole plant	16.99	98.10	3087	4.60	9.82	40.32	28.18	12.14	1.84
Commercial Feed	87.58	95.86	3234	16.00	1.63	10.70	2.67	16.92	4.14

Note: Values represent the mean of replicated laboratory analyses of feed samples.

3.2 Average daily feed intake and feed refusal of native pigs

The voluntary feed intake and average feed refusal of native pigs fed different arrowroot-based feedstuffs are presented in Table 2. Average daily feed intake (ADFI) of native pigs was significantly affected by diet ($P = 0.0114$), with intake increasing from ensiled arrowroot whole plant to commercial feed. Pigs fed commercial feed recorded the highest ADFI (304.17 g/day), followed by fresh arrowroot whole plant (232.08 g/day[1]) and arrowroot tuber meal (202.08 g/day), while the lowest intake was observed in pigs fed ensiled arrowroot whole plant (114.17 g/day). The reduced intake in pigs fed ensiled whole-plant arrowroot indicates lower palatability, likely associated with higher fiber content and fermentation end products, such as organic acids. High dietary fiber levels have been reported to reduce voluntary feed intake in pigs due to increased gut fill and slower gastric emptying, thereby limiting feed consumption in monogastric animals [23]. In addition, fermentation acids formed during ensiling may negatively affect feed palatability and reduce intake, as reported by Simwaka et al. [12]. Despite lower intake compared with commercial feed, fresh arrowroot whole plant and tuber meal demonstrated acceptable intake levels, suggesting that native pigs can adapt to alternative feed resources. Native pig breeds have been reported to tolerate fibrous and unconventional feed ingredients, owing to enhanced hindgut fermentation and greater feeding adaptability compared with improved breeds [23].

Table 2. Voluntary feed intake (ADFI) and average feed refusal (AFR) of native pigs fed with different arrowroot feedstuffs and commercial feed

Diets	ADFI (g)	ADFR (g)
Ensilaged arrowroot whole plant	114.17b	0.01
Arrowroot tuber meal	202.08ab	0.03
Fresh arrowroot whole plant	232.08ab	0.02
Commercial Feed	304.17a	0.06
SEM	25.84	0.02
P-Value	0.0114	0.4006

Means with the same letter are not significantly different at ($p > 0.05$).

Average feed refusal (AFR) was not significantly affected by diet ($p = 0.4006$), indicating similar acceptance across treatments. Although pigs fed commercial feed showed numerically higher refusal (0.06 g) than those fed arrowroot-based diets (0.01–0.03 g), the differences were minimal and statistically non-significant. The low feed refusal across treatments suggests that all diets were generally acceptable to native pigs and resulted in minimal feed wastage. Similar findings were reported in studies involving indigenous pig breeds, where acceptable palatability of alternative feed ingredients resulted in low feed refusal and efficient feed utilization [14].

3.3 Coefficient of Digestibility of arrowroot-based diets

True coefficient of energy digestibility (COD_{energy}) was not significantly affected by diet ($p = 0.1779$), although fresh arrowroot whole plant showed higher numerical values (90.42%) next to commercial feed (92.54%), arrowroot tuber meal (89.51%), and ensiled arrowroot whole plant (86.94%). The higher COD_{energy} in fresh arrowroot indicates better energy availability from readily digestible carbohydrates, while the slightly lower values in ensiled material suggest possible energy losses during fermentation. These results are consistent with the growing interest in plant-based and forage resources as sustainable alternative feeds for livestock in tropical regions [23]. Similar findings were reported by Coulibaly et al. [11], who noted that ensiling tropical forages may reduce energy availability due to fermentation-associated nutrient losses. Comparable variation in the estimated metabolizable energy of fermented agricultural biomass and cassava-based by-products has likewise been reported in ruminant feeding studies [24], underscoring how processing method influences the energy contribution of alternative feedstuffs.

Table 3. Nutrient metabolizability of arrowroot-based feedstuffs and commercial diet in native pigs

Diets	COD_{energy} (%)	$COD_{protein}$ (%)	COD_{fiber}	
			NDF (%)	ADF (%)
Ensilaged arrowroot whole plant	86.94	68.27[b]	86.48	86.47[b]
Arrowroot tuber meal	89.51	72.50[b]	88.97	87.56[b]
Fresh arrowroot whole plant	90.42	88.27[a]	94.69	96.07[a]
Commercial Feed	92.54	93.61[a]	93.99	94.91[a]
SEM	1.53	3.15	1.82	2.04
P-Value	0.1779	0.0034	0.0513	0.0330

Means with the same letter are not significantly different at ($P>0.05$.

True $COD_{protein}$ was significantly affected by diet ($p = 0.0034$), with commercial feed (93.61%) and fresh arrowroot whole plant (88.27%) showing higher values compared with ensiled arrowroot whole plant (68.27%) and arrowroot tuber meal (72.50%). This indicates improved protein utilization in commercial feed and fresh plant material, while processing through ensiling or tuber extraction reduced protein availability. The reduced $COD_{protein}$ in fermented feeds may be associated with protein degradation and formation of less digestible nitrogen compounds during ensiling, as similarly observed in tropical silage systems [12] and supported by reports on antinutritional factors affecting protein utilization in root crops [9]. Neutral detergent fiber (NDF) digestibility was not significantly affected by diet ($p = 0.0513$), although fresh arrowroot whole plant exhibited

the highest numerical value (95.69%), followed by commercial feed (93.99%), arrowroot tuber meal (88.97%), and ensiled whole plant (86.48%). The higher fiber utilization in fresh arrowroot suggests efficient microbial fermentation of structural carbohydrates in the hindgut of native pigs. This supports the findings of Ngoc et al. [25], who reported that native pigs possess a strong fiber-digesting capacity due to enhanced hindgut fermentation. Acid detergent fiber (ADF) digestibility was significantly affected by diet ($p = 0.0330$), with fresh arrowroot whole plant (96.07%) and commercial feed (94.91%) showing higher values compared with arrowroot tuber meal (87.56%) and ensiled whole plant (86.47%). The higher ADF digestibility in fresh arrowroot indicates improved digestibility of cellulose and lignified fractions when fed in fresh form, consistent with previous reports that forage freshness enhances fiber degradation in monogastric herbivores [11]. Despite these findings, several limitations should be considered. The study used a small sample size ($n = 3$ per treatment) due to the high cost and limited availability of native pigs, which may affect the statistical power of the results. In addition, the metabolism trial was conducted under controlled conditions with restricted feeding, which may not fully reflect practical production systems. Antinutritional factors (ANFs) were not directly measured, as the study focused on the metabolizability of energy, protein, and fiber and relied on existing literature for ANF-related explanations. Furthermore, economic analysis was not included in this study, as it is being addressed in a separate ongoing investigation.

4. Conclusions

This study evaluated the coefficient of digestibility and voluntary feed intake of arrowroot-based feedstuffs in native pigs under controlled metabolism trial conditions. The results showed that fresh arrowroot whole plant exhibited the highest numerical values for true coefficient of energy and fiber utilization, while ensiled arrowroot generally resulted in lower intake and reduced nutrient metabolizability compared with other treatments. True coefficient of protein digestibility was significantly higher in commercial feed and fresh arrowroot whole plant, indicating better protein utilization in these diets, whereas arrowroot tuber meal and ensiled forms showed lower values, reflecting limited protein availability and possible processing-related losses. However, this study was limited to measurements of digestibility and intake under a controlled experimental setup. Therefore, further studies are recommended to evaluate growth performance, feed efficiency, carcass characteristics, and economic viability, and to optimize processing methods, such as ensiling, to improve nutrient utilization and reduce antinutritional factors.

5. Acknowledgments

The authors wish to thank the Department of Science and Technology – Accelerated Science and Technology Human Resource Development Program – Science Education Institute (DOST-ASTHRDP-SEI) for the scholarship and financial support that made this study possible.

Author Contributions: R.Y.I.J & S.M.L.V: Data collection, recording, discussion, interpretation of results validation, and editing; U.A.C, J.V.A, G.A.AV, & M.D.G.J: Conceptualization, methodology, Literature review, proofreading, and critiquing. All authors have read and agreed to the published version of the manuscript.

Funding: This study was funded by the Department of Science and Technology–Accelerated Science and Technology Human Resource Development Program–Science Education Institute (DOST-ASTHRDP-SEI).

Conflicts of Interest: The authors declare no conflict of interest.

References

[1] Prehaten, D.; Hardiwinoto, S.; Na'iem, M.; Supriyo, H.; Widiyatno, W.; Rodiana, D. Productivity of Arrowroots and Taro Grown under Superior Teak Clones with Several Levels of Stand Density. *Biosaintifika: Journal of Biology & Biology Education* **2021**, *13*(1), 51–57. https://doi.org/10.15294/biosaintifika.v13i1.26428

[2] Faridah, D. N.; Fardiaz, D.; Andarwulan, N.; Sunarti, T. Physicochemical Characterisation of Arrowroot Starch (*Maranta arundinacea*). *Agritech* **2014**, *34*(1), 14–21.

[3] Malki, M. K. S.; Wijesinghe, J. A. A. C.; Ratnayake, R. H. M. K.; Thilakarathna, G. C. Characterization of Arrowroot (*Maranta arundinacea*) Starch as a Potential Starch Source for the Food Industry. *Heliyon* **2023**, *9*(9), e20033. https://doi.org/10.1016/j.heliyon.2023.e20033

[4] Kumari, S.; Singh, A.; Tamrakar, P. Arrowroot—Gluten-Free, Multipurpose Crops. *Int. J. Multidiscip. Res.* **2022**, *4*(4), 179–190. https://doi.org/10.36948/ijfmr.2022.v04i04.021

[5] Erdman, M. D.; Erdman, B. A. Arrowroot (*Maranta arundinacea*): Food, Feed, Fuel, and Fiber Resource. *Econ. Bot.* **1984**, *38* (3), 332–341. https://doi.org/10.1007/BF02859011

[6] Heuzé, V.; Tran, G. Arrowroot (*Maranta arundinacea*). *Feedipedia*, 2022. https://www.feedipedia.org /node/545 (accessed 2026-06-07).

[7] Tarique, J.; Sapuan, S. M.; Khalina, A.; Sherwani, S. F. K.; Yusuf, J.; Ilyas, R. A. Recent Developments in Sustainable Arrowroot (*Maranta arundinacea* Linn) Starch Biopolymers, Fibres, Biopolymer Composites and Their Potential Industrial Applications: A Review. *J. Mater. Res. Technol.* **2021**, *13*, 1191–1219. https://doi.org/10.1016/j.jmrt.2021.05.047

[8] Jayakumar, A.; Suganthi, A. Biochemical and Phytochemical Analysis of *Maranta arundinacea* (L.) Rhizome. *Int. J. Res. Pharm. Pharm. Sci.* **2017**, *2*(3), 26–30.

[9] Iamkeng, S.; Santibenchakul, S.; Sooksawat, N. Potential of *Maranta arundinacea* Residues for Recycling: Analysis of Total Phenolic, Flavonoid, and Tannin Contents. *Biodiversitas* **2022**, *23*(3). https://doi.org/10.13057/biodiv/d230303

[10] Samtiya, M.; Aluko, R. E.; Dhewa, T. Plant Food Antinutritional Factors and Their Reduction Strategies: An Overview. *Food Prod. Process. Nutr.* **2020**, *2*(1), 2–14. https://doi.org/10.1186/s43014-020-0020-5

[11] Coulibaly, A.; Kouakou, B.; Chen, J. Phytic Acid in Cereal Grains: Structure, Healthy or Harmful Ways to Reduce Phytic Acid in Cereal Grains and Their Effects on Nutritional Quality. *Am. J. Plant Nutr. Fertil. Technol.* **2011**, *1*(1), 1–22. https://doi.org/10.3923/ajpnft.2011.1.22

[12] Simwaka, J. E.; Chamba, M. V. M.; Huiming, Z.; Masamba, K. G.; Luo, Y. Effect of Fermentation on Physicochemical and Antinutritional Factors of Complementary Foods from Millet, Sorghum, Pumpkin and Amaranth Seed Flours. *Int. Food Res. J.* **2017**, *24*(5), 1869–1879.

[13] Falculan, K. N. Phenotypic Characterization of Native Pig in Romblon Province, Philippines. *Technium BioChemMed* **2021**, *2*(3), 1–17. https://doi.org/10.47577/biochemmed.v2i3.4373

[14] Muth, P. C.; Pohlmann, I. K.; Bae, S.; Reiber, C.; Bondoc, O. L.; Valle Zárate, A. Does Backyard-Keeping of Native Sows by Smallholders in Quezon, Philippines, Offer Sustainability Benefits Compared to More Intensive Management of Exotic Sow Breeds? *J. Agric. Rural Dev. Trop. Subtrop.* **2020**, *121*(1), 43–55. https://doi.org/10.17170/KOBRA-202002281033

[15] Santiago, R.; Palima, C.; Rosales, B. O. Native Pigs: A Climate Resilient Business Enterprise. *BAI-NSPRDC Bulletin* **2020**, 8–11.

[16] Hang, L.; Preston, T.; Ba, N.; Dung, D. Effect of Biochar on Growth and Methane Emissions of Goats Fed Fresh Cassava Foliage. *Livest. Res. Rural Dev.* **2019**, *31*(5).

[17] Lan, L.; Hung, L.; Thu, N.; Loc, H.; Liang, J.; Thiet, N.; Ngu, N. Effects of Substituting Taro (*Colocasia esculenta*) Wastes Silage in Diets on Growth and Nutrient Digestibility in Pigs. *J. Anim. Health Prod.* **2021**, *9*(2), 112–118. https://doi.org/10.17582/journal.jahp/2021/9.2.112.118

[18] Bai, J.; Ding, Z.; Su, R.; Wang, M.; Cheng, M.; Xie, D.; Guo, X. Storage Temperature Is More Effective than Lactic Acid Bacteria Inoculations in Manipulating Fermentation and Bacterial Community Diversity, Co-Occurrence, and Functionality of Whole-Plant Corn Silage. *Microbiol. Spectr.* **2022**, *10*(2), e00101-22. https://doi.org/10.1128/spectrum.00101-22

[19] Moughan, P. J.; Smith, W. C.; Schrama, J.; Smits, C. Chromic Oxide and Acid-Insoluble Ash as Fecal Markers in Digestibility Studies with Young Growing Pigs. *N. Z. J. Agric. Res.* **1991**, *34*(1), 85–88. https://doi.org/10.1080/00288233.1991.10417796

[20] Dong, W.; Wang, Q.; Chen, J.; Liu, L.; Zhang, S. Apparent Total Tract Digestibility of Nutrients and the Digestible and Metabolizable Energy Values of Five Unconventional Feedstuffs Fed to Growing Pigs. *J. Appl. Anim. Res.* **2019**, *47*(1), 273–279. https://doi.org/10.1080/09712119.2019.1625778

[21] AOAC International. *Official Methods of Analysis*, 22nd ed.; AOAC International: Gaithersburg, MD, USA, 2023.

[22] Hellström, D.; Johansson, E.; Grennberg, K. Storage of Human Urine: Acidification as a Method to Inhibit Decomposition of Urea. *Ecol. Eng.* **1999**, *12*(3–4), 253–269. https://doi.org/10.1016/S0925-8574(98)00074-3

[23] Napalinga, C. P. Plant-Based Feed and Forage Research for Livestock: A Bibliometric Review. *ASEAN J. Sci. Technol. Rep.* **2025**, *28*(5). https://doi.org/10.55164/ajstr.v28i5.259394

[24] Jirawattanasomkul, N.; Roschat, W.; Leelatam, T.; Phanphli, S.; Chaipikun, W.; Thammayod, A.; Khotsuno, N.; Yeemin, P.; Wongma, N.; Phewphong, S. Evaluation of the Nutritional, Mineral, and Estimated Metabolizable Energy Values of Agricultural Biomass Raw Materials Used for the Development of Concentrated Fermented Feed for Beef Cattle in Mukdahan Province, Northeast Thailand. *ASEAN J. Sci. Technol. Rep.* **2026**, *29*(4). https://doi.org/10.55164/ajstr.v29i4.262452

[25] Ngoc, T. T. B.; Oanh, N. C.; Hong, T. T. T.; Dang, P. K. Effects of Dietary Fiber Sources on Bacterial Diversity in Separate Segments of the Gastrointestinal Tract of Native and Exotic Pig Breeds Raised in Vietnam. *Vet. World* **2021**, *14*(10), 2579–2587. https://doi.org/10.14202/vetworld.2021.2579-2587

ASEAN
Journal of Scientific and Technological Reports
Online ISSN:2773-8752

Research article

Development and Evaluation of a Web-Based GIS-Enabled Demographic Profiling System for Data-Driven Local Government Policy Making

Anna Monica Paculaba[1*]

[1] Samar State University, Catbalogan City, Samar, 6700, Philippines
* Correspondence: monica.paculaba@ssu.edu.ph

Citation:
Paculaba, M.A. Development and evaluation of a web-based gis-enabled demographic profiling system for data-driven local government policy making *ASEAN J. Sci. Tech. Report.* **2026**, *29*(7), e262067. https://doi.org/10.55164/ajstr.v29i7.262067

Article history:
Received: October 26, 2025
Revised: April 12, 2026
Accepted: May 13, 2026
Available online: June 14, 2026

Publisher's Note:
This article is published and distributed under the terms of the Thaksin University.

Abstract: Timely and accurate demographic data have become an important factor for effective local governance. However, many municipalities in the 2nd District of Samar have yet to gather and collate household data automatically. Advanced methods often yield siloed datasets that clutter analysis and reduce the likelihood of spatial visualization. Consequently, the information generated is less useful in formulating effective sub-national policies. Furthermore, current demographic information systems are not integrated with GIS or web-based applications, creating a disconnect between data collection and information generation. This study aimed to fill the gap by developing a web-based GIS-enabled demographic profiling system to strengthen evidence-based policy-making among local government units (LGUs) in the 2nd District of Samar. The system integrates household-level demographic records and visualizes them through interactive GIS maps and dashboards for easier access, management, and spatial analysis. A descriptive research design was used to evaluate the system's functionality, reliability, usability, efficiency, maintainability, and portability, following the ISO 9126/25010 software quality framework. Further, the system's development follows the Waterfall System Development Life Cycle (SDLC) model. Results showed that the system met essential software quality standards and substantially improved how demographic data are accessed and analyzed. Thus, the system enhances Samar's LGUs' ability to design well-informed, inclusive, and community-oriented local policies.

Keywords: Information system development; waterfall model; ISO 9126/25010 quality model; web-based system; information system assessment

1. Introduction

Effective governance requires timely, relevant, and spatially referenced population information. Governments at the global, national, and local levels are recognizing that health services, infrastructure, disaster preparedness, and social protection plans require population and household statistics [1,2]. Over the past decade, the convergence of web technologies and Geographic Information Systems (GIS) has transformed how such data are collected, analyzed, and presented. Web-based information systems provide real-time data capture and integration, while GIS adds spatial intelligence, enabling decision-makers to visualize and query demographic indicators across

geographic scales [3-5]. Together, these technologies provide actionable insights for evidence-based policy formulation on raw demographic data.

Web-based GIS platforms can be applied in various governance and planning contexts, demonstrating potential to transform spatial decision-making. The effects of the systems impacted forest conservation, climate change, urban planning, and public health significantly[3]. These tools also enable data-driven decision-making by providing new, innovative capabilities to manage resources and respond to crises [6]. For example, a web-GIS platform design for sustainable waste governance in Istanbul that enabled stakeholder participation and real-time data sharing [7]. Also, the technology's utilization in urban governance has strengthened through visualization, enabling informed decision-making and enhancing citizen participation [9]. Thus, web-based GIS is vital for modern collaborative governance. Furthermore, many studies suggest that demographic profiling, along with spatial analysis, can significantly improve policy-making capabilities. The evidence indicates that a range of policies can create a certain impact. This shows how geodemography can help gain an understanding of our population and allow for more targeted interventions in urban planning, public health, and disaster management [9]. Also, spatial integration enables the identification of asynchronous data across different levels of government and provides useful geographic perspectives for demographic policy-making [10].

The Philippines faces significant challenges in leveraging Web-GIS platforms and spatial analytics for evidence-based policy-making, despite promising technological initiatives. The Community-Based Monitoring System (CBMS) pertains to a major national initiative that aims to enhance local-level data[11]. While the national Community-Based Monitoring System (CBMS) provides vital socioeconomic indicators, there is a recognized opportunity to enhance local agility by bridging the time between national data collection and real-time local application. Many local government units (LGUs) still use manual, paper-based workflows, which can result in fragmented data. [12]. Furthermore, existing systems primarily focus on single-sector issues, such as health surveillance or disaster mapping, rather than integrated household-level profiling. Studies reveal that Web-GIS technologies can support real-time integrated spatial analysis and decision-making systems [13]. Limited disaggregation, pooling of local government spending data, and sub-national survey capacity are the key challenges. It restricts the accurate measurement of many development indicators and the impacts of policies. Web-based GIS tools in the Philippines demonstrate significant potential for demographic analysis but remain fragmented across sector-specific applications. Research highlights diverse implementations, including health surveillance[14], election monitoring[15], and population data management[16]. Although these studies validate the feasibility of web-GIS applications in the Philippines, they mostly focus on a single sectoral problem, such as health surveillance, disaster mapping, or housing gaps. Furthermore, they rarely integrate household-level demographic profiling with dynamic, interactive spatial analysis to inform policy formulation.

The Eastern Visayas region in the Philippines, particularly Samar Province, urgently requires integrated demographic information systems due to its vulnerability to poverty and natural hazards[17]. Within this province, the 2nd District faces a persistent problem with household-level demographic data. Municipal Rural Health Units and Planning Offices rely heavily on manual processes to gather, tabulate, and extract information. The delay in updates, bad transcription, and limited mapping of household locations, sanitation conditions, and unmet need for family-planning services are due to these paper-based workflows. The Community-Based Monitoring System (CBMS) has provided numerous socioeconomic indicators. However, CBMS has yet to have an integrated LGU-managed web-based GIS platform capable of converting raw household data into decision-ready, spatially explicit information [11]. Consequently, it is difficult for local government units in the 2nd District of Samar to identify spatial patterns of vulnerability, create targeted interventions, and monitor development outcomes. Moreover, while there are studies on web-based GIS and demographic profiling, a distinct gap exists: there is no published research on the development and evaluation of a web-based, GIS-enabled demographic profiling system by the local government in the context of the Philippine LGU operationalized at the district scale. Existing Philippine systems do not usually have interactive spatial dashboards, nor are they designed for broad purposes. What is needed instead is an end-

to-end solution that integrates household data, visualizes indicators on sanitation and family planning, and allows for evidence-based policy formulation.

The present study aims to fill this gap by creating a web-based GIS-enabled demographic profiling system for the 2nd District of Samar. The system aims to strengthen local policy-making, service delivery, and data-driven governance in an environment where manual workflows hamper effective decision-making by converting household data generated manually into interactive, spatially explicit, and query-ready information. This system is designed to complement the national Community-Based Monitoring System (CBMS) by providing a localized, real-time interface tailored for immediate LGU operations. While the CBMS serves as a vital national initiative for comprehensive socioeconomic data, this platform offers the 2nd District of Samar the agility to process and visualize household-level data in real time, facilitating rapid, evidence-based local interventions.

2. Materials and Methods

2.1 Materials

2.1.1 Research Design

This study utilized developmental-descriptive research, a type of research common in information systems research, in which functional prototypes are designed, implemented, and evaluated as the subject of research [18-19]. The design's development stage was realized through the application of the Waterfall Software Development Life Cycle (SDLC) model, comprising requirements analysis, system design, implementation, testing, deployment, and maintenance [20]. On the other hand, the descriptive aspect of the study was incorporated during the assessment phase. Specifically, the system's effectiveness was evaluated using the ISO 9126 quality model. While ISO 25010 is the newer standard, ISO 9126 was chosen to focus strictly on the six core characteristics (Functionality, Reliability, Usability, Efficiency, Maintainability, and Portability) most critical for software deployment in resource-constrained local government environments. The evaluation used standardized tools, including validated questionnaires and usability testing, ensuring that findings were quantifiable and replicable.

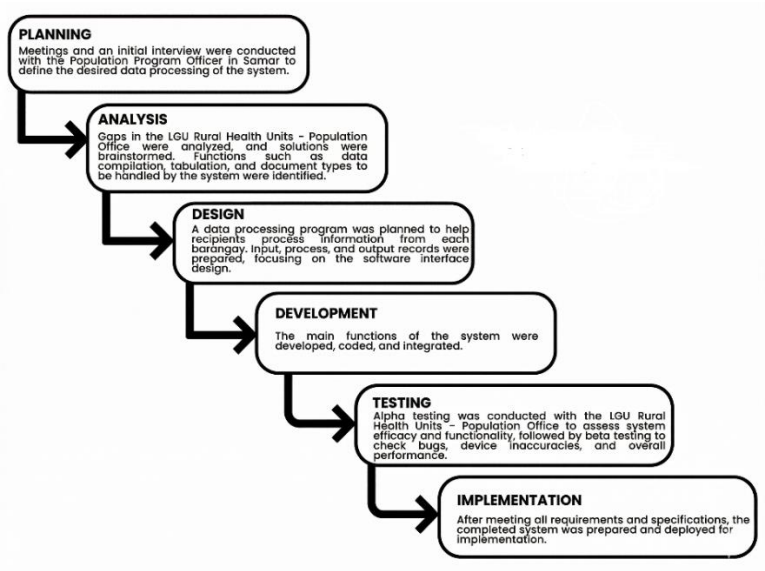


Figure 1. Waterfall Software Development Life Cycle

2.1.2 Data Sources

Two primary data sources were employed in this study. The first dataset consisted of household-level socio-demographic variables, including household composition, sanitation facilities, family planning utilization, and socio-economic characteristics. Initially, household-level demographic data were taken from the paper forms as administered by Local Government Unit (LGU) personnel and Rural Health Unit (RHU) staff in the 2nd District of Samar. The initial input used for the study comprised these records, which included socio-demographic and economic data. The information system developed will enable the encoding,

integration, and storage of collected data for analysis and incorporation into the digital environment. The second dataset comprises evaluation data from the end users. This was evaluative feedback from LGU personnel and RHU officers who were purposely selected as respondents. The officials selected were the primary users of the developed system for demographic profiling, program implementation, and policy formulation at the municipal level. The feedback was collected through standardized questionnaires based on the ISO 9126 framework that assesses the quality of software in terms of effectiveness, usability, reliability, and relevance to the functioning of local governance. To achieve an evaluation process, the participants were LGUs and RHUs, the primary users of the system at the municipal level and the ones directly implementing demographic profiling, programs, and policies.

2.1.3 Respondents

The evaluation of the system involved 30 respondents purposively selected from various municipalities within the 2nd District of Samar. The participant group comprised a representative mix of target end-users, specifically Local Government Unit (LGU) Planning and Development Officers, Population Program Officers, and Rural Health Unit (RHU) staff. The selection criteria required that respondents be directly involved in the manual preparation of demographic profiles, policy drafting, or health program implementation. Their domain expertise was leveraged to ensure a credible assessment of the system's functionality and its practical applicability within the local governance context. Information on their specific roles and expertise was used to validate the system's usability across different technical skill levels.

2.1.4 Instrument

A questionnaire was utilized, derived from the quality model (ISO 9126/25010), to evaluate the software. The tool was organized into six dimensions: functionality, usability, reliability, efficiency, maintainability, and portability. For each item, a five-point effectiveness scale was administered. The scales for the categories are as follows: not effective (NE) is between 1.00-1.50, slightly effective (SE) is between 1.51-2.50, moderately effective (ME) is between 2.51-3.50, highly effective (HE) is between 3.51-4.50, and extremely effective (EE) is between 4.51-5.00.

For data analysis, descriptive statistics were used. The average enabled the researcher to obtain a measure of the central tendency of responses for each software quality dimension. The standard deviation (SD) is a measure of the variability of user perceptions. If the SD is lower, that means the evaluators have the same answer. If the SD is higher, that means they have different answers. Using the SD along with the mean strengthened the analysis of the question, as both results indicate the effectiveness of the solution and the degree of agreement across respondents.

2.2 Methods

2.2.1 System Development Approach

The Waterfall Software Development Life Cycle (SDLC) model was used to develop this Web-Based GIS-Enabled Demographic Profiling System. This model comprises the following phases: analysis, system design, implementation, testing, deployment, and maintenance. The Waterfall model was chosen as the software development life cycle, as it has clearly defined study objectives and suitable documentation for long-term sustainability in the local government context. Each phase produced deliverables that informed subsequent phases, ensuring that design ambiguity was kept to a minimum while verification was carried out systematically.

2.2.2 Tools and Technologies

The system was designed and implemented using a set of open-source technologies. This was done to apply major cost savings while ensuring adaptability and sustainability in resource-poor environments. The selected technologies were chosen for their ability to ensure scalability and maintainability, as well as compatibility with government IT infrastructure standards. The tools cover server-side scripting, client-side interactivity, geospatial processing, and database management and deployment across different layers of system development.

Table 1. Tools and Technologies Used in System Development

Technology/Tool	Purpose/Function
PHP	A server-side scripting language used to implement system logic/functions.
Laravel Framework	It provides an automatic MVC (Model-View-Controller) architecture, which leads to easy scalability, maintainability, and secure development of web applications.
JavaScript	Enables dynamic client-side interaction and handles requests asynchronously for better responsiveness.
Leaflet.js	An open-source JavaScript library for visualization functions and mapping geospatial data.
QGIS	A desktop GIS application mainly used for pre-processing spatial data sets for validation and projection consistency.
PostgreSQL	Household-level demographic data were stored in a relational database system.
PostGIS Extension	Improves PostgreSQL to store spatial data and run geospatial queries.
HTML5, CSS3, Bootstrap	Front-end tools to create a responsive, user-friendly interface.
Apache Web Server	A web server is used to host the application.
Linux Environment	The deployment platform was chosen to be compatible with open-source standards and the existing LGU IT infrastructure.

Table 1 summarizes the various tools and technologies used, along with their major functions in the system. The combined use of these technologies yielded a system that will be technically robust and more practical for Local Government Units (LGUs) to adopt. Their combined application made the system more efficient, easier to use, and scalable, thereby supporting improved data-driven governance and policy formulation.

Table 2. System Features and Functions of the Web-Based GIS-Enabled Demographic Profiling System

Module	Description	Core Functions/Capabilities
Data Entry and Compilation Module	It allows Local Government Unit staff and Rural Health Unit officers to input and upload household demographic information.	Web-based applications for individual household entry Batch uploading of demographic records Data validation during entry to reduce errors
Data Management Module	This provides a secure mechanism for storage, retrieval, and updating household datasets.	Centralized database management CRUD operations (Create, Read, Update, Delete) Version control and audit logging
GIS Visualization and Analysis Module	Translates demographic data into geographical maps and supports geospatial analysis.	Interactive map visualization using GIS tools Detection of spatial clusters (e.g., poverty, sanitation) Query functions for targeted analysis
Reporting and Dashboard Module	Provides dynamic dashboards and custom reporting for evidence-based decision making.	Real-time statistical summaries Customizable charts and graphs Exportable reports (PDF, Excel) for official use
User Access and Security Module	Prevents unauthorized users from accessing and manipulating data to preserve the confidentiality of information.	Role-based access control Authentication and authorization mechanisms Secure data transmission and storage

2.2.3 System Features and Functions

The developed system comprised five core modules, each designed to address specific functional requirements and support evidence-based decision-making for LGUs.

This modular design enhanced the system's usability and aligned its functionality with the actual flow of operations in the planning and management of health services in LGUs.

2.2.4 Evaluation Procedure

The assessment of the developed system was carried out using the ISO 9126/25010 software quality model, which provides a dimensional framework for software quality evaluation. It involves functionality, reliability, usability, efficiency, maintainability, and portability. These dimensions were chosen as they are internationally recognized benchmarks of software quality.

The respondents were purposively selected as evaluators among the Local Government Unit (LGU) staff and Rural Health Unit (RHU) officers from the 2nd District of Samar, as they serve as the primary end-users of the system and are involved in demographic profiling and policy formulation. Before the assessment, the respondents were oriented on system features and guided to undertake hands-on exercises such as data entry, report generation, and GIS-based visualization.

Two primary instruments were used for the evaluation:

A questionnaire standardized based on ISO 9126/25010 – this tool was adapted to measure user perception of system effectiveness across the six quality dimensions. It used a five-point Likert scale with responses ranging from 1 (Not Effective) to 5 (Very Effective).

System's usability testing sessions – respondents were asked to perform the system's key functionality: entering demographic data, visualizing household distributions, and generating statistical reports. To capture ease of use, task completion time, and user errors, observational notes were used to identify items that could provide additional insights.

2.2.5 Data Analysis

The data collected from the respondents were evaluated using descriptive statistics, including the mean and standard deviation (SD). The mean was used to calculate the central tendency of responses from participants regarding functionality, reliability, usability, efficiency, maintainability, and portability. To assess the level of variation in responses, the standard deviation was computed, which helps in understanding users' perceptions. If SD values are low, it indicates that respondents agree. If they are high, it signifies that the respondents do not agree. The mean value was interpreted from an effectiveness scale 4.51 to 5.00 Extremely Effective (EE), 3.51 to 4.50 Highly Effective (HE), 2.51 to 3.50 Moderately Effective (ME), 1.51 to 2.50 Slightly Effective (SE), and 1.00 to 1.50 Not Effective (NE). Including the SD with the mean not only represented the effectiveness rating but also clearly showed the consistency of the analysis.

2.2.6 System architecture and Data Flow

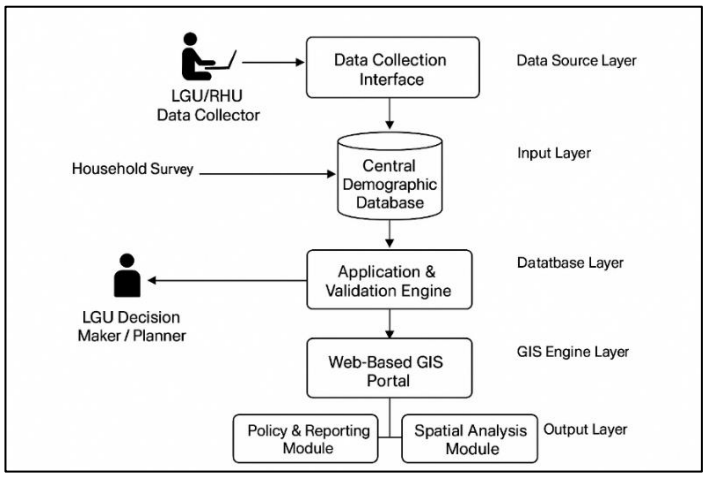


Figure 2. System architecture and Data Flow Diagram of the Web-Based GIS-Enabled Demographic Profiling System.

Figure 2 shows the system architecture of the proposed Web-Based GIS-Enabled Demographic Profiling System, which enables seamless acquisition, processing, and spatial visualization of demographic and sanitation data to support evidence-based decision-making at the local government unit (LGU) level. The data source layer initiates data acquisition through LGU and Rural Health Unit (RHU) personnel who conduct structured household surveys and field interviews. Using the Data Collection Interface, field staff directly encode demographic and sanitation information, reducing transcription errors and eliminating inefficiencies common in paper-based workflows. On the other hand, at the input layer, household information flows into the Central Demographic Database, a secure, centralized repository designed for the immediate storage and retrieval of household composition, socio-economic attributes, and sanitation indicators. Systematic data handling at this stage enables accurate information for the downstream processing. Moreover, the Application and Validation Engine ensures data integrity and consistency in the database layer. The component automatically checks, collects records, and controls the use of the dataset for spatial and statistical analysis, enabling timely decisions based on reliable data. Furthermore, the GIS engine layer serves as the analytical and visualization core, linking verified demographic and sanitation data to geographic coordinates through the Web-Based GIS Portal. The resulting GIS-based maps provide an overview of household locations and sanitation status. This enables spatial pattern searches, service gaps, and areas of vulnerability. Finally, the output layer provides insights through the Policy and Reporting Module and the Spatial Analysis Module. The use of interactive dashboards, dynamic map displays, and real-time reports provides ample evidence for LGU decision-makers and planners to formulate policies, target interventions, and continuously monitor development indicators.

3. Results and Discussion

3.1 System's Interface

This section illustrates the main system interfaces of the developed web-based GIS-enabled demographic profiling system. The system supports various modules, such as user login, demographic data entry, GIS information visualization, and report generation. All forms are accompanied by a description of how the system enables the LGU to manage household demographic information at the household level. Through these interfaces, the study highlights the system's user-oriented design and its ability to encourage evidence-based decision-making at the local level.

3.1.1 Login Form

As shown in Figure 3, the login page can be accessed only by authorized personnel from the Local Government Unit (LGU) and Rural Health Unit (RHU). A standard username and password authentication mechanism was employed to protect confidential demographic information from unauthorized access. The design is minimalist for ease of use, allowing users to enter their credentials and access the main dashboard easily.

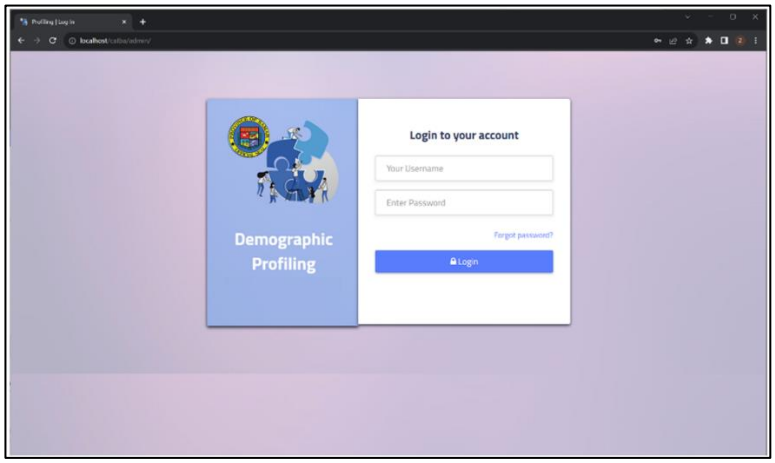


Figure 3. Log-In Form of the Web-Based GIS-Enabled Demographic Profiling System

3.1.2 Data Entry Form

As shown in Figure 4, the data entry module allows authorized personnel to enter household-level demographic information, such as family composition, economic status, and health-related information. The design consists of intuitive fields and dropdown menus, along with validations for incorrect input, to facilitate error-free data entry. This feature enables the digital encoding of bulk household data, eliminating the need for paper records.

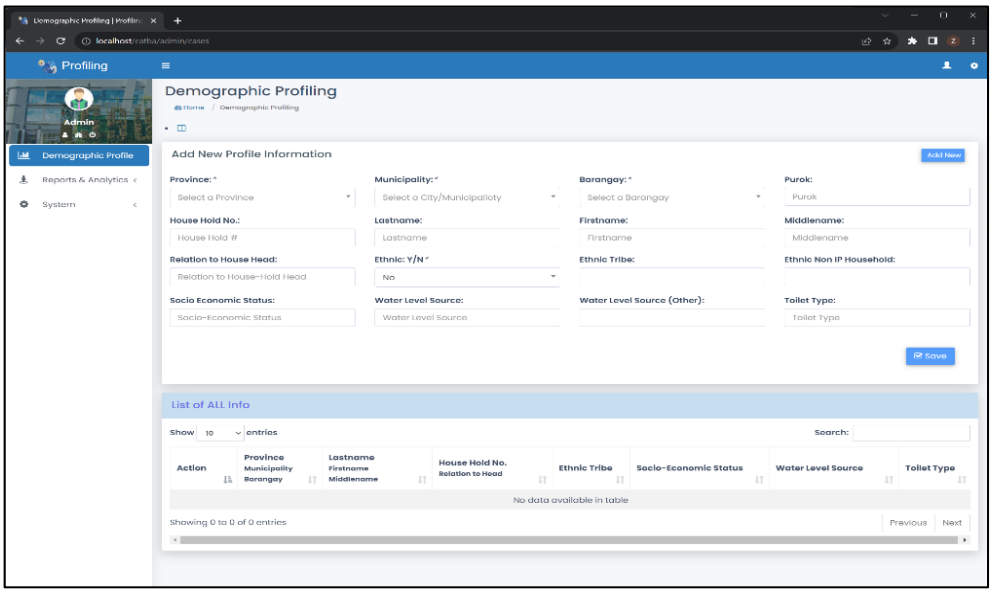
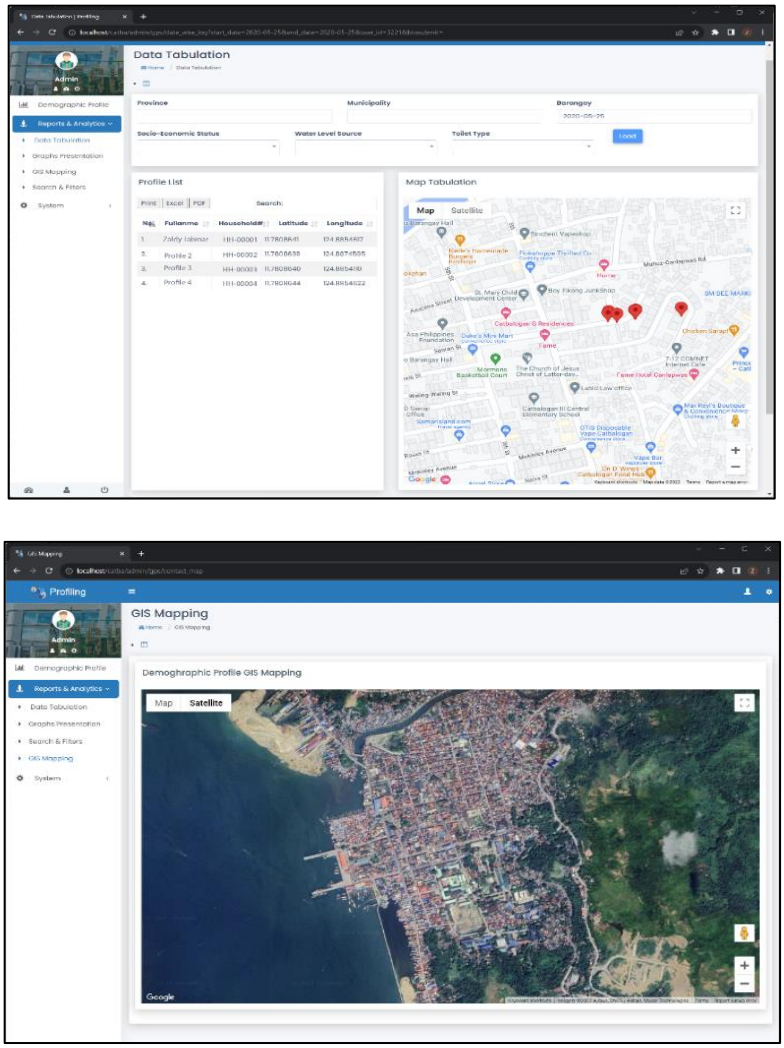


Figure 4. Data Entry Form of the Web-Based GIS-Enabled Demographic Profiling System

3.1.3 Reports/GIS Visualization

The reporting module provides a summary of household demographic data in table and graphical forms, as well as GIS visualization, as shown in Figure 5. Along with numerical indicators, such as household size composition, socio-economic classification, and population counts, the module also presents GIS-based maps showing the distribution of households and sanitation status. Using GIS-enabled reporting, a user can find the exact locations of households and their sanitation status within a community. It will also help identify clusters of households without facilities. This feature strengthens the decision-making process by providing a dual perspective—statistical and spatial—thereby allowing Local Government Units (LGUs) to prioritize interventions, allocate resources efficiently, and design policies grounded in both quantitative data and geographic evidence.

During the system's pilot implementation in the 2nd District of Samar, a Municipal Planning Officer used the GIS Visualization module to assess the local sanitation program. By filtering the dataset for 'No Sanitary Toilet Facility,' the system immediately identified a dense geographic cluster in an isolated purok that had been overlooked in previous aggregated, paper-based reports. This spatial evidence empowered the Municipal LGU to pivot its policy, shifting from a general, town-wide subsidy to a targeted sanitation infrastructure project specifically for the georeferenced households in that cluster. This transition from broad-based to evidence-based intervention ensured that limited municipal resources were allocated with maximum impact, directly addressing a critical public health gap identified through the system.



Figures 5. Reports/GIS Visualization Forms of the Web-Based GIS-Enabled Demographic Profiling System

3.2 System's Evaluation Results

Table 3. Level of Effectiveness of the System along Functionality as Assessed by the Respondents (n = 30)

Indicators	Mean (M)	Standard Deviation (SD)	Interpretation
The system performs the required task	4.30	0.55	Highly Effective
The system displays an accurate result	4.70	0.46	Extremely Effective
The system can interact with another system	4.30	0.52	Highly Effective
The system prevents unauthorized access	4.60	0.48	Extremely Effective
Grand Mean	4.48	0.50	Highly Effective

[3] Legend: 4.51–5.00 = Extremely Effective (EE); 3.51–4.50 = Highly Effective (HE); 2.51–3.50 = Moderately Effective (ME); 1.51–2.50 = Slightly Effective (SE); 1.00–1.50 = Not Effective (NE)

The functionality of the Web-Based GIS-Enabled Demographic Profiling System was assessed and evaluated by 30 respondents across four indicators, as shown in Table 3. The grand mean was 4.48 (SD = 0.50), indicating a Highly Effective (HE) level. The result suggests that the system effectively executes its main functions, produces accurate results, supports interoperability, and provides secure access. In terms of the

system's effectiveness, the display of accurate results ranked highest (M = 4.70, SD = 0.46). This means that respondents have confidence in the outputs' reliability for decision-making or for drawing demographic profiles. The indicator on preventing unauthorized access received an average score of 4.60 with a standard deviation of 0.48, indicating it was Extremely Effective. This reflects that the system prevents unauthorized access to sensitive household-level data.

On the other hand, performing required tasks and interaction with other platforms obtained a mean score of 4.30 (Highly Effective) with slightly higher SD (0.52–0.55). This implies that respondents largely agreed that the system is effective, but not all shared the same opinions as the previous indicators. This means that further improvement, particularly concerning interoperability, can enhance the system's long-term viability for LGUs.

The low SD values across all indicators indicate consistent evaluations, strengthening the overall credibility of the findings. The obtained results confirm that the system responds to functional requirements from the ISO 9126/25010 quality model, which aligns with previous studies that found that functional requirements are the backbone of government information systems [21-22].

Table 4. Level of Effectiveness of the System along Reliability as Assessed by the Respondents (n = 30)

Indicators	Mean (M)	Standard Deviation (SD)	Interpretation
The system is error-free	4.60	0.48	Extremely Effective
The system is capable of handling errors	4.40	0.52	Highly Effective
The system can resume and restore lost data after failure	4.40	0.50	Highly Effective
The system presents integrated reports	4.40	0.51	Highly Effective
Grand Mean	4.45	0.50	Highly Effective

[4] Legend: 4.51–5.00 = Extremely Effective (EE); 3.51–4.50 = Highly Effective (HE); 2.51–3.50 = Moderately Effective (ME); 1.51–2.50 = Slightly Effective (SE); 1.00–1.50 = Not Effective (NE)

Table 4 shows that the system's reliability was rated by respondents at a grand mean of 4.45 (SD = 0.50), indicating Highly Effective (HE). As indicated, users found that the system was stable, reliable, and performed its task appropriately without major problems. The indicator rated Extremely Effective (EE) was "The system is error-free" (M = 4.60, SD = 0.48), which had the highest mean score in the evaluation. This means users strongly believe the system can operate robustly and without critical failures. In the meantime, the error handling, data recovery after failure, and integrated report generation indicators obtained a mean score of 4.40, indicating Highly Effective (HE). Based on these findings, while the system has good handling and recovery measures, users still see opportunities to improve its long-term resilience and fault tolerance. The low standard deviation values of 0.48-0.52 indicate greater consensus among the respondents, suggesting confidence in the system's reliability. These findings support the ISO 9126/25010 quality model, which says reliability is an essential factor in user trust and continued use of a system. This result aligns with other studies that state that a reliable system improves the continuity of digital service delivery in governance and public administration [23-24].

As shown in Table 5, the system's overall usability achieved a grand mean of 4.58 (SD = 0.50), indicating Extremely Effective (EE). The rating shows that respondents agree that the system's operation requires minimal effort. Moreover, the system is intuitive and easy to learn. The findings imply that the user interface design and overall user experience were tailored to the needs of Local Government Unit (LGU) staff and Rural Health Unit (RHU) officers. The consistently high mean scores across indicators demonstrate that the system successfully balanced technical complexity with user accessibility. The simplicity and learnability of the system were appreciated by the respondents, as they play an important role in its adoption. The mean rating of 4.45 for interface aesthetics, while somewhat lower, is still within the Highly Effective range. This means that while users found the interface's graphics acceptable, further enhancements to design and layout can increase engagement. The standard deviation scores of 0.31 to 0.52 across all indicators reveal a consensus

among respondents with low variations. Thus, regardless of their technical skill levels, they found the system usable. This finding agrees with previous studies, which state that usability is an important factor for user acceptance and continued use of digital governance platforms [25-26].

Table 5. Level of Effectiveness of the System along Usability as Assessed by the Respondents (n = 30)

Indicators	Mean (M)	Standard Deviation (SD)	Interpretation
The system is easy to use	4.67	0.47	Extremely Effective
The user can learn to use the system easily	4.62	0.49	Extremely Effective
The user can use the system without much effort	4.57	0.50	Extremely Effective
The interface of the system looks good	4.45	0.52	Highly Effective
Grand Mean	4.58	0.50	Extremely Effective

[5] Legend: 4.51–5.00 = Extremely Effective (EE); 3.51–4.50 = Highly Effective (HE); 2.51–3.50 = Moderately Effective (ME); 1.51–2.50 = Slightly Effective (SE); 1.00–1.50 = Not Effective (NE)

Table 6. Level of Effectiveness of the System along Efficiency as Assessed by the Respondents (n = 30)

Indicators	Mean (M)	Standard Deviation (SD)	Interpretation
The system responds quickly	4.60	0.47	Extremely Effective
The system can handle predicted volumes of data in a timely and efficient manner	4.70	0.46	Extremely Effective
The system uses an internal search facility to let users find what they want quickly and efficiently	4.50	0.50	Highly Effective
This system has all the functions and capabilities that the user expects it to have	4.40	0.52	Highly Effective
Grand Mean	4.60	0.49	Extremely Effective

[6] Legend: 4.51–5.00 = Extremely Effective (EE); 3.51–4.50 = Highly Effective (HE); 2.51–3.50 = Moderately Effective (ME); 1.51–2.50 = Slightly Effective (SE); 1.00–1.50 = Not Effective (NE)

The Web-Based GIS-Enabled Demographic Profiling System's efficiency was rated by the respondents as Extremely Effective (EE), as indicated by a grand mean of 4.60 (SD = 0.49) in Table 6. The result shows that the system can respond to user commands quickly, manage large volumes of demographic data, and provide access to important information on time for decision-making. The system is rated highest in being able to handle expected volumes of data (M = 4.70, SD = 0.46), which shows the respondents trust the system would be able to manage and process large quantities of data. In local government settings, information that requires regular updates and multi-stakeholder access must be demographic in nature. The system's ability to respond quickly to commands was also highly rated, further demonstrating on-time results.

While both are still in the Highly Effective range, the internal search facility and system capabilities scored slightly lower than user expectations (M = 4.50 and 4.40, respectively). The research indicates that this system meets the key efficiency requirements. However, enhancements to many advanced searches, as well as the system's general features, will yield better user satisfaction. The low value of SD, that is, (0.46 - 0.52) across the indicators, indicates agreement among respondents and thus reflects consensus on efficiency. The results are consistent with the ISO 9126/25010 quality model, which identifies efficiency as a key factor for software performance. In addition, the result aligns with previous studies that efficient systems enable real-time data management and policy decision-making in governance contexts [27-28].

Table 7. Level of Effectiveness of the System along Portability as Assessed by the Respondents (n = 30)

Indicators	Mean (M)	Standard Deviation (SD)	Interpretation
The system can be moved to other environments	4.40	0.50	Highly Effective
The system is easy to install	4.30	0.55	Highly Effective
The system complies with the portability standard	4.60	0.48	Extremely Effective
The system can easily integrate with other software	4.50	0.51	Highly Effective
Grand Mean	4.45	0.51	Highly Effective

[7] Legend: 4.51–5.00 = Extremely Effective (EE); 3.51–4.50 = Highly Effective (HE); 2.51–3.50 = Moderately Effective (ME); 1.51–2.50 = Slightly Effective (SE); 1.00–1.50 = Not Effective (NE)

Table 7 shows that the portability of the Web-Based GIS-Enabled Demographic Profiling System was evaluated as Highly Effective (HE), with a grand mean of 4.45 (SD = 0.51). This illustrates that the said system is adaptable across various locations, easy to operate and set up, and highly portable and interoperable with standard software applications used by local governments and government environments. The system's adherence to portability standards received the highest rating (M = 4.60, SD = 0.48). This means that respondents consider the system meets recognized standards, which ensure it is sustainable and can be applied widely. In government settings, the ability to scale and transfer in multiple jurisdictions is especially advantageous. Likewise, the integration indicator (M = 4.50, SD = 0.51) was rated Highly Effective, suggesting system flexibility in communicating with other platforms to support collaborative governance and data sharing.

System transferability to other environments (M = 4.40; SD = 0.50) and ease of installation (M = 4.30; SD = 0.55) also impact the overall impression, yet received lower ratings, although still Highly Effective. These findings imply that the system can largely be moved and installed without too much trouble. Improving procedures and automating installation tools could, however, further improve portability and reduce the burden on users. The SD values (0.48–0.55) for the indicators indicate that respondents have similar perceptions and agree on system portability. According to the ISO 9126/25010 quality model, portability is an important factor that determines sustainability. The ISO 9126/25010 quality model recognizes portability as an essential factor in software sustainability, and the psychometric results confirm this. These findings support previous research, which affirms that portable, interoperable systems are most likely to be used in local government. Further, portability and integration features strengthen cross-sectoral collaboration [29-31].

4. Conclusions

The development and evaluation of the Web-Based GIS-Enabled Demographic Profiling System provide a transformative framework for data-driven local government policymaking. By digitalizing manual, paper-based registries through a robust geospatial architecture, the system empowers local government units (LGUs) with the spatial intelligence required to identify geographic clusters of community needs and implement targeted interventions with unprecedented agility. Evaluated as highly effective across all ISO 9126 software quality dimensions, the study demonstrates that integrating international technical benchmarks is a vital prerequisite for modernizing local governance tools. In practice, this platform serves as a high-impact, localized companion to national programs like the CBMS, offering real-time reporting and administrative flexibility to bridge the gap between data collection and immediate policy application. While the implementation highlights the need to address technical dependencies, such as connectivity and data integrity, it establishes a scalable digital foundation for more resilient and inclusive governance. Future advancements in predictive analytics will further enable local authorities to anticipate demographic shifts and vulnerabilities before they manifest, ensuring that local policies remain proactive, evidence-based, and community-oriented.

5. Acknowledgments

The author acknowledged the Samar Island Center for Good and Local Governance (SICGLG) of Samar State University for its support in making this study possible.

Author Contributions: Conceptualization, methodology, validation, formal analysis, resources, data curation, writing—original draft preparation, writing—review and editing, funding acquisition, project administration, and supervision are contributed by A.M.P.

Funding: Samar Island Center for Good and Local Governance (SICGLG) of Samar State University.

Conflicts of Interest: The author declares no conflict of interest.

References

[1] Chen, C.-W.; Wei, J. C.-C. Employing Digital Technologies for Effective Governance: Taiwan's Experience in COVID-19 Prevention. *Health Policy Technol.* **2023**, *12*(2), 100755. https://doi.org/10.1016/j.hlpt.2023.100755

[2] Jones, M.; Moeller, E. A.; Meara, J. G.; Juran, S. The Importance of Geographic and Demographic Data from Census for Locating and Mapping Vulnerable Populations. *Stat. J. IAOS* **2021**, *37*(1), 13–17. https://doi.org/10.3233/SJI-200760

[3] Vinueza-Martinez, J.; Correa-Peralta, M.; Ramirez-Anormaliza, R.; Franco Arias, O.; Vera Paredes, D. Geographic Information Systems (GISs) Based on WebGIS Architecture: Bibliometric Analysis of the Current Status and Research Trends. *Sustainability* **2024**, *16*(15), 6439. https://doi.org/10.3390/su16156439

[4] Duarte, L.; Teodoro, A. C. GIS Open-Source Plugins Development: A 10-Year Bibliometric Analysis on Scientific Literature. *Geomatics* **2021**, *1*(2), 206–245. https://doi.org/10.3390/geomatics1020013

[5] Lata, K.; Sood, A.; Kaur, K.; Benipal, A. K.; Pateriya, B. Web-GIS Based Dashboard for Real-Time Data Visualization & Analysis Using Open Source Technologies. *J. Geomat.* **2022**, *16*(2), 134–146. https://doi.org/10.58825/jog.2022.16.2.42

[6] Rita Uchenna Attah; Baalah Matthew Patrick Garba; Ifechukwu Gil-Ozoudeh; Obinna Iwuanyanwu. Leveraging Geographic Information Systems and Data Analytics for Enhanced Public Sector Decision-Making and Urban Planning. *Magna Sci. Adv. Res. Rev.* **2024**, *12*(2), 152–163. https://doi.org/10.30574/msarr.2024.12.2.0191

[7] Karademir, M.; Özbakır Acımert, B. A. Sustainable Waste Governance Framework via Web-GIS: Kadikoy Case. *Sustainability* **2024**, *16*(16), 7171. https://doi.org/10.3390/su16167171

[8] Li, Y.; Lai, Y.; Lin, Y. The Role of Diversified Geo-Information Technologies in Urban Governance: A Literature Review. *Land* **2024**, *13*(9), 1408. https://doi.org/10.3390/land13091408

[9] Gnyawali, B.; Sigdel, U. Geodemography: Geospatial Stream of Demographic Analysis. *Janajyoti J.* **2025**, *3*(1), 173–187. https://doi.org/10.3126/jj.v3i1.83307

[10] Wijaya, A. P.; Nugraha, A. L.; Sukmono, A.; Firdaus, H. S. Study on the Analysis of Demographic Data Based on Spatial Information Systems. *IOP Conf. Ser. Earth Environ. Sci.* **2022**, *1098*(1), 012029. https://doi.org/10.1088/1755-1315/1098/1/012029

[11] Reyes, C.; Vargas, A. R.; Arboneda, A. *Evidence-Based Local Planning and Budgeting Using the CBMS*; Research Paper Series; Philippine Institute for Development Studies, 2022. https://doi.org/10.62986/rps2022.02

[12] Abidoye, B.; Orlic, E. Localizing the Sustainable Development Goals: A Case for Investment in Data and Impact Evaluation. *Stat. J. IAOS* **2022**, *38*(3), 863–878. https://doi.org/10.3233/SJI-220058.

[13] Daud, M.; Ugliotti, F. M.; Osello, A. Comprehensive Analysis of the Use of Web-GIS for Natural Hazard Management: A Systematic Review. *Sustainability* **2024**, *16*(10), 4238. https://doi.org/10.3390/su16104238

[14] Belizario, Jr., V. Y.; Delos Trinos, J. P. C. R.; Lentejas, N.; Alonte, A. J.; Cuayzon, A. N.; Isiderio, M. E.; Delgado, R.; Tejero, M.; Molina, V. B. Use of Geographic Information System as a Tool for

Schistosomiasis Surveillance in an Endemic Municipality in Eastern Samar, The Philippines. *Geospatial Health* **2021**, *16*(1). https://doi.org/10.4081/gh.2021.957

[15] Salubre, H. C.; Dela Cerna, M. A.; Chua, F. V. A.; Buniel, G. G.; Tiu, G. D. Web-Based Election Monitoring Integrating Barangay Geospatial Mapping. In *2022 IEEE 3rd Global Conference for Advancement in Technology (GCAT)*; IEEE: Bangalore, India, 2022; pp 1–8. https://doi.org/10.1109/GCAT55367.2022.9971959

[16] Sasmito, G. W.; Ratono, R. WebGIS Development to Integrate, Visualize, Map, and Disseminate Population Data. In *2023 International Conference on Computer Science, Information Technology and Engineering (ICCoSITE)*; IEEE: Jakarta, Indonesia, 2023; pp 784–789. https://doi.org/10.1109/ICCoSITE57641.2023.10127778

[17] Pantolla, H.; Atibagos-Nacion, N. Spatial Analysis of Poverty Incidence and Road Networks in Eastern Visayas Region, Philippines. *Philipp. J. Sci.* **2023**, *152*(4). https://doi.org/10.56899/152.04.01

[18] Faza, A.; Prasetiawan, I.; Donovan, D.; Eldora, K.; Zethro, Z.; Indrawan, S. R.; Kurniawan, M. I. Design and Development of an Audit Information System Prototype. In *2024 International Conference on Informatics Engineering, Science & Technology (INCITEST)*; IEEE: Bandung, Indonesia, 2024; pp 1–7. https://doi.org/10.1109/INCITEST64888.2024.11121485

[19] M, S.; R, B. L.; Balakkrishnan, M.; H, A. The Development of a Design Theory for Web Based Information Systems. *J. Comput. Nat. Sci.* **2023**, 113–123. https://doi.org/10.53759/181X/JCNS202303011

[20] Pargaonkar, S. A Comprehensive Research Analysis of Software Development Life Cycle (SDLC) Agile & Waterfall Model Advantages, Disadvantages, and Application Suitability in Software Quality Engineering. *Int. J. Sci. Res. Publ.* **2023**, *13*(8), 120–124. https://doi.org/10.29322/IJSRP.13.08.2023.p14015

[21] Suparto, H. S.; Dai, R. H. Evaluasi Kualitas Sistem Informasi Pengukuran Prestasi Kerja Berdasarkan ISO/IEC 25010. *Jambura J. Inform.* **2021**, *3*(2), 109–120. https://doi.org/10.37905/jji.v3i2.11744

[22] Ariyani, S.; Sudarma, M.; Wicaksana, P. A. Analysis of Functional Suitability and Usability in Sales Order Procedure to Determine Management Information System Quality. *INTENSIF J. Ilm. Penelit. Dan Penerapan Teknol. Sist. Inf.* **2021**, *5*(2), 234–248. https://doi.org/10.29407/intensif.v5i2.15537

[23] AbdulKareem, A. K.; Oladimeji, K. A. Cultivating the Digital Citizen: Trust, Digital Literacy and e-Government Adoption. *Transform. Gov. People Process Policy* **2024**, *18*(2), 270–286. https://doi.org/10.1108/TG-11-2023-0196

[24] Hakeem, M. J.; Sulphey, M. M. Investigating the Adoption of Smart Local Government Services: The Impact of Service Quality, Trust, and Social Influence. *Transform. Gov. People Process Policy* **2024**, *18*(4), 785–802. https://doi.org/10.1108/TG-06-2024-0136

[25] Master of Science in Management Information Systems, Lamar University, Texas, USA.; Barua, T.; Rahman, M. A.; MBA in Management Information System, International American University, Los Angeles, USA. A Systematic Literature Review Of User-Centric Design In Digital Business Systems Enhancing Accessibility, Adoption, And Organizational Impact. *Am. J. Sch. Res. Innov.* **2023**, *02*(02), 193–216. https://doi.org/10.63125/36w7fn47

[26] Bastardo, R.; Pavão, J.; Rocha, N. P. Methodological Quality of User-Centered Usability Evaluation of Digital Applications to Promote Citizens' Engagement and Participation in Public Governance: A Systematic Literature Review. *Digital* **2024**, *4*(3), 740–761. https://doi.org/10.3390/digital4030038

[27] Hamdat, A.; B, C.; Samalam, A. G.; Rizal, M.; Lawalata, I. L. D. The Impact of Management Information Systems on Decision-Making Efficiency. *Vifada Manag. Digit. Bus.* **2024**, *1*(2), 56–74. https://doi.org/10.70184/qpw1rq78

[28] Ortega, J. H. J. C.; Lagman, A. C.; De Angel, R. M.; Alix, A. L.; Lagrazon, P. G. G. Evaluation of Program Completion Decision-Based Recommendation System with the ISO Software Quality Model. In *2023 IEEE 15th International Conference on Humanoid, Nanotechnology, Information Technology, Communication and Control, Environment, and Management (HNICEM)*; IEEE: Coron, Palawan, Philippines, 2023; pp 1–6. https://doi.org/10.1109/HNICEM60674.2023.10589184

[29] Martin, C. P.; Cochanco, A.; Cochanco, R. A. HighDro: An Intelligent Asset and Pressure Management Application for Local Water Utilities Using GIS. *QUEST J. Multidiscip. Res. Dev.* **2024**, *3*(1). https://doi.org/10.60008/thequest.v3i1.132

[30] Manun-og, M.; Flores, J. B. Optimizing Registry of Inhabitants' Record Management: The Development of Municipal Consolidation System for Local Governance. *SciEnggJ* **2023**, *17*(1), 1–7. https://doi.org/10.54645/VTHW47150

[31] Purbaratri, W.; Hartomo, K. D.; Hendry; Tambotoh, J. J. C. The New Smart Government Software Quality Framework Uses Modifications to ISO/IEC 25010. In *2023 Eighth International Conference on Informatics and Computing (ICIC)*; IEEE: Manado, Indonesia, 2023; pp 1–6. https://doi.org/10.1109/ICIC60109.2023.10382109

ASEAN
Journal of Scientific and Technological Reports
Online ISSN:2773-8752

Research article

Dietary Lecithin Modulates Growth, Selected Hemato-immunological Indices, and Glutathione Peroxidase Activity of Hoven's Carp (*Leptobarbus hoevenii*)

Poosana Keawkong[1, 2], Nutt Nuntapong[1, 2], and Naraid Suanyuk[1, 2*]

[1] Faculty of Natural Resources, Prince of Songkla University, Songkhla, 90110, Thailand
[2] Discipline of Excellence in Sustainable Aquaculture, Prince of Songkla University, Songkhla, 90110, Thailand
* Correspondence: naraid.s@psu.ac.th

Citation:
Keawkong, P.; Nuntapong, N.; Suanyuk, N. Dietary lecithin modulates growth, selected hemato-immunological indices, and glutathione peroxidase activity of Hoven's carp (*Leptobarbus hoevenii*). *ASEAN J. Sci. Tech. Report.* **2026**, *29*(7), e262095. https://doi.org/10.55164/ajstr.v29i7.262095

Article history:
Received: October 28, 2025
Revised: April 20, 2026
Accepted: April 30, 2026
Available online: June 14, 2026

Publisher's Note:
This article is published and distributed under the terms of the Thaksin University.

Abstract: Beneficial effects of dietary phospholipids on growth performance, hemato-immunological parameters, and antioxidant status in Hoven's carp (*Leptobarbus hoevenii*) are reported in this study. Experimental fish were fed four isoproteic (40%) and isolipidic (13%) experimental diets supplemented with lecithin at 0, 1, 3, and 5% for 90 days. The results showed that at 30, 60, and 90 days into the feeding trial, fish fed dietary supplementation containing 3% or 5% lecithin showed significantly improved total length, mean body weight, feed conversion ratio, and specific growth rate compared to the control group ($p<0.05$). No significant differences in condition factor and survival rate were observed between fish receiving dietary lecithin at any tested concentration and the control group ($p>0.05$). A study on hemato-immunological parameters of fish fed the experimental diets for 90 days revealed the highest red blood cell count in those receiving the 1% lecithin diet ($p<0.05$), whereas the white blood cell count was significantly higher in fish fed 3% and 5% lecithin diets ($p<0.05$). In addition, fish fed a 3% lecithin diet showed significantly higher glutathione peroxidase activity than those fed with the control diet or the 1% lecithin diet ($p<0.05$). These findings suggest that dietary supplementation with lecithin modulates growth and some hematological and immunological parameters, as well as antioxidant activity, in this fish species. Based on the findings, dietary supplementation with lecithin at 3-5% could promote growth, stimulate the immune response, and enhance antioxidant activity in Hoven's carp.

Keywords: Hoven's carp; lecithin; growth; immunity; antioxidant activity

1. Introduction

Hoven's carp (*Leptobarbus hoevenii*), also known as Sultan fish, Jelawat [1], and mad carp [2], is a native fish found in rivers and lakes in Malaysia, Cambodia, Indonesia, Laos, Vietnam, and Thailand [3]. This species is a commercially important freshwater fish with high potential for aquaculture production as a food and ornamental fish in Southeast Asian countries [3-4]. Despite this fish being a valuable aquatic species, only a few studies have reported on its nutritional management. Previously, Sunarno [4] reported that the maximum growth and high feed conversion efficiency of this fish were observed at about 40% protein level. Furthermore, Farahiyah *et al*. [5] reported that the optimal protein level for this fish's growth was 38%. In addition,

nutritional management of Hoven's carp broodstock, larvae, and juveniles in culture systems has been reviewed recently [3].

Phospholipids, defined as lipids containing phosphorus, are well-known important precursors of biologically active mediators involved in physiology and metabolism [6]. However, fish may have a limited capacity to synthesize phospholipids, insufficient to fully meet their requirements at larval and early juvenile stages [6]. Regarding this concern, lecithin has been used as a ubiquitous phospholipid source in aquafeed [7]. Lecithin is a glycerol phospholipid with varying amounts of sphingosyl phospholipids, glycolipids, triglycerides, and fatty acids [7], and lecithin can be found in both plants and animals, especially in soybean, sunflower, rapeseed, corn, camelina seed, canola, rice bran, egg yolk, dairy products, and marine products [8]. Previous studies have reported beneficial effects of dietary lecithin on growth performance, survival rate, immunity, and antioxidant capacity in aquaculture species. Incorporating lecithin at an optimum dose of 3.56% in the diet enhances survival, overall growth performance, and improves carcass composition of early juvenile milkfish (*Chanos chanos*) [9]. Furthermore, the optimum dose of lecithin required for better productivity and health performances of striped catfish (*Pangasianodon hypophthalmus*) is 3.65-4.42% [10]. Moreover, 4% dietary lecithin could not only improve growth, hematological indices, antioxidant capabilities, immune responses, and intestinal functions, but also alleviate inflammatory responses in largemouth bass (*Micropterus salmoides*) juveniles [11]. Therefore, the present study aimed to investigate the effects of dietary lecithin on growth performance, blood parameters, and antioxidant activity of Hoven's carp. The results of this study can serve as guidelines for developing Hoven's carp aquaculture in Southeast Asia.

2. Materials and Methods

2.1 Ethics statement

This study was carried out in accordance with the "Ethical Principles and Guidelines for the Use of Animals for Scientific Purposes", National Research Council, Thailand, and has been approved by the Institutional Animal Care and Use Committee, Prince of Songkla University, under permission number Ref. AQ069/2022.

2.2 Experimental fish

Healthy Hoven's carp with an average weight of 0.1 g obtained from Songkhla Inland Aquaculture Research and Development Center were used in this study. The fish were reared in 3,000 L fiberglass tanks containing 2,000 L of dechlorinated tap water with aeration until reaching approximately 2.0 g. During the cultivation period, water exchange was performed every 3 days at 80%. Experimental fish were fed to satiation with commercial feed twice daily at 9:00 AM and 4:00 PM.

2.3 Experimental diets

Sunflower lecithin powder (NOW Foods, IL, USA) was used in the present study. Four experimental diets were formulated to be isoproteic at 40% and isolipidic at 13% (Table 1). The experimental diets were designed to contain lecithin at 0%, 1%, 3%, and 5%. The raw materials were ground to a fine particle size, passed through an 80-mesh sieve, mixed, and pelleted using the HOBART machine (LEGACY®, OH, USA). The pellet-form fish feed was then dried in a hot-air oven at 60 °C for 3 h to obtain a moisture content not exceeding 10%. The experimental diets were analyzed for moisture, crude protein, crude lipid, crude fiber, and ash content, according to AOAC [12].

2.4 Experimental design

The experiment was carried out with 600 fish stocked in fiberglass tanks (120×50×40 cm) each containing 180 liters of dechlorinated tap water and equipped with an aeration system. Each tank was stocked with thirty fish. The experiment was conducted in a completely randomized design with 4 treatments and 5 replications: T1 (Control; 0% lecithin), T2 (1% lecithin), T3 (3% lecithin), and T4 (5% lecithin). During the rearing period, fish were fed to satiation twice daily at 9:00 AM and 4:00 PM for 90 days. Uneaten feed was siphoned out daily. Water exchange was performed every day at 30%. The water quality parameters, temperature, and dissolved oxygen, were measured using a DO meter (Pro20, YSI); pH was determined using a pH meter (Starter 3100-F, gibthai); and total ammonia-nitrogen, nitrite-nitrogen, and alkalinity were analyzed by standard methods following Boyd and Tucker [13] every 7 days.

Table 1. Ingredients and proximate chemical compositions of the experimental diets.

Ingredient	Dietary lecithin supplementation (%)			
	0	**1**	**3**	**5**
Fish meal	32.00	32.00	32.00	32.00
Defatted-soybean meal	17.00	17.00	17.00	17.00
Rice bran	9.00	9.00	9.00	9.00
Corn meal	5.00	5.00	5.00	5.00
Poultry meal	15.00	15.00	15.00	15.00
Crude palm oil	9.00	8.20	6.60	5.00
Tapioca starch	9.00	8.80	8.40	8.00
NaCl	1.00	1.00	1.00	1.00
Vitamin premix[1]	0.50	0.50	0.50	0.50
Mineral premix[2]	0.50	0.50	0.50	0.50
Carboxymethyl cellulose	2.00	2.00	2.00	2.00
Sunflower lecithin	0.00	1.00	3.00	5.00
Total	100.00	100.00	100.00	100.00
Proximate composition (% as fed basis)[3]				
Moisture	9.38 ± 0.10	7.32 ± 0.13	7.78 ± 0.02	7.10 ± 0.16
Crude protein	40.21 ± 0.12	40.34 ± 0.10	40.48 ± 0.19	40.88 ± 0.15
Crude lipid	12.66 ± 0.22	12.84 ± 0.09	12.97 ± 0.42	12.83 ± 0.86
Crude fiber	1.80 ± 0.02	1.79 ± 0.02	1.79 ± 0.01	1.78 ± 0.02
Ash	10.17 ± 0.58	9.96 ± 0.07	10.11 ± 0.03	10.26 ± 0.07

[1] Vitamin premix delivers the following per 100g of diet: Retinal (A) 250 IU; Cholecalciferol (D3) 50 IU; Tocopherol (E) 2.5 mg; Menadione sodium bisulfite (K) 1 mg; Thiamine (B1) 1.25 mg; Riboflavin (B2) 0.5 mg; Pyridoxine (B6) 0.5 mg; Cobalamin (B12) 0.005 mg; Ascorbic acid (C) 5 mg; Niacin 1.5 mg; Calcium pantothenate 1.5 mg; Folic acid 0.15 mg; Inositol (B8) 0.5 mg; and Biotin 0.005 mg.

[2] Mineral premix delivers the following per 100g of diet: Ca 50 mg; P 40 mg; Cu 1.25 mg; Fe 0.6 mg; Mn 0.6 mg; Zn 0.77 mg; K 0.13 mg; I 0.37 mg; Mg 1.08 mg; Se 0.005 mg; and Co 0.12 mg

[3] Proximate compositions are expressed as mean ± SD of triplicates.

2.5 Growth performance and survival rate

At 30, 60, and 90 days into the feeding trial, all experimental Hoven's carp were fasted for 24 h before being counted, weighed, and measured for body length. Total length was measured according to the method of Upasit *et al*. [14]. Condition factor (CF) was calculated according to the method of Kliangtapong *et al*. [15]. Feed conversion ratio (FCR), specific growth rate (SGR), and survival rate were calculated according to the method of Kamnerddee *et al*. [16]. The growth performance and survival rate were calculated as follows.

$CF = [\text{body weight (g)} / \text{total length (cm)}^3] \times 100$

$FCR = \text{total feed consumed (g)} / \text{weight gained (g)}$

$SGR\ (\%/\text{day}) = \{[\ln \text{final weight} - \ln \text{initial weight}]/\text{time interval (day)}\} \times 100$

$\text{Survival rate} = [\text{final number of fish} / \text{initial number of fish}] \times 100$

2.6 Proximate compositions in muscle tissue of Hoven's carp

At the end of the feeding trial, 2 fish from each replication (10 fish/treatment) were randomly selected and analyzed for proximate composition. Moisture, crude protein, crude lipid, and ash were analyzed for muscle tissue using the methods of AOAC [12].

2.7 Hemato-immunological parameter analysis

At the end of the experiment, two fish from each replication were randomly collected (10 fish/experiment) for blood parameter analyses. Fish were anesthetized with clove oil at a concentration of 40 mg/L [17]. Blood was withdrawn from the caudal vein/artery for the study of blood parameters, namely red blood cell and

white blood cell counts, hematocrit, and hemoglobin, measured using the method of Suwannasang *et al*. [18]. Wintrobe erythrocyte indices (mean corpuscular volume, mean corpuscular hemoglobin, and mean corpuscular hemoglobin concentration) were measured according to the method of Malawa *et al*. [19]. Serum protein was measured using the Lowry *et al*. [20] method. The nitroblue tetrazolium reduction was assayed using the modified method of Stasiak and Baumann [21]. Lysozyme activity was measured according to the method of Demers and Bayne [22]. Glucose content was measured according to the method of Hyvärinen and Nikkilä [23]. Alkaline phosphatase in blood serum was determined using a Cobas 8000 analyzer (Roche Diagnostics).

2.8 Antioxidant activity and thiobarbituric acid reactive substances in liver

At the end of the experiment, liver samples from two fish from each replication (10 fish/treatment) were collected for antioxidant activity analysis. Tissue samples were preserved in liquid nitrogen before enzyme extraction, as described by Ávila-Villa *et al*. [24]. The antioxidant activities determined were catalase (CAT) activity, analyzed according to the method of Trasviña-Arenas *et al*. [25], and Glutathione peroxidase (GPx) activity, determined using the Glutathione Peroxide Assay Kit No. 703102 (Cayman, USA). Thiobarbituric acid reactive substances (TBARs) were determined according to the method of Senphan and Benjakul [26].

2.9 Statistical analysis

Data are expressed as mean±standard deviation. Data that are percentages were subjected to arcsine transformation before analysis of variance. Significant differences were analyzed using one-way analysis of variance. Differences between treatments were then confirmed using Duncan's multiple range test, with $p<0.05$ required for statistical significance.

3. Results and Discussion

3.1 Growth performance and survival rate

In aquafeed, phospholipids are an essential component as they provide energy for metabolic activities and promote the digestion and absorption of other dietary lipids [7]. Accordingly, soybean lecithin has been widely used as a phospholipid source in aquafeed [11, 27-30]. However, growing genetically modified organisms (GMOs) and environmental concerns have led to a demand for developing alternative sources of vegetable lecithin, but research on these alternatives remains limited compared to extensive studies on soybean lecithin [31]. This study documents the growth performance, hematological and immunological parameters, and antioxidant status of Hoven's carp fed a diet supplemented with sunflower lecithin. In this study, the experimental diets were prepared to contain 40% protein and 13% fat, consistent with a study by Sunarno [4], who reported that a feed containing 40% protein and 14% fat is optimal for this fish species, resulting in maximum growth. Growth performance and survival rate of the experimental fish receiving dietary supplementation with lecithin at various concentrations are shown in Table 2. At 30, 60, and 90 days of the feeding trial, fish fed with dietary supplementation of lecithin at the concentrations 3% or 5% showed significantly improved total length, average body weight, FCR, and SGR, in comparison to the control group ($p<0.05$). In addition, no significant differences in CF or survival rate were observed between fish receiving dietary supplementation with lecithin at any tested concentration and the control group ($p>0.05$). Water quality parameters in all the experimental tanks during the experimental period were within the acceptable ranges for aquaculture [32-33]: temperature was 26.49 ± 0.35 °C, pH was 7.06 ± 0.04, dissolved oxygen was 5.33 ± 0.44 mg/L, total ammonia-nitrogen was 0.74 ± 0.07 mg/L, nitrite-nitrogen was 0.08 ± 0.01 mg/L, and alkalinity was 20.05 ± 2.6 mg/L.

Vegetable lecithins, containing primarily phosphatidylcholine, phosphatidylethanolamine, phosphatidylinositol, and phosphatidic acid, are typically produced from soybean, rapeseed, or sunflower [34-36]. According to van Nieuwenhuyzen and Tomás [35], the distribution of the main phospholipid components of sunflower lecithin is considerably similar to that of soybean lecithin. Additionally, sunflower lecithin is considered an attractive alternative to soybean lecithin due to its similar composition [35] and its advantage of being derived from a non-GMO source [36]. The phospholipid composition in sunflower lecithin used in this study includes 25% phosphatidylcholine, 18% phosphatidylinositol, and 11% phosphatidylethanolamine.

Phospholipids are vital precursors for a range of highly biologically active mediators of metabolism and physiology [6]. The improved growth of aquaculture species induced by dietary lecithin has been previously investigated. Batista *et al.* [29] reported that Nile tilapia (*Oreochromis niloticus*) fed a diet supplemented with soybean lecithin at 42-50 g/kg showed better growth, lipid digestibility, and body composition. Moreover, Amer *et al*. [10] reported that the final weight, weight gain, SGR, feed intake, and protein efficiency ratio were markedly higher in striped catfish treated with 2-4% soybean lecithin than in the control treatment group (0% soybean lecithin). In addition, Sink and Lochmann [27] reported that dietary supplementation with soybean lecithin at concentrations of 0-4% did not affect the survival rate of juvenile channel catfish (*Ictalurus punctatus*). In this study, however, no significant difference in growth performance was observed between Hoven's carp fed a diet supplemented with 1% soybean lecithin and the control group ($p>0.05$). This is consistent with Ciji *et al*. [37], who reported that dietary supplementation with 0-2% lecithin did not show significant differences in growth performance, measured as percentage weight gain, SGR, and survival rate, in golden mahseer (*Tor putitora*). In contrast, Butler *et al*. [38] reported that increasing the lipid content from 10% to 15%, combined with 1% sunflower lecithin inclusion, enhanced the weight gain of juvenile giant grouper (*Epinephelus lanceolatus*) by 12.14%. The differences in our findings compared to prior studies may be attributed to effects from fish species, the size of experimental subjects, and culture conditions.

Table 2. Growth performance of Hoven's carp fed with dietary supplementation with lecithin at various concentrations for 90 days.

Treatment	Dietary lecithin supplementation (%)				p-value
	0	1	3	5	
Average total length (cm)					
Initial total length	5.86 ± 0.03	5.88 ± 0.03	5.85 ± 0.02	5.85 ± 0.02	0.244
Day 30	8.20 ± 0.20^{a}	8.40 ± 0.20^{a}	8.65 ± 0.12^{b}	8.63 ± 0.13^{b}	0.002
Day 60	9.91 ± 0.16^{a}	10.11 ± 0.43^{ab}	10.56 ± 0.26^{b}	10.54 ± 0.35^{b}	0.017
Day 90	11.24 ± 0.17^{a}	11.49 ± 0.27^{ab}	11.68 ± 0.27^{b}	11.80 ± 0.32^{b}	0.023
Average body weight (g)					
Initial body weight	2.25 ± 0.01	2.26 ± 0.01	2.24 ± 0.01	2.25 ± 0.02	0.388
Day 30	6.94 ± 0.07^{a}	7.21 ± 0.40^{a}	7.82 ± 0.26^{b}	7.86 ± 0.42^{b}	0.001
Day 60	13.96 ± 0.55^{a}	14.52 ± 1.10^{a}	15.74 ± 0.45^{b}	16.76 ± 0.63^{b}	<0.001
Day 90	22.06 ± 1.13^{a}	22.41 ± 1.87^{a}	25.08 ± 1.03^{b}	26.67 ± 1.02^{b}	<0.001
Condition factor					
Day 30	1.26 ± 0.10	1.21 ± 0.04	1.21 ± 0.05	1.22 ± 0.06	0.620
Day 60	1.44 ± 0.11	1.41 ± 0.13	1.34 ± 0.09	1.44 ± 0.14	0.631
Day 90	1.56 ± 0.12	1.47 ± 0.06	1.58 ± 0.06	1.63 ± 0.11	0.099
Feed conversion ratio					
Day 0-30	2.13 ± 0.03^{b}	2.06 ± 0.18^{b}	1.77 ± 0.07^{a}	1.79 ± 0.15^{a}	<0.001
Day 0-60	2.02 ± 0.10^{b}	1.90 ± 0.16^{b}	1.68 ± 0.05^{a}	1.59 ± 0.08^{a}	<0.001
Day 0-90	1.77 ± 0.11^{b}	1.75 ± 0.15^{b}	1.52 ± 0.07^{a}	1.45 ± 0.06^{a}	<0.001
Specific growth rate (%/day)					
Day 0-30	3.75 ± 0.03^{a}	3.86 ± 0.20^{a}	4.16 ± 0.11^{b}	4.17 ± 0.18^{b}	0.001
Day 0-60	3.04 ± 0.07^{a}	3.10 ± 0.14^{a}	3.25 ± 0.05^{b}	3.35 ± 0.06^{b}	<0.001
Day 0-90	2.53 ± 0.06^{a}	2.54 ± 0.09^{a}	2.68 ± 0.05^{b}	2.75 ± 0.04^{b}	<0.001
Survival rate (%)					
Day 0-90	100.00 ± 0.00	99.33 ± 1.49	100.00 ± 0.00	100.00 ± 0.00	0.454

Values within the same row with different superscripts are significantly different ($p<0.05$).

3.2 Proximate compositions in muscle tissue of Hoven's carp

Proximate composition of muscle tissue was significantly affected by dietary supplementation with lecithin (Table 3). The fish fed with 1-5% lecithin had significantly higher crude lipid than those in the control

group ($p<0.05$). There were no statistical differences in moisture, crude protein, or ash content of the muscles of fish examined in this study ($p>0.05$). The enhanced lipid digestion and absorption of fish in response to lecithin supplementation is associated with the emulsifying property of lecithin [9, 39]. Balito-Liboon *et al*. [9] reported that the highest tissue protein and lipid contents were observed in early juvenile milkfish fed a diet with 3% soybean lecithin, and declines in tissue protein and lipid contents were observed beyond this dose level. The lipid composition in the muscle of the fish consisted of non-phospholipids and phospholipids. Major lipid component of the muscle from red sea bream (*Pagrus major*), amberjack (*Seriola dumerili*), and striped jack (*Caranx delicatissimus*) was triglyceride. At the same time, phospholipids, including phosphatidylcholine and phosphatidylethanolamine, were the main lipid components in the muscle of puffer (*Takifugu rubripes*) and flounder (*Paralichthys olivaceus*) [40]. Generally, freshwater fish are an important source of n-3 fatty acids, especially eicosapentaenoic acid and docosahexaenoic acid [41-42]. Several studies have shown that consuming freshwater fish has beneficial effects on human health [41]. The deposition of fatty acids in fish tissue is influenced by the fatty acid profiles of the diets [43]. In addition, lipid distribution patterns are related to flesh quality and the yield rate of aquaculture products. A preferable lipid distribution pattern, characterized by small lipid depots evenly distributed in the edible part of muscle, positively impacts consumers' taste perception [44]. This study, however, did not analyze lipid class and fatty acid composition, as well as lipid distribution, in the fillet of Hoven's carp. Further research on dietary lecithin and its effects on flesh quality should be conducted to promote this fish species as a valuable source of nutrition.

Table 3. Proximate compositions (% wet weight basis) of muscle tissue of fish fed experimental diets supplemented with various concentrations of lecithin for 90 days.

Treatment	Dietary lecithin supplementation (%)				p-value
	0	1	3	5	
Moisture	75.44 ±0.28	74.88 ± 0.59	75.12 ± 0.93	75.59 ± 1.14	0.512
Crude protein	19.45 ± 0.41	19.55 ± 0.49	19.61 ± 1.32	19.36 ± 0.83	0.968
Crude lipid	1.95 ± 0.04^{a}	2.84 ± 0.04^{b}	2.83 ± 0.12^{b}	2.73 ± 0.10^{b}	<0.001
Ash	1.30 ± 0.17	1.25 ± 0.08	1.36 ± 0.07	1.40 ± 0.14	0.232

Values within the same row with different superscripts are significantly different ($p<0.05$).

3.3 Hemato-immunological parameters

Hemato-immunological parameters have been used to monitor fish growth and health status [45-46]. Red blood cells transport oxygen [46]. In the present study, significantly higher red blood cell count was observed in fish fed with dietary supplementation of 1% lecithin in comparison to the other treatments ($p<0.05$) (Table 4), suggesting that 1% lecithin provides an optimal supply of phospholipids necessary to support membrane fluidity and stability potentially involved in enhancing erythropoiesis and oxygen-carrying capacity in Hoven's carp. In addition, the fish fed a diet supplemented with 1% lecithin showed lower mean corpuscular volume and mean corpuscular hemoglobin values than other groups, although the difference was not statistically significant ($p>0.05$). This could be the result of variation in cell size and hemoglobin content, which may have had physiological consequences for the fish [47]. The results from the present study are consistent with the results for striped catfish fed with dietary soy lecithin, which showed significantly higher red blood cells at 2% compared to the control group, with the highest level observed at 6% supplementation, followed by a reduction when fed beyond this level ($p<0.05$) [48]. Similarly, significantly increased red blood cell counts have also been reported in female shark catfish (*Pangasius nasutus*), where the red blood cell count increased with phospholipid supplementation, with the highest value recorded in the 2.0-2.5% group [49]. In this study, fish fed diets supplemented with 3-5% lecithin showed significantly higher white blood cell counts than those in the other treatments ($p<0.05$) (Table 4). The results from the present study resemble those in a previous study on juvenile largemouth bass fed diets supplemented with 2-4% soybean lecithin [11], and on stellate sturgeon (*Acipenser stellatus*) fed diets supplemented with 4-8% soybean lecithin [28]: these had significantly higher white blood cell counts in comparison to the control group ($p<0.05$). While white blood cells are involved in both acquired and innate immunity [46], increasing white blood cell counts of fish fed

with experimental diet supplementation with lecithin may be related to phospholipids and their unsaturated fatty acids, which can maintain fluidity and permeability of cell membranes and enhance fish immunity [28, 50]. In this study, however, no significant differences were observed in hematocrit, hemoglobin, mean corpuscular volume, mean corpuscular hemoglobin, mean corpuscular hemoglobin concentration, serum protein, lysozyme, nitroblue tetrazolium reduction, glucose, or alkaline phosphatase between the dietary treatment groups ($p>0.05$). This finding is consistent with a study by Sink and Lochmann [27], who reported that channel catfish fed dietary supplementation of 0-4% soybean lecithin showed no significant differences in hematocrit, hemoglobin, mean corpuscular hemoglobin concentration, or lysozyme activity. Additionally, Pagheh *et al*. [51] reported that silvery-black porgy (*Sparidentex hasta*) fed with dietary supplementation of 0-9% soybean lecithin had no significant differences in red blood cell count, hemoglobin, hematocrit, mean corpuscular volume, mean corpuscular hemoglobin, mean corpuscular hemoglobin concentration, or white blood cell count ($p>0.05$).

Table 4. Hemato-immunological parameters of fish fed experimental diets supplemented with various concentrations of lecithin for 90 days.

Parameter	Dietary lecithin supplementation (%)				p-value
	0	1	3	5	
RBC (x10^9 cell/mL)	2.63 ± 0.18^a	3.17 ± 0.41^b	2.66 ± 0.28^a	2.42 ± 0.57^a	0.005
WBC (×10^7 cell/mL)	2.12 ± 0.21^a	2.51 ± 0.87^a	3.74 ± 0.85^b	3.85 ± 1.03^b	<0.001
Hct (%)	22.51 ± 5.78	24.30 ± 2.55	23.19 ± 1.81	21.82 ± 1.28	0.409
Hb (g/dL)	5.49 ± 0.96	5.65 ± 0.44	5.71 ± 0.97	5.11 ± 0.32	0.274
MCV (femtoliter)	89.94 ± 10.55	79.69 ± 16.87	85.78 ± 6.37	83.06 ± 11.70	0.429
MCH (picogram)	20.97 ± 3.87	17.71 ± 1.59	21.79 ± 4.03	22.55 ± 7.04	0.221
MCHC (g/dL)	25.32 ± 5.52	23.59 ± 3.78	24.63 ± 3.72	23.44 ± 1.08	0.664
Serum protein (mg/mL)	33.16 ± 0.59	32.31 ± 2.35	33.03 ± 1.26	32.98 ± 1.66	0.728
Lysozyme (µg/mL)	22.04 ± 8.86	21.09 ± 7.36	24.42 ± 6.18	32.81 ± 12.40	0.235
NBT reduction	2.90 ± 0.89	3.13 ± 0.65	3.01 ± 0.62	2.85 ± 0.44	0.824
Blood glucose (mg %)	27.15 ± 2.97	28.66 ± 4.30	28.39 ± 3.73	28.68 ± 3.89	0.771
ALP (U/L)	24.80 ± 3.35	21.40 ± 1.67	25.00 ± 5.92	23.80 ± 4.44	0.515

RBC; red blood cell, WBC; white blood cell, Hct; hematocrit, Hb; hemoglobin, MCV; mean corpuscular volume, MCH; mean corpuscular hemoglobin, MCHC; mean corpuscular hemoglobin concentration, NBT; nitroblue tetrazolium, ALP; Alkaline phosphatase

Values within the same row with different superscripts are significantly different ($p<0.05$).

3.4 Antioxidant status

It is widely recognized that reactive oxygen species (ROS), such as superoxide and hydrogen peroxide, can be generated in all cells by mitochondrial and enzymatic sources. These ROS can cause oxidative damage to DNA, proteins, and membrane lipids [52]. GPx and CAT are intracellular enzymatic antioxidants that are involved in the detoxification of hydrogen peroxide; GPx catalyzes the reduction of hydrogen peroxide into water [52], whereas the CAT catalyzes the decomposition of hydrogen peroxide into water and oxygen [53], thereby protecting tissue against oxidative damage. In this study, fish fed a diet supplemented with 3% lecithin showed significantly higher GPx activity compared to those that received dietary lecithin at 0 or 1% ($p<0.05$) (Fig. 1b), indicating that lecithin may provide protective effects against oxidative damage. This result is similar to those reported for largemouth bass juveniles fed with dietary soybean lecithin at 4% [11]. In this current study, however, no significant differences were found in CAT activity among the treatments at 90 days of the feeding trial ($p>0.05$) (Fig. 1a). Several studies on the antioxidative status in fish have reported that antioxidative enzyme activities vary among different growth phases [54], organs [55], and feeding and starvation conditions [56]. This is consistent with a previous study, which found that fish receiving dietary soybean lecithin did not show differences in CAT [51]. Basically, malondialdehyde, a TBAR, is an important indicator of lipid peroxidation. It is endogenously formed during intracellular oxidative stress and its reaction

with DNA, leading to cellular damage [57]. This study observed a decrease, though not statistically significant, in TBAR levels in fish fed 1-5% lecithin compared to the control group, indicating that lecithin may reduce oxidative stress in fish.

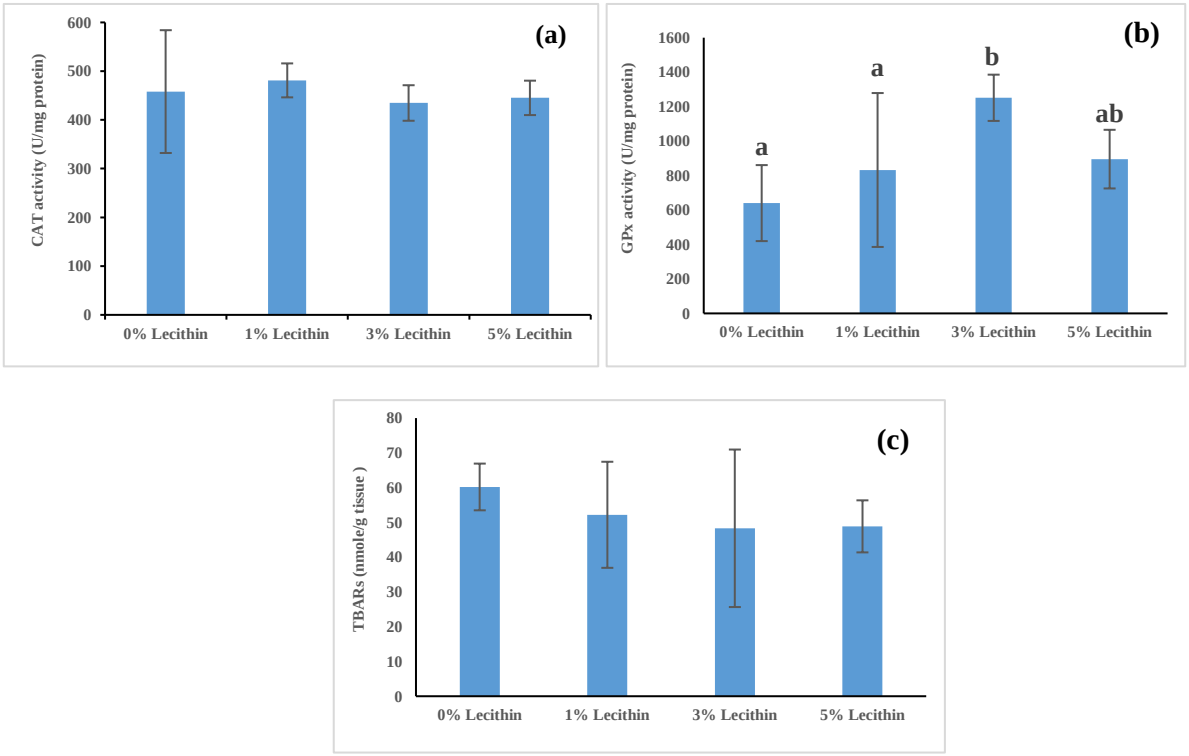


Figure 1. CAT activity (a), GPx activity (b), and TBARs (c) of Hoven's carp fed experimental diets supplemented with lecithin at various concentrations for 90 days.

4. Conclusions

Our findings from the present study indicate that dietary 3-5% lecithin modulates growth, hemato-immunological indices, and antioxidant activity in Hoven's carp. However, this study was conducted in small-sized experimental fish under laboratory conditions. Further investigation into a long-term field-based study may provide additional insights and improve the practical applicability of the findings. In addition, studies on the effects of lecithin on lipid class and fatty acid composition, as well as lipid distribution, in the fillet of Hoven's carp could provide more valuable information.

5. Acknowledgments

Thanks to Akkarawit Issaro, Chalanda Kamnerddee, Ratchakrit Konrian, Suchanun Eamsakul, and Wiroonsak Thongsupa for excellent technical assistance in the laboratory.

Author Contributions: Conceptualization, P.K., N.N., and N.S.; methodology, P.K., N.N., and N.S.; software, P.K. and N.S.; validation, N.S.; formal analysis, P.K., N.N., and N.S.; investigation, P.K., N.N., and N.S.; resources, N.S.; data curation, P.K. and N.S.; writing—original draft preparation, P.K., N.N., and N.S.; writing—review and editing, P.K., N.N., and N.S.; supervision, N.S.; funding acquisition, N.S. All authors have read and agreed to the published version of the manuscript.

Funding: This research was funded by the Discipline of Excellence in Sustainable Aquaculture, Prince of Songkla University.

Conflicts of Interest: The authors declare no conflict of interest.

References

[1] Srithongthum, S.; Au, H. L.; Amornsakun, T.; Musikarun, P.; Fatihah, S. N.; Halid, N. F. A.; Lim, L. S. Observation on the Embryonic Development of Sultan Fish, *Leptobarbus hoevenii*. *AACL Bioflux* **2021**, *14*(3), 1359–1364.

[2] Kwanmuang, S.; Kraisurasi, S.; Phetrit, N.; Jiamton, W. Ah... Is There Fish Too? Pla Baa. *Thai Fish. Gaz.* **2016**, *69*(1), 77–79.

[3] Au, H. L.; Lim, L. S.; Amornsakun, T.; Rahmah, S.; Liew, H. J.; Musikarun, P.; Promkaew, P.; Mok, W. J.; Kawamura, G.; Yong, A. S.; Shapawi, R.; Mustafa, S. Feeding and Nutrients Requirement of Sultan Fish, *Leptobarbus hoevenii*: A Review. *Int. J. Aqu. Sci.* **2020**, *11*(1), 3–12.

[4] Sunarno, M. T. D. Growth and Nutrient Digestibility of Jelawat (*Leptobarbus hoevenii*) Fry Fed with Various Dietary Protein Levels. *Indones. Fish. Res. J.* **2002**, *8*(1), 19–25. https://doi.org/10.15578/ifrj.8.1.2002.19-25.

[5] Farahiyah, I. J.; Zainal Abidin, A. R.; Ahmad, A.; Wong, H. K. Optimum Protein Requirement for the Growth of Jelawat Fish (*Leptobarbus hoevenii*). *Mal. J. Anim. Sci.* **2017**, *20*(2), 39–46.

[6] Tocher, D. R.; Bendiksen, E. Å.; Campbell, P. J.; Bell, J. G. The Role of Phospholipids in Nutrition and Metabolism of Teleost Fish. *Aquaculture* **2008**, *280*(1–4), 21–34. https://doi.org/10.1016/j.aquaculture.2008.04.034

[7] Ukwela, E. J.; Muhammad, S. R. S.; Mazelan, S.; Mohamad, S. J.; Chian, W. C.; Vethamony, P.; Al-Khayat, J.; Rosas, V. T.; Jung, L. H. Benefits of Phospholipids in Aquafeed Development: A Review. *Planet. Sust.* **2024**, *2*(1), 5–24. https://doi.org/10.46754/ps.2024.01.002

[8] Wee, W.; Téllez-Isaías, G.; Abdul Kari, Z.; Cheadoloh, R.; Kabir, M. A.; Mat, K.; Mohamad Sukri, S. A.; Rahman, M. M.; Rusli, N. D.; Wei, L. S. The Roles of Soybean Lecithin in Aquafeed: A Crucial Need and Update. *Front. Vet. Sci.* **2023**, *10*, 1188659. https://doi.org/10.3389/fvets.2023.1188659

[9] Balito-Liboon, J. S.; Ferdinand, R.; Traifalgar, M.; Pagapulan, M. J. B. B.; Mameloco, E. J. G.; Temario, E. E.; Corre, V. L., Jr. Dietary Soybean Lecithin Enhances Growth Performance, Feed Utilization Efficiency and Body Composition of Early Juvenile Milkfish, *Chanos chanos*. *Isr. J. Aquacult.-Bamid.* **2018**, *70*. https://doi.org/10.46989/001c.20927

[10] Amer, A.-R.; Eweedah, N. M.; Amer, A. A.; Gewaily, M. S.; Younis, N. A.; Ahmed, H. A.; Dawood, M. A. O. Dietary Effect of Soybean Lecithin on the Growth Performance, Digestive Enzyme Activity, Blood Biomarkers, and Antioxidative Status of Striped Catfish, *Pangasianodon hypophthalmus*. *PLoS One* **2023**, *18*(10), e0291954. https://doi.org/10.1371/journal.pone.0291954

[11] Wu, J.; Yang, W.; Song, R.; Li, Z.; Jia, X.; Zhang, H.; Zhang, P.; Xue, X.; Li, S.; Xie, Y.; Zhang, R.; Ye, J.; Zhou, Z.; Wu, C. Dietary Soybean Lecithin Improves Growth, Immunity, Antioxidant Capability and Intestinal Barrier Functions in Largemouth Bass *Micropterus salmoides* Juveniles. *Metabolites* **2023**, *13*(4), 512. https://doi.org/10.3390/metabo13040512

[12] AOAC. *Official Methods of Analysis of AOAC International*, 18th ed.; AOAC International: Gaithersburg, MD, USA, 2005.

[13] Boyd, C. E.; Tucker, C. S. *Water Quality and Pond Soil Analyses for Aquaculture*; Alabama Agricultural Experiment Station, Auburn University: Alabama, USA, 1992.

[14] Upasit, D.; Chiayvareesajja, J.; Chiayvareesajja, S. Reproductive Biology of *Johnius carouna* (Cuvier, 1830) off the Coast of Songkhla Province. *Thaksin Univ J.* **2017**, *20*(3), 43–50.

[15] Kliangtapong, A.; Thongprajukaew, K.; Rodjaroen, S. Growth Performance of Oranda Goldfish (*Carassius auratus*) Fed Diets Containing Cyanobacteria *Hapalosiphon welwitschii* TISTR 8237. *RMUTSV Res. J.* **2018**, *10*(3), 356–367.

[16] Kamnerddee, C.; Puangpee, S.; Kaewkong, P.; Nuntapong, N.; Wanlem, S.; Suanyuk, N. Dietary Supplementation with *Zooshikella marina* Improves Growth Performance, Haemato-Immunological Parameters and Disease Resistance against *Streptococcus agalactiae* in Nile Tilapia (*Oreochromis niloticus*). *Songklanakarin J. Sci. Technol.* **2024**, *46*(2), 83–91.

[17] Mylonas, C. C.; Cardinaletti, G.; Sigelaki, I.; Polzonetti-Magni, A. Comparative Efficacy of Clove Oil and 2-Phenoxyethanol as Anesthetics in the Aquaculture of European Sea Bass (*Dicentrarchus labrax*) and Gilthead Sea Bream (*Sparus aurata*) at Different Temperatures. *Aquaculture* **2005**, *246*(1–4), 467–481. https://doi.org/10.1016/j.aquaculture.2005.02.046

[18] Suwannasang, A.; Dangwetngam, M.; Issaro, A.; Phromkunthong, W.; Suanyuk, N. Pathological Manifestations and Immune Responses of Serotypes Ia and III *Streptococcus agalactiae* Infections in Nile Tilapia (*Oreochromis niloticus*). *Songklanakarin J. Sci. Technol.* **2014**, *36*(5), 499–506.

[19] Malawa, S.; Nuntapong, N.; Suanyuk, N.; Thongprajukaew, K. Addition of Different Concentrations of Indian Almond (*Terminalia catappa*) Leaf Extract to Aquarium Water Resulted in Improved Water Quality and Increased Bubble Nest Formation by Male Siamese Fighting Fish (*Betta splendens*) without Having Any Consistent Negative Effects on Growth Metrics and Blood Chemistry. *Aquacult. Int.* **2022**, *30*, 3269–3288. https://doi.org/10.1007/s10499-022-00960-1

[20] Lowry, O. H.; Rosebrough, N. J.; Farr, A. L.; Randall, R. J. Protein Measurement with the Folin-Phenol Reagent. *J. Biol. Chem.* **1951**, *193*(1), 265–275. https://doi.org/10.1016/S0021-9258(19)52451-6

[21] Stasiak, S. A.; Baumann, P. C. Neutrophil Activity as a Potential Bioindicator for Contaminant Analysis. *Fish Shellfish Immunol.* **1996**, *6*(7), 537–539. https://doi.org/10.1006/fsim.1996.0050

[22] Demers, N. E.; Bayne, C. J. The Immediate Effects of Stress on Hormones and Plasma Lysozyme in Rainbow Trout. *Dev. Comp. Immunol.* **1997**, *21*(4), 363–373. https://doi.org/10.1016/S0145-305X(97)00009-8

[23] Hyvärinen, A.; Nikkilä, E. A. Specific Determination of Blood Glucose with *o*-Toluidine. *Clin. Chim. Acta* **1962**, *7*(1), 140–143. https://doi.org/10.1016/0009-8981(62)90133-X.

[24] Ávila-Villa, L. A.; Fimbres-Olivarria, D.; Garcia-Sánchez, G.; Gollas-Galván, T.; Hernández-López, J.; Martínez-Porchas, M. Physiological and Immune Responses of White Shrimp (*Litopenaeus vannamei*) Infected with Necrotizing Hepatopancreatitis Bacterium. *Aquaculture* **2012**, *324–325*, 14–19. https://doi.org/10.1016/j.aquaculture.2011.09.010

[25] Trasviña-Arenas, C. H.; Garcia-Triana, A.; Peregrino-Uriarte, A. B.; Yepiz-Plascencia, G. White Shrimp *Litopenaeus vannamei* Catalase: Gene Structure, Expression and Activity under Hypoxia and Reoxygenation. *Comp. Biochem. Physiol. B Biochem. Mol. Biol.* **2013**, *164*, 44–52. https://doi.org/10.1016/j.cbpb.2012.10.004

[26] Senphan, T.; Benjakul, S. Compositions and Yield of Lipids Extracted from Hepatopancreas of Pacific White Shrimp (*Litopenaeus vannamei*) as Affected by Prior Autolysis. *Food Chem.* **2012**, *134*(2), 829–835. https://doi.org/10.1016/j.foodchem.2012.02.188

[27] Sink, T. D.; Lochmann, R. T. The Effects of Soybean Lecithin Supplementation to a Practical Diet Formulation on Juvenile Channel Catfish, *Ictalurus punctatus*: Growth, Survival, Hematology, Innate Immune Activity, and Lipid Biochemistry. *J. World Aquac. Soc.* **2014**, *45*(2), 163–172. https://doi.org/10.1111/jwas.12108

[28] Jafari, F.; Agh, N.; Noori, F.; Tokmachi, A.; Gisbert, E. Effects of Dietary Soybean Lecithin on Growth Performance, Blood Chemistry and Immunity in Juvenile Stellate Sturgeon (*Acipenser stellatus*). *Fish Shellfish Immunol.* **2018**, *80*, 487–496. https://doi.org/10.1016/j.fsi.2018.06.023

[29] Batista, R. O.; Richter, B. L.; Banze, J. F.; Schleder, D. D.; Salhi, M.; Nobrega, R. O.; Silva, M. F. O.; Mattioni, B.; Pettigrew, J. E.; Fracalossi, D. M. Soy Lecithin Supplementation Promotes Growth and Increases Lipid Digestibility in GIFT Nile Tilapia Raised at Suboptimal Temperature. *Fishes* **2023**, *8*(8), 404. https://doi.org/10.3390/fishes8080404

[30] Yang, W.; Wu, J.; Song, R.; Li, Z.; Jia, X.; Qian, P.; Zhang, H.; Zhang, P.; Xue, X.; Li, S.; Xie, Y.; Ye, J.; Dong, G.; Wu, C. Effects of Dietary Soybean Lecithin on Growth Performance, Body Composition, Serum Biochemical Parameters, Digestive and Metabolic Abilities in Largemouth Bass *Micropterus salmoides*. *Aquac. Rep.* **2023**, *29*, 101528. https://doi.org/10.1016/j.aqrep.2023.101528

[31] Robert, C.; Couëdelo, L.; Vaysse, C.; Michalski, M. C. Vegetable Lecithins: A Review of Their Compositional Diversity, Impact on Lipid Metabolism and Potential in Cardiometabolic Disease Prevention. *Biochimie* **2020**, *169*, 121–132. https://doi.org/10.1016/j.biochi.2019.11.017

[32] Boyd, C. E. *Water Quality for Pond Aquaculture*; Research and Development Series No. 43; International Center for Aquaculture and Aquatic Environments, Alabama Agricultural Experiment Station, Auburn University: Alabama, USA, 1998.

[33] Lucas, J. S.; Southgate, P. C.; Tucker, C. S. *Aquaculture: Farming Aquatic Animals and Plants*, 3rd ed.; John Wiley & Sons Ltd.: Chichester, UK, 2019.

[34] Wu, Y.; Wang, T. Soybean Lecithin Fractionation and Functionality. *J. Am. Oil Chem. Soc.* **2003**, *80*, 319–326. https://doi.org/10.1007/s11746-003-0697-x

[35] van Nieuwenhuyzen, W.; Tomás, M. C. Update on Vegetable Lecithin and Phospholipid Technologies. *Eur. J. Lipid Sci. Technol.* **2008**, *110*(5), 472–486. https://doi.org/10.1002/ejlt.200800041

[36] Guiotto, E. N.; Tomás, M. C.; Diehl, B. W. K. Sunflower Lecithin. In *Polar Lipids*; Ahmad, M. U., Xu, X., Eds.; Elsevier: Amsterdam, The Netherlands, 2015; pp 57–75. https://doi.org/10.1016/B978-1-63067-044-3.50007-8

[37] Ciji, A.; Akhtar, M. S.; Tripathi, P. H.; Pandey, A.; Rajesh, M.; Kamalam, B. S. Dietary Soy Lecithin Augments Antioxidative Defense and Thermal Tolerance but Fails to Modulate Non-Specific Immune Genes in Endangered Golden Mahseer (*Tor putitora*) Fry. *Fish Shellfish Immunol.* **2021**, *109*, 34–40. https://doi.org/10.1016/j.fsi.2020.11.031

[38] Butler, G.; Candebat, C. L.; Das, S. K.; Nankervis, L. Improving Lipid Utilization and Growth through Lecithin Inclusion in Diets for Giant Grouper (*Epinephelus lanceolatus*). *Anim. Feed Sci. Technol.* **2025**, *326*, 116393. https://doi.org/10.1016/j.anifeedsci.2025.116393

[39] Sivaramakrishnan, T.; Ambasankar, K.; Kumaraguru Vasagam, K. P.; Syama Dayal, J.; Sandeep, K. P.; Bera, A.; Makesh, M.; Kailasam, M.; Vijayan, K. K. Effect of Dietary Soy Lecithin Inclusion Levels on Growth, Feed Utilization, Fatty Acid Profile, Deformity and Survival of Milkfish (*Chanos chanos*) Larvae. *Aquac. Res.* **2021**, *52*, 5366–5374. https://doi.org/10.1111/are.15406

[40] Ando, S.; Mori, Y.; Nakamura, K.; Sugawara, A. Characteristics of Lipid Accumulation Types in Five Species of Fish. *Nippon Suisan Gakkaishi* **1993**, *59*(9), 1559–1564. https://doi.org/10.2331/suisan.59.1559

[41] Steffens, W.; Wirth, M. Freshwater Fish—An Important Source of *n*-3 Polyunsaturated Fatty Acids: A Review. *Arch. Pol. Fish.* **2005**, *13*(1), 5–16.

[42] Talukdar, H.; Kalita, D.; Singh, K. B. Current Perspective on Omega-3 Fatty Acids in Freshwater Fish from India: A Review of Scientific Progress. *Int. J. Zool. Appl. Biosci.* **2025**, *10*(6), 173–180. https://doi.org/10.55126/ijzab.2025.v10.i06.019

[43] Bahurmiz, O. M.; Ng, W. K. Effects of Dietary Palm Oil Source on Growth, Tissue Fatty Acid Composition and Nutrient Digestibility of Red Hybrid Tilapia, *Oreochromis* sp., Raised from Stocking to Marketable Size. *Aquaculture* **2007**, *262*(2–4), 382–392. https://doi.org/10.1016/j.aquaculture.2006.11.023

[44] Khieokhajonkhet, A.; Klongchai, S.; Maphum, O.; Kaneko, G. Lipid Distribution Patterns of Nine Commercial Fish in Thailand. *Aquac. Res.* **2019**, *50*, 1348–1360. https://doi.org/10.1111/are.14011

[45] Monir, M. S.; Yusoff, S. M.; Zulperi, Z. M.; Hassim, H. A.; Mohamad, A.; Ngoo, M. S. M. H.; Ina-Salwany, M. Y. Haemato-Immunological Responses and Effectiveness of Feed-Based Bivalent Vaccine against *Streptococcus iniae* and *Aeromonas hydrophila* Infections in Hybrid Red Tilapia (*Oreochromis mossambicus* × *O. niloticus*). *BMC Vet. Res.* **2020**, *16*, 226. https://doi.org/10.1186/s12917-020-02443-y

[46] Esmaeili, M. Blood Performance: A New Formula for Fish Growth and Health. *Biology* **2021**, *10*(12), 1236. https://doi.org/10.3390/biology10121236

[47] Torsabo, D.; Idris, N.; Iber, B. T.; Arome, A. G.; Chu, I. K. C.; Abduh, M. Y.; Noordin, N. M.; Azra, M. N.; Impellitteri, F.; Faggio, C.; Abdol-Munafi, A. B. Effects of Dietary Phospholipids on Growth, Biochemical Composition, Fatty Acid Profiles, Blood Metrics, and Sex Steroid Hormone of Male *Pangasius nasutus* Broodstock. *Aquac. Stud.* **2025**, *25* (1), 47–63. https://doi.org/10.4194/AQUAST1935

[48] Torsabo, D.; Iber, B. T.; Idris, N.; Okomoda, V. T.; Koh, I. C. C.; Abduh, M. Y.; Noordin, N. M.; Abdol-Munafi, A. B. Phospholipid-Supplemented Diet Impacts on Growth, Blood Metrics, Reproductive Indices, and Fatty Acid Profiles of *Pangasianodon hypophthalmus*. *Aquac. Rep.* **2023**, *33*, 101802. https://doi.org/10.1016/j.aqrep.2023.101802

[49] Torsabo, D.; Iber, B. T.; Idris, N.; Arome, A. G.; Okomoda, V. T.; Chu, I. K. C.; Abduh, M. Y.; Noordin, N. M.; Abdol-Munafi, A. B. Dietary Phospholipid Supplementation Affects Blood Metrics, Reproductive Indices, and Biochemical Parameters of Female Shark Catfish, *Pangasius nasutus*. *J. Fish. Environ.* **2025**, *49*(1), 46–66.

[50] Balfry, S. K.; Higgs, D. A. Influence of Dietary Lipid Composition on the Immune System and Disease Resistance of Finfish. In *Nutritional and Fish Health*; Lim, C., Webster, C. D., Eds.; The Haworth Press: New York, NY, USA, 2001; pp 213–234.

[51] Pagheh, E.; Agh, N.; Marammazi, J. G.; Nouri, F.; Sepahdari, A.; Gisbert, E.; Torfi Mozanzadeh, M. Dietary Soybean Lecithin Affects Growth Performance, Fillet Biochemical Composition and Digestive Enzyme Activity in *Sparidentex hasta* Juveniles. *J. Appl. Anim. Res.* **2019**, *47*(1), 24–33. https://doi.org/10.1080/09712119.2018.1557663

[52] Lubos, E.; Loscalzo, J.; Handy, D. E. Glutathione Peroxidase-1 in Health and Disease: From Molecular Mechanisms to Therapeutic Opportunities. *Antioxid. Redox Signal.* **2011**, *15*(7), 1957–1997. https://doi.org/10.1089/ars.2010.3586

[53] Anwar, S.; Alrumaihi, F.; Sarwar, T.; Babiker, A. Y.; Khan, A. A.; Prabhu, S. V.; Rahmani, A. H. Exploring Therapeutic Potential of Catalase: Strategies in Disease Prevention and Management. *Biomolecules* **2024**, *14*, 697. https://doi.org/10.3390/biom14060697

[54] Mourente, G.; Díaz-Salvago, E.; Bell, J. G.; Tocher, D. R. Increased Activities of Hepatic Antioxidant Defence Enzymes in Juvenile Gilthead Sea Bream (*Sparus aurata* L.) Fed Dietary Oxidised Oil: Attenuation by Dietary Vitamin E. *Aquaculture* **2002**, *214*(1–4), 343–361. https://doi.org/10.1016/S0044-8486(02)00064-9

[55] Zhang, H.; Mu, Z.; Xu, L.; Xu, G.; Liu, M.; Shan, A. Dietary Lipid Level Induced Antioxidant Response in Manchurian Trout, *Brachymystax lenok* (Pallas) Larvae. *Lipids* **2009**, *44*, 643–654. https://doi.org/10.1007/s11745-009-3313-7

[56] Zengin, H. The Effects of Feeding and Starvation on Antioxidant Defence, Fatty Acid Composition and Lipid Peroxidation in Reared *Oncorhynchus mykiss* Fry. *Sci. Rep.* **2021**, *11*, 16716. https://doi.org/10.1038/s41598-021-96204-y

[57] Annamalay, S. D. Effects of Antioxidants on Oxidative Stress: Assessing MDA in Urine Samples. *Int. J. Clin. Nutr. Diet.* **2018**, *4*, 135. https://doi.org/10.15344/2456-8171/2018/135

ASEAN
Journal of Scientific and Technological Reports
Online ISSN:2773-8752

Research article

Comparative Analysis of Forecasting Models for Hourly Solar Irradiance in Southern Thailand

Mojtaba Safari[1], Suttipan Aksornniem[1], Tanawat Srirugsa[1, 2], Wiwat Su-hren[1, 2] and Supachai Kaewpoung[1, 2*]

[1] Faculty of Engineering, Thaksin University, Phatthalung 93210, Thailand
[2] Center of Excellence for Agricultural Innovation and Bioproducts of Thaksin University, Thaksin University, Phatthalung, 93210, Thailand
* Correspondence: supachai.ka@tsu.ac.th

Citation:
Safari, M., Aksornniem, S., Srirugsa, T., Su-hren, W., Kaewpoung, S., Comparative analysis of forecasting Models for hourly solar irradiance in southern Thailand. *ASEAN J. Sci. Tech. Report.* **2026**, *29*(7), e262134. https://doi.org/10.55164/ajstr.v29i7.262134

Article history:
Received: October 30, 2025
Revised: April 11, 2026
Accepted: April 12, 2026
Available online: June 14, 2026

Publisher's Note:
This article is published and distributed under the terms of the Thaksin University.

Abstract: Accurate forecasting of short-term solar irradiance is essential to optimize energy supply, improve grid stability, and increase the economic viability of photovoltaic systems. This study compares several forecasting models for predicting hourly solar irradiance using real-world data from Southern Thailand. Eight models were evaluated, including six forecasting models (Prophet, LSTM, GRU, XGBoost, Random Forest, and SARIMA with walk-forward validation) and two benchmarks (Naive and Seasonal Naive), using RMSE, MAE, and MAPE metrics. The results demonstrate that ensemble-based machine learning models significantly outperformed traditional statistical and deep learning approaches. Specifically, XGBoost achieved the best performance with RMSE of 79.43 W/m², MAE of 59.63 W/m², and MAPE of 30.07%, followed closely by Random Forest with RMSE of 83.00 W/m² and MAPE of 29.36%. Compared to the best benchmark model, XGBoost reduced RMSE by 50.3% and MAPE by 47.1%. The GRU model outperformed LSTM, demonstrating greater efficiency in capturing short-term temporal dependencies. The findings confirm that ensemble methods effectively capture complex temporal patterns and nonlinear meteorological dependencies, making them highly suitable for real-time solar forecasting applications in tropical climates.

Keywords: Solar irradiance forecasting; southern Thailand; machine learning; deep learning

1. Introduction

Currently, solar energy is a critical renewable energy source driving environmental and economic progress worldwide. As global energy demand continues to rise, transitioning to solar energy has become essential for reducing greenhouse gas emissions, advancing sustainable development, and decreasing reliance on fossil fuels [1]. However, solar power generation is inherently variable and intermittent, depending on weather conditions, time of day, and seasonal factors. These fluctuations pose significant challenges for power generation and distribution management, potentially affecting electrical grid stability [2–3]. Consequently, developing accurate forecasting models for solar irradiance has become crucial for optimizing energy generation, storage, and management in modern renewable energy systems [4–5].

Accurate short-term solar irradiance forecasting, particularly at hourly resolution, is essential for real-time control of photovoltaic (PV) systems and for optimizing energy storage devices, such as batteries, and load control mechanisms [6]. Statistical models such as ARIMA and SARIMA have been

widely used in time-series analysis due to their effectiveness in capturing seasonal patterns and linear trends [7–8]. However, these models often struggle to capture nonlinear relationships between climatic variables [9]. The rapid development of machine learning (ML) and deep learning (DL) techniques has introduced new approaches for time-series forecasting [10–11]. Ensemble methods such as Random Forest (RF) and XGBoost have gained popularity due to their ability to handle large datasets and model complex interactions [12–13].

Deep neural network architectures such as Long Short-Term Memory (LSTM) and Gated Recurrent Unit (GRU) have demonstrated strong capabilities for retaining long-term temporal information and learning sequential dependencies, making them particularly suitable for analyzing complex, time-varying solar irradiance patterns [14–17]. Additionally, Facebook's Prophet model was created especially to handle data with changing temporal trends and varied seasonalities. For extremely variable environmental and energy datasets, it has shown especially favorable results [18–19]. Consequently, evaluating the effectiveness of statistical, machine learning, and deep learning models offers a crucial foundation for determining the best method for forecasting solar irradiance, especially in tropical areas like Thailand [20–21].

This study aims to develop and evaluate hourly solar irradiance forecasting models using real-world data from a solar monitoring station at the Faculty of Engineering, Thaksin University, Southern Thailand. The dataset includes solar irradiance and key meteorological variables that influence solar radiation on PV surfaces: ambient temperature, panel temperature, relative humidity, wind speed, and wind direction [22–23]. The proposed framework encompasses baseline models (Naive and Seasonal Naive (SNaive)) for performance benchmarking, statistical models (SARIMA and Prophet), machine learning models (XGBoost and Random Forest), and deep learning models (LSTM and GRU) [24–25].

The key contributions of this study include: (1) a comprehensive comparison of eight forecasting approaches under tropical conditions, (2) empirical evidence on the relative performance of traditional statistical methods versus modern machine learning and deep learning techniques for solar forecasting, and (3) practical guidance on computational efficiency and model selection for real-time applications. These findings are expected to support the development of intelligent solar energy management systems and enhance renewable energy integration in tropical regions with high solar potential [26].

The remainder of this paper is organized as follows: Section 2 presents the methodology, including data preprocessing, model descriptions, and evaluation metrics. Section 3 describes the exploratory data analysis, discusses the experimental setup, and compares model performance. Finally, Section 5 concludes with key findings, practical implications, and recommendations for future research.

2. Methodology

This study develops and compares multiple forecasting models to predict hourly solar irradiance. The methodology includes three types of techniques: statistical models (SARIMA and Prophet), ML models (XGBoost and RF), and DL models (LSTM and GRU). Each model is designed to capture different characteristics of solar irradiance patterns, including seasonal changes, nonlinear relationships, and the influence of weather variables. Furthermore, two simple benchmark models are used: the Naive method and the SNaive method, which provide a baseline for comparison. Finally, the performance of these models is evaluated using three key metrics: RMSE, MAE, and MAPE [27].

2.1 Pre-processing and normalization

Before building the forecasting models, the raw dataset was checked for missing or incorrect values that might have resulted from sensor failures. Missing hourly values were filled using a two-step method based on climatology patterns. In the second step, a Day-of-Year × Hour matrix was created and linearly interpolated across both days and hours to smooth any remaining gaps. This process produced a complete and physically consistent hourly dataset. All variables were then aligned to a uniform hourly timestamp format to ensure temporal consistency. After cleaning the data, all variables were normalized using Min-Max scaling, which maps values to the range [0, 1]. This normalization was applied separately to the training set (80% of the data) and the testing set (20% of the data) to prevent data leakage. The Min-Max scaling formula is:

$$Z = \frac{X - X_{min}}{Xmin_{max}} \quad (1)$$

Where X is the original value of a feature, X_{min} is the minimum value of that feature in the training data, X_{max} is the maximum value of that feature in the training data, and Z is the normalized value.

2.2 Forecasting models

2.2.1 Walk-forward SARIMA model

The Seasonal Autoregressive Integrated Moving Average (SARIMA) model extends the classical ARIMA framework by accounting for both regular patterns and seasonal patterns in time series data [28]. The general form of a SARIMA model is expressed as:

$$SARIMA\ (p, d, q)\ (P, D, Q)_S \quad (2)$$

where the parameters$p$, d, and $q$represents the non-seasonal autoregressive order, non-seasonal differencing, and non-seasonal moving average order, respectively, and the parameters P,D, Q, and Srefer to the seasonal autoregressive order, seasonal differencing, seasonal moving average order, and length of the seasonal cycle, respectively. The mathematical formulation of the SARIAM model can be defined as [29]:

$$\phi_p(B)\phi_P(B^S)(1-B)^d(1-B^S)^D Y_t = \theta_q(B)\theta_Q(B)^S\varepsilon_t \quad (3)$$

where:
$\phi_p(B) = 1 - \phi_1 B - \phi_2 B^2 - \ldots - \phi_p B^p$,
$\phi_P(B^S) = 1 - \phi_1 B^S - \phi_2 B^{2S} - \ldots - \phi_P B^{PS}$,
$\theta_q(B) = 1 - \theta_1 B - \theta_2 B^2 - \ldots - \theta_q B^q$,
$\theta_Q(B^S) = 1 - \theta_1 B^S - \theta_2 B^{2S} - \ldots - \theta_Q B^{QS}$,
where $\phi_1, \ldots, \phi_p$, and $\phi_1, \ldots, \phi_P$, are non-seasonal and seasonal autoregressive coefficients, while $\theta_1, \ldots, \theta_q$, and $\theta_1, \ldots, \theta_Q$ are the coefficients for the non-seasonal and seasonal moving-average terms. B is the backshift operator, whose effect on a time seriesY_t, and ε_t is a white noise sequence.

To evaluate the SARIMA model under realistic forecasting conditions, a walk-forward validation strategy was used. This approach is widely recommended in time series forecasting literature [29-30], because it provides a more reliable assessment of how well statistical models like SARIMA generalize to unseen data. Unlike a single train-test split, walk-forward validation continuously retrains the model as new data becomes available, ensuring that all forecasts are made on truly future data. This study used a fixed-length rolling window approach for the walk-forward validation. Specifically, at each forecasting step, the model was trained on the most recent observations within a window of approximately 720 hours. After making a forecast, the window moved forward by one hour: the oldest observation was removed, and the newest observation was added. The model was retrained at every step to capture short-term patterns and adapt to local changes in solar irradiance. The mathematical representation of the walk-forward validation process is as follows:

Let $y_1, y_2, \ldots, y_t$ represent the observed irradiance series of length t. At each step t(where$t \geq W$), the model is trained on a fixed window of the most recent W observations as follows:

$$D_t = y_{t-W+1}, y_{t-W+2}, \ldots, y_t \quad (4)$$

Using this training window, the model estimates its parameters θ_t and produces a one-step-ahead forecast:

$$\hat{y}_{t+1} = f(D_t; \theta_t) \quad (5)$$

After generating the forecast, the window is advanced by one time step, discarding the oldest observation and adding the newest actual value y_{t+1}:

$$D_{t+1} = y_{t-W+2}, y_{t-W+3}, \ldots, y_{t+1} \quad (6)$$

This process repeats until the end of the testing period. The forecasting performance is evaluated by comparing each predicted value $\hat{y}_{t+1}$ to its corresponding actual valuey_{t+1}.

2.2.2 LSTM model

The LSTM network is a specialized type of Recurrent Neural Network (RNN) designed to capture temporal patterns in sequential data. Traditional RNNs struggle to learn long-term dependencies due to vanishing or exploding gradients during training. LSTMs overcome this limitation by using memory cells and gating mechanisms that control which information to retain or discard over extended time periods. Each LSTM unit includes three gates that control information flow [31]. Which data from the prior cell state should be erased is decided by the forget gate. Which fresh data should be added to the cell state is controlled by the input gate. The output gate controls the amount of cell-state data sent to the next time step. These gates work together to selectively update and propagate information through the network, enabling the model to learn both short-term and long-term dependencies in the data. The operations within an LSTM unit at time step t are mathematically expressed as follows:

The forget gate f_t determines what information to discard from the previous cell state:

$$f_t = \sigma(W_{hf} h_{t-1} + W_{xf} X_t + b_{hf} + b_{xf}) \tag{7}$$

The input gate i_t decides which new information should be added to the cell state:

$$i_t = \sigma(W_{xi} X_t + W_{hi} h_{t-1} + b_i) \tag{8}$$

The candidate cell state $\tilde{c}_t$ represents new information that could be added to the cell:

$$\tilde{c}_t = tanh(W_{xc} X_t + W_{hc} h_{t-1} + b_c) \tag{9}$$

The cell state c_t is updated by combining the forgotten information and new information:

$$c_t = f_t \odot c_{t-1} + i_t \odot \tilde{c}_t \tag{10}$$

The output gate o_t controls what information from the cell state to output:

$$o_t = \sigma(W_{xo} X_t + W_{ho} h_{t-1} + b_o) \tag{11}$$

The hidden state (h_t output of the LSTM unit) is computed as:

$$h_t = o_t \odot tanh(c_t) \tag{12}$$

where X_t represents the input vector at the time step t, h_{t-1} is the previous hidden state, c_{t-1} refers to the previous cell state, tanh is the hyperbolic tangent activation function, $W_{xf}, W_{hf}, W_{xi}, W_{hi}, W_{xc}, W_{hc}, W_{xo}, W_{ho}$ are weights for forget gate, input gate, candidate cell state, and output gate, respectively, and b_{xf}, b_i, b_c, b_o are bias values for forget gate, input gate, candidate cell state, and output gate, respectively. The symbol $\odot$ denotes element-wise multiplication.

2.2.3 GRU model

The Gated Recurrent Unit (GRU) is a simplified variant of the LSTM network, also designed to capture temporal dependencies in sequential data while addressing the vanishing gradient problem. GRUs achieve comparable performance to LSTMs but with a more simplified architecture that uses fewer parameters, making them computationally more efficient and faster to train [31]. Unlike LSTMs, which use separate memory cells and hidden states, GRUs combine these into a single hidden state. Each GRU unit contains two gates that control information flow:

- Reset gate: Determines how much of the previous hidden state should be discarded,
- Update gate: Controls how much of the previous hidden state to retain and how much new information to add.

These two gates enable the GRU to selectively retain relevant information from previous time steps while incorporating new inputs. The operations within a GRU unit at time step $t$are mathematically expressed as follows:

The reset gate r_t determines how much past information to forget:

$$r_t = \sigma(W_{xr}X_t + W_{hr}h_{t-1} + b_r) \tag{13}$$

The update gate z_t controls the balance between retaining old information and adding new information:

$$z_t = \sigma(W_{xz}X_t + W_{hz}h_{t-1} + b_z) \tag{14}$$

The candidate's hidden state $\tilde{h}_t$ represents new information based on the current input and resets the past state:

$$\tilde{h}_t = tanh(W_{xh}X_t + W_{hh}(r_t \odot h_{t-1}) + b_h) \tag{15}$$

The hidden state h_t is updated by combining the previous hidden state and the candidate hidden state:

$$h_t = (1 - z_t) \odot h_{t-1} + z_t \odot \tilde{h}_t \tag{16}$$

where X_t is the input vector at time step t, h_{t-1} is the previous hidden state, σ is the sigmoid activation function, $tanh$ is the hyperbolic tangent activation function, $W_{xr}, W_{hr}, W_{xz}, W_{hz}, W_{xh}, W_{hh}$ are weight matrices for the reset gate, update gate, and candidate hidden state, respectively, and b_r, b_z, b_h are bias terms for the reset gate, update gate, and candidate hidden state, respectively.

2.2.4 Prophet model

Prophet is a time-series forecasting model developed by Facebook designed to handle data with strong seasonal patterns and multiple seasonality components [32]. Prophet uses an additive decomposition framework that automatically detects and models trends, seasonality, and holiday effects, making it particularly suitable for business and environmental forecasting applications. The Prophet model decomposes a time series into three main components: trend, seasonality, and holidays. The general formulation of the Prophet model is expressed as:

$$y(t) = g(t) + s(t) + h(t) + \varepsilon_t \tag{17}$$

where $y(t)$ is the forecasted value at time t, $g(t)$ represents the trend component that captures long-term changes in the data, $s(t)$ represents the seasonal component that captures periodic patterns (daily, weekly, or yearly), $h(t)$ represents the holiday or special event effects, and ε_t is the error term representing random noise? The trend component $g(t)$ models non-periodic changes in the time series. Prophet uses a piecewise linear or logistic growth model to capture trends that may change over time:

$$g(t) = (k + a(t)^T\delta) \cdot t + (m + a(t)^T\gamma) \tag{18}$$

where k is the growth rate, δ contains rate adjustments at changepoints, m is the offset parameter, and $a(t)$ is an indicator function for the changepoint. The seasonality component $s(t)$ captures periodic patterns using the Fourier series:

$$s(t) = \sum_{n=1}^{N}(a_n\, cos(\frac{2\pi nt}{P}) + b_n\, sin(\frac{2\pi nt}{P})) \tag{19}$$

where P is the period, $N$is the number of Fourier terms, and a_n and $b_n$are the Fourier coefficients estimated from the data.

2.2.5 Random Forest

An ensemble machine learning approach called Random Forest (RF) combines multiple decision trees to produce more reliable and accurate predictions. The model averages predictions from numerous trees, each trained on a random subset of the data and features, to address the overfitting issue sometimes encountered with single decision trees. The RF algorithm operates through the following process [33]: (1) Bootstrap sampling creates multiple subsets of the training data through random sampling with replacement; (2) Tree construction builds a decision tree for each subset, where at each node, only a random subset of features is considered for splitting; and (3) Aggregation produces the final prediction by averaging the outputs of all individual trees for regression tasks. The prediction of a Random Forest model for a given input X is mathematically expressed as:

$$\hat{y} = \frac{1}{n_{trees}} \sum_{i=1}^{n_{trees}} T_i(X) \tag{20}$$

where $\hat{y}$ is the predicted value, n_{trees} is the total number of decision trees in the forest, and $T_i(X)$ is the prediction from the i -th decision tree. Each decision tree in the forest learns different patterns from the data due to the randomness in both data sampling and feature selection. This diversity among trees reduces the model's variance and improves its generalization ability. The RF model includes several key hyperparameters, including the number of trees (n_{trees}), the maximum depth of each tree (max_{depth}), and the minimum number of samples required to split a node ($min_{samples}$).

2.2.6 XGBoost model

XGBoost (Extreme Gradient Boosting) is an advanced ensemble machine learning algorithm that builds a series of decision trees sequentially, where each new tree attempts to correct the errors made by the previous trees. Unlike RF, which builds trees in parallel, XGBoost uses a boosting approach in which trees are added one at a time, with each tree learning from the mistakes of its predecessors. The XGBoost model optimizes a regularized objective function that balances prediction accuracy and model complexity [34]:

$$L = \sum_{i=1}^{n} l(y_i, \hat{y}_i) + \sum_{k=1}^{K} \Omega(f_k) \tag{21}$$

where $l(y_i, \hat{y}_i)$ is the loss function measuring the difference between the actual value y_i and the predicted value $\hat{y}_i, \Omega(f_k)$ is the regularization term that penalizes model complexity to prevent overfitting, n is the number of samples, and K is the number of trees. The final prediction is obtained by summing the predictions from all trees:

$$\hat{y}_i = \sum_{k=1}^{K} f_k(x_i) \tag{22}$$

where $\hat{y}_i$ is the predicted value for the sample i, f_k represents the k -th tree, and x_i is the input feature vector. XGBoost employs gradient descent to iteratively minimize the loss function. At each iteration, a new tree is added that approximates the negative gradient of the loss function, effectively moving the predictions closer to the true values. The algorithm also incorporates several advanced techniques, including tree pruning, handling of missing values, and parallel processing, which contribute to its computational efficiency and superior performance. The key hyperparameters of the XGBoost model include the number of trees ($n_{estimators}$), the learning rate (η) that controls the contribution of each tree, the maximum tree depth (max_{depth}), the minimum loss reduction required to make a split(γ), and regularization parameters (λ and α) that control model complexity.

2.2.7 Benchmark models

To evaluate the performance of the forecasting models, two simple benchmark methods were implemented: the Naive model and the Seasonal Naive (SNaive) model. These benchmarks provide baseline comparisons and help assess whether the more complex models offer meaningful improvements over straightforward forecasting approaches. These two benchmark models were selected because hourly solar irradiance typically exhibits both short-term continuity and daily cyclical behavior, making persistence-based and seasonal-repeat baselines appropriate reference models for performance evaluation. The Naive model is

the simplest forecasting method, which assumes that the next value will be equal to the most recent observed value. Mathematically, the Naive forecast at time t is expressed as:

$$\hat{y}_i = y_{t-1} \tag{23}$$

where $\hat{y}_i$ is the predicted value at time t, and y_{t-1} is the actual value at the previous time step. This model is particularly useful for data without strong trends or seasonal patterns and serves as a minimum performance threshold that any sophisticated model should exceed. SNaive model accounts for seasonal patterns in the data by using the value from the same period in the previous seasonal cycle as the forecast. For hourly solar irradiance data with a daily seasonal pattern, the SNaive forecast is expressed as:

$$\hat{y}_i = y_{t-S} \tag{24}$$

where S is the seasonal period. In this study, S = 12 hours, corresponding to the 12 daylight hours retained after preprocessing. This means the forecast for a given hour is based on the irradiance value from the same hour on the previous day. The SNaive model is particularly effective for data with strong and stable seasonal patterns, making it a more challenging benchmark than the simple Naive model for solar irradiance forecasting. Both benchmark models require minimal computational resources and no parameter tuning. Their performance serves as a reference point to determine whether the added complexity of statistical, machine learning, and deep learning models translates into tangible forecasting improvements.

2.3 Evaluation metrics

To assess and compare the forecasting performance of all models, three widely used evaluation metrics were employed: RMSE, MAE, and MAPE.

$$RMSE = \sqrt{\frac{1}{n}\sum_{i=1}^{n}(y_i - \hat{y}_i)^2} \tag{25}$$

$$MAE = \frac{1}{n}\sum_{i=1}^{n}|y_i - \hat{y}_i| \tag{26}$$

$$MAPE = \frac{100}{n}\sum_{i=1}^{n}\left|\frac{y_i - \hat{y}_i}{y_i}\right| \tag{27}$$

where n is the number of observations, y_i is the actual value at time i, and $\hat{y}_i$ is the predicted value at time i. Lower values of all three metrics indicate better forecasting performance.

3. Experiment and numerical results

This section presents the experimental framework and the numerical results obtained from evaluating the forecasting models. All experiments were conducted using Python 3.11 on a system equipped with an Intel Core i7 processor and 16 GB of RAM. The models were trained on 80% of the dataset and tested on the remaining 20% to assess their generalization performance. Model accuracy was evaluated using three performance metrics: MAE, RMSE, and MAPE, which enable direct comparison across all models.

3.1 Exploratory data analysis

Before developing the forecasting models, an exploratory data analysis was conducted to understand the dataset's temporal and statistical characteristics. This study uses data recorded by a solar photovoltaic monitoring station at the Faculty of Engineering, Thaksin University, Thailand. The monitoring system continuously measures key meteorological and operational parameters that influence solar irradiance and energy generation. The dataset spans the period from May 2024 to April 2025 and consists of 4,406 hourly records. The variables included in the dataset are:

- Irradiance (W/m²): The target variable representing the solar power received per unit area on the panel surface,
- Environmental Temperature (Env Temp, °C): The ambient air temperature measured near the panel installation site,
- Panel Temperature (Panel Temp, °C): The surface temperature of the PV panel,
- Wind Speed (m/s): The average wind speed measured at sensor height,
- Wind Angle (°): The direction of wind flow, which influences panel cooling,
- Environmental Humidity (Env Humidity, %): The ambient moisture content in the air.

These data were collected using several sensors connected to a data logger, which was synchronized to local time to ensure data accuracy and consistency. Figure 1(a) illustrates the temporal distribution of solar irradiance throughout the dataset, highlighting the daily and monthly patterns. The figure shows that solar irradiance has a strong daily cycle, with peak intensity concentrated around midday (11:00-13:00). This pattern is typical of tropical solar conditions [35-36]. The visualization also reveals seasonal variations in irradiance levels across different months of the year. Since the original dataset includes nighttime hours with zero irradiance values, these non-productive hours were excluded from the analysis to improve forecasting. Only daytime hours with meaningful solar activity were retained, ensuring that the models are trained on relevant data. Figure 1(b) shows the filtered dataset after removing nighttime observations, which consists of 12 daylight hours per day.

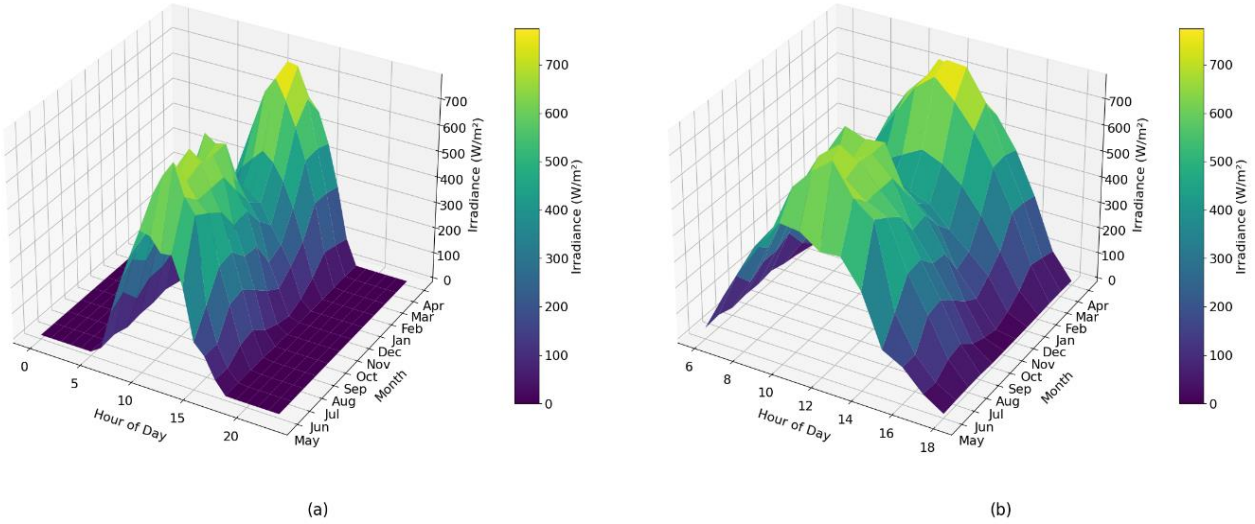


Figure 1. Temporal distribution of solar irradiance: (a) complete 24-hour dataset showing daily and seasonal patterns, (b) filtered daytime-only dataset (12 hours) used for model training and testing.

Figure 2 presents the monthly distributions of all measured variables, with boxplots and trend lines overlaid on the monthly averages. The analysis reveals clear seasonal patterns across all meteorological parameters. Irradiance and temperature variables (both panel and environmental) exhibit a positive correlation and show higher values from February to May, corresponding to the hot, dry season in Thailand. Conversely, these variables reach their lowest levels during the monsoon season from October to December. Relative humidity displays an inverse relationship with irradiance, reaching its highest values during the wet season (October to December) and decreasing as irradiance levels increase during the dry months. Wind speed gradually increases throughout the year, with higher values observed from December to April. Wind angle shows significant seasonal variation, likely influenced by local monsoon patterns that shift the direction of prevailing winds. These seasonal patterns demonstrate that meteorological and climatic factors strongly influence solar energy generation. The observed correlations between irradiance and weather variables justify

the inclusion of environmental predictors (temperature, humidity, and wind characteristics) in the forecasting models, as they contain valuable information that can improve prediction accuracy. Wind speed and wind direction were recorded using an anemometer positioned at approximately 12.5 meters above ground level, consistent with standard meteorological guidelines, since wind behavior changes markedly with height due to surface friction. Atmospheric wind conditions affect solar irradiance indirectly by influencing cloud development, cloud transport, and air turbulence. Stronger winds are commonly linked to faster cloud movement, which can produce abrupt variations in incoming solar radiation, while wind direction provides insight into dominant weather systems, particularly during tropical monsoon periods. For this reason, wind parameters were incorporated into the forecasting models as meteorological inputs to represent atmospheric processes that drive short-term fluctuations in solar irradiance.

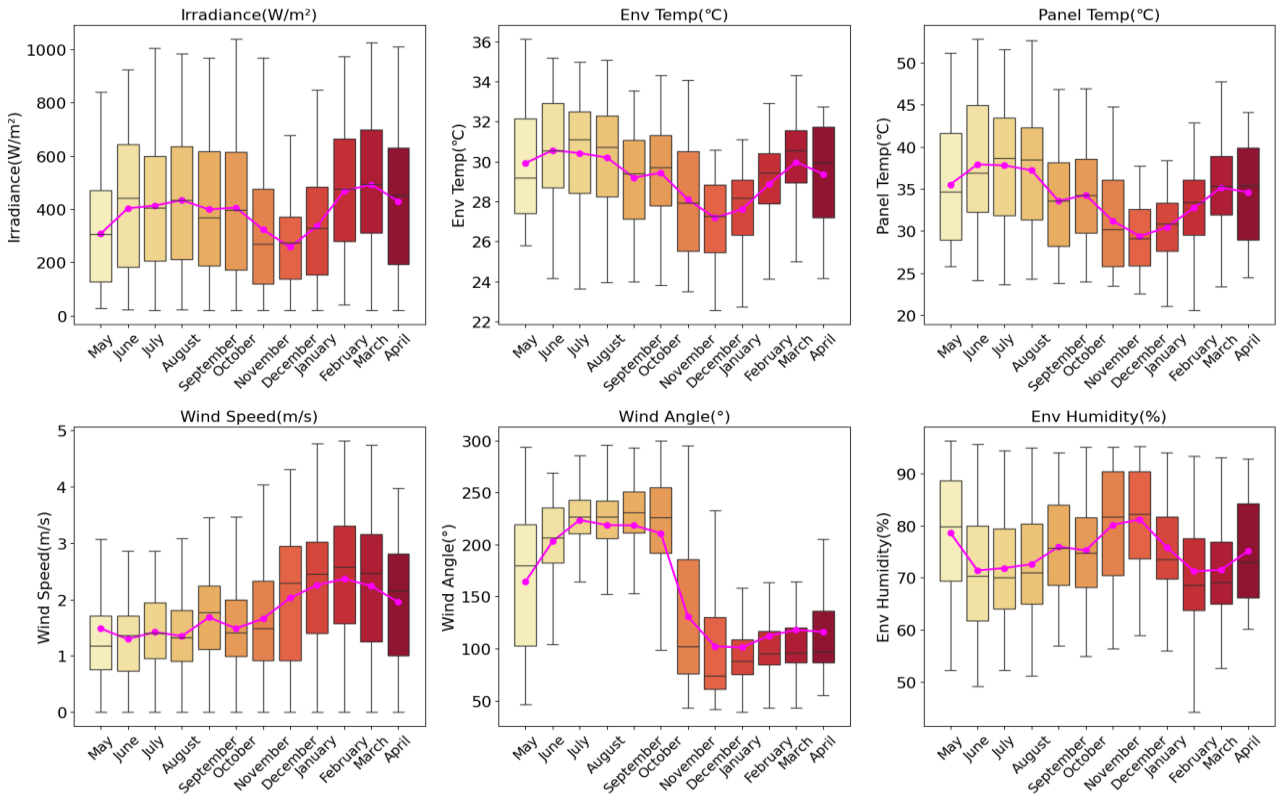


Figure 2. The monthly boxplots of irradiance and meteorological variables.

In this study, "sun irradiance" refers to the Global Horizontal Irradiance (GHI) recorded at an actual monitoring site. GHI, or the total amount of solar radiation incident on a horizontal surface, is composed of diffuse radiation scattered by the atmosphere and direct beam radiation from the sun. Because the irradiance sensor was positioned horizontally, the observed values are appropriate for GHI-based analysis and predictions.

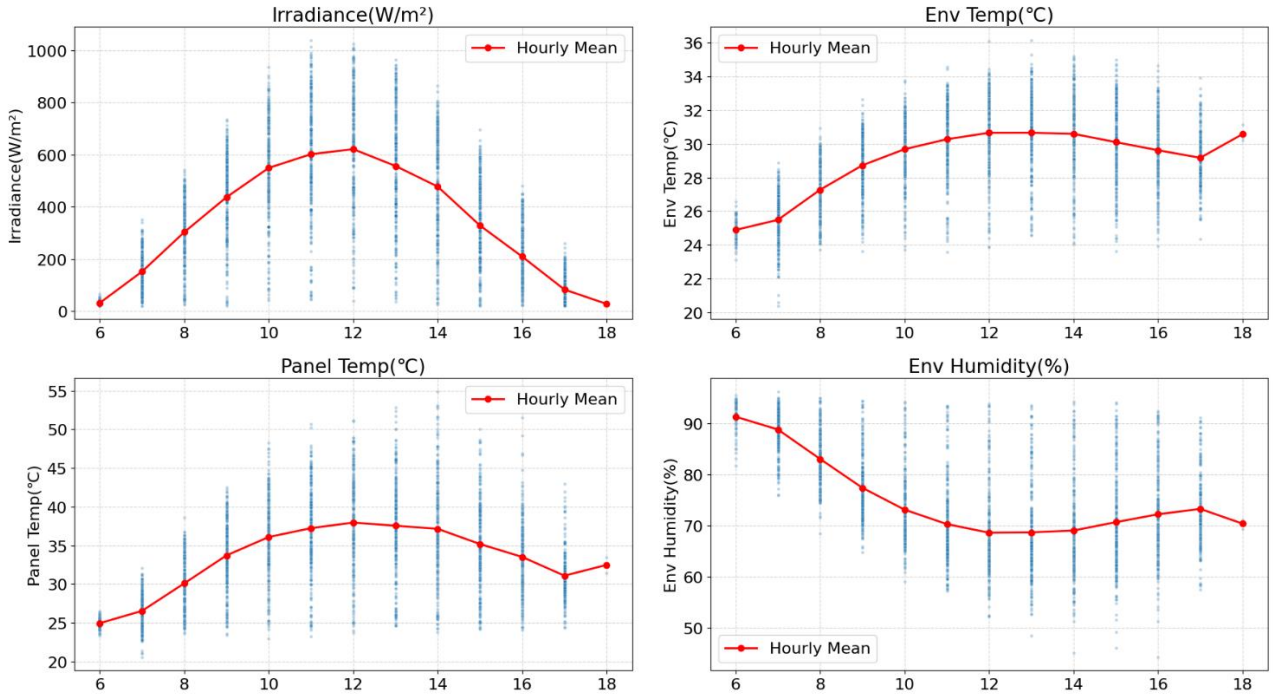


Figure 3. The hourly distribution of the main variables.

Panel temperature is closely related to solar irradiance. As solar radiation increases, the surface temperature of photovoltaic modules also rises. Therefore, under high irradiance, some of the incoming solar energy is converted into electricity, while the rest is converted into heat, which raises the panel's temperature. Moreover, the panel's temperature directly affects how well the photovoltaic (PV) system operates, as higher temperatures often reduce its energy conversion efficiency. Consequently, it serves as a useful indirect indicator of both solar radiation intensity and the system's operational condition. In forecasting applications, panel temperature is treated as an external (exogenous) variable to account for the PV system's thermal response to fluctuating atmospheric conditions. By providing supplementary information beyond irradiance data, panel temperature improves the precision of predictions.

From a daily perspective, Figure 3 presents the hourly distributions of the main variables using histograms, along with the trend line for the hourly mean. The Irradiance curve shows a bell-shaped pattern, with a peak between 11:00 and 13:00, corresponding to maximum solar exposure. Both environmental and panel temperatures increase during the morning, reach their highest values around midday, and then decline toward evening. In contrast, relative humidity decreases as irradiance and temperature rise, then increases in the late afternoon. These results confirm a strong diurnal relationship between solar radiation and atmospheric conditions, supporting the importance of these meteorological variables for enhancing short-term irradiance forecasting accuracy.

3.2 Model hyperparameter configuration

To ensure a fair comparison across all forecasting models, each model was systematically optimized via hyperparameter tuning on the training dataset. For the SARIMA model, a comprehensive grid search was conducted across multiple combinations of non-seasonal (p, d, q) and seasonal P, D, Q, S parameters. The search space included reasonable ranges derived from the observed autocorrelation and partial autocorrelation structures of the irradiance series. Specifically, the orders p, q, P, and Q were varied between 0 and 2, while the differencing orders d and D were restricted to 0 or 1 to maintain model simplicity and avoid over-differencing. The seasonal period was set to S = 12, corresponding to the 12 daylight hours retained after preprocessing. In total, 325 unique parameter combinations were evaluated. Each candidate model was trained on 80% of the data (the training set) and assessed using two criteria: the Akaike Information Criterion

(AIC) and the Bayesian Information Criterion (BIC). These metrics balance model accuracy with model complexity by penalizing models that have too many parameters. The model with the lowest AIC and BIC values was selected as the optimal configuration. Figure 4(a) shows the AIC and BIC values for the top 10 model combinations, with the best-performing model being SARIMA (1, 1, 2) (2, 0, 2, 12). Figure 4(b) analyzes the relationship between model complexity and performance. Model complexity is measured by the total number of parameters ($p + d + q + P + D + Q$). The results show that very simple models (2-4 parameters) perform worse than moderately complex models (6-8 parameters). Beyond 8 parameters, there is no significant improvement, and some models with 9-10 parameters actually perform worse.

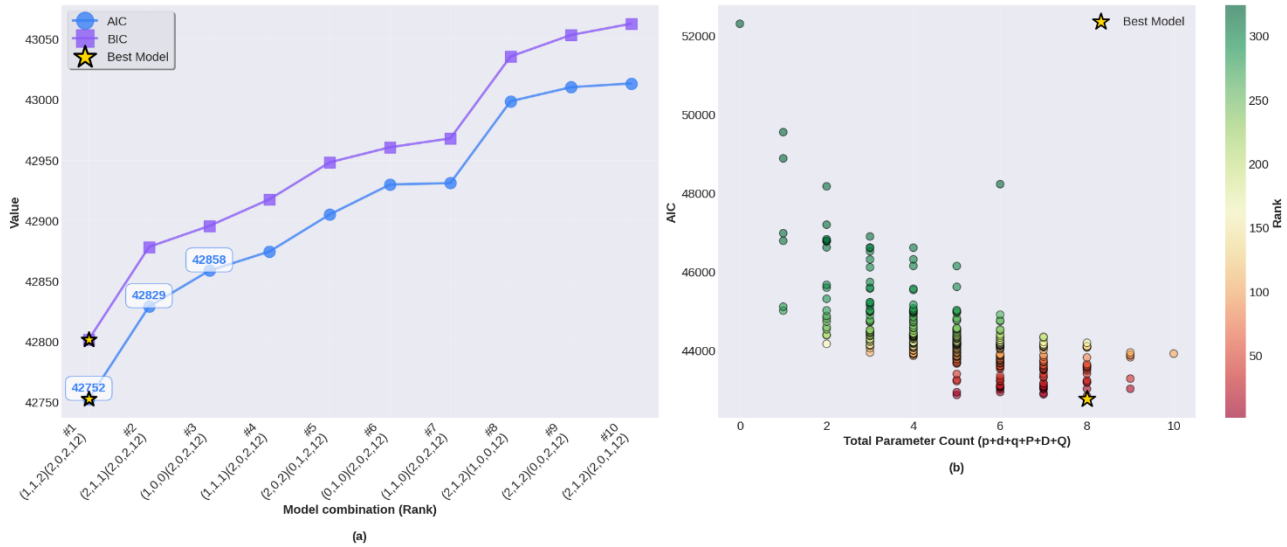


Figure 4. a) AIC and BIC across the top 10 model combinations, b) model complexity versus performance.

The Prophet model was configured to capture daily and weekly seasonality with four meteorological variables (environmental temperature, panel temperature, wind speed, and relative humidity) incorporated as exogenous regressors. Both XGBoost and Random Forest models utilized lag features at 1-hour, 24-hour, and 168-hour intervals, combined with meteorological variables, with all features standardized using a StandardScaler fitted to the training set. The LSTM and GRU networks used a 24-hour lookback window, with all features standardized, and their architectures included a recurrent layer, a dense layer with ReLU activation, and an output layer. Training used the Adam optimizer with early stopping (patience: 5-6 epochs) and learning rate reduction at plateaus. The final hyperparameter configurations for all models are summarized in Table 1.

Table 1. Summary of model hyperparameters and configurations.

Model	Key Hyperparameters	Configuration
SARIMA	$(p, d, q)(P, D, Q, s)$	(1,1,2) (2,0,2,12)
Prophet	Seasonality, Regressors	Daily and weekly, variables
XGBoost	Estimators, Learning rate, Max depth, Lags	500, 0.05, 6, (1, 24, 168)
RF	Estimators, Max depth, Min samples split, Lags	500, 15, 5, (1, 24, 168)
LSTM	Neurons, Batch size, Epochs, Lookback	64, 128, 50, 24
GRU	Neurons, Batch size, Epochs, Lookback	64, 128, 50, 24

3.3 Forecasting results

Six forecasting models, which are SARIMA, Prophet, LSTM, GRU, XGBoost, and RF, were trained on the training set spanning from May 6, 2024, 06:00 to February 1, 2025, 06:00 (3,524 hours, representing 80% of the dataset). The performance of these models was evaluated on the test set from February 1, 2025, 07:00 to April 9, 2025, 17:00 (885 hours, representing 20% of the dataset) and compared against two benchmark models:

the Naive and SNaive methods. Model performance was assessed using three evaluation metrics: RMSE, MAE, and MAPE.

The numerical results are presented in Table 2, which provides a comprehensive comparison of all forecasting models against the benchmark methods. Furthermore, Figure 5 presents a visual comparison of forecasted versus actual irradiance values for all models across the entire test period. The plots reveal that all forecasting models successfully capture the daily cyclic pattern of solar irradiance, with peaks around midday and troughs in the early morning and late afternoon. However, notable differences in tracking accuracy are evident across models. As shown in Table 2, all advanced forecasting models substantially outperformed both benchmark approaches, confirming their ability to capture the complex temporal patterns and meteorological dependencies inherent in solar irradiance data. Between the two benchmarks, the Naive model performed considerably better than the SNaive model, with RMSE improvements of 34.06 W/m² and MAPE reductions of 22.78%. This suggests that short-term persistence (hour-to-hour continuity) is a more reliable forecasting assumption than daily periodicity for this tropical solar irradiance dataset.

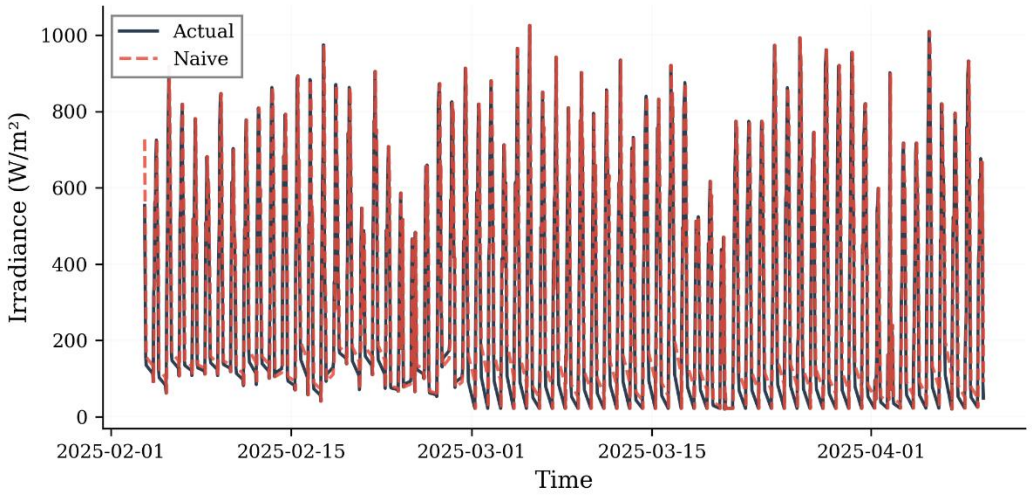
Table 2. Forecasting performance comparison across all models.

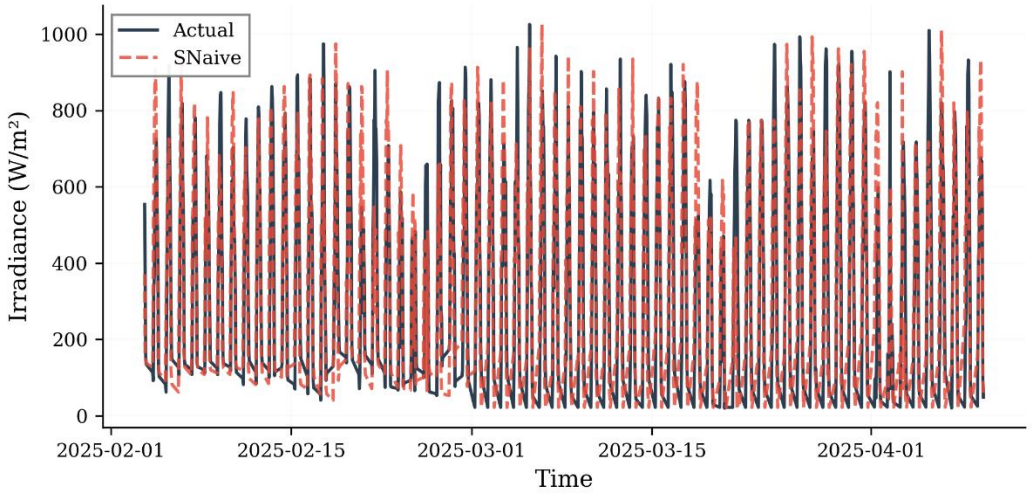
Model type	Models	Evaluation metrics		
		RMSE	**MAE**	**MAPE %**
Forecasting models	SARIMA	110.79	83.78	49.29
	Prophet	94.31	74.59	41.85
	LSTM	140.36	105.86	43.79
	GRU	106.94	78.24	35.98
	XGboost	79.43	59.63	30.07
	RF	83.00	61.98	29.36
Benchmark models	Naive	159.80	129.48	56.89
	SNaive	193.86	153.06	79.67

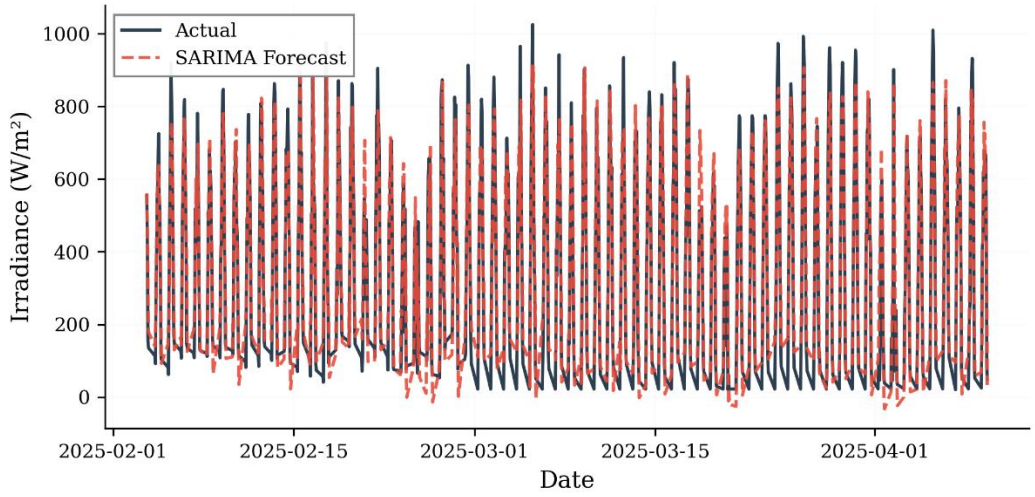
Among the forecasting models, the ensemble-based machine learning approaches demonstrated superior performance. XGBoost achieved the best overall results across all metrics, yielding the lowest RMSE (79.43 W/m²) and MAE (59.63 W/m²), with a MAPE of 30.07%. RF produced comparable results, achieving the lowest MAPE (29.36%) while maintaining competitive RMSE (83.00 W/m²) and MAE (61.98 W/m²) values. The strong performance of both ensemble methods can be attributed to their ability to effectively model nonlinear feature-target relationships and capture complex interactions between meteorological variables and solar irradiance. Compared to the best benchmark (Naive), XGBoost reduced RMSE by 50.3%, MAE by 53.9%, and MAPE by 47.1%, demonstrating substantial improvements in forecasting accuracy.

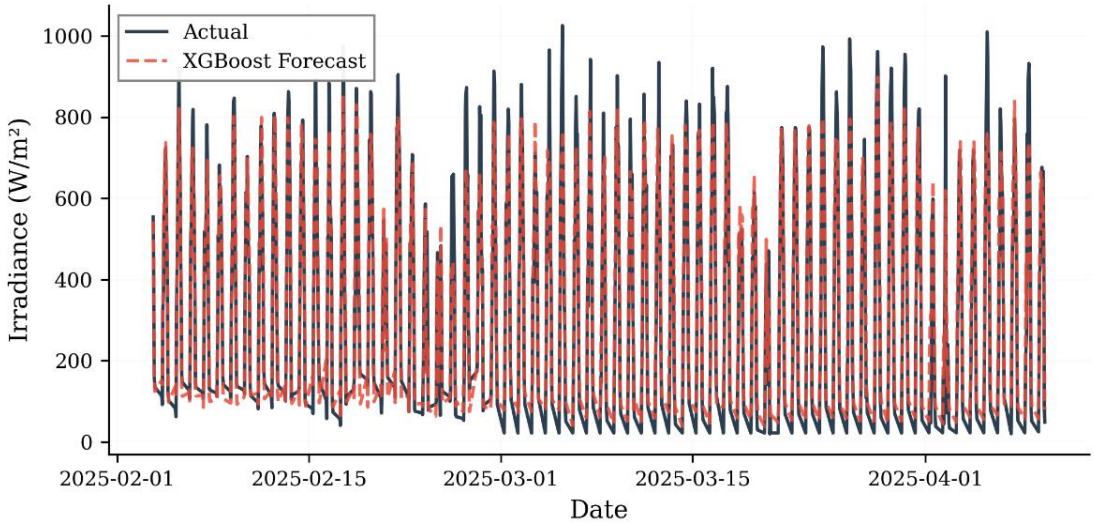
The deep learning models exhibited mixed results. The GRU model outperformed the LSTM across all metrics, achieving an RMSE of 106.94 W/m² compared to the LSTM's 140.36 W/m², and reducing MAPE from 43.79% to 35.98%. This performance difference highlights GRU's greater efficiency in modelling short-term temporal dependencies with fewer parameters and its superior stability during training. However, both recurrent neural network architectures were outperformed by the machine learning ensemble methods, suggesting that the added complexity of deep learning may not be necessary for this particular forecasting task, given the dataset size and temporal structure.

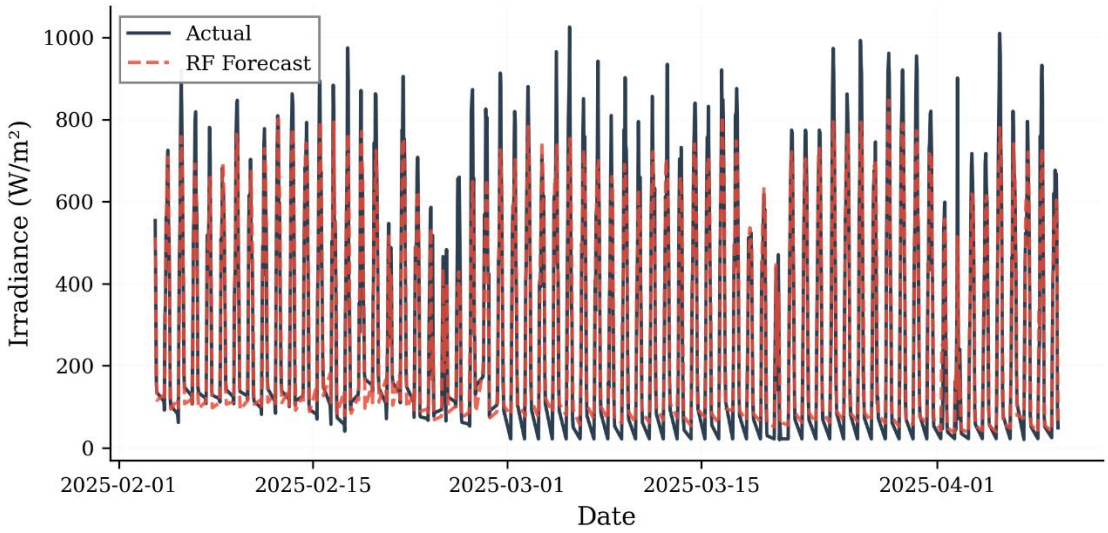
Among the statistical and hybrid models, Prophet demonstrated competitive performance with an RMSE of 94.31 W/m² and an MAPE of 41.85%, substantially outperforming SARIMA (RMSE: 110.79 W/m², MAPE: 49.29%). Prophet's strength lies in its ability to decompose automatically and model trend and seasonal components while incorporating exogenous meteorological variables with minimal parameter tuning. In contrast, despite the comprehensive grid search optimization and rigorous walk-forward validation employed for SARIMA, the model achieved the second-worst performance among all forecasting methods, only surpassing LSTM.

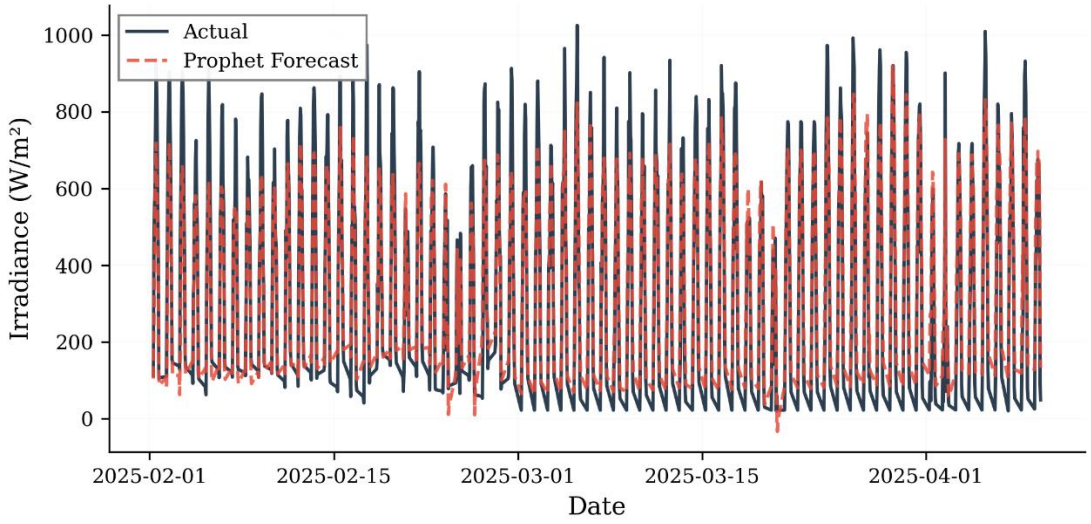

Actual
Naive
Irradiance (W/m²)
0
200
400
600
800
1000
2025-02-01
2025-02-15
2025-03-01
2025-03-15
2025-04-01
Time


Actual
SNaive
Irradiance (W/m²)
0
200
400
600
800
1000
2025-02-01
2025-02-15
2025-03-01
2025-03-15
2025-04-01
Time


Actual
SARIMA Forecast
Irradiance (W/m²)
0
200
400
600
800
1000
2025-02-01
2025-02-15
2025-03-01
2025-03-15
2025-04-01
Date


Actual
XGBoost Forecast
Irradiance (W/m²)
1000
800
600
400
200
0
2025-02-01
2025-02-15
2025-03-01
2025-03-15
2025-04-01
Date


Actual
RF Forecast
Irradiance (W/m²)
1000
800
600
400
200
0
2025-02-01
2025-02-15
2025-03-01
2025-03-15
2025-04-01
Date


Actual
Prophet Forecast
Irradiance (W/m²)
1000
800
600
400
200
0
2025-02-01
2025-02-15
2025-03-01
2025-03-15
2025-04-01
Date

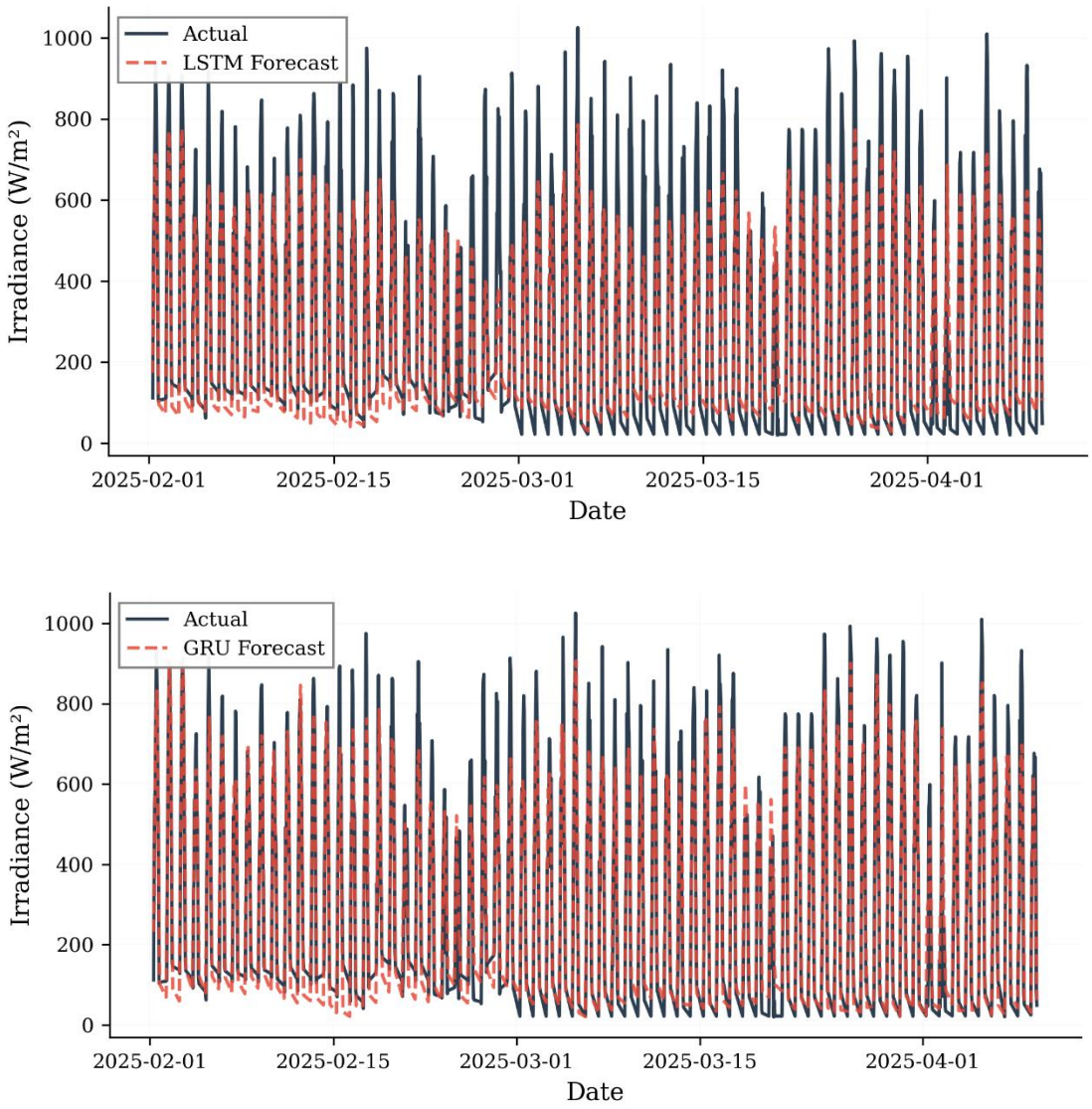


Figure 5. Time series comparison of actual versus forecasted irradiance for all models over the test period. Black solid lines represent actual values, while red dashed lines show model predictions.

In addition to forecasting accuracy, computational efficiency was evaluated for all models. The machine learning and deep learning models (XGBoost, RF, LSTM, and GRU) required 5-10 minutes each for the complete training and prediction cycle, making them highly suitable for real-time or near-real-time forecasting applications. In contrast, the walk-forward SARIMA model required approximately 170 minutes (2 hours and 50 minutes) to complete its training and walk-forward forecasting, due to iterative retraining at each time step—a computationally intensive but methodologically rigorous approach recommended in the time series forecasting literature to ensure temporal robustness and prevent data leakage.

In conclusion, the results demonstrate that ensemble-based machine learning models (XGBoost and Random Forest) provide the most accurate and computationally efficient forecasts for hourly solar irradiance prediction. These models effectively exploit both temporal persistence and nonlinear meteorological effects, making them well-suited for short-term solar forecasting in tropical climates. The GRU model offers a viable alternative when sequential modelling is preferred, outperforming LSTM while maintaining reasonable computational efficiency. Prophet provides a practical compromise between statistical rigor and forecasting accuracy, particularly valuable when model interpretability and automatic seasonality detection are priorities. Overall, the findings confirm that modern machine learning approaches significantly outperform traditional statistical methods for this application, both in terms of accuracy and computational efficiency.

3.4 Practical implications for intelligent solar energy management

Accurate short-term solar irradiance forecasting is crucial for advanced energy management systems, especially in regions with substantial renewable energy integration. The models developed in this research support real-time operational decision-making processes, including load management strategies, maintaining grid stability, and optimal coordination of energy storage units. This capacity is especially vital in tropical areas, such as Southern Thailand, where the monsoon's influence on cloud dynamics and seasonal shifts substantially affects solar irradiance. Accurate predictions empower operators to anticipate fluctuations in power generation, thereby facilitating proactive strategies, such as activating backup generators or adjusting battery charging and discharging protocols. Consequently, the strong efficacy demonstrated by ensemble machine learning methods highlights their applicability in automated energy management systems, thereby optimizing the utilization of renewable energy sources, diminishing dependence on fossil-fuel-based backup systems, and enhancing overall system functionality. In accordance with this premise, the research outcomes provide substantial support for the advancement of advanced solar energy management systems, specifically designed to promote extensive renewable integration within tropical environments [37].

4. Conclusions

This study developed and evaluated multiple forecasting models for predicting hourly solar irradiance using data collected from a photovoltaic monitoring station at Thaksin University, Thailand. The research compared six forecasting approaches, namely SARIMA, Prophet, LSTM, GRU, XGBoost, and Random Forest, against two benchmark models (Naive and SNaive). The results showed that ensemble machine learning models performed best, with XGBoost achieving the highest overall accuracy (RMSE = 79.43 W/m², MAE = 59.63 W/m², and MAPE = 30.07%), followed by Random Forest. In contrast, the statistical and deep learning models showed lower predictive performance under the conditions of this dataset. These findings indicate that ensemble methods are highly effective for short-term solar irradiance forecasting in tropical environments and can support more reliable solar energy management. These findings align with previous research in similar climatic regions. A study conducted in Rajasthan, India (another tropical region with high solar potential) found that Random Forest achieved the best performance with an average error below 20%, outperforming linear regression by 19.47%. This consistency across different tropical locations suggests that ensemble methods are particularly well-suited for solar irradiance forecasting in regions with complex meteorological dynamics and strong seasonal variations. Future work should evaluate hybrid models and longer, multi-year datasets to improve generalizability and forecasting robustness further.

5. Acknowledgments

We would like to sincerely thank Thaksin University's Faculty of Engineering for providing important facilities, necessary equipment, and useful data that made this research much easier to complete. Additionally, we would like to express our gratitude to Thaksin University for making academic resources accessible and for their outstanding assistance throughout this research.

Author Contributions: The simulation strategy and techniques were conceptualized and designed by M.S., S.A., T.S., and S.K. M.S. and S.K. implemented the simulation, collected the data, analyzed the results, and reached the conclusion. The authors M.S., S.A., T.S., W.S., and S.K. contributed to the writing and the general content modification.

Funding: This study was funded by the Researcher and Research for Industry Development Program (RRID), which is managed by the National Research Council of Thailand (NRCT), Ministry of Higher Education, Science, Research, and Innovation.

Conflicts of Interest: The study's authors hereby declare that they have no competing interests.

References

[1] Antonanzas, J.; Osorio, N.; Escobar, R.; Urraca, R.; Martinez-de-Pison, F. J.; Antonanzas-Torres, F. Review of photovoltaic power forecasting. *Sol. Energy* **2016**, *136*, 78–111. https://doi.org/10.1016/j.solener.2016.06.069

[2] Armstrong, B.; Collopy, F. Error measures for generalizing about forecasting methods. *Int. J. Forecast.* **1992**, *8* (1), 69–80. https://doi.org/10.1016/0169-2070(92)90008-W

[3] Hussain, D.; Hossain, S.; Talukder, J.; Mia, A.; Shamsuzzaman, H. M. Solar energy integration into smart grids: Challenges and opportunities. *Lett. High Energy Phys.* **2024**, *4*, 2313–2324

[4] Sammar, M. J.; Saeed, M. A.; Mohsin, S. M.; Akber, S. M.; Bukhsh, R.; Abazeed, M.; Ali, M. Illuminating the future: A comprehensive review of AI-based solar irradiance prediction models. *IEEE Access* **2024**, *12*, 114394–114415. https://doi.org/10.1109/ACCESS.2024.3402096

[5] Teixeira, R.; Cerveira, A.; Pires, E. J. S.; Baptista, J. Advancing renewable energy forecasting: A comprehensive review of renewable energy forecasting methods. *Energies* **2024**, *17*(14), 3480. https://doi.org/10.3390/en17143480

[6] Cho, K.; van Merriënboer, B.; Gulcehre, C.; Bahdanau, D.; Bougares, F.; Schwenk, H.; Bengio, Y. Learning phrase representations using RNN encoder–decoder for statistical machine translation. In *Proceedings of the 2014 Conference on Empirical Methods in Natural Language Processing (EMNLP)*; Association for Computational Linguistics: Doha, Qatar, 2014; pp 1724–1734. https://doi.org/10.3115/v1/D14-1179

[7] Crone, A.; Goel, S.; Billings, S. Forecasting with computational intelligence: An overview. In *Computational Intelligence in Forecasting*; Springer: Cham, Switzerland, 2020; pp 1–24.

[8] Diagne, M.; David, M.; Lauret, P.; Boland, J.; Schmutz, N. Review of solar irradiance forecasting methods and a proposition for small-scale insular grids. *Renew. Sustain. Energy Rev.* **2013**, *27*, 65–76. https://doi.org/10.1016/j.rser.2013.06.042

[9] Assaf, A. M.; Haron, H.; Abdull Hamed, H. N.; Ghaleb, F. A.; Qasem, S. N.; Albarrak, A. M. A review on neural network based models for short-term solar irradiance forecasting. *Appl. Sci.* **2023**, *13*(14), 8332. https://doi.org/10.3390/app13148332

[10] Friedman, J. H. Greedy function approximation: A gradient boosting machine. *Ann. Stat.* **2001**, *29*(5), 1189–1232. https://doi.org/10.1214/aos/1013203451

[11] Goodfellow, I.; Bengio, Y.; Courville, A. *Deep Learning*; MIT Press: Cambridge, MA, 2016.

[12] Hochreiter, S.; Schmidhuber, J. Long short-term memory. *Neural Comput.* **1997**, *9*(8), 1735–1780. https://doi.org/10.1162/neco.1997.9.8.1735

[13] Hyndman, R. J.; Athanasopoulos, G. *Forecasting: Principles and Practice*, 2nd ed.; OTexts: Melbourne, Australia, 2018.

[14] International Energy Agency (IEA). *Renewable Energy Market Update*; IEA: Paris, France, 2023.

[15] Kumari, P.; Toshniwal, D. Deep learning models for solar irradiance forecasting: A comprehensive review. *J. Clean. Prod.* **2021**, *318*, 128566. https://doi.org/10.1016/j.jclepro.2021.128566

[16] Hossain, M. A.; Rahman, M. M.; Hasan, S. S.; Mahmud, A.; Bai, L. Analysis and forecasting of meteorological drought using PROPHET and SARIMA models deploying machine learning technique for southwestern region of Bangladesh. *Environ. Sustain. Indic.* **2025**, *25*, 100761. https://doi.org/10.1016/j.indic.2025.100761

[17] Tsai, W. C.; Tu, C. S.; Hong, C. M.; Lin, W. M. A review of state-of-the-art and short-term forecasting models for solar PV power generation. *Energies* **2023**, *16* (14), 5436. https://doi.org/10.3390/en16145436

[18] Mellit, A.; Kalogirou, S. A. Artificial intelligence techniques for photovoltaic applications: A review. *Prog. Energy Combust. Sci.* **2008**, *34* (5), 574–632. https://doi.org/10.1016/j.pecs.2008.01.001

[19] Ministry of Energy, Department of Alternative Energy Development and Efficiency. *Thailand Solar Energy Potential Report*; Ministry of Energy: Bangkok, Thailand, 2022.

[20] Baloch, M.; Honnurvali, M. S.; Kabbani, A.; Ahmed, T.; Chauhdary, S. T.; Saeed, M. S. Solar energy forecasting framework using Prophet-based machine learning model: An opportunity to explore solar energy potential in Muscat, Oman. *Energies* **2025**, *18*(1), 205. https://doi.org/10.3390/en18010205

[21] Reikard, G. Predicting solar radiation at high resolutions: A comparison of time series forecasts. *Sol. Energy* **2009**, *83*(3), 342–349. https://doi.org/10.1016/j.solener.2008.08.007

[22] Raschka, S.; Liu, Y. H.; Mirjalili, V. *Machine Learning with PyTorch and Scikit-Learn: Develop Machine Learning and Deep Learning Models with Python*, 2nd ed.; Packt Publishing: Birmingham, U.K., 2022.

[23] Obando, E. D.; Carvajal, S. X.; Agudelo, J. P. Solar radiation prediction using machine learning techniques: A review. *IEEE Lat. Am. Trans.* **2019**, *17*(4), 684–697. https://doi.org/10.1109/TLA.2019.8891934

[24] Siami-Namini, H.; Tavakoli, N.; Namin, A. S. A comparison of ARIMA and LSTM in forecasting time series. In *Proceedings of the 17th IEEE International Conference on Machine Learning and Applications (ICMLA 2018)*; IEEE: Orlando, FL, USA, 2018; pp 1394–1401. https://doi.org/10.1109/ICMLA.2018.00227

[25] Chaves, R. R.; Oliveira, A. F.; Rubinger, R. M.; Silva, A. J. Recurrent neural networks (LSTM and GRU) in the prediction of current–voltage characteristics curves of polycrystalline solar cells. *Electronics* **2025**, *14*(17), 3342. https://doi.org/10.3390/electronics14173342

[26] Voyant, C.; Notton, G.; Kalogirou, S.; Nivet, M. L.; Paoli, C.; Motte, F.; Fouilloy, A. Machine learning methods for solar radiation forecasting: A review. *Renew. Energy* **2017**, *105*, 569–582. https://doi.org/10.1016/j.renene.2016.12.095

[27] Willmott, C. J.; Matsuura, K. Advantages of the mean absolute error (MAE) over the root mean square error (RMSE) in assessing average model performance. *Clim. Res.* **2005**, *30*(1), 79–82. https://doi.org/10.3354/cr030079

[28] Box, G. E. P.; Jenkins, G. M.; Reinsel, G. C.; Ljung, G. M. *Time Series Analysis: Forecasting and Control*, 5th ed.; John Wiley & Sons: Hoboken, NJ, 2015.

[29] Safari, M.; Nakharutai, N.; Awiphan, S. Beyond traditional models: Predicting cryptocurrency prices with SARIMA, RNNs, and hybrid SARIMA–RNNs. *J. Financ. Data Sci.* **2025**, *7*(3). https://doi.org/10.3905/jfds.2025.1.193

[30] Hyndman, R. J.; Athanasopoulos, G. *Forecasting: Principles and Practice*, 2nd ed.; OTexts: Melbourne, Australia, 2018.

[31] Safari, M.; Nakharutai, N.; Chiawkhun, P.; Phetpradap, P. DEA-RNNs: An ensemble approach for portfolio selection in the Thailand stock market. In *Proceedings of ECONVN2024*; Ho Chi Minh City, Vietnam, January 9–11, 2024; Springer Nature: Singapore, 2025. https://doi.org/10.1007/978-3-031-59110-5_30

[32] Taylor, S. J.; Letham, B. Forecasting at scale. *Am. Stat.* **2018**, *72*(1), 37–45. https://doi.org/10.1080/00031305.2017.1380080

[33] Breiman, L. Random forests. *Mach. Learn.* **2001**, *45*(1), 5–32. https://doi.org/10.1023/A:1010933404324

[34] Chen, T.; Guestrin, C. XGBoost: A scalable tree boosting system. In *Proceedings of the 22nd ACM SIGKDD International Conference on Knowledge Discovery and Data Mining (KDD '16)*; ACM: San Francisco, CA, USA, August 13–17, 2016; pp 785–794. https://doi.org/10.1145/2939672.2939785

[35] Tantanasiriwong, R.; Tantanasiriwong, S. The solar radiation climate of Thailand. *Sol. Energy* **1976**, *18*(1), 43–49. https://doi.org/10.1016/0038-092X(76)90062-1

[36] Wang, X.; Zhang, Y.; Tan, L. Solar radiation and daily light integral characteristics of photovoltaic-green roof system in tropical area: A case study in Singapore. *Sol. Energy* **2024**, *274*, 117–129. https://doi.org/10.1016/S0038-092X(24)00502-4

[37] Tandon, A.; Awasthi, A.; Pattnayak, K. C.; Tandon, A.; Choudhury, T.; Kotecha, K. Machine learning-driven solar irradiance prediction: Advancing renewable energy in Rajasthan. *Discover Appl. Sci.* **2025**, *7*(2), 107. https://doi.org/10.1007/s42452-025-06490-8

ASEAN
Journal of Scientific and Technological Reports
Online ISSN:2773-8752

Research article

Enhancing Oil Palm (*Elaeis guineensis* Jacq.) Growth Using Microbial Consortia: Roles of Phosphate Solubilization and Nitrogen Fixation

Korakot Nakkanong[1], Thanyakorn Rongsawat[2], Charassri Nualsri[1], Palakrit Jiwanit[1], Nurainee Salaemae[2], and Natthakorn Woraathasin[2*]

[1] Faculty of Natural Resources, Prince of Songkla University, Hat Yai Campus, Songkhla, 90110, Thailand
[2] Faculty of Science and Technology, Prince of Songkla University, Pattani, 94000, Thailand
* Correspondence: natthakorn.w@psu.ac.th

Citation:
Nakkanong, K.; Rongsawat, T.; Nualsri, C.; Jiwanit, P.; Salaemae, N.; Woraathasin, N. Enhancing oil palm (*Elaeis guineensis* Jacq.) growth using microbial consortia: roles of phosphated solubilization and nitrogen fixation. *ASEAN J. Sci. Tech. Report.* **2026**, *29*(7), e262347. https://doi.org/10.55164/ajstr.v29i7.262347

Article history:
Received: November 13, 2025
Revised: April 26, 2026
Accepted: April 30, 2026
Available online: June 14, 2026

Publisher's Note:
This article is published and distributed under the terms of the Thaksin University.

Abstract: In Thailand, oil palm is a vital economic crop, primarily cultivated in the southern region. Farmers are expanding plantations by establishing new sites and replanting previous crop areas. Proper maintenance from the seedling stage is essential for growth. Agriculturists place rock phosphate at the planting hole base to speed seedling recovery after transplantation. Converting rock phosphate into water-soluble phosphate, essential for root development and pre-planting, is a labor-intensive process dependent on microbial activity. The objective of this investigation is to identify microbes capable of converting insoluble phosphate into a soluble form in water. Furthermore, oil palm seedlings require a significant amount of nitrogen. Therefore, nitrogen-fixing microorganisms are also screened. Several phosphate-soluble microorganisms have been identified, especially the NN311 strain, which is the most effective at releasing water-soluble phosphate, both qualitatively and quantitatively. For nitrogen fixation, strain NT7 performed best. NN311 was classified as *Pseudomonas* sp., whereas NT7 was classified as *Bacillus* sp., according to nucleic acid sequence analysis in comparison to the NCBI database. In the absence of antagonistic interactions between NN311 and NT7, they were assessed simultaneously in nursery research. The results indicated that the application of these microorganisms, individually or in combination, markedly enhanced seedling growth compared to the control group. Nonetheless, combining them yields optimal outcomes. The combination of NN311 and NT7 with rock phosphate in the planting hole enhances seedling growth post-transplantation. After 18 months, seedlings treated with both strains of bacteria exhibit much superior growth compared to those that do not receive microorganisms.

Keywords: Oil palm seedling; plant growth promotion; phosphorus releasing; nitrogen fixation

1. Introduction

The oil palm (*Elaeis guineensis* Jacq.) is a crop of significant economic value that has received government backing to incentivize farmers to increase its cultivation in response to the energy crisis in Thailand and globally.

Moreover, oil palm products can be used in many consumer and industrial products, making it a crucial crop for the nation in line with national strategies outlined in the Oil Palm Industry Development Plan. Furthermore, Thailand's tropical environment is well-suited to oil palm cultivation, giving it a competitive edge over alternative oil-producing crops. Southern Thailand hosts the majority of oil palm farms, covering 0.86 million ha out of a total of 1 million ha [1]. Despite government subsidies, domestic oil palm production falls short of meeting demand, and we anticipate rising demand for palm oil products in the future. Agricultural producers face difficulties, including price fluctuations, rising production costs, and climate change, which lead to income instability. To augment oil palm output, two primary strategies can be employed: expanding cultivation areas and enhancing yield per unit area. Cultivating high-yielding cultivars with elevated oil content can enhance yield per unit area. Fertilization is crucial, and chemical fertilizers are predominantly preferred. Prolonged application of chemical fertilizers results in environmental degradation, diminishes soil fertility, reduces beneficial microbes and soil-dwelling creatures, and disrupts ecological equilibrium. It also escalates production expenses. To alleviate these challenges and decrease expenses, the utilization of plant growth-promoting microorganisms offers a viable solution. Farmers can economically produce microbial inoculants, offering a sustainable approach to increasing oil palm yield while minimizing environmental impact.

Plant Growth-Promoting Rhizobacteria (PGPRs) are increasingly employed in contemporary agriculture owing to their capacity to stimulate plant growth through direct and indirect mechanisms. These advantageous root-colonizing bacteria enhance plant growth by fixing atmospheric nitrogen, solubilizing vital nutrients such as phosphorus and potassium, and synthesizing siderophores that augment iron availability. Furthermore, PGPRs excrete phytohormones that promote cell division and elongation in roots, shoots, and leaves, and accelerate seed germination, flowering, and fruiting [2]. They indirectly inhibit plant pathogens by competitive exclusion and stimulate systemic resistance in plants. Prevalent genera of PGPRs encompass *Pseudomonas*, *Bacillus*, *Enterobacter*, and *Erwinia* [3]. The PGPRs isolated from the oil palm rhizosphere have exhibited considerable growth-promoting properties, including nitrogen fixation, enhanced nutrient uptake, and improved root and shoot development [4, 5]. The PGPRs have demonstrated encouraging results in enhancing yields of several crops, such as peanuts, canola, safflower, and rapeseed, underscoring their potential for sustainable agricultural use [6, 7, 8, 9].

This research investigates the impact of microbial inoculation on the physical and biological alterations during the initial growth phase of oil palm seedlings. Despite increasing interest in beneficial microorganisms in agriculture, a substantial information gap persists regarding the application of microbial consortia, particularly in oil palm cultivation during the nursery stage, where such methods are either restricted or not yet implemented. Therefore, this study addresses these unresolved questions by: (1) evaluating the impact of selected PGPR strains on the physical and biological growth parameters of oil palm seedlings during the nursery stage; (2) identifying microbial strains or consortia that most effectively enhance germination, root development, shoot elongation, and seedling vigor in oil palm; and (3) giving insight into the potential of PGPRs as a sustainable alternative to chemical fertilizers in oil palm nurseries. The results will aid the development of more effective and sustainable cultivation methods for oil palm seedlings, potentially reducing dependence on chemical inputs while enhancing seedling quality and uniformity. This study is especially important given the rising global demand for palm oil and the need for more sustainable agricultural practices.

2. Materials and Methods

2.1 Oil Palm Seedling Preparation

The experiment used oil palm seeds of the Tenera hybrid variety, obtained from the Suratthani Oil Palm Research Center, Department of Agriculture, Thailand. The seeds were surface sterilized before germination by being washed with 70% ethanol, submerged in 5% sodium hypochlorite for 10 min, and then rinsed with sterile distilled water. The sterilized seeds were kept at 30°C for 60 days to facilitate germination. After this period, germinating seedlings were sprayed with sterile distilled water and kept at 30°C for an

additional 7 days. Seeds with root lengths of 2.0–2.5 cm and shoot lengths of 1.0–1.5 cm [10] were selected and transplanted into 6 × 12-inch polyethylene bags containing 0.5 L of sterile peat moss.

2.2 Screening of PGPRs

Soil samples were collected from the rhizosphere of oil palms across eight different zones in Hat Yai District, Songkhla Province, Thailand. From each sample, 20 g of soil was placed in a 50 mL Erlenmeyer flask and vigorously shaken with 30 mL of sterile saline solution (0.85% NaCl) for 2 min. After shaking, the mixture was allowed to settle for one hour. The supernatant was then carefully decanted, while the sediment was discarded [11]. The resulting eluent was serially diluted 10-fold before being spread onto selective media for phosphate-solubilizing and nitrogen-fixing bacteria.

2.2.1 Phosphate Solubilization Capacity

Pikovskaya's agar plates (15 cm in diameter) were covered with a 100 µL aliquot of the diluted sample. Each liter of Pikovskia's agar medium comprises 0.5 g $(NH_4)_2SO_4$, 0.2 g NaCl, 0.1 g $MgSO_4 \cdot 7H_2O$, 0.002 g $MnSO_4$, 0.002 g $FeSO_4 \cdot 7H_2O$, 0.2 g KCl, 0.5 g yeast extract, 10 g glucose, 5 g $Ca_3(PO_4)_2$, and 15 g agar with a pH adjusted to 7.0 ± 0.02. Bacterial colonies with clear zones showing phosphate dissolution can be transferred using aseptic loops into a 100 ml Erlenmeyer with 50 ml of NB media. The cultures were grown at 30°C with continuous agitation at 200 rpm for 24 h. Centrifugation was then used for 20 min at 8,000 rpm to obtain the bacterial cells. The pellet was rinsed twice with sterile distilled water and resuspended in sterile saline (0.85% NaCl) to achieve a turbidity corresponding to the 0.5 McFarland standard. One milliliter of the bacterial suspension was then added to 100 mL of Pikovskaya's broth, and the mixture was agitated (at 200 rpm) for 7 days at 30°C. After incubation, the culture was centrifuged (8,000 rpm, 20 min), and the supernatant was collected for quantification of soluble phosphate using KH_2PO_4 as the standard [12].

2.2.2 Nitrogen Fixation Capacity

A 100 µL diluted sample was applied to nitrogen-free agar medium. The inoculation plates were then incubated for 7 days at 37°C. Bacterial colonies that developed on the nitrogen-free medium were aseptically inoculated into 50 mL of nutrient broth using a sterile loop. All broths were subsequently incubated at 37°C with continuous agitation at 200 rpm for 24 hours. The bacterial cells were collected by centrifugation at 8,000 rpm for 20 min, rinsed twice with sterile distilled water, and then resuspended in sterile saline solution to achieve a turbidity matching the 0.5 McFarland standard. One mL of the bacterial suspension was introduced into 100 mL of nitrogen-free bromothymol blue medium [13] and cultured at 30°C with shaking at 200 rpm for 7 days. After incubation, the culture was centrifuged at 8,000 rpm for 20 min, and the supernatant was collected for total nitrogen analysis by the Kjeldahl method [14].

2.3 PGPRs identification

This study focused on identifying microbial strains that possess superior phosphate-solubilizing and nitrogen-fixing abilities. DNA was extracted from the microorganisms [15], and the 16S rRNA gene fragment was amplified by PCR using universal eubacterial primers (fD1 and rD1). The amplification approach consisted of an initial denaturation at 94°C for 1 min, followed by annealing at 55°C for 1 min, and extension at 72°C for 1 min, repeated for 30 cycles, terminating with a final extension at 72°C for 1 min [16]. The amplified 16S rRNA gene region was subsequently ligated into the pGEM-T easy vector for sequencing applications. The resulting nucleotide sequences were aligned with data in the NCBI database [17] to identify the microbial type precisely.

2.4 Microbial Compatibility Assessment

The compatibility of phosphate-solubilizing and nitrogen-fixing strains was evaluated using a modified cross-streak assay [18]. Nutrient agar plates (15 cm in diameter) were inoculated with 100 µL of strain 1 (adjusted to 10^3 CFU mL^{-1}) and evenly distributed to get isolated colonies. A sterile filter paper strip (0.5 × 12 cm, Whatman No. 1) was aseptically placed on the inoculated medium, followed by the addition of 500 µL of strain 2 suspension (10^3 CFU mL^{-1}) along the strip. Plates were incubated aerobically for 18 h at 37 ± 0.5°C. The inhibition zones at the interface between Strains 1 and 2 were examined to assess antagonism. Three biological replicates were performed for each strain combination.

2.5 Effect of PGPRs on oil palm seedlings in the nursery

The selected rhizobacteria that fix nitrogen and solubilize phosphate were cultivated in 100 mL of nutrient broth at 30°C while being continuously shaken at 200 rpm for 24 h. The bacterial cells were obtained by centrifugation (8,000 rpm, 20 min), rinsed twice with sterile distilled water, and then resuspended in PBS buffer (10 mM NaH_2PO_4 in 0.85% NaCl, pH 6.5) to reach a McFarland-standard concentration of 10^9 CFU mL^{-1}. Oil palm seedlings were divided into four treatment groups: (1) bacteria that fix nitrogen, (2) bacteria that solubilize phosphate, (3) bacteria that fix nitrogen and solubilize phosphate, and (4) control (sterile distilled water). Two experimental runs, three replicates per treatment, and ten seedlings per replication were used in the investigation, which was conducted in the greenhouse at the Faculty of Natural Resources, Prince of Songkla University in Thailand, using a randomized complete block design (RCBD). Physical growth factors and levels of carotenoids and chlorophyll were monitored over the 5 months during which treatments were given monthly. At 5 months of age, seedlings underwent destructive analysis to measure: (1) biomass parameters: fresh weight (total, stem, root), dry weight (total, stem, root), and (2) morphological parameters: leaf length, total leaf number, root area, leaf area, and root: shoot ratio. The second leaf from the shoot apex was collected, flash-frozen in liquid nitrogen, and ground to a fine powder for pigment analysis. Exactly 0.2 g of leaf powder was extracted with 20 mL of 90% acetone in darkness [19]. Chlorophyll and carotenoid contents were determined spectrophotometrically at 663 nm, 647 nm, and 480 nm and calculated using the following equations:

$$\text{Chlorophyll a } (\mu g\ cm^{-2}) = [(12.64 \times A_{664} - 2.99 \times A_{647}) \times V]/(LA \times 100)$$

$$\text{Chlorophyll b } (\mu g\ cm^{-2}) = [(23.26 \times A_{647} - 5.06 \times A_{664}) \times V]/(LA \times 100)$$

$$\text{Total chlorophyll } (\mu g\ cm^{-2}) = [(20.27 \times A_{647} + 7.04 \times A_{664}) \times V]/(LA \times 100)$$

$$\text{Carotenoids } (\mu g\ cm^{-2}) = [(1000 \times A_{480} - 1.12 \times \text{Chl a} - 34.07 \times \text{Chl b})/245 \times V]/(LA \times 100)$$

Where:

A = Absorbance at specified wavelength

V = Solvent volume (mL)

LA = Leaf area (cm^2)

Chl a = Chlorophyll a

Chl b = Chlorophyll b

2.6 Effect of PGPR on oil palm in the field

The field experiment utilized 14-month-old Deli × Ghana oil palm seedlings transplanted into clay soil (pH < 4.5, Total N < 100 ppm, Available P < 5 ppm, and organic matter 1%) in a 4.8 ha plantation in Ko Nang Kham Subdistrict, Phatthalung Province, Thailand (7.285094°N, 100.410708°E). The experiment used two co-selected microbial species known for their enhanced phosphorus solubility and nitrogen-fixation capabilities. Before planting the oil palm seedlings, prepare the base of each hole by mixing 500 mL of each microbial suspension (10^9 CFU mL-1) with 500 g of phosphate rock (0-3-0, P_2O_5 available = 3%) and 5 L of dehydrated cow manure. An RCBD experiment was conducted with four replications, each containing five seedlings. Control plots were included and received the same amendments, but did not receive microbial inoculation. Evaluate the growth performance by measuring plant height 18 months after cultivation to assess the effectiveness of microbial application on seedling formation and development in real growing conditions.

2.7 Statistical analysis

All experimental data were analyzed using one-way analysis of variance (ANOVA). When significant differences were detected, means were compared using Tukey's honest significant difference (HSD) post-hoc test. Results are presented as mean values ± standard error of the mean (SE) with three biological replicates (n = 3). A probability level of $p \leq 0.05$ was considered statistically significant for all analyses.

3. Results and Discussion

3.1 Microbial Selection

3.1.1 Screening for Phosphate-Solubilizing Microorganisms

The ability to transform insoluble phosphate into a water-soluble form is a key criterion for selecting microorganisms that promote plant growth. An examination of dishes using Pikovskaya's agar, which contains solid nutrients, reveals a milky-white color due to insoluble phosphate in the medium. Microorganisms were collected from various soil sources associated with plant roots. They were cultivated on Pikovskaya's agar at 30 ± 5°C for 7 days. Their presence was indicated by distinct, clear zones around the colonies, as shown in Figure 1; however, most of these zones were small, suggesting limited phosphate solubilization capacity. A few isolated microbial colonies exhibited substantial clear zones, suggesting their exceptional ability to convert phosphate into a water-soluble form. The microorganisms initially selected displayed phosphate solubilization efficiency values outlined in Table 1. Their ability to quantitatively convert phosphate into a water-soluble form was evaluated against a standard graph of KH_2PO_4, as shown in Table 2. Colonies that strongly converted phosphate to its soluble form also showed higher quantitative values.

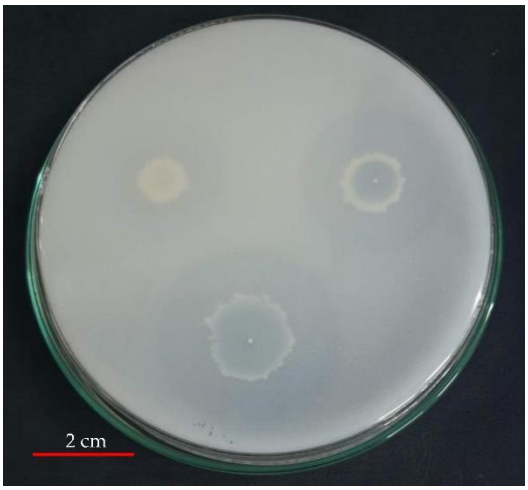


Figure 1. Microbial colonies exhibiting phosphate-solubilizing activity on Pikovskaya's agar medium, demonstrated by clear halo zones surrounding colonies.

Table 1. Qualitative assessment of phosphate solubilization efficiency by microbial isolates, as indicated by clear zone formation on Pikovskaya's agar medium

Microbial isolate	Phosphate Solubilization Efficiency (PSE)
D122	2.53 ± 0.15b
BS	2.23 ± 0.12a
D321	2.00 ± 0.00a
NN321	2.28 ± 0.11ab
D111	2.32 ± 0.19ab
NN322	2.42 ± 0.04b
NN311	3.37 ± 0.19c

The table presents calculated PSE ratios from the measured clear zone diameters for each microbial strain, demonstrating their relative phosphate-solubilizing capabilities. Data represent mean ± SE. Means followed by the same lowercase letter do not differ significantly (Tukey's HSD test, $p \leq 0.05$).

Table 2. Quantitative analysis of phosphate solubilization capacity by selected microbial isolates

Microbial isolate	Total soluble phosphate (μg mL^{-1})
D122	0.60 ± 0.07b
BS	0.31 ± 0.00a
D321	0.54 ± 0.02b
NN321	0.84 ± 0.03c
D111	0.33 ± 0.00a
NN322	0.30 ± 0.00a
NN311	1.77 ± 00.05d

The table presents solubilized phosphate concentrations measured spectrophotometrically against a KH_2PO_4 standard curve. Data represent mean ± SE. Means followed by the same lowercase letter do not differ significantly (Tukey's HSD test, $p \leq 0.05$).

3.1.2 Screening for Nitrogen-Fixing Microorganisms

The nitrogen-fixing capacity of microbial isolates was evaluated using the Kjeldahl method. Among the tested isolates, 66.67% demonstrated nitrogen-fixing activity, with strain NT7 exhibiting the highest nitrogen fixation rate, fixing 1.1204 mg L^{-1} of nitrogen. Other notable isolates included: PSB1 (0.8870 mg L^{-1}), NT4 (0.8403 mg L^{-1}), PSB2 (0.7469 mg L^{-1}), BS (0.4668 mg L^{-1}), and NT3 (0.4202 mg L^{-1}). These quantitative results, summarized in Table 3, highlight NT7 as the most efficient nitrogen-fixing strain, suggesting strong potential to enhance nitrogen availability in agricultural systems.

Table 3. Nitrogen fixation capacity of isolated microbial strains quantified using the Kjeldahl method

Microbial isolate	Total N (mg L^{-1})
control	ND
NT3	0.4202 ± 0.0154a
NT4	0.8403 ± 0.0755b
NT7	1.1204 ± 0.0461c
NT8	ND
BS	0.4668 ± 0.0034a
PSB1	0.8870 ± 0.1084b
PSB2	0.7469 ± 0.0649b
NN311	ND
NN411	ND

Data represent mean ± SE. Means followed by the same lowercase letter do not differ significantly (Tukey's HSD test, $p \leq 0.05$). ND = Not Detected

3.2 Microbial Strain Identification

Upon selecting the most proficient phosphate-solubilizing and nitrogen-fixing isolates, microbial strain identification was conducted to confirm their genus. DNA extraction and PCR amplification of the 16S rRNA gene (~1,500 bp) employing universal primers (fD1/rD1) produced distinct fragments, which were then sequenced and analyzed using BLAST against the NCBI database. The phosphate-solubilizing isolate NN311 demonstrated significant sequence similarity to *Pseudomonas* sp., a genus extensively recognized for its capacity to solubilize inorganic phosphorus via organic acid secretion [20-22]. Simultaneously, the nitrogen-fixing isolate NT7 exhibited a strong association with *Bacillus* sp., a genus known for its capacity to function as a diazotroph in soil ecosystems. The molecular identifications validate the taxonomic classification of the strains and correspond with their presumed functions in nutrient cycling, as *Pseudomonas* and *Bacillus* species are often associated with improving soil fertility through phosphorus mobilization and atmospheric nitrogen fixation, respectively [23, 24, 25, 26]. The amalgamation of molecular and functional data underlines the promise of these isolates as bioinoculants for sustainable agriculture, especially in nutrient-deficient soils.

3.3 Microbial compatibility test

The cross-streak compatibility assay revealed the absence of antagonistic interactions between the nitrogen-fixing *Bacillus* sp. (NT7) and the phosphate-solubilizing *Pseudomonas* sp. (NN311), as shown by the absence of inhibition zones (Figuer 2). The compatibility of these organisms is crucial for their potential combined application in agricultural systems, as microbial antagonism may diminish the efficacy of bioinoculants in agriculture. The observed coexistence indicates that these strains may engage in synergistic interactions rather than competitive exclusion, a characteristic that is advantageous for the formation of microbial consortia that provide various plant growth-promoting functions [27].

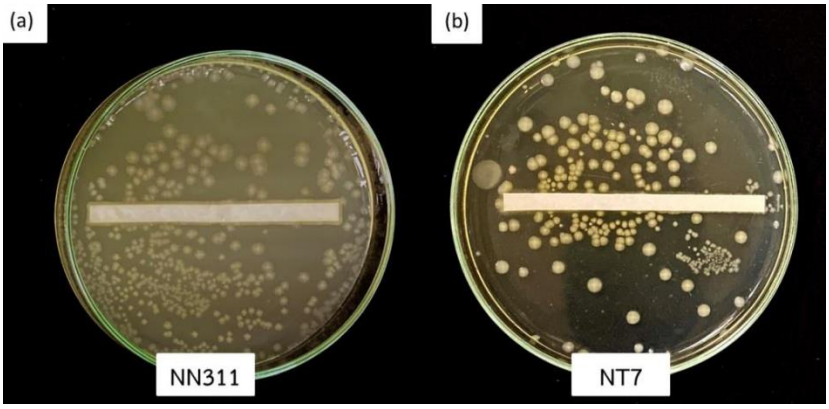


Figure 2. Microbial antagonism assay between the two selected isolates. The absence of inhibition zones confirms a non-antagonistic interaction. (a) Inhibition test of isolate NT7 against NN311 on paper strip, (b) Inhibition test of isolate NN311 against NT7 on paper strip

The absence of inhibitory effects between NT7 and NN311 suggests that their metabolic activities do not impede each other, potentially owing to niche differentiation or complementary resource utilization [28]. This compatibility is particularly advantageous in rhizosphere environments, where microbial cooperation can improve nutrient availability, such as through nitrogen fixation by *Bacillus* and phosphate solubilization by *Pseudomonas*, without causing cross-inhibition [29]. The lack of antagonism enhances their potential for use in biofertilizer formulations, as microbial synergy can more effectively enhance plant performance than single-strain inoculants [30].

3.4 Influence of Microorganisms on Oil Palm Growth

3.4.1 Physical Growth

The study used pre-germinated oil palm seeds with emerging shoots (1.0-1.5 cm) and roots (2.0-2.5 cm) to evaluate the effects of microbes on growth promotion. Seedlings received weekly microbial treatments for 5 months before physical growth parameters were measured, including fresh/dry weights (whole plant, shoot, root), leaf length, and leaf count. The results, although derived from different functional mechanisms, indicated that *Bacillus* sp. NT7, a nitrogen fixer, and *Pseudomonas* sp. NN311, a phosphate solubilizer, significantly enhances the growth of oil palm seedlings (Figure. 3, Table 4). The notable increase in root biomass (5.84 g vs. 5.01 g in NT7) was likely due to organic acids facilitating phosphorus mobilization, which in turn encourages root growth [31]. Conversely, NT7 enhanced leaf elongation (38.43 cm vs. 36.45 cm in NN311), which is consistent with its function in the assimilation of nitrogen for the development of shoots [32]. This functional complementarity demonstrates the benefits of consortia-based biofertilizers, as the simultaneous supply of phosphorus and nitrogen can mitigate single-nutrient deficiencies in tropical soils [33]. The discovery demonstrated the functional complementarity between nitrogen-fixing and phosphate-solubilizing microorganisms, indicating that their combined application provides greater growth benefits than inoculations of individual strains. The results suggested that using microbial consortia could be an effective biofertilizer strategy for oil palm cultivation.



Figure 3. Physical growth characteristics of oil palm seedlings under different treatments: (a) Control (untreated) seedlings, (b) Seedlings inoculated with NT7, (c) Seedlings inoculated with NN311, and (d) Seedlings co-inoculated with NN311+NT7.

3.4.2 Chlorophyll and Carotenoid Content

Chlorophyll is a crucial component of plant photosynthesis, working synergistically with carotenoids. Carotenoids absorb light for photosynthesis and shield chlorophyll from photodamage in high-light conditions [34], while chlorophyll transforms light energy into chemical energy to synthesize organic compounds, especially sugars, which act as precursors for numerous other organic molecules [35]. The molecular structure of chlorophyll includes nitrogen, enabling sufficient nitrogen availability, which is crucial for optimal plant growth [36]. After 5 months of growth, the levels of carotenoids and chlorophyll in the leaves were assessed to evaluate the effects of plant growth-promoting microorganisms on oil palm seedlings. The increased levels of chlorophyll and carotenoids in microbially treated oil palm seedlings highlighted the essential role of plant growth-promoting microorganisms in photosynthetic efficiency. The findings indicated that seedlings exposed to growth-promoting microorganisms showed markedly elevated leaf chlorophyll and carotenoid concentrations compared with the control group (Table 5). Significantly, the application of NT7, whether used independently or in conjunction with NN311, resulted in higher pigment concentrations than NN311 treatment alone. The study indicated that nitrogen-fixing microorganisms (NT7) significantly enhance photosynthetic pigment production, mainly by increasing nitrogen availability for chlorophyll synthesis. The enhanced efficacy of the NT7+NN311 treatment suggested a possible synergistic interaction between nitrogen fixation and phosphate solubilization, thereby improving photosynthetic efficiency and photoprotective mechanisms in oil palm seedlings. This physiological enhancement is associated with observed improvements in plant growth metrics, underscoring the significance of microbial-mediated nutrient acquisition for optimal plant development. Enhancing biofertilizer formulations for oil palm cultivation requires a thorough understanding of the specific effects of both individual and combinatorial microbial treatments.

Table 4. Physical growth parameters of oil palm seedlings under different microbial treatments

Treatment	gross weight (g)	stem weight (g)	root weight (g)	root shoot ratio (wet)	leaf length (cm)	total leave	gross dry weight (g)	stem dry weight (g)	root dry weight (g)	root shoot ratio (dry)
Control	12.4±1.0a	7.2±0.7a	2.5±0.1a	0.36±0.02a	33.9±2.4a	5.2±0.2a	2.8±0.2a	1.9±0.2a	0.88±0.04a	0.46±0.02b
NN311	23.7±3.4c	13.6±1.7b	5.8±1.0b	0.42±0.03b	36.4±2.9b	6.0±0.0b	5.3±0.8c	3.4±0.3c	1.89±0.47c	0.54±0.78c
NT7	21.5±0.8b	12.1±0.4b	5.0±0.2b	0.41±0.02b	38.4±1.4bc	5.5±0.03a	4.3±0.1b	2.9±0.1b	1.41±0.04b	0.48±0.04b
NN311+ NT7	24.0±0.8c	15.0±0.5c	5.4±0.6b	0.36±0.04a	41.8±1.0c	6.0±0.0b	5.0±0.3c	3.7±0.2c	1.37±0.13b	0.37±0.03a

Data represent mean ± SE. Means followed by the same lowercase letter do not differ significantly (Tukey's HSD test, $p \leq 0.05$).

Table 5. Chlorophyll and carotenoid content in oil palm (*E. guineensis* Jacq.) seedling leaves

Treatment	Chlorophyll a (μg cm^{-2})	Chlorophyll b (μg cm^{-2})	Total Chlorophyll (μg cm^{-2})	Carotenoid (μg cm^{-2})
Control	0.22 ± 0.01a	0.09 ± 0.00a	0.30 ± 0.01a	0.06 ± 0.00a
NN311	0.31 ± 0.00b	0.13 ± 0.00b	0.42 ± 0.01b	0.09 ± 0.00b
NT7	0.36 ± 0.02c	0.16 ± 0.01c	0.50 ± 0.03c	0.10 ± 0.01b
NN311+ NT7	0.40 ± 0.00c	0.18 ± 0.00c	0.55 ± 0.01c	0.12 ± 0.00c

Data represent mean ± SE. Means followed by the same lowercase letter do not differ significantly (Tukey's HSD test, $p \leq 0.05$).

3.4.3 Effects of Microorganisms on Oil Palm Growth After Field Transplantation

The field study revealed that the co-inoculation of *Pseudomonas* sp. NN311 and *Bacillus* sp. NT7 markedly enhanced oil palm establishment in clay soils. Treated seedlings exhibited a height increase of 70.9% (3.1 m compared to 1.8 m) and displayed enhanced stem morphology in comparison to the control group (Table 6, Figure 4 and 5). This growth enhancement resulted from synergistic nutrient cycling: NN311's organic acid-mediated phosphate solubilization augmented rock phosphate availability (from 500 g applications), while NT7's nitrogen fixation mitigated the typically low nitrogen retention in clay soils [37]. The 4.8 ha scale results validate laboratory findings and address a significant agricultural issue: clay soils impede root growth and nutrient absorption [38]. The treatment's efficacy (about 2 years of normal growth in 18 months) suggested the possibility of reducing the unproductive juvenile phase in oil palm farming, which often lasts 3-4 years [39]. The enduring effects suggested the ecological resilience of introduced strains, possibly via biofilm formation in the manure-amended rhizosphere [40]. This research provides empirical evidence that microbial consortia can serve as a sustainable alternative to chemical fertilizers in perennial crop systems, especially in clay soils.



Figure 4. Oil palm growth performance 18 months after field transplantation with microbial-augmented planting material.



Figure 5. Oil palm growth performance 18 months after field transplantation without microbial-augmented planting material.

Table 6. Oil palm growth performance 18 months after field transplantation with and without microbial-augmented planting material

Treatment	Height (m)	Stem girth (cm)	Number of fronds
Control	1.8 ± 0.2a	38.2 ± 0.02a	13.8 ± 1.0a
NN311+ NT7	3.1 ± 0.3b	66.7 ± 0.02b	33.8 ± 1.0b

Data represent mean ± SE. Means (same column) followed by the same lowercase letter do not differ significantly (ANOVA, $p \leq 0.05$).

4. Conclusions

This research isolated and characterized two efficacious microbial strains for oil palm cultivation: NN311 (*Pseudomonas* sp.), distinguished by its phosphate-solubilizing properties, and NT7 (*Bacillus* sp.), acknowledged for its nitrogen-fixing capabilities. Among the microbial colonies analyzed, NN311 and NT7 demonstrated the most substantial performance in both qualitative and quantitative assessments. These strains demonstrated no antagonistic effects when co-inoculated, enabling their combined application. Field tests demonstrated that both individual and combined applications of NN311 and NT7 significantly enhanced oil palm seedling growth compared to the control group, with the combined treatment yielding the most favorable results. After 18 months, the inoculated seedlings exhibited significantly superior growth compared to the untreated seedlings when these microorganisms were applied in agricultural fields alongside rock phosphate-enriched planting material. This research demonstrates that the simultaneous application of phosphate-solubilizing (*Pseudomonas* sp.) and nitrogen-fixing (*Bacillus* sp.) microorganisms constitutes an effective biological approach for improving the establishment and growth of oil palm seedlings. This microbial consortium offers a sustainable method to enhance nutrient availability and reduce dependence on chemical fertilizers in oil palm cultivation.

5. Acknowledgments

This work was supported by the Faculty of Science and Technology Research Fund, Prince of Songkla University, Pattani Campus, contract No. SAT6104054S and the Program Management Unit on Area-Based Development (PMU A).

Author Contributions: conceptualization, methodology, and validation, Korakot Nakkanong; visualization, Thanyakorn Rongsawat; resources and data curation, Charassri Nualsri; methodology and formal analysis, Palakrit Jiwanit; visualization, Nurainee Salaemae; supervision, conceptualization, writing—original draft—review, and editing, Natthakorn Woraathasin

Funding: This research was funded by the Faculty of Science and Technology Research Fund, Prince of Songkla University, Pattani Campus, contract No. SAT6104054S and the Program Management Unit on Area-Based Development (PMU A).

Conflicts of Interest: The authors declare no conflict of interest.

Declarations: The authors used AI-assisted technologies solely to paraphrase selected sentences to improve clarity and flow. All scientific content, data interpretation, and conclusions are the original work of the authors.

References

[1] Office of Agricultural Economics. *Thailand Agricultural Production Index*. https://www.ceicdata.com/en/thailand/agricultural-production-index-office-of-agricultural-economics (accessed Dec 12, 2024).

[2] Wulandari, D.; Baskoro, K.; Mahmuudah, Y.; Kusmiyati, F.; Pratiwi, A. R.; Budiharjo, A. Bioprospecting of Rhizobia as Plant Growth Promoting Rhizobacteria Potential from Root Nodules of Groundnut (*Arachis hypogaea* L.). *Trends Sci*. **2024**, 7651–7651. https://doi.org/10.48048/tis.2024.7651

[3] Danesh, Y. R.; Pellegrini, M.; Akköprü, A.; Farda, B.; Boyno, G.; Djebaili, R. Plant Growth–Promoting Rhizobacteria: Their Potential as Biological Control Agents in Sustainable Agriculture. *Sustainable Agricultural Practices* **2024**, pp. 145–159. https://doi.org/10.1016/B978-0-443-19150-3.00015-1

[4] Oktari, I.; Mustamu, N. E.; Walida, H. Ultisols Fertility and Morphological Characteristics of N-Fixing Bacteria from Oil Palm Rhizosphere. *Pesqui. Agropecu. Trop.* **2021**, 51, e68559. https://doi.org/10.1590/1983-40632021v5168559

[5] Hidayat, F.; Pane, R. D. P.; Sapalina, F.; Listia, E.; Lubis, M. E. S.; Oshiro, M.; Sakai, K.; Tashiro, Y. Novel Multifunctional Plant Growth-Promoting Bacteria Isolated from the Oil Palm Rhizosphere under Long-Term Organic Matter Application. *J. Biosci. Bioeng.* **2024**, 138, 406–414. https://doi.org/10.1016/j.jbiosc.2024.07.008

[6] Van Chuong, N. Effect of Three Different Nitrogen Rates and Three Rhizosphere N2-Fixing Bacteria on Growth, Yield and Quality of Peanuts. *Trends Sci.* ***2024***, 21, 7281–7281. https://doi.org/10.48048/tis.2024.7281

[7] de Aquino, G. S.; Shahab, M.; Moraes, L. A.; Moreira, A. Plant Growth Promoting Rhizobacteria Increased Canola Yield and Root System. *J. Plant Nutr.* **2023**, 46, 1400–1406. https://doi.org/10.1080/01904167.2022.2068441

[8] Nosheen, A.; Yasmin, H.; Naz, R.; Keyani, R.; Mumtaz, S.; Hussain, S. B.; Hassan, M. N.; Alzahrani, O. M.; Noureldeen, A.; Darwish, H. Phosphate Solubilizing Bacteria Enhanced Growth, Oil Yield, Antioxidant Properties and Biodiesel Quality of Kasumbha. *Saudi J. Biol. Sci.* **2022**, 35, 1574–1581. https://doi.org/10.1016/j.sjbs.2021.09.068

[9] Farhat, F.; Tariq, A.; Waseem, M.; Masood, A.; Raja, S.; Ajmal, W.; Iftikhar, I.; Zulfiqar, U.; Maqsood, M. F. Plant Growth Promoting Rhizobacteria (PGPR) Induced Improvements in the Growth, Photosynthesis, Antioxidants, and Nutrient Uptake of Rapeseed (*Brassica napus* L.). *Gesunde Pflanzen* **2023**, 75, 2075–2088. https://doi.org/10.1007/s10343-023-00845-0

[10] Azri, M. H.; Ismail, S.; Abdullah, R. An Endophytic *Bacillus* Strain Promotes Growth of Oil Palm Seedling by Fine Root Biofilm Formation. *Rhizosphere* **2018**, 5, 1–7. https://doi.org/10.1016/j.rhisph.2017.10.003

[11] Son, J. S.; Sumayo, M.; Hwang, Y. J.; Kim, B. S.; Ghim, S. Y. Screening of Plant Growth-Promoting Rhizobacteria as Elicitor of Systemic Resistance against Gray Leaf Spot Disease in Pepper. *Appl. Soil Ecol.* **2014**, 73, 1–8. https://doi.org/10.1016/j.apsoil.2013.07.016

[12] King, E. J. The Colorimetric Determination of Phosphorus. *Biochem. J.* **1932**, 26, 292. https://doi.org/10.1042/bj0260292

[13] Dobereiner, J.; Marriel, I.; Nery, M. Ecological Distribution of *Spirillum lipoferum* Beijerinck. *Can. J. Microbiol.* **1976**, 22, 1464-1473. https://doi.org/10.1139/m76-217

[14] Bradstreet, R. B. Kjeldahl Method for Organic Nitrogen. *Anal. Chem.* **1954**, 26, 185–187. https://doi.org/10.1021/ac60085a028

[15] Sambrook, J.; Fritsch, E. F.; Maniatis, T. *Molecular Cloning: A Laboratory Manual*, 2nd ed.; Cold Spring Harbor Laboratory Press: Cold Spring Harbor, NY, **1989**.

[16] Weisburg, W. G.; Barns, S. M.; Pelletier, D. A.; Lane, D. J. 16S ribosomal DNA amplification for phylogenetic study. *J. Bacteriol.* **1991**. https://doi.org/10.1128/jb.173.2.697-703.1991

[17] Basic Local Alignment Search Tool. http://www.ncbi.nlm.nih.gov/blast/Blast.cgi (accessed July 9, **2024**).

[18] Hossain, T. J. Methods for screening and evaluation of antimicrobial activity: A review of protocols, advantages, and limitations. *Eur. J. Microbiol. Immunol.* **2024**, 14, 97–115. https://doi.org/10.1556/1886.2024.00035

[19] Johan, F.; Jafri, M.; Lim, H.; Maznah, W. W. Laboratory Measurement: Chlorophyll-a Concentration Measurement with Acetone Method Using Spectrophotometer. In *Proceedings of the 2014 IEEE International Conference on Industrial Engineering and Engineering Management*; IEEE: Piscataway, NJ, **2014**, pp 744-748. https://doi.org/10.1109/IEEM.2014.7058737

[20] Amri, M.; Rjeibi, M. R.; Gatrouni, M.; Mateus, D. M.; Asses, N.; Pinho, H. J.; Abbes, C. Isolation, identification, and characterization of phosphate- solubilizing bacteria from Tunisian soils. *Microorganisms* **2023**, 11, 783. https://doi.org/10.3390/microorganisms11030783

[21] Ahmad, R.; Khan, S.; Hayat, M.; Afzal, S. M.; Muhammad, J. Plant Growth-Promoting Rhizobacteria/*Pseudomonas* as a Biofertilizer. In Biofertilizers for Sustainable Soil Management; CRC Press, **2023**, pp 179–201.

[22] Ahmad, A.; Haq, T.; Karim, A.; Saleem, M.; Hasan, K.; Liaqat, I.; Zafar, U. Designing of Phosphate Rich Compost Inoculated with Environmental Strain *Pseudomonas aeruginosa* AAC1 As a Phosphate Solubilizer. *Int. J. Environ. Sci. Technol.* **2024**. 1–20. https://doi.org/10.1007/s13762-024-06278-0

[23] Idress, M.; Khan, P.; Nawab, J.; Khan, A.; Khan, S.; Ali, R.; Rehman, A.; Alam, A.; Ayaz, S.; Bayabil, H. Improving Phosphorus Availability in Saline-Alkaline Agricultural Soils through Biochar and Phosphorus Solubilizing Bacteria (PSB) Inoculation: A Greenhouse Experiment. *Int. J. Phytoremediation* **2025**, 27, 1042–1056. https://doi.org/10.1080/15226514.2025.2473594

[24] Jain, S.; Varma, A.; Choudhary, D. K. Perspectives on Nitrogen-Fixing *Bacillus* Species. In *Soil Nitrogen Ecology*; Springer: Cham, Switzerland, **2021**, 359–369. https://doi.org/10.1007/978-3-030-71206-8_18

[25] Patani, A.; Patel, M.; Islam, S.; Yadav, V. K.; Prajapati, D.; Yadav, A. N.; Sahoo, D. K.; Patel, A. Recent advances in *Bacillus*- mediated plant growth enhancement: a paradigm shift in redefining crop resilience. *World J. Microbiol. Biotechnol.* **2024**, 40, 77. https://doi.org/10.1007/s11274-024-03903-5

[26] Kumar, A.; Patel, J. S.; Meena, V. S.; Srivastava, R. Recent Advances of PGPR Based Approaches for Stress Tolerance in Plants for Sustainable Agriculture. *Biocatal. Agric. Biotechnol.* **2019**, 20, 101271. https://doi.org/10.1016/j.bcab.2019.101271

[27] dos Reis, G. A.; Martínez-Burgos, W. J.; Pozzan, R.; Pastrana Puche, Y.; Ocán-Torres, D.; de Queiroz Fonseca Mota, P.; Rodrigues, C.; Lima Serra, J.; Scapini, T.; Karp, S. G. Comprehensive Review of Microbial Inoculants: Agricultural Applications, Technology Trends in Patents, and Regulatory Frameworks. *Sustainability* **2024**, 16, 8720. https://doi.org/10.3390/su16198720

[28] Lin, Q.; Li, L.; Adams, J. M.; Heděnec, P.; Tu, B.; Li, C.; Li, T.; Li, X. Nutrient Resource Availability Mediates Niche Differentiation and Temporal Co-Occurrence of Soil Bacterial Communities. *Appl. Soil Ecol.* **2021**, 163, 103965. https://doi.org/10.1016/j.apsoil.2021.103965

[29] Ge, J.; Li, D.; Ding, J.; Xiao, X.; Liang, Y. Microbial Coexistence in the Rhizosphere and the Promotion of Plant Stress Resistance: A Review. *Environ. Res.* **2023**, 222, 115298. https://doi.org/10.1016/j.envres.2023.115298

[30] Singh, M.; Jha, S.; Pathak, D.; Maisnam, G. Advancing Biofertilizers: The Evolution from Single-Strain Formulations to Synthetic Microbial Communities (SynCom) for Sustainable Agriculture. *Discov. Plants* **2025**, 2, 226. https://doi.org/10.1007/s44372-025-00318-w

[31] Zhao, Y.; Zhang, M.; Liu, Z.; Yang, F. Migration and Transformation of Soil Phosphorus by Organic Acids: A Global Meta-Analysis. *J. Soils Sediments* **2024**, 24, 589–602. https://doi.org/10.1007/s11368-023-03665-x

[32] Zhang, W.; Ni, K.; Long, L.; Ruan, J. Nitrogen Transport and Assimilation in Tea Plant (*Camellia sinensis*): A Review. *Front. Plant Sci*. **2023**. https://doi.org/10.3389/fpls.2023.1249202

[33] Seghouani, M.; Bravin, M. N.; Mollier, A. Crop Response to Nitrogen-Phosphorus Colimitation: Theory, Experimental Evidences, Mechanisms, and Models. A Review. *Agron. Sustain. Dev.* **2024**, 44, 3. https://doi.org/10.1007/s13593-023-00939-z

[34] Zulfiqar, S.; Sharif, S.; Saeed, M.; Tahir, A. Role of Carotenoids in Photosynthesis. In Carotenoids: Structure and Function in the Human Body; *Springer*: Cham, Switzerland, **2021**, pp. 147–187. https://doi.org/10.1007/978-3-030-46459-2_5

[35] Berg, J. M.; Tymoczko, J. L.; Gatto, G. J.; Stryer, L. Photosynthetic organisms convert light energy into chemical energy to produce sugars as precursors for other organic molecules. Biochemistry, 8th ed.; W.H. Freeman: New York, **2015**; pp. 765–790.

[36] Fathi, A. Role of Nitrogen (N) in Plant Growth, Photosynthesis Pigments, and N Use Efficiency: A. *Agrisost* **2022**, 28, 1–8. https://doi.org/10.5281/zenodo.7143588

[37] Melero, S.; Madejón, E.; Ruiz, J. C.; Herencia, J. F. Chemical and Biochemical Properties of a Clay Soil under Dryland Agriculture System as Affected by Organic Fertilization. *Eur. J. Agron.* **2007**, 26, 327–334. https://doi.org/10.1016/j.eja.2006.11.004

[38] Huntley, B. J. Soil, Water and Nutrients. In Ecology of Angola: Terrestrial Biomes and Ecoregions; *Springer*: Cham, Switzerland, **2023**, pp. 127–147. https://doi.org/10.1007/978-3-031-18923-4_6

[39] Corley, R. H. V.; Tinker, P. B. *The Oil Palm*, 5th ed.; Wiley-Blackwell: Chichester, UK, **2016**.

[40] Ajijah, N.; Fiodor, A.; Pandey, A. K.; Rana, A.; Pranaw, K. Plant Growth-Promoting Bacteria (PGPB) with Biofilm-Forming Ability: A Multifaceted Agent for Sustainable Agriculture. *Diversity* **2023**, 15, 112. https://doi.org/10.3390/d15010112

ASEAN
Journal of Scientific and Technological Reports
Online ISSN:2773-8752

Research article

Development of High-performance Activated Carbon Derived from Longan Peel for Caffeine Removal in Ion-rich Hospital Wastewater

Chetnipat Kunawong[1], Napaphat Datpratoom[1], Panupong Uprajong[1], Jidapa Pimthong[2], and Sakdinun Nuntang[2*]

[1] Montfort College, Chiang Mai, 50000, Thailand
[2] Faculty of Science, Maejo University, Chiang Mai, 50290, Thailand
* Correspondence: Sakdinun.nt@gmail.com

Citation:
Kunawong , C.; Datpratoom , N.; Uprajong , P.; Pimthong, J; Nuntang, S. Development of a novel activated carbon derived from longan peel for removing of caffeine from synthetic hospital wastewater . *ASEAN J. Sci. Tech. Report.* **2026**, *29*(7), e262381. https://doi.org/10.55164/ajstr.v29i7.262381

Article history:
Received: November 17, 2025
Revised: April 25, 2026
Accepted: April 30, 2026
Available online: June 14, 2026

Publisher's Note:
This article is published and distributed under the terms of the Thaksin University.

Abstract: This study presents the development of activated carbon derived from longan peel (LPAC) as an efficient and low-cost adsorbent for the removal of caffeine (CAF) from synthetic hospital wastewater. Longan peel was carbonized and chemically activated at 600 °C and 700 °C, producing LPAC-600 and LPAC-700, respectively. The structural, textural, and functional properties of the adsorbents were characterized using XRD, FTIR, N_2 adsorption–desorption analysis, and SEM. The results indicated that increasing the activation temperature significantly enhanced surface area, pore volume, and graphitic carbon structure, with LPAC-700 exhibiting the highest BET surface area (1401.8 m^2/g) and mesoporosity. Batch adsorption experiments demonstrated that LPAC-700 achieved superior CAF removal compared to LPAC-600 in both deionized water and synthetic hospital wastewater, although ion-rich conditions reduced removal efficiency due to competitive adsorption. The optimal adsorbent dosage was 0.3 g/L, yielding up to 94.23% CAF removal at an initial concentration of 100 ppm. Solution pH strongly influenced adsorption, with maximum removal at pH 7, attributed to favorable π–π interactions and hydrogen bonding. These findings confirm that LPAC-700 is a promising bio-derived adsorbent for caffeine removal in complex wastewater systems.

Keywords: Activated carbon; longan peel; caffeine; synthetic hospital wastewater

1. Introduction

Caffeine (CAF) is among the most widely ingested bioactive compounds worldwide, functioning as a central nervous system stimulant and appearing in a broad spectrum of commercial products, including beverages, functional foods, dietary supplements, and pharmaceutical formulations [1-3]. Because of its extensive global consumption and relatively low metabolic transformation in humans, a significant proportion of ingested caffeine is excreted unmetabolized. Consequently, CAF is increasingly observed in natural and engineered aquatic environments, where it is now recognized as an emerging anthropogenic contaminant of environmental relevance. Regulatory agencies, including the United States Environmental Protection Agency (EPA), have reported that caffeine serves as a reliable marker for domestic and sanitary wastewater contamination, providing insight into the performance and integrity of water treatment systems [4].

Concerns over caffeine's ecological implications, such as its potential effects on aquatic organisms, persistence in water matrices, and co-occurrence with other pharmaceutical residues, have driven ongoing efforts to develop efficient removal technologies. Wastewater originating from hospitals frequently contains relatively high concentrations of caffeine, partly due to the extensive use of CAF-containing medications and diagnostic agents [4-6]. Moreover, such effluents generally exhibit elevated ionic strength, which adds additional complexity to the removal processes. High ionic concentrations can interfere with adsorption or catalytic reactions by competing for active sites or altering surface charge interactions, making remediation of caffeine in these matrices particularly challenging. Previous investigations have reported that CAF removal can be achieved using advanced oxidation systems, ozonation, membrane-based separations, and adsorption-based technologies; however, limitations in operational cost, energy consumption, and maintenance often restrict their practical application [7-9].

Among the various technologies, adsorption remains an especially promising approach for removing caffeine and other pharmaceutical contaminants. This method offers multiple advantages, including low operational cost, ease of implementation, compatibility with existing treatment infrastructures, and minimal generation of harmful by-products. A variety of adsorbent materials, such as zeolites, activated carbon, mesoporous silica materials, and metal-organic frameworks (MOFs), have been examined for their capacity to remove pharmaceuticals from water [9-12]. Despite their effectiveness, many of these materials have drawbacks, including high production costs, difficulty in regeneration, or limited sustainability. Activated carbon, in contrast, is a well-established adsorbent widely used across industrial sectors due to its high porosity, tunable surface chemistry, and substantial adsorption capacity for organic and inorganic pollutants [6,10]. Nonetheless, reliance on conventional raw materials and the challenges associated with separating powdered activated carbon from aqueous systems have prompted growing interest in alternative biomass-derived sources. Agricultural waste provides a renewable, abundant feedstock for producing cost-efficient activated carbon while contributing to waste valorization. Longan peel, rich in carbonaceous content and widely available in Southeast Asia, has recently emerged as a promising precursor for generating activated carbon with desirable structural properties [13].

The present study investigates the feasibility of producing activated carbon derived from longan peel (LPAC) through chemical activation at different temperatures, to assess its performance in removing caffeine from synthetic hospital wastewater. Comprehensive structural, functional, and morphological characterization techniques, including XRD, FTIR, N_2 adsorption–desorption analysis, and SEM, were employed to elucidate the influence of activation temperature on the physicochemical properties of the prepared materials. Additionally, the stability of LPAC after exposure to caffeine-containing solutions was examined to determine its potential as a robust, sustainable bioadsorbent. By evaluating LPAC performance in a highly ionized wastewater system, this work aims to establish the viability of longan peel-derived activated carbon as an environmentally friendly, economically feasible candidate for advanced wastewater treatment applications.

2. Materials and Methods

2.1 Chemicals and reagents for preparation of longan peel activated carbon (LPAC)

Sodium hydroxide (NaOH; analytical grade 99%) was acquired from Sigma-Aldrich. All chemical solutions were prepared using deionized (DI) water from RCI Labscan, which was also used to rinse and clean the samples. Longan peel, a common agricultural residue material, was collected from Rim Rong Housewives Community Enterprise, Makhuea Chae Subdistrict, Mueang District, Lamphun Province, Thailand.

2.2 Preparation of longan peel activated carbon (LPAC)

The following process was used to produce the longan peel activated carbon. Before being stored in silica gel desiccators, the raw longan peel was crushed and sieved to achieve a particle size of 100 mesh. Then, it was dried in an oven at 100°C for 10 h to remove any water absorbed on the surface. The dried longan peel was carbonized for 1.5 h at 400 °C. After cooling to room temperature, the resulting carbon was crushed. Sodium hydroxide (NaOH) was combined with the carbonized material in a 1:2 (w/w) ratio. The mixture was

then activated at 600 and 700 C for 1.5 h. The resulting activated carbons from the longan peel were labeled as LPAC-600 and LPAC-700, respectively. Then, they were cooled to room temperature and washed with distilled water until their pH reached 7. The LPAC materials were then dried in a hot air oven at 80 °C for 24 h. The yield of LPAC-600 and LPAC-700 was estimated to be in the range of 18–25 wt%, which is consistent with previously reported values for NaOH-activated longan seed-derived carbons prepared at high temperatures [14].

2.3 Characterization of adsorbents

Structural information about the materials was obtained by powder X-ray diffraction (XRD) using an Empyrean 3 Panalytical diffractometer with Cu Kα radiation at 40 kV and 40 mA. N_2 adsorption-desorption measurements were performed at -196 °C utilizing an Anton Paar Nova 600 to determine the textural properties of the materials. The sample weight, initially approximately 40 mg, was precisely measured following pretreatment at 150 °C for 2 hours. Fourier-transform infrared spectroscopy (FTIR) was utilized to identify functional groups in the composites, employing a Perkin-Elmer spectrometer with the KBr technique. Sixty-four scans were averaged for each spectrum, covering the range of 400-4000 cm^{-1}at a resolution of 4 cm^{-1}. The morphology of the sample was assessed using scanning electron microscopy (SEM). The SEM images were captured using a TESCAN VEGA3 scanning electron microscope functioning at 10 kV. The samples on carbon tape were examined with a gold coating applied.

2.4 Preparation of synthetic hospital wastewater (HP wastewater)

The synthetic hospital effluent was prepared to represent a substantial volume of ionized wastewater, following the methodology reported by Tiwari et al. (2019) [15]. The mixture comprised $(NH_4)_2SO_4$ at 353.57 ppm, KH_2PO_4 at 92.19 ppm, $MgSO_4$ at 34.68 ppm, $CaCl_2{\cdot}2H_2O$ at 22.10 ppm, $FeCl_3$ at 11.63 ppm, $CuSO_4$ at 0.07 ppm, $Na_2MoO_4{\cdot}2H_2O$ at 0.10 ppm, $MnSO_4{\cdot}H_2O$ at 0.12 ppm, $ZnCl_2$ at 0.23 ppm, $CoSO_4{\cdot}7H_2O$ at 0.48 ppm, Na_2CO_3 at 428.60 ppm, and $C_6H_{12}O_6$ at 938.35 ppm. Furthermore, 100 ppm of caffeine ($C_8H_{10}N_4O_2$, CAF) was incorporated into the synthetic hospital wastewater. The chemicals utilized were of analytical grade and obtained from Sigma-Aldrich. A batch adsorption study was performed for 48 hours at 150 rpm and room temperature. The samples passed filtration, and the total removal was determined by analyzing the UV-Vis spectra over 200 to 800 nm.

2.5 Adsorption experiment

Adsorption studies of CAF on longan peel-activated carbon were conducted in a batch system using 50-mL Erlenmeyer flasks containing CAF solution and dried absorbents. The adsorption experiments were performed by shaking the flasks in a shaker under specified conditions. The concentration of the CAF solution post-adsorption was quantified using a UV–vis spectrophotometer at 273.5 nm. The characteristic absorption of caffeine, and no significant interference was observed. Additionally, calibration using standard solutions ensures reliable quantification. The amount of CAF removal and adsorption capacity was calculated according to a mass balance on the CAF concentration using Eq (1) and Eq. (2), respectively:

$$\% \text{ CAF Removal} = \frac{(C_i - C_e)}{C_i} \times 100 \quad (1)$$

$$Q_e = \frac{(C_i - C_e)}{W} \times V \quad (2)$$

where C_i is the initial concentration of CAF (ppm, mg/L), C_e is the equilibrium concentration of CAF in solution (ppm, mg/L), Q_e is the adsorption capacity at adsorption equilibrium (mg/g, dried adsorbent), V is the volume of initial solution (L), and W is the weight of dried adsorbent (g). All experiments were conducted in duplicate, and the reproducibility of the data was verified with deviations within an acceptable range (<5%).

3. Results and Discussion

3.1 Characterization of LPAC adsorbents

Figure 1 presents the XRD patterns of activated carbon derived from longan peel, specifically LP-600 and LP-700. Two distinct peaks were observed in both materials. The prominent peak observed at 15-30° is

likely attributable to reflection plane C(002), indicative of a disordered aromatic carbon structure, while the peak at 43.96° corresponds to reflection plane C(100/101) associated with graphitic or organized carbon [16]. The signal intensity of the graphitic carbon in LPAC-700 was significantly greater than that in LPAC-600, suggesting that the elevated activation temperature led to an improvement in the graphitic carbon structure.

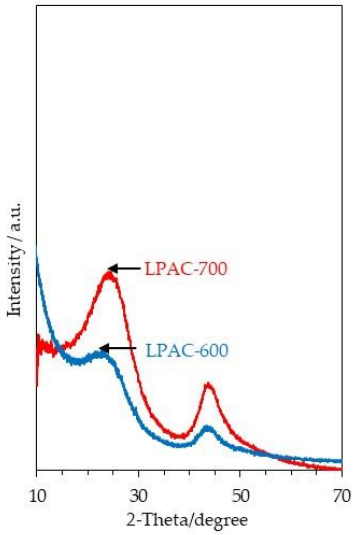


Figure 1. XRD patterns of LPAC adsorbents.

The FT-IR analysis provided information for identifying the chemical functional groups in longan peel activated carbon at different activation temperatures. Figure 2 shows the FTIR spectra of LPAC-600 and LPAC-700 materials. The broad band at approximately 3440 cm^{-1} was attributed to the O-H stretching of hydroxyl groups and adsorbed water. The C–H stretching vibration characteristic of the alkyl structure in the aliphatic group was observed at 2920 cm^{-1} [17]. The band at 1630 cm^{-1} could be assigned to C–C vibrations in aromatic rings and C=O stretching vibrations of carboxyl and carbonyl groups. The bands within the range of 1000 – 1300 cm^{-1} were attributed to oxidized carbons, specifically the C–O stretching vibrations associated with carboxylic acids, alcohols, phenols, ethers, and esters [17,18]. The intensity of the LPAC-700 peak was observed to be lower than that of the LPAC-600 peak. The results indicated that higher activation temperatures led to the decomposition of these organic compounds [19].

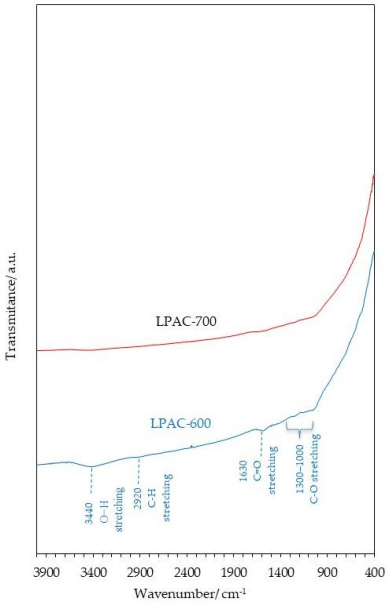


Figure 2. FT-IR spectra of LPAC adsorbents.

Figure 3 shows the N_2 adsorption–desorption isotherms and pore size distributions of LPAC materials. According to IUPAC, the isotherms of these materials could be classified as type IV, which are characteristic of materials with well-developed mesoporous structures. The LPAC-700 exhibited a higher N_2 adsorbed volume than the LPAC-600 (Figure 3A), corresponding to the specific surface area of these materials, as shown in Table 1. These results indicated that the activation temperature resulted in the textural properties of the activated carbon. In addition, the pore size distribution of LPAC materials, as shown in Figure 3b, indicated that most pores were distributed in the 2–10 nm size range, confirming the material's mesoporosity. However, the LPAC-600 exhibited a lower pore volume and average pore diameter (Table 1) than that of the LPAC-700. These results suggested that increasing the activation temperature resulted in distinct pore structures.

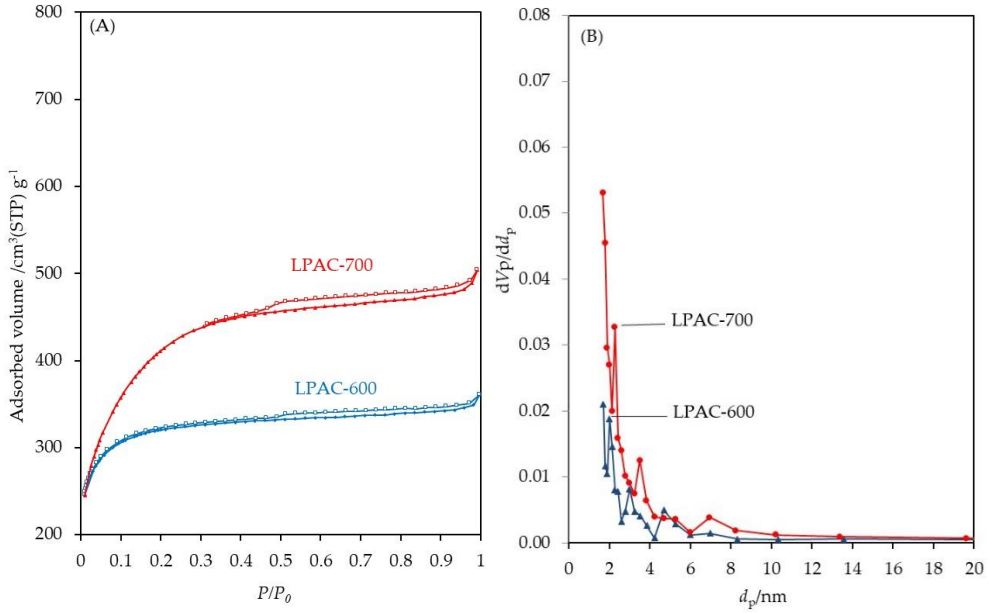


Figure 3. N_2 adsorption-desorption isotherms (A) and BJH pore size distribution (B) of LPAC adsorbents.

Table 1. Textural properties of LPAC adsorbents.

Sample	Specific surface area (m^2/g)	Pore volume (cm^3g^{-1})	Average Pore diameter (nm)
LPAC-600	1004.5	0.66	8.5
LPAC-700	1401.8	0.82	9.2

3.2 Caffeine adsorption studies

In the present study, we investigated how different types of activated carbons affect the CAF adsorption process using an initial concentration of 100 ppm of CAF dissolved in DI water and in synthetic hospital wastewater (representative of high ionized wastewater), as shown in Figure 4. The LPAC adsorbents were examined for their effectiveness in removing CAF from aqueous solutions, both with and without the ion present, as illustrated in Figures 4A and 4B, respectively. The adsorption conditions included an adsorbent/solution (M/V) ratio of 0.1 g/L, a CAF concentration of 100 ppm, a time duration of 120 minutes, a shaking speed of 120 rpm, and room temperature. The longan peel activated carbon produced at higher activation temperatures showed a higher percentage of CAF removal (LPAC-600 < LPAC-700), which correlated with BET surface area and pore volume, as shown in Table 1. The findings indicated that the highest CAF removal was contingent on the adsorbent's textural properties. Consequently, the LPAC-700 proved to be an appropriate adsorbent for subsequent investigations. However, the CAF removal from synthetic hospital wastewater with high ion concentrations showed lower adsorption for both adsorbents, as shown in Figure 4B.

A significant decrease in CAF removal was observed in synthetic hospital effluent compared with deionized water, indicating the influence of coexisting ions on adsorption efficacy. This phenomenon cannot be ascribed solely to mere competition but also encompasses other physical factors. Multivalent cations,

including Ca^{2+} and Mg^{2+}, may compete with CAF molecules for adsorption sites, especially those linked to oxygen-containing functional groups. Moreover, increased ionic strength results in electrostatic screening, diminishing the effective interaction between caffeine molecules and the adsorbent surface. Furthermore, hydration shells encasing dissolved ions may impede the diffusion of CAF into porous matrices, consequently diminishing adsorption efficiency [6]. These results were confirmed by comparing FTIR spectra obtained before and after caffeine adsorption in synthetic wastewater, as shown in Figure 5. The FTIR spectra of LPAC after adsorption showed multiple peaks corresponding to caffeine molecules adsorbed on its surface.

In addition, the synthesized activated carbons exhibited an adsorption capacity for CAF comparable to that of the commercial activated carbon (AC) with a BET surface area of 1200 m2/g, reported by Rajkamal et al. to be around 71.7 mg/g, depending on operational conditions and surface properties [20]. Furthermore, Figure 6 shows SEM images of LPAC materials before and after CAF adsorption in synthetic HP wastewater. The LPAC exhibited a particle size of 50–125 nm and a high porosity. After adsorption of CAF in synthetic HP wastewater, the LPAC showed no difference in morphology from the initial.

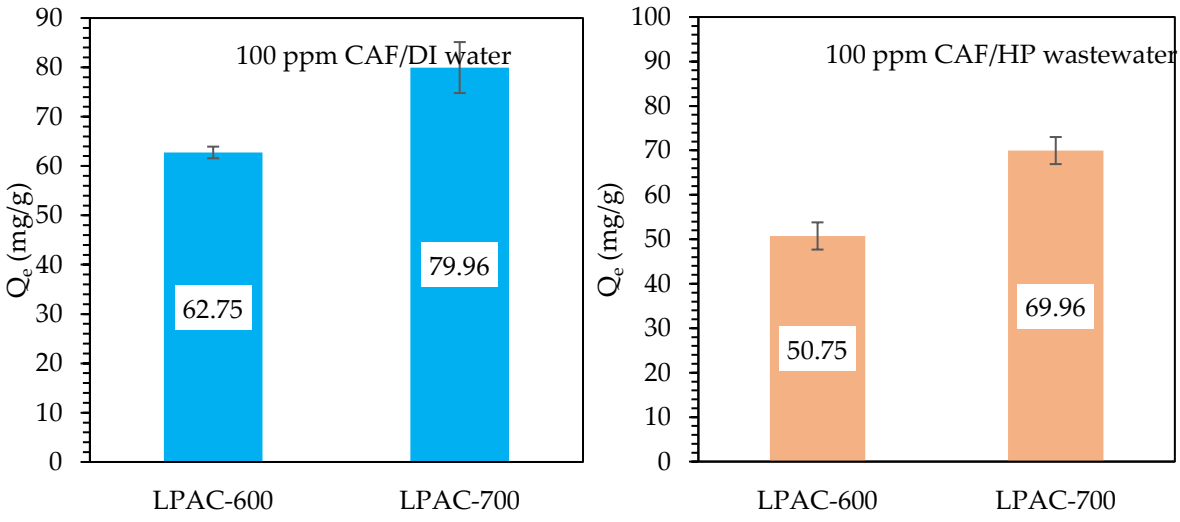


Figure 4. Effect of type of LPAC adsorbents on CAF removal in (A) DI water, (B) synthetic HP wastewater.

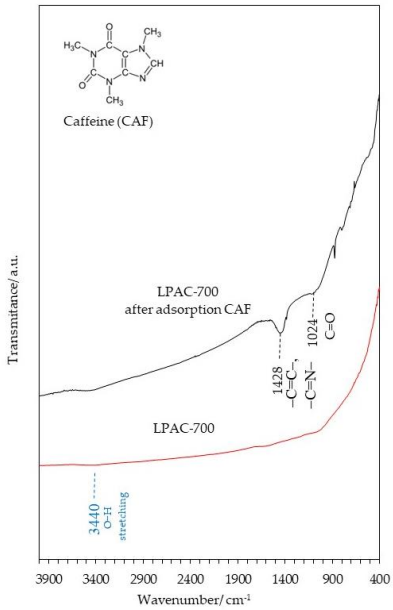


Figure 5. FT-IR spectra of LPAC-700 before and after adsorption of CAF in synthetic HP wastewater.

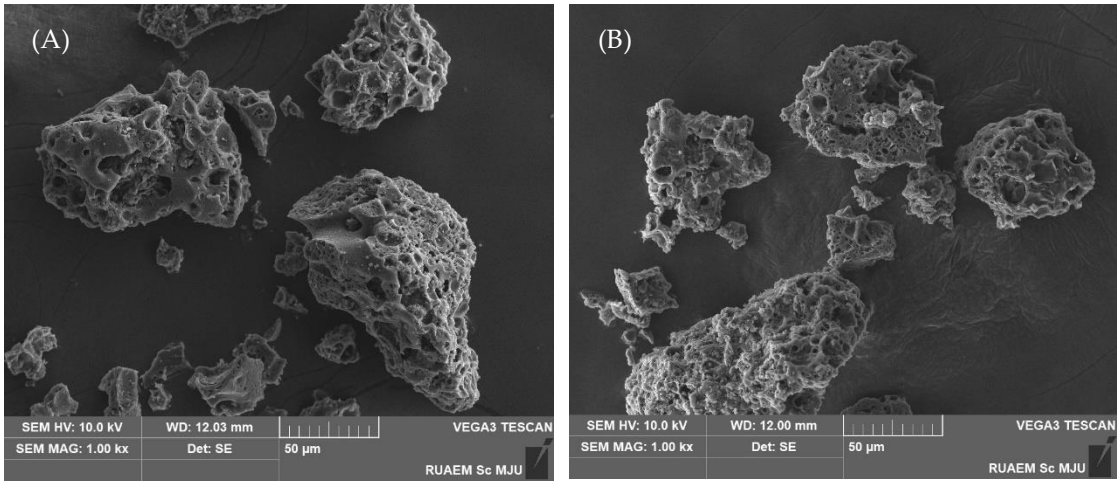


Figure 6. SEM images of LPAC materials (A) before and (B) after adsorption of CAF in synthetic HP wastewater.

Figure 7 illustrates the impact of the mass of adsorbent per volume of CAF solution (M/V) on the removal of CAF by LPAC-700. The adsorption conditions comprised an adsorbent/solution (M/V) ratio of 0.1-0.3 g/L, a CAF concentration of 100 ppm, a duration of 120 minutes, a shaking speed of 120 rpm, and ambient temperature. Increasing M/V from 0.1 g/L to 0.3 g/L resulted in an increase in CAF removal percentage from 69.96 to 94.23. An increase in the mass of adsorbent per volume led to a corresponding increase in pore volume and the presence of functional groups (–COOH, -OH, and aliphatic –C=C–) in the material. The physicochemical adsorption capacity of this adsorbent for CAF removal was superior. The results indicate that 0.3 g/L is the optimal mass-to-volume ratio for treating 1 L of CAF solution at 100 ppm.

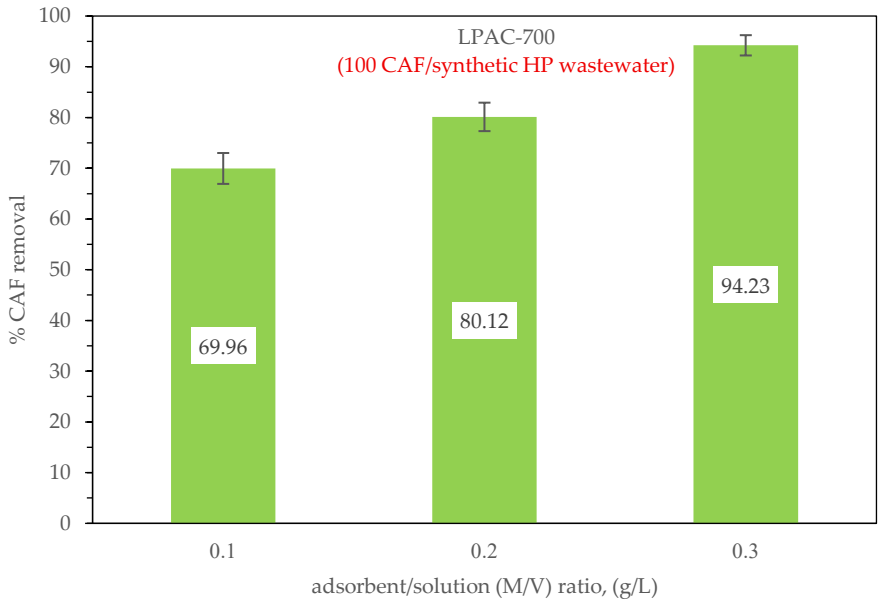


Figure 7. Effect of LPAC adsorbent dose on CAF removal.

The pH of a solution significantly affects adsorption processes by influencing the interactions between adsorbents and adsorbates. Variations in pH can alter the surface charge of adsorbents and affect the protonation state of functional groups on the adsorbent surface. The effect of pH on the CAF removal of LPAC-700 are shown in Figure 8. The adsorption conditions were as follows: pH range of 4-10, adsorbent/solution (M/V) ratio of 0.3 g/L, CAF concentration of 100 ppm, duration of 120 minutes, shaking speed of 120 rpm, and maintained at room temperature. The findings indicate that the maximum percentage of CAF removal was

achieved at pH 7, with a notable reduction at pH 10. The findings align with those of Beltrame et al. [10], who observed a significant pH change during the removal of CAF utilizing mesoporous activated carbon fibers derived from pineapple plant leaves. At pH 7, the predominance of the neutral form of CAF and the activated carbon's negative surface charge created optimal conditions for CAF removal. Many processes influence the adsorption of CAF onto LPAC. The aromatic configuration of CAF facilitates π–π interactions with the graphitic domains of LPAC, which are more evident in LPAC-700 owing to increased graphitization. Furthermore, mesopores (2–10 nm) correspond well with the molecular dimensions of CAF (~0.8 nm), promoting pore-filling adsorption [18,19]. The increase in solution pH led to a decrease in CAF removal, indicating repulsion between CAF molecules and the negatively charged surface of the activated carbon [10].

Although full isotherm modeling was not conducted, the adsorption behavior is expected to follow Langmuir-type monolayer adsorption due to the activated carbon's homogeneous surface, as reported in similar systems. Furthermore, CAF adsorption on activated carbon is commonly described by pseudo-second-order kinetics, consistent with the chemisorption mechanisms reported by Rajkamal et al. [20]. However, these materials will be further studied for their adsorption behavior and kinetics compared to commercially available activated carbon. Importantly, this study demonstrates that LPAC maintains reasonable adsorption efficiency even under ion-rich conditions, which are representative of real hospital wastewater. This highlights its potential applicability in practical wastewater treatment systems.

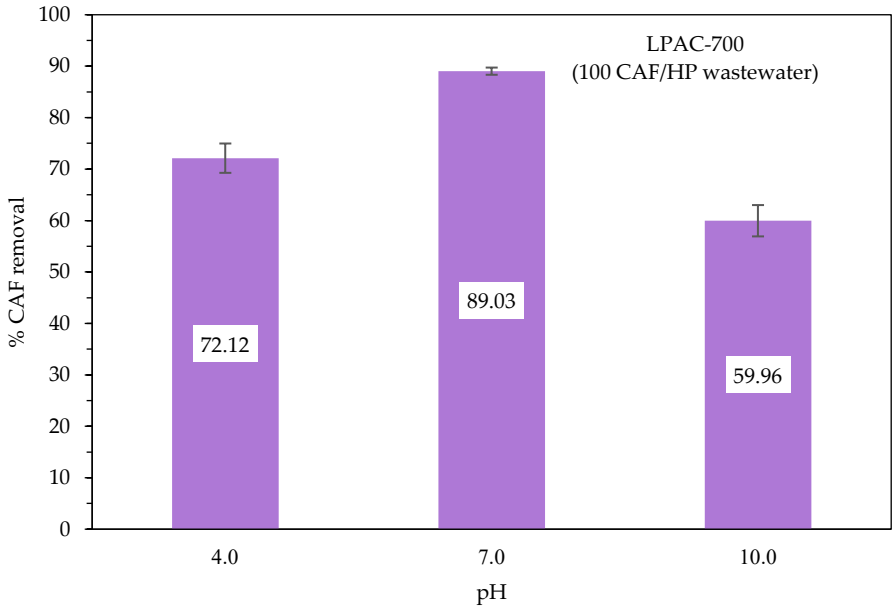


Figure 8. Effect of pH on CAF removal.

4. Conclusions

Activated carbon produced from longan peel demonstrated high potential for removing caffeine from aqueous systems, particularly LPAC-700, which offered superior textural and structural properties due to higher activation temperature. The mesoporous structure, large specific surface area, and suitable functional groups contributed to its high adsorption efficiency. Although ion-rich synthetic hospital wastewater reduced caffeine adsorption through competitive interactions, LPAC-700 still maintained substantial removal capability. Adsorbent dosage and solution pH were critical parameters, with optimal performance observed at 0.3 g/L and neutral pH. Overall, longan peel-derived activated carbon is an effective, sustainable, and inexpensive adsorbent, demonstrating its applicability for treating pharmaceutical-contaminated wastewater in real-world settings.

5. Acknowledgments

The authors gratefully acknowledge all staff of the Industrial Chemistry Innovation Program, Faculty of Science, Maejo University, and Montfort College for their support in providing the facilities for this study.

Author Contributions: Conceptualization, S.N.; methodology, C.K., N.D., P.U. and J.P.; software, J.P. and S.N.; validation, J.P. and S.N.; formal analysis, J.P. and S.N.; investigation, S.N.; resources, C.K., N.D., P.U. and J.P.; data curation, J.P. and S.N.; writing—original draft preparation, J.P. and S.N.; writing—review and editing, S.N.; visualization, C.K., N.D., P.U. and J.P.; supervision, S.N.; project administration, S.N.; funding acquisition, S.N. All authors have read and agreed to the published version of the manuscript.

Funding: This research was funded by Thailand Science Research and Innovation (TSRI), as stated in the annual government statement B.E. 2563.

Conflicts of Interest: The authors declare no conflict of interest.

References

[1] Colombo, R.; Papetti, A. An Outlook on the Role of Decaffeinated Coffee in Neurodegenerative Diseases. *Crit. Rev. Food Sci. Nutr.* **2020**, *60*, 760–779. https://doi.org/10.1080/10408398.2018.1550384

[2] Bachmann, S. A. L.; Calvete, T.; Féris, L. A. Caffeine Removal from Aqueous Media by Adsorption: An Overview of Adsorbents Evolution and the Kinetic, Equilibrium and Thermodynamic Studies. *Sci. Total Environ.* **2021**, *767*, 144229. https://doi.org/10.1016/j.scitotenv.2020.144229

[3] Li, S.; He, B.; Wang, J.; Liu, J.; Hu, X. Risks of Caffeine Residues in the Environment: Necessity for a Targeted Ecopharmacovigilance Program. *Chemosphere* **2020**, *243*, 125343. https://doi.org/10.1016/j.chemosphere.2019.125343

[4] Vieira, L. R.; Soares, A. M. V. M.; Freitas, R. Caffeine as a Contaminant of Concern: A Review on Concentrations and Impacts in Marine Coastal Systems. *Chemosphere* **2022**, *286*(2), 131675. https://doi.org/10.1016/j.chemosphere.2021.131675

[5] Buerge, I. I.; Poiger, T.; Müller, M. D.; Buser, H.-R. Caffeine: An Anthropogenic Marker for Wastewater Contamination of Surface Waters. *Environ. Sci. Technol.* **2003**, *37*(4), 691–700. https://doi.org/10.1021/es020125z

[6] Quesada, H. B.; de Araújo, T. P.; Cusioli, L. F.; de Barros, M. A. S. D.; Gomes, R. G.; Bergamasco, R. Caffeine Removal by Chitosan/Activated Carbon Composite Beads: Adsorption in Tap Water and Synthetic Hospital Wastewater. *Chem. Eng. Res. Des.* **2022**, *184*, 1–12. https://doi.org/}10.1016/j.cherd.2022.05.044

[7] Thomas, T.A.; Stüber, J.; Herrmann, N.; McDowell, D.; Ried, A.; Kampmann, M.; Bernhard, T. Ozonation: A Tool for Removal of Pharmaceuticals, Contrast Media and Musk Fragrances from Wastewater. *Water Res.* **2003**, *37*(8), 1976–1982. https://doi.org/10.1016/S0043-1354(02)00570-5

[8] Afonso-Olivares, C.; Fernández-Rodríguez, C.; Ojeda-González, R. J.; Sosa-Ferrera, Z.; Santana-Rodríguez, J. J.; Doña Rodríguez, J. M. Estimation of Kinetic Parameters and UV Doses Necessary to Remove Twenty-Three Pharmaceuticals from Pre-Treated Urban Wastewater by UV/H_2O_2. *J. Photochem. Photobiol. A* **2016**, *329*, 130–138. https://doi.org/10.1016/j.jphotochem.2016.06.018

[9] Ptaszkowska-Koniarz, M.; Gościańska, J.; Pietrzak, R. Synthesis of Carbon Xerogels Modified with Amine Groups and Copper for Efficient Adsorption of Caffeine. *Chem. Eng. J.* **2018**, *345*, 13–21. https://doi.org/10.1016/j.cej.2018.03.132

[10] Beltrame, K. K.; Cazetta, A. L.; de Souza, P. S. C.; Spessato, L.; Silva, T. L.; Almeida, V. C. Adsorption of Caffeine on Mesoporous Activated Carbon Fibers Prepared from Pineapple Plant Leaves. *Ecotoxicol. Environ. Saf.* **2018**, *147*, 64–71. https://doi.org/10.1016/j.ecoenv.2017.08.034

[11] Essam, A.; Eldek, S. I.; Shehata, N. Management of Caffeine in Wastewater Using MOF and Perovskite Materials: Optimization, Kinetics, and Adsorption Isotherm Modelling. *J. Environ. Health Sci. Eng.* **2024**, *22*, 345–360. https://doi.org/10.1007/s40201-024-00904-2

[12] Hua, Y.; Liu, G.; Lin, Z.; Jie, Z.; Zhao, C.; Han, J.; Chen, G.; Li, L.; Huang, X.; Liu, Z.; Lv, J.; Xu, D. Engineering of Zeolitic Imidazolate Frameworks Based on Magnetic 3D Graphene for Adsorption and

Removal of Caffeine from Tea Samples. *Food Chem.* **2024**, *431*, 137143. https://doi.org/10.1016/j.foodchem.2023.137143

[13] Hoa, N. T. H.; Quynh, N. T.; Nguyen, V. D.; Nguyen, T. N.; Huy, B. Q.; Thanh, N. T.; Loan, H. T.; Hoa, N. T. Q.; Nghia, N. T. Adsorptive Removal of Reactive Black 5 by Longan Peel-Derived Activated Carbon. *Water* **2025**, *17*, 1678. https://doi.org/10.3390/w17111678

[14] Yang, J.; Yu, M.; Chen, W. Adsorption of Hexavalent Chromium from Aqueous Solution by Activated Carbon Prepared from Longan Seed: Kinetics, Equilibrium and Thermodynamics. *J. Ind. Eng. Chem.* **2015**, *21*, 414–422. https://doi.org/10.1016/j.jiec.2014.02.054

[15] Tiwari, B.; Sellamuthu, B.; Piché-Choquette, S.; Drogui, P.; Tyagi, R. D.; Vaudreuil, M. A.; Sauvé, S.; Buelna, G.; Dubé, R. The Bacterial Community Structure of Submerged Membrane Bioreactor Treating Synthetic Hospital Wastewater. *Bioresour. Technol.* **2019**, *286*, 121362. https://doi.org/10.1016/j.biortech.2019.121362

[16] Cazetta, A. L.; Martins, A. C.; Pezoti, O.; Bedin, K. C.; Beltrame, K. K.; Asefa, T.; Almeida, V. C. Synthesis and Application of N,S-Doped Mesoporous Carbon Obtained from Nanocasting. *Chem. Eng. J.* **2016**, *315*, 54–63. https://doi.org/10.1016/j.cej.2016.04.124

[17] Yakout, S. M.; El-Deen, G. S. Characterization of Activated Carbon Prepared by Phosphoric Acid Activation of Olive Stones. *Arab. J. Chem.* **2016**, *9*, 1155–1162. https://doi.org/10.1016/j.arabjc.2011.12.002

[18] Zhu, D.; Pignatello, J. J. Characterization of Aromatic Compound Interactions with Black Carbon (Charcoal) Assisted by Graphite as a Model. *Environ. Sci. Technol.* **2005**, *39*, 2033–2041. https://doi.org/10.1021/es0491376

[19] Yang, R.; Liu, G.; Xu, X.; Li, M.; Zhang, J.; Hao, X. Surface Texture, Chemistry and Adsorption Properties of Acid Blue 9 of Hemp (*Cannabis sativa L.*) Bast-Based Activated Carbon Fibers Prepared by Phosphoric Acid Activation. *Biomass Bioenergy* **2011**, *35*, 437–445. https://doi.org/10.1016/j.biombioe.2010.08.061

[20] Rajkamal, A.; Kim, H. Theoretical Verification on Adsorptive Removal of Caffeine by Carbon- and Nitrogen-Based Surfaces: Role of Charge Transfer, π-Electron Occupancy, and Temperature. *Chemosphere* **2023**, *339*, 139667. https://doi.org/10.1016/j.chemosphere.2023.139667

ASEAN
Journal of Scientific and Technological Reports
Online ISSN:2773-8752

Research article

A Contextual Framework for Agricultural IoT Adoption: Integrating TAM, Innovation–Decision Process, and Governmental Support in Smart Farming Contexts

Sompoch Tongnamtiang[1], Manirath Wongsim[1], and Natarpha Satchawatee[1*]

[1] Mahasarakham Business School, Mahasarakham University, Maha Sarakham, 44150, Thailand
* Correspondence: natarpha.s@msu.ac.th

Citation:
Tongnamtiang, S.; Wongsim, M.; Satchawatee, N. A Contextual framework for agricultural IoT adoption: integrating TAM, innovation–decision process, and governmental support in smart farming contexts. *ASEAN J. Sci. Tech. Report.* **2026**, *29*(7), e262844. https://doi.org/10.55164/ajstr.v29i7.262844

Article history:
Received: December 17, 2025
Revised: April 24, 2026
Accepted: April 26, 2026
Available online: June 14, 2026

Publisher's Note:
This article is published and distributed under the terms of the Thaksin University.

Abstract: Agricultural Internet of Things (IoT) adoption in developing contexts remains constrained by a fragmented understanding of cognitive, behavioral, and contextual factors. A contextual framework is developed by integrating the Technology Acceptance Model (TAM), selected components of the Innovation–Decision Process (IDP), and key enabling conditions to explain continued use intention in smart farming environments. Data from 250 Thai agricultural stakeholders with prior exposure to or implementation experience with IoT-based agricultural applications were analyzed using partial least squares structural equation modeling (PLS-SEM). Results indicate that perceived usefulness is the strongest predictor of attitude toward use, which in turn drives continued use intention. Knowledge plays a critical role as a precursor, shaping perceived ease of use, persuasion, and perceived usefulness, underscoring the importance of cognitive readiness even among experienced users. Facilitating conditions significantly support continued use intention, whereas governmental support shows no direct effect. Perceived ease of use does not significantly influence attitude, suggesting that functional value may outweigh usability considerations in post-adoption or experience-based contexts. The framework offers a context-sensitive explanation of agricultural IoT adoption by linking cognitive processes with operational support mechanisms, while the model-fit results indicate that conclusions should be interpreted with appropriate caution.

Keywords: Agricultural Internet of things; smart farming; technology acceptance model; innovation–decision process; continued use intention

1. Introduction

Global agriculture is undergoing rapid transformation driven by advanced digital technologies, particularly the Internet of Things (IoT). In agricultural contexts, IoT systems enable real-time monitoring and automated management through integrated sensor networks, data analytics, and cloud platforms. These capabilities support precision irrigation, soil assessment, pest detection, and remote farm supervision, thereby enhancing productivity, resource efficiency, and sustainability [1-3].

In Thailand, the Ministry of Agriculture and Cooperatives has introduced the "Digital Agriculture Development Plan (2021–2027)" to accelerate the adoption of smart technologies. Despite these national initiatives,

adoption among smallholder farmers remains limited, particularly in rural areas characterized by insufficient connectivity and support services. A nationwide survey by the Digital Economy Promotion Agency indicates that fewer than 25% of farmers have implemented IoT technologies, largely due to technological complexity, infrastructural gaps, and limited access to training and financial support [4]. These constraints suggest that technology availability alone does not necessarily lead to successful adoption outcomes in resource-constrained environments. From a technical perspective, prior studies demonstrate that IoT-based smart agriculture systems enable data-driven decision-making and automation through architectures integrating sensor nodes, microcontrollers, communication protocols (e.g., MQTT and HTTP), cloud platforms, and user interfaces. Empirical evidence has been reported across applications such as precision irrigation and water-use efficiency improvement [5, 6], low-power sensor-based irrigation automation [7, 8], and greenhouse monitoring using real-time environmental data and dashboards [9, 10]. Research also highlights cost-effective, modular approaches that improve accessibility in smallholder and peri-urban farming contexts [11, 12].

Recent developments further demonstrate the integration of artificial intelligence (AI) with IoT to enhance agricultural monitoring and decision support. For example, an AI-driven smart farming system combining environmental sensing with image-based plant health analysis has demonstrated improved accuracy in detecting nutrient deficiencies and enabling automated responses in real-world deployments [13]. Similarly, IoT-based automation in livestock environments has shown the ability to monitor environmental conditions and optimize operational efficiency, including reductions in mortality rates and improvements in farm productivity [14]. Related IoT-enabled systems in laboratory education, healthcare monitoring, and smart-learning contexts further illustrate the broader regional diffusion of IoT applications and the need to understand user readiness and contextual support across applied domains [15-18]. These developments reinforce the practical potential of IoT-enabled systems while highlighting the importance of system integration, real-time control, and user interaction in agricultural applications.

Comprehensive reviews highlight ongoing trends toward interoperability, energy efficiency, and scalable platform design, while also emphasizing persistent deployment challenges such as sensor calibration, unreliable connectivity, and limited user readiness [19, 20]. System-level perspectives emphasize the importance of modularity and scalability in IoT ecosystems [21], whereas cross-sector insights indicate that institutional support and platform readiness function as critical enabling conditions for adoption in developing economies [22]. Successful deployment and sustained use depend not only on technical feasibility but also on user acceptance and decision-making processes. Behavioral and contextual factors—such as perceived usefulness (PU), perceived ease of use (PEOU), social influence, and institutional support—play a central role in determining whether available technologies are used [5, 6]. Consequently, adoption research has relied extensively on theoretical models to explain how users form attitudes and intentions toward smart farming technologies.

Among these models, the Technology Acceptance Model (TAM) proposed by Davis [23] remains widely applied, with perceived usefulness and perceived ease of use consistently identified as key predictors of attitude and behavioral intention. Empirical evidence across agricultural and related domains supports the robustness of TAM relationships, while also revealing contextual variability across user groups and environments [24-28]. To better capture real-world complexity, researchers have extended TAM by incorporating complementary frameworks such as UTAUT, TOE, and innovation diffusion theory. These hybrid approaches highlight enabling conditions and governmental support as structural determinants that may either facilitate or constrain adoption, particularly in smallholder farming contexts [6, 29-32]. Broader synthesis studies further suggest that agricultural technology adoption is a socio-technical process that requires alignment across economic, organizational, and infrastructural dimensions [33, 34].

Regional evidence underscores the context-dependent nature of agricultural IoT adoption. Studies conducted in Thailand and Southeast Asia emphasize the role of institutional facilitation and policy support [24, 31, 32], whereas findings from China highlight technological complexity and organizational readiness [30, 35]. Research in Nepal identifies self-efficacy and anxiety as critical psychological determinants [27], while studies

in Sub-Saharan Africa emphasize systemic barriers and the importance of trust and actual use considerations [36]. A scoping review across low- and middle-income contexts consistently reports challenges related to high costs, limited digital literacy, insufficient training, and weak technical support infrastructures [37]. Collectively, these findings indicate that agricultural IoT adoption models must incorporate both behavioral determinants and contextual enablers to reflect real-world conditions accurately.

Despite these advances, several research gaps remain. Existing studies predominantly emphasize behavioral intention while paying limited attention to process-based dynamics and early-stage cognitive determinants that shape user perceptions before adoption. In addition, contextual factors such as governmental support and infrastructural readiness are often acknowledged but not consistently operationalized within unified analytical frameworks. Empirical evidence focusing on Thai users with direct agricultural IoT experience also remains limited. These gaps highlight the need for a context-sensitive, empirically grounded, and process-oriented framework that integrates behavioral beliefs, cognitive stages, and external enabling mechanisms.

Accordingly, a hybrid framework is proposed and empirically validated by integrating the Technology Acceptance Model (TAM) with selected components of Rogers' Innovation–Decision Process (IDP), while explicitly incorporating facilitating conditions and governmental support as contextual enablers. Quantitative data from 250 Thai agricultural IoT stakeholders with prior exposure to or implementation experience with agricultural IoT applications were analyzed using partial least squares structural equation modeling (PLS-SEM), providing empirical insights into how cognitive, behavioral, and contextual factors jointly shape adoption and continued use intention in smart farming contexts.

2. Materials and Methods

A quantitative research approach underpins the empirical examination of agricultural Internet of Things (IoT) adoption and continued use among Thai agricultural stakeholders. Methodological design follows a hypothetico-deductive paradigm, integrating behavioral, cognitive, and contextual perspectives to evaluate the proposed framework. Structural equation modeling (SEM) is employed as the primary analytical technique, enabling simultaneous assessment of measurement validity and structural relationships among latent constructs.

2.1 Conceptual Framework and Hypotheses Development

Integration of the Technology Acceptance Model (TAM) with selected components of Rogers' Innovation–Decision Process (IDP) underpins the proposed conceptual framework, complemented by two contextual enablers: facilitating conditions (FC) and governmental support (GS). Framework design seeks to explain agricultural Internet of Things (IoT) adoption and continued use by capturing interactions among early-stage cognitive processes, perceived system value, and external support mechanisms within resource-constrained farming contexts. Within this structure, TAM provides the core behavioral foundation through perceived ease of use (PEOU) and perceived usefulness (PU), both of which shape attitude toward use (ATT) and subsequently influence behavioral intention (BI) [38]. In the present study, behavioral intention reflects continued use intention, emphasizing sustained engagement with IoT technologies among respondents with prior experience. To extend explanatory capacity beyond conventional TAM, two constructs derived from the Innovation–Decision Process (IDP)—knowledge (KN) and persuasion (PS)—are incorporated to represent early-stage cognitive dynamics preceding attitude formation. Knowledge captures awareness and understanding of agricultural IoT technologies, whereas persuasion reflects evaluative influence shaped by communication, social interaction, and perceived relevance during initial exposure and early adoption phases [39]. The selection of these constructs aligns with cognitive and evaluative stages of innovation processing, which remain particularly relevant in cross-sectional analyses focusing on user perception rather than longitudinal adoption trajectories.

Contextual influences are represented through two external enabling mechanisms. Facilitating conditions capture perceived availability of infrastructure, technical support, and training necessary for

effective IoT utilization at the operational level [6]. Governmental support reflects policy initiatives, financial incentives, and extension services designed to reduce adoption barriers and enhance readiness for digital agriculture [40, 41]. Within the proposed framework, governmental support is conceptualized as a macro-level contextual driver, whereas facilitating conditions operate at a more immediate and operational level of technology use. This configuration is intended to extend conventional TAM-based adoption models in three ways. First, knowledge and persuasion are selected from the IDP because they represent the cognitive and evaluative stages most directly observable in a cross-sectional perception study; later IDP stages, such as decision, implementation, and confirmation, require stronger longitudinal evidence. Second, persuasion is modeled as an evaluative mechanism shaped by peer communication, community influence, and perceived relevance, allowing it to directly affect attitude while also being tested for its direct influence on continued use intention. Third, governmental support is modeled as a direct antecedent of behavioral intention to examine whether policy-level support is visible enough to shape users' intentions beyond immediate facilitating conditions. This arrangement therefore tests whether cognitive readiness, technology beliefs, and contextual support mechanisms jointly enhance explanatory value in a Thai smart farming context. Figure 1 illustrates the integrated conceptual framework, highlighting hypothesized relationships among cognitive, behavioral, and contextual constructs. Knowledge influences perceived ease of use, perceived usefulness, and persuasion (H1–H3), while persuasion contributes to both attitude and behavioral intention (H4–H5). Perceived ease of use affects perceived usefulness and attitude (H6–H7), whereas perceived usefulness and persuasion jointly shape attitude (H8). Attitude subsequently determines behavioral intention (H9), while facilitating conditions and governmental support are modeled as direct predictors of behavioral intention (H10–H11).

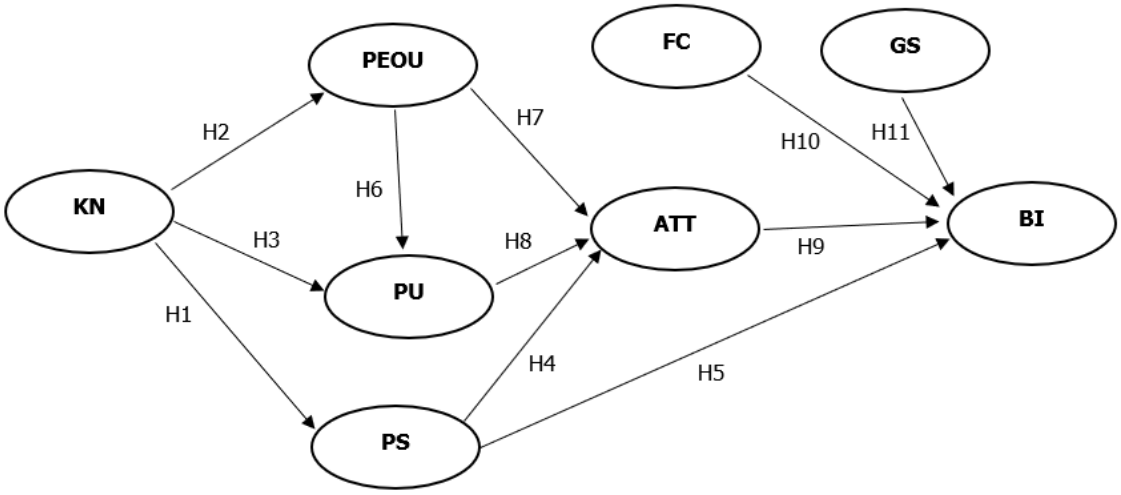


Figure 1. Conceptual framework for agricultural IoT adoption and continued use. *KN = Knowledge; PS = Persuasion; PEOU = Perceived Ease of Use; PU = Perceived Usefulness; ATT = Attitude toward Use; BI = Behavioral Intention; FC = Facilitating Conditions; GS = Governmental Support*

Empirical evaluation is conducted using Partial Least Squares Structural Equation Modeling (PLS-SEM), which is well-suited for complex models involving multiple latent constructs and predictive-oriented research objectives. This approach enables simultaneous estimation of direct and indirect effects, providing a comprehensive understanding of how cognitive, behavioral, and contextual factors jointly shape agricultural IoT adoption and continued use.

2.2 Research Objectives

Building on the integrated conceptual framework, this study addresses the following research objectives:

1. Examination of the effects of perceived usefulness (PU) and perceived ease of use (PEOU) on attitude toward use (ATT) and continued behavioral intention (BI), to assess the applicability of the Technology Acceptance Model in agricultural IoT contexts.

2. Investigation of how cognitive factors derived from the Innovation–Decision Process—specifically knowledge (KN) and persuasion (PS)—shape early-stage awareness, evaluation, and attitudinal development associated with agricultural IoT adoption.
3. Evaluation of the influence of contextual enablers, namely facilitating conditions (FC) and governmental support (GS), on continued behavioral intention toward agricultural IoT use in resource-constrained environments.

2.3 Research Hypotheses

Grounded in the proposed conceptual framework, eleven hypotheses are specified to examine relationships among cognitive determinants, technology acceptance constructs, and contextual influences shaping agricultural Internet of Things (IoT) adoption and continued use.

2.3.1 Cognitive Determinants (Innovation-Decision Process)

Cognitive factors derived from the Innovation–Decision Process capture early-stage awareness and evaluative mechanisms that precede attitude formation. Knowledge is expected to strengthen persuasion while also shaping perceptions of system usability and usefulness. Accordingly:

H1: Knowledge (KN) positively influences persuasion (PS).
H2: Knowledge (KN) positively influences perceived ease of use (PEOU).
H3: Knowledge (KN) positively influences perceived usefulness (PU).

Persuasion reflects evaluative influence shaped by communication and social interaction and is expected to contribute to both attitudinal responses and continued behavioral intentions toward technology use. Thus:

H4: Persuasion (PS) positively influences attitude toward use (ATT).
H5: Persuasion (PS) positively influences continued behavioral intention (BI).

2.3.2 Technology Acceptance Constructs

Relationships among perceived ease of use, perceived usefulness, attitude, and behavioral intention follow the core structure of the Technology Acceptance Model. Perceived ease of use enhances perceived usefulness and contributes to attitude formation, while perceived usefulness reinforces positive attitudes that drive continued intention. Accordingly:

H6: Perceived ease of use (PEOU) positively influences perceived usefulness (PU).
H7: Perceived ease of use (PEOU) positively influences attitude toward use (ATT).
H8: Perceived usefulness (PU) positively influences attitude toward use (ATT).
H9: Attitude toward use (ATT) positively influences continued behavioral intention (BI).

2.3.3 Contextual Determinants

Contextual influences represent external conditions that shape technology use beyond individual perception. Facilitating conditions are expected to directly support continued use through operational resources and infrastructure, while governmental support reflects broader institutional mechanisms that may influence intention formation. Accordingly:

H10: Facilitating conditions (FC) positively influence continued behavioral intention (BI).
H11: Governmental support (GS) positively influences continued behavioral intention (BI).

Table 1 summarizes the proposed hypotheses and their theoretical foundations.

Table 1. Constructs and Associated Hypotheses

Hypothesis	Source Construct	Target Construct	Framework
H1	Knowledge (KN)	Persuasion (PS)	IDP
H2	Knowledge (KN)	Perceived ease of use (PEOU)	IDP
H3	Knowledge (KN)	Perceived usefulness (PU)	IDP
H4	Persuasion (PS)	Attitude toward use (ATT)	IDP
H5	Persuasion (PS)	Continued behavioral intention (BI)	IDP
H6	Perceived ease of use (PEOU)	Perceived usefulness (PU)	TAM
H7	Perceived ease of use (PEOU)	Attitude toward use (ATT)	TAM
H8	Perceived usefulness (PU)	Attitude toward use (ATT)	TAM
H9	Attitude toward use (ATT)	Continued behavioral intention (BI)	TAM
H10	Facilitating conditions (FC)	Continued behavioral intention (BI)	Contextual
H11	Governmental support (GS)	Continued behavioral intention (BI)	Contextual

2.4 Research Design

A cross-sectional quantitative design underpins data collection using a structured questionnaire administered to Thai agricultural stakeholders with direct experience in agricultural IoT technologies. The design choice supports the statistical validation of relationships among latent constructs derived from the Technology Acceptance Model (TAM), the Innovation–Decision Process (IDP), and contextual adoption perspectives. Structural equation modeling is adopted as the primary analytical approach due to its capacity to simultaneously evaluate measurement reliability and validity, account for measurement error, and estimate complex structural relationships among constructs.

2.5 Sample and Data Collection

The target population comprises Thai agricultural stakeholders with prior exposure to or experience implementing IoT-based agricultural applications, including automated irrigation systems, environmental monitoring sensors, and digital farm management platforms. The term "stakeholders" is used deliberately because smart farming adoption in Thailand involves not only farm owners and direct users but also agricultural officers, extension personnel, technology service providers, private-sector practitioners, and organizational actors who support implementation. Therefore, the study does not claim to represent farmers exclusively; rather, it captures perceptions within the broader agricultural IoT adoption ecosystem. Data collection was conducted using a standardized questionnaire distributed through both online and offline channels. Offline administration was supported by agricultural extension officers and farming cooperatives, whereas online distribution leveraged smart agriculture networks and social media platforms. Screening questions were used to ensure that participants had direct familiarity with agricultural IoT applications, either through personal use, implementation support, technical operation, advisory roles, or institutional involvement. This mixed-mode approach improved geographical and role-based coverage, particularly across rural and remote areas. Recommended minimum sample size for structural equation modeling exceeds 200 observations [42]. The final dataset comprises 250 valid responses, meeting commonly accepted thresholds for model estimation and statistical power. Ethical approval is obtained prior to data collection, and informed consent is obtained from all participants.

2.6 Measurement Instrument

Data collection is conducted using a structured questionnaire comprising two sections. The first section captures demographic characteristics to contextualize respondent profiles. The second section measures eight latent constructs derived from the proposed framework: knowledge (KN), persuasion (PS), perceived ease of use (PEOU), perceived usefulness (PU), attitude toward use (ATT), continued behavioral intention (BI), facilitating conditions (FC), and governmental support (GS). Measurement items were adapted from established and validated scales, including Davis [23], Rogers [39], and Venkatesh et al. [43], and

subsequently modified to reflect the agricultural IoT context. Construct wording was reviewed to ensure relevance to smart farming applications such as sensor-based monitoring, irrigation automation, and digital farm management. All constructs were operationalized as reflective measures using three to five items per construct. Responses were recorded on a five-point Likert scale ranging from 1 ("strongly disagree") to 5 ("strongly agree"). Item codes, adapted item content, source references, and outer loadings are provided in Supplementary Table S1. Content validity is established through expert evaluation involving three domain specialists in agricultural technology and information systems. Pilot testing involving 30 smart farming practitioners is conducted to assess clarity, wording, and contextual relevance. Feedback from the pilot phase is incorporated to refine the measurement instrument before full-scale data collection. Construct definitions are summarized in Table 2, while detailed measurement items and corresponding factor loadings are provided in the supplementary materials.

Table 2. Construct Definitions

Construct	Definition
Knowledge (KN)	Understanding of IoT functionality and its applications in agriculture.
Persuasion (PS)	Influence of peers and community on acceptance of IoT.
Perceived ease of use (PEOU)	The degree to which IoT systems are perceived as easy to operate.
Perceived usefulness (PU)	The extent to which IoT use is seen as beneficial to farming.
Attitude toward use (ATT)	Users' affective evaluation of using IoT technologies.
Continued behavioral intention (BI)	Intention to continue using and engaging with IoT systems in agricultural operations.
Facilitating conditions (FC)	Availability of infrastructure and technical support for IoT.
Governmental support (GS)	Perceived support from the government in adopting IoT technologies.

Common method bias was mitigated through procedural remedies, including anonymity assurance, neutral wording of questionnaire items, separation of construct blocks, and clarification that there were no right or wrong answers. In addition, post hoc diagnostics were conducted. Harman's single-factor test indicated that the first unrotated factor did not account for a majority of the total variance, and the structural collinearity assessment showed that VIF values remained below the conservative threshold of 3.3. These results suggest that common method variance is unlikely to substantially bias the findings, although the cross-sectional self-report design remains a limitation.

2.7 Data Analysis

A variance-based PLS-SEM approach is applied to evaluate the proposed framework [42]. The first stage focuses on assessing the measurement model, including internal consistency reliability, convergent validity, and discriminant validity. Reliability is examined using Cronbach's alpha and composite reliability (CR), with values above 0.70 indicating acceptable internal consistency [44]. Convergent validity is assessed using average variance extracted (AVE), with a threshold of 0.50 [45]. Discriminant validity is evaluated using the Fornell–Larcker criterion and the heterotrait–monotrait (HTMT) ratio, where values below 0.90 indicate adequate discriminant validity [46]. The second stage evaluates the structural model by estimating path coefficients, t-values, p-values, confidence intervals, effect sizes (f^2), and inner VIF values obtained through bootstrapping with 5,000 resamples. VIF values are examined to assess potential collinearity among predictor constructs. Model explanatory power and predictive relevance are assessed using the coefficient of determination (R^2), effect size (f^2), and Stone–Geisser's Q^2. Model fit is examined using the standardized root mean square residual (SRMR), while acknowledging that SRMR is a diagnostic indicator rather than a sole acceptance criterion in predictive-oriented PLS-SEM. Key evaluation criteria are summarized in Table 3.

Table 3. Model Fit Criteria

Fit Index	Threshold
SRMR	< 0.08 (commonly recommended guideline)
Cronbach's Alpha	≥ 0.70
Composite Reliability (CR)	≥ 0.70
Average Variance Extracted (AVE)	≥ 0.50
Fornell–Larcker Criterion	The square root of AVE exceeds inter-construct correlations
HTMT Ratio	< 0.90
R^2	≥ 0.10 (minimum acceptable level)
Q^2	> 0.00 (predictive relevance)
f^2	≥ 0.02 (small effect size)

Note: Threshold values are based on commonly recommended guidelines in PLS-SEM literature and should be interpreted with caution depending on model context.

3. Results and Discussion

This section presents and interprets the empirical findings derived from the structural equation modeling analysis. Results are discussed in relation to the proposed hypotheses and relevant theoretical perspectives, integrating statistical evidence with prior research to explain agricultural Internet of Things (IoT) adoption and continued use in resource-constrained contexts.

3.1 Respondent Profile and Descriptive Overview

A total of 250 valid responses from Thai agricultural stakeholders with direct experience in or close involvement with agricultural IoT technologies are included in the analysis, as summarized in Table 4. Male participants constitute the majority (95.6%), while the largest age group falls between 45–54 years (48.4%), indicating a mature user base. Educational attainment is relatively high, with most respondents holding at least a bachelor's degree (57.1%), suggesting sufficient capacity to engage with digital technologies. Occupational distribution extends beyond farmers, with substantial representation from government or state enterprises (39.6%) and the private sector (26.4%), as well as business owners and other roles. This profile indicates that the sample represents a mixed group of agricultural IoT stakeholders rather than farmers alone. Many respondents were involved in implementation, advisory, technical support, extension, or organizational decision-making activities related to smart farming. Accordingly, the findings should be interpreted as reflecting stakeholder-based continued use intention within the agricultural IoT ecosystem, not as a population estimate of Thai farmers as a whole.

Table 4. Demographic Profile of Respondents (N = 250)

Variable	Category	Percentage (%)
Gender	Male	95.6
	Female / Other	4.4
Age	Below 25 years	3.0
	25–34 years	12.1
	35–44 years	23.1
	45–54 years	48.4
	55 years and above	13.2
Education Level	Secondary school	5.5
	Vocational diploma (Voc. Cert. / High Voc.)	2.2
	Bachelor's degree	57.1
	Postgraduate degree	35.2
Occupation	Farmer	11.0
	Government/State enterprise employee	39.6
	Private sector employee	26.4
	Business owner	11.0
	Other	12.1

Observed demographic patterns suggest a stakeholder composition aligned with early adoption of smart farming technologies in Thailand, where institutional and public-sector channels play a central role in technology diffusion. This context provides a critical lens for interpreting subsequent behavioral and contextual effects, particularly the influence of external support mechanisms on continued technology use.

3.2 Measurement Model Results

The measurement model is evaluated before structural analysis to ensure adequate reliability and validity of the latent constructs. The assessment focuses on internal consistency reliability, convergent validity, and discriminant validity, following the established PLS-SEM procedure.

3.2.1 Internal Consistency and Convergent Validity

Internal consistency reliability is assessed using Cronbach's alpha and composite reliability (CR). All constructs exceed the recommended threshold of 0.70, indicating satisfactory reliability. Convergent validity is evaluated using average variance extracted (AVE) and indicator loadings. Most constructs achieve AVE values above 0.50, while outer loadings are generally above 0.70, supporting adequate convergent validity and strong indicator reliability. A marginal deviation is observed for persuasion (PS), where AVE falls slightly below the recommended threshold (AVE = 0.482). This construct was retained for three reasons. First, Cronbach's alpha and composite reliability exceed acceptable levels, indicating adequate internal consistency. Second, most indicators show acceptable loadings, while the lower-loading item reflects the social-communication dimension of persuasion that is theoretically central to the Innovation–Decision Process. Third, removing the item would narrow the conceptual domain of persuasion and reduce content validity. Consequently, PS is retained but interpreted cautiously, especially for paths involving behavioral intention. Detailed results, including Cronbach's alpha, composite reliability, AVE, and indicator loadings, are presented in Table 5.

Table 5. Measurement Model Results: Reliability and Convergent Validity

Construct	Cronbach's α	Composite Reliability (CR)	AVE	Loading Range
ATT	0.949	0.961	0.833	0.829 – 0.970
BI	0.956	0.966	0.850	0.898 – 0.945
FC	0.837	0.883	0.601	0.720 – 0.844
GS	0.932	0.949	0.788	0.796 – 0.949
KN	0.937	0.953	0.803	0.806 – 0.956
PEOU	0.919	0.940	0.759	0.780 – 0.947
PS	0.773	0.818	0.482	0.533 – 0.860
PU	0.937	0.952	0.800	0.840 – 0.921

3.2.2 Discriminant Validity

Discriminant validity is evaluated using the Fornell–Larcker criterion. Results show that the square roots of the AVEs for each construct exceed their correlations with other constructs, indicating adequate discriminant validity across the measurement model. Moderate correlations observed among selected constructs (e.g., ATT and BI) remain within acceptable limits and reflect expected theoretical relationships rather than measurement overlap. Detailed results are presented in Table 6.

Table 6. Discriminant Validity Assessment (Fornell–Larcker Criterion)

Construct	ATT	BI	FC	GS	KN	PEOU	PS	PU
ATT	0.913							
BI	0.768	0.922						
FC	0.479	0.565	0.775					
GS	0.372	0.359	0.591	0.888				
KN	0.511	0.554	0.550	0.366	0.896			
PEOU	0.552	0.471	0.583	0.391	0.685	0.871		
PS	0.589	0.495	0.454	0.592	0.467	0.467	0.695	
PU	0.787	0.615	0.578	0.442	0.566	0.704	0.579	0.894

Further assessment of discriminant validity is conducted using the heterotrait–monotrait (HTMT) ratio. All HTMT values remain below the recommended threshold of 0.90, supporting adequate discriminant validity across constructs. The highest HTMT value is observed between attitude toward use (ATT) and perceived usefulness (PU), reflecting a strong conceptual relationship while remaining within acceptable limits. These results confirm that the constructs are empirically distinct despite their theoretical interrelatedness. Detailed HTMT results are presented in Table 7.

Table 7. Discriminant Validity Assessment (HTMT Ratios)

Construct	ATT	BI	FC	GS	KN	PEOU	PS	PU
ATT								
BI	0.805							
FC	0.512	0.600						
GS	0.392	0.371	0.678					
KN	0.536	0.586	0.626	0.389				
PEOU	0.589	0.500	0.657	0.422	0.732			
PS	0.538	0.435	0.576	0.768	0.536	0.478		
PU	0.832	0.647	0.638	0.468	0.596	0.756	0.566	

3.3 Structural Model Results and Hypothesis Testing

Hypothesis testing was conducted using a bootstrapping procedure with 5,000 resamples to evaluate the significance of the proposed structural relationships. Standardized path coefficients (β), t-values, p-values, effect sizes (f^2), and VIF values are reported in Table 8. All reported VIF values remain below the commonly recommended threshold, indicating that collinearity among predictor constructs is not a major concern.

Table 8. Structural Path Coefficients, Collinearity Diagnostics, and Hypothesis Testing Results

Hypothesis	Path	β	t-value	p-value	f^2	Result	VIF	95% CI
H1	KN → PS	0.467	6.820	< 0.001	0.278	Supported	1.000	[0.333, 0.601]
H2	KN → PEOU	0.685	17.934	< 0.001	0.885	Supported	1.000	[0.610, 0.760]
H3	KN → PU	0.157	2.141	0.037	0.027	Supported	1.885	[0.013, 0.301]
H4	PS → ATT	0.203	4.561	< 0.001	0.077	Supported	1.558	[0.116, 0.290]
H5	PS → BI	0.026	0.398	0.637	0.001	Not Supported	1.617	[-0.102, 0.154]
H6	PEOU → PU	0.597	8.051	< 0.001	0.385	Supported	1.885	[0.452, 0.742]
H7	PEOU → ATT	-0.029	0.552	0.553	0.001	Not Supported	2.259	[-0.132, 0.074]
H8	PU → ATT	0.689	12.888	< 0.001	0.570	Supported	2.444	[0.584, 0.794]
H9	ATT → BI	0.640	11.427	< 0.001	0.676	Supported	1.678	[0.530, 0.750]
H10	FC → BI	0.284	4.890	< 0.001	0.129	Supported	1.584	[0.170, 0.398]
H11	GS → BI	-0.062	1.272	0.210	0.006	Not Supported	1.626	[-0.158, 0.034]

Results indicate that several hypothesized relationships are statistically supported. Perceived usefulness (PU) exerts a strong positive effect on attitude toward use (ATT) ($\beta = 0.689$, $t = 12.888$, $p < 0.001$), confirming its central role in shaping users' evaluations of agricultural IoT technologies. Attitude toward use subsequently demonstrates a strong positive effect on continued behavioral intention (BI) ($\beta = 0.640$, $t = 11.427$, $p < 0.001$), reinforcing its critical role in sustained technology adoption. Persuasion (PS) significantly influences attitude ($\beta = 0.203$, $t = 4.561$, $p < 0.001$), indicating that social and evaluative processes contribute to attitude formation. Facilitating conditions (FC) also show a significant positive effect on behavioral intention ($\beta = 0.284$, $t = 4.890$, $p < 0.001$), highlighting the importance of infrastructure and technical support. In contrast, governmental support (GS) does not exhibit a significant direct effect on behavioral intention ($\beta = -0.062$, $t = 1.272$, $p = 0.210$), suggesting a potential gap between policy-level initiatives and user-perceived support. Similarly, persuasion does not significantly influence behavioral intention ($\beta = 0.026$, $t = 0.398$, $p = 0.637$), indicating that its effect is

primarily indirect. Perceived ease of use (PEOU) does not significantly influence attitude (β = -0.029, t = 0.552, p = 0.553), suggesting that usability plays a limited role in post-adoption contexts. However, PEOU significantly influences perceived usefulness (β = 0.597, t = 8.051, p < 0.001), consistent with TAM. Knowledge (KN) significantly influences perceived ease of use (β = 0.685, t = 17.934, p < 0.001), persuasion (β = 0.467, t = 6.820, p < 0.001), and perceived usefulness (β = 0.157, t = 2.141, p = 0.037), confirming its foundational role in shaping early-stage perceptions.

3.4 Model Explanatory Power and Predictive Relevance

Explanatory power is assessed using the coefficient of determination (R^2), representing the proportion of variance explained in each endogenous construct. As shown in Table 9, the model demonstrates strong explanatory capability for the key outcome variables. Attitude toward use (ATT) and behavioral intention (BI) exhibit high R^2 values of 0.646 and 0.643, respectively, indicating that the integrated framework explains a substantial proportion of the variance in users' attitudinal and behavioral intentions toward agricultural IoT adoption.

Table 9. Coefficient of determination (R^2).

Construct	R^2	Adjusted R^2
ATT	0.646	0.642
BI	0.643	0.637
PEOU	0.470	0.467
PS	0.218	0.215
PU	0.509	0.505

Perceived usefulness (PU) and perceived ease of use (PEOU) present moderate explanatory power (R^2 = 0.509 and 0.470), while persuasion (PS) shows a lower yet acceptable level of explained variance (R^2 = 0.218), consistent with its role as an early-stage cognitive construct. Model fit is further evaluated using the standardized root mean square residual (SRMR). The SRMR values are 0.090 for the saturated model and 0.135 for the estimated model, both exceeding the commonly suggested threshold of 0.08. This indicates that the model does not fully meet conventional model-fit criteria. Therefore, the results should be interpreted with caution, and SRMR is treated as a limitation of the study. Accordingly, model interpretation relies on a combination of explanatory and predictive metrics, including R^2 and Q^2, rather than SRMR alone. Predictive relevance is assessed using the blindfolding procedure, which yields the cross-validated redundancy measure (Q^2). A Q^2 value greater than zero indicates predictive capability. As reported in Table 10, all endogenous constructs demonstrate Q^2 values above zero, confirming the model's predictive relevance. Behavioral intention (Q^2 = 0.401) and attitude toward use (Q^2 = 0.356) exhibit strong predictive power, while perceived usefulness and perceived ease of use show moderate predictive relevance. Persuasion, although lower in magnitude, remains meaningful in capturing early-stage evaluative processes within the adoption mechanism. Overall, the combined evidence from R^2 and Q^2 assessments suggests that the integrated TAM–IDP framework provides meaningful explanatory and predictive relevance for key endogenous constructs. However, the elevated SRMR values indicate that the model should be interpreted as a useful but not definitive representation of agricultural IoT adoption. Additional statistics, including effect sizes, indirect effects, item-level measurement diagnostics, and supplementary predictive diagnostics, are provided in Supplementary Tables S1–S4.

Table 10. Predictive relevance (Q^2).

Construct	Q^2 Value
Behavioral intention (BI)	0.401
Attitude toward use (ATT)	0.356
Perceived usefulness (PU)	0.291
Perceived ease of use (PEOU)	0.243
Persuasion (PS)	0.198

Note: Q^2 values greater than zero indicate the model's predictive relevance.

3.5 Integrated Discussion

Findings provide empirical support for the usefulness of the integrated TAM–IDP framework in explaining agricultural IoT adoption. Perceived usefulness (PU) and attitude toward use (ATT) emerge as the most influential determinants of continued behavioral intention (BI), confirming that perceived value remains the primary driver of adoption decisions. This pattern aligns with prior TAM-based studies, which show that functional benefits outweigh other considerations in shaping user acceptance, particularly in task-oriented and outcome-driven environments. The non-significant effect of perceived ease of use (PEOU) on attitude suggests that usability considerations become less salient once users have experience with agricultural IoT technologies. In post-adoption or experience-based contexts, users may evaluate systems less by simplicity and more by whether the technology produces tangible operational benefits such as improved monitoring, reduced labor, or better farm decisions. The significant PEOU → PU path supports this interpretation: ease of use appears to matter indirectly by strengthening perceived usefulness rather than directly shaping attitude.

Integration of knowledge (KN) and persuasion (PS) from the Innovation–Decision Process provides additional explanatory depth by capturing early-stage cognitive dynamics. Knowledge significantly influences perceived ease of use, perceived usefulness, and persuasion, highlighting its foundational role in shaping users' mental models of technology. Persuasion contributes to attitude formation but does not directly influence behavioral intention, indicating that peer communication and evaluative influence may first shape favorable attitudes before becoming behavioral commitment. This finding supports a mediated interpretation of persuasion rather than a simple direct-intention mechanism. Facilitating conditions (FC) have a significant positive effect on behavioral intention, underscoring the roles of infrastructure, training, and technical support in enabling adoption. In contrast, governmental support (GS) does not exhibit a significant direct effect, suggesting a disconnect between policy-level initiatives and users' perceived or experienced support. Several explanations are plausible: policy support may be unevenly visible to users, may operate indirectly through facilitating conditions, or may be perceived as too general to influence day-to-day technology decisions. Future studies should test mediation or moderation mechanisms linking governmental support to more immediate operational enablers. Collectively, the integration of cognitive, behavioral, and contextual dimensions offers a comprehensive explanation of IoT adoption in resource-constrained agricultural environments. Results highlight that successful digital transformation in agriculture requires more than technological functionality; it depends on informed users, effective knowledge dissemination, and operational support systems that translate institutional intent into practical adoption.

4. Limitations and Future Research

Several limitations should be acknowledged. First, the study uses a cross-sectional survey design; therefore, the findings support associative interpretation rather than strong causal claims. Longitudinal research is needed to examine how knowledge, persuasion, attitude, and continued use intention evolve across the full innovation-decision process. Second, the sample represents agricultural IoT stakeholders rather than farmers exclusively. Although this broader stakeholder perspective is appropriate for smart farming ecosystems, it limits the extent to which findings can be generalized to the wider population of Thai farmers. Future studies should compare farmers, extension officers, technology providers, and policy actors as separate groups. Third, all variables were measured using self-reported questionnaire data collected at one point in time. Procedural and statistical checks suggest that common method bias is unlikely to dominate the results, but it cannot be fully eliminated. Future research should incorporate objective usage data, field observations, or multi-source measures. Fourth, the persuasion construct has an AVE value slightly below the recommended threshold, and the SRMR values exceed the common guideline. These issues indicate that the model should be interpreted cautiously and may benefit from further refinement of the measurements. Future studies should test alternative item specifications, additional contextual mediators, and multi-group comparisons across regions and farm types. Finally, governmental support was modeled as a direct predictor of continued use intention. The non-significant result suggests that policy-level support may operate indirectly by facilitating conditions, improving access to training, enhancing perceived affordability, or fostering trust. Future research should examine these mediating pathways and evaluate the effectiveness of specific policy interventions.

5. Conclusions

Determinants associated with agricultural Internet of Things (IoT) adoption were examined through an integrated framework combining the Technology Acceptance Model (TAM), the Innovation–Decision Process (IDP), and contextual enablers, including facilitating conditions and governmental support. Empirical validation based on survey data from 250 Thai agricultural stakeholders, analyzed using partial least squares structural equation modeling (PLS-SEM), provides insight into how cognitive, behavioral, and environmental factors are associated with continued use intention for IoT adoption in smart farming contexts. Findings confirm the continued relevance of TAM, with perceived usefulness and attitude toward use emerging as the most influential drivers of behavioral intention. Incorporation of IDP constructs, particularly knowledge and persuasion, extends existing adoption models by highlighting the importance of early-stage cognitive and evaluative processes that precede attitude formation. Facilitating conditions demonstrate a significant role in enabling adoption, emphasizing the importance of infrastructure availability, technical support, and training in resource-constrained environments. In contrast, governmental support does not exhibit a statistically significant direct effect, suggesting a gap between policy-level initiatives and user-perceived or operational support. From a theoretical perspective, a context-sensitive adoption framework is established that integrates cognitive processes, behavioral beliefs, and environmental enablers to enhance explanatory and predictive capabilities beyond traditional TAM-based approaches. From a practical perspective, results indicate that strategies to promote agricultural IoT adoption should prioritize perceived system value, strengthen user knowledge, and improve accessible support mechanisms rather than relying solely on top-down policy interventions. Overall, the findings provide empirical evidence from a developing-country context and offer a validated, yet cautiously interpreted, framework for future research on smart farming and digital agriculture. Addressing the socio-technical complexity of technology adoption contributes to more effective, inclusive, and sustainable digital transformation in the agricultural sector. Future research may extend the proposed framework using longitudinal designs and cross-country validation to enhance generalizability.

6. Acknowledgments

Grateful appreciation is extended to all participants who contributed to this study for their valuable time, experiences, and insights. Sincere thanks are also extended to agricultural extension officers and local community representatives for facilitating data collection and field access. Further appreciation is given to colleagues and anonymous reviewers for their constructive feedback, which contributed to enhancing the clarity, rigor, and overall quality of this manuscript.

Author Contributions: Conceptualization, S.T.; methodology, S.T.; formal analysis, S.T.; investigation, S.T.; data curation, S.T.; writing—original draft preparation, S.T.; writing—review and editing, S.T., M.W., and N.S.; supervision, N.S.; project administration, N.S.; validation, N.S.; visualization, S.T.; resources, M.W.; conceptual support, M.W. All authors have read and agreed to the published version of the manuscript.

Funding: This research was funded by Mahasarakham Business School, Mahasarakham University, Thailand.

Conflicts of Interest: The authors declare no conflict of interest.

Ethical Approval: The research protocol was approved by the Ethics Committee for Research Involving Human Subjects, Mahasarakham University, Thailand (Approval No. 393-338/2025, approved on 24 June 2025; valid until 23 June 2026). All procedures involving human participants were conducted in accordance with institutional ethical standards. Informed consent was obtained from all participants. Participation was voluntary, and respondents were free to withdraw at any time without penalty.

References

[1] Charania, I. L.; Xinrong. Smart Farming: Agriculture's Shift from a Labor Intensive to Technology Native Industry. *Internet Things* **2020**, *9*, 100142. https://doi.org/10.1016/j.iot.2019.100142

[2] Wolfert, S.; Ge, L.; Verdouw, C.; Bogaardt, M. J. Big Data in Smart Farming—A Review. *Agric. Syst.* **2017**, *153*, 69–80. https://doi.org/10.1016/j.agsy.2017.01.023

[3] Kamilaris, A.; Kartakoullis, A.; Prenafeta-Boldú, F. X. Agri-IoT: A Semantic Framework for Internet of Things-Enabled Smart Farming Applications. In *Proceedings of the 2016 IEEE 3rd World Forum on Internet of Things (WF-IoT)*; IEEE, 2016. https://doi.org/10.1109/WF-IoT.2016.7845467

[4] Digital Economy Promotion Agency. *Thailand Digital Outlook Report 2021*; Digital Economy Promotion Agency: Bangkok, Thailand, 2021.

[5] Koech, R.; Langat, P. Improving Irrigation Water Use Efficiency: A Review of Advances, Challenges and Opportunities in the Australian Context. *Water* **2018**, *10*, 1771. https://doi.org/10.3390/w10121771

[6] Morchid, A.; et al. IoT-Based Smart Irrigation Management System to Enhance Agricultural Water Security Using Embedded Systems, Telemetry Data, and Cloud Computing. *Results Eng.* **2024**, *23*, 102829. https://doi.org/10.1016/j.rineng.2024.102829

[7] Al Mamun, M. R.; et al. IoT-Enabled Solar-Powered Smart Irrigation for Precision Agriculture. *Smart Agric. Technol.* **2025**, *10*, 100773. https://doi.org/10.1016/j.atech.2025.100773

[8] Thameeza; Mohammed Tanzeem, A. IoT Based Smart Irrigation System for Precision Agriculture. *Int. J. Eng. Res. Appl.* **2021**, *11*, 66–69.

[9] Song, Y.; Bi, J.; Wang, X. Design and Implementation of Intelligent Monitoring System for Agricultural Environment in IoT. *Internet Things* **2024**, *25*, 101029. https://doi.org/10.1016/j.iot.2023.101029

[10] Chinedu, P. U.; Isah, Y.; Chinedu, N. B. An Internet of Things (IoT)-Based Smart Agriculture Monitoring System for Enhanced Productivity in a Controlled Farm Environment. *J. Sci. Technol. Educ.* **2022**, *10*, 122–136.

[11] Fatima, S. F.; Ali, S.; Shinde, U. Overview of IoT-Based Agriculture Monitoring System. *Int. J. Innov. Eng. Res. Technol.* **2020**, *7*, 37–40.

[12] Rabak, A.; et al. Sensor System for Precision Agriculture Smart Watering Can. *Results Eng.* **2023**, *19*, 101297. https://doi.org/10.1016/j.rineng.2023.101297

[13] Serin, J.; et al. AI-Driven Smart Farming for Automated Plant Health Monitoring and Nutrient Deficiency Detection. *ASEAN J. Sci. Technol. Rep.* **2026**, *29*, e258175. https://doi.org/10.55164/ajstr.v29i1.258175

[14] Singh, J. P.; et al. Design and Development of a Smart Automated System for Poultry Farm Management Using Internet of Things (IoT). *ASEAN J. Sci. Technol. Rep.* **2026**, *29*, e260601. https://doi.org/10.55164/ajstr.v29i4.260601

[15] Chomanee, J.; et al. An Experimental Set for Studying the Changing State of Matter with Smart Learning Media Displayed through the IoT System for Smart-Lab. *ASEAN J. Sci. Technol. Rep.* **2024**, *27*, 42–49. https://doi.org/10.55164/ajstr.v25i4.247317

[16] Chomanee, J.; et al. Development of an Apparatus for Educational Heat of Reaction in Chemical Laboratory with Digital Thermal Sensor and IoT on Smartphone. *ASEAN J. Sci. Technol. Rep.* **2024**, *27*, 70–78.

[17] Otanasap, N.; Kanchanawongkul, V.; Chalermsuk, C. Design and Development of Saline Infusion Administration System Using IoT. *ASEAN J. Sci. Technol. Rep.* **2024**, *27*, 41–49. https://doi.org/10.55164/ajstr.v25i1.244460

[18] Sangkhiew, N.; et al. A Study of Disruptive Technology Impacts on Industrial Engineering Professionals under the Context of Thailand 4.0. *ASEAN J. Sci. Technol. Rep.* **2024**, *27*, 1–9.

[19] Gzar, D. A.; Mahmood, A. M.; Al-Adilee, M. K. A. Recent Trends of Smart Agricultural Systems Based on Internet of Things Technology: A Survey. *Comput. Electr. Eng.* **2022**, *104*, 108453. https://doi.org/10.1016/j.compeleceng.2022.108453

[20] Rajak, P.; et al. Internet of Things and Smart Sensors in Agriculture: Scopes and Challenges. *J. Agric. Food Res.* **2023**, *14*, 100776. https://doi.org/10.1016/j.jafr.2023.100776

[21] Zhang, Q.-Y.; Zhang, T.-T. Introduction to the System of Agricultural Internet of Things. In *Design, Manufacturing and Mechatronics*; pp 548–557. https://doi.org/10.1142/9789814730518_0066

[22] Jabeen, M.; Ishaq, K. Adoption of Internet of Things in Telecommunications: An Emerging Market Case. *Int. J. Innov. Technol. Manage.* **2024**, *21*, 2450020. https://doi.org/10.1142/S0219877024500202

[23] Davis, F. D. Perceived Usefulness, Perceived Ease of Use, and User Acceptance of Information Technology. *MIS Q.* **1989**, *13*, 319–340. https://doi.org/10.2307/249008

[24] Duang-Ek-Anong, S.; Pibulcharoensit, S.; Phongsatha, T. Technology Readiness for Internet of Things (IoT) Adoption in Smart Farming in Thailand. *Int. J. Simul. Syst. Sci. Technol.* **2019**. https://doi.org/10.5013/IJSSST.a.20.05.12

[25] Thomas, R. J.; et al. Development of a Scale to Measure Technology Acceptance in Smart Agriculture. *arXiv* **2022**, arXiv:2203.15423.

[26] Alzahrani, A. Analysis of the Technology Acceptance Model TAM in Understanding Faculty's Behavioral Intention to Use Internet of Things IOT. *Int. J. Educ. Res. Innov.* **2023**, 153–169. https://doi.org/10.46661/ijeri.7461

[27] Mishra, N.; et al. Technology in Farming: Unleashing Farmers' Behavioral Intention for the Adoption of Agriculture 5.0. *PLoS One* **2024**, *19*, e0308883. https://doi.org/10.1371/journal.pone.0308883

[28] Okai, G.; Agangiba, W.; Agangiba, M. Assessment of Farmers' Acceptance of Intelligent Agriculture System Using Technology Acceptance Model. *Int. J. Comput. Appl.* **2024**, *186*, 16–22. https://doi.org/10.5120/ijca2024923953

[29] Rodzoan, M. Smart Farming: Integrating IoT and UAV Technologies for Precision Agriculture through the Lens of Technology Acceptance and the UTAUT2 Model. *Pak. J. Life Soc. Sci.* **2024**, *22*. https://doi.org/10.57239/PJLSS-2024-22.2.00468

[30] Li, L.; et al. The Influence Mechanism Analysis on the Farmers' Intention to Adopt Internet of Things Based on UTAUT-TOE Model. *Sci. Rep.* **2024**, *14*, 15016. https://doi.org/10.1038/s41598-024-65415-4

[31] Bahari, M.; et al. Driving Agricultural Transformation: Unraveling Key Factors Shaping IoT Adoption in Smart Farming with Empirical Insights. *Sustainability* **2024**, *16*, 2129. https://doi.org/10.3390/su16052129

[32] Jaroenwanit, P.; et al. Risk Management in the Adoption of Smart Farming Technologies by Rural Farmers. *Uncertain Supply Chain Manage.* **2023**, *11*, 533–546. https://doi.org/10.5267/j.uscm.2023.2.011.

[33] Dibbern, T.; Romani, L. A. S.; Massruhá, S. M. F. S. Main Drivers and Barriers to the Adoption of Digital Agriculture Technologies. *Smart Agric. Technol.* **2024**, *8*, 100459. https://doi.org/10.1016/j.atech.2024.100459

[34] Far, S. T.; Rezaei-Moghaddam, K. Impacts of the Precision Agricultural Technologies in Iran: An Analysis of Experts' Perception and Their Determinants. *Inf. Process. Agric.* **2018**, *5*, 173–184. https://doi.org/10.1016/j.inpa.2017.09.001

[35] Zhang, X.; et al. Acceptance of New Agricultural Technology among Small Rural Farmers. *Humanit. Soc. Sci. Commun.* **2024**, *11*, 1641. https://doi.org/10.1057/s41599-024-04163-2

[36] Okai, G.; et al. Evaluation of Rice Farmers' Acceptance of a Knowledge Management System Using the Technology Acceptance Model. *Int. J. Comput. Appl.* **2025**, *186*, 45–53. https://doi.org/10.5120/ijca2025924744

[37] Zhahir, A.; et al. Smart Farming Adoption—A Scoping Review. *Konstelasi: Konvergensi Teknol. Sist. Inf.* **2024**, *4*, 14–23. https://doi.org/10.24002/konstelasi.v4i1.9257

[38] Venkatesh, V.; Bala, H. Technology Acceptance Model 3 and a Research Agenda on Interventions. *Decis. Sci.* **2008**, *39*, 273–315. https://doi.org/10.1111/j.1540-5915.2008.00192.x

[39] Rogers, E. M. *Diffusion of Innovations*, 3rd ed.; Free Press: New York, NY, 1983.

[40] Food and Agriculture Organization of the United Nations. *In Brief to The State of Food and Agriculture 2020: Overcoming Water Challenges in Agriculture*; FAO: Rome, Italy, 2020.

[41] Li, L.; et al. Investigating the Intention and Behavior of Vegetable Farmers to Adopt IoT Technology: Survey-Based Evidence from China. *Front. Sustain. Food Syst.* **2024**, *8*. https://doi.org/10.3389/fsufs.2024.1340874

[42] Hair, J. F.; Hult, G. T. M.; Ringle, C. M.; Sarstedt, M. *Partial Least Squares Structural Equation Modeling (PLS-SEM) Using R*; SAGE Publications: Thousand Oaks, CA, 2019. https://doi.org/10.3926/oss.37

[43] Venkatesh, V. Determinants of Perceived Ease of Use: Integrating Control, Intrinsic Motivation, and Emotion into the Technology Acceptance Model. *Inf. Syst. Res.* **2000**, *11*, 342–365. https://doi.org/10.1287/isre.11.4.342.11872

[44] Cronbach, L. J. Coefficient Alpha and the Internal Structure of Tests. *Psychometrika* **1951**, *16*, 297–334. https://doi.org/10.1007/BF02310555

[45] Fornell, C.; Larcker, D. F. Evaluating Structural Equation Models with Unobservable Variables and Measurement Error. *J. Mark. Res.* **1981**, *18*, 39–50. https://doi.org/10.2307/3151312

[46] Henseler, J.; Ringle, C. M.; Sarstedt, M. A New Criterion for Assessing Discriminant Validity in Variance-Based Structural Equation Modeling. *J. Acad. Mark. Sci.* **2015**, *43*, 115–135. https://doi.org/10.1007/s11747-014-0403-8

Supplementary Materials

Supplementary Table S1. Measurement items, sources, and outer loadings

Item	Construct	Adapted measurement item	Source	Loading
KN1	Knowledge	I understand the basic functions of IoT systems used in agriculture.	Rogers [39]	0.806
KN2	Knowledge	I am aware of how sensors and connected devices can support farm operations.	Rogers [39]	0.882
KN3	Knowledge	I understand the benefits and limitations of agricultural IoT applications.	Rogers [39]	0.956
KN4	Knowledge	I can explain how IoT data can be used for farm decision-making.	Rogers [39]	0.931
PS1	Persuasion	People in my agricultural network encourage the use of IoT technologies.	Rogers [39]	0.533
PS2	Persuasion	Opinions from peers or communities influence my evaluation of agricultural IoT.	Rogers [39]	0.681
PS3	Persuasion	Agricultural IoT is perceived as relevant to improving farm practices.	Rogers [39]	0.860
PS4	Persuasion	Communication and demonstrations make agricultural IoT more convincing.	Rogers [39]	0.748
PEOU1	Perceived ease of use	Learning to operate agricultural IoT systems is easy for me.	Davis [23]; Venkatesh [43]	0.780
PEOU2	Perceived ease of use	Interacting with agricultural IoT systems is clear and understandable.	Davis [23]; Venkatesh [43]	0.865
PEOU3	Perceived ease of use	I find agricultural IoT systems easy to use in farm-related tasks.	Davis [23]; Venkatesh [43]	0.947
PEOU4	Perceived ease of use	It is easy to become proficient with agricultural IoT systems.	Davis [23]; Venkatesh [43]	0.882
PU1	Perceived usefulness	Using agricultural IoT improves the effectiveness of farm management.	Davis [23]	0.840
PU2	Perceived usefulness	Agricultural IoT helps improve productivity and resource efficiency.	Davis [23]	0.901
PU3	Perceived usefulness	Agricultural IoT supports better monitoring and decision-making.	Davis [23]	0.921

Supplementary Table S1. Measurement items, sources, and outer loadings. (continued)

Item	Construct	Adapted measurement item	Source	Loading
PU4	Perceived usefulness	Overall, agricultural IoT is useful for farming operations.	Davis [23]	0.912
ATT1	Attitude toward use	Using agricultural IoT is a good idea for modern farming.	Davis [23]	0.829
ATT2	Attitude toward use	I have a positive attitude toward the use of agricultural IoT technologies.	Davis [23]	0.902
ATT3	Attitude toward use	Using agricultural IoT is beneficial for agricultural work.	Davis [23]	0.970
ATT4	Attitude toward use	I support the use of IoT technologies in farming.	Davis [23]	0.942
BI1	Continued use intention	I intend to continue using or supporting agricultural IoT technologies.	Venkatesh et al. [43]	0.898
BI2	Continued use intention	I plan to use or promote agricultural IoT in future agricultural activities.	Venkatesh et al. [43]	0.924
BI3	Continued use intention	I expect to remain engaged with agricultural IoT systems.	Venkatesh et al. [43]	0.945
BI4	Continued use intention	I would recommend continued use of agricultural IoT technologies.	Venkatesh et al. [43]	0.918
FC1	Facilitating conditions	Necessary infrastructure is available to support agricultural IoT use.	Venkatesh et al. [43]	0.720
FC2	Facilitating conditions	Technical support is available when using agricultural IoT systems.	Venkatesh et al. [43]	0.801
FC3	Facilitating conditions	Training or guidance is available for agricultural IoT operations.	Venkatesh et al. [43]	0.844
FC4	Facilitating conditions	Resources needed for agricultural IoT use are reasonably accessible.	Venkatesh et al. [43]	0.732
GS1	Governmental support	Government policies support the adoption of agricultural IoT technologies.	Li et al. [41]	0.796
GS2	Governmental support	Government agencies provide useful information about smart farming.	Li et al. [41]	0.887
GS3	Governmental support	Government programs help reduce barriers to agricultural IoT adoption.	Li et al. [41]	0.949
GS4	Governmental support	Public support mechanisms encourage the implementation of agricultural IoT.	Li et al. [41]	0.912

Supplementary Table S2. Effect size (f^2) statistics

This table reports the effect size (f^2) values for all structural relationships in the proposed model. Effect sizes reflect the relative contribution of each exogenous construct to its corresponding endogenous construct. According to Hair et al. [42], f^2 values of 0.02, 0.15, and 0.35 indicate small, medium, and large effects, respectively.

Exogenous Construct	Endogenous Construct	f^2 Value	Effect Magnitude
PEOU	ATT	0.001	Negligible
PS	ATT	0.077	Small
PU	ATT	0.570	Large
ATT	BI	0.676	Large
FC	BI	0.129	Small–Medium
GS	BI	0.006	Negligible
PS	BI	0.001	Negligible
KN	PEOU	0.885	Large
KN	PS	0.278	Medium
KN	PU	0.027	Small
PEOU	PU	0.385	Large

Note: Interpretation of effect sizes follows Hair et al. (2019): $f^2 \geq 0.02$ (small), ≥ 0.15 (medium), and ≥ 0.35 (large).

Supplementary Table S3. Indirect effects and mediation analysis

This table presents the indirect effects among constructs to examine mediation mechanisms in the proposed model. Indirect effects were estimated using a bootstrapping procedure with 5,000 resamples. Statistical significance of the indirect paths provides evidence for the presence and strength of mediation relationships among cognitive, behavioral, and contextual constructs.

Indirect Path	Indirect Effect (β)	t-value	p-value	Mediation Type	Result	95% CI
KN → PEOU → PU	0.409	6.85	<0.001	Partial	Significant	[0.292, 0.526]
KN → PU → ATT	0.108	2.03	0.042	Partial	Significant	[0.004, 0.212]
PU → ATT → BI	0.441	9.77	<0.001	Partial	Significant	[0.353, 0.529]
PS → ATT → BI	0.130	2.98	0.003	Full	Significant	[0.044, 0.216]
KN → PS → ATT	0.095	2.76	0.006	Partial	Significant	[0.028, 0.162]

Note: Indirect effects were evaluated using bootstrapping (5,000 resamples). Significance is determined at $p < 0.05$. Mediation type is classified based on the significance of direct and indirect effects.

Supplementary Table S4. Predictive relevance diagnostics for endogenous constructs.

This table summarizes predictive relevance diagnostics for endogenous constructs based on Q^2 values. These indicators complement the explanatory power (R^2) and predictive relevance results reported in the main text (Tables 9 and 10).

Construct	Q^2 Value	Predictive Strength	Interpretation
BI	0.401	High	Strong predictive relevance
ATT	0.356	High	Strong predictive relevance
PU	0.291	Moderate	Moderate predictive relevance
PEOU	0.243	Moderate	Moderate predictive relevance
PS	0.198	Moderate	Moderate predictive relevance

Note: Q^2 values greater than zero indicate predictive relevance. Values of approximately 0.02, 0.15, and 0.35 suggest small, medium, and large predictive relevance, respectively.

ASEAN
Journal of Scientific and Technological Reports
Online ISSN:2773-8752

Research article

Genetic Relationship Assessment of Micropropagated *Nymphaea colorata* Peter Seedlings using HAT-RAPD

Itsaraphong Khaenthong[1, 2], Theerachai Thanananta[2], and Narumol Thanananta[3*]

[1] Division of Central Administration, Office of the President, Rajamangala University of Technology Thanyaburi, Pathum Thani, 12110, Thailand; https://orcid.org/0000-0003-2307-577X
[2] Faculty of Science and Technology, Thammasat University, Pathum Thani, 12120, Thailand
[3] Faculty of Science and Technology, Valaya Alongkorn Rajabhat University Under The Royal Patronage, Pathum Thani, 13180, Thailand
[*] Correspondence: narumol@vru.ac.th

Citation:
Khaenthong, I.; Thanananta, T.; Thanananata, N. Genetic relationship assessment of micropropagated *Nymphaea colorata* Peter seedlings using HAT-RAPD. *ASEAN J. Sci. Tech. Report.* **2026**, *29*(7), e262883. https://doi.org/10.55164/ajstr.v29i7.262883

Article history:
Received: December 19, 2025
Revised: May 10, 2026
Accepted: May 16, 2026
Available online: June 14, 2026

Publisher's Note:
This article is published and distributed under the terms of the Thaksin University.

Abstract: *Nymphaea colorata* Peter and its natural hybrids are typical African waterlily cultivars with beautiful, blue-flowered shading, which were precisely selected to be subjects in this study. We have proposed to assess the genetic relationships and variability of *in vitro* seedlings derived from cross pollination of three *N. colorata* cultivars. The surface-sterilized mature seeds were cultured on half Murashige and Skoog's (1/2MS) semi-solid medium supplemented with 1.5% (w/v) sucrose and 1.0 mg/L 6- (N^6)-benzylaminopurine (6-BAP). After 4 weeks of culture, leafy-shooted seedlings (microgreens) were observed in all cultivars. For *ex situ* conservation and certain germplasm utilization, it is necessary to confirm that true-to-type waterlily species, wildtype and hybrid cultivars, are identified by their genetic backgrounds and genotyping. Thus, high-temperature random amplified polymorphic DNA (HAT-RAPD) markers were applied to examine genetic relationships among *in vitro* cultured seedlings compared with their field grown seed donor plants. Fourteen random primers were screened and selected from seventy-two universal primers for polymerase chain reaction (PCR) amplification and DNA fingerprinting. Genetic distances were represented as similarity coefficients ranging from 0.64 to 0.94 and then classified into two main clusters : the parental plant populations and their next generation populations. Therefore, HAT-RAPD might be effective for analyzing genetic relationships and variability in these waterlily cultivars. These scientific findings will support further conservation, breeding, genetic engineering and production of waterlily germplasm.

Keywords: *Nymphaea*; micropropagation; genetic relationship; HAT-RAPD

1. Introduction

Waterlilies are commonly known and called as 'Bua Sai' (in Thai), they are frequently represented to be the iconic queen of aquatic plants and aquarium landscapes, which includes an approximately 40 to 50 waterlily species and are the largest group in genus *Nymphaea* L., family Nymphaeaceae, followed by about discovered 800 waterlily species belonging to the order Nymphaeales [1, 2, 4, 7, 8, 9, 14, 15, 16, 17, 24, 25, 29, 31, 35]. Subgenus *Bachyceras* is recognized to various tropical day-blooming waterlilies, which are described as blooming time starting from 6.00 a.m. – 2.00 p.m. in each circadian rhythm. They are normally used for living plant collection, water gardening, traditional propagation, and

breeding [7, 8, 22, 25, 28, 29, 30, 35]. Members of this subgenus are considered diverse in both phenotypic and genotypic traits [3, 30]. Due to their pan-, core-, and niche-wide distribution, they are widely distributed and have adapted to propagate in several world regions, except Antarctica, under both hot and cold extreme conditions [20, 28, 29, 30, 32, 34]. However, different ecosystems, habitat fragmentation, and urbanization also affect their botanical characteristics and genetic backgrounds, both directly and indirectly. Likewise, *Nymphaea colorala* Peter (Subgenus *Bachyceras*, Genus *Nymphaea* L., Family Nymphaeaceae), a tropical day-blooming waterlily with floral uniqueness characteristics and notably blue flowered bloomer, is widely distributed from East Africa to the other tropical zones, which is usually used as a plant model in waterlily research [1, 5, 6, 10, 11, 18, 29, 30, 32, 33]. The niche conservation of native, exotic, and alien waterlily species has been investigated in numerous experiments and studies, thereby fostering species diversification in this group. In addition to *in situ* and *ex situ* conservation, *N. colorata* and its hybrids, including natural and artificial hybrid lines/cultivars, are chosen as plant models and plant materials for developing precision biotechnologies, especially mass-propagation and ornamental crop production systems, germplasm preservation, and breeding programs. For instance, *Nymphaea* 'Chalong Khwan' or *Nymphaea* 'King of Siam', an artificial waterlily hybrid with its commercially valuable traits of amaranth-flowered flowers, which was created by outcrossing between *Nymphaea* 'Larpprasert' and *Nymphaea colorata*. This waterlily hybrid cultivar was officially registered to the International Waterlily and Water Gardening Society (IWGS) by Thai breeder Chaiyaphon Thamasuwan [1, 7, 13, 18]. Moreover, the natural hybrids of *N. colorata* are also required for hybridization, varietal improvement, and genetic manipulation. Though the conservation and utilization of the waterlily genetic resource are necessary for understanding, they are essential for reliable, sustainable biological resource management within the ecosystem. In the context of novel agricultural biotechnologies, precision procedures are important for adaptive responses and innovation in the face of climate change. Thus, we aimed to develop suitable molecular markers for germplasm detection and genetic identification of *N. colorata* and its natural hybrids, which were tested in both parental plants and *in vitro* seedlings, and to assess the genetic relationships of these vulnerable waterlilies using HAT-RAPD markers.

2. Materials and Methods

2.1 Plant material preparation and *in vitro* seed culture

Mature seeds of three *N. colorata* cultivars obtained from outcrosses of the first day-bloomers as maternal (seed) plants with the second and third day-blooming flowers, which were from the same cultivar as paternal (pollen) plants, which caused from the protogynous phenomena (data were shown in figure 1A-F). After waterlily germplasm sampling, seed samples were used as explants and then disinfected with suitable sterilization protocols. Surface-sterilized seeds were cultured on half Murashige and Skoog's (1/2MS) semi-solid medium supplemented with 1.5% (w/v) sucrose and 1.0 mg/L 6- (N^6)-benzylaminopurine (6-BAP) for primary *in vitro* seed culture establishment. The results showed that germination and survival percentages of *in vitro* seedlings ranged approximately 30–45% after 4 weeks of culture. 1-2 cm-long, leafy-shooted seedlings representing microgreens were selected to test the genetic background and identify them, compared with their field grown seed donor plants. *In vitro* propagated seedlings were continuously maintained in standard tissue culture conditions until which were finally transplanted to the nursery [26, 27].

Table 1. List of twelve *N. colorata* accessions used in this study.

Sample No.	Sample Name: the concise details†	Sample Code
1	*Nymphaea colorata* Peter (a blue-petal cultivar; wildtype): Field-grown seed donor plant/wildtype #1	NCB1_WT
2	*Nymphaea colorata* Peter (a blue-petal cultivar): Field-grown seed donor plant/wildtype #2	NCB2
3	*Nymphaea colorata* Peter (a light purple-petal cultivar): Field-grown seed donor plant/natural waterlily hybrid line No. 1 #1	NCL1
4	*Nymphaea colorata* Peter (a light purple-petal cultivar): Field-grown seed donor plant/natural waterlily hybrid line No. 1 #2	NCL2

Table 1. List of twelve *N. colorata* accessions used in this study (continued).

Sample No.	Sample Name: the concise details[†]	Sample Code
5	*Nymphaea colorata* Peter (a purple-petal cultivar): Field-grown seed donor plant/natural waterlily hybrid line No. 2 #1	NCP1
6	*Nymphaea colorata* Peter (a purple-petal cultivar): Field-grown seed donor plant/natural waterlily hybrid line No. 2 #2	NCP2
7	*Nymphaea colorata* Peter (a blue-petal cultivar): *In vitro* grown seedling/wildtype #1	NCB_IS1
8	*Nymphaea colorata* Peter (a blue-petal cultivar): *In vitro* grown seedling/wildtype #2	NCB_IS2
9	*Nymphaea colorata* Peter (a light purple-petal cultivar): *In vitro* grown seedling/natural waterlily hybrid line No. 1 #1	NCL_IS1
10	*Nymphaea colorata* Peter (a light purple-petal cultivar): *In vitro* grown seedling/natural waterlily hybrid line No. 1 #2	NCL_IS2
11	*Nymphaea colorata* Peter (a purple-petal cultivar): *In vitro* grown seedling/natural waterlily hybrid line No. 2 #1	NCP_IS1
12	*Nymphaea colorata* Peter (a purple-petal cultivar): *In vitro* grown seedling/natural waterlily hybrid line No. 2 #2	NCP_IS2

[†] 12 accessions tested: the individually randomized plant samples were collected and selected from field grown seed donor plants and *in vitro* grown seedlings, which covered all *N. colorata* and its natural hybrids.

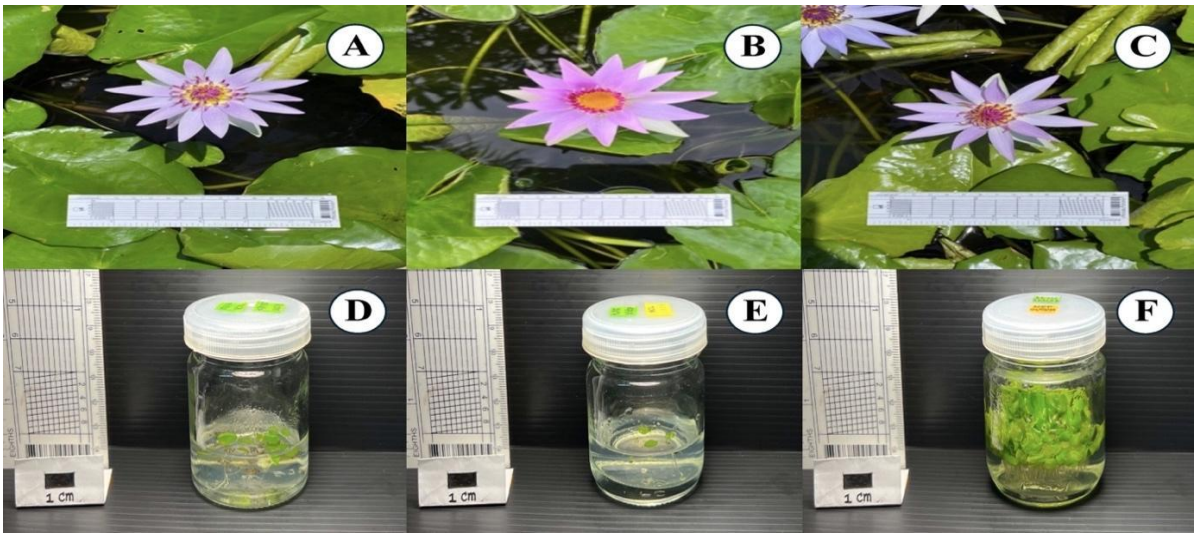


Figure 1. This is a picture of the (A) field grown seed donor plant of *N. colorata* (a blue-petal cultivar; wildtype), (B) field grown seed donor plant of *N. colorata* (a light purple-petal cultivar; natural waterlily hybrid line no. 1), (C) field grown seed donor plant of *N. colorata* (a purple-petal cultivar; natural waterlily hybrid line no. 2), (D) *in vitro* cultured seedlings of *N. colorata* (a blue-petal cultivar; wildtype), (E) *in vitro* cultured seedlings of *N. colorata* (a light purple-petal cultivar; natural waterlily hybrid line no. 1), and (F) *in vitro* cultured seedlings of *N. colorata* (a purple-petal cultivar; natural waterlily hybrid line no. 2). White ruler bar = 14 cm., Black bar = 1 cm.

2.2 DNA extraction and quantification

Fresh leaves were collected from vigorous seed donor plants that were planted and grown in the fields of Lotus and Waterlily Museum, Division of Central Administration, Office of the President, Rajamangala University of Technology Thanyaburi (RMUTT) (data were shown in figure 1A-C and table 1). Three cultivars of *N. colorata* were chosen to examine in this experiment, especially wildtype (a blue-petal cultivar), natural hybrid line no. 1 (a light purple-petal cultivar), and natural hybrid line no. 2 (a purple-petal cultivar). Healthy leaves were picked from the fields before pre-sterilization with mild detergent, then washed three times with running tap water. Fresh leaf samples were stored at -20 °C in a refrigerator before use. The Cetyltrimethyl ammonium bromide (CTAB) extraction used in this experiment was modified and then followed by the traditional CTAB extraction procedure that reported by Doyle and Doyle in 1987 [12, 16, 24, 25]. Genomic DNA (gDNA) pellets were dissolved in 500 µl TE buffer and stored at -20 °C. For *in vitro* cultured explant samples, about 100 mg of six-month-old *in vitro N. colorata* seedlings and its natural hybrids were also gently prepared for gDNA extraction using the modified CTAB extraction method as above (data showed in figure 1D-F and table 1) [12, 16, 24, 25]. The quantity of all stock gDNA samples was examined by spectrophotometer at the wavelength of optical density (OD) at 260 and 280 nanometer (nm), which were used to evaluate the amount of extracted gDNA samples, DNA concentration, and purification, respectively. At the same time, gDNA samples were also used for quality control by 0.8% (w/v) smart agarose gel electrophoresis and then visualized under UV trans-illumination.

2.3 Genetic analysis by high annealing temperature-random amplified polymorphic DNA (HAT-RAPD)

Polymerase chain reaction (PCR-based) technique was studied by using HAT-RAPD, which has been applied to investigate genetic relationship and identification in various *Nymphaea* species and their hybrids, and then reported by Suksakul et al., 2018 [16]. Seventy-two primers containing 12 nucleotides were also tested and produced DNA bands on the agarose gel. PCR reactions of the HAT-RAPD technique were applied and conducted in a BIO-RAD T100™ Thermal Cycler. A total reaction mixture was prepared for each PCR reaction, adjusted to 30 µl, containing about 100 ng/µl gDNA template. PCR amplification conditions were performed by involving in initial denaturation of 1 cycle of 94 °C for 3 minutes (the main step no. 1), following by the main step no. 2 contained 40 cycles of 94 °C for 45 seconds (Denaturation), 46 °C for 45 seconds (Annealing), 72 °C for 1 minute (Extension) and then a final cycle in the main step no. 3: 1 cycle of 72 °C for 5 minutes (Final Extension) [16]. After the thermal cycling procedure was finished, the amplified PCR products were stored at 4 °C overnight before the gel electrophoresis. PCR amplified products were electrophoresed on 1.5% (w/v) smart agarose gel that was incubated in 1X TAE (Tris-Acetate-EDTA) Buffer Solution at 100 V (Voltage), with running time (~ 30 minutes), depending on PCR product size, and stained with 6X ready-to-use (RTU) loading dye solution. The different stained DNA sizes of PCR amplicons were verified against a volume of 10 µl 0.1% (µg/µl) VC 100 bp Plus ready-to-use (RTU) DNA ladder molecular size standard (Vivantis Technologies Sdn Bhd, Malaysia), which was used as a DNA marker, compared to the negative control lane (deionized water, DI). The electrophoresed gels were stained with 0.1% (w/v) ethidium bromide (EtBr) solution for 10 minutes before gel documentation. The reproducibly obtained DNA fragments were repeated at least three times. Clearly, the resultant bands were counted and analyzed using a binary coding system (1/0). For all genotypes, amplified banding results were scored using a 1/0 coding method, where '1' indicated the presence of a DNA band and '0' its absence at the loci used for each HAT-RAPD primer. Numeric data generated from each primer were recorded and then compared between samples using the Numerical Taxonomy System Package (NTSYS-pc, version 2.01e) (Applied Biostatistics Inc., New York, USA) [16, 24, 25]. Leading to a genetic similarity index and phylogenetic dendrogram, the SimQual and SAHN modules were also used to compute the similarity coefficient, as the resultant similarity matrix was utilized for constructing an accurate phylogenetic dendrogram throughout an unweighted pair group method with arithmetic mean (UPGMA)-based technique (Applied Biostatistics Inc., New York, USA) [16, 24, 25].

3. Results and Discussion

Regarding to the micropropagated seedlings grown *in vitro*, no abnormal morphological characteristics or malformed leafy seedlings were observed; however, germination and growth performance showed significant differences among *N. colorata* cultivars and treatments. Fourteen primers containing twelve nucleotides were also screened and then selected that these HAT-RAPD markers for PCR product amplification and DNA fingerprinting on the 1.5% (w/v) smart agarose gel, especially primer A32, B22, B23, B27, B32, C21, C24, C28, C29, D23, E24, E32, F23, and F31 (data were shown in figure 2 and table 2). Depending on the HAT-RAPD technique, twenty-fifth waterlily accessions contained in both tropical and hardy waterlily hybrids have also been demonstrated by precisely selected seventeen primers out of seventy-two primers (i.e. A22, A24, A27, A29, A30, B21, C28, C29, C31, D23, D31, E22, E24, E32, F23, F25, and F31), which produced the total clearly scored of 226 bands (sized in ~ 200-3,000 bp). It gave a total polymorphic loci percentage of 98.67%. While the genetic similarities among all accessions ranged from 0.47 to 0.88, they were used to infer their genetic relationships with three major groups [16]. Therefore, genetic variation assessment and analysis could be investigated to understand the genetic basis of various biological phenomena in plants [21]. In particular, true-to-type plantlets grown *in vitro* have also been shown to exhibit clonal fidelity in tissue-cultured plants using DNA-based markers, such as ISSR, RAPD, and HAT-RAPD, which were investigated in *Aloe vera* and *Hedychium longicornutum* Griff. ex Baker [21, 26]. Interestingly, some HAT-RAPD markers, including primer E32, could be used to characterize *in vitro* regenerated banana plantlets (*Musa* spp., AAA genome) induced to mutate using gamma ray radiation [25]. From our molecular marker detection, the DNA amplicons showed clear bands, which were counted and scored in numeric results (data showed in Table 2). Numeric data from each effective primer yielded a total of 240 distinct DNA bands, with an average frequency of 17.14 bands per primer, spanning approximately 150-3000 base pairs (bps) (data showed in Table 2). The genetic distance matrix obtained for individual samples of three cultivars/populations according to the field grown seed donor plants and their seedlings grown *in vitro* showed that the genetic distance among twelve genotypes ranged from moderate to high values of 0.64 to 0.94, with an average of 0.82 (data were shown in figures 3-4). Hence, the polymorphic loci obtained from HAT-RAPD genotyping of appropriate markers were analyzed for total polymorphic loci percentage (73.33%) and then compared for genetic similarities between the samples using the program NTSYS-pc (data showed in figures 2-4 and table 2). From the accurately generated dendrogram, each sample was constructed and classified into two main clusters, especially cluster no. 1: field-grown seed donor plants and cluster no. 2: *in vitro* grown seedlings, respectively. Each clustering group revealed genetic relationships within and between *N. colorata* cultivars (data were shown in Figures 3 and 4). Whilst the genetic similarities within the same cultivars according to blue-petal cultivars versus (vs.) blue-petal cultivars, light-purple petal cultivars vs. light-purple petal cultivars, and purple-petal cultivars vs. purple-petal cultivars showed closer genetic relationship than another cultivar, except in some individuals of cluster no. 2 that showed the genetic variation during the outcrossing. Leading to some blue-petal *N. colorata* individual samples being particularly separated as another genotypic trait with different genetic inheritances, caused by occurrences and possibilities in both natural and artificial hybridization, apart from somaclonal variation in *in vitro* grown seedlings and plantlets. However, the specifically designed DNA-based markers and advanced high-throughput data derived from the multiple omics technologies are still more importantly applied to characterize and double-check in the genetic relationship assessment and variability of the living plants and certain germplasms of *N. colorata* than the one-trial or one-dimensional laboratory practice [1, 21, 22, 23, 24]. Using primer C24 of HAT-RAPD yielded a unique monomorphic set of PCR products and the lowest percentage of polymorphic loci (60%) among the others (data showed in Figure 2A-D and Table 2). By contrast, primer C21 not only yielded a monomorphic set of amplified PCR products, but also generated different alleles within the same locus, as shown in the alliant alleles, and this occurred in some individual plant samples. They are caused by genetic manipulation, for instance, gene introgression, nucleotide insertion, nucleotide deletion, nucleotide duplication, and so on (data were shown in Figure 2A-D and Table 2). Previous studies have confirmed the genetic uniformity and clonal fidelity of micropropagated *Aloe* plants derived from shoot-tip explants [21]. On the other hand, RAPD markers also showed consistent genetic uniformity and maintained genetic fidelity in the field-grown mother plants and *in vitro*-propagated plantlets of *H. longicornutum* [21].

Application of some efficient molecular markers in the tropical and hardy waterlilies, the selected DNA-based markers of ISSR, RAPD, PCR-RFLPs, HAT-RAPD and SCoT techniques and additive nuclear internal transcribed spacer (nrITS sized in approximately 900 bps) characterized sequences containing the partial regions of *18S*, *ITS1*, *5.8S*, *ITS2*, and *26S* rRNA genes were also used to identify and classified the interspecific, intersubgeneric (ISG) waterlily hybrid cultivars and several waterlily species [3, 4, 6, 7, 8, 15, 16, 17, 19, 21, 22, 23, 24, 25, 28, 29, 30]. Thus, we have aimed to assess and identify the genetic relationship and variation among the field grown seed donor or mother plants and *in vitro* grown seedlings by using reasonable molecular markers that will not be an arduous procedure for confirming the genetic relationship and authentication of *N. colorata* and its natural hybrids, but also used to characterize its artificial hybrids and mutant lines/cultivars in further studies.

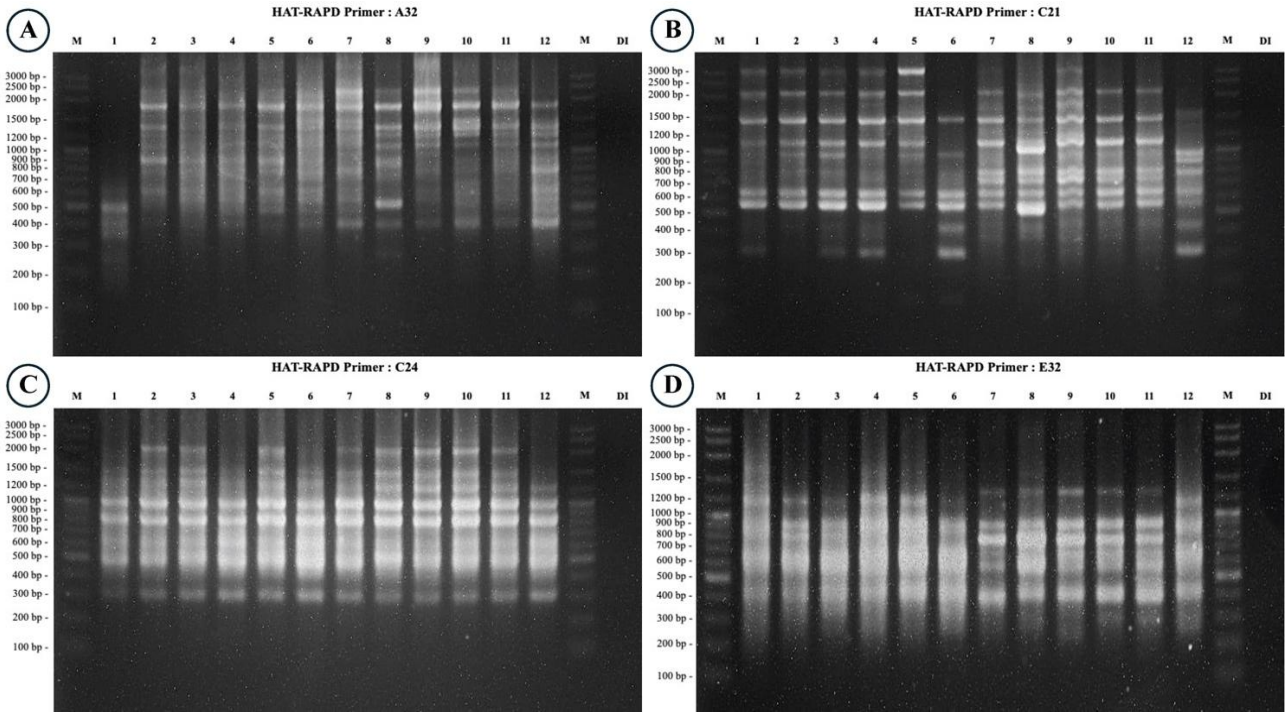


Figure 2. Representing pictures of polymerase chain reaction (PCR) amplified with the screened and selected high annealing temperature (HAT-RAPD) primers from *in vitro* cultured seedlings and their field grown seed donor plants of *N. colorata* and its natural hybrids. Primers used: (A) HAT-RAPD Primer-A32, (B) HAT-RAPD Primer-C21, (C) HAT-RAPD Primer-C24, and (D) HAT-RAPD Primer-E32. Lane M represents 100 bp Plus DNA ladder RTU, Lane DI represents deionized water (negative control), Lanes 1-6 represent field-grown seed donor plants of *N. colorata* and its natural hybrids, and Lanes 7-12 represent *in vitro* cultured seedlings of *N. colorata* and its natural hybrids. The sample loading lanes (lanes 1-12) were assigned to the sample codes in Table 1.

Table 2. List of high annealing temperature – random amplified polymorphic DNA (HAT-RAPD) primers used for genetic relationship and fidelity assessment of *in vitro* cultured *N. colorata* seedlings, compared to their field grown seed donor plants. The nucleotide sequences of selected primers, PCR product sizes, the number of total bands, and the percentage of polymorphic loci are shown in the column.

Primer name	Nucleotide sequence (5′→ 3′)	Approximately amplified DNA range/ PCR products sized (bp)	Total scorable bands (Sb/p†)	Polymorphic loci examined with scorable bands	Polymorphic loci percentage (%)
A32	TTGCCGGGACCA	200 – 2250	20	14	70.00
B22	GGTGACTGGTGG	300 – 2250	16	13	81.25
B23	GGTGCCGGAGCA	300 – 3000	19	14	73.68
B27	GGCGGTTATGAA	150 – 2250	20	14	70.00
B32	ATCGCGGCTTAT	250 – 2250	15	12	80.00
C21	GGAGAGCGGACG	150 – 3000	23	18	78.26
C24	CCTTGGCATCGG	300 – 2250	15	9	60.00
C28	GTCGACGCATCA	300 – 3000	13	9	69.23
C29	GTCGCCTTACCA	150 – 3000	17	11	64.71
D23	ACCATCAAACGG	300 – 1800	12	10	83.33
E24	CCGGAGTGGATG	200 – 2500	18	14	77.78
E32	CAGGAACAGCAA	250 – 1300	12	8	66.67
F23	CCATCCGCACGA	200 – 3000	20	15	75.00
F31	ATCGTGACGCCG	200 – 2750	20	15	75.00
Total numeric result (s)		~ 150 – 3000	240	176	73.33

† Sb/p = total scorable amplified DNA bands per primer.

NCB1_WT	1.00											
NCB2	0.91	1.00										
NCL1	0.87	0.92	1.00									
NCL2	0.82	0.86	0.94	1.00								
NCP1	0.82	0.84	0.87	0.88	1.00							
NCP2	0.76	0.80	0.82	0.84	0.86	1.00						
NCB_IS1	0.68	0.71	0.74	0.74	0.73	0.76	1.00					
NCB_IS2	0.64	0.66	0.66	0.66	0.70	0.67	0.81	1.00				
NCL_IS1	0.68	0.72	0.73	0.71	0.72	0.72	0.91	0.81	1.00			
NCL_IS2	0.67	0.72	0.72	0.71	0.72	0.74	0.84	0.74	0.89	1.00		
NCP_IS1	0.67	0.69	0.71	0.70	0.68	0.70	0.81	0.73	0.83	0.84	1.00	
NCP_IS2	0.68	0.69	0.71	0.71	0.71	0.73	0.75	0.67	0.74	0.79	0.86	1.00
Sample	NCB1_WT	NCB2	NCL1	NCL2	NCP1	NCP2	NCB_IS1	NCB_IS2	NCL_IS1	NCL_IS2	NCP_IS1	NCP_IS2

Figure 3. The similarity coefficient matrix of HAT-RAPD data of the 12 *N. colorata* accessions with 14 primers.

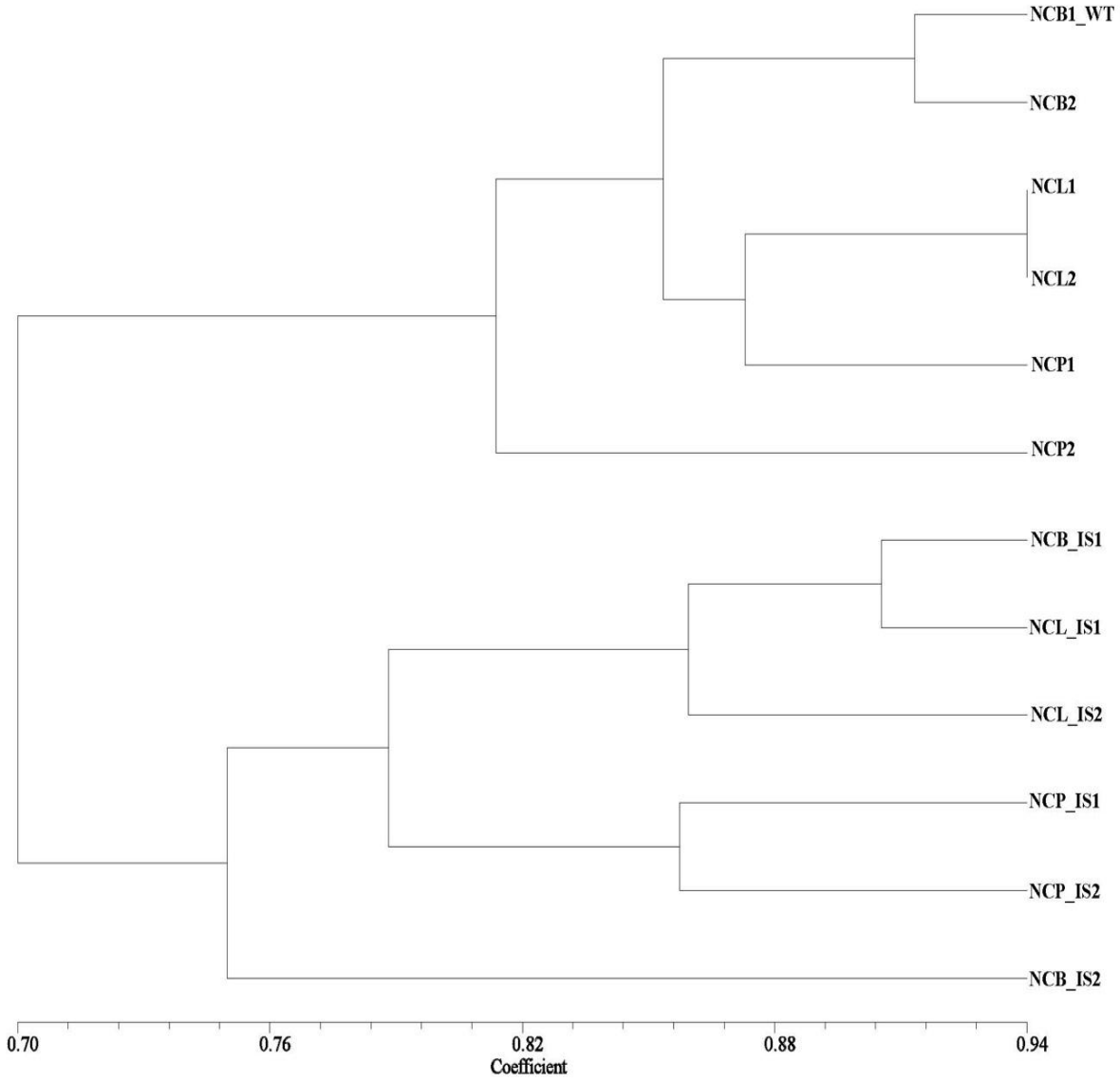


Figure 4. Phylogenetic dendrogram constructed by cluster analysis (UPGMA) of HAT-RAPD data of twelve *N. colorata* accessions with 14 primers.

4. Conclusions

This is the HAT-RAPD application specifically reported for *N. colorata* accessions and their *in vitro* progenies, which distinguishes it from previous studies. It has the potential to serve as molecular markers for assessing genetic relationships, species-specific identification, authentication, variability, and heterogeneity that expected due to reciprocal outcrosses and cross pollination among the field grown seed donor plants. However, *in vitro* seed culture and storage of these *N. colorata* cultivars will be demonstrated in further studies. Our research results not only served as a precise database for micropropagation and genetic characterization of *N. colorata* and its hybrids, but also developed effective molecular markers for seed-derived plants, true-to-type species, and pedigree analysis. Hence, a combination of plant biotechnological approaches would be useful for establishing *in situ* and *ex situ* conservation of all *N. colorata* hybrid lines/cultivars. There are also opportunities to apply in commercial ornamental crop production, breeding technology, genetic engineering, and the utilization of certain waterlily germplasm resources.

5. Acknowledgments

This research was financially supported by the Internationalization, Education and Research Promotion Scholarship from Thammasat University (TU) (Contract No. 4/2563). At the same time, Itsaraphong Khaenthong would like to thank all academic and supporting staffs driven the Doctor of Philoshophy Program in Biotechnology and Agriculture, Department of Biotechnology, Faculty of Science and Technology, Thammasat University, Rangsit Campus, and the executives and the up-skilled/re-skilled university staff committees for supporting the personnel development funds for education and research that approved and provided by Rajamangala University of Technology Thanyaburi (RMUTT) due to related authors during year 2020-2026, which were referred to the Contract No. 0022/2563, Contract No. 0001/2567, Contract No. 0002/2567, Contract No. 0005/2567, Contract No. 0006/2567, Contract No. 0004/2568, Contract No. 012/2569 and the related RMUTT official working contracts and commitments.

The authors also acknowledge the full supports, which are perfectly provided by Lotus and Waterlily Museum, Division of Central Administration, Office of the President, Rajamangala University of Technology Thanyaburi (RMUTT), joined with Plant Genetic Conservation Project Under The Royal Initiative of Her Royal Highness Princess Maha Chakri Sirindhorn (RSPG) and Department of Biotechnology, Faculty of Science and Technology, Thammasat University (TU), Rangsit Campus, Pathum Thani, Thailand for providing all laboratory equipment and facilities, according to waterlily genetic resources and germplasms, living plant materials grown in the field study sites and sampling.

Author Contributions: Conceptualization, I.K., T.T., and N.T.; methodology, I.K., T.T., and N.T.; software, I.K.; validation, I.K.; formal analysis, I.K., T.T., and N.T.; investigation, I.K., T.T., and N.T.; resources, I.K., T.T., and N.T.; data curation, I.K.; writing—original draft preparation, I.K., T.T., and N.T.; writing—review and editing, I.K., T.T., and N.T.; visualization, T.T. and N.T.; supervision and project administration. All authors have read and agreed to the published version of the manuscript.

Funding: During year 2020-2026, this research was funded by Internationalization, Education and Research Promotion Scholarship from Thammasat University (TU) (Contract No. 4/2563) and the personnel development funds for education and research from Rajamangala University of Technology Thanyaburi (RMUTT), which were referred to the Contract No. 0022/2563, Contract No. 0001/2567, Contract No. 0002/2567, Contract No. 0005/2567, Contract No. 0006/2567, Contract No. 0004/2568, Contract No. 012/2569 and the related RMUTT official working contracts and commitments.

Conflicts of Interest: The authors declare no conflict of interest.

References

[1] Yu, C.; Qiao, G.; Qiu, W.; Yu, D.; Zhou, S.; Shen, Y.; Yu, G.; Jiang, J.; Han, X.; Liu, M.; Zhang, L.; Chen, F.; Chen, Y.; Zhuo, R. Molecular breeding of water lily: Engineering cold stress tolerance into tropical water lily. *Hortic. Res.* **2018**, *5*, 73. https://doi.org/10.1038/s41438-018-0086-2

[2] Borsch, T.; Hilu, K. W.; Wiersema, J. H.; Löhne, C.; Barthlott, W.; Wildes, V. Phylogeny of *Nymphaea* (Nymphaeaceae): Evidence from substitutions and microstructural changes in the chloroplast *trnT-trnF* region. *Int. J. Plant Sci.* **2007**, *168*(5), 639–671. https://doi.org/10.1086/513476

[3] Nzei, J. M.; Médez, N. M.; Mwanzia, V. M.; Kurauka, J. K.; Wang, Q. F.; Li, Z. Z.; Chen, J. M. Climatic niche evolution and niche conservation of *Nymphaea* species in Africa, South America, and Australia. *BMC Plant Biol.* **2024**, *24*, 476. https://doi.org/10.1186/s12870-024-05141-1

[4] Borsch, T.; Wiersema, J. H.; Hellquist, C. B.; Löhne, C.; Govers, K. Speciation in North American water lilies: Evidence for the hybrid origin of the newly discovered Canadian endemic *Nymphaea loriana* sp. nov. (Nymphaeaceae) in a past contact zone. *Botany* **2014**, *92*, 867–882. https://doi.org/10.1139/cjb-2014-0060

[5] Löhne, C.; Borsch, T.; Jacobs, S. W. L.; Hellquist, C. B.; Wiersema, J. H. Nuclear and plastid DNA sequences reveal complex reticulate patterns in Australian waterlilies (*Nymphaea* subgenus *Anecphya*, Nymphaeaceae). *Aust. Syst. Bot.* **2008**, *21*, 229–250. https://doi.org/10.1071/SB07010

[6] Borsch, T.; Löhne, C.; Wiersema, J. Phylogeny and evolutionary patterns in Nymphaeales: Integrating genes, genomes and morphology. *Taxon* **2008**, *57*(4), 1052–1081. https://doi.org/10.1002/tax.574004

[7] Sangsri, N.; Kuleung, C.; Hongtrakul, V. Analysis of nrITS sequence in Thai waterlilies, *Nymphaea* spp. *Thai J. Sci. Technol.* **2018**, *8*(3), 258–270.

[8] Songpanich, P.; Hongtrakul, V. Intersubgeneric cross in *Nymphaea* spp. L. to develop a blue hardy waterlily. *Sci. Hortic.* **2010**, *124*, 475–481. https://doi.org/10.1016/j.scienta.2010.01.024

[9] Parveen, S.; Singh, N.; Adit, A.; Kumaria, S.; Tandon, R.; Agarwal, M.; Jagannath, A.; Goel, S. Contrasting reproductive strategies of two *Nymphaea* species affect existing natural genetic diversity as assessed by microsatellite markers: Implications for conservation and wetlands restoration. *Front. Plant Sci.* **2022**, *13*, 773572. https://doi.org/10.3389/fpls.2022.773572

[10] Murashige, T.; Skoog, F. A revised medium for rapid growth and bio-assays with tobacco tissue culture. *Physiol. Plant.* **1962**, *15*(3), 473–497. https://doi.org/10.1111/j.1399-3054.1962.tb08052.x

[11] Khan, S.; Al-Qurainy, F.; Nadeem, M. Biotechnological approaches for conservation and improvement of rare and endangered plants of Saudi Arabia. *Saudi J. Biol. Sci.* **2012**, *19*(1), 1–11. https://doi.org/10.1016/j.sjbs.2011.11.001

[12] Doyle, J. J.; Doyle, J. L. A rapid DNA isolation procedure for small quantities of fresh leaf tissue. *Phytochem. Bull.* **1987**, *19*(1), 11–15.

[13] Noimai, Y.; Charoenwattana, P. Effects of BA and IAA on *in vitro* shoot induction of *Nymphaea* sp. 'King of Siam'. *Agric. Sci. J.* **2012**, *43*(2, Suppl.), 249–252.

[14] Khaenthong, I.; Chuenboonngarm, N.; Muengkrut, A. *In vitro* self and cross pollinated seed culture of *Nymphaea rubra* 'Maeploi', a night-blooming tropical waterlily hybrid (Nymphaeaceae) from Thailand. *Res. J. Rajamangala Univ. Technol. Thanyaburi* **2021**, *20*(1), 123–133. https://doi.org/10.14456/rj-rmutt.2021.12

[15] Pereva, P. I. P.; Attanayaka, D. P. S. T. G.; Yakandawala, K.; Yakandawala, D. M. D.; Fernando, C. N.; Arachchi, U. P. E.; Gunawardhana, W. P. D. S.; Weerashighe, W. D. C. D. *In vitro* culture of *Nymphaea nouchali* seeds: A conservation approach for a vulnerable species. *J. Natl. Sci. Found. Sri Lanka* **2021**, *49*(3), 393–402. https://doi.org/10.4038/jnsfsr.v49i3.10305

[16] Suksakul, S.; Thanananta, T.; Thanananta, N. Genetic relationship assessment and identification of *Nymphaea* sp. and their hybrids using HAT-RAPD. *Thai J. Sci. Technol.* **2018**, *7*(4, Suppl.), 418–426. https://doi.org/10.14456/tjst.2018.39

[17] Poczai, P.; Mátyás, K. K.; Szabó, I.; Vanga, I.; Hyvönen, J.; Cernák, I.; Gorji, A. M.; Decsi, K.; Taller, J. Genetic variability of thermal *Nymphaea* (Nymphaeaceae) populations based on ISSR markers: Implications on relationships, hybridization, and conservation. *Plant Mol. Biol. Rep.* **2011**, *29*, 906–918. https://doi.org/10.1007/s11105-011-0302-9

[18] Rodboot, N.; Yenchon, S.; Te-chato, S. Optimization of explant sterilization and plant growth regulators for enhancing the *in vitro* propagation of *Nymphaea colorata* Peter. *Plant Cell Tissue Organ Cult.* **2024**, *159*, 59. https://doi.org/10.1007/s11240-024-02911-5

[19] Williams, J. G. K.; Kubelik, A. R.; Livak, K. J.; Rafalski, J. A.; Tingey, S. V. DNA polymorphisms amplified by arbitrary primers are useful as genetic markers. *Nucleic Acids Res.* **1990**, *18*(22), 6531–6535. https://doi.org/10.1093/nar/18.22.6531

[20] Lin, F.; Kang, Y.; Huqail, A. A. A.; Alshehri, D.; Li, Y.; Guo, Y.; Yang, G.; Tang, F.; Yin, J.; Ding, Z.; Eissa, M. A. Novel cultivation techniques for water lily (*Nymphaea micrantha* Guill. & Perr.) production based on *in vitro* technology. *Plant Methods* **2025**, *21*, 56. https://doi.org/10.1186/s13007-025-01377-6

[21] Khatun, M. M.; Tanny, T.; Yesmin, S.; Salimullah, M.; Alam, I. Evaluation of genetic fidelity of *in vitro*-propagated *Aloe vera* plants using DNA-based markers. *ScienceAsia* **2018**, *44*, 87–91. https://doi.org/10.2306/scienceasia1513-1874.2018.44.087

[22] Chen, F.; Liu, X.; Yu, C.; Chen, Y.; Tang, H.; Zhang, L. Water lilies as emerging models for Darwin's abominable mystery. *Hortic. Res.* **2017**, *4*, 17051. https://doi.org/10.1038/hortres.2017.51

[23] Dong, S.; Zhao, C.; Chen, F.; Liu, Y.; Zhang, S.; Wu, H.; Zhang, L.; Liu, Y. The complete mitochondrial genome of the early flowering plant *Nymphaea colorata* is highly repetitive with low recombination. *BMC Genomics* **2018**, *19*, 614. https://doi.org/10.1186/s12864-018-4991-4

[24] Suksakul, S.; Thanananta, T.; Thanananta, N. Genetic relationship assessment and identification of *Nymphaea* sp. and their hybrids using SCoT markers. *Thai J. Sci. Technol.* **2018**, *7*(6), 570–579.

[25] Kashima, S.; Thanananta, T.; Kachonpadungkitti, Y.; Bodhipadma, K. Induced mutation in *Musa* spp. genomes AAA using acute gamma ray and determination with HAT-RAPD markers. *Thai J. Sci. Technol.* **2020**, *9*(5), 668–679.

[26] Chuengpanya, R.; Muangkroot, A.; Jenjittikul, T.; Thammasiri, K.; Umpunjun, P.; Viboonjun, U.; Chuenboonngarm, N. *In vitro* propagation and genetic fidelity assessment of *Hedychium longicornutum* Griff. ex Baker, a vulnerable zingiberaceous plant of Thailand. *Curr. Appl. Sci. Technol.* **2022**, *22* (6), 1–21. https://doi.org/10.55003/cast.2022.06.22.012

[27] Rittirat, S.; Thammasiri, K.; Klaocheed, S. *In vitro* rapid multiplication of a highly valuable ornamental aquatic plant *Anubias heterophylla*. *Trends Sci.* **2021**, *18* (19), 3. https://doi.org/10.48048/tis.2021.3

[28] Zhang, L.; Chen, F.; Zhang, X.; Li, Z.; Zhao, Y.; Lohaus, R.; Chang, X.; Dong, W.; Ho, S. Y. W.; Liu, X.; Song, A.; Chen, J.; Guo, W.; Wang, Z.; Zhuang, Y.; Wang, H.; Chen, X.; Hu, J.; Liu, Y.; Tang, H. The water lily genome and the early evolution of flowering plants. *Nature* **2020**, *577*(7788), 79–84. https://doi.org/10.1038/s41586-019-1852-5

[29] Tang, H.; Zhang, L.; Chen, F.; Zhang, X.; Chen, F.; Ma, H.; Van de Peer, Y. *Nymphaea colorata* (Blue-Petal Water Lily). *Trends Genet.* **2020**, *36* (9), 718–719. https://doi.org/10.1016/j.tig.2020.06.004

[30] Xiong, X.; Zhang, J.; Yang, Y.; Chen, Y.; Su, Q.; Zhao, Y.; Wang, J.; Xia, Z.; Wang, L.; Zhang, L.; Chen, F. Water lily research: Past, present, and future. *Trop. Plants* **2023**, *2*(1), 1–8. https://doi.org/10.48130/TP-2023-0001

[31] Khaenthong, I.; Phairin, U.; Mattisinlapin, P.; Subudom, S.; Sripan, S.; Boonthongto, A.; Malaithong, S. The effects of seed coat scarification, priming, and cold stratification on seed germination of a tropical night-blooming waterlily hybrid *Nymphaea rubra* 'Maeploi'. *Acta Hortic.* **2020**, *1298*, 581–586. https://doi.org/10.17660/ActaHortic.2020.1298.80

[32] Orban, I.; Bouharmont, J. Megagametophyte development of *Nymphaea nouchali* Burm. f. (Nymphaeaceae). *Bot. J. Linn. Soc.* **1998**, *126*, 339–348. https://doi.org/10.1111/j.1095-8339.1998.tb01386.x

[33] Rodboot, N.; Te-chato, S.; Yenchon, S. Influence of MS medium strengths and types on *in vitro* shoot multiplication and development of *Nymphaea colorata*. *ASEAN J. Sci. Technol. Rep.* **2025**, *28*(4), e258176. https://doi.org/10.55164/ajstr.v28i4.258176

[34] Khaenthong, I.; Akkarakultron, P. Seed coat scarification of some Australian *Nymphaea* species by vinegar. *Agric. Sci. J.* **2016**, *47*(2, Suppl.), 537–540.

[35] Song, W.; Shi, W.; Wang, H.; Zhang, Z.; Tao, R.; Liu, J.; Wang, S.; Engel, M. S.; Shi, C. Comparative analysis of 12 water lily plastid genomes reveals genomic divergence and evolutionary relationships in early flowering plants. *Mar. Life Sci. Technol.* **2024**, *6*, 425–441. https://doi.org/10.1007/s42995-024-00242-0

ASEAN
Journal of Scientific and Technological Reports
Online ISSN:2773-8752

Research article

Development of a Sustainable Wood Treatment Process for Palmyra Palm Fronds toward Furniture Production

Palachai Khaonuan[1], Noppadon Podkumnerd[1*], Kosin Teeparuksapun[1], Jirapat Phookwantong[1], Supranee Wunsri[1], Nuntachai Chusilp[2], and Mahamasuhaimi Masae[2]

[1] Faculty of Liberal Arts, Rajamangala University of Technology Srivijaya, Songkhla, 90000, Thailand
[2] Faculty of Engineering, Rajamangala University of Technology Srivijaya, Songkhla, 90000, Thailand
* Correspondence: Noppadon.p@rmutsv.ac.th

Citation:
Khaonuan, P.; Podkumnerd, N.; Teeparuksapun, K.; Phookwantong, J.; Wunsri, S.; Chusilp, N.; Masae, M. Development of a sustainable wood treatment process for palmyra palm fronds toward furniture production. *ASEAN J. Sci. Tech. Report.* **2026**, *29*(7), e263161. https://doi.org/10.55164/ajstr.v29i7.263161

Article history:
Received: January 8, 2026
Revised: May 6, 2026
Accepted: May 13, 2026
Available online: June 14, 2026

Publisher's Note:
This article is published and distributed under the terms of the Thaksin University.

Abstract: This study investigated the potential of Palmyra palm frond wood preservation treatments as an alternative material for furniture production. The palm fronds were composed of 74.94 ± 2.05% moisture, 30.61 ± 17.67% cellulose, 23.54 ± 1.00% hemicellulose, and 45.36 ± 0.55% lignin. Specimens (2.5x2.5 cm) were treated with boron compounds (boric acid: borax, 1:1.5) or wood vinegar at concentrations of 1%, 3%, and 5%, and then tested for fungal resistance, termite resistance, and mechanical properties. The 3% boron compound treatment demonstrated optimal performance, with 55.62 ± 1.96% absorption after 6 days, significantly higher than 3% wood vinegar (46.91 ± 1.58%). Termite resistance testing revealed weight loss of 5.83 ± 0.17% for the 3% boron-treated samples compared to 11.21 ± 0.35% for wood vinegar and 23.90 ± 1.40% for untreated controls after 45 days. Mechanical testing showed numerically higher flexural strength values for boron-treated specimens (34.87 ± 4.48 N/mm^2) than for controls (27.85 ± 1.10 N/mm^2), although the difference was not statistically significant ($p>0.05$). Color stability remained acceptable with L-values decreasing from 68.60 ± 0.53 to 59.30 ± 0.44 after three months. Microscopic examination confirmed preservative penetration into the cellular structure. The optimized 3% boron compound treatment provided an economically viable and environmentally sustainable solution for utilizing abundant Palmyra palm resources in Southern Thailand, creating durable furniture components while reducing the pressure on endangered hardwood species.

Keywords: Palmyra palm wood; wood preservation; boron compounds; termite resistance; sustainable furniture

1. Introduction

Based on the 2021 global greenhouse gas emissions scenario, carbon dioxide (CO_2) emissions are expected to rise by 4.8% due to the accelerating economic recovery [1]. Biomass, produced through photosynthesis in green plants under sunlight, is among the Earth's most significant organic materials [2]. Thailand is an agrarian-based nation, with approximately 28% of its population employed in the agricultural sector [3]. The increasing demand for naturally durable wood species like Blackwood, Ironwood, and Teak, which command high market prices, is leading to significant depletion of resources. Thailand primarily uses rubberwood as a raw material for furniture production, but its low natural durability, due to its high carbohydrate content, makes it susceptible to wood-destroying pests, including fungi, powder-post beetles,

and termites [4-6]. Thai processed rubber wood typically requires treatment with boron compounds (a mixture of borax and boric acid) to enhance resistance against these destructive agents, thereby increasing its cost [7, 8]. The need for alternative wood sources has prompted research into other plant species, including the Palmyra palm (*Borassus flabellifer*), which is an important economic plant in Southern Thailand, particularly in the Sathing Phra Peninsula of Songkhla Province. Palmyra palms are typically planted in rice fields at a density of 20 trees per rai (1,600 m^2), with the number growing from 1 million trees in 2007 to 3 million in Songkhla Province. The Palmyra palm has become integrated into local community lifestyles and culture [9, 10]. The wood is economically significant in Southern Thailand and primarily utilized for furniture or interior structural work due to its lightweight properties, moderate strength, and ease of processing [11]. However, Palmyra palm wood has low natural durability, making it vulnerable to termites, fungi, and other pests.

Treatments using boron compounds and wood vinegar offer effective protection against wood-destroying organisms through simple soaking and coating methods that are easy to apply, time- and labor-efficient, and that extend the service life of the wood. Wood vinegar, produced through wood pyrolysis, contains various organic acids and alcohols derived from hemicellulose and cellulose decomposition, as well as phenolic compounds from lignin breakdown [12]. Wood vinegar is primarily water, with organic acids and other organic compounds in smaller proportions. These substances are highly acidic and have specific gravities only slightly higher than that of water. These properties vary depending on the type of wood used as raw material [13, 14]. Boron compounds offer advantages as wood preservatives by preventing termite, powder-post beetle, and fungal infestation [15]. These substances are particularly suitable for treating wood due to their low toxicity to humans and mammals, transparent appearance when dissolved in water, preservation of wood color after treatment, affordability, and availability [16]. Previous research has shown that the processed plywood treated with boron compounds containing borax and boric acid demonstrated increased resistance to decay fungi (*Trametes versicolor* and *Fomitopsis palustris*) and termites (*Coptotermes formosamus*) compared to untreated wood [17]. In 2007, Kartal and co-workers reported that wood soaked in 6% borax and boric acid solutions exhibited enhanced resistance against subterranean termites (Coptotermes formosanus Shiraki), with weight loss of 3% to 5% after three weeks of termite exposure, compared to 23.9% in untreated samples [18].

This study aimed to develop an effective preservation process for wood from Palmyra palm fronds by first examining its fundamental composition, then evaluating the performance of boron compounds and wood vinegar as treatment agents, followed by formulating a suitable treatment process, and finally testing the treated wood for termite resistance, durability, and mechanical strength.

2. Materials and Methods

2.1 Materials

2.1.1 Palm frond samples

Palmyra palm frond samples were obtained from the Palmyra palm community in Bang Khiad Subdistrict, Singhanakhon District, Songkhla Province. The samples were cut into small pieces and dried at 95 ± 5°C for 5 hours in a hot-air oven until constant weight, for subsequent physical and chemical analysis.

2.1.2 Chemicals

Boric acid (analytical grade, ≥99.5% purity; Ajax Finechem, Thailand) and borax (sodium tetraborate decahydrate, analytical grade, ≥99.0% purity; Ajax Finechem, Thailand) were used to prepare boron compound solutions at a boric acid:borax molar ratio of 1:1.5 Wood vinegar (pH 2.8-3.2, specific gravity 1.015-1.020; obtained from a local charcoal kiln in Songkhla Province, Thailand) was used as the second preservative agent. Solutions were prepared at concentrations of 1%, 3%, and 5% (w/v) in distilled water immediately before use. All glassware was rinsed with distilled water before use.

2.2 Methods

2.2.1 Physical and chemical composition analysis

The physical and chemical properties analyzed included moisture content, ash content, pH (Electrometric Method), fat (Direct Extraction Methods), cellulose, hemicellulose, and lignin (Klason Lignin

method). Carbohydrate content was determined using the Anthrone Method [19], and reducing sugars were measured using the Dinitrosalicylic Acid Method [20].

2.2.2 Treatment methods

Palmyra palm frond samples measuring 2.5 x 2.5 cm were prepared and dried at 95 ± 5 °C for 5 hours in a hot-air oven until constant weight. Three treatment methods were employed. Method 1: The samples were soaked in boron compound solutions (boric acid: borax at 1::1.5 ratio) at concentrations of 1%, 3%, and 5% for 12 hours. After soaking, the samples were dried at 95±5°C for 5 hours and weighed. Method 2: The samples were soaked in wood vinegar solutions at 1%, 3%, and 5% for 12 hours, then subjected to the same procedures as in Method 1. Method 3: The control sample was soaked in tap water for 12 hours, and then subjected to the same procedures as Method 1.

2.2.3 Fungal resistance testing

The treated palm frond samples (4-5 pieces per treatment) were placed on trays with air circulation to allow fungal growth for 45 days. After the testing period, the samples were examined by swabbing to calculate fungal contamination. The dominant fungal species observed were *Aspergillus niger* and *Trichoderma* spp., identified by colony morphology and microscopic examination of conidia structure on potato dextrose agar (PDA) after 7 days at 28°C.

2.2.4 Termite resistance testing

Termite resistance was investigated using the method described in ASTM D 3345-74 [21]. Briefly, treated palm frond samples (4-5 pieces per treatment) of known constant weight were exposed to 1 g of termites (0.9 g worker termites and 0.1 g soldier termites) per sample piece for 45 days. The termites used were *Microcerotermes crassus* Snyder, collected from naturally infested Palmyra palm trunks in the Singhanakhon District, Songkhla Province. Species identity was confirmed by an entomologist at Rajamangala University of Technology Srivijaya through morphological examination of soldier caste head-capsule characteristics. After the testing period, the samples were dried to constant weight. The termite damage was calculated as equation (1).

$$\text{Termite damage (weight loss) (\%)} = \frac{(\text{Initial weight} - \text{Final weight}) \times 100}{\text{Initial weight}} \quad (1)$$

2.2.5 Water absorption testing

Water absorption was investigated using the ASTM D7264 method [22]. Test specimens (5 x 5 cm) were immersed in distilled water at 25 ± 2 °C for 6 days. The water absorption was calculated using equation (2).

$$\text{Water absorption (\%)} = \frac{(t_2 - t_1)}{t_1} \times 100 \quad (2)$$

Where t_1 and t_2 are the weights before and after water immersion (g), respectively.

2.2.6 Flexural strength and elastic modulus testing

Flexural strength (FS) and elastic modulus (E) were determined using a Universal Testing Machine (QC-506M1F Extend) in three-point bending mode. The span between the lower supports was 70 mm, and the testing speed was 10 mm/min. The FS and E were calculated using equations (3) and (4), respectively.

$$\text{Flexural strength (FS)} = \frac{L^3 m}{4bh^3} \quad (3)$$

$$\text{Elastic modulus } (\sigma) = \frac{3PL}{2bh^2} \quad (4)$$

where P is the maximum load the specimen can bear (N), L is the span of the supports (mm), m is the load increase in the linear region of the graph (N), b is the width at the center of the specimen (mm), and h is the thickness at the center of the specimen (mm).

2.2.7 Morphological examination

The morphology of the palm frond wood was examined using a Trinocular Fluorescence Stereo Microscope (Leica M205FCA).

2.2.8 Statistical analysis

All data were expressed as mean ± standard deviation (SD). Statistical comparisons among treatment groups were performed using one-way analysis of variance (ANOVA) followed by Duncan's multiple-range test for post hoc comparisons, with statistical significance set at $p<0.05$ and $p<0.01$ as indicated. A paired t-test was used to compare absorption rates between two treatment groups at each time point. All statistical analyses were performed using R statistical software.

3. Results and Discussion

3.1 Basic physical and chemical composition of palm fronds

Analysis of Palmyra palm frond wood revealed a moisture content of 74.94 ± 2.05%, ash content of 27.91 ± 0.47%, cellulose content of 30.61 ± 17.67%, hemicellulose content of 23.54 ± 1.00%, and lignin content of 45.36 ± 0.55%. Carbohydrate and reducing sugar contents were 9.00 ± 0.47 and 4.33 ± 0.56 g/L, respectively, with a pH value of 7.43 ± 0.10 (Table 1). The high carbohydrate content rendered this material susceptible to biological degradation, as the oil palm leaflets and fronds contain a high amount of cellulose [23]. Palmyra palm fronds contain a gradient of vascular bundle density from the dense peripheral zone to the looser central parenchyma, resulting in large sample-to-sample variation in cellulose content.

Table 1. Physical and chemical composition of Palmyra palm frond wood

Component	Value
Moisture content (%)	74.94 ± 2.05
Ash content (%)	27.91 ± 0.47
pH	7.43 ± 0.10
Carbohydrate (g/L)	9.00 ± 0.47
Reducing sugar (g/L)	4.33 ± 0.56
Cellulose (%)	30.61 ± 17.67
Hemicellulose (%)	23.54 ± 1.00
Lignin (%)	45.36 ± 0.55

3.2 Effectiveness of treatment solutions against fungi and termites

After 45 days of testing, the control sample showed the highest fungal contamination at 1.13 ± 0.16 log CFU/g. Samples treated with different solutions demonstrated significantly lower contaminations ranging from 0.69 ± 0.21 log CFU/g to 0.94 ± 0.06 log CFU/g (Table 2), indicating improved resistance to fungal growth. These results aligned with Puttinun [11] findings regarding the antifungal properties of wood vinegar. Termite resistance testing revealed that boron compound treatments provided superior protection, with weight-loss percentages ranging from 5.48 ± 0.58% to 8.79 ± 1.53%. The wood vinegar-treated samples showed moderate protection (9.54 ± 0.95% to 12.46 ± 1.80% weight loss), while the control sample suffered the highest damage (23.90 ± 1.40% weight loss). The termites were identified as *Microcerotermes crassus* Snyder. These results concurred with a previous study reporting significantly reduced weight loss in boron-treated wood compared to untreated samples [18].

Table 2. Fungal contamination (log CFU/g) and termite damage (weight loss, %) after 45 days

Treatment method	Soaking time (hours)	Fungal contamination (log CFU/g)	Termite damage (weight loss, %)
Water (control)	12	1.13±0.16^{b}	23.90±1.40^{d}
1% Boron compounds	12	0.88±0.16^{ab}	8.79±1.53^{ab}
3% Boron compounds	12	0.77±0.21^{a}	5.83±0.17^{a}
5% Boron compounds	12	0.69±0.21^{a}	5.48±0.58^{a}
1% Wood vinegar	12	0.94±0.06^{ab}	12.46±1.80^{c}
3% Wood vinegar	12	0.89±0.11^{ab}	11.21±0.35^{bc}
5% Wood vinegar	12	0.82±0.11^{a}	9.54±0.95^{bc}

Different superscript letters indicate statistically significant differences at $p<0.05$

3.3 Absorption rates of treatment solutions

The absorption rate of the 3% boron compound solution reached 55.62±1.96% after 6 days, while the 3% wood vinegar solution achieved 46.91±1.58% (Table 3). The highest absorption rate occurred on days 1 and 2, with a gradual decrease from days 3 to 6. Statistically significant differences ($p<0.01$) between the solutions suggested better penetration of boron compounds into the wood structure [17]. Ionic borate species ($B(OH)_4^-$) form reversible covalent bonds with polyol hydroxyl groups in hemicelluloses, facilitating diffusion into the cell wall matrix; wood vinegar's complex mixture of organic acids and phenolics may interact non-specifically with surface sites, limiting deeper penetration [24].

Table 3. Absorption rates (%) of 3% boron compounds and 3% wood vinegar solutions over time

Soaking time (days)	Absorption rate (%)		t-value	p-value
	3% Boron compounds	3% Wood vinegar		
0	0.00±0.00	0.00±0.00	-	-
1	38.42±2.07	23.93±2.05	8.624**	<0.001
2	47.21±1.03	36.80±0.51	15.636**	<0.001
3	51.18±1.61	40.89±0.90	9.658**	<0.001
4	52.94±2.10	43.15±1.24	6.940**	0.002
5	54.20±1.98	44.88±1.48	6.530**	0.003
6	55.62±1.96	46.91±1.58	5.977**	0.004

** Significant difference at $p<0.01$

3.4 Color analysis before and after treatment

The color analysis (L, a*, b* values) showed that palm frond wood treated with 3% boron compounds maintained high brightness (L values 68.60±0.53 to 59.30±0.44) compared to wood vinegar-treated samples (47.57±1.90 to 44.70±4.20). All samples showed decreased brightness after 3 months, with wood vinegar causing greater darkening (Table 4). This applies to the control and boron compound groups, while wood vinegar-treated samples maintained consistently low brightness values throughout from time zero. For color change: phenolic compounds from lignin pyrolysis in wood vinegar bind to cell wall surfaces and undergo oxidative polymerization under ambient conditions, producing irreversible brown-black chromophores [13]. These findings aligned with a previous report showing that both treatments could maintain wood appearance with minimal color changes over time.

3.5 Mechanical strength after treatment

Ultimate strength testing of the samples treated with 3% boron compounds, 3% wood vinegar, and the control sample yielded values of 29.19±5.24 N, 26.71±1.61 N, and 29.65±1.27 N, respectively. The elastic modulus values were 29.40±7.18 N/mm², 29.04±7.47 N/mm², and 27.27±4.04 N/mm², with flexural strength 34.87±4.48 N/mm², 32.07±3.83 N/mm², and 27.85±1.10 N/mm², respectively (Table 5). The improved mechanical properties in the boron-treated samples were attributed to the adhesive properties of borax, which enhanced bonding to cellulose hydroxyl groups, as noted in previous studies [25].

Table 4. Color analysis (L, a*, b*) of Palmyra palm frond wood before and after treatment

Treatment	Time (months)	Color parameters		
		L	a*	b*
Control	0	71.17±0.58^{d}	9.87±0.74^{b}	22.13±0.25^{c}
	1	68.57±0.12^{c}	10.37±0.60^{b}	21.13±0.50^{b}
	2	63.63±1.69^{b}	10.93±1.03^{b}	37.30±0.26^{a}
	3	60.70±1.10^{a}	13.90±0.35^{a}	37.20±0.46^{a}
3% Boron compounds	0	68.60±0.53^{c}	12.10±0.70^{a}	21.03±0.38^{a}
	1	66.63±0.93^{b}	12.80±0.75^{a}	22.57±0.59^{b}
	2	60.13±0.67^{a}	13.30±0.20^{a}	37.43±0.25^{c}
	3	59.30±0.44^{a}	15.43±0.91^{b}	37.73±0.61^{c}
3% Wood vinegar	0	47.57±1.90^{a}	11.03±0.15^{a}	34.03±0.93^{a}
	1	47.43±0.81^{a}	12.10±07.0^{a}	34.33±0.55^{a}
	2	46.20±0.26^{a}	13.97±0.59^{b}	33.73±0.31^{a}
	3	44.70±4.20^{a}	14.20±0.66^{b}	32.77±2.61^{a}

Different superscript letters indicate statistically significant differences at $p<0.05$ within each treatment group

Table 5. Mechanical properties of Palmyra palm frond wood after different treatments

Treatment	Ultimate Strength (N)	Elastic Strength at P.L. (N/mm²)	Elastic modulus (N/mm²)	Flexural strength (N/mm²)
Control	29.65±1.27^{a}	26.32±1.56^{a}	27.27±4.04^{a}	27.85±1.10^{a}
3% Boron compounds	29.19±5.24^{a}	28.26±4.89^{a}	29.40±7.18^{a}	34.87±4.48^{a}
3% Wood vinegar	26.71±1.61^{a}	23.27±2.20^{a}	29.04±7.47^{a}	32.07±3.83^{a}

The same superscripts indicate no statistically significant differences at $p<0.05$

3.6 Morphological characteristics

Microscopic examination revealed that the treated samples showed evidence of preservative penetration into the cellular structure (Table 6, Figure 1), confirming the effectiveness of the treatment methods in reaching the internal structure of the Palmyra palm frond wood. This penetration is essential for long-term protection against biodegradation [26-27].

Table 6. Morphological analysis of Palmyra palm frond wood before and after treatment

Treatment	Surface texture	Fiber arrangement	Visible treatment penetration
Untreated	Rough, porous	Longitudinal, parallel	N/A
3% Boron compounds	Smooth, less porous	Maintained structure	Visible in cross-section
3% Wood vinegar	Smooth, slightly darkened	Maintained structure	Visible in surface layers

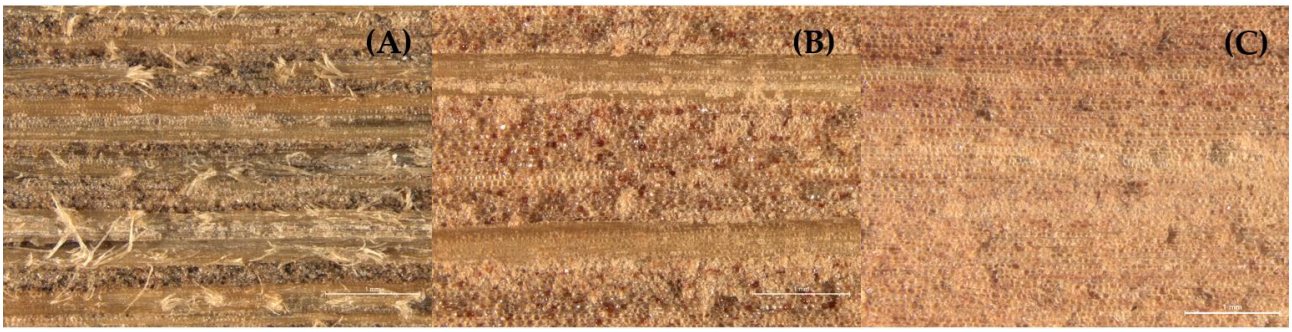


Figure 1. The morphology of the Palmyra palm frond wood was examined using a Trinocular Fluorescence Stereo Microscope; (A) Untreated, (B) 3% Boron compounds, and (C) 3% Wood vinegar

4. Conclusions

Treatment with 3% boron compounds (boric acid:borax at a 1:1.5 ratio) provided superior protection for Palmyra palm frond wood against fungal growth and termite attack, while also enhancing mechanical properties. The 12-hour soaking period was effective for treatment penetration, with 3% boron compound absorption reaching 55.62±1.96% after 6 days. Palmyra palm frond wood treated with 3% boron compounds showed multiple advantages for furniture production applications, including enhanced durability against biodegradation, improved mechanical strength (flexural strength of 3,487.60±448.75 N/mm²), and minimal color alteration (higher brightness than wood vinegar treatment). These characteristics are suitable for indoor furniture components, decorative elements, and non-structural applications requiring moderate strength. The economic benefits include utilizing an abundant local resource from Southern Thailand, with 3 million Palmyra palm trees in Songkhla Province. This treatment process is cost-effective, using readily available preservatives applied through simple soaking methods, and requires minimal equipment or specialized facilities. Small-scale local furniture producers and community enterprises can utilize this technology. The environmental benefits include reduced pressure on endangered hardwood species by providing an alternative material source. Boron compounds have lower environmental toxicity than other conventional wood preservatives, aligning with sustainable production practices. This preservation process extends the service life of Palmyra palm wood products, reducing replacement frequency and resource consumption. It should be noted that boron compounds are water-soluble and susceptible to leaching under repeated wetting conditions, which is a recognized limitation for long-term use in humid tropical environments. The treated products are therefore recommended for indoor applications where direct water contact is minimized. Future research should investigate the long-term performance of treated products under various environmental conditions and explore additional treatment combinations to further the effectiveness and production efficiency of Palmyra palm frond wood preservation.

5. Acknowledgments

The authors express their deepest gratitude to Rajamangala University of Technology Srivijaya and the Fundamental Fund (FF) for supporting the research project "Development of palm frond furniture products from the wisdom of the Songkhla lake basin community to the cultural tourism of palmyra palm community, Songkhla Province, using innovation" for fiscal year 2023 under contract number FRB660020/0172. Special thanks are due to the anonymous reviewers for their constructive comments and suggestions to improve the quality of this manuscript.

Author Contributions: Conceptualization, N.P., P.K., and K.T.; methodology, N.P., P.K., J.P., S.W., N.C., and M.M.; software, P.K.; validation, N.P., P.K., and K.T.; formal analysis, P.K.; investigation, N.P., S.W., and K.T.; resources, N.P. and N.C.; data curation, P.K., M.M., and J.P.; writing original draft preparation, N.P., P.K., and K.T.; writing, review and editing, N.P. and P.K.; visualization, P.K.; supervision, N.P., and P.K.; project administration, N.P. and P.K.; funding acquisition, N.P. and P.K.; statistics, P.K. and J.P.

Funding: This research was funded by the Ministry of Higher Education, Thailand Science Research and Innovation (TSRI), and the Fundamental Fund (FF) for fiscal year 2023.

Conflicts of Interest: The authors declare no conflicts of interest. The funders had no role in the study's design, data collection, analysis, or interpretation, the writing of the manuscript, or the decision to publish the results.

References

[1] Kaewmanee, J.; Pradabphetrat, P.; Rangpan, V. Carbon Footprint Assessment Based on Life Cycle Assessment of Biomass Power Plant. *ASEAN J. Sci. Tech. Report*. **2024**, *27*(1), 92-101. https://doi.org/10.55164/ajstr.v27i1.250754

[2] Jangsawang, W. Preliminary Experimental of Biomass Gasification Process with Open Core Throat Less Downdraft Gasifier. *ASEAN J. Sci. Tech. Report*. **2022**, *26*(1), 1-10. https://doi.org/10.55164/ajstr.v26i1.247166

[3] Jirawattanasomkul, N.; Roschat, W.; Leelatam, T.; Phanphli, S.; Chaipikun, W.; Thammayod, A.; Khotsuno, N.; Yeemin, P.; Wongma, N.; Phewphong, S. Evaluation of the nutritional, mineral, and Estimated Metabolizable Energy values of agricultural biomass raw materials used for the development of concentrated fermented feed for beef cattle in Mukdahan Province, Northeast Thailand. *ASEAN J. Sci. Tech. Report.* **2026**, *29*(4), e262452. https://doi.org/10.55164/ajstr.v29i4.262452

[4] Shigematsu, A.; Mizoue, N.; Kajisa, T..; Yoshida, S. Importane of Rubberwood in Wood Export of Malaysia and Thailand. *New For*. **2011**, *41*, 179-189. https://doi.org/10.1007/s11056-010-9219-7

[5] Teoh, Y. P.; Don, M. M.; Ujang, S. Assessment of the Properties, Utilization, and Preservation of Rubberwood (*Hevea brasiliensis*): A Case Study in Malaysia. *J. Wood Sci.* **2011**, *57*, 255-266. https://doi.org/10.1007/s10086-011-1173-2

[6] Tamiz, A.; Alfredsen, G.; Eikenes, M.; Terziev, N. Decay Resistance of Wood Treated with Boric Acid and Tall Oil Derivates. *Bioresour. Technol*. **2008**, *99*, 2102-2106. https://doi.org/10.1016/j.biortech.2007.08.052

[7] Intharapat, P.; Nakason, C.; Kongnoo, A. Preparation of Boric Acid Suppored Natural Rubber as A Reactive Flame Retardant and Its Properties. Decay Resistance of Wood Treated with Boric Acid and Tall Oil Derivates. *Bioresour. Technol*. **2008**, *99*, 2102-2106. https://doi.org/10.1016/j.biortech.2007.08.052

[8] Suwanno, T.; Veenin, T.; Jarusombuti, S. Study on Fire Retardant Treatment of Rubberwood by Boron Compounds. *J. For.* **2017**, *36*, 129-135 (In Thai).

[9] Pankong, A.; Komoltree, B.; Tepsing, P. The Existences of Sugar Palms Wisdom in Sathing Phra Peinsula in The Midst. GTHJ. **2023**, *29*(20), 236-248 (In Thai).

[10] Worachetwarawat, P.; Pungchompoo, S.; Worachetwarawat, P.; Kuniart, B.; Podkumnerd, N. Furniture Product Design and Development Based on Consumer Demands: A Case Study of Products Made from Palmyra Palm Leaf Stalk in the Singha Nakhon Peninsula, Songkhla Province. *ECBAJ-TSU*. **2026**, *8*(1), 27-42 (In Thai).

[11] Pantamanatsopa, P.; Srivabut, C.; Homkhiew, C.; Boonchouytan, W.; Rawangwong, S.; Thongmung

[12] Kamnerdwam, A. Comparative Analysis of Rubberwood, Plywood, and Wood-Plastic Composites for Safe Elderly Toy Applications. *ASEAN J. Sci. Tech. Report*. **2025**, *29*(4), e260685. https://doi.org/10.55164/ajstr.v29i4.260685

[13] Yang, J. F.; Yang, C. H.; Liang, M. T.; Gao, Z. J.; Wu, Y. W.; Chuang, L. Y. Chemical Composition, Antioxidant, and Antibacterial Activity of Wood Vinegar from *Litchi chinensis*. *Molecules* **2016**, *21*, 1150. https://doi.org/10.3390/molecules21091150

[14] Ratanapisit, J.; Apiraksakul, S.; Rerngnarong, A.; Chungsiriporn, J.; Bunyakarn, C. Preliminary Evaluation of Production and Characterization of Wood Vinegar from Rubberwood. *Songklanakarin J. Sci. Technol*. **2009**, *31*, 343-349.

[15] Puttinun, P. Wood Vinegar. *Nat. Agric*. **2011**, *9*, 928–933 (In Thai).

[16] Grace, J. K.; Yamamoto, R. T. Repeated Exposure of Borate-Treated Douglas-Fir Lumber of Formosan Subterranean Termites in an Accelerated Field Test. *For. Prod. J.* **1994**, *44*, 65-67.

[17] Williams, L. H. Borate Wood-Protection Compounds: A Review of Research and Commercial Use. *APT Bull. J. Preser. Tech*. **1996**, *27*, 46-51- doi: 10.2307/1504564

[18] Kartal, S. N.; Ayrilmis, N. Blockboard with Boron-Treated Veneers: Laboratory Decay and Termite Resistance Tests. *Int. Biodeterior. Biodegrad.* **2005**, *55*, 93-98. https://doi.org/10.1016/j.ibiod.2004.08.001

[19] Kartal, S. N.; Ayrilmis, N.; Imamura, Y. Decay and Termite Resistance of Plywood Treated with Various Fire Retardants. *Build. Environ.* **2007**, *42*, 1207-1211. https://doi.org/10.1016.j.buildenv.2005.12.011

[20] Morris, D. L. Quantitative Determination of Carbohydrates with Dreywood's Anthrone Reagent. *Science* **1948**, *107*, 254-255. https://doi.org/10.1126/science.107.2775.254

[21] Miller, G. L. Use of Dinitrosalicylic Acid Reagent for Determination of Reducing Sugar. *Anal. Chem.* **1959**, *31*, 426-428. https://doi.org/10.1021/ac60147a030

[22] ASTM. *Standard Test Method for Laboratory Evaluation of Wood and Other Cellulosic Materials for Resistance to Termites*; ASTM D 3345-74; American Society for Testing and Materials: West Conshohocken, PA, 1999.

[23] ASTM. *Standard Test Method for Flexural Properties of Polymer Matrix Composite Materials*; ASTM D7264/D7264M-07; ASTM International: West Conshohocken, PA, 2007.

[24] Manosong, W.; Nuanla-ong, M.; Udomvech, A. Isolation of fiber-cellulose and characterization from oil palm frond for 3D and 4D printing materials application. *ASEAN J. Sci. Tech. Report*. **2024**, *27*(5), e253216. https://doi.org/10.55164/ajstr.v27i5.253216

[25] Yanjuan, W.; Yanxiong, F.; Wei, T.; Chunying, L. Preservation of Aged Paper Using Borax in Alcohols and the Supercritical Carbon Dioxide System. *J. Cult. Herit.* **2013**, *14*, 16-22. https://doi.org/10.1016/j.culher.2012.03.003

[26] Pedieu, R.; Bentis, A.; Riedl, B.; Wang, X. M.; Deng, J.; Braghiroli, F. L.; Koubaa, A. Enhancing Fire Resistance and Mechanical Properties of Wood Strand Boards by Impregnation with Sodium Bicarbonate and Sodium Borate. Polymers. **2025**, *17*, 2943. https:// doi.org/10.3390/polym17212943

[27] Tsunoda, K. Preservative Properties of Vapor-Boron-Treated Wood and Wood-Based Composites. J. Wood. Sci. **2001**, *47*(2), 149-153. https://doi.org/1007/bf00780565

[28] Anggraini, R.; Khabibi, J.; Ridho, M. R. Utilization of Wood Vinegar as a Natural Preservative for Sengon Wood (*Falcataria moluccana* Miq.) against Fungal Attack (*Schizophyllum commune* Fries). J. Sylva Lestari. **2021**, *9*(2), 302-313. https://doi.org/10.23960/jsl29302-313

ASEAN
Journal of Scientific and Technological Reports
Online ISSN:2773-8752

Research article

FlexIoU: Modularity and Flexibility IoU for Bounding Box Regression in Agricultural Disease Detection

Naphat Keawpibal[1, 2*], Ajaree Naco[1], Kanida Sinmai[1], and Noppamas Pukkhem[1]

[1] Faculty of Science and Digital Innovation, Thaksin University, Phatthalung, 93210, Thailand
[2] Research Center for Indigenous Plant Species in ASEAN Culture, Thaksin University, Phatthalung, 93210, Thailand
* Correspondence: naphat.k@tsu.ac.th

Citation:
Keawpibal, N.; Naco, A.; Sinmai, K.; Pukkhem, N. FlexIou: Modularity and flexibility IoU for bounding box regression in agricultural disease detection. *ASEAN J. Sci. Tech. Report.* **2026**, *29*(7), e263179. https://doi.org/10.55164/ajstr.v29i7.263179

Article history:
Received: January 9, 2026
Revised: June 3, 2026
Accepted: June 6, 2026
Available online: June 14, 2026

Publisher's Note:
This article is published and distributed under the terms of the Thaksin University.

Abstract: Accurate bounding-box regression plays a crucial role in object detection, particularly in agricultural disease detection, where target objects are often small, irregular, and weakly bounded. Although Intersection over Union (IoU)-based losses such as CIoU and EIoU have improved localization performance, their fixed geometric penalty formulations limit adaptability to domain-specific object characteristics. In this work, we propose FlexIoU, a flexible and lightweight IoU-based regression loss that introduces tunable geometric penalties to enhance localization robustness. FlexIoU provides explicit control over center-distance, width, and height penalties, enabling more adaptive regression behavior for irregular lesion shapes commonly observed in agricultural imagery. The proposed loss integrates seamlessly into the YOLO training pipeline as a drop-in replacement for conventional IoU-based losses, without modifying classification or distribution focal loss components, thereby preserving inference efficiency. We evaluate FlexIoU within a YOLOv11 detection framework on a tomato leaf disease dataset under identical experimental settings and across three random seeds to ensure statistical reliability. Experimental results demonstrate that FlexIoU consistently outperforms the default YOLOv11 regression objective as well as CIoU and EIoU in terms of mAP@0.5:0.95 and overall detection balance, while maintaining stable inference speed comparable to baseline losses. These findings indicate that FlexIoU provides an effective and practical solution for improving bounding-box regression in agricultural disease detection. While the results demonstrate promising robustness across two tomato disease datasets, further validation on additional agricultural and general object detection datasets is required.

Keywords: Object detection; IoU-based loss; FlexIoU; agricultural disease detection; precision agriculture

1. Introduction

Precision agriculture has emerged as a key strategy for increasing crop productivity, reducing resource consumption, and improving early detection of plant diseases [1-3]. Accurate identification and localization of diseased regions on leaves enable timely interventions, minimize pathogen spread, and support automated decision-making in smart farming systems. With the rapid advancement of deep learning, object detection models—especially the YOLO family [4-10], have become widely adopted for real-time object detection. Recent studies have successfully applied YOLO-based models to agricultural disease detection tasks, including tomato disease recognition and plant pest

identification [11-15]. However, the effectiveness of these models depends not only on architectural design but also heavily on the loss function used to guide bounding-box regression during training. In plant-disease imagery, lesions often appear as small, irregular, partially occluded, or non-uniformly shaped regions [3,11]. Leaves vary widely in size, aspect ratio, orientation, and deformation, creating additional challenges for bounding-box localization. These characteristics underscore the importance of a regression loss that effectively penalizes geometric discrepancies between predicted and ground-truth boxes [16]. A loss function that behaves well on general object detection datasets may perform poorly in agricultural settings, where lesion boundaries are subtle and precise localization is crucial for accurate disease diagnosis [3,11,14].

The most fundamental metric for bounding-box regression is the Intersection over Union (IoU), which measures the overlap ratio between predicted and ground-truth boxes [16-18]. Although IoU is widely used, it suffers from a major limitation: the gradient vanishes when boxes do not overlap, leading to unstable early-stage optimization. To address this, several extensions have been proposed. Complete IoU (CIoU) [19] incorporates center-distance and aspect-ratio terms to accelerate convergence, while Enhanced IoU (EIoU) [20] decouples width and height deviations for more stable regression. These methods have improved performance on general object detection tasks, yet they still rely on fixed penalty formulations [21, 22]. Such fixed penalties may not generalize well across agricultural datasets where object geometry varies significantly. Moreover, CIoU and EIoU lack explicit control over the influence of different geometric components, limiting their adaptability to datasets with imbalanced lesion sizes or highly elongated leaf structures.

Beyond distance- and scale-decomposition, recent work incorporates directional or angular components to enhance regression performance. SIoU [23] introduces an angle-based penalty that encourages predicted boxes to move toward the ground-truth direction more efficiently, potentially accelerating convergence. While SIoU improves early-stage regression, its angle-based formulation introduces additional computational cost and is sensitive to noisy boxes. MPDIoU [24] and Minimum-Point-Distance approaches aim to unify area overlap, center-distance, and width–height deviation using geometric projections. These losses demonstrate competitive performance in certain domains; however, they typically involve more complex geometric transformations and do not provide explicit modularity or tunable weighting for different penalty terms. In oriented object detection, such as in aerial imagery and scene text recognition, the limitations of axis-aligned IoU become more pronounced. Losses such as Rotated IoU [25], FPDIoU [26], and EPIoU loss [27] account for rotation angles and corner distances to guide regression. Although effective for rotated bounding boxes, these methods introduce substantial computational overhead, making them unsuitable for mainstream real-time detectors like YOLO unless specifically targeting rotated domains.

Given these limitations, there is a strong need for a flexible, tunable IoU-based regression loss that can adapt to the diverse geometric characteristics of agricultural imagery. A loss function that allows independent control over center distance, aspect ratio, and side-length deviations would provide better localization performance and enable tailored optimization strategies for different plant species or disease types. Such tunability is particularly valuable when working with datasets that exhibit class imbalance, size variation, or high lesion irregularity, all of which are common in real-world farming scenarios.

To address these limitations, this study introduces FlexIoU, a modular, tunable IoU-based regression loss that enhances bounding-box regression for plant-disease detection. FlexIoU decomposes the geometric relationship into interpretable, weighted components, allowing for flexible adaptation. Extensive evaluations on a benchmark tomato leaf disease dataset, along with preliminary validation, demonstrate that FlexIoU achieves superior localization robustness and improved regression performance compared to state-of-the-art IoU-based losses, such as CIoU and EIoU.

The main contributions of this work are as follows:

1. We introduce a modular geometric formulation that enhances regression stability and interpretability compared to existing IoU-based losses.
2. We propose FlexIoU, a tunable IoU-based regression loss that allows explicit control over center-distance, aspect-ratio, width, and height penalties, enabling flexible adaptation to agricultural imagery.

3. FlexIoU integrates seamlessly with the YOLO loss pipeline without modifying the classification or DFL components, enabling a drop-in replacement for CIoU.
4. We evaluate FlexIoU on agricultural datasets, including tomato leaf disease imagery, demonstrating improved localization robustness for small and irregular disease symptoms.
5. We conduct comparative experiments across multiple random seeds, demonstrating consistent regression behavior and providing insights into the impact of tuning geometric weights.

2. Materials and Methods

This section describes the research framework, baseline loss functions, and the proposed FlexIoU formulation. The overall methodology follows a unified training–evaluation pipeline in which each loss function is tested under identical experimental settings and repeated across three random seeds to ensure statistical stability.

2.1 Research Framework

This study follows a unified experimental framework designed to systematically evaluate the impact of different IoU-based loss functions on bounding-box regression performance. The overall pipeline is illustrated in Figure 1 and consists of dataset preparation, model training with interchangeable regression losses, and performance evaluation on held-out test sets.

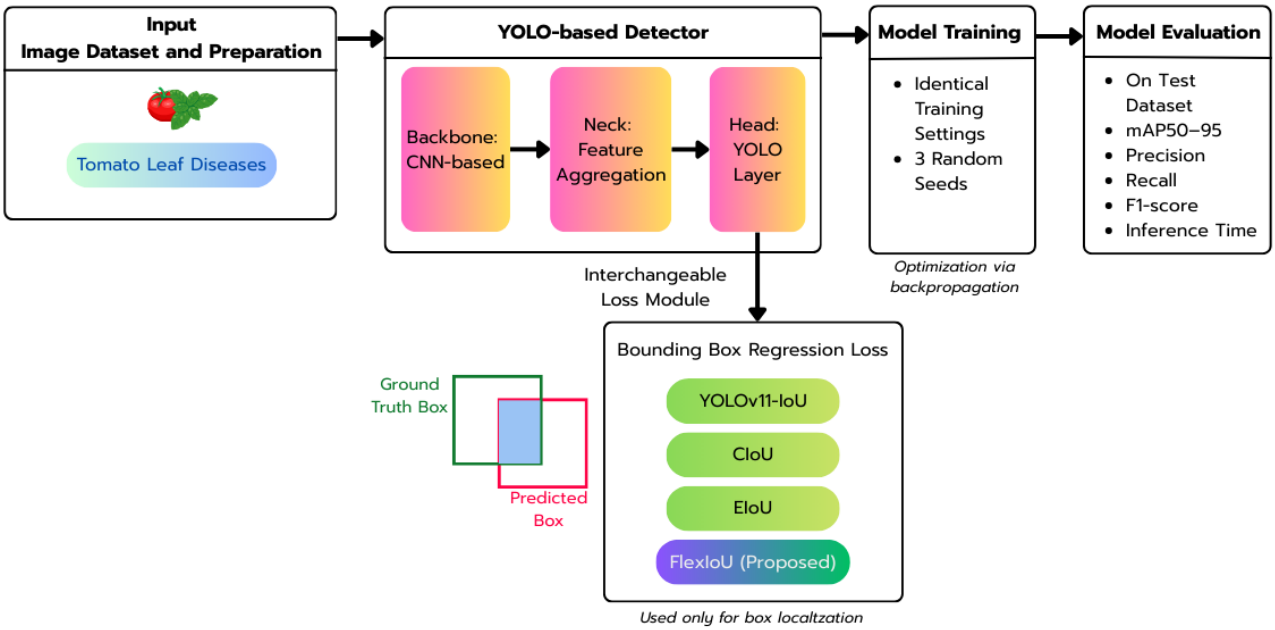


Figure 1. Overview of the research framework.

Given an input image, object detection is performed using a YOLO-based architecture, which jointly predicts class probabilities and bounding-box parameters. The dataset is first divided into training, validation, and test subsets to ensure unbiased evaluation. During training, images from the training set are passed through the YOLO backbone and detection head to generate predicted bounding boxes. These predictions are then compared against the corresponding ground-truth annotations through an IoU-based regression loss.

To enable a fair comparison, the regression loss component is treated as a modular element within the YOLO training pipeline. Specifically, four different loss functions—IoU, CIoU, EIoU, and the proposed FlexIoU—are independently integrated into the bounding-box regression branch while keeping all other components unchanged. Classification loss and objectness loss follow the default YOLO configuration, ensuring that observed performance differences are primarily due to the regression loss design.

Each model is trained using identical hyperparameters and optimization settings, and the training process is repeated using three fixed random seeds. This multi-seed strategy reduces stochastic variance and

provides a more reliable assessment of loss stability and convergence behavior. After training, the final models are evaluated on the test set, where detection performance is measured using standard object detection metrics such as mean Average Precision (mAP) and inference time. This framework allows the proposed FlexIoU loss to be evaluated under controlled, reproducible conditions, while enabling direct comparisons with established IoU-based losses. By isolating the effect of the regression loss within the YOLO architecture, the framework provides clear insight into how different geometric penalty formulations influence localization accuracy, convergence stability, and generalization performance.

2.2 Baseline IoU-based Loss Functions

Bounding-box regression is a core component of modern object detection frameworks, determining how effectively a detector localizes objects of interest. In YOLO-based models, this regression traditionally relies on IoU-driven losses because Intersection over Union remains the most intuitive and widely adopted measure of spatial overlap between predicted and ground-truth bounding boxes. However, IoU alone is insufficient for ensuring stable optimization, motivating the development of extended formulations such as CIoU and EIoU. In this section, we describe these baseline losses in detail to establish a clear foundation for evaluating the proposed FlexIoU.

2.2.1. IoU Loss

Intersection over Union (IoU) evaluates the geometric overlap between two bounding boxes:

$$IoU = \frac{|B_p \cap B_g|}{|B_p \cup B_g|} \tag{1}$$

where $B_p \cap B_g$ refers to the intersection region between the two boxes and $B_p \cup B_g$ is their union.

The loss function corresponding to this measure is:

$$\mathcal{L}_{IoU} = 1 - IoU \tag{2}$$

This loss directly penalizes low overlap and reaches its minimum when the predicted and ground-truth boxes coincide exactly. However, despite its conceptual simplicity, IoU suffers from two well-known limitations. First, when B_p and B_g do not intersect, $|B_p \cap B_g| = 0$, leading to $IoU = 0$ and a zero gradient with respect to box coordinates. In such cases, the model receives no meaningful signal to guide the predicted box toward the target, which can severely slow convergence during early training. Second, IoU depends solely on the overlapping area and does not encode any information about the distance between box centers, their relative position, or their shape similarity. As a result, two pairs of boxes may yield the same IoU value even if one pair is well-aligned but slightly shifted, while the other is far apart but happens to overlap marginally. These weaknesses often lead to slow and sometimes unstable optimization, especially in datasets containing small or sparsely distributed objects, such as agricultural disease lesions, where slight misalignments can drastically affect detection quality.

2.2.2. CIoU Loss

To overcome the limitations of IoU, Zheng et al. introduced the Complete IoU (CIoU) loss, which augments the original formulation with additional geometric constraints. While IoU considers only the overlapping area, CIoU integrates (1) the distance between bounding-box centers and (2) the discrepancy in aspect ratio. These additional terms enable more stable and discriminative gradients during optimization.

Let $p = (x_p, y_p)$ and $g = (x_g, y_g)$ denote the center coordinates of the predicted and ground-truth bounding boxes, respectively. Let $\rho(p, g)$ represent the Euclidean distance between the two centers:

$$\rho(p, g) = \sqrt{(x_p - x_g)^2 + (y_p - y_g)^2} \tag{3}$$

Let c be the diagonal length of the smallest enclosing box that contains both the predicted and ground-truth boxes. CIoU is defined as:

$$\mathcal{L}_{CIoU} = 1 - IoU + \frac{\rho^2(p,g)}{c^2} + \alpha v, \tag{4}$$

where v represents the aspect-ratio penalty term, defined as

$$v = \frac{4}{\pi^2}\left(\tan^{-1}\frac{w_g}{h_g} - \tan^{-1}\frac{w_p}{h_p}\right)^2 \tag{5}$$

Here,

- w_p, h_p: width and height of the predicted box,
- w_g, h_g: width and height of the ground-truth box

The first additional term, ρ^2/c^2, directly penalizes deviations in box location, providing meaningful gradients even when IoU is zero (i.e., when boxes do not overlap). The second term, αv, penalizes aspect-ratio discrepancies, with α dynamically balancing the contribution of the shape penalty to ensure stable and proportional regression.

Despite its advantages, CIoU employs fixed, hard-coded balancing between its distance and aspect-ratio components. Models trained on domains with highly variable object shapes—such as diseased leaves, which exhibit irregular lesions—may require different penalization strengths, but CIoU does not allow such adaptation. This motivates the development of more flexible formulations, such as the proposed FlexIoU.

2.2.3. EIoU Loss

Extended IoU (EIoU) addresses another limitation of CIoU: its aspect-ratio penalty indirectly influences width and height without explicitly optimizing them. In many real-world cases—especially agricultural images where lesions vary dramatically in width, elongation, and local deformation—separating width and height regression can significantly improve convergence.

Let (w_p, h_p) and (w_g, h_g) denote the width-height pairs of the predicted and ground-truth boxes, respectively. Let w_c and h_c be the width and height of the smallest enclosing box containing both boxes. EIoU is defined as:

$$\mathcal{L}_{EIoU} = 1 - IoU + \frac{(w_p - w_g)^2}{w_c^2} + \frac{(h_p - h_g)^2}{h_c^2} \tag{6}$$

The additional terms explicitly penalize width and height differences:

- $\frac{(w_p - w_g)^2}{w_c^2}$: width deviation
- $\frac{(h_p - h_g)^2}{h_c^2}$: height deviation

This decomposition enables direct supervision of the predicted box's shape, generally yielding faster convergence and more stable regression than CIoU, especially for narrow, elongated, or irregularly shaped targets. However, similar to CIoU, EIoU employs fixed penalty strengths, applying the same geometric constraints uniformly across datasets regardless of object morphology or scale variation. Thus, although EIoU improves optimization behavior, it still lacks the adaptability required for domain-specific tuning—an issue that the proposed FlexIoU addresses by introducing user-configurable weighting for each geometric component.

2.3 Proposed FlexIoU Loss

Accurate bounding box regression is fundamental to YOLO-based object detectors, as localization quality directly influences both classification confidence and final detection accuracy. Although IoU-based loss functions have been widely adopted to improve localization by incorporating geometric constraints, most existing formulations employ fixed penalty terms that treat all geometric components equally across different datasets. In practice, however, object characteristics such as scale, shape, and spatial distribution can vary substantially, particularly in agricultural imagery where objects often exhibit irregular shapes, elongated structures, or small target regions. Motivated by this observation, we propose FlexIoU, a flexible IoU-based loss function that allows explicit and independent control over key geometric components involved in

bounding box regression. Rather than enforcing a rigid formulation, FlexIoU enables adaptive weighting of center alignment and shape-related penalties, thereby improving robustness across diverse detection scenarios while preserving the efficiency of the original YOLO training pipeline.

2.3.1 Formulation of FlexIoU

Let $B_p = (x_p, y_p, w_p, h_p)$ denote the predicted bounding box and $B_g = (x_g, y_g, w_g, h_g)$ denote the corresponding ground-truth bounding box, where (x, y) represent the box center coordinates, and w and h denote width and height, respectively. FlexIoU is defined as a similarity score composed of the standard IoU term and multiple weighted geometric penalties:

$$FlexIoU(B_p, B_g) = IoU - (\lambda_c \mathcal{L}_{center} + \lambda_a \mathcal{L}_{aspect} + \lambda_w \mathcal{L}_{width} + \lambda_h \mathcal{L}_{height}) \quad (7)$$

where λ_c, λ_a, λ_w and λ_h are tunable weight coefficients that regulate the relative importance of each penalty term. This formulation decomposes bounding box regression into interpretable components, allowing each term to contribute independently to the optimization process.

2.3.2 IoU Term

The Intersection over Union (IoU) between B_p and B_g is computed as

$$IoU = \frac{|B_p \cap B_g|}{|B_p \cup B_g|} \quad (8)$$

The term IoU serves as the primary overlap-driven objective, directly encouraging the predicted box to maximize its intersection with the ground truth. However, IoU alone provides limited gradient information when predicted and ground-truth boxes do not overlap, which often occurs during early training stages. Consequently, additional geometric constraints are required to better guide the regression process.

2.3.3 Center Distance Penalty

To address spatial misalignment between bounding boxes, FlexIoU incorporates a center distance penalty defined as

$$\mathcal{L}_{center} = \frac{(x_p - x_g)^2 + (y_p - y_g)^2}{c^2} \quad (9)$$

where (x_p, y_p) and (x_g, y_g) denote the center coordinates of the predicted and ground-truth boxes, respectively. The normalization term c^2 represents the squared diagonal length of the smallest enclosing (convex) box that covers both B_p and B_g, and is defined as $c^2 = w_c^2 + h_c^2$, where w_c and h_c denote the width and height of the smallest enclosing box, respectively.

This normalization ensures scale invariance and prevents excessively large gradients for objects of different sizes. By explicitly penalizing large center offsets, this term provides meaningful gradient signals even when the predicted and ground-truth boxes do not overlap. The influence of spatial alignment can be adjusted via the weighting coefficient λ_c, which is particularly beneficial for small or sparsely distributed objects commonly found in agricultural imagery.

2.3.4 Aspect Ratio Penalty

To account for shape discrepancies caused by aspect-ratio differences, FlexIoU adopts an aspect-ratio penalty inspired by CIoU.

$$\mathcal{L}_{aspect} = \alpha \cdot \frac{4}{\pi^2} \left(\tan^{-1} \frac{w_g}{h_g} - \tan^{-1} \frac{w_p}{h_p} \right)^2 \quad (10)$$

where α is a dynamic balancing factor following the original CIoU formulation, designed to regulate the contribution of the aspect-ratio term relative to IoU, this penalty encourages consistent proportional scaling between predicted and target boxes, reducing oscillation caused by shape mismatch.

Although the CIoU formulation inspires the aspect-ratio term, FlexIoU extends its role through an independent weighting mechanism rather than introducing a new aspect-ratio equation. Unlike CIoU, where the aspect-ratio penalty is incorporated as a fixed component of the regression loss, FlexIoU allows the contribution of the aspect-ratio term to be explicitly adjusted through λa. This design enables the aspect-ratio

penalty to be strengthened, reduced, or disabled entirely (λa = 0) based on object characteristics and dataset requirements. Consequently, the novelty of FlexIoU lies not in redefining the aspect-ratio penalty itself, but in transforming the fixed CIoU penalty structure into a flexible weighting framework that allows center-distance, aspect-ratio, width, and height penalties to be independently controlled. This provides greater adaptability than the fixed-weighting strategy used by CIoU.

2.3.5 Width and Height Penalties

In addition to spatial alignment, accurate shape estimation is essential for precise localization. FlexIoU therefore introduces independent penalties for width and height discrepancies:

$$\mathcal{L}_{width} = \frac{(w_p - w_g)^2}{w_c^2}, \mathcal{L}_{height} = \frac{(h_p - h_g)^2}{h_c^2} \tag{11}$$

where w_c and h_c represent the width and height of the smallest enclosing box, respectively.

Unlike aspect-ratio-based penalties that couple width and height into a single term, this decomposition allows FlexIoU to handle anisotropic shape variations more effectively. In agricultural detection tasks, objects such as leaves or disease regions often exhibit elongated or irregular geometries, where width and height errors may have different semantic importance. The independent weighting coefficients λ_w and λ_h enable targeted shape refinement without imposing unnecessary constraints.

2.3.6 Integration into YOLO Training

During training, FlexIoU replaces only the bounding-box regression component of the default YOLOv11 localization loss. The Distribution Focal Loss (DFL) remains unchanged and follows the standard YOLOv11 implementation. The overall training objective is expressed as

$$\mathcal{L}_{Total} = \lambda_{box}(1 - FlexIoU) + \lambda_{cls}\mathcal{L}_{cls} + \lambda_{dfl}\mathcal{L}_{dfl} \tag{12}$$

In the baseline YOLOv11 implementation, the localization term is computed using the default IoU-based regression loss together with DFL. In the proposed approach, only the localization term is replaced with FlexIoU, while all other training components and hyperparameters are kept identical for a fair comparison.

No additional prediction branches or inference-time operations are introduced. As a result, it preserves the computational efficiency and inference speed of the original YOLO architecture, making it suitable for deployment on resource-constrained and edge devices.

2.3.7 Practical Interpretation

FlexIoU's flexibility allows the loss function to be tailored to specific detection scenarios. Emphasizing the center penalty improves convergence stability for small objects, while increasing width or height penalties enhances shape accuracy for elongated targets. This tunable design enables FlexIoU to adapt across both generic benchmarks and domain-specific datasets without architectural modifications. To facilitate practical deployment and reproducibility, the proposed FlexIoU loss defined in Section 2.3 is summarized in Algorithm 1. The algorithm explicitly follows the mathematical formulation presented in Eqs. (7) - (11), detailing the computation of overlap, spatial alignment, and shape discrepancy terms used during bounding box regression. This algorithm is applied during the training phase of YOLO-based detectors to compute the localization loss for each matched prediction–ground-truth pair.

Algorithm 1. FlexIoU Bounding Box Regression

Input: predicted box $B_p = (x_p, y_p, w_p, h_p)$, ground-truth box $B_g = (x_g, y_g, w_g, h_g)$, weights λ_c, λ_a, λ_w, λ_h
Output: FlexIoU similarity score and bounding-box regression loss ($FlexIoU$ and $\mathcal{L}_{box}$)

function FlexIoU(B_p, B_g, λ_c, λ_a, λ_w, λ_h)

Step 1: Convert (center, w, h) → box corners for overlap computation
$x_{p1} \leftarrow x_p - w_p/2;\ y_{p1} \leftarrow y_p - h_p/2;$
$x_{p2} \leftarrow x_p + w_p/2;\ y_{p2} \leftarrow y_p + h_p/2;$
$x_{g1} \leftarrow x_g - w_g/2;\ y_{g1} \leftarrow y_g - h_g/2;$
$x_{g2} \leftarrow x_g + w_g/2;\ y_{g2} \leftarrow y_g + h_g/2;$

Step 2: Compute intersection area
$x_{i1} \leftarrow \max(x_{p1}, x_{g1});\ y_{i1} \leftarrow \max(y_{p1}, y_{g1});$
$x_{i2} \leftarrow \min(x_{p2}, x_{g2});\ y_{i2} \leftarrow \min(y_{p2}, y_{g2});$
$i_w \leftarrow \max(0, x_{i2} - x_{i1})$
$i_h \leftarrow \max(0, y_{i2} - y_{i1})$
$A_{int} \leftarrow i_w * i_h$

Step 3: Compute union area and IoU
$A_p \leftarrow w_p * h_p$
$A_g \leftarrow w_g * h_g$
$A_{union} \leftarrow A_p + A_g - A_{int} + \varepsilon$
$IoU \leftarrow A_{int}/A_{union}$

Step 4: Smallest enclosing box (for normalization terms)
$x_{c1} \leftarrow \min(x_{p1}, x_{g1});\ y_{c1} \leftarrow \min(y_{p1}, y_{g1});$
$x_{c2} \leftarrow \max(x_{p2}, x_{g2});\ y_{c2} \leftarrow \max(y_{p2}, y_{g2});$
$w_c \leftarrow (x_{c2} - x_{c1}) + \varepsilon$
$h_c \leftarrow (y_{c2} - y_{c1}) + \varepsilon$
$d^2 \leftarrow w_c^2 + h_c^2 + \varepsilon$

Step 5: Center distance penalty
$d_x \leftarrow x_p - x_g$
$d_y \leftarrow y_p - y_g$
$\mathcal{L}_{center} \leftarrow (d_x^2 + d_y^2)/d^2$

Step 6: Aspect ratio penalty
$v \leftarrow 4/\pi^2 \times \left(\tan^{-1}(w_g/h_g) - \tan^{-1}(w_p/h_p)\right)^2$
$\alpha \leftarrow v/(v - IoU + (1 + \varepsilon))$
$\mathcal{L}_{aspect} \leftarrow \alpha \times v$

Step 7: Width/height penalties
$\mathcal{L}_{width} \leftarrow (w_p - w_g)^2/w_c^2$
$\mathcal{L}_{height} \leftarrow (h_p - h_g)^2/h_c^2$

Step 7: FlexIoU similarity
$FlexIoU \leftarrow IoU - (\lambda_c \times \mathcal{L}_{center} + \lambda_a \times \mathcal{L}_{aspect} + \lambda_w \times \mathcal{L}_{width} + \lambda_h \times \mathcal{L}_{height})$

Step 8: Final FlexIoU loss
$\mathcal{L}_{box} \leftarrow 1 - FlexIoU$

return $FlexIoU$, $\mathcal{L}_{box}$
end function
* ε is a small constant (e.g., 10^{-7} to avoid division by zero)

Algorithm 1 is invoked for each positive–ground-truth pair during training and used exclusively to compute the bounding-box regression loss within the YOLO detection head. The resulting FlexIoU loss is then combined with classification and DFL as described in Eq. (12) and optimized via backpropagation.

2.4 Experimental Setup

This section describes the datasets, data preparation, training configuration, and implementation details used to evaluate the proposed FlexIoU loss under controlled and reproducible conditions. All experiments were designed to ensure a fair comparison between baseline IoU-based losses and the proposed method by keeping the detection architecture and training settings identical across all configurations.

2.4.1 Datasets

Experiments were conducted on the Tomato Leaf Disease dataset, which is publicly available on Kaggle under the CC0 (Public Domain) license at: https://www.kaggle.com/datasets/farukalam/tomato-leaf-diseases-detection-computer-vision. This dataset represents a practical agricultural object detection scenario, consisting of images of tomato leaves affected by multiple disease types. The diseased regions exhibit irregular lesion shapes, varying object scales, and fine-grained visual patterns, which pose significant challenges for accurate bounding-box localization. Such characteristics make the dataset particularly suitable for evaluating the effectiveness of IoU-based regression losses under complex geometric variations. In particular, small lesion regions, non-uniform shapes, and ambiguous boundaries highlight the limitations of fixed geometric penalties and motivate the need for more flexible loss formulations. The dataset contains a total of 1,082 images, which were divided into 938 training images, 96 validation images, and 48 test images using a consistent split strategy to ensure unbiased evaluation. The test set was completely excluded from both training and validation and used exclusively for final performance assessment. This separation allows the reported results to reflect true generalization performance rather than memorization of training data. Detailed dataset statistics, including the number of images per class and their distribution across training, validation, and test splits, are summarized in Table 1.

Table 1. Dataset statistics of the tomato leaf disease dataset

Class	Train	Validation	Test	Total
Bacterial Spot	45	3	2	**50**
Black Spot	191	21	9	**221**
Early Blight	321	31	15	**367**
Healthy	162	19	7	**188**
Late Blight	144	13	9	**166**
Leaf Mold	45	4	4	**53**
Target Spot	30	5	2	**37**
Total	**938**	**96**	**48**	**1,082**

It should be noted that the dataset exhibits class imbalance across disease categories. For example, the Early Blight class contains substantially more training images than the Target Spot class. No class weighting, oversampling, or resampling techniques were applied in this study, as the objective was to evaluate the effect of the proposed regression loss within the standard YOLO training pipeline.

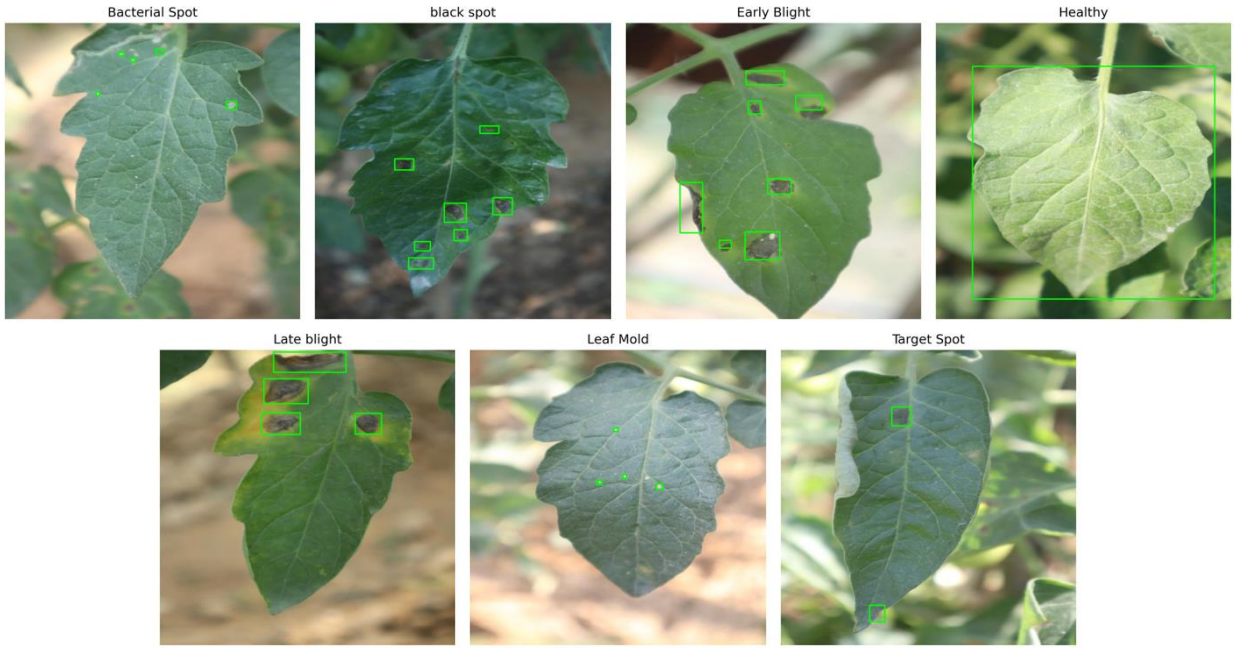


Figure 2. Samples of the tomato leaf disease dataset with ground-truth annotations.

To provide a qualitative understanding of the dataset, Figure 2 presents representative training samples with ground-truth annotations. Each image includes a green bounding box indicating the annotated disease region. The examples illustrate substantial variability in lesion size, shape, and visual appearance across different disease categories, further emphasizing the challenges of bounding-box regression in agricultural disease detection.

2.4.2 Data Preprocessing and Annotation

All images were resized to 640 × 640 pixels before training and evaluation, following the default YOLOv11 preprocessing pipeline. Ground-truth annotations were converted to the standard YOLO bounding-box format, representing each object as normalized center coordinates, width, and height. No dataset-specific geometric augmentation was introduced to avoid biasing the regression behavior toward a particular loss formulation.

2.4.3 Training Configuration

All models were trained using the same YOLOv11 detector architecture, with the bounding-box regression loss being the only interchangeable component. The classification loss and Distribution Focal Loss (DFL) formulations remained unchanged throughout the experiments. Training was performed with identical hyperparameters across all experiments, including the learning rate schedule, batch size, optimizer settings, image resolution, and number of epochs, as shown in Table 2.

Table 2. Training hyperparameters used in all experiments

Hyperparameter	Value
Input Resolution	640 × 640
Epochs	100
Batch Size	16
Optimizer	MuSGD
Initial Learning Rate	0.01
Momentum	0.90
Random Seeds	0, 1, 2
Device	NVIDIA L4

To investigate the tunability of the proposed FlexIoU loss, a sensitivity analysis was conducted by varying the geometric penalty coefficients λ_c, λ_a, λ_w, and λ_h. Eight coefficient combinations were evaluated, as summarized in Table 3. In addition, different loss-weighting settings for λ_{cls} and λ_{box} were investigated to examine the influence of balancing classification and localization objectives during training, as shown in Table 4. To reduce stochastic variance and improve statistical reliability, each experiment was repeated with three fixed random seeds, yielding three independently trained models per configuration. Results were reported as the mean performance across the three runs. The final FlexIoU configuration was selected based on validation performance and subsequently evaluated on the independent test set.

Table 3. FlexIoU coefficient configurations evaluated in the sensitivity analysis

Weight ID	λ_c	λ_a	λ_w	λ_h
W1	1.0	0.0	1.0	1.0
W2	1.0	0.5	1.0	1.0
W3	1.0	0.5	1.0	1.5
W4	1.0	0.5	1.5	1.0
W5	1.0	0.5	1.5	1.5
W6	1.0	1.0	1.0	1.0
W7	1.5	0.5	1.0	1.0
W8	1.5	0.5	1.5	1.5

Table 4. Loss-weighting configurations evaluated for FlexIoU

Loss ID	λ_{cls}	λ_{box}
C1	1.0	1.0
C2	1.0	1.5
C3	1.0	2.0
C4	1.2	1.5
C5	1.2	2.0

2.4.4 Implementation Details

All experiments were implemented using the Ultralytics YOLO framework. Training and evaluation were conducted on Google Colab with an Nvidia L4 GPU-enabled system to ensure consistent computational performance. During inference, identical post-processing steps, including non-maximum suppression, were applied to all models to ensure a fair comparison of both detection accuracy and inference efficiency. This experimental setup ensures that any observed performance differences among YOLOv11-IoU, CIoU, EIoU, and the proposed FlexIoU losses can be attributed primarily to the loss formulation itself rather than to architectural or training discrepancies.

2.5 Evaluation Metrics

To comprehensively assess the effectiveness of the proposed FlexIoU loss, detection performance was evaluated using standard metrics widely adopted in object detection research. These metrics capture both localization accuracy and computational efficiency, enabling a balanced comparison between baseline IoU-based losses and the proposed method. Detection accuracy was primarily measured using mean Average Precision (mAP), which evaluates the quality of predicted bounding boxes and classification confidence across different Intersection over Union thresholds. Specifically, mAP@0.5:0.95 was adopted, where Average Precision is computed at IoU thresholds from 0.5 to 0.95 with a step size of 0.05, then averaged. This metric provides a stringent evaluation of localization performance, as higher IoU thresholds require more precise alignment between predicted and ground-truth boxes. In addition to mAP, Precision and Recall were reported to analyze detection behavior further. Precision reflects the proportion of correctly predicted objects among all detections, while Recall measures the proportion of ground-truth objects that are successfully detected. Together, these metrics provide insight into the trade-off between false positives and false negatives and help interpret the impact of different regression losses on detection confidence. Beyond accuracy, inference efficiency is a critical consideration, particularly for real-time and edge-device applications. Inference

performance was evaluated by measuring the average inference time per image during the testing phase under identical hardware conditions. All models were evaluated using the same input resolution and post-processing configuration to ensure fair comparison. By jointly considering detection accuracy and inference efficiency, this evaluation protocol enables a comprehensive assessment of how different IoU-based loss functions affect both localization quality and practical deployment performance.

3. Results and Discussion

This section presents the experimental results of evaluating the proposed FlexIoU loss within a YOLOv11 detection framework on the tomato leaf disease dataset. The objective of this analysis is to examine whether introducing tunable geometric penalties can improve bounding-box regression performance within a controlled training pipeline while maintaining practical efficiency. To ensure a fair comparison, all models were trained using identical settings, and only the bounding-box regression loss was varied across four configurations: the default YOLOv11 regression (hereafter referred to as YOLOv11-IoU), CIoU, EIoU, and the proposed FlexIoU. All experiments were repeated across three random seeds, and performance is reported as mean values with corresponding standard deviations to reflect both effectiveness and stability

3.1 Hyperparameter Sensitivity Analysis of FlexIoU

Since FlexIoU introduces four tunable geometric penalty coefficients, an additional sensitivity analysis was conducted to identify promising coefficient configurations before performing the final evaluation. Eight coefficient combinations were evaluated under identical training conditions using λ_{cls} = 1.0 and λ_{box} = 1.0. To avoid selecting configurations solely based on localization accuracy, a weighted ranking score was used to consider localization quality, precision, and recall jointly. Specifically, a weight of 0.5 was assigned to mAP@0.5:0.95, while precision and recall were assigned weights of 0.2 and 0.3, respectively. The larger weight assigned to mAP@0.5:0.95 reflects its role as the primary evaluation metric for object detection, as it summarizes localization performance across multiple IoU thresholds. Precision was included to penalize excessive false-positive detections, whereas recall was given slightly higher importance to ensure that diseased regions were not overlooked. This weighting strategy was designed to favor configurations that achieve a balanced trade-off between localization accuracy and detection reliability rather than optimizing a single metric. The corresponding results are summarized in Table 5. Configurations ranked among the top five by weighted score are highlighted in bold and were subsequently selected for further investigation under different λcls and λbox settings.

Table 5. Sensitivity analysis of FlexIoU geometric penalty coefficients using λ_{cls} = 1.0 and λ_{box} = 1.0

Weight	mAP@0.5:0.95	Precision	Recall	F1-score
W1	**0.504 ± 0.005**	**0.801 ± 0.033**	**0.725 ± 0.003**	**0.761 ± 0.016**
W2	0.491 ± 0.006	0.760 ± 0.023	0.732 ± 0.036	0.746 ± 0.030
W3	**0.491 ± 0.014**	**0.775 ± 0.071**	**0.743 ± 0.036**	**0.756 ± 0.015**
W4	0.494 ± 0.001	0.719 ± 0.048	0.730 ± 0.043	0.723 ± 0.023
W5	**0.493 ± 0.008**	**0.754 ± 0.051**	**0.781 ± 0.033**	**0.766 ± 0.022**
W6	0.495 ± 0.006	0.767 ± 0.029	0.738 ± 0.031	0.751 ± 0.004
W7	**0.492 ± 0.017**	**0.768 ± 0.016**	**0.768 ± 0.017**	**0.768 ± 0.007**
W8	**0.498 ± 0.001**	**0.784 ± 0.051**	**0.728 ± 0.046**	**0.753 ± 0.008**

As shown in Table 5, different coefficient combinations led to noticeable variations in detection performance, confirming that FlexIoU's behavior is sensitive to the choice of geometric penalties. Although several configurations achieved similar mAP@0.5:0.95 values, differences in precision and recall led to different weighted scores. This observation indicates that evaluating coefficient configurations using a single metric may overlook important trade-offs between localization accuracy and detection reliability. Therefore, the weighted ranking strategy was adopted to identify configurations that provide a more balanced overall performance. Interestingly, configurations with different λ_a values produced different performance trends, suggesting that the contribution of the aspect-ratio penalty is dataset-dependent and may not always be

beneficial when applied with a fixed weight. This observation further supports the motivation behind FlexIoU, where the aspect-ratio penalty can be flexibly adjusted or completely disabled depending on object characteristics and localization requirements. The top-ranked configurations were subsequently evaluated under additional λ_{cls} and λ_{box} settings to investigate the interaction between geometric penalties and loss-weight balancing. The results of this second-stage sensitivity analysis are presented in Table 6.

Table 6. Performance of selected FlexIoU configurations under different λ_{cls} and λ_{box} settings.

Weight	λ_{cls}	λ_{box}	mAP@0.5:0.95	Precision	Recall	F1-score
W1	1.0	1.0	0.504 ± 0.005	0.801 ± 0.033	0.725 ± 0.003	0.761 ± 0.016
	1.0	1.5	0.504 ± 0.011	0.782 ± 0.042	0.746 ± 0.032	0.763 ± 0.007
	1.0	2.0	0.491 ± 0.003	0.774 ± 0.015	0.747 ± 0.009	0.760 ± 0.010
	1.2	1.5	0.492 ± 0.005	0.760 ± 0.040	0.739 ± 0.047	0.748 ± 0.013
	1.2	2.0	0.496 ± 0.016	0.753 ± 0.046	0.737 ± 0.015	0.744 ± 0.022
W3	1.0	1.0	0.491 ± 0.014	0.775 ± 0.071	0.743 ± 0.035	0.756 ± 0.015
	1.0	1.5	0.494 ± 0.011	0.765 ± 0.014	0.737 ± 0.026	0.751 ± 0.018
	1.0	2.0	0.482 ± 0.007	0.748 ± 0.042	0.739 ± 0.030	0.742 ± 0.005
	1.2	1.5	0.484 ± 0.004	0.738 ± 0.038	0.734 ± 0.009	0.736 ± 0.022
	1.2	**2.0**	**0.510 ± 0.010**	**0.784 ± 0.058**	**0.752 ± 0.046**	**0.765 ± 0.006**
W5	1.0	1.0	0.493 ± 0.008	0.754 ± 0.051	0.781 ± 0.033	0.766 ± 0.022
	1.0	1.5	0.499 ± 0.016	0.783 ± 0.018	0.732 ± 0.041	0.756 ± 0.014
	1.0	2.0	0.488 ± 0.009	0.750 ± 0.044	0.735 ± 0.015	0.742 ± 0.028
	1.2	1.5	0.495 ± 0.005	0.798 ± 0.010	0.721 ± 0.049	0.757 ± 0.023
	1.2	2.0	0.498 ± 0.008	0.721 ± 0.034	0.761 ± 0.020	0.740 ± 0.014
W7	1.0	1.0	0.492 ± 0.017	0.768 ± 0.016	0.768 ± 0.017	0.768 ± 0.007
	1.0	1.5	0.498 ± 0.017	0.751 ± 0.018	0.755 ± 0.007	0.753 ± 0.013
	1.0	2.0	0.487 ± 0.008	0.734 ± 0.015	0.735 ± 0.024	0.734 ± 0.005
	1.2	1.5	0.511 ± 0.012	0.786 ± 0.015	0.724 ± 0.035	0.754 ± 0.025
	1.2	2.0	0.503 ± 0.002	0.799 ± 0.012	0.742 ± 0.021	0.770 ± 0.007
W8	1.0	1.0	0.498 ± 0.001	0.784 ± 0.051	0.728 ± 0.046	0.753 ± 0.008
	1.0	1.5	0.489 ± 0.005	0.743 ± 0.035	0.715 ± 0.000	0.728 ± 0.016
	1.0	2.0	0.492 ± 0.005	0.756 ± 0.022	0.737 ± 0.020	0.746 ± 0.017
	1.2	1.5	0.503 ± 0.006	0.781 ± 0.018	0.755 ± 0.017	0.768 ± 0.017
	1.2	2.0	0.498 ± 0.002	0.769 ± 0.022	0.739 ± 0.008	0.754 ± 0.014

The results indicate that the optimal performance of FlexIoU depends not only on the geometric penalty coefficients but also on the balance between localization and classification objectives. Increasing λ_{box} generally places greater emphasis on bounding-box regression, whereas increasing λ_{cls} encourages improved classification performance. However, the influence of these parameters varies across coefficient configurations, suggesting that the best-performing setting cannot be determined solely from a single evaluation metric. To provide a more balanced assessment, the final configuration was selected using the weighted ranking score defined in Section 3.1, which combines mAP@0.5:0.95, precision, and recall with weights of 0.5, 0.2, and 0.3, respectively. Based on this criterion, configuration W3 (λ_c = 1.0, λ_a = 0.5, λ_w = 1.0, λ_h = 1.5, λ_{cls} = 1.2, and λ_{box} = 2.0) achieved the highest overall score and was therefore selected for final evaluation on the independent test set.

3.2 Quantitative Results on the Tomato Leaf Disease Dataset

Table 7 reports the quantitative performance of the evaluated bounding-box regression losses on the tomato leaf disease test set. Overall, the proposed FlexIoU achieves the highest mean mAP@0.5:0.95 among all compared methods, indicating improved localization accuracy across multiple IoU thresholds. This improvement is particularly relevant for tomato disease detection, where disease symptoms often appear as small, irregular, and weakly bounded regions that are challenging to localize accurately.

Table 7. Quantitative performance comparison on the tomato leaf disease test set

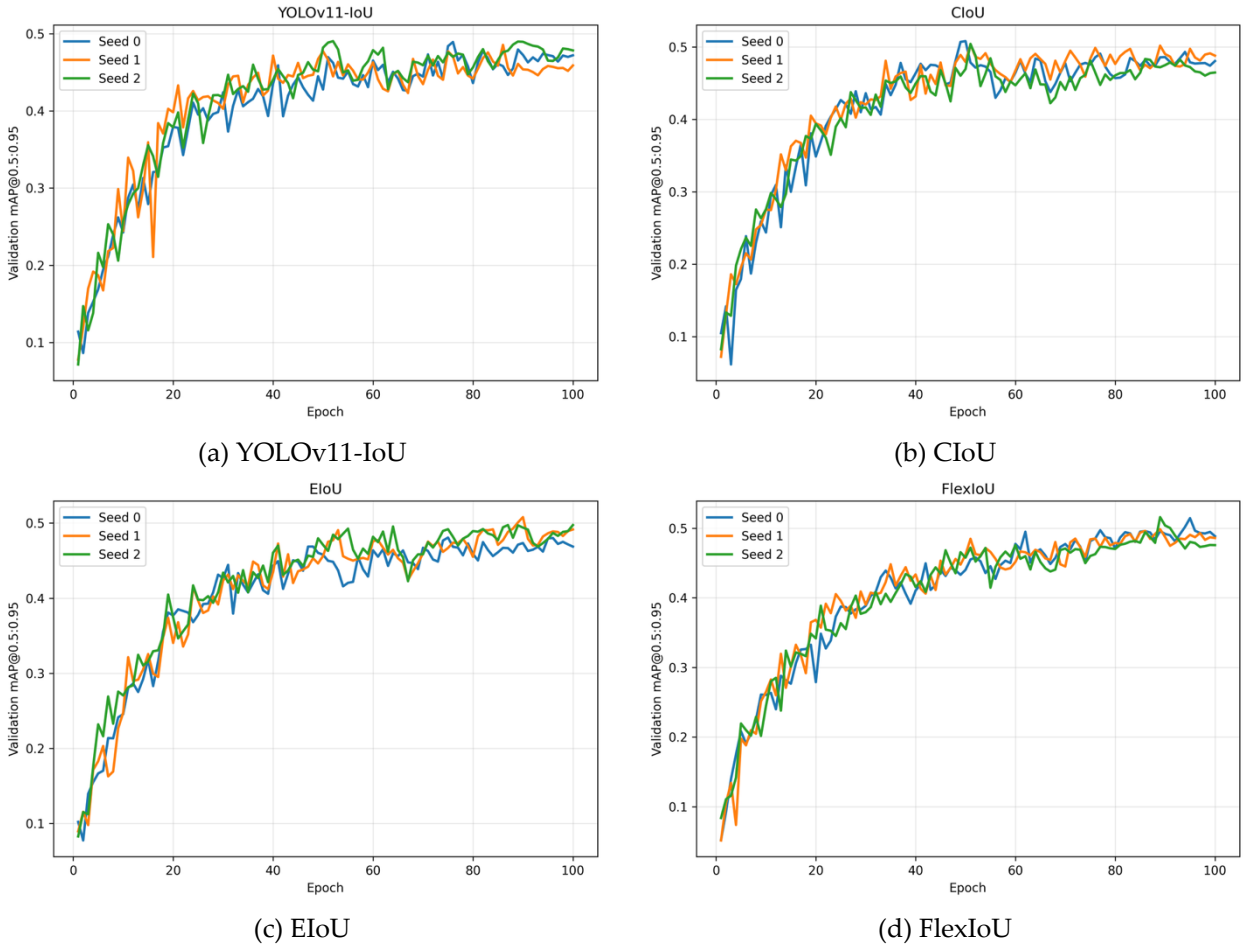
Loss	mAP@0.5:0.95	Precision	Recall	F1-score	Inference Time (ms)	FPS
YOLOv11-IoU	0.473 ± 0.029	0.690 ± 0.044	0.739 ± 0.064	0.711 ± 0.018	14.117 ± 0.133	70.842 ± 0.669
CIoU	0.464 ± 0.006	0.695 ± 0.082	0.742 ± 0.021	0.715 ± 0.035	14.147 ± 0.112	70.691 ± 0.563
EIoU	0.464 ± 0.015	0.632 ± 0.066	0.755 ± 0.029	0.687 ± 0.038	14.211 ± 0.102	**70.372 ± 0.507**
FlexIoU	**0.488 ± 0.005**	**0.751 ± 0.012**	**0.768 ± 0.005**	**0.759 ± 0.003**	**14.116 ± 0.083**	70.844 ± 0.419

Compared with the default YOLOv11 regression loss, FlexIoU improves mAP@0.5:0.95, precision, recall, and F1-score, indicating that introducing tunable geometric penalties can enhance localization performance. Among all evaluated methods, FlexIoU achieves the highest mean values across all reported detection metrics, suggesting a favorable balance between localization accuracy and classification reliability. While CIoU and EIoU provide alternative geometric formulations for bounding-box regression, their overall mAP@0.5:0.95 remains lower than both YOLOv11-IoU and FlexIoU on this dataset. As shown in Table 7, EIoU achieves the highest recall among the baseline methods, indicating a tendency to detect a larger proportion of disease regions. However, this behavior is accompanied by reduced precision, resulting in a lower overall F1-score. In contrast, FlexIoU simultaneously achieves the highest precision, recall, and F1-score, indicating a more balanced trade-off between false-positive and false-negative detections. Such a balance is particularly important in agricultural disease detection, where missed lesions may delay treatment decisions, while excessive false detections may lead to unnecessary interventions. Importantly, the performance improvements achieved by FlexIoU are not limited to a single training run. The relatively low standard deviations reported in Table 7 indicate stable performance across three independent random seeds. This observation suggests that the proposed loss function produces consistent detection behavior under different initialization conditions and does not rely on a specific random seed to achieve improved performance. Table 8 presents the statistical significance analysis of mAP@0.5:0.95 for FlexIoU relative to the baseline regression losses. FlexIoU achieved higher mean mAP@0.5:0.95 values than all evaluated baselines, with mean improvements of +0.0152, +0.0244, and +0.0248 over YOLOv11-IoU, CIoU, and EIoU, respectively.

Table 8. Statistical significance analysis of mAP@0.5:0.95 between FlexIoU and baseline losses across three random seeds

Comparison	FlexIoU mean	Baseline mean	Mean difference	Paired t-test p-value	Wilcoxon p-value
FlexIoU vs YOLOv11-IoU	0.4884	0.4732	+0.0152	0.5135	1.0000
FlexIoU vs CIoU	0.4884	0.4640	+0.0244	**0.0218**	0.2500
FlexIoU vs EIoU	0.4884	0.4636	+0.0248	0.0980	0.2500

The paired t-test revealed a statistically significant improvement of FlexIoU over CIoU ($p = 0.0218$). In contrast, the comparisons against YOLOv11-IoU ($p = 0.5135$) and EIoU ($p = 0.0980$) did not reach statistical significance under the current experimental setting. Similarly, the Wilcoxon signed-rank test did not indicate significant differences between FlexIoU and the baseline methods. These results should be interpreted in the context of the limited number of repeated runs used in this study. Although statistical significance was observed only for the comparison with CIoU, FlexIoU consistently achieved the highest mean values for mAP@0.5:0.95, precision, recall, and F1-score among all evaluated methods. Therefore, the overall experimental evidence suggests that FlexIoU provides a competitive and reliable improvement in localization performance on the tomato leaf disease dataset, while additional experiments with more repeated runs and a wider range of datasets would be beneficial for further validation. To further analyze the quantitative results, Figure 3 presents the convergence behavior of each regression loss across three independent random seeds in terms of validation mAP@0.5:0.95 over training epochs. By visualizing all three runs for each method, the figure provides a clearer view of training stability and reproducibility under different initialization conditions. Overall, the convergence trajectories exhibit similar trends across seeds, indicating that a single favorable run does not drive the reported performance.



(a) YOLOv11-IoU (b) CIoU

(c) EIoU (d) FlexIoU

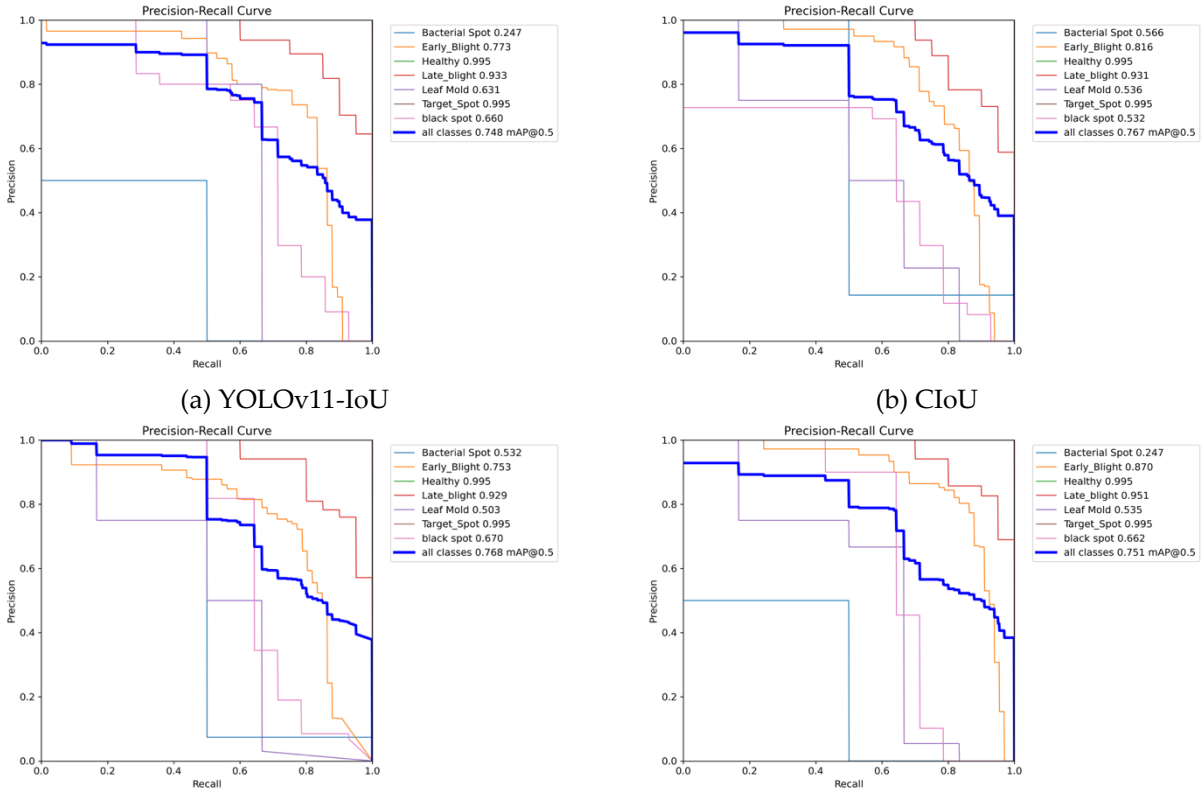
Figure 3. Convergence behavior of YOLOv11-IoU, CIoU, EIoU, and FlexIoU across three independent random seeds in terms of validation mAP@0.5:0.95.

Although minor variations can be observed among individual runs, all evaluated regression losses converge to stable performance levels during later training epochs. FlexIoU maintains competitive validation performance throughout training and demonstrates consistent convergence behavior across different random seeds. This observation is consistent with the statistical results reported in Table 8, where FlexIoU achieves the highest mean mAP@0.5:0.95 among the evaluated methods while maintaining relatively low variation across repeated runs. These findings suggest that the proposed tunable geometric penalties do not introduce unstable optimization dynamics and can maintain reliable training behavior under different initialization conditions. The convergence analysis therefore, provides additional evidence that the performance improvements achieved by FlexIoU are not dependent on a particular random seed and are consistently observed across repeated experiments.

3.3 Comparison with Baseline Loss Functions

To further analyze the behavior of the proposed FlexIoU loss beyond aggregate performance metrics, this section compares the precision–recall curves and confusion matrices of YOLOv11-IoU, CIoU, EIoU, and FlexIoU on the tomato leaf disease test set. While Table 7 summarizes the overall quantitative performance, Figures 4 and 5 provide additional insight into class-wise prediction behavior, precision-recall characteristics, and error distribution across disease categories. Figure 4 presents the precision-recall curves of all evaluated regression losses. Overall, the four methods exhibit similar precision–recall curves, indicating that the underlying detector architecture remains effective across different regression loss formulations. Although the differences among the curves are relatively moderate, variations can still be observed for individual disease categories. In particular, classes such as Early Blight, Late Blight, and Target Spot maintain strong precision

across a wide range of recall values, whereas classes with fewer samples, such as Bacterial Spot and Leaf Mold, exhibit greater performance fluctuations. These observations are consistent with the class imbalance characteristics discussed in Section 2.4.

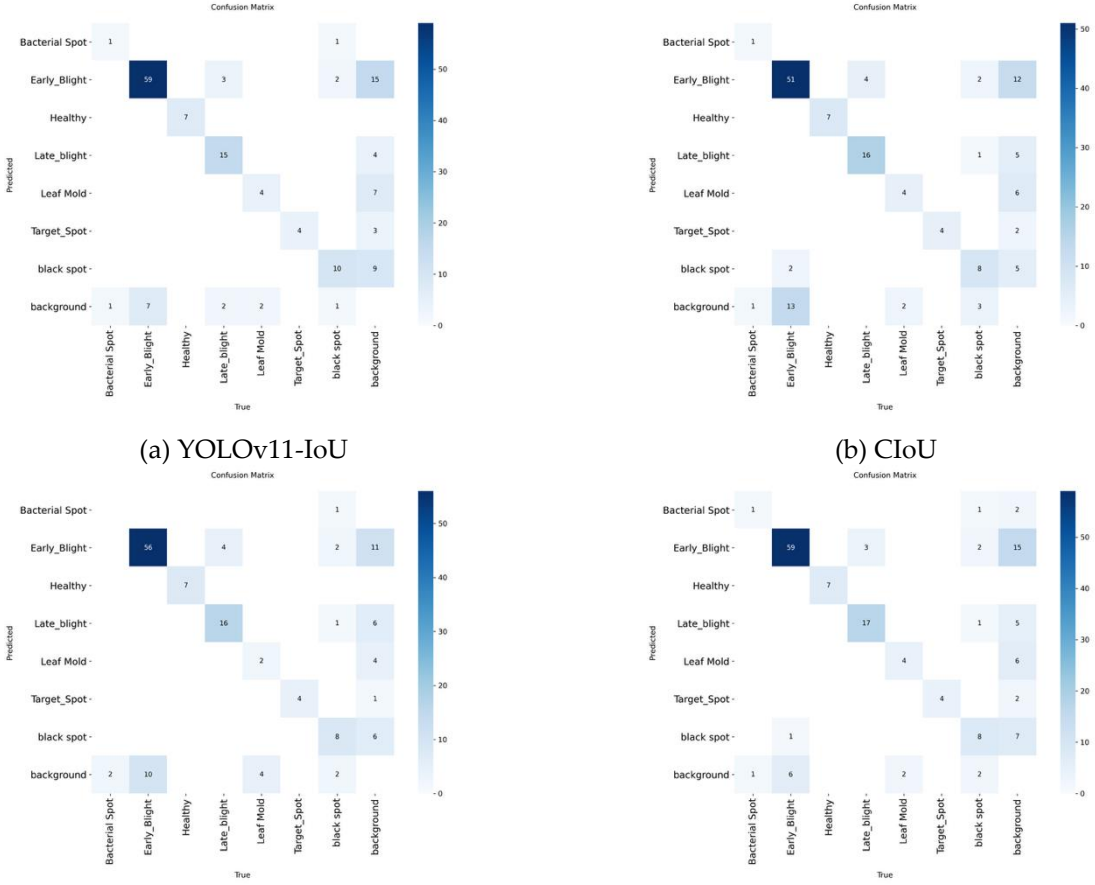


(a) YOLOv11-IoU (b) CIoU

(c) EIoU (d) FlexIoU

Figure 4. Precision–recall curves of YOLOv11-IoU, CIoU, EIoU, and FlexIoU on the tomato test set.

Figure 5 presents the confusion matrices of the evaluated methods. Across all regression losses, most predictions are concentrated along the diagonal, indicating that the detector correctly identifies the majority of disease instances. The remaining errors are primarily due to visually similar disease categories and background confusion, as expected in tomato leaf disease detection given overlapping lesion textures, color patterns, and disease morphology. Compared with the baseline losses, FlexIoU exhibits prediction patterns that are generally consistent with the quantitative results reported in Table 7. The confusion matrix shows strong diagonal dominance across major disease categories, while maintaining relatively limited confusion with background regions. These observations suggest that the proposed tunable geometric penalties improve localization quality without introducing excessive false-positive detections. When considered together with the quantitative results, the qualitative analyses help explain the performance differences observed among the evaluated losses. CIoU incorporates center-distance and aspect-ratio penalties, whereas EIoU further introduces explicit width and height penalties. FlexIoU extends this concept by allowing independent control of multiple geometric penalty terms through tunable coefficients. This flexibility enables the regression objective to be adapted to dataset-specific characteristics and may contribute to the improved localization performance observed in the tomato leaf disease dataset. Overall, the qualitative evidence provided by Figures 4 and 5 complements the quantitative results reported in Section 3.2. While the differences among the evaluated losses are not dramatic at the visual level, the combined quantitative and qualitative analyses suggest that FlexIoU provides a favorable balance between localization accuracy, detection reliability, and prediction consistency.



(a) YOLOv11-IoU (b) CIoU

(c) EIoU (d) FlexIoU

Figure 5. Confusion matrices of YOLOv11-IoU, CIoU, EIoU, and FlexIoU on the tomato test set

3.4 Additional Evaluation on an Independent Tomato Disease Dataset

To further assess the robustness of the proposed FlexIoU loss, an additional evaluation was conducted on an independent tomato leaf disease dataset obtained from a different public source. Unlike the primary dataset used in Sections 3.2 and 3.3, this dataset exhibits distinct class distributions, lesion characteristics, and annotation properties, providing a complementary evaluation setting to assess whether FlexIoU's effectiveness can be maintained under varying data conditions. The dataset was obtained from a publicly available Kaggle repository from https://www.kaggle.com/datasets/vasantharank/tomato-leaf-disease-detection-yolov8-dataset and is distributed under the CC BY-NC-SA 4.0 license. To ensure a balanced and reproducible evaluation protocol, the original dataset was re-partitioned using a stratified class-wise split of 70%, 20%, and 10% for training, validation, and testing, respectively. The resulting dataset contains 10 tomato disease categories: Tomato Bacterial Spot, Early Blight, Late Blight, Leaf Mold, Septoria Leaf Spot, Spider Mites, Target Spot, Yellow Leaf Curl Virus, Healthy, and Mosaic Virus. After re-splitting, the dataset consisted of 7,476 training images, 2,131 validation images, and 1,080 testing images. The purpose of this experiment was not to perform an additional hyperparameter search, but rather to evaluate whether the coefficient configuration selected in Section 3.1 remains effective when applied to a different tomato disease dataset. Therefore, the best-performing FlexIoU configuration identified from the primary dataset was directly transferred to this independent dataset without further coefficient optimization. All baseline methods were trained using identical experimental settings to ensure a fair comparison. Based on the sensitivity analysis presented in Section 3.2, the selected FlexIoU configuration employed λ_c = 1.0, λ_a = 0.5, λ_w = 1.0, λ_h = 1.5, λ_{cls} = 1.2, and λ_{box} = 2.0. This configuration was transferred directly to the independent dataset without further tuning to evaluate its robustness across different data distributions. Table 9 presents the quantitative

performance comparison between YOLOv11-IoU, CIoU, EIoU, and the proposed FlexIoU on the independent tomato disease dataset.

Table 9. Quantitative performance comparison on the independent tomato disease dataset

Loss	mAP@0.5:0.95	Precision	Recall	F1-score	Inference Time (ms)	FPS
YOLOv11-IoU	0.883 ± 0.005	0.970 ± 0.014	0.954 ± 0.004	0.962 ± 0.006	14.715 ± 0.131	67.962 ± 0.608
CIoU	0.873 ± 0.003	0.954 ± 0.008	0.956 ± 0.002	0.955 ± 0.003	15.022 ± 0.251	66.579 ± 1.104
EIoU	0.843 ± 0.013	0.906 ± 0.023	0.960 ± 0.013	0.932 ± 0.009	14.955 ± 0.146	66.872 ± 0.653
FlexIoU	0.858 ± 0.007	0.944 ± 0.025	0.928 ± 0.012	0.936 ± 0.017	14.895 ± 0.140	67.139 ± 0.628

As shown in Table 9, the performance trends observed on the independent dataset differ from those reported on the primary tomato leaf disease dataset. While FlexIoU achieved the best overall performance on the primary dataset, YOLOv11-IoU obtained the highest mAP@0.5:0.95, precision, and F1-score on the independent dataset. Nevertheless, FlexIoU remained competitive and achieved performance comparable to the evaluated IoU-based regression losses, indicating that the proposed formulation can maintain reasonable detection effectiveness under different dataset characteristics. It is important to note that the independent dataset differs substantially from the primary dataset in terms of class distribution, lesion composition, and annotation characteristics. In particular, the rebalanced split provides a more uniform distribution across disease categories and generally contains larger lesion regions than those observed in the primary dataset. Under these conditions, the advantage of emphasizing width and height penalties may become less pronounced, which could partially explain the reduced performance gap between FlexIoU and the baseline methods. These observations suggest that the effectiveness of individual geometric penalty terms depends on dataset-specific object characteristics. Despite not achieving the highest performance on this dataset, FlexIoU continued to produce competitive results while maintaining inference efficiency comparable to the baseline losses. This behavior is consistent with the findings of the sensitivity analysis in Section 3.2, which demonstrated that the contribution of geometric penalty components depends on the underlying data distribution. Therefore, the additional evaluation provides useful evidence that the proposed weighting framework remains applicable across different tomato disease datasets, although the optimal coefficient configuration may vary depending on lesion size, shape, and annotation properties. Overall, the results indicate that FlexIoU is not universally superior across all tomato disease datasets but remains a competitive regression loss under varying dataset conditions. These findings highlight both the potential and limitations of tunable geometric penalties, underscoring the importance of dataset-specific coefficient selection when applying FlexIoU across different detection scenarios.

3.5 Inference Speed and Computational Overhead

In addition to detection accuracy, computational efficiency is a key factor for real-world deployment, particularly in agricultural monitoring systems where real-time or near-real-time inference is often required. To evaluate whether the proposed FlexIoU loss incurs additional runtime cost, inference latency, and throughput, these metrics were measured under controlled benchmarking conditions. To reduce measurement variability caused by model initialization and GPU stabilization effects, all timing experiments were conducted after a dedicated warm-up phase before latency measurement. The resulting inference latency and throughput are summarized in Table 7. As shown in Table 7, FlexIoU achieves inference time and FPS comparable to those of CIoU and EIoU. Across all evaluated configurations, the average inference latency remains nearly identical, with only negligible variations. This result is expected, as IoU-based regression losses are applied exclusively during training, whereas inference relies solely on forward propagation through the trained detection network. Consequently, modifying the regression loss formulation does not alter the inference-time computational graph. Following the controlled warm-up procedure, all evaluated methods exhibited low variance in both latency and FPS measurements. The resulting consistency indicates that the reported inference performance is stable and largely independent of runtime initialization effects. Furthermore, the comparable latency observed across YOLOv11-IoU, CIoU, EIoU, and FlexIoU confirms that modifications to the regression loss do not introduce additional computational overhead during inference.

Overall, these results confirm that FlexIoU enhances localization robustness without introducing additional inference-time overhead. The absence of measurable computational cost makes FlexIoU suitable for deployment in resource-constrained environments and practical agricultural applications, where maintaining efficiency is as critical as improving detection accuracy.

3.6 Discussion

The experimental results demonstrate that improvements in bounding-box localization can be achieved without introducing additional architectural complexity or inference-time overhead. On the primary tomato leaf disease dataset, FlexIoU achieved the highest mAP@0.5:0.95, precision, recall, and F1-score among the evaluated methods while maintaining inference efficiency comparable to YOLOv11-IoU, CIoU, and EIoU. Furthermore, the relatively low variation observed across three independent random seeds suggests that the proposed loss provides stable optimization behavior under different initialization conditions. A key finding of this study is that the effectiveness of bounding-box regression depends on how geometric penalties are weighted. The sensitivity analysis showed that different combinations of λ_c, λ_a, λ_w, λ_h produced noticeably different detection outcomes, indicating that the contribution of individual geometric constraints is not uniform across all datasets. This observation supports the central motivation of FlexIoU: to provide a flexible weighting framework rather than relying on a fixed penalty structure. The findings are generally consistent with previous studies showing that incorporating additional geometric information beyond conventional IoU can improve localization performance. Similar to CIoU, EIoU, SIoU, and MPDIoU, the proposed method leverages geometric relationships between predicted and ground-truth boxes. However, unlike these approaches, FlexIoU emphasizes adaptability through independently tunable penalty terms, allowing the regression objective to be adjusted according to dataset characteristics and application requirements. Figure 6 presents representative detection results obtained using the FlexIoU-based detector. The qualitative results are consistent with the quantitative findings reported in Section 3.2, demonstrating that the model can successfully localize disease regions across multiple tomato leaf disease categories while maintaining visually coherent bounding-box predictions.

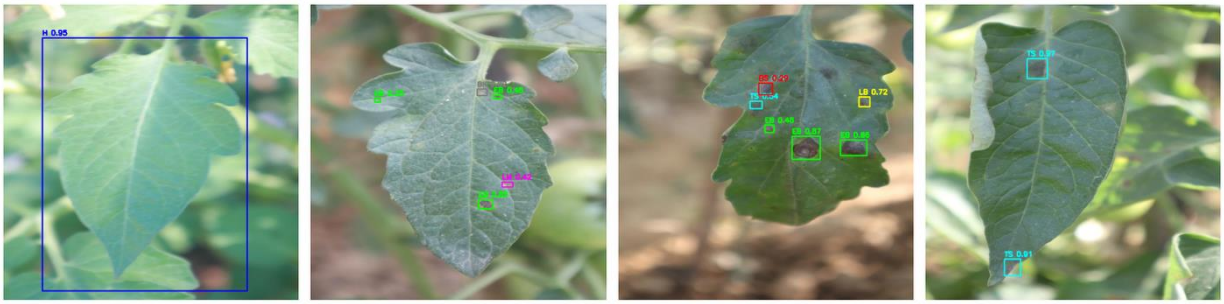


Figure 6. Detection results produced by the FlexIoU on the test dataset.

Another important observation is that the localization improvements achieved by FlexIoU do not come at the expense of increased computational cost. Since the proposed modifications affect only the training objective and do not alter the inference-time computation graph, latency and throughput remain comparable to those of the baseline losses. This characteristic is particularly important for agricultural monitoring systems and edge-device deployments where computational resources are limited. The additional evaluation on an independent tomato disease dataset further highlights the importance of dataset-specific coefficient selection. Although FlexIoU achieved the best performance on the primary dataset, YOLOv11-IoU achieved slightly higher mAP@0.5:0.95 on the secondary dataset. This result suggests that no single coefficient configuration is universally optimal and reinforces the need to introduce tunable geometric penalties that can be adapted to different data distributions. Finally, it should be noted that recent regression losses such as SIoU [23] and MPDIoU [24] were not included in the experimental comparison. Therefore, the reported improvements should be interpreted relative to the evaluated baselines (YOLOv11-IoU, CIoU, and EIoU) rather than all existing IoU-based regression losses. Additional comparisons with more recent loss formulations and evaluations across diverse datasets would provide a more comprehensive assessment of FlexIoU's strengths and limitations.

4. Conclusion

This study introduced FlexIoU, a flexible and lightweight IoU-based regression loss designed to improve bounding-box localization in YOLO-based object detection, with a particular focus on agricultural disease imagery. By incorporating tunable geometric penalties into the regression objective, FlexIoU enables independent control of center-distance, aspect-ratio, width, and height constraints, providing greater flexibility than conventional fixed-penalty IoU-based losses. Experimental results on the tomato leaf disease dataset demonstrated that FlexIoU achieved the highest mean mAP@0.5:0.95, precision, recall, and F1-score among the evaluated regression losses. Furthermore, the proposed loss maintained stable performance across three independent random seeds while preserving inference efficiency comparable to the baseline methods. These findings suggest that introducing tunable geometric penalties can improve localization performance without sacrificing computational efficiency. An additional contribution of this work is the introduction of a configurable regression framework that enables geometric penalty terms to be adjusted based on dataset characteristics. The sensitivity analysis showed that different coefficient configurations produce different performance behaviors, highlighting the importance of adaptive geometric weighting in bounding-box regression. This flexibility represents a practical advantage over fixed-penalty formulations such as CIoU and EIoU. Despite these promising results, several limitations should be acknowledged. First, the experimental evaluation was conducted on a tomato leaf disease dataset, which may limit the generalizability of the findings to other agricultural domains and object detection tasks. Second, the comparative experiments were restricted to YOLOv11-IoU, CIoU, and EIoU, while more recent IoU-based losses such as SIoU [23] and MPDIoU [24] were not included. Third, although statistical significance was observed when comparing FlexIoU with CIoU, the limited number of repeated runs may restrict the strength of statistical conclusions for some comparisons. Furthermore, the dataset exhibits noticeable class imbalance across disease categories. Although all methods were trained under identical conditions, class imbalance may have influenced category-specific detection performance and represents an additional limitation of the current study. Future work will focus on evaluating FlexIoU on additional agricultural and general-purpose object detection datasets, as well as extending comparisons to more recent IoU-based regression losses. Further research will also investigate adaptive and data-driven approaches for automatic coefficient selection. In addition, extending the proposed formulation to support rotated and oriented bounding-box regression represents a promising direction for improving localization performance in more complex detection scenarios.

5. Acknowledgments

The authors would like to thank all individuals who provided valuable support and feedback during the development of this study.

Author Contributions: Conceptualization, N.K.; methodology, N.K.; software, N.K.; validation, N.K., A.N., K.S. and N.P.; formal analysis, N.K.; investigation, N.K.; resources, N.K.; data curation, N.K.; writing—original draft preparation, N.K.; writing—review and editing, N.K., K.S. and N.P.; visualization, N.K., K.S; supervision, A.N. and N.P.; project administration, N.K. All authors have read and agreed to the published version of the manuscript.

Funding: This research received no external funding.

Conflicts of Interest: The authors declare no conflict of interest. The funders had no role in the design of the study, in the collection, analysis, or interpretation of data, in the writing of the manuscript, or in the decision to publish the results.

References

[1] Nagababu, P.; Nageena, S.; Dharani, V.; Naveen, D. Plant Disease Detection and Diagnosis. In *Proceedings of the 2024 5th International Conference for Emerging Technology (INCET)*; Belgaum, India, 2024; pp 1–6. https://doi.org/10.1109/INCET61516.2024.10593371

[2] Lokhande, N.; Thool, V.; Vikhe, P. Comparative Analysis of Different Plant Leaf Disease Classification and Detection Using CNN. In *Proceedings of the 2024 International Conference on Recent Innovation in Smart and Sustainable Technology (ICRISST)*; Bengaluru, India, 2024; pp 1–4. https://doi.org/10.1109/ICRISST59181.2024.10921975

[3] Kusuma, S.; Jothi, K. R. Early Betel Leaf Disease Detection Using Vision Transformer and Deep Learning Algorithms. *Int. J. Inf. Technol.* **2024**, *16*(1), 169–180. https://doi.org/10.1007/s41870-023-01647-3

[4] Redmon, J.; Divvala, S.; Girshick, R.; Farhadi, A. You Only Look Once: Unified, Real-Time Object Detection. In *Proceedings of the IEEE Conference on Computer Vision and Pattern Recognition (CVPR)*; Las Vegas, NV, USA, 2016; pp 779–788. https://doi.org/10.1109/CVPR.2016.91

[5] Bochkovskiy, A.; Wang, C.-Y.; Liao, H.-Y. M. YOLOv4: Optimal Speed and Accuracy of Object Detection. *arXiv* **2020**, arXiv:2004.10934.

[6] Jocher, G. *Ultralytics YOLOv5*, Version 7.0; Ultralytics, 2020. https://github.com/ultralytics/yolov5 (accessed 2025-12-13). https://doi.org/10.5281/zenodo.3908559

[7] Wang, C.-Y.; Bochkovskiy, A.; Liao, H.-Y. M. YOLOv7: Trainable Bag-of-Freebies Sets New State-of-the-Art for Real-Time Object Detectors. In *Proceedings of the IEEE/CVF Conference on Computer Vision and Pattern Recognition (CVPR)*; IEEE, 2023; pp 7464–7475. https://doi.org/10.1109/CVPR52729.2023.00721

[8] Varghese, R.; Sambath, M. YOLOv8: A Novel Object Detection Algorithm with Enhanced Performance and Robustness. In *Proceedings of the 2024 International Conference on Advances in Data Engineering and Intelligent Computing Systems (ADICS)*; Chennai, India, 2024; pp 1–6. https://doi.org/10.1109/ADICS58448.2024.10533619

[9] Wang, A.; Chen, H.; Liu, L.; Chen, K.; Lin, Z.; Han, J. YOLOv10: Real-Time End-to-End Object Detection. *Adv. Neural Inf. Process. Syst.* **2024**, *37*, 107984–108011

[10] Jocher, G.; Qiu, J. *Ultralytics YOLO11*, Version 11.0.0; Ultralytics, 2024. https://github.com/ultralytics/ultralytics (accessed 2025-12-13).

[11] Ramesh, M.; Sherin, S. D.; Deepak A, V.; Dhanin, G.; Kodeeswari, K.; Nathiya, T. Tomato Plant Disease Classification with Pesticide Suggestion Using YOLOv8 Algorithm. In *Proceedings of the 2025 3rd International Conference on Advancements in Electrical, Electronics, Communication, Computing and Automation (ICAECA)*; Coimbatore, India, 2025; pp 1–6. https://doi.org/10.1109/ICAECA63854.2025.11012147

[12] Wei, Y.; Pan, X. Improvement Algorithm Analysis and Implementation of Plant Disease and Pest Recognition Based on YOLO. In *Proceedings of the 5th International Conference on Computer Vision, Image and Deep Learning (CVIDL 2024)*; Zhuhai, China, 2024; pp 442–446. https://doi.org/10.1109/CVIDL62147.2024.10603557

[13] Pathan, F.; Sakalle, V.; Munir, S. An Efficient Machine Learning Technique for Agricultural Plant Leaf Disease Prediction Using Image Processing. In *Proceedings of the 2025 International Conference on Engineering Innovations and Technologies (ICoEIT)*; Bhopal, India, 2025; pp 612–617. https://doi.org/10.1109/ICoEIT63558.2025.11211659

[14] David, F.; Mukunthan, M. A. Betel Leaf Diseases Classification Using Machine Learning Algorithm: A Feasible Approach. *J. Adv. Res. Appl. Sci. Eng. Technol.* **2024**, *40*(1), 74–86. https://doi.org/10.37934/araset.40.1.7486

[15] Mamart, S.; Sangamuang, S.; Sugunnasil, P. Deep Learning-Based Classification of Apple Leaf Diseases under Field Conditions. *ASEAN J. Sci. Technol. Rep.* **2026**, *29*(3), e261221. https://doi.org/10.55164/ajstr.v29i3.261221

[16] Yu, J.; Jiang, Y.; Wang, Z.; Cao, Z.; Huang, T. UnitBox: An Advanced Object Detection Network. In *Proceedings of the 24th ACM International Conference on Multimedia*; ACM: New York, NY, 2016; pp 516–520. https://doi.org/10.1145/2964284.2967274

[17] Rezatofighi, H.; Tsoi, N.; Gwak, J. Y.; Sadeghian, A.; Reid, I.; Savarese, S. Generalized Intersection over Union: A Metric and a Loss for Bounding Box Regression. In *Proceedings of the IEEE/CVF Conference on Computer Vision and Pattern Recognition (CVPR)*; Long Beach, CA, USA, 2019; pp 658–666. https://doi.org/10.1109/CVPR.2019.00075

[18] Zheng, Z.; Wang, P.; Liu, W.; Li, J.; Ye, R.; Ren, D. Distance-IoU Loss: Faster and Better Learning for Bounding Box Regression. *Proc. AAAI Conf. Artif. Intell.* **2020**, *34*(7), 12993–13000. https://doi.org/10.1609/aaai.v34i07.6999

[19] Zheng, Z.; Wang, P.; Ren, D.; Liu, W.; Ye, R.; Hu, Q.; Zuo, W. Enhancing Geometric Factors in Model Learning and Inference for Object Detection and Instance Segmentation. *IEEE Trans. Cybern.* **2022**, *52*(8), 8574–8586. https://doi.org/10.48550/arXiv.2005.03572

[20] Yang, Z.; Wang, X.; Li, J. EIoU: An Improved Vehicle Detection Algorithm Based on VehicleNet Neural Network. *J. Phys.: Conf. Ser.* **2021**, *1924* (1), 012001. https://doi.org/10.1088/1742-6596/1924/1/012001.

[21] Sun, Y.; Wang, J.; Wang, H.; Zhang, S.; You, Y.; Yu, Z.; Peng, Y. Fused-IoU Loss: Efficient Learning for Accurate Bounding Box Regression. *IEEE Access* **2024**, *12*, 37363–37377. https://doi.org/10.1109/ACCESS.2024.3359433

[22] Xiao, Z.; Zhao, H.; Guo, J.; Yu, H.; Li, J. CRIoU: A Complete and Relevant Bounding Box Regression Method. In *Proceedings of the 2022 International Symposium on Advances in Informatics, Electronics and Education (ISAIEE)*; IEEE: Piscataway, NJ, 2022; pp 511–518. https://doi.org/10.1109/ISAIEE57420.2022.00111

[23] Gevorgyan, Z. SIoU Loss: More Powerful Learning for Bounding Box Regression. *arXiv* **2022**, arXiv:2205.12740.

[24] Ma, S.; Xu, Y. MPDIoU: A Loss for Efficient and Accurate Bounding Box Regression. *arXiv* **2023**, arXiv:2307.07662.

[25] Zheng, Y.; Zhang, D.; Xie, S.; Lu, J.; Zhou, J. Rotation-Robust Intersection over Union for 3D Object Detection. In *Computer Vision – ECCV 2020*; Springer: Cham, Switzerland, 2020; pp 464–480. https://doi.org/10.1007/978-3-030-58565-5_28

[26] Ma, S.; Xu, Y. FPDIoU Loss: A Loss Function for Efficient Bounding Box Regression of Rotated Object Detection. *Image Vis. Comput.* **2025**, *154*, 105381. https://doi.org/10.1016/j.imavis.2024.105381.

[27] Li, W.; Shang, R.; Ju, Z.; Feng, J.; Xu, S.; Zhang, W. Ellipse IoU Loss: Better Learning for Rotated Bounding Box Regression. *IEEE Geosci. Remote Sens. Lett.* **2024**, *21*, 1–5. https://doi.org/10.1109/LGRS.2023.334588

ASEAN
Journal of Scientific and Technological Reports
Online ISSN:2773-8752

Research article

Carbon Footprint Assessment and GHG Reduction Guidelines for the Rubberwood Processing Industry in Yala Province

Jutamas Kaewmanee[1*], and Adulsman Sukkaew[2]

[1] Faculty of Public Health and Allied Health Sciences, Yala Rajabhat University, Yala, 95000, Thailand
[2] Faculty of Science Technology and Agriculture, Yala Rajabhat University, Yala, 95000, Thailand
* Correspondence: jutamas.k@yru.ac.th

Citation:
Kaewmanee, J. Carbon Footprint assessment and GHG reduction guidelines for the rubberwood processing industry in Yala province. *ASEAN J. Sci. Tech. Report.* **2026**, *29*(7), e263215. https://doi.org/10.55164/ajstr.v29i7.263215

Article history:
Received: January 14, 2026
Revised: April 28, 2026
Accepted: May 16, 2026
Available online: June 14, 2026

Publisher's Note:
This article is published and distributed under the terms of the Thaksin University.

Abstract: This study presents a Cradle-to-Gate carbon footprint assessment (CFP) of a representative rubberwood (Hevea brasiliensis) processing factory in Yala Province, Thailand, conducted in accordance with the Life Cycle Inventory (LCI) framework and ISO 14067:2018. The functional unit was defined as one cubic meter (1 m^3) of processed rubberwood leaving the factory gate. The total greenhouse gas (GHG) emission intensity was calculated as 40.83 $kgCO_2$-eq/m^3, with raw materials and processing residues identified as the dominant emission sources, accounting for approximately 90% of total emissions. Electricity (2.33 $kgCO_2$-eq/m^3) and diesel fuel (0.11 $kgCO_2$-eq/m^3) constituted secondary contributors, while consumables and auxiliary materials contributed negligibly. The findings should be interpreted as a single-factory case study rather than an industry-wide representative baseline. Potential mitigation pathways, drawn from analogous studies, include optimized inventory management (15–30% reduction potential), biomass fuel substitution (50–85%), operational efficiency improvements through preventive maintenance and AI-assisted optimization (5–15%), and waste valorization through biochar conversion. These hotspots align with Thai national policy frameworks, including the Nationally Determined Contribution (NDC), Carbon Neutrality (2050), Net Zero (2065), the TGO Carbon Label Program, the EU Carbon Border Adjustment Mechanism (CBAM), the Bio-Circular-Green (BCG) economic model, and the energy policies under the Power Development Plan (PDP) and the Department of Alternative Energy Development and Efficiency (DEDE). The study provides empirical baseline data for the rubberwood processing sector and serves as a methodological reference for future, larger-scale assessments.

Keywords: Carbon footprint; greenhouse gas emissions; rubberwood processing; cradle-to-gate

1. Introduction

Rubberwood is a principal timber resource for the wood-based industries in Southeast Asia [1]. The rubber tree (Hevea brasiliensis) is primarily cultivated for latex production, and its wood is widely used as a raw material in furniture manufacturing and other downstream applications [2]. The Thai rubber sector is a major component of the national economy. In 2022, rubber plantations covered approximately 28,736 km^2, and the sector recorded an average annual growth rate of 15.15% during 2019–2022, positioning Thailand as the world's second-largest natural rubber producer after Indonesia [3]. Approximately 40% of the Thai workforce is employed in agriculture [4]. The

total area under rubber cultivation increased to 32,276.8 km² by 2018, with the southern region accounting for the largest share (61%), followed by the northeast (22%), the central region (11%), and the north (6%). Rubber plantations supply raw material to several downstream industries, including rubberwood processing, furniture manufacturing, and biomass-based power generation.

In Thailand's southern border provinces — Yala, Narathiwat, and Pattani — rubber is among the most economically significant crops, with Yala possessing the largest plantation area among the three. Consequently, the rubberwood processing industry has become an important source of livelihood in this region. In 2022, 51 rubberwood processing factories were licensed in Yala Province, of which 29 were operational, with a combined annual production capacity of approximately 357,395 m³. Processed rubberwood from this region is exported primarily to Malaysia and China, in addition to supplying domestic downstream industries [5]. The global mean surface temperature in 2023 reached 1.45 °C above pre-industrial levels, approaching the 1.5 °C threshold established under the Paris Agreement. The Intergovernmental Panel on Climate Change (IPCC) has emphasized the need to achieve net-zero CO_2 emissions globally by 2050 [6]. Thailand has committed to attaining Carbon Neutrality by 2050 and Net Zero Emissions by 2065 [7], and has set a Nationally Determined Contribution (NDC) target to reduce GHG emissions by 30%–40% below the Business-as-Usual (BAU) projection by 2030 [8].

Despite this policy momentum, factory-level empirical data on GHG emissions from rubberwood processing in Yala Province remain limited. Quantifying the product carbon footprint (CFP) and identifying emission hotspots within the LCI framework are therefore essential for evidence-based mitigation planning. This study provides a Cradle-to-Gate carbon footprint assessment of one operational rubberwood processing factory in Yala Province as an empirical case study. The contribution of this work is the provision of factory-level baseline data; it is not intended as a methodological advance, and its findings should be interpreted within the context of the single-factory scope.

2. Materials and Methods

This study employed an applied research design to quantify GHG emissions from a rubberwood processing facility. The environmental impact was evaluated using Global Warming Potential (GWP) and reported as the Product Carbon Footprint (CFP), expressed in kilograms of carbon dioxide equivalent ($kgCO_2$-eq).

2.1 Study scope and system boundary

GHG quantification was conducted within the LCI framework and adopted a Cradle-to-Gate system boundary, in accordance with ISO 14067:2018 (Greenhouse gases, Carbon footprint of products, Requirements and guidelines for quantification). A single rubberwood processing factory in Yala Province, Thailand (255/16 Moo 97, Sateng Nok Subdistrict, Mueang Yala District), was selected through purposive sampling as the case-study site. Selection was based on the factory's willingness to disclose detailed monthly inventory data and its operational status during the study period. The facility occupies approximately 8,000 m² and produces 832,000 kg (1,280 m³) of pallet rubberwood annually [9]. It employs 62 administrative staff and 20 production workers, and operates 15 sawing/processing machines, 15 cyclones, and 7 forklifts. The selected factory's annual processed-wood output (~9,645 m³) represents only a small fraction of the total provincial capacity (357,395 m³). Consequently, this study should be interpreted as a single-factory case study rather than a statistically representative baseline for the Yala rubberwood industry as a whole. The system boundary encompasses the in-factory production stage, from the receipt of raw or semi-finished rubberwood to the dispatch of finished processed wood at the factory gate. Inclusions: rubberwood input, in-factory unit operations (sawing, cutting, sorting), energy consumption (electricity and diesel), auxiliary consumables (lubricants, cleaning agents, personal protective equipment, lighting fixtures), and on-site solid-waste handling. Exclusions: upstream processes (plantation establishment, silvicultural management, harvesting, and inbound transport), downstream processes (use phase and end-of-life), and land-use change (LUC) effects. The detailed material flows, in-factory unit operations, and the established Cradle-to-Gate system boundary are illustrated in the schematic diagram shown in Figure 1.

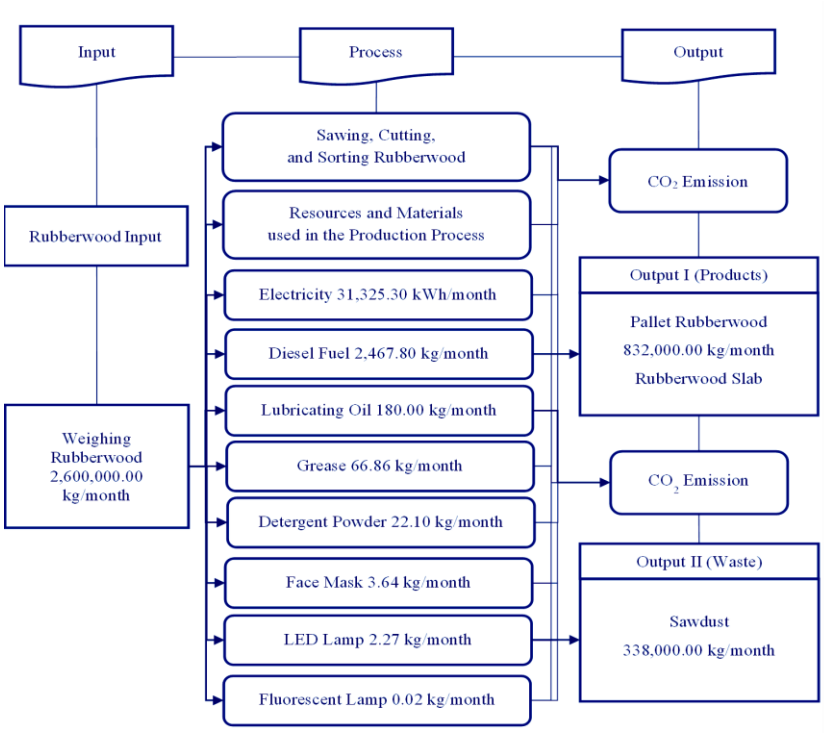


Figure 1. Process-flow diagram showing inputs, in-factory unit operations (receiving → sawing → cutting → sorting → drying/finishing → dispatch), outputs, and the Cradle-to-Gate system boundary of the rubberwood processing factory

2.2 Treatment of biogenic carbon

Rubberwood is a biogenic material whose carbon content was sequestered from atmospheric CO_2 during tree growth. In accordance with ISO 14067:2018 (Annex D), biogenic CO_2 emissions and removals associated with the use of biomass should be reported separately from fossil GHG emissions. The emission factors applied to rubberwood inputs and outputs in this study (Table 1) were derived from the factory's internal life cycle inventory data [9] and represent the on-site processing-related GHG burdens (predominantly fossil-derived from electricity, diesel, and lubricants used during processing) attributable to each unit mass of material handled. They do not represent the biogenic CO_2 stock contained within the wood itself, nor do they reflect plantation-level sequestration or land-use change. Consequently, the long-term biogenic carbon storage embodied in finished rubberwood products is not quantified in this assessment. This exclusion is acknowledged as a limitation; comprehensive treatment would require an extended Cradle-to-Grave LCA incorporating plantation carbon-stock dynamics, which is beyond the scope of this single-factory baseline.

2.3 Functional unit

The functional unit (FU) was defined as one cubic meter (1 m^3) of processed rubberwood leaving the factory gate. This FU is consistent with international wood-industry CFP studies, including the carbon footprint assessment of rubberwood sawmilling in Peninsular Malaysia by Ratnasingam et al. [1] and the supply-chain CFP for imported timber-based wooden furniture by Wang et al. [10], thereby enabling regional benchmarking.

2.4 Inventory data collection

Activity data were obtained from the factory's 2022 annual production report [9] each month (N = 12) and aggregated into monthly averages, yielding a 13-line inventory (N = 13) covering all inputs and outputs within the system boundary. Because reference [9] is an unpublished internal factory document, all activity data and the corresponding emission factors derived from it are reproduced in full in Table 1 to support transparency and reproducibility. Cross-verification against the publicly available Thailand Greenhouse Gas

Management Organization (TGO) emission-factor database [13] and the Climatiq emission-factor repository [14] was conducted for energy and selected consumable inputs; the values used in the calculation are within the same order of magnitude as those publicly reported.

The inventory comprises:

- Raw materials (inputs and outputs): rubberwood, pallet rubberwood, rubberwood slab, sawdust
- Energy: electricity (kWh) and diesel fuel (kg)
- Consumables: grease, lubricating oil, detergent powder, fabric gloves, face masks, fluorescent lamps, LED lamps (kg)

2.5 Carbon footprint calculation

The total CFP was calculated using the standard equation:

CFP ($kgCO_2$-eq) = Activity Data × Emission Factor (EF)

where Activity Data denotes the quantity of input or output (kg, kWh, etc.) and EF ($kgCO_2$-eq/Unit) represents the GHG emissions per unit of activity. EFs for energy and most consumables were drawn from peer-reviewed and database sources [10–16]; EFs for rubberwood materials originated from the factory's internal LCI documentation [9]. The emission factors of 0.0471 $kgCO_2$-eq/kg (rubberwood and pallet rubberwood inputs) and 0.0829 $kgCO_2$-eq/kg (rubberwood slab and sawdust outputs) are interpreted as the on-site, processing-stage GHG burden per unit mass of material handled within the factory. The slightly higher EF for slab and sawdust reflects the additional processing energy and material-handling steps (sorting, conveying, on-site management) associated with these intermediate output streams before they leave the factory gate. The values represent fossil-derived emissions from material handling and do not capture biogenic CO_2 flows. As these EFs originate from a single internal source, the resulting emission estimates should be regarded as indicative rather than definitive; this constraint is discussed further in Section 3.4.

2.6 Data analysis

Total GHG emissions were obtained by summing the monthly $kgCO_2$-eq values for all inventory items. The factory-level CFP intensity was derived by dividing the total monthly GHG emissions by the total monthly volume of processed wood (8,037.19 m^3). Emission hotspots were identified by ranking the percentage contribution of each inventory item. The calculated percentage contributions of all 13 inventory items are presented in Figure 2, utilizing a custom segmented linear scale on the X-axis to ensure legibility across widely disparate data ranges. The Consumables (Combined) category accounts for 0.074% of the total CO_2 emissions, which is broken down into Lubricating Oil, Grease, Detergent Powder, Fabric Gloves, LED Lamp, Face Mask, and Fluorescent.

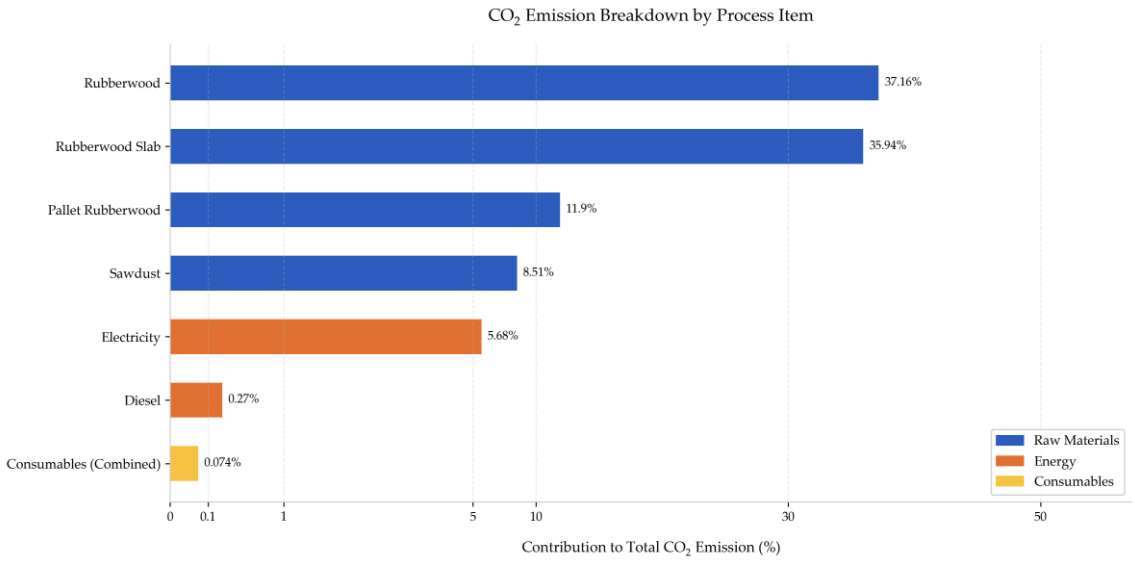


Figure 2. Percent CO_2 Emissions of the Rubberwood Processing Factory

2.7 Uncertainty considerations

Quantitative uncertainty propagation (e.g., Monte Carlo simulation) was not performed because parameter distributions for the internally derived rubberwood EFs were unavailable. A discussion of qualitative uncertainty is presented in Section 3.4. Key uncertainty sources include: (i) reliance on a single-year (2022) inventory that may not capture inter-annual or seasonal variability; (ii) use of internally derived EFs for rubberwood that have not been peer-reviewed; (iii) the single-factory scope, which precludes generalization to the provincial industry; and (iv) the exclusion of upstream, downstream, and land-use-change emissions. The environmental inventory data, including the category, item, and greenhouse gas (GHG) emissions of the rubberwood processing factory are presented in Table 1.

Table 1. Environmental Inventory Data (Cradle-to-Gate) of the Rubberwood Processing Factory

Category	Item	Unit	Inventory Data /month	EF ($kgCO_2$-eq/Unit)	CO_2 Emission /Month ($kgCO_2$-eq)	GHG ($kgCO_2$-eq/m^3)	% CO_2
Raw Materials	Rubberwood	kg	2,600,000	0.0471 [9]	122,460.00	15.24	37.16
	Pallet Rubberwood	kg	832,000	0.0471 [9]	39,187.20	4.88	11.95
	Rubberwood Slab	kg	1,430,000	0.0829 [9]	118,547.00	14.74	36.13
	Sawdust	kg	338,000	0.0829 [9]	28,020.20	3.49	8.54
Energy	Electricity	kWh	31,325.3	0.5986 [13]	18,751.32	2.33	5.71
	Diesel	kg	2,467.8	0.3522 [13]	869.16	0.11	0.26
Consumables	Grease	kg	66.86	1.0547 [10]	70.52	0.009	0.02
	Lubricating Oil	kg	180	0.8319 [14]	149.74	0.019	0.05
	Detergent Powder	kg	22.1	0.405 [12]	8.95	0.0011	0.003
	Fabric Gloves	kg	1.63	2.11 [14]	3.44	0.00043	0.001
	Face Mask	kg	3.64	0.02 [15]	0.07	0.000009	0.00002
	Fluorescent Lamp	kg	0.02	0.477 [14]	0.01	0.000001	0.000002
	LED Lamp	kg	2.27	0.5986 [14]	1.36	0.00017	0.0004
				Total	**328,068.50**	**40.83**	**100.00**

Notes: Inventory data (N = 13 items) include all inputs and outputs within the Cradle-to-Gate boundary. Functional Unit (FU): 1 m^3 of processed rubberwood leaving the factory gate; total processed-wood output sums to 8,037.19 m^3/month. EFs cited as [9] are derived from the factory's internal LCI documentation and represent on-site, processing-stage GHG burdens (predominantly fossil-derived). Biogenic CO_2 stock within the wood and plantation-level sequestration is not included in these EFs. The total intensity per FU (40.83 $kgCO_2$-eq/m^3) is the sum of all line-item intensities and supersedes any single-item intensity (e.g., the slab line at 14.74 $kgCO_2$-eq/m^3) for factory-level reporting.

3. Results and Discussion

3.1 Inventory results and emission hotspots

Table 1 presents the complete environmental inventory and corresponding monthly GHG emissions for the studied factory. Total monthly GHG emissions amount to 328,068.50 $kgCO_2$-eq. With a total monthly processed-wood output of 8,037.19 m^3, the factory-level CFP intensity is 40.83 $kgCO_2$-eq/m^3 (see Table 4). This figure represents the aggregate GHG emission per functional unit and supersedes any per-line-item intensity (such as the 14.74 $kgCO_2$-eq/m^3 value associated specifically with the rubberwood-slab line in Table 1) when

characterizing factory-level performance. Raw materials (rubberwood input, pallet rubberwood, rubberwood slab, and sawdust output) collectively contribute approximately 308,214 $kgCO_2$-eq/month, or about 93.9% of total monthly emissions. Within this category, rubberwood input alone accounts for 37.16% of the total, while rubberwood slab accounts for 36.13%. Electricity is the most significant non-material contributor (5.71%), followed by diesel (0.26%); all other consumables collectively contribute less than 0.1%. The rubberwood-slab and sawdust line items represent intermediate output streams that undergo additional in-factory handling (sorting, conveying, on-site temporary storage) before leaving the gate. The associated EFs, therefore, capture the processing-stage GHG burden per unit mass handled rather than emissions generated by the materials themselves. If these output streams were excluded from the boundary, only the rubberwood and pallet-rubberwood input lines would remain attributable to material handling, and the energy share of total emissions would rise correspondingly.

3.2 Comparison with related studies

The dominance of raw materials in the CFP of this rubberwood processing factory is qualitatively consistent with prior wood-industry LCA studies. Ratnasingam et al. [1] reported that raw materials and energy are the principal drivers of the carbon footprint in Peninsular Malaysian rubberwood sawmilling. Wang et al. [10] found that upstream processes account for 74.6%–80.7% of total CFP for imported timber-based wooden furniture supply chains. By contrast, Srichat et al. [11] reported the dominance of energy use in wood-pellet production — a finding that differs from the present study (in which raw-material handling rather than energy dominates), reflecting the substantially higher thermal-energy intensity of pelletization compared with sawmilling. This contrast underscores the need to tailor mitigation strategies to the specific operational profile of each wood-processing sub-sector. The CFP intensity reported here (40.83 $kgCO_2$-eq/m^3) is broadly within the same order of magnitude as that reported in the Malaysian sawmilling study, although direct numerical comparison is constrained by differences in system boundaries, EF sources, and biogenic-carbon treatment. Table 2 summarizes the thematic alignment of the present findings with related studies, with citations corrected to reflect each study's actual focus.

3.3 Mitigation strategies and policy linkages

Table 3 outlines potential GHG reduction measures relevant to the rubberwood processing industry. The numerical reduction ranges (15–30% for inventory optimization; 50–85% for biomass substitution; ~4% for renewable electricity; 5–15% for operational efficiency) are drawn from analogous studies in related sub-sectors and are presented as *indicative potentials*. They have not been derived directly from the present factory's data, and their applicability to a sawmilling-type operation such as the studied facility may differ from the source contexts (for example, the 50–85% biomass-substitution range originates from a thermal-energy-intensive wood-pellet study [11], whereas sawmilling is comparatively electricity-dominant). Site-specific feasibility assessment would therefore be required before adopting any of these ranges as concrete reduction targets for the studied factory. Table 4 connects the identified carbon hotspots to relevant Thai national policy instruments. Optimized inventory management of raw materials and offcuts supports the national NDC, Carbon Neutrality (2050), and Net Zero (2065) targets [17]. Reporting CFP at the product level enables manufacturers to participate in the TGO Carbon Label Program [18] and supports compliance with the EU Carbon Border Adjustment Mechanism (CBAM), thereby enhancing export competitiveness in environmentally stringent markets. Conversion of sawdust and offcuts into biochar is consistent with the Bio-Circular-Green (BCG) economic model and Circular Economy policy [19], offering both waste reduction and potential long-term carbon sequestration. Substitution of fossil thermal energy with biomass and the adoption of rooftop solar PV are aligned with the Power Development Plan (PDP) and the DEDE energy-conservation policy [20]. The consistency comparison with prior studies and the GHG reduction measures are presented in Table 2 and Table 3, respectively.

Table 2. Consistency of Research Findings with Related Studies

Thematic Area	Supporting Study	Key Findings	Consistency with Current Study
I. Raw-material dominance in GHG emissions	Ratnasingam et al. [1]	Raw materials and energy are the main drivers of the carbon footprint in rubberwood sawmilling. Indicative GHG reduction potential: 15–30% through inventory optimization.	Confirms that rubberwood inventory management is the most critical intervention point for carbon reduction in the present case (~90% of CO_2 emissions).
II. Upstream-stage dominance in supply-chain CFP	Wang et al. [10]	Upstream processes accounted for 74.6%–80.7% of total CFP in imported timber-based wooden-furniture supply chains. Indicative GHG reduction potential: ~4% through renewable-electricity transition.	Confirms that material/upstream inventory is the primary carbon hotspot. Energy is a secondary but actionable factor.
III. Energy-dominated profile in pelletization (CONTRAST)	Srichat et al. [11]	Most GHG emissions in wood-pellet production originate from energy consumption. Indicative GHG reduction potential: 50–85% through biomass-fuel substitution.	Differs from the present sawmilling case (raw materials dominate, not energy). The contrast is attributed to the higher thermal energy intensity during pelletization. Reduction from this source primarily applies to thermal-energy-intensive processes.
IV. Operational-energy and machinery-fuel contribution	Thaipradith et al. [12]	Fossil-fuel consumption in production is a significant contributor to GHG emissions—indicative GHG reduction potential: 5–15% through operational efficiency improvements.	Supports the strategy of targeted mitigation of diesel and lubricating oil use in machinery.

Table 3. Indicative GHG Reduction Measures Drawn from Analogous Studies

Mitigation Strategy	Focus Area	Indicative Reduction	Source Context and Applicability
Optimized inventory management	Raw-material handling; reducing spoilage	15–30%	From rubberwood sawmilling [1]; directly relevant to the present case, given the dominance of raw-material emissions.
Biomass-fuel substitution	Thermal energy (drying/heat)	50–85%	From wood-pellet production [11], it is directly applicable only to thermal-energy-intensive operations. The present sawmilling case has limited drying/thermal demand, so the realizable reduction is expected to be lower.
Renewable electricity	Electricity consumption	~4%	From hard-to-abate industrial sectors [10], modest but actionable for the present factory's electricity load.
Operational efficiency (machinery maintenance + AI-assisted scheduling)	Diesel/fuel optimization	5–15%	From the CFP of wooden-chair production [12], applicable to forklift and machinery operations.
Waste valorization (sawdust → biochar)	Carbon sequestration	Indicative ~3–6% global CO_2 avoidance per global biochar literature	From global biochar studies [16], site-specific feasibility depends on local biochar uptake and end-use markets.

3.4 Limitations and uncertainty

Several limitations should be considered when interpreting these results. **(1)** The study is based on a single factory selected by purposive sampling; the selected facility's annual output (~9,645 m^3) is approximately 2.7% of the total Yala provincial capacity (357,395 m^3 across 29 active factories), and the findings cannot be assumed to be representative of the industry as a whole. **(2)** Activity data are drawn from a single calendar year (2022), and seasonal or inter-annual variability is not captured. **(3)** The EFs for rubberwood-related items are derived from an unpublished internal factory document [9] and have not been peer-reviewed. However, the values are reproduced transparently in Table 1 and were cross-checked against external databases [13,14] for energy and consumable items; independent verification of the rubberwood-specific factors was not feasible. **(4)** Biogenic CO_2 stock within rubberwood, plantation-level sequestration, and land-use change are excluded, in line with the Cradle-to-Gate boundary; a complete biogenic-carbon balance would require a Cradle-to-Grave or Cradle-to-Cradle assessment. **(5)** Formal uncertainty propagation (e.g., Monte Carlo simulation) was not performed because parameter distributions for the internally derived EFs were unavailable. Future research should expand to multi-factory sampling within Yala Province, incorporate peer-reviewed or independently audited EFs for rubberwood, include biogenic carbon and land-use-change effects, and conduct quantitative uncertainty and sensitivity analyses. The policy analysis and associated GHG mitigation impacts for the industry are presented in Table 4.

Table 4. Policy Analysis and GHG Mitigation Impact in the Rubberwood Industry

Key Finding (Carbon Hotspot)	Proposed Mitigation Strategy	Relevant National Policy / Goal	Policy Linkage and Significance
Raw materials and wood offcuts (~90% of GHG)	Optimized inventory management (15%–30% indicative reduction)	NDC (30%–40% reduction by 2030), Carbon Neutrality (2050), and Net Zero (2065) [17]	Factory-level data provide the empirical basis for setting GHG-reduction strategies in the industrial sector that align with national NDCs and long-term goals.
Total CFP intensity = 40.83 $kgCO_2$-eq/m^3 (corrected total)	GHG reduction based on CFP data	TGO Carbon Labeling Program [18] and EU CBAM	Supports manufacturers in using CFP data for the Carbon Label and trade competitiveness in environmentally stringent export markets.
Wood offcuts/sawdust (production residues)	Waste valorization (sawdust → biochar)	BCG Economic Model and Circular Economy Policy [19]	Promotes resource efficiency by converting residues into high-value products with potential long-term carbon sequestration.
Energy (electricity and diesel) — secondary driver	Biomass-fuel substitution and renewable energy (e.g., rooftop solar)	Power Development Plan (PDP) and DEDE Energy Conservation Policy [20]	Supports national energy policy to reduce reliance on fossil fuels and promote clean-energy and energy-saving measures within factories.

4. Conclusions

This study provides a Cradle-to-Gate baseline carbon footprint assessment for one operational rubberwood processing factory in Yala Province, Thailand. The factory-level CFP intensity is 40.83 $kgCO_2$-eq/m^3, with raw materials and processing residues responsible for approximately 90% of total emissions, and electricity and diesel fuel acting as secondary contributors. The findings are presented as single-factory empirical evidence rather than a provincial baseline. Indicative mitigation pathways drawn from the literature — optimized inventory management, biomass-fuel substitution, operational efficiency, and biochar-based waste valorization — offer entry points for evidence-based emission-reduction planning, conditional on site-specific feasibility evaluation. These hotspots align with Thailand's NDC, Carbon Neutrality, and Net Zero targets; the TGO Carbon Label Program and the EU CBAM; the Bio-Circular-Green economic model; and the PDP/DEDE energy framework. The study is constrained by its single-factory scope, single-year inventory, exclusion of biogenic carbon and land-use change, and reliance on internally derived EFs for rubberwood; multi-factory studies with independently verified EFs and quantitative uncertainty analysis are recommended as next steps.

5. Acknowledgments

The researcher would like to express sincere gratitude to the rubberwood processing factory for their kind cooperation, support, and facilitation in the data collection process for this study.

Author Contributions: Conceptualization, J.K.; methodology, J.K.; software, J.K.; validation, J.K.; formal analysis, J.K.; investigation, J.K.; resources, J.K.; data curation, J.K.; writing—original draft preparation, J.K.; writing—review and editing, J.K.; visualization, J.K.; supervision, J.K.; project administration, J.K.The author has read and agreed to the published version of the manuscript.. All authors have read and agreed to the published version of the manuscript.

Funding: This research received no external funding.

Conflicts of Interest: The authors declare no conflict of interest.

References

[1] Ratnasingam, J.; Ramasamy, G.; Ioras, F.; Parasuraman, N. Assessment of the Carbon Footprint of Rubberwood Sawmilling in Peninsular Malaysia: Challenging the Green Label of the Material. *BioResources* **2017**, *12*(2), 3490–3503. https://doi.org/10.15376/biores.12.2.3490-3503

[2] Eshun, J. F.; Marfo, E. D.; Quartey, G. A. Evaluation of the Carbon Footprint of Rubberwood Lumber Production in Ghana. *Eur. J. Appl. Sci.* **2022**, *10*(4), 803–810. https://doi.org/10.14738/aivp.104.12951

[3] Jawjit, S.; Jawjit, W.; Pibul, P.; Wongcharee, S.; Suwannahong, K. Enhancing the Sustainability of the Sawn Rubberwood Industry through Resource-Efficient and Cleaner Production Approaches. *J. Clean. Prod.* **2024**, *479*, 143913. https://doi.org/10.1016/j.jclepro.2024.143913

[4] Chaichana, T.; Thongdee, S.; Pechurai, W. Carbon Footprint and Carbon Stock Volume for Para Rubber Production in Southern Thailand. In *2020 International Conference on Energy, Environment and Climate Change (ICUE)*; 2020; pp 1–6. https://doi.org/10.1109/ICUE49301.2020.9307004

[5] Yala Provincial Industry Office. *Industrial Investment Movement Report of Yala Province as of January 2022*; Yala Provincial Industry Office: Yala, Thailand, 2022.

[6] He, K.; Dong, X.; Gong, C.; Yu, Q.; Ye, Q.; Guo, Q.; Varbanov, P. S.; Wang, X. Spatiotemporal Prediction of Greenhouse Gas Emissions from Rubber Wood Furniture Industry, Taking Hainan as the Case. *J. Clean. Prod.* **2024**, *480*, 144049. https://doi.org/10.1016/j.jclepro.2024.144049

[7] Office of Natural Resources and Environmental Policy and Planning. *Thailand's Long-Term Low Greenhouse Gas Emission Development Strategy (LT-LEDS)*; ONEP: Bangkok, Thailand, 2021.

[8] Office of Natural Resources and Environmental Policy and Planning. *Thailand's Second Updated Nationally Determined Contribution (NDC)*; ONEP: Bangkok, Thailand, 2022.

[9] Rubberwood Processing Factory. *Annual Production Report 2022*; Internal Document; Yala, Thailand, 2022.

[10] Wang, H.; Wu, J.; Chen, Z. Carbon Footprint Accounting and Low-Carbon Path Optimization for Imported Timber-Based Wooden Furniture Supply Chains. *BioResources* **2021**, *16*(4), 6870–6890. https://doi.org/10.15376/biores.16.4.6870-6890

[11] Srichat, P.; Nanthasamroeng, P.; Bonnet, S. Life Cycle Assessment of Wood Pellet Production in Thailand. *Sustainability* **2020**, *12*(17), 6996. https://doi.org/10.3390/su12176996.

[12] Thaipradith, P.; Tuprakay, S.; Ratcha, M.; Suwannahong, K. Assessing the Carbon Footprint of a Product: A Case Study of the Wooden Chair Production Process. *J. Health Environ. Educ.* **2023**, *8*(3), 178–186.

[13] Thailand Greenhouse Gas Management Organization. *Emission Factors by Industrial Sector*; TGO: Bangkok, Thailand, 2025.

[14] Climatiq. *The Largest Database of Vetted Emission Factors*; Climatiq, 2025.

[15] Türkmen, B. A. Life Cycle Environmental Impacts of Disposable Medical Masks. *Environ. Sci. Pollut. Res.* **2022**, *29*, 25496–25506. https://doi.org/10.1007/s11356-021-17430-5.

[16] Kwon, K.-S.; Lee, H.-S. Sustainable Development of Sawdust Biochar as a Green and Promising Material for CO_2 Capture Technologies. *Materials* **2025**, *18*(14), 3243. https://doi.org/10.3390/ma18143243.

[17] Department of Climate Change and Environment. *National Greenhouse Gas Emission Reduction Action Plan 2021–2030*; DCCE: Bangkok, Thailand, 2021.

[18] Thailand Greenhouse Gas Management Organization. *National Guideline Carbon Footprinting for Organization*; TGO: Bangkok, Thailand, 2025.

[19] Office of the National Economic and Social Development Council. *Driving the BCG Economic Model (Bio-Circular-Green Economy)*; NESDC: Bangkok, Thailand, 2025.

[20] Department of Alternative Energy Development and Efficiency. *Thailand's Energy Conservation Plan and Renewable Energy Development Plan*; DEDE: Bangkok, Thailand, 2025.

ASEAN
Journal of Scientific and Technological Reports
Online ISSN:2773-8752

Research article

Trichoderma asperelloides TSUxPT3.5 Exhibits Antifungal Activity Against Plant Pathogenic Fungi and Enhances the Growth of Mini Cos Lettuce (*Lactuca sativa* L.)

Wankuson Chanasit[1], Prisana Wonglom[2], Nakarin Suwannarach[3, 4], Jaturong Kumla[3, 4], Anurag Sunpapao[5], Kamonthip Jiadkong[2], Monthon Lertworapreecha[1], Nugul Intrasungkha[1], Panadda Promjun[1], Chaisit Niyasom[1], and Pumin Nutaratat[1*]

[1] Faculty of Science and Digital Innovation, Thaksin University, Phatthalung, 93210, Thailand
[2] Faculty of Agriculture, Thaksin University, Phatthalung, 93210, Thailand
[3] Center of Excellence in Microbial Diversity and Sustainable Utilization, Chiang Mai University, Chiang Mai, 50200, Thailand
[4] Office of Research Administration, Chiang Mai University, Chiang Mai, 50200, Thailand
[5] Faculty of Natural Resources, Prince of Songkla University, Songkhla, 90112, Thailand
* Corresponding: pumin.n@tsu.ac.th

Citation:
Chanasit, W.; Wonglom, P.; Suwannarach, N.; Kumla, J.; Sunpapao, A.; Jiadkong, K.; Lertworapreecha, M.; Intrasungkha, N.; Promjun , P.; Niyasom, C.; Nutaratat, P. *Trichoderma asperelloides* TSUxPT3.5 exhibits antifungal activity against plant pathogenic fungi and enhances the growth of mini cos lettuce (*Lactuca sativa* L.). *ASEAN J. Sci. Tech. Report.* **2026**, *29*(7), e264555. https://doi.org/10.55164/ajstr.v29i7.264555

Article history:
Received: March 25, 2026
Revised: May 28, 2026
Accepted: May 30, 2026
Available online: June 14, 2026

Publisher's Note:
This article is published and distributed under the terms of the Thaksin University.

Abstract: *Trichoderma* species are widely recognized as effective biological control agents due to their multifaceted antagonistic mechanisms and plant growth-promoting activities. In this study, an indigenous fungal strain, TSUxPT3.5, was isolated from organic agricultural soil in southern Thailand. Molecular identification based on multi-locus sequence analysis of the ITS, *tef1*, and *rpb2* regions confirmed the strain as *Trichoderma asperelloides*. This fungus was further characterized for its plant growth-promoting traits through both direct and indirect mechanisms. *Trichoderma asperelloides* TSUxPT3.5 produced indole compounds and exhibited antagonistic activity against economically important plant pathogenic fungi, including *Curvularia aeria* and *Corynespora cassiicola*, causal agents of leaf spot disease in lettuce. Its biocontrol mechanisms involved competition for nutrients and space, production of cell wall-degrading enzymes (chitinase and cellulase), and emission of volatile organic compounds (VOCs). Among the detected VOCs, 2-ethylhexan-1-ol was the predominant compound. Additionally, 6-pentyl-2H-pyran-2-one, 2,4-Di-tert-butylphenol, and 2-methyl-1-propanol, a well-known antifungal metabolite, were also identified. Application of *T. asperelloides* TSUxPT3.5 significantly enhanced the growth of mini cos lettuce (*Lactuca sativa* L.), increasing fresh weight and improving plant vigor compared with the untreated control. In addition, disease severity was markedly reduced in treated plants. These findings demonstrate that the indigenous *T. asperelloides* TSUxPT3.5 possesses multifunctional antagonistic and plant growth–promoting traits, highlighting its potential as an eco-friendly biological control agent for sustainable lettuce production.

Keywords: Biological control; indole compounds; plant growth promotion; *Trichoderma*; volatile organic compounds

1. Introduction

Plant diseases caused by fungal pathogens represent a major constraint on global agricultural productivity, resulting in substantial yield losses and posing serious threats to food security worldwide [1]. In recent years, the

incidence and severity of fungal plant diseases have increased markedly, largely due to climate change-related factors such as rising temperatures, altered precipitation, increased humidity, and more frequent extreme climate events [2, 3]. These changing environmental conditions can induce pathogen germination, survival, reproduction, and spread, while simultaneously weakening host plant resistance [4-6]. For instance, crops grown under protected cultivation systems, including leafy vegetables such as lettuce (*Lactuca sativa*), have become increasingly vulnerable to fungal diseases [7-9]. Addressing fungal diseases in the context of climate change has therefore become a critical challenge for sustainable agricultural production.

Effective plant disease management relies on accurate disease diagnosis and the application of appropriate control strategies, including biological, chemical, and mechanical approaches. Chemical control provides rapid, broad-spectrum efficacy in suppressing fungal pathogens and inducing plant defense responses [10]. However, the extensive use of synthetic fungicides has led to several negative consequences, including environmental contamination, adverse effects on non-target microorganisms, risks to human health, and the rapid emergence of fungicide-resistant pathogens [11-13]. Given these limitations, there is increasing interest in alternative, environmentally friendly, and sustainable disease management strategies. Among them, biological control using beneficial microorganisms has emerged as an effective and sustainable approach for suppressing plant pathogens while reducing reliance on chemical inputs [14].

Among the diverse group of antagonistic biological control agents (BCAs), species of the genus *Trichoderma* are among the most extensively studied and commercially exploited fungi for plant disease control. *Trichoderma* spp. suppress plant pathogenic fungi through multiple mechanisms, including competition for nutrients and space, mycoparasitism, production of antimicrobial secondary metabolites, emission of volatile organic compounds (VOCs), and secretion of hydrolysis enzymes [15-18]. Furthermore, *Trichoderma* spp. are well recognized for their ability to promote plant growth and development by producing phytohormones, including indole compounds (e.g., indole-3-acetic acid), and to enhance systemic resistance against several pathogens [19-21]. Interestingly, accumulating evidence revealed that these biocontrol and plant growth-promoting traits are highly strain-dependent, even within the same *Trichoderma* species, highlighting the importance of identifying and characterizing effective indigenous strains adapted to local environmental conditions [22]. Although several strains of *T. asperelloides* have previously been reported for their biocontrol activity and volatile-mediated antifungal effects [16–18], information regarding the biological characteristics and plant growth-promoting potential of *T. asperelloides* strain TSUxPT3.5 remains limited. In particular, its antifungal activity, extracellular enzyme production, volatile organic compound emission, indole compound production, and plant growth-promoting potential in lettuce systems have not been comprehensively characterized.

Lettuce (*Lactuca sativa* L.) is one of the most widely cultivated and consumed leafy vegetables worldwide and represents an economically important crop in the fresh vegetable market. It includes a wide range of horticultural types, such as mini cos (baby romaine), crisphead (iceberg), butterhead, loose-leaf, and stem lettuce, which vary in morphology, texture, and consumer preference. Global production of lettuce and chicory exceeds 27 million tonnes annually [23], reflecting its high market demand and economic importance. Among lettuce types, mini cos lettuce has gained increasing popularity due to its compact size, crisp texture, and suitability for fresh consumption. Mini cos lettuce is increasingly cultivated as a high-value leafy vegetable under protected and semi-protected cultivation systems to meet the growing demand for fresh produce. However, fungal diseases such as leaf spot and leaf blight remain major constraints on lettuce production, causing both quality and yield losses under warm, humid conditions [7, 24]. *Trichoderma* species are widely recognized as effective BCAs and plant growth promoters, owing to their multiple mechanisms of antagonism against plant pathogens. Therefore, the objective of this study was to identify and characterize an indigenous *Trichoderma* isolate from agricultural soil and evaluate its antagonistic activity against economically important plant pathogenic fungi associated with lettuce diseases, as well as its plant growth-promoting potential.

2. Materials and Methods

2.1 Source of *Trichoderma* and fungal pathogens

Trichoderma sp. strain TSUxPT3.5 were isolated from organic agricultural soil collected from Tha Chamuang subdistrict, Rattaphum district, Songkhla province, Thailand, by the serial dilution spread plate method. It has been preserved at the Culture Collection of the Department of Biological Science, Faculty of Science and Digital Innovation, Thaksin University, Phatthalung, Thailand. *Curvularia aeria* and *Corynespora cassiicola*, causal agents of leaf spot disease in lettuce [7, 25], were obtained from the Culture Collection of the Department of Plant Pathology, Faculty of Natural Resources, Prince of Songkla University, Thailand. Both *Trichoderma* and fungal pathogens were cultured on potato dextrose agar (PDA) and incubated at 30 ± 2°C for 5 days before use in the bioassay.

2.2 Identification of the *Trichoderma* sp. strain TSUxPT3.5

The *Trichoderma* sp. strain TSUxPT3.5 was identified using morphology and molecular taxonomic methods. For morphological identification, the fungus was cultured on PDA to assess growth and macroscopic features. Microscopic features of hyphae, conidiophores, phialides, and conidia were observed under a compound microscope. For molecular identification, genomic DNA was extracted from fungal mycelia using the FavoPrep® DNA Extraction Mini Kit (Favorgen, Taiwan) according to the manufacturer's instructions. Genus-level identification was performed using the internal transcribed spacer (ITS) region, which was PCR-amplified from fungal genomic DNA with the primers ITS4 and ITS5 [26]. Species-level identification was conducted using partial sequences of the translation elongation factor 1-alpha (*tef1*) and the second largest subunit of RNA polymerase II (*rpb2*). The *tef1* gene was amplified using the primer pairs EF1/EF2 [27] and EF1-728F/tef1-LLErevR [28, 29], while the *rpb2* gene was amplified using the primer pair RPB2-5F/RPB2-7cR [30]. The obtained ITS, *tef1*, and *rpb2* sequences were compared with reference sequences of type strains available in the GenBank database (https://www.ncbi.nlm.nih.gov). Phylogenetic trees based on *tef1* and *rpb2* sequences were constructed from evolutionary distance data using the general time-reversible (GTR) model and maximum likelihood methods [31] with the MEGA12 (molecular evolutionary genetics analysis) software [32]. Bootstrap confidence values were obtained using 1000 resamplings [33]. The sequence was aligned with the closest strains of the species using multiple sequence comparison by log-expectation (MUSCLE) [34]. *Nectria aurantiaca* was used as an outgroup.

2.3 Evaluation of antagonistic activity of *Trichoderma* sp. strain TSUxPT3.5 against plant pathogenic fungi

In vitro antagonistic activity was evaluated using the dual culture method [35]. A mycelial plug of *Trichoderma* sp. strain TSUxPT3.5, and a plug of the tested phytopathogen were placed 65 mm apart on 90 mm Petri dishes containing PDA and incubated at 30 ± 2 °C. The phytopathogenic fungi used in this study are *C. aeria* and *Co. cassiicola.* Control plates containing only the phytopathogen were included for comparison. Radial mycelial growth was measured after 3 and 5 days of incubation, and the percentage inhibition of mycelial growth was calculated using Equation (1):

$$\text{Percentage inhibition} = [(R_1 - R_2)/R_1] \times 100 \quad (1)$$

where R_1 represents the radial growth of the phytopathogen in the control plates, and R_2 represents the radial growth in the presence of *Trichoderma* sp. strain TSUxPT3.5. All assays were performed in triplicate.

2.4 Qualitative chitinase and cellulase activity of *Trichoderma* sp. strain TSUxPT3.5

The inoculum of the *Trichoderma* sp. strain TSUxPT3.5 was prepared on PDA and incubated at 30 ± 2 °C for 5 days. Mycelial plugs (5 mm in diameter) obtained from the actively growing margins of the colonies were transferred onto carboxymethyl cellulose (CMC) agar and chitin agar, as described by Kamala and Indira [36], for the primary detection of cellulase and chitinase activities, respectively. For cellulase activity analysis, the agar plates were flooded with 0.1% (w/v) Congo red solution for 10 min, then destained with 1 N NaCl. The formation of clear hydrolysis zones around the fungal colonies indicated enzyme activity. Chitinase activity was detected by the formation of purple-colored zones on chitin agar, indicating chitin degradation and dye-substrate complex formation. All experiments were conducted in triplicate.

2.5 *In vitro* antifungal activity of VOCs produced by *Trichoderma* sp. strain TSUxPT3.5

The antifungal activity of volatile organic compounds (VOCs) produced by *Trichoderma* sp. strain TSUxPT3.5 was examined using a sealed plate assay. A mycelial plug of *Trichoderma* sp. strain TSUxPT3.5, and a plug of the fungal pathogen were placed at the center of two separate PDA plates of the same size. The plates were paired face-to-face, sealed with parafilm, and incubated at 30 ± 2 °C for 3 and 5 days. Control plates were prepared in the same manner without inoculation of *Trichoderma*. The percentage inhibition of mycelial growth was calculated using Equation (2):

$$\text{Percentage inhibition (\%)} = (C - T) / C \times 100 \quad (2)$$

where C is the colony diameter of the fungal pathogen in the control, and T is the colony diameter in the treatment.

2.6 Evaluation of volatile organic compounds produced by *Trichoderma* sp. strain TSUxPT3.5

Volatile organic compounds (VOCs) produced by *Trichoderma* sp. strain TSUxPT3.5 were analyzed using solid-phase microextraction (SPME) coupled with gas chromatography–mass spectrometry (GC–MS), following the method described by Suwannarach et al. [37]. A 50/30 μm divinylbenzene/carboxen/ polydimethylsiloxane (DVB/CAR/PDMS) StableFlex fiber (Supelco, USA) was exposed to the headspace above each fungal culture for 45 min. The adsorbed fiber was then inserted into the splitless injection port of a gas chromatograph (GC-2010, Shimadzu, Japan) equipped with a DB-Wax capillary column (0.25 mm × 30 m, 0.25 μm film thickness, Supelco, USA). The column temperature was programmed to 40°C for 2 min and then increased to 200 °C at 5°C min^{-1}. Helium (ultra-high purity) was used as the carrier gas at an initial column head pressure of 60 kPa. The fiber was desorbed at 250°C for 57 min under a helium flow, then the volatiles were trapped. A 30 s injection time was used to introduce the adsorbed volatiles into the gas chromatograph (GC) interfaced with a mass spectrometer (MS-QP2010 Plus, Shimadzu, Japan). The mass spectrometer was operated at unit mass resolution. Software systems performed data acquisition and data processing. The VOCs produced by *Trichoderma* sp. strain TSUxPT3.5 were tentatively identified through a library comparison with the NIST database.

2.7 Detection of indole compounds produced by *Trichoderma* sp. strain TSUxPT3.5

Trichoderma sp. strain TSUxPT3.5 was cultured on PDA and incubated at 30 ± 2 °C for 5 days. After incubation, five mycelial plugs (5 mm in diameter) obtained from the actively growing margins of the colonies were transferred into 50 mL of potato dextrose broth (PDB) supplemented with 0.1% (w/v) L-tryptophan. The cultures were incubated on an orbital shaker at 170 rpm and 30 °C for 7 days. The culture supernatants were collected by centrifugation and used to determine indole compounds [38]. Briefly, 1 mL of culture supernatant was mixed with 2 mL of Salkowski's reagent (containing 0.5 M $FeCl_3$, 2 mL, and 35% $HClO_4$, 98 mL and incubated in the dark for 30 min. The development of a pink-to-red color indicated the presence of a positive indole compound. All experiments were conducted in triplicate.

2.8 Effects of *Trichoderma* sp. strain TSUxPT3.5 on plant growth parameters and reduction of leaf disease caused by natural infection

Mini cos lettuce seedlings aged 18 days after sowing were transplanted into experimental plots at a spacing of 20 × 20 cm, with one plant per planting hole. Plants were irrigated using a drip irrigation system, and additional overhead misting was applied three times daily to reduce temperature and increase relative humidity. The experiment was conducted in a protected greenhouse under conditions of 28–34 °C and approximately 70–85% relative humidity. The experiment consisted of three treatments: (i) *Trichoderma* sp. strain TSUxPT3.5, (ii) *Trichoderma asperellum* (commercial strain used to serve as a positive control), and (iii) untreated control. *Trichoderma* suspensions, adjusted to 1×10^6 spores mL^{-1} using a hemocytometer according to standard fungal inoculum preparation procedures [15], were applied as foliar sprays every three days in the evening, starting 14 days after transplanting. Plant growth parameters, including plant height, number of leaves per plant, and fresh weight, were recorded during the experiment. Each treatment consisted of ten replicates, and the experiment was conducted twice. Natural infection and leaf disease were observed in protected cultivation. Disease severity was assessed using a rating scale of 0–5, where 0 = no spots, 1 = spot

area of 0–20%, 2 = 20–40%, 3 = 40–60%, 4 = 60–80% with approximately 50% spot coalescence, and 5 = 80–100% with more than 75% spot coalescence. Disease severity scores were converted to a disease severity index (DSI) according to Equation (3):

$$\text{DSI (\%)} = \frac{\Sigma\,(scale \times amount\ of\ plants)}{maximum\ level \times total\ number\ of\ plant} \times 100 \quad (3)$$

2.9 Statistical Analysis

The effects of *Trichoderma* treatment on plant growth were analyzed using one-way analysis of variance (ANOVA). When significant differences were detected, treatment means were separated using the least significant difference (LSD) test at $P < 0.05$.

3. Results

3.1 Identification of *Trichoderma* sp. strain TSUxPT3.5

Morphological observations of *Trichoderma* sp. strain TSUxPT3.5 were conducted on PDA at 28 ± 2 °C after 1–4 days of incubation. Conidia germinated on PDA within 24 h, and colonies reached a diameter of 85 mm after four days of incubation. Colonies initially produced white, downy mycelia that gradually turned pale green and, with age, dark green. Conidiophores were branched and produced in pustules with the formation of secondary branches. These secondary branches were typically paired and asymmetric, terminating in either a single phialide or a whorl of two to three divergent phialides. Phialides were ampulliform. Conidia were dark green and subglobose (Figure 1).

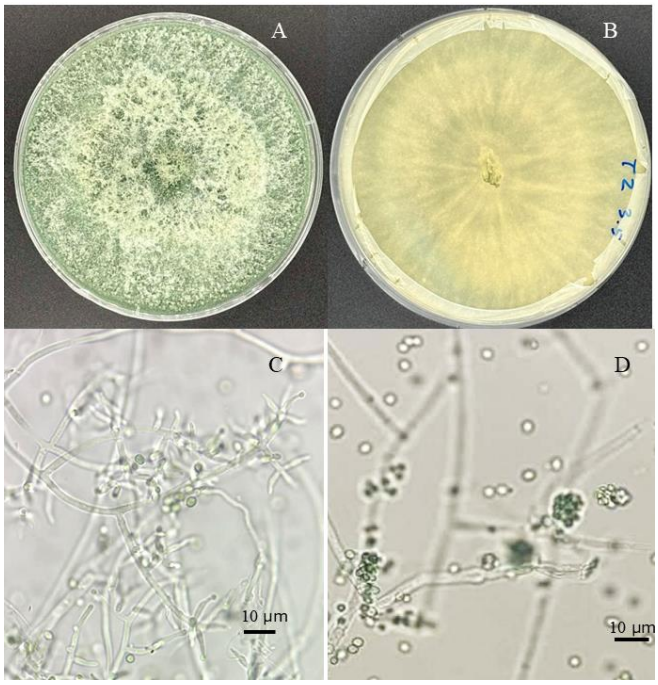


Figure 1. Morphological characteristics of the fungal strain TSUxPT3.5. Colony morphology on potato dextrose agar (PDA) showing the top view (A) and bottom view (B); microscopic structures including conidiophores and phialides (C); and conidia (D). Scale bars = 10 µm.

Based on ITS region sequence analysis, the fungal strain TSUxPT3.5 was identified as a member of the genus *Trichoderma*. Species-level identification was subsequently performed using multi-locus phylogenetic analysis of the *tef1* and *rpb2* gene regions. Strain TSUxPT3.5 exhibited high sequence similarity to *Trichoderma asperelloides*, showing 99.81% and 100% identity for the *tef1* and *rpb2* genes, respectively. According to the molecular identification guidelines proposed by Cai and Druzhinina [39], a query strain can be reliably assigned to an existing *Trichoderma* species when sequence similarity is ≥97% for *tef1* and ≥99% for *rpb2*, provided that both loci indicate the same species. Phylogenetic analysis further revealed that strain TSUxPT3.5

clustered within a strongly supported monophyletic clade of *Trichoderma asperelloides* with 100% bootstrap support (Figure 2). In the present study, multi-locus phylogenetic analysis consistently assigned strain TSUxPT3.5 to *T. asperelloides*, thereby confirming its taxonomic placement in accordance with established molecular identification criteria.

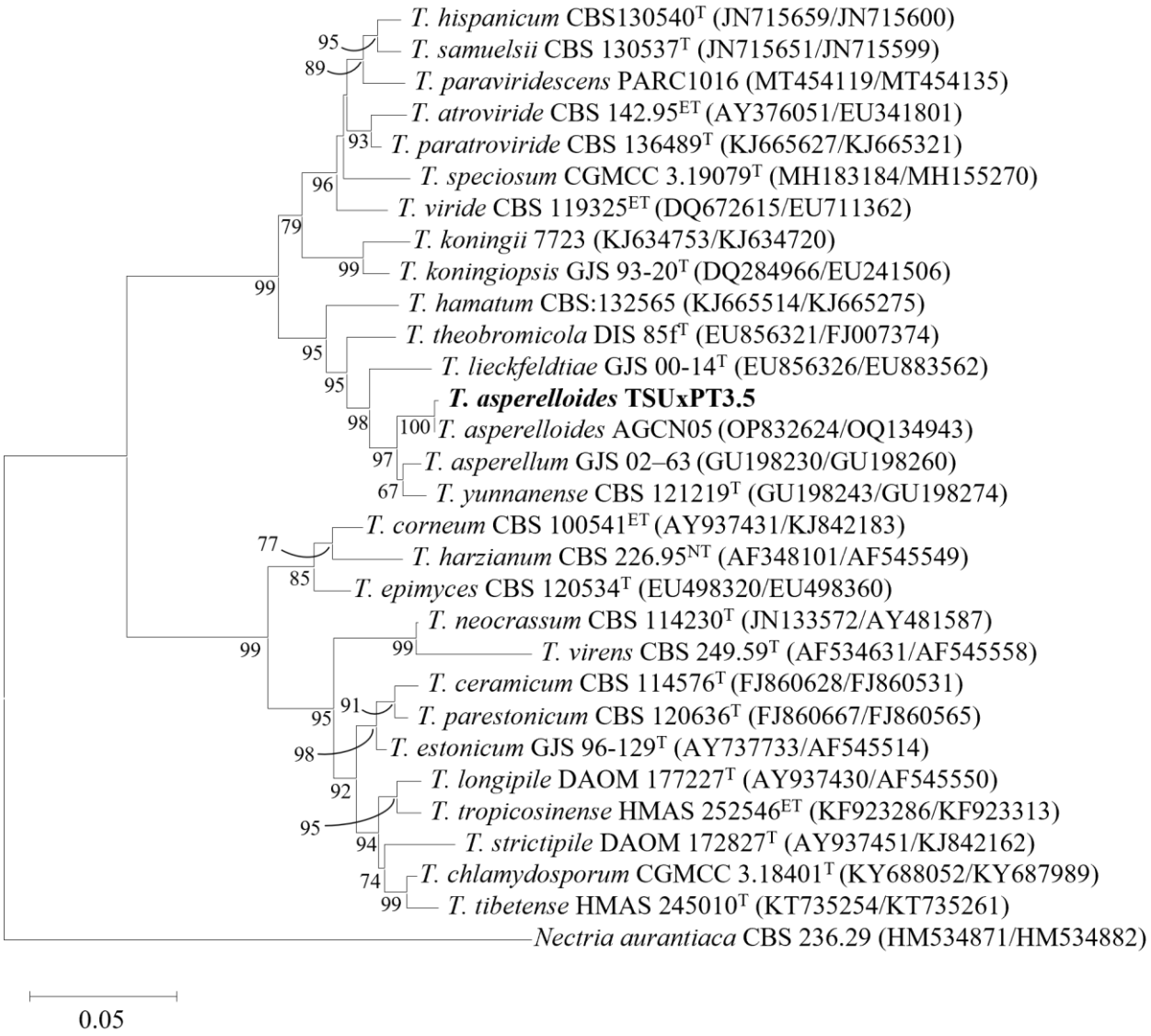


Figure 2. Phylogenetic tree based on combined *tef1* and *rpb2* gene sequences, constructed using the maximum likelihood method with the General Time Reversible (GTR) model, showing the phylogenetic relationships of *Trichoderma* sp. strain TSUxPT3.5 with representative species of the genus *Trichoderma* and related taxa. The numbers in parentheses are GenBank accession numbers of the *tef1*/*rpb2* sequences. *Nectria aurantiaca* was used as an outgroup in these analyses. Sequences of fungal species obtained in this study are bold. Superscript T, ET, and NT represent type, epitype, and neotype culture, respectively.

3.2 Competitive ability of *Trichoderma asperelloides* strain TSUxPT3.5 in dual culture assay

The results showed that strain TSUxPT3.5 inhibited the mycelial growth of the tested pathogens, *C. aeria* and *Co. cassiicola*. After 3 days of incubation, *T. asperelloides* TSUxPT3.5 began to grow toward the pathogen colonies, and an interaction zone was observed between the mycelia of the antagonist and the pathogens (Figure 3). The growth of both pathogens was noticeably restricted compared with the control

plates. After 5 days of incubation, *T. asperelloides* TSUxPT3.5 rapidly colonized the culture medium and overgrew the pathogen colonies. The mycelia of *Trichoderma* intertwined with those of the pathogens, and browning was observed at the interaction zone. The inhibition rates of *T. asperelloides* TSUxPT3.5 against *C. aeria* and *Co. cassiicola* were 49.78% and 59.81%, respectively, indicating stronger antagonistic activity against *Co. cassiicola*.

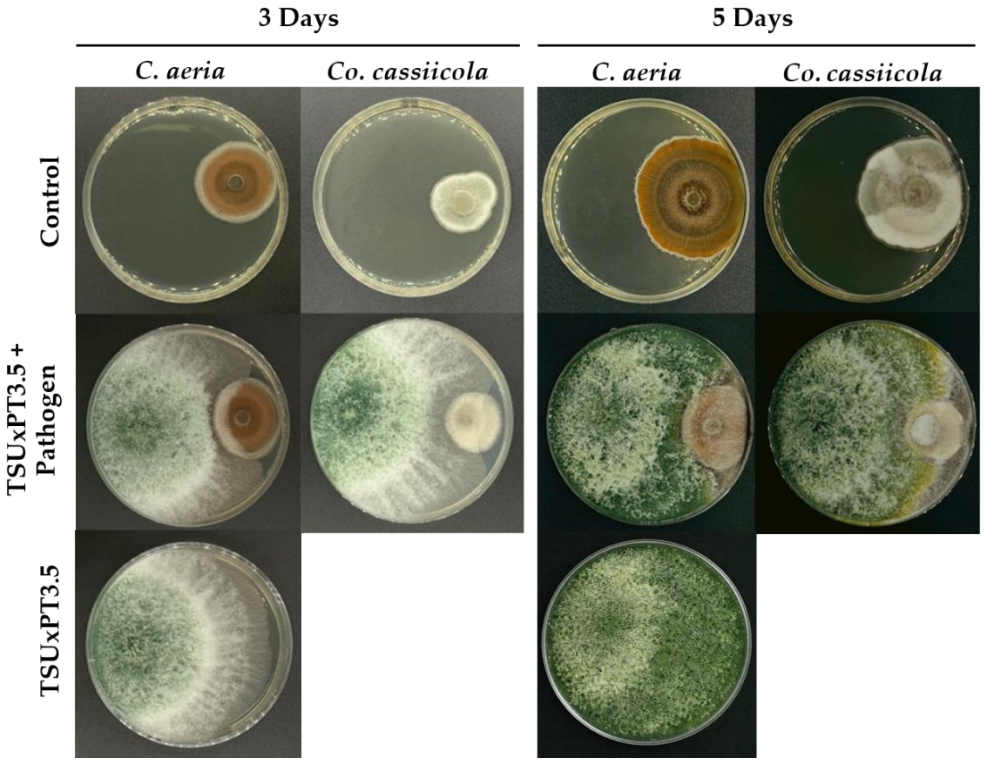


Figure 3. Dual culture assay illustrating the antagonistic interaction between *T. asperelloides* strain TSUxPT3.5 and the plant pathogenic fungi *C. aeria* and *Co. cassiicola* on potato dextrose agar after 3 and 5 days of incubation. Control plates containing only the pathogens and plates containing *T. asperelloides* TSUxPT3.5 alone are included for comparison.

3.3 Qualitative chitinase and cellulase activity of *Trichoderma asperelloides* strain TSUxPT3.5

In the present study, *T. asperelloides* TSUxPT3.5 exhibited positive activity for both cellulase and chitinase production. However, cellulolytic activity was relatively weak, as indicated by the formation of a narrow substrate degradation zone beneath the fungal colony. In contrast, chitinase activity was more pronounced, as evidenced by a broader clear zone on chitin agar (Figure 4).

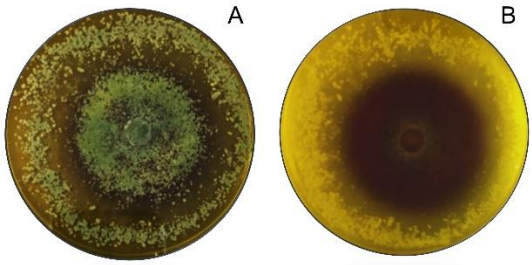


Figure 4. Chitinase activity of *T. asperelloides* TSUxPT3.5 on chitin agar: (A) top view and (B) bottom view.

3.4 *In vitro* antifungal activity of VOCs produced by *Trichoderma asperelloides* strain TSUxPT3.5

The inhibitory effect of VOCs produced by *T. asperelloides* TSUxPT3.5 against the tested pathogens differed between species. For *C. aeria*, the percentage inhibition was 7.15%. In contrast, *Co. cassiicola* showed a

higher level of inhibition, with a 27.24% inhibition. These results suggest that VOCs produced by *T. asperelloides* TSUxPT3.5 may contribute to inhibiting fungal pathogens (Figure 5).

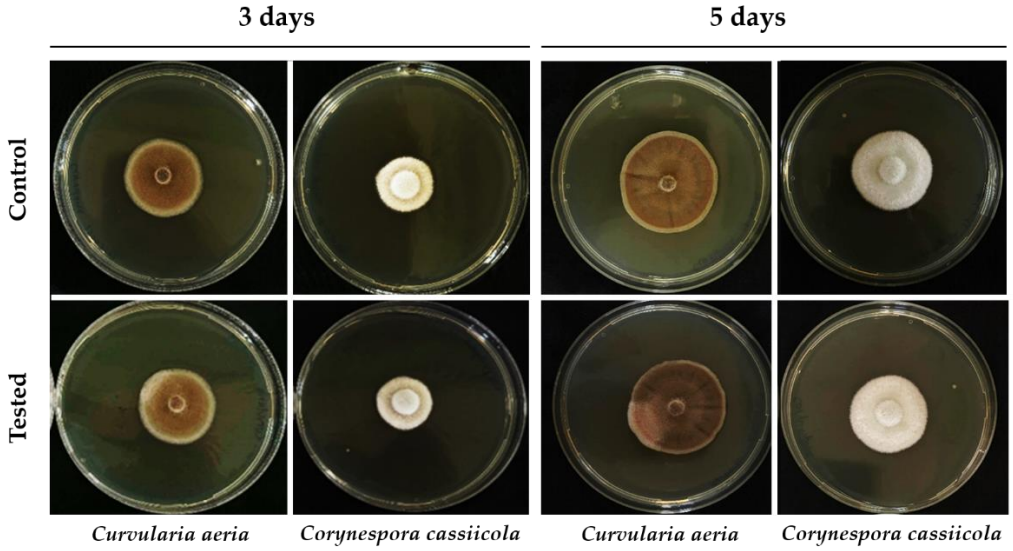


Figure 5. Antifungal activity of volatile organic compounds (VOCs) produced by *Trichoderma asperelloides* strain TSUxPT3.5 against *C. aeria* and *Co. cassiicola* using a sealed plate assay. Fungal growth was assessed after 3 and 5 days of incubation. Control plates represent pathogen growth without exposure to *Trichoderma*, while tested plates represent pathogen growth exposed to VOCs emitted by strain TSUxPT3.5.

3.5 Volatile organic compounds produced by *Trichoderma asperelloides* strain TSUxPT3.5

Volatile organic compounds (VOCs) produced by *Trichoderma* spp. have been widely reported to exhibit antifungal activity. In this study, the VOCs emitted by *T. asperelloides* TSUxPT3.5 were analyzed using solid-phase microextraction coupled with gas chromatography–mass spectrometry (SPME/GC–MS). A total of six volatile compounds with ≥90% similarity were tentatively identified by comparison with the NIST mass spectral library (Table 1). Among the detected compounds, 2-ethylhexan-1-ol was the predominant, followed by 6-pentyl-2H-pyran-2-one, a well-known antifungal metabolite produced by *Trichoderma* species. These results indicate that strain TSUxPT3.5 can produce multiple VOCs, which may contribute to its antifungal activity.

Table 1. International Union of Pure and Applied Chemistry (IUPAC) names of volatile compounds produced by *T. asperelloides* TSUxPT3.5 identified by SPME/GC/MS analysis

Retention time (min)	Libraries identify with the IUPAC name	Formula	Similarity (%)	Area (%)
7.80	2-Methyl-1-propanol	$C_4H_{10}O$	90	1.34
13.52	2-Ethylhexan-1-ol	$C_8H_{18}O$	90	14.66
27.75	6-Pentyl-2H-pyran-2-one	$C_{10}H_{14}O_2$	91	5.12
27.91	4-Isopropyl-1,6-dimethylnaphthalene	$C_{15}H_{18}$	98	1.86
29.86	2,4-Di-tert-butylphenol	$C_{14}H_{22}O$	94	2.32
31.09	Diethyl benzene-1,2-dicarboxylate	$C_{12}H_{14}O_4$	96	1.11

3.6 Indole compounds production by *Trichoderma asperelloides* strain TSUxPT3.5

Indole-producing fungi have been widely recognized for their potential to enhance plant growth and alleviate abiotic stress, thereby improving agricultural productivity. In this study, *T. asperelloides* TSUxPT3.5 was evaluated for its ability to produce the indole compounds. *Trichoderma asperelloides* TSUxPT3.5 exhibited positive indole compound production, as indicated by the development of pink coloration in the culture supernatant, whereas no visible color change was observed in the control (Figure 6).

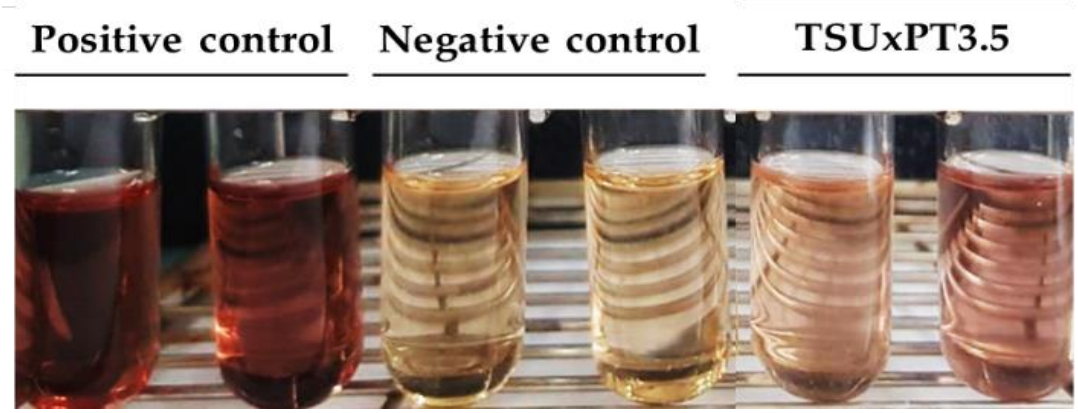


Figure 6. Colorimetric assay of indole compound production of *T. asperelloides* TSUxPT3.5.

3.7 *Trichoderma asperelloides* strain TSUxPT3.5 enhances plant growth and reduces leaf disease severity

At 29 days after planting, plants treated with commercial *T. asperellum* (33.00 cm) and *T. asperelloides* TSUxPT3.5 (33.90 cm) showed no significant difference in plant height; however, both treatments produced significantly taller plants than the untreated control (27.53 cm). Similarly, the number of leaves per plant was higher in plants treated with *T. asperelloides* TSUxPT3.5 (28.40 leaves plant^{-1}) and *T. asperellum* (27.04 leaves plant^{-1}) than in the control (24.72 leaves plant^{-1}), with no significant difference between the two *Trichoderma* treatments (Table 2 and Figure 7). Fresh weight was significantly affected by the treatments, with *T. asperelloides* TSUxPT3.5 exhibiting the highest (81.00 g plant^{-1}), followed by T. asperellum (68.00 g plant^{-1}), while the untreated control showed the lowest (63.00 g plant^{-1}). For disease severity, no disease symptoms were observed in plants treated with *T. asperelloides* TSUxPT3.5 (0.00%), whereas low disease severity was observed in *T. asperellum*-treated plants (0.80%). The highest disease severity was found in the untreated control (2.20%). However, since the experiment was conducted under natural infection conditions with relatively low overall disease pressure, these results should be interpreted cautiously regarding the efficacy of disease suppression. The F-test indicated significant differences among treatments for all measured parameters at $P < 0.01$, indicating good treatment discrimination (Figure 7).

Table 2. Effects of *T. asperelloides* TSUxPT3.5 on plant growth parameters and disease severity of mini cos lettuce at 29 days after planting.

Treatment	Plant height (cm)	Leaves plant-^{1}	Marketable fresh weight (g plant-^{1})	Disease severity (%)
Trichoderma asperellum	33.00 ± 0.83^{a}	27.04 ± 1.45^{a}	68.00 ± 0.44^{b}	0.80 ± 0.55^{b}
Trichoderma asperelloides TSUxPT3.5	33.90 ± 0.86^{a}	28.40 ± 1.53^{a}	81.00 ± 0.52^{a}	0.00 ± 0.00^{b}
Control	27.53 ± 0.70^{b}	24.72 ±1.33^{b}	63.00 ± 0.40^{c}	2.20± 1.50^{a}
C.V. (%)	2.53	5.38	0.64	68.31
F-Test	**	**	**	**

**, significant at $P < 0.01$.

Means within a column followed by different letters are significantly different according to the least significant difference (LSD) test at $P < 0.05$.

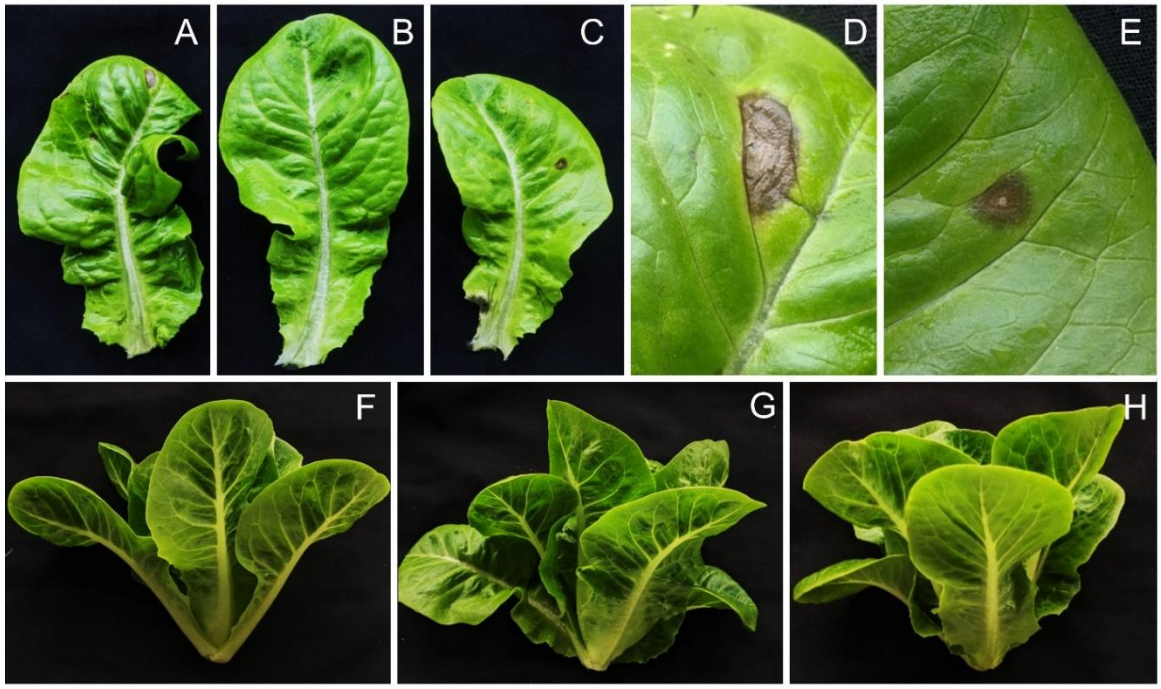


Figure 7. Disease symptoms and plant growth of mini cos lettuce (*Lactuca sativa* L.) under natural infection with different treatments. Control (A), *T. asperelloides* strain TSUxPT3.5 (B), and *Trichoderma asperellum* (C). Close-up of leaf spot symptoms in the control (D) and *T. asperellum*–treated plants (E) caused by *Corynespora cassiicola*. Growth of mini cos lettuce under different treatments: control (F), *T. asperelloides* TSUxPT3.5 (G), and *T. asperellum* (H).

4. Discussion

The antagonistic activity of *T. asperelloides* TSUxPT3.5 against the plant pathogenic fungi *C. aeria* and *Co. cassiicola* can be explained by several well-established biocontrol mechanisms. These include competition for nutrients and space, the production of extracellular cell wall–degrading enzymes such as chitinases and cellulases, and the emission of volatile organic compounds (VOCs) [15-18, 40]. Cell wall–degrading enzymes play a crucial role in weakening pathogen structures and facilitating mycoparasitism, whereas VOCs enable *Trichoderma* spp. to inhibit pathogen growth without direct physical contact [41]. Chitinase is a key cell wall–degrading enzyme that hydrolyzes chitin, a major structural component of fungal cell walls, including those of many phytopathogenic fungi. The production of chitinase is a well-established biocontrol mechanism employed by antagonistic fungi, which degrades the pathogen's cell wall by hydrolyzing β-1,4 linkages between N-acetylglucosamine residues, ultimately leading to cell lysis and death. In the present study, 2-ethylhexan-1-ol was the predominant VOC produced by strain TSUxPT3.5, which is consistent with previous reports identifying this compound among volatile metabolites emitted by *Trichoderma* species [42], followed by 6-pentyl-2H-pyran-2-one. Several of the detected VOCs, including 2-ethylhexan-1-ol [43-45], 6-pentyl-2H-pyran-2-one [46-49], 2,4-di-tert-butylphenol [50-52], and 2-methyl-1-propanol [53], have previously been reported to inhibit fungal growth. The combined presence of multiple VOCs may also result in synergistic antifungal effects, thereby enhancing the inhibitory activity against plant pathogenic fungi. Among the detected VOCs, 6-pentyl-2H-pyran-2-one, a well-known antifungal metabolite commonly produced by *Trichoderma*, and 2,4-di-tert-butylphenol, a phenolic compound previously reported to exhibit antifungal activity, may contribute to the inhibition of plant pathogenic fungi observed in this study. In addition, 2-ethylhexan-1-ol, the major VOC detected in this study, has been reported to exhibit antifungal activity against several plant pathogenic fungi. It should be noted that only VOCs with similarity scores ≥90% were tentatively identified and included in this study. Therefore, additional unidentified volatile compounds may also contribute to the observed antifungal activity of *T. asperelloides* TSUxPT3.5. The inhibitory effects observed in the VOC assay were lower than those obtained in the dual culture assay, suggesting that volatile compounds

alone may contribute only partially to the antagonistic activity of *T. asperelloides* TSUxPT3.5. The stronger inhibition observed in dual culture assays may result from the combined effects of multiple biocontrol mechanisms, including nutrient and space competition, secretion of extracellular hydrolytic enzymes, and the production of both volatile and diffusible antifungal metabolites. The coexistence of multiple antagonistic mechanisms suggests that strain TSUxPT3.5 employs a multifaceted mode of action, which is advantageous for durable disease suppression and may reduce the risk of resistance development in target pathogens.

The present study demonstrated that *Trichoderma asperelloides* TSUxPT3.5 produced indole compounds, as detected by the Salkowski colorimetric assay. This assay is widely used as a rapid method for screening indole compound production by microorganisms [38, 54]. Although the reagent reacts with several indole compounds, including indole-3-acetic acid (IAA), indolepyruvic acid, and indoleacetamide [55], IAA has been reported as the predominant auxin produced by many plant-associated microorganisms [56]. Therefore, high-performance liquid chromatography (HPLC) or gas chromatography–mass spectrometry (GC–MS) may be used in future studies to precisely identify and quantify the indole compounds produced by strain TSUxPT3.5. Generally, *Trichoderma*-mediated plant growth promotion is associated with the production of fungal signaling metabolites that diffuse through the soil and exhibit hormone-like effects, including indole compounds [57]. Consistent with this observation, application of strain TSUxPT3.5 resulted in a statistically significant enhancement of mini cos lettuce growth compared with the untreated control. Similar observations have been reported in previous studies, where plant growth promotion by *Trichoderma* spp. was attributed to auxin-like compounds, modification of root system architecture, and improved nutrient acquisition, even in the absence of direct IAA quantification [58, 59]. Therefore, the observed growth-promoting effect supports the functional role of strain TSUxPT3.5 as a plant growth-promoting fungus under the experimental conditions.

Trichoderma asperelloides has been extensively reported as an effective biological control agent against a wide range of soilborne and foliar plant pathogens, as well as a promoter of plant growth in diverse cropping systems [16-18]. The findings of this study further support the concept that biocontrol efficacy is highly strain-dependent, underscoring the importance of selecting indigenous strains well adapted to local environmental conditions [60]. The multifunctional traits exhibited by strain TSUxPT3.5, including antagonistic activity, enzyme production, VOC emission, and plant growth promotion, underscore its strong potential for use in sustainable lettuce production. Future studies should focus on the precise identification and quantification of bioactive metabolites, validation under field conditions, and the development of suitable formulations to enhance shelf life and field efficacy. Such efforts will facilitate the integration of *T. asperelloides* TSUxPT3.5 into practical biological control programs and sustainable crop management strategies.

5. Conclusions

This study demonstrated that the indigenous fungus *Trichoderma asperelloides* strain TSUxPT3.5 possesses strong biocontrol potential against multiple economically important plant pathogenic fungi, as well as the ability to promote plant growth in mini cos lettuce (*Lactuca sativa*). Strain TSUxPT3.5 exhibited broad-spectrum antagonistic activity mediated by a combination of mechanisms, including competition for nutrients and space, production of fungal cell wall-degrading enzymes, and emission of antifungal volatile organic compounds. In addition to its antagonistic properties, *T. asperelloides* TSUxPT3.5 produced indole compounds and significantly enhanced lettuce growth, resulting in increased fresh weight and improved plant vigor compared with the untreated control. These findings highlight the potential of *T. asperelloides* TSUxPT3.5 as an eco-friendly biological control agent and plant growth promoter for sustainable lettuce production. Further studies focusing on metabolite characterization, formulation development, and field validation will be essential to support its practical application in integrated disease management programs and to maximize its contribution to sustainable agriculture.

6. Acknowledgments

The authors would like to express their sincere gratitude to the Faculty of Science and Digital Innovation and the Faculty of Agriculture, Thaksin University, for providing laboratory facilities and research support, and to Prince of Songkla University for partial support. The authors also gratefully acknowledge the

Office of the Permanent Secretary, Ministry of Higher Education, Science, Research and Innovation for financial support during the fiscal year 2020.

Author Contributions: Conceptualization, W.C. and P.N.; methodology, W.C., P.N., N.S., J.K. and A.S.; validation, W.C., P.N., P.W., N.S., J.K. and A.S.; formal analysis, W.C., P.N., P.W., N.S., J.K. and A.S.; investigation, W.C., P.N., P.W., P.P., N.S., J.K. and A.S.; resources, W.C., P.N., P.W., P.P., N.S., J.K. and A.S.; data curation, W.C., P.N., P.W., N.S., J.K. and A.S.; data curation, W.C., P.N., P.W., N.S., J.K. and A.S.; writing—original draft preparation, W.C., P.N., P.W., N.S., J.K., K.J. and A.S.; visualization, W.C., P.N., P.W., N.S., J.K. and A.S.; supervision, W.C. and P.N.; project administration, W.C. and P.N.; funding acquisition, W.C., P.N., M.L., N.I., P.P. and C.N. All authors have read and agreed to the published version of the manuscript.

Funding: This research was funded by the Office of the Permanent Secretary, Ministry of Higher Education, Science, Research and Innovation (fiscal year 2020), and partially funded by Thaksin University and Prince of Songkla University.

Conflicts of Interest: The authors declare no conflict of interest.

References

[1] Savary, S.; Willocquet, L.; Pethybridge, S.J.; Esker, P.; McRoberts, N.; Nelson, A. The global burden of pathogens and pests on major food crops. *Nat. Ecol. Evol.* **2019**, *3*(3), 430–439. https://doi.org/10.1038/s41559-018-0793-y

[2] Garrett, K.A.; Dendy, S.P.; Frank, E.E.; Rouse, M.N.; Travers, S.E. Climate change effects on plant disease: Genomes to ecosystems. *Annu. Rev. Phytopathol.* **2006**, *44*, 489–509. https://doi.org/10.1146/annurev.phyto.44.070505.143420

[3] Chakraborty, S.; Newton, A.C. Climate change, plant diseases and food security: An overview. *Plant Pathol.* **2011**, *60*(1), 2–14. https://doi.org/10.1111/j.1365-3059.2010.02411.x

[4] Elad, Y.; Pertot, I. Climate change impacts on plant pathogens and plant diseases. *J. Crop. Improv.* **2014**, *28*(1), 99–139. https://doi.org/10.1080/15427528.2014.865412

[5] Thithuan, N.; Bunjonsiri, P.; Sunpapao, A. Morphology and behavior of gametes and zoospores from the plant-parasitic green algae, *Cephaleuros* (Chlorophyta, Ulvophyceae) 1. *Pac. Sci.* **2019**, *73*(3), 403–410. https://doi.org/10.2984/73.3.7

[6] Wonglom, P.; Thithuan, N.; Sunpapao, A. Occurrence and seasonal development of plant parasitic algae *Cephaleuros* (Chlorophyta, Ulvophyceae) in southern Thailand. *Chiang Mai J. Sci.* **2026a**; *53*(1), e2026013 https://doi.org/10.12982/CMJS.2026.013

[7] Pornsuriya, C.; Ito, S.I.; Sunpapao, A. First report of leaf spot on lettuce caused by *Curvularia aeria*. *J. Gen. Plant Pathol.* **2018**, *84*(4), 296–299. https://doi.org/10.1007/s10327-018-0782-7

[8] Wonglom, P.; Ito, S.; Sunpapao, A. First report of *Curvularia lunata* causing leaf spot on *Barsica rapa* subsp. *pekinensis* in Thailand. *New Dis. Rep.* **2018**, *38*, 15. https://doi.org/10.5197/j.2044-0588.2018.038.015

[9] Liu, H.; Wang, H.; Zhong, J.; Lu, X.; Pan, X.T.; Zhu, H.J.; Zhou, Q. First report of *Stemphylium lycopersici* and *Stemphylium vesicarium* causing leaf spot on lettuce (*Lactuca sativa*) in China. *Plant Dis.* **2019**, *103*(11), 2957. https://doi.org/10.1094/PDIS-05-19-1052-PDN

[10] Thaochan, N.; Pornsuriya, C.; Chairin, T.; Sunpapao, A. Roles of systemic fungicide in antifungal activity and induced defense responses in rubber tree (*Hevea brasiliensis*) against leaf fall disease caused by *Neopestalotiopsis cubana*. *Physiol. Mol. Plant Pathol.* **2020**, *111*, 101511. https://doi.org/10.1016/j.pmpp.2020.101511

[11] Samarghandi, M.R.; Mohammadi, M.; Karami, A.; Tabandeh, L.; Dargahi, A.; Amirian, F. Residue analysis of pesticides, herbicides, and fungicides in various water sources using gas chromatography-mass detection. *Pol. J. Environ. Stud*, **2017**, *26*(5), 2189–2195. https://doi.org/10.15244/pjoes/70387

[12] Santísima-Trinidad, A.B.L.; del Mar Montiel-Rozas, M.; Diéz-Rojo, M.Á.; Pascual, J.A.; Ros, M. Impact of foliar fungicides on target and non-target soil microbial communities in cucumber crops. *Ecotoxicol. Environ. Saf.* **2018**, *166*, 78–85. https://doi.org/10.1016/j.ecoenv.2018.09.074

[13] Fungicide Resistance Action Committee (FRAC). FRAC Website. Available online: https://www.frac.info/#open-tour (accessed on 2 January 2026).

[14] Omar, I.; O'neill, T.M.; Rossall, S. Biological control of Fusarium crown and root rot of tomato with antagonistic bacteria and integrated control when combined with the fungicide carbendazim. *Plant Pathol.* **2006**, *55*(1), 92–99. https://doi.org/10.1111/j.1365-3059.2005.01315.x

[15] Baiyee, B.; Ito, S.; Sunapapo, A. *Trichoderma asperellum* T1 mediated antifungal activity and induced defense response against leaf spot fungi in lettuce (*Lactuca sativa* L.). *Physiol. Mol. Plant Pathol.* **2019a**, *106*, 96–101. https://doi.org/10.1016/j.pmpp.2018.12.009

[16] Phoka, N.; Suwannarach, N.; Lumyong, S.; Ito, S.I.; Matsui, K.; Arikit, S.; Sunpapao, A. Role of volatiles from the endophytic fungus *Trichoderma asperelloides* PSU-P1 in biocontrol potential and in promoting the plant growth of *Arabidopsis thaliana*. *J. Fungi* **2020**, *6*, 341. https://doi.org/10.3390/jof6040341

[17] Ruangwong, O.U.; Wonglom, P.; Phoka, N.; Suwannarach, N.; Lumyong, S.; Ito, S.I.; Sunpapao, A. Biological control activity of *Trichoderma asperelloides* PSU-P1 against gummy stem blight in muskmelon (*Cucumis melo*). *Physiol. Mol. Plant Pathol.* **2021a**, *115*, 101663. https://doi.org/10.1016/j.pmpp.2021.101663

[18] Ruangwong, O.U.; Wonglom, P.; Suwannarach, N.; Kumla, J.; Thaochan, N.; Chomnunti, P.; Pitija, K.; Sunpapao, A. Volatile organic compound from *Trichoderma asperelloides* TSU1: Impact on plant pathogenic fungi. *J. Fungi* **2021b**, 7, 187. https://doi.org/10.3390/jof7030187

[19] Singh, B.N.; Singh, A.; Singh, B.R.; Singh, H.B. *Trichoderma harzianum* elicits induced resistance in sunflower challenged by *Rhizoctonia solani*. *J. Appl. Microbiol.* **2014**, *116*(3), 654–666. https://doi.org/10.1111/jam.12387

[20] Herrera-Jiménez, E.; Alarcón, A.; Larsen, J.; Ferrera-Cerrato, R.; Cruz-Izquierdo, S.; Ferrera-Rodríguez, M.R. Comparative effects of two indole-producing *Trichoderma* strains and two exogenous phytohormones on the growth of *Zea mays* L., with or without tryptophan. *J. Soil Sci. Plant Nutr.* **2018**, *18*(1), 188–201. http://dx.doi.org/10.4067/S0718-95162018005000704

[21] Nancha, N.; Hendarto, Z.; Bowchauy, S.; Wonglom, P. Efficacy of various *Trichoderma* spp. in controlling anthracnose disease in white Chaiburi pepper (*Capsicum frutescens*). *AgriSci. Soc. J.* **2025,** 1(*1*), 1–7. https://li02.tci-thaijo.org/index.php/NRJ/article/view/1139

[22] Hermosa, R.; Viterbo, A.; Chet, I.; Monte, E. Plant-beneficial effects of *Trichoderma* and of its genes. *Microbiology* **2012**, *158*(1), 17–25. https://doi.org/10.1099/mic.0.052274-0

[23] FAO. FAOSTAT: Crops and Livestock Products. Food and Agriculture Organization of the United Nations. Available online: https://www.fao.org/faostat/. 2023.

[24] Baiyee, B.; Pornsuriya, C.; Ito, S.; Sunapapo, A. *Trichoderma spirale* T76-1 displays biocontrol activity on lettuce (*Lactuca sativa* L.) caused by *Corynespora cassiicola* or *Curvularia aeria*. *Biol. Control* **2019b**, *129*, 195–200. https://doi.org/10.1016/j.biocontrol.2018.10.018

[25] Chairin, T.; Pornsuriya, C.; Thaochan, N.; Sunpapao, A. Corynespora cassiicola causes leaf spot disease on lettuce (Lactuca sativa) cultivated in hydroponic systems in Thailand. *Australas. Plant Dis. Notes* **2017**, *12*(1), 16. https://doi.org/10.1007/s13314-017-0241-x

[26] White, T.J.; Burns, T.; Lee, S.; Taylor, J.W. Amplification and direct sequencing of fungal ribosomal RNA genes for phylogenetics. In M.A. Innis, D.H. Gelfand, J.J. Sninsky & T.J. White (Eds.) *PCR protocols: a guide to methods and applications* (pp. 315– 322). **1990.** https://doi.org/10.1016/B978-0-12-372180-8.50042-1

[27] O'Donnell, K.; Kistler, H.C.; Cigelnik, E.; Ploetz, R.C. Multiple evolutionary origins of the fungus causing Panama disease of banana: Concordant evidence from nuclear and mitochondrial gene genealogies. *Proc. Natl. Acad. Sci. U.S.A.* **1998**, *95*, 2044–2049. https://doi.org/10.1073/pnas.95.5.2044

[28] Carbone, I.; Kohn, L.M. A method for designing primer sets for speciation studies in filamentous ascomycetes. *Mycologia* **1999**, *91*(3), 553–556. https://doi.org/10.1080/00275514.1999.12061051

[29] Samuels, G.J.; Dodd, S.L.; Gams, W.; Castlebury, L.A.; Petrini, O. *Trichoderma* species associated with the green mold epidemic of commercially grown *Agaricus bisporus*. *Mycologia* **2002**, *94*(1), 146–170. https://doi.org/10.1080/15572536.2003.11833257

[30] Liu, Y.J.; Whelen, S.; Hall, B.D. Phylogenetic relationships among ascomycetes: evidence from an RNA polymerse II subunit. *Mol. Biol. Evol.* **1999**, *16*(12), 1799–1808. https://doi.org/10.1093/oxfordjournals.molbev.a026092

[31] Nei, M.; Kumar, S. *Molecular Evolution and Phylogenetics*; Oxford University Press: New York, USA, 2000.

[32] Kumar, S.; Stecher G.; Suleski, M.; Sanderford, M.; Sharma, S.; Tamura, K. Molecular Evolutionary Genetics Analysis Version 12 for adaptive and green computing. *Mol. Biol. Evol.* **2024**, *41*, 1–9. https://doi.org/10.1093/molbev/msae263

[33] Felsenstein, J. Confidence limits on phylogenies: An approach using the bootstrap. *Evolution* **1985**, *39*, 783–791. https://doi.org/10.2307/2408678

[34] Edgar, R.C. MUSCLE: multiple sequence alignment with high accuracy and high throughput. *Nucleic Acids Res.* **2004**, *32*, 1792–1797. https://doi.org/10.1093/nar/gkh340

[35] Nuangmek, W.; Aiduang, W.; Kumla, J.; Lumyong, S.; Suwannarach, N. Evaluation of a newly identified endophytic fungus, *Trichoderma phayaoense* for plant growth promotion and biological control of gummy stem blight and wilt of muskmelon. *Front. Microbiol.* **2021**, *12*, e634772. https://doi.org/10.3389/fmicb.2021.634772

[36] Kamala, T.; Indira, S. Evaluation of indigenous *Trichoderma* isolates from Manipur as biocontrol agent against *Pythium aphanidermatum* on common beans. *3 Biotech* **2011**, *1*, 217–225. https://doi.org/10.1007/s13205-011-0027-3

[37] Suwannarach, N.; Kaewyana, C.; Yodmeeklin, A.; Kumla, J.; Matsui, K.; Lumyong, S. Evaluation of *Muscodor cinnamomi* as an egg biofumigant for the reduction of microorganisms on eggshell surfaces and its effect on egg quality. *Int. J. Food Microbiol.* **2017**, *244*, 52–61. https://doi.org/10.1016/j.ijfoodmicro.2016.12.021

[38] Gordon, S.A.; Weber, R.P. Colorimetric estimation of indoleacetic acid. *Plant Physiol.* **1951**, *26*, 192–195. https://doi.org/10.1104/pp.26.1.192

[39] Cai, F.; Druzhinina, I.S. In honor of John Bissett: authoritative guidelines on molecular identification of *Trichoderma*. *Fungal Divers.* **2021**, *107*, 1-69. https://doi.org/10.1007/s13225-020-00464-4

[40] Wonglom, P.; Suwannarach, N.; Kumla, J.; Pitija, K.; Sunpapao, A. Biocontrol mechanisms and field efficacy of *Trichoderma asperelloides* Z2-02 against anthracnose of torch ginger caused by *Colletotrichum atlanticum*. *Physiol. Molec. Plant Pathol.* **2026b,** *142*, 103133. https://doi.org/10.1016/j.pmpp.2026.103133

[41] Vinale, F.; Sivasithamparam, K.; Ghisalberti, E.L.; Marra, R.; Woo, S.L.; Lorito, M. *Trichoderma*–plant–pathogen interactions. *Soil Biol. Biochem.* **2008**, *40*(1), 1–10. https://doi.org/10.1016/j.soilbio.2007.07.002

[42] Wonglom, P.; Ito, S.I.; Sunpapao, A. Volatile organic compounds emitted from endophytic fungus *Trichoderma asperellum* T1 mediate antifungal activity, defense response and promote plant growth in lettuce (*Lactuca sativa*). *Fungal Ecol.* **2020** *43*, 100867. https://doi.org/10.1016/j.funeco.2019.100867

[43] Zhang, Y.; Li, Z.; Wei, S.; Xu, C.; Chen, M.; Sang, J.; Han, L.; Yan, H.; Li., Z.; Cui, Z.; Ye, X. Antifungal activity and mechanisms of 2-ethylhexanol, a volatile organic compound produced by *Stenotrophomonas* sp. NAU1697, against Fusarium oxysporum f. sp. cucumerinum. *J. Agric. Food Chem.* **2024**, *72*(27), 15213-15227. https://doi.org/10.1021/acs.jafc.3c09851

[44] Marcomini, E.K.; Rezende, P.S.T.; Gomes, J.; Leite, C.R.; de Oliveira, K.M.P.; Pomini, A.M.; Svidzinski, T.I.E.; Negri, M. 2-ethyl-1-hexanol: a promising molecule against priority fungal pathogens. *J. Appl. Microbiol.* **2025**, *136*(7), lxaf165. https://doi.org/10.1093/jambio/lxaf165

[45] Wang, Z.; Duan, W.; Duan, B.; He, H.; Nan, J.; Yan, X.; Lei, S.; Bin, Y.; Chen, C.; Yue, X.; Xu, X.; Yuan, S.; Zuo, J.; Liu, J.; Xu, X.; Wang, Q. 2-Ethylhexanol inhibit Botrytis cinerea by interfering in sugar and amino acid metabolism. *npj Sci. Food* **2026** https://doi.org/10.1038/s41538-026-00753-3

[46] Jeleń, H.; Błaszczyk, L.; Chełkowski, J.; Rogowicz, K.; Strakowska, J. Formation of 6-n-pentyl-2H-pyran-2-one (6-PAP) and other volatiles by different *Trichoderma* species. *Mycol. Progress* **2014**, *13*(3), 589-600. https://doi.org/10.1007/s11557-013-0942-2

[47] Jin, X.; Guo, L.; Jin, B.; Zhu, S.; Mei, X.; Wu, J.; Liu, T.; He, X. Inhibitory mechanism of 6-Pentyl-2H-pyran-2-one secreted by *Trichoderma atroviride* T2 against *Cylindrocarpon destructans*. *Pestic. Biochem. Physiol.* **2020**, *170*, 104683. https://doi.org/10.1016/j.pestbp.2020.104683

[48] Xing, M.; Zhao, J.; Zhang, J.; Wu, Y.; Khan, R.A.A.; Li, X.; Wang, R.; Li, T.; Liu, T. 6-Pentyl-2 H-pyran-2-one from *Trichoderma erinaceum* is fungicidal against litchi downy blight pathogen Peronophythora litchii and preservation of litchi. *J. Agric. Food Chem.* **2023**, *71*(49), 19488-19500. https://doi.org/10.1021/acs.jafc.3c03872

[49] Wu, Y.; Li, X.; Dong, L.; Liu, T.; Tang, Z.; Lin, R.; Norvienyeku, J.; Xing, M. A new insight into 6-pentyl-2h-pyran-2-one against peronophythora litchii via TOR pathway. *J. Fungi* **2023**, *9*(8), 863. https://doi.org/10.3390/jof9080863

[50] Dharni, S.; Sanchita; Maurya, A.; Samad, A.; Srivastava, S.K.; Sharma, A.; Patra, D.D. Purification, characterization, and in vitro activity of 2, 4-di-tert-butylphenol from *Pseudomonas monteilii* PsF84: conformational and molecular docking studies. *J. Agric. Food. Chem.* **2014**, *62*(26), 6138-6146. https://doi.org/10.1021/jf5001138

[51] Varsha, K.K.; Devendra, L.; Shilpa, G.; Priya, S.; Pandey, A.; Nampoothiri, K.M. 2, 4-Di-tert-butyl phenol as the antifungal, antioxidant bioactive purified from a newly isolated *Lactococcus* sp. *Int. J. Food Microbiol.* **2015**, *211*, 44-50. https://doi.org/10.1016/j.ijfoodmicro.2015.06.025

[52] Fan, K.; Yu, Y.; Hu, Z.; Qian, S.A.; Zhao, Z.; Meng, J.; Zheng, S.; Huang, Q.; Zhang, Z.; Nie, D.; Han, Z. Antifungal activity and action mechanisms of 2, 4-Di-tert-butylphenol against *Ustilaginoidea virens*. *J. Agric. Food Chem.* 2023, 71, 46, 17723–17732. https://doi.org/10.1021/acs.jafc.3c05157

[53] Di Francesco, A.; Ugolini, L.; Lazzeri, L.; Mari, M. Production of volatile organic compounds by *Aureobasidium pullulans* as a potential mechanism of action against postharvest fruit pathogens. *Biol. Control* **2015**, *81*, 8-14. https://doi.org/10.1016/j.biocontrol.2014.10.004

[54] Rahman, A.; Sitepu, I.R.; Tang, S.Y.; Hashidoko, Y. Salkowski's reagent test as a primary screening index for functionalities of rhizobacteria isolated from wild dipterocarp saplings growing naturally on medium-strongly acidic tropical peat soil. *Biosci., Biotechnol., Biochem.* **2010**, *74*(11), 2202-2208. https://doi.org/10.1271/bbb.100360

[55] Glickmann, E.; Dessaux, Y. A critical examination of the specificity of the Salkowski reagent for indolic compounds produced by phytopathogenic bacteria. *Appl. Environ. Microbiol.* **1995**, *61*(2), 793-796. https://doi.org/10.1128/aem.61.2.793-796.1995

[56] Guardado-Fierros, B.G.; Tuesta-Popolizio, D.A.; Lorenzo-Santiago, M.A.; Rodriguez-Campos, J.; Contreras-Ramos, S.M. Comparative study between Salkowski reagent and chromatographic method for auxins quantification from bacterial production. *Front. Plant Sci.* **2024**, *15*, 1378079. https://doi.org/10.3389/fpls.2024.1378079

[57] Contreras-Cornejo, H.A.; Schmoll, M.; Esquivel-Ayala, B.A.; González-Esquivel, C.E.; Rocha-Ramírez, V.; Larsen, J. Mechanisms for plant growth promotion activated by *Trichoderma* in natural and managed terrestrial ecosystems. *Microbiol. Res.* **2024**, *281*, 127621. https://doi.org/10.1016/j.micres.2024.127621

[58] Contreras-Cornejo, H.A.; Macías-Rodríguez, L.; Cortés-Penagos, C.; López-Bucio, J. *Trichoderma virens*, a plant beneficial fungus, enhances biomass production and promotes lateral root growth through an auxin-dependent mechanism in *Arabidopsis*. *Plant Physiol.* **2009**, *149*, 1579–1592. https://doi.org/10.1104/pp.108.130369

[59] Woo, S.L.; Pepe, O. Microbial consortia: promising probiotics as plant biostimulants for sustainable agriculture. *Front. Plant Sci.* **2018**, *9*, 1801. https://doi.org/10.3389/fpls.2018.01801

[60] Saba, H.; Vibhash, D.; Manisha, M.; Prashant, K.S.; Farhan, H.; Tauseef, A. *Trichoderma*–a promising plant growth stimulator and biocontrol agent. *Mycosphere* **2012**, *3*(4), 524–531. https://doi.org/10.5943/mycosphere/3/4/14

ASEAN
Journal of Scientific and Technological Reports
Online ISSN:2773-8752

Research article

Phytochemical Characterization, Curcuminoid Quantification by HPLC, and Biological Activities of Ethanolic and Aqueous Extracts of *Zingiber cassumunar* and *Curcuma longa* Prepared by Ultrasonic-Assisted Extraction

Aurawan Boonyataeng[1*], Ratchaneekorn Reudhabibadh[1], Lukman Sueree[1], Khanittha Yottrai[1], Nattakan Nin-On[2], and Thanawat Pitakpornpreecha[3]

[1] Faculty of Science and Technology, Hatyai University, Songkhla, 90110, Thailand
[2] Faculty of Health and Sports Science, Thaksin University, Phatthalung, 93210, Thailand
[3] Faculty of Science, Prince of Songkla University, Songkhla, 90110, Thailand
* Correspondence: aurawan.boo@hu.ac.th

Citation:
Boonyataeng, A.; Reudhabibadh, R.; Suree, L; Yottrai, K.; Nin-On, N.; Pitakpornpreecha, T. Phytochemical characterization, curcuminoid quantification by HPLC, and biological activities of ethanolic and aqueous extracts of *Zingiber cassumunar* and *Curcuma longa* prepared by ultrasonic-assisted extraction. *ASEAN J. Sci. Tech. Report.* **2026**, *29*(7), e264707. https://doi.org/10.55164/ajstr.v29i7.262844

Article history:
Received: April 3, 2026
Revised: April 11, 2026
Accepted: April 30, 2026
Available online: June 14, 2026

Publisher's Note:
This article is published and distributed under the terms of the Thaksin University.

Abstract: *Zingiber cassumunar* and *Curcuma longa* are widely used medicinal plants in Southeast Asia, with therapeutic properties attributed to curcuminoids, phenolics, and flavonoids. This study evaluated the effects of solvent type and ultrasonic pretreatment on extraction efficiency and phytochemical composition. Herbal powders were extracted using water and ethanol under ultrasonic conditions. Extraction yields were determined, and phytochemical contents were analyzed using HPLC for curcuminoids and UV–VIS spectrophotometry for total phenolic content (TPC) and total flavonoid content (TFC). The results demonstrated that extraction efficiency was significantly influenced by solvent selection. Ethanolic extraction produced higher yields and significantly greater concentrations of curcuminoids, phenolics, and flavonoids compared to aqueous extraction. Curcuminoids were predominantly detected in ethanolic extracts, with *Curcuma longa* showing the highest content (13.951% w/w). Similarly, TPC and TFC were markedly higher in ethanolic extracts (412,105.51 mg GAE/kg and 659,001.92 mg QE/kg, respectively), whereas aqueous extracts showed limited recovery due to poor solubility of hydrophobic and semi-polar compounds in water. The enhanced recovery observed with ethanol was attributed to improved solvent penetration and solubilization capacity, further enhanced by ultrasonic cavitation, which promoted cell wall disruption and mass transfer. Additionally, both aqueous and ethanolic extracts of *Z. cassumunar* and *C. longa* demonstrated significant anti-inflammatory activity (inhibition of nitric oxide production in LPS-stimulated macrophages) and antioxidant activity (reduction of intracellular ROS), regardless of solvent type. Overall, the combination of ethanol and ultrasonic pretreatment was identified as a more efficient, less solvent-intensive method for maximizing phytochemical extraction than conventional maceration, supporting its application in functional foods, nutraceuticals, and herbal pharmaceuticals.

Keywords: *Zingiber cassumunar*, *Curcuma longa*, ultrasonic extraction, phytochemical analysis, HPLC

1. Introduction

The *Zingiberaceae* family (*Zingiber cassumunar* and *Curcuma longa*), which includes several economically and pharmacologically significant species,

has been used in traditional medicine, nutraceutical products, and culinary practices in many parts of the world [1]. The quality and pharmacological standardization of these plants, including cassumunar ginger, have been progressively established [2, 3, 4]. It has been determined that the rhizomes of plants in this family are abundant in a variety of bioactive compounds with substantial medicinal potential [5]. Because of its high concentration of curcuminoids, specifically curcumin, demethoxycurcumin, and bisdemethoxycurcumin, which give it its distinctive yellow pigmentation and a variety of biological activities, *C. longa* has drawn a lot of scientific attention among these species [6, 7]. Numerous studies have demonstrated the potent antioxidant, anti-inflammatory, antimicrobial, and anticancer properties of these extracts [8, 9]. Furthermore, phenolic compounds, flavonoids, and terpenoids have been identified in other members of the Zingiberaceae family, further enhancing their therapeutic versatility and health-promoting properties [10, 11]. The development of functional foods, nutraceuticals, and contemporary pharmaceutical products has therefore been seen to depend on the isolation, characterization, and quantification of these phytochemicals.

Because extraction conditions directly affect the yield, purity, and stability of target bioactive compounds, the extraction method used significantly influences the effectiveness and quality of herbal formulations [12]. Long extraction times, high solvent consumption, and possible degradation of thermolabile compounds have been linked to traditional extraction methods such as maceration and percolation [12]. As a result, one of the main goals of current phytochemical research is to develop effective, rapid, and environmentally friendly extraction technologies. In this context, a variety of polar and semi-polar compounds, such as glycosides and curcuminoids, have been proposed for extraction from complex plant matrices using a combination of aqueous and methanolic solvent systems [1]. Ultrasonic-assisted extraction (UAE) has been recognized as a green, innovative technique for phytochemical recovery. This method relies on the generation of acoustic cavitation by applying high-frequency sound waves, leading to the formation and collapse of microbubbles in the solvent medium [13]. The resulting localized high pressure and micro-jets facilitate the disruption of plant cell walls, enhance solvent penetration, and promote the release of intracellular metabolites. As a result, the UAE has been shown to improve extraction efficiency, reduce solvent and energy consumption, and significantly shorten extraction time when compared with conventional extraction methods [13, 14, 15, 16]. Furthermore, because the UAE is a non-thermal, energy-efficient process, the structural integrity and biological activity of thermolabile phytochemicals can be better preserved [17].

In this study, aqueous and ethanolic extracts of Zingiber cassumunar and Curcuma longa prepared using ultrasonic pretreatment were analyzed for phytochemicals. The concentrations and profiles of bioactive constituents were evaluated. An optimized, efficient, and scalable extraction protocol was established. The result of this study is expected to provide an extraction method, the phytochemical composition of these medicinal plants, and to support their potential industrial application in the development of high-value functional and therapeutic products. However, despite the growing literature on individual species, a direct comparison of UAE efficiency using water versus ethanol for both Z. cassumunar and C. longa simultaneously, combined with integrated curcuminoid HPLC quantification and cellular biological activity assessment, has not been comprehensively reported. This study addresses that gap by evaluating the combined effect of solvent polarity and ultrasonic pretreatment on phytochemical yield, curcuminoid content, TPC, TFC, and biological activities of both species in a single systematic investigation.

2. Materials and Methods

2.1 Herbal Extraction Process

The dried herbs of *Z. cassumunar* and *C. longa* were used in this study and purchased from Fa Sen Herbal Shop (Hatyai, Songkla, Thailand). They were ground into a fine powder and stored in a desiccator until further extraction. To ensure environmental safety, water and 95% (v/v) ethanol were selected as solvents due to their differing charge properties, and the extraction employed a combination of solvent extraction and ultrasonic pretreatment to maximize efficiency. Each herbal sample was extracted at a solid-to-solvent ratio of 1:10, with 10 g of powdered plant material weighed and mixed with 100 mL of water or ethanol. The mixture was agitated using a magnetic stirrer and subsequently incubated for two hours (as a pre-soaking maceration step to promote initial diffusion of soluble compounds before sonication) to facilitate the complete diffusion of bioactive

compounds into the solvent [12]. The mixture was then subjected to ultrasonic pretreatment using an ultrasonic bath operating at 40 kHz and a nominal power output of 150 W (continuous duty cycle) for 60 minutes at a temperature of 40 °C, with the application of ultrasound intended to promote acoustic cavitation and thereby improve mass transfer efficiency within the solvent system [13]. Following pretreatment, the crude extract was separated from the solid residue by filtration, after which the solvent was removed using a rotary evaporator under reduced pressure (approximately 40–50 mbar) at a temperature below 40 °C to prevent thermal degradation of sensitive compounds. The dried extract was used to calculate the extraction yield (%) using equation (1). The extract was stored in a freezer until further use. Finally, the optimized extraction conditions were scaled up by doubling the amounts of both the herbal materials and the solvents to obtain sufficient extract for subsequent characterization.

$$(\text{wt.}\%) = \frac{\text{m\_extract}}{\text{m\_raw material}} \times 100 \quad (1)$$

A limitation of this study lies in the potential influence of seasonal variation on the phytochemical composition of the plant materials. The raw materials used were collected from a specific location and at a particular time, which may affect the concentration and profile of bioactive compounds. Variations in environmental factors, such as climate, soil conditions, and the harvesting season, are known to influence the biosynthesis and accumulation of phytochemicals. Therefore, the extraction yields and phytochemical contents reported in this study may not fully represent samples from different regions or harvest periods.

2.2 Characterization of Herbal Extracts

The extracts were evaluated for their sensory and physical characteristics, including appearance, color, odor, clarity, consistency, and phase separation. A series of curcumin standard solutions at concentrations of 0.1, 0.5, 2, 4, 6, 8, 10, and 12 μg/mL was prepared and analyzed by HPLC, with linearity evaluated using the coefficient of determination (R^2) and the relationship between peak area and curcumin concentration established from the calibration curve. Chromatographic analysis was performed using a Shimadzu Nexera LC-40Dx3 Series HPLC system equipped with an autosampler and a photodiode-array (PDA) detector. Separation was achieved on a Zorbax C18 column (150 mm × 4.60 mm, 5 μm particle size), and the mobile phase consisted of 0.1% (v/v) formic acid in water and acetonitrile at a ratio of 50:50 (v/v). Isocratic elution was maintained at 1.0 mL/min, the column temperature was set to 40 °C, and an injection volume of 10 μL was used for all analyses. Detection of curcumin was carried out at a wavelength of 420 nm. The peak was identified by comparing retention times with those of the curcumin standard (Figure 2), and the contents in the extracts were quantified based on peak area.

2.3 Total Phenolic Content (TPC)

The total phenolic content (TPC) was determined using the Folin–Ciocalteu colorimetric method, as previously described [25]. The phenolic content of the samples was quantified based on a gallic acid standard calibration curve (n = 3), and the results were expressed as milligrams of gallic acid equivalents per kilogram of dry extract (mg GAE/kg).

2.4 Total Flavonoid Content (TFC)

The identification and quantification of flavonoids were performed according to the method described by Lin *et al*. [11]. Detection was performed at 364 nm using a UV–visible detector. Quercetin and apigenin were employed as reference standards for the identification of flavonoid compounds in the samples. Briefly, 0.1 mL of each sample was mixed with 0.3 mL of 5% (w/v) $AlCl_3$ in methanol and 0.3 mL of 1 M potassium acetate, and the mixture was incubated at room temperature for 30 minutes. Absorbance was measured at 415 nm. Results were expressed as milligrams of quercetin equivalents per kilogram of dry extract (mg QE/kg, n = 3).

3. Results and Discussion

3.1 Extracts yield of *Zingiber cassumunar* and *Curcuma longa* from water and ethanol combined with ultrasonic pretreatment

The extraction yields of *Z. cassumunar* and *C. longa* were evaluated using water and ethanol as extraction solvents. There was no significant difference in the percentage yield when the extraction scale was doubled (data not shown). The extraction yields of *Z. cassumunar* using water and ethanol as solvents were 13.07% and 8.77%, respectively. In contrast, the extraction yields of *C. longa* using water and ethanol as solvents were 9.63% and 9.90%, respectively (Figure 1). The result demonstrated that comparative extraction of *Z. cassumunar* performance between the two solvents showed differences in efficiency, depending on solvent polarity and the chemical-specific properties of the target phytochemicals. When water was used as the extraction solvent with *C. longa*, a lower yield was obtained. This finding is consistent with the documented poor aqueous solubility of curcuminoids, which restricts their extraction efficiency in water-based systems [6]. In contrast, ethanolic extraction yielded substantially higher curcumin, ranging from approximately 8.0% to 12.0%. The improved recovery observed with ethanol has been attributed to its ability to dissolve curcuminoids effectively and facilitate deeper solvent penetration into the plant matrix, thereby enhancing mass transfer and extraction efficiency [8, 9]. These results align with previous reports indicating that alcoholic solvents are more suitable for curcumin extraction than aqueous solvents [8, 9]. A similar extraction trend was observed for *Z. cassumunar*. Aqueous extraction, including hydrodistillation or soaking methods, yielded a relatively higher extraction yield of 13.07% by total mass; however, this yield is expected to be largely composed of water-soluble components (polysaccharides, proteins, and other hydrophilic compounds) rather than the non-polar bioactive phenylbutanoids that confer medicinal properties. This limitation has been reported in earlier studies, where water-based extraction methods were found to be ineffective for selectively recovering non-volatile phenylbutanoids such as DMPBD [11]. In contrast, ethanol use significantly increased the total extractable yield to approximately 6–8%. This improvement was attributed to the efficient recovery of non-volatile bioactive compounds, particularly (E)-1-(3,4-dimethoxyphenyl) butadiene (DMPBD), which has limited water solubility but is readily extracted with organic solvents [11]. These findings further suggest that ethanol is more suitable than water for extracting a broader spectrum of bioactive constituents from *Z. cassumunar*. A significant variation in extraction efficiency was observed between aqueous and ethanolic solvents. Ethanol was shown to be a more effective solvent for plant materials than water. This outcome has been attributed to the physicochemical properties of the major bioactive constituents present in *Z. cassumunar* and *C. longa*, specifically curcuminoids and phenylbutanoids, which exhibit limited solubility in water but higher affinity for polar organic solvents [1, 6]. Previous studies have similarly reported that ethanol enhances the extraction of hydrophobic and semi-polar compounds by penetrating plant cell walls and dissolving a wider range of secondary metabolites [17]. Overall, the results indicate that ethanol is a more effective solvent than water for extracting bioactive compounds from both Z. cassumunar and C. longa, supporting its use in developing phytochemical-rich extracts for functional and therapeutic applications.

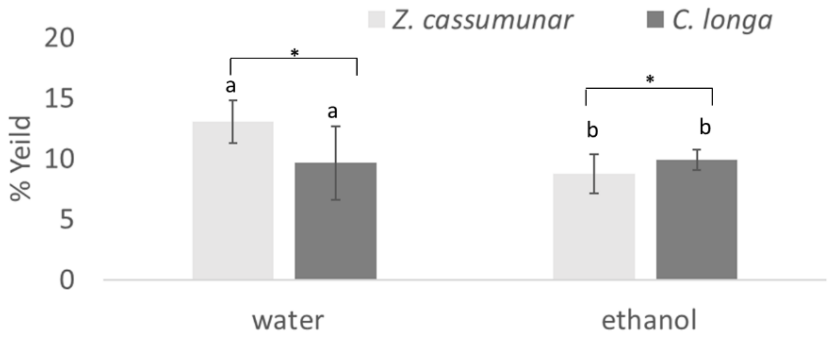


Figure 1. Extraction Yield *of Z. cassumunar* and *C. longa* using water and ethanol as extraction solvents combined with ultrasonic pretreatment. Statistical significance was determined using a one-way analysis of variance (ANOVA) followed by a post hoc test for mean comparison (n=3). Different superscript

letters indicate statistical differences in extraction efficiency between solvents ($p < 0.05$), while asterisks indicate statistical differences between the plant species ($p < 0.05$).

The stability of herbal compress extracts, both in individual and formulaic forms, was evaluated at 4 °C for 90 days. The physical appearance and color of the extracts remained unchanged throughout the study period (data not shown). These findings are consistent with previous reports suggesting that low-temperature storage effectively preserves the organoleptic properties and chemical integrity of bioactive compounds in *Zingiberaceous* plants [18]. Regarding solubility, the extracts of *Z. cassumunar* and *C. longa* obtained via aqueous extraction were found to be highly soluble in water. Conversely, the ethanolic extracts exhibited limited water solubility but were highly soluble in ethanol. This behavior is attributed to the presence of non-polar curcuminoids and essential oil components, which require organic solvents for optimal dissolution [19]. Furthermore, all extracts obtained exhibited a viscous, fine-textured consistency that adhered to the container walls. It was also observed that no phase separation occurred upon prolonged standing, indicating a high degree of physical homogeneity and structural stability within the extract matrix. The concentration of curcumin in the extracts was quantified by High-Performance Liquid Chromatography (HPLC), with results expressed as a percentage by weight (%w/w).

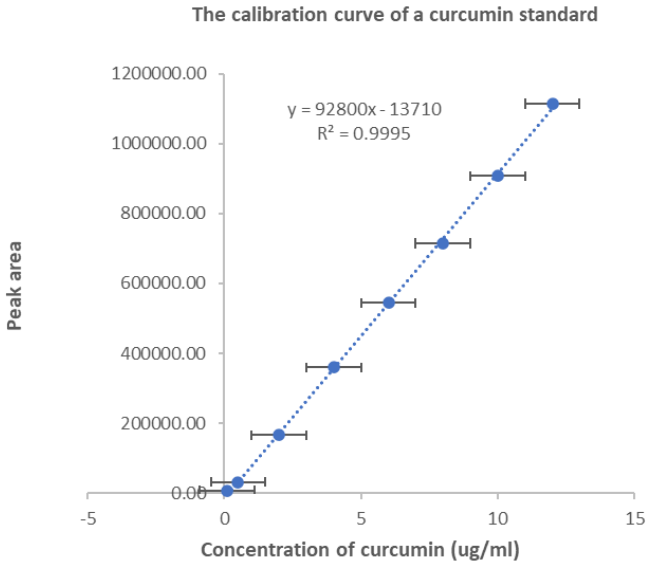


Figure 2. A calibration curve for curcumin at concentrations of 0.1, 0.5, 2, 4, 6, 8, 10, and 12 μg/mL was generated to provide a range of standard concentrations for quantification. (t-test analysis ± SD, n = 3)

A significant disparity in curcumin recovery was observed between the aqueous and ethanolic extraction methods. For the extracts of *Z. cassumunar* (PH_2O) and *C. longa* (CH_2O) prepared using water, the curcumin content was determined to be below the Limit of Detection (< LOD). These observations are consistent with the existing literature, which states that curcumin has extremely low solubility in aqueous media, severely limiting its recovery when water is used as the primary solvent [19].

Table 1. Curcumin Content in *Z. cassumunar* and *C.longa*

Sample	Curcumin (ug/ml±SD)	Curcumin (%w/w±SD)
Z. cassumunar - Water	ND	<LOD[A]
C. longa - Water	ND	<LOD[A]
Z. Cassumunar - Ethanol	0.87 ± 0.03	0.659 ± 0.016
C. longa - Ethanol	6.18 ± 0.37	13.951 ± 0.478

Note: ND= not detection, LOD=0.05μg/mL.

Conversely, the use of ethanol as a solvent facilitated a substantial increase in the extraction of these bioactive compounds. The highest curcuminoid concentration was recorded in the ethanolic *C. longa* extract at

13.951 ± 0.478 %w/w. The ethanolic *Z. cassumunar* extract exhibited a comparatively lower concentration of 0.659 ± 0.016 %w/w (Table 1). Correlated to the phytochemicals analysis of *Z. cassumunar*, which found a phenylbutenoid as a major compound, while the yield of curcumin was 0.2% by weight [20]. These results confirm that organic polar solvents, such as ethanol, are required to effectively penetrate the plant matrix and solubilize hydrophobic polyphenols, such as curcumin [18]. Consistent with previous research on the optimization of component extraction from Curcuma xanthorrhiza using Ultrasound-Assisted Extraction (UAE), a high curcumin concentration (39.73% w/w) was obtained [21]. The HPLC analysis also revealed that the ethanolic extract of *C. longa* contained three principal curcuminoids, namely bisdemethoxycurcumin, demethoxycurcumin, and curcumin, with curcumin detected as the dominant compound based on peak area and intensity. The peak area of the ethanolic extract showed a higher peak and greater intensity than those of the aqueous extract (Figures 2 and 3).

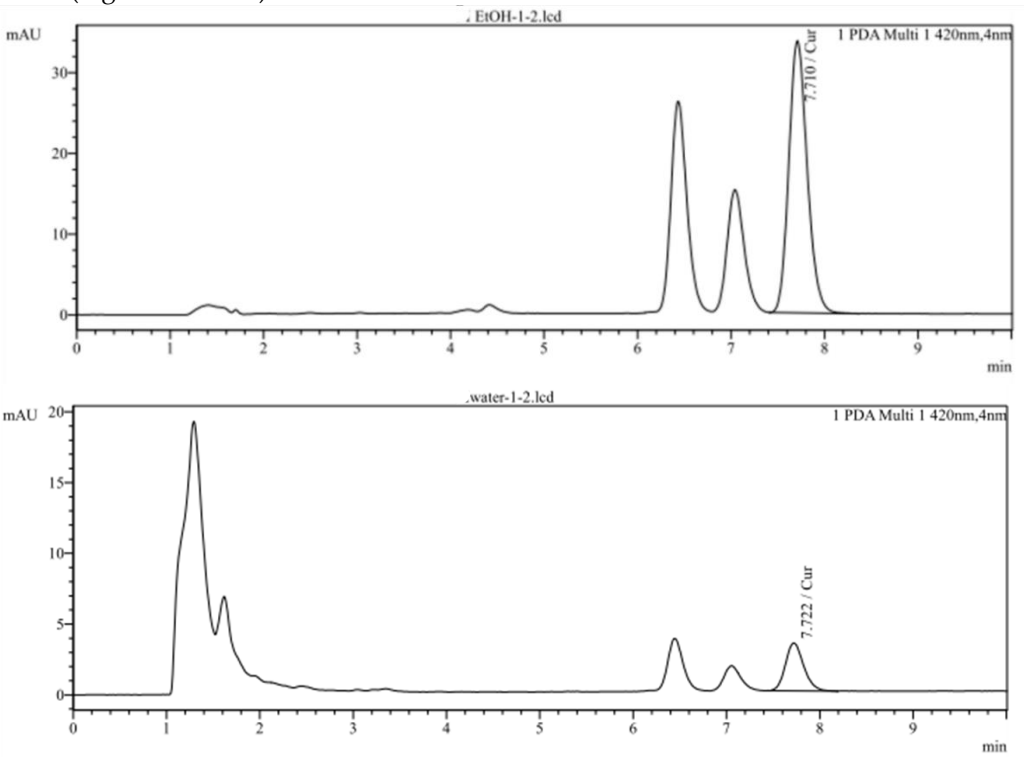


Figure 3. Representative HPLC chromatograms of *C. longa* and *Z. cassumunar* plant extracts showing resolved curcuminoid peaks (bisdemethoxycurcumin, demethoxycurcumin, and curcumin annotated with respective retention times): (top) extract obtained using ethanol as the solvent, and (bottom) extract obtained using water as the solvent.

3.2 Determination of Total Phenolic Content (TPC)

The total phenolic content (TPC) of the herbal extracts was determined using the Folin-Ciocalteu colorimetric method and measured with a UV–VIS spectrophotometer (JASCO V-770). The results were expressed as milligrams of gallic acid equivalents per kilogram of extract (mg GAE/kg ± SD). The quantitative outcomes are summarized in Table 2 and described below. A substantial difference in the recovery of phenolic compounds was observed between the two extraction solvents. For all samples, TPC values were significantly higher when ethanol was used as the extraction medium than when water was used. The highest phenolic concentration was detected in the ethanolic extract of *C. longa*, with a value of 412,105.51 ± 23,450.00 mg GAE/kg. This observation is consistent with previous findings reporting that polar organic solvents, particularly ethanol, exhibit superior efficiency in extracting phenolic compounds from plant matrices when compared with aqueous systems [18]. For *Z. cassumunar*, the phenolic content of the ethanolic extract was determined to be 104,457.14 ± 7,379.86 mg GAE/kg, which was approximately fourfold higher than that obtained from the aqueous extract (28,159.69 ± 2,215.06 mg GAE/kg). In the case of *C. longa*, the most pronounced difference between solvents was observed. The ethanolic extract exhibited a TPC value of 412,105.51 ± 23,450.00 mg GAE/kg, whereas the

aqueous extract yielded only 17,602.16 ± 584.06 mg GAE/kg. The elevated phenolic contents detected in the ethanolic extracts were attributed to the enhanced solubilization of hydrophobic and semi-polar compounds, including curcuminoids and phenylbutanoids, which are known to possess strong antioxidant activity [19]. These findings further confirm the suitability of ethanol as an effective solvent for maximizing the recovery of phenolic constituents from medicinal plant materials.

Table 2. Total Phenolic Content of Herbal Extracts Measured via UV-VIS Spectrophotometry (n=3).

Sample Source	Solvent	Total Phenolic Content (mgGAE/kg±SD)
Z. cassumunar	Water (H_2O)	28,159.69 ± 2,215.06
C. longa	Water (H_2O)	17,602.16 ± 584.06
Z. cassumunar	Ethanol	104,457.14 ± 7,379.86
C. longa	Ethanol	412,105.51 ± 23,450.00

The total flavonoid content (TFC) of the extracts was quantified using UV–VIS spectrophotometry with a JASCO V-770 system. The results were expressed as milligrams of quercetin equivalents per kilogram of extract (mg QE/kg ± SD) and are presented in Table 3.

Table 3. Total Flavonoid Content of Herbal Extracts Measured via UV-VIS Spectrophotometry (n=3).

Sample Source	Solvent	Total Flavonoid Content (mgQE/kg±SD)
Z. cassumunar	Water (H_2O)	8,863.20 ± 27.15
C. longa	Water (H_2O)	9,383.57 ± 22.41
Z. cassumunar	Ethanol	70,111.68 ± 2,831.50
C. longa	Ethanol	659,001.92 ± 7,206.92

A marked variation in flavonoid recovery was observed depending on the solvent employed for extraction. Across all samples, TFC values were significantly higher in ethanolic extracts than in aqueous extracts. The highest flavonoid concentration was detected in the ethanolic extract of *C. longa*, with a value of 659,001.92 ± 7,206.92 mg QE/kg. This outcome is consistent with previous reports showing that polar organic solvents, such as ethanol, enhance the solubility and extraction efficiency of polyphenolic compounds, including flavonoids, through favorable solvent–solute interactions [22]. For *Z. cassumunar*, the TFC of the ethanolic extract was determined to be 70,111.68 ± 2,831.50 mg QE/kg, approximately eightfold higher than that of the aqueous extract (8,863.20 ± 27.15 mg QE/kg). In the case of *C. longa*, the ethanolic extract exhibited a markedly higher flavonoid concentration (659,001.92 ± 7,206.92 mg QE/kg) than the aqueous extract, which contained only 9,383.57 ± 22.41 mg QE/kg. The superior recovery of flavonoids in ethanolic extracts was attributed to the enhanced ability of ethanol to penetrate plant cell walls and solubilize semi-polar and non-polar bioactive compounds. Additionally, ethanol facilitates disruption of hydrogen bonds between flavonoids and cell wall polysaccharides, thereby promoting their release into the extraction medium [23].

3.3 Comparative Analysis of Total Phenolic and Flavonoid Contents

A comparative evaluation of total phenolic content (TPC) and total flavonoid content (TFC) in *Z. cassumunar* and *C. longa* was conducted to assess the influence of solvent selection on the recovery of bioactive compounds. The results are summarized below and illustrated in the corresponding graphical representation. A pronounced disparity in phenolic and flavonoid concentrations was observed between aqueous and ethanolic extraction methods. For both plant species, significantly higher levels of bioactive compounds were obtained with ethanol than with water. In *C. longa*, the ethanolic extract exhibited a total phenolic content of 412,105.51 ± 23,450.00 mg GAE/kg and a total flavonoid content of 659,001.92 ± 7,206.92 mg QE/kg. In contrast, the aqueous extract yielded substantially lower concentrations: 17,602.16 ± 584.06 mg GAE/kg for TPC and 9,383.57 ± 22.41 mg QE/kg for TFC. A similar extraction pattern was observed for *Z. cassumunar*. The ethanolic extract produced higher concentrations of phenolics and flavonoids, with TPC and TFC values of 104,457.14 ± 7,379.86 mg GAE/kg and 70,111.68 ± 2,831.50 mg QE/kg, respectively. Conversely, the aqueous extract yielded markedly lower values of 28,159.69 ± 2,215.06 mg GAE/kg for TPC and 8,863.20 ± 27.15 mg QE/kg for TFC.

The relationship between phenolic and flavonoid contents was found to be strongly influenced by both plant species and extraction solvent. In aqueous extracts, TPC values were generally higher than TFC values for *Z. cassumunar*, whereas *C. longa* exhibited relatively balanced but overall low concentrations of both compound classes (Figure 4). In contrast, ethanolic extracts of *C. longa* demonstrated a markedly higher flavonoid content compared to phenolic content, with TFC values exceeding TPC by more than 50%. This observation is consistent with the high solubility of curcuminoids, which are flavonoid-related polyphenols, in polar organic solvents such as ethanol. Although flavonoids are a subclass of phenolic compounds, the higher TFC values compared to TPC may be attributed to differences in assay principles and calibration standards (quercetin vs. gallic acid equivalents), as well as the strong complex-forming capacity of flavonoids with $AlCl_3$ [24, 25]. Based on the comparative results, ethanol was identified as the superior solvent for the efficient recovery of both phenolic and flavonoid compounds from *Z.cassumunar* and *C. longa* rhizomes. The predominance of hydrophobic and semi-polar bioactive constituents in these species necessitates the use of a polar organic solvent to maximize extraction efficiency and enhance the potential therapeutic value of the resulting extracts.

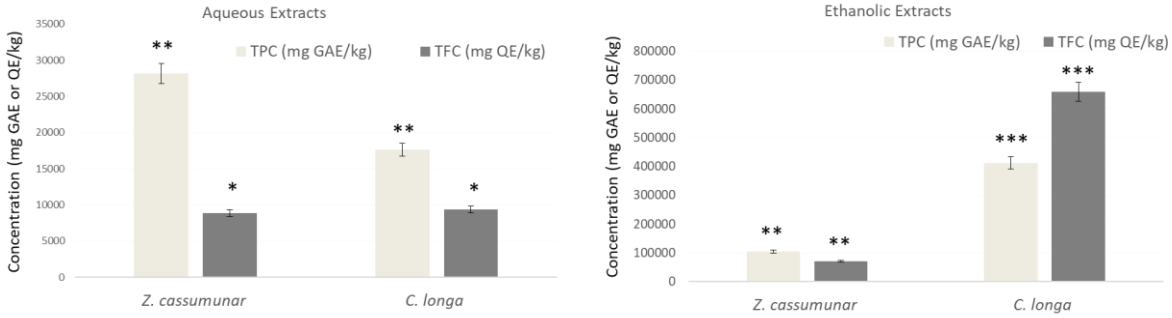


Figure 4. Comparison of total Phenolic and Flavonoid content in *Zingiber cassumunar* and *Curcuma longa.* For comparison of the mean values, one-way ANOVA followed by post hoc was used ($p < 0.05$, $n = 3$).). Asterisks indicate statistical differences in TPC and TFC content between different plants (* no differences in TFC content, ** and *** differences in TPC and TFC content)

3.4 Biological activities of *Zingiber cassumunar* and *Curcuma longa* extracts

The cytotoxic effects of *Z. cassumunar* and *C. longa* extracts were evaluated using the MTT assay following 24-hour incubation with macrophage cells at concentrations of 0.25, 0.5, 1, 2, 5, and 10 μg/mL. The results indicated that aqueous extracts from both plant species did not induce cytotoxicity, as cell viability remained comparable to that of the control group (data not shown). In contrast, the ethanolic extract of *C. longa* exhibited concentration-dependent cytotoxicity, with cell viability remaining above 85% at concentrations ranging from 0.25 to 5 μg/mL, while a significant reduction in cell viability was observed at 10 μg/mL. Meanwhile, the ethanolic extract of *Z. cassumunar* did not exhibit cytotoxicity at any tested concentration (Figure 5).

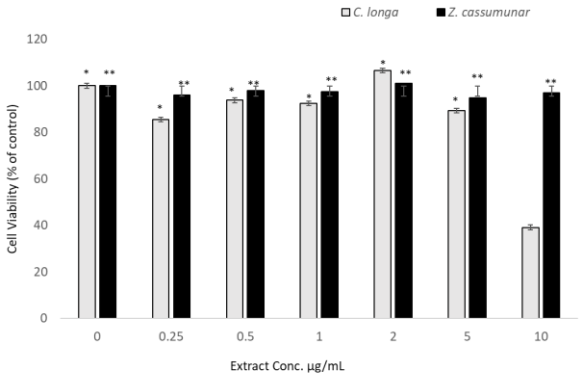


Figure 5. Cell viability of macrophage cells treated with *Z. cassumunar* and *C. longa* extracts at concentrations of 0.25, 0.5, 1, 2, 5, and 10 μg/mL. For comparison of the mean values, one-way ANOVA followed by post hoc tests was used ($p < 0.05$; $n = 3$). *Cell viability with 85% of *C. longa* extracts ** no difference of cell viability

Nitric oxide production in LPS-stimulated macrophage cells was evaluated following 24-hour treatment with *Z. cassumunar* and *C. longa* extracts. The results demonstrated that both aqueous and ethanolic extracts at 5 μg/mL significantly reduced NO production to levels comparable to those of the untreated control group (without LPS stimulation), without inducing significant cytotoxicity (data not shown). Therefore, a concentration of 5 μg/mL was determined to be the optimal concentration for extracts derived from both herbal sources. Both aqueous and ethanolic extracts at 5 μg/mL significantly reduced nitric oxide levels to levels comparable to those of the non-LPS control group (Fig. 6). Similar inhibitory effects were observed for both plant extracts, and no substantial differences in nitric oxide suppression were detected between water and ethanol extracts at the same concentration. These findings indicate that both *Z. cassumunar* and *C. longa* extracts exhibited anti-inflammatory activity (Figure 6), regardless of the solvent used [26, 27, 28].

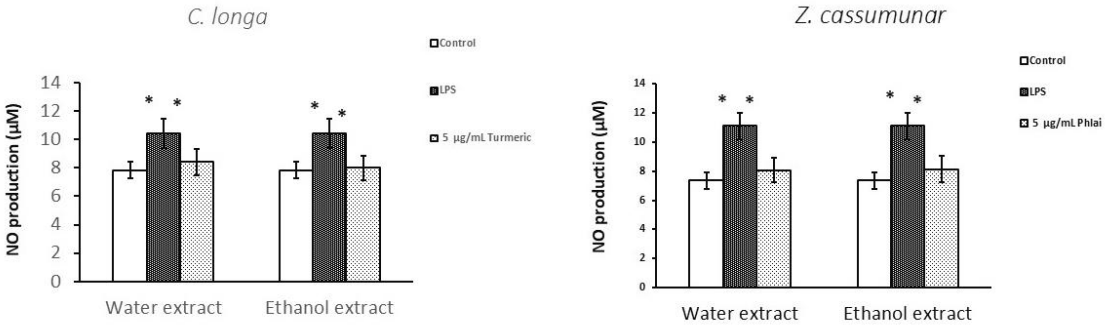


Figure 6. Nitric oxide production in LPS-stimulated macrophage cells was evaluated following 24-hour treatment with *Z. cassumunar* and *C. longa* extracts. For comparison of mean values, a one-way ANOVA followed by post hoc tests was used. * * $p < 0.05$ vs. LPS-treated control (n = 3).

The optimal incubation period for antioxidant activity assessment was determined using RAW 264.7 macrophage cells stimulated with LPS and incubated for 1, 3, 6, 12, and 24 hours. Intracellular reactive oxygen species (ROS) levels were measured using a microplate reader. The highest ROS production was observed after 3 hours of incubation (Fig. 7); therefore, this time point was selected as the optimal condition for subsequent antioxidant assays. Under these conditions, the antioxidant activities of Z. cassumunar and C. *longa* extracts were evaluated. At a concentration of 5 μg/mL, both aqueous and ethanolic *Z. cassumunar* extracts significantly reduced ROS levels compared with the LPS-treated control group, indicating effective antioxidant activity. Similarly, both aqueous and ethanolic C. longa extracts at the same concentration markedly decreased ROS production relative to the LPS control. Overall, antioxidant effects were demonstrated for both *Z. cassumunar* and *C. longa* extracts, regardless of solvent type, as evidenced by a significant reduction in intracellular ROS under LPS-induced oxidative stress conditions [29, 32].

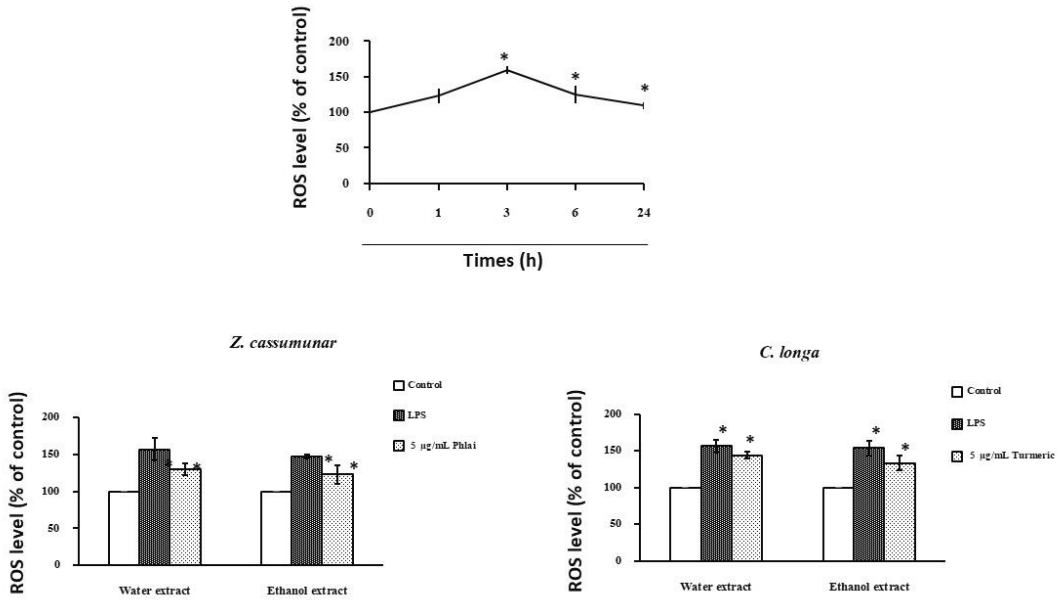


Figure 7. Intracellular reactive oxygen species (ROS) levels of *Zingiber cassumunar and Curcuma longa* from aqueous and ethanolic extracts. The y-axis label "ROS level (% of control)" is expressed relative to the untreated control group (= 100%). LPS-stimulated cells exceeding 100% at 3 h indicate elevated oxidative stress above baseline, consistent with the expected positive-control response. Authors should clarify this in the legend text to avoid confusion. Statistical significance indicators * $p < 0.05$ vs. LPS-treated group (one-way ANOVA with Tukey's post-hoc test; n = 3).

4. Conclusion

This study demonstrated that solvent selection significantly influences the extraction efficiency of bioactive compounds from *Z. cassumunar* and *C. longa*. Ethanol proved to be superior to water, yielding higher concentrations of curcuminoids, phenolics, and flavonoids, as confirmed by HPLC, TPC, and TFC analyses. Enhanced recovery is attributed to ethanol's ability to solubilize semi-polar and hydrophobic phytochemicals. Furthermore, ultrasonic pretreatment combined with ethanolic extraction improved overall extraction efficiency while maintaining phytochemical integrity. These findings support the use of ethanol as an optimal solvent and provide a scientific basis for developing standardized extraction protocols for functional foods, nutraceuticals, and herbal pharmaceuticals. Collectively, the results demonstrated that ethanol is the most suitable solvent for the extraction of phenolics, flavonoids, and curcuminoids from *Z. cassumunar* and *C. longa*. The combined use of ultrasonic pretreatment and ethanolic extraction was shown to enhance extraction efficiency while preserving phytochemical integrity. These findings provide a scientifically validated basis for optimizing extraction protocols and support the potential industrial application of these medicinal plants in the development of functional foods, nutraceuticals, and herbal pharmaceutical products [30, 31]. Nevertheless, several limitations of the present study should be acknowledged. Biological activity was assessed at a single concentration (5 μg/mL) only, precluding the calculation of IC_{50} values and dose-response relationships. Cytotoxicity of the extracts toward RAW 264.7 cells was not evaluated, and confirmation that the observed reduction in NO and ROS reflects true pharmacological activity rather than cell death requires further investigation. Additionally, plant materials were sourced commercially without voucher specimen deposition, which limits batch-to-batch reproducibility. Future studies should employ multi-concentration biological assays with full IC_{50} determination, conduct in vivo validation, include cytotoxicity controls, use authenticated herbarium-vouched plant material, and explore encapsulation or formulation strategies to enhance the bioavailability of the predominantly hydrophobic bioactive compounds identified.

5. Acknowledgments

Author Contributions: Conceptualization, T.P. and A.B..; methodology, L.S.; software, T.P..; validation, R.R.,., and A.B..; formal analysis, K.Y..; investigation, A.B..; resources, L.S..; data curation, N.N..; writing—original draft preparation, A.B..; writing—review and editing, T.P..; visualization, L.S..; supervision, T.P..; project administration, A.B..; funding acquisition, A.B.. All authors have read and agreed to the published version of the manuscript.

Funding: This research was funded by the National Science Research and Innovation Fund (NSRF) under the Fundamental Fund (FF) [Grant Number: 4778762] through the Faculty of Science and Technology, Hatyai University, Hatyai, Songkhla, Thailand.

Conflicts of Interest: The authors declare no conflict of interest.

References

[1] Sumi, M. J.; Zaman, S. B.; Imran, S.; Sarker, P.; Rhaman, M. S. A Review on the Ethnopharmacological Importance and Biochemical Composition of Medicinal Plants within the Zingiberaceae Family. *Plant Sci. Today* **2024**, *11*(sp1). https://doi.org/10.14719/pst.3514

[2] Srisuwan, T.; Keereekoch, T.; Chikasem, I.; Da-o, A.; Salaemae, M.; Saleh, A.; Subhadhirasakul, S. Development of the Preparation Methods for Qualified Cassumunar Ginger Powder Based on Thai Herbal Pharmacopoeia Standards. *Thaksin Univ. J.* **2016**, *19*(2) 53–65.

[3] Khamsopa, N.; Vanichanon, A.; Sukrakanchana, N. Efficacy of Essential Oils from Clove (*Syzygium aromaticum*) and Cassumunar Ginger (*Zingiber montanum*) as Anesthetic Agents for Fruit Fly (*Drosophila melanogaster*). *ASEAN J. Sci. Technol. Rep.* **2018**, *21*(3), 58–64.

[4] Pascual, P. R. L.; Remedios, E. A.; Abello, N. F.; Carabio, D. E.; Pascual, V. U.; Alburo, R. P. Vegetative, Photosynthetic, and Anthocyanin Content of Turmeric (*Curcuma longa* L.) Applied with Organic Foliar Fertilizers. *ASEAN J. Sci. Technol. Rep.* **2025**, *28*(5), e257477. https://doi.org/10.55164/ajstr.v28i5.257477

[5] Ali, A. M. A.; El-Nour, M. E. M.; Yagi, S. M. Total Phenolic and Flavonoid Contents and Antioxidant Activity of Ginger (*Zingiber officinale* Rosc.) Rhizome, Callus and Callus Treated with Some Elicitors. *J. Genet. Eng. Biotechnol.* **2018**, *16*(2), 677–682. https://doi.org/10.1016/j.jgeb.2018.03.003

[6] Aggarwal, B. B.; Harikumar, K. B. Potential Therapeutic Effects of Curcumin, the Anti-Inflammatory Agent, against Neurodegenerative, Cardiovascular, Pulmonary, Metabolic, Autoimmune and Neoplastic Diseases. *Int. J. Biochem. Cell Biol.* **2009**, *41*(1), 40–59. https://doi.org/10.1016/j.biocel.2008.06.010

[7] Keereekoch, T.; Srisuwan, T.; Taleh, R.; Hemtrakoonwong, R.; Chesa-E, S.; Subhadhirasakul, S. Effects of Steam Sterilization Time and Temperature on Quality of Turmeric Powder. *Thaksin Univ. J.* **2014**, *17*(1), 57–67.

[8] Akbik, D.; Ghadiri, M.; Chrzanowski, W.; Rohanizadeh, R. Curcumin as a Wound Healing Agent. *Life Sci.* **2014**, *116*(1), 1–7. https://doi.org/10.1016/j.lfs.2014.08.016

[9] Kocaadam, B.; Şanlier, N. Curcumin, an Active Component of Turmeric (*Curcuma longa*), and Its Effects on Health. *Crit. Rev. Food Sci. Nutr.* **2017**, *57*(13), 2889–2895. https://doi.org/10.1080/10408398.2015.1077195

[10] Rawat, G.; Geetha, S. J.; Pandit, S.; et al. Flavonoids as Antioxidants and Anti-Inflammatory Agents in Cancer Prevention. *Vegetos* **2026**. https://doi.org/10.1007/s42535-026-01670-2

[11] Lin, L. Z.; Mukhopadhyay, S.; Robbins, R. J.; Harnly, J. M. Identification and Quantification of Flavonoids of Mexican Oregano (*Lippia graveolens*) by LC-DAD-ESI/MS Analysis. *J. Food Compos. Anal.* **2007**, *20*(5), 361–369. https://doi.org/10.1016/j.jfca.2006.09.005

[12] Pauner, R.; Hamzah, A. S. Phenylbutanoid Compounds from *Zingiber cassumunar* and Their Pharmacological Activities. *J. Ethnopharmacol.* **2022**, *289*, 115016

[13] Chemat, F.; Rombaut, N.; Zill-e-Huma; Khan, M. K. Ultrasonic-Assisted Extraction of Food Ingredients. *Ultrason. Sonochem.* **2017**, *34*, 540–549. https://doi.org/10.1016/j.ultsonch.2016.06.035

[14] Saenge Chooklin, C.; Chooklin, S. Optimized Extraction of Total Phenolic Compounds from 'Tubtim Siam' Pummelo Peel Using Ultrasonic Technique and Response Surface Methodology. *ASEAN J. Sci. Technol. Rep.* **2021**, *24*(1), 61-70. https://doi.org/10.55164/ajstr.v24i1.240796

[15] Buachoon, N. Development of Ultrasonic Extraction Techniques for Bioactive Compounds from Banana Peel Waste: A Comparative Study of Biological Activities. *ASEAN J. Sci. Technol. Rep.* **2025**, *29*(1), e258852. https://doi.org/10.55164/ajstr.v29i1.258852

[16] Panyo, J.; Klomklao, S. Microwave-Assisted Extraction of Phenolic Compounds from *Smilax ovalifolia* Roxb. and Chemical Compositions. *Thaksin Univ. J.* **2013**, 45–51. https://doi.org/10.55164/ajstr.v26i3.249604

[17] Sridhar, N.; Veer-Anjaneyulu, A.; Arora, A. Phytochemical Analysis and Biological Activities of Ethanolic Extract of *Curcuma longa* Rhizome. *Braz. J. Biol.* **2021**, *81*(3), 737–740. https://doi.org/10.1590/1519-6984.230628

[18] Peram, M. R.; Jalalpure, S. S.; Palkar, M. B.; Diwan, P. V. Stability Studies of Pure and Mixture Form of Curcuminoids by Reverse Phase-HPLC Method under Various Experimental Stress Conditions. *Food Sci. Biotechnol.* **2017**, *26*(3), 591–602. https://doi.org/10.1007/s10068-017-0087-1

[19] Revathy, S.; Elumalai, S.; Bennita, M. A.; Prathapa, S. T. Isolation, Purification and Identification of Curcuminoids from *Curcuma longa* L. by Column Chromatography. *J. Exp. Sci.* **2011**, *2*(7), 21–25.

[20] Han, A.-R.; Kim, H.; Piao, D.; Jung, C.-H.; Seo, E. K. Phytochemicals and Bioactivities of *Zingiber cassumunar* Roxb. *Molecules* **2021**, *26*(8), 2377. https://doi.org/10.3390/molecules26082377

[21] Azemi, N.; Basar, N.; Toemen, S. Ultrasound-Assisted Extraction (UAE) of Phytochemicals with Response Surface Methodology (RSM) in *Curcuma xanthorrhiza*. *Ann. Trop. Med. Public Health* **2020**, *13*(8). https://doi.org/10.36295/ASRO.2020.231306

[22] Rajchasom, S.; Sombatnan, P.; Vuthijumnonk, J. T.; Suphiratwanich, P. Comparison of Different Extraction Methods for Bioactive Compounds from Kao-Kum Doi-Saket (*Oryza sativa* L.). *ASEAN J. Sci. Technol. Rep.*, 38–46. https://doi.org/10.55164/ajstr.v26i4.249961

[23] Ruiz-Vasquez, L.; Ruiz Mesia, L.; Maco, M. M.; Zapata, J. A.; Ricopa Cotrina, H.; Cobos, M.; Pinedo-Cancino, V.; Tello, F.; Castro, J. C. Optimized Folin-Ciocalteu Method for Determination of Total Polyphenols in Medicinal Plants of the Peruvian Amazon: Validation and Application to Twelve Species. *AppliedChem* **2026**, *6*(1), 17. https://doi.org/10.3390/appliedchem6010017

[24] Chang, C. C.; Yang, M. H.; Wen, H. M.; Chern, J. C. Estimation of Total Flavonoid Content in Propolis by Two Complementary Colorimetric Methods. *J. Food Drug Anal.* **2002**, *10*(3), 178–182. https://doi.org/10.38212/2224-6614.2748

[25] Singleton, V. L.; Orthofer, R.; Lamuela-Raventós, R. M. Analysis of Total Phenols and Other Oxidation Substrates and Antioxidants by Means of Folin-Ciocalteu Reagent. *Methods Enzymol.* **1999**, *299*, 152–178. https://doi.org/10.1016/S0076-6879(99)99017-1

[26] Chaijan, S.; Chaijan, M.; Uawisetwathana, U.; Panya, A.; Phonsatta, N.; Shetty, K.; Panpipat, W. Phenolic and Metabolic Profiles, Antioxidant Activities, Glycemic Control, and Anti-Inflammatory Activity of Three Thai Papaya Cultivar Leaves. *Foods* **2024**, *13*(11), 1692. https://doi.org/10.3390/foods13111692

[27] Bunkaew, K.; Ponpichai, P.; Lertworapreecha, M.; Maitip, J.; Chanasit, W. Phytochemical Analysis and Biological Activities of Propolis from *Geniotrigona thoracica*: Evaluating Its Therapeutic Applications. *ASEAN J. Sci. Technol. Rep.* **2024**, *27*(5), e253219. https://doi.org/10.55164/ajstr.v27i5.253219

[28] Sueree, L.; Madaka, F.; Jongrungruangchok, S.; Vipunngeun, N.; Songsak, T. Comprehensive Pharmacognostic Analysis and Quality Control Parameters of *Cannabis sativa* L. subsp. *sativa*: Evaluating Leaves and Flowers for Medicinal Applications. *ASEAN J. Sci. Technol. Rep.* **2025**, *28*(6), e259515. https://doi.org/10.55164/ajstr.v28i6.259515

[29] Altaweel, D. Enhancement of Bioactive Compounds and Nutrient Content in Rosemary (*Salvia rosmarinus*) Using Nano-Magnesium and NPK Fertilization: A GC-MS Analysis. *ASEAN J. Sci. Technol. Rep.* **2025**, *28*(6), e261168. https://doi.org/10.55164/ajstr.v28i6.261168

[30] Worawut, K.; Phungpis, B.; Noppawan, P. Valorization of White Shrimp Shell Waste: Development of Chitosan-Based Pellet Feed for Enhanced Nile Tilapia (*Oreochromis niloticus*) Nutrition. *ASEAN J. Sci. Technol. Rep.* e260098. **2026**, *29*(2), e260098. https://doi.org/10.55164/ajstr.v29i2.260098

[31] Sang-Ngam, S.; Chaowiset, W.; Theerapisit, S.; Promprao, S.; Sintupachee, S. Ecological Factors Governing the Persistence of Khlong-Saeng Durian: Implications for Conservation. *ASEAN J. Sci. Technol. Rep.* e259593. **2025**, *28*(5), https://doi.org/10.55164/ajstr.v28i5.259593

[32] Tongkasee, P.; Srithat, D.; Srithupthai, K.; Wechvitan, P.; Thititanaapipong, P.; Insuwan, W.; Kamsri, P.; Khotpakdee, P. Extraction and Phytochemical Profile of Three Herbal Weeds: *Chromolaena odorata* L., *Amaranthus viridis* L., and *Cyperus rotundus* L. for Green Synthesis of Silver Nanoparticles. *ASEAN J. Sci. Technol. Rep.* **2023**, *26*(3), 10–23. https://doi.org/10.55164/ajstr.v26i3.249267

ASEAN
Journal of Scientific and Technological Reports
Online ISSN:2773-8752

Research article

Numerical Solutions of Fractional Integro-Differential Equations with Weakly Singular Kernel by Using a Hybrid of Block-Pulse Functions and Taylor Polynomials

Weerachai Thadee[1], Onuma Ruksachol[2], Walisa Intarapak[2], Rattiya Rittichuai[2], and Nattinee Khongnual[2*]

[1] Faculty of Liberal Arts, Rajamangala University of Technology Srivijaya, Songkhla, 90000, Thailand
[2] Faculty of Science and Technology, Nakhon Si Thammarat Rajabhat University, Nakhon Si Thammarat, 80280, Thailand
* Correspondence: nattinee_kho@nstru.ac.th

Citation:
Thadee, W.; Ruksachol, O.; Intarapak, W.; Rittichual, R.; Khongnual, N. Numerical solutions of fractional integro-differential equations with weakly singular kernal by using a hybrid of block-pulse functions and taylor polynomials. *ASEAN J. Sci. Tech. Report.* **2026**, *29*(7), e262844. https://doi.org/10.55164/ajstr.v29i7.262844

Article history:
Received: April 3, 2026
Revised: April 11, 2026
Accepted: April 30, 2026
Available online: June 14, 2026

Publisher's Note:
This article is published and distributed under the terms of the Thaksin University.

Abstract: Fractional integro-differential equations (FIDEs) with weakly singular kernels arise in mathematical models of viscoelasticity, anomalous diffusion, and hereditary systems, yet closed-form solutions are rarely attainable. This study proposes a numerical scheme based on a hybrid combination of block-pulse functions and Taylor polynomials for solving both linear and nonlinear FIDEs with weakly singular kernels of the form $(t-s)^{-\beta}$, $0<\beta<1$, formulated within the Caputo fractional derivative framework. The fractional problem is transformed into an equivalent system of algebraic equations by constructing a Riemann–Liouville operational matrix and applying Newton–Cotes collocation nodes, yielding a computationally straightforward solver. Three illustrative examples were examined, including two linear equations with exact solutions $u(t)=t^2+t^3$ and $u(t)=-t+t^2$, and one nonlinear equation with an exact solution $u(t)=t^2$. The proposed method achieved absolute errors below 1.0×10^{-4} across all test points using N = 1, 2 block-pulse intervals and M = 2, 3 Taylor polynomial terms. Comparison with the Legendre wavelet method (LWM) demonstrates that the present scheme matches or surpasses LWM accuracy at most collocation points while requiring fewer basis functions. These results confirm that the hybrid block-pulse–Taylor polynomial approach offers a reliable and efficient alternative for solving FIDEs encountered in applied science and engineering.

Keywords: Hybrid functions; fractional differential equations; taylor polynomials; integro-differential equations; weakly singular kernel

1. Introduction

In general calculus, derivatives of order n are considered only for the particular case when n is a positive integer. The next logical direction is to explore generalized definitions of derivatives and integrals that are valid for arbitrary real orders. This area of mathematics is known as fractional calculus, with origins traceable to 1695, when L'Hospital posed the question to Leibniz: 'What could $\frac{d^{\frac{1}{2}}}{dx^{\frac{1}{2}}} f(x)$ mean?' For more than two centuries, this subject remained largely within pure mathematics. Pioneering mathematicians such as Euler, Fourier, Abel, Liouville, Riemann, and Hadamard contributed significantly to

the early development of fractional operators by introducing various definitions and examining their fundamental properties. In recent decades, however, fractional calculus has expanded considerably, demonstrating applicability across a wide range of natural and applied sciences.

The growing significance of fractional differential equations (FDEs) in various fields of science and engineering has led to increasing research interest [1–12]. Fractional calculus provides a powerful framework for modelling memory effects and hereditary properties in complex systems, making it particularly valuable in applications ranging from viscoelasticity to anomalous diffusion processes [13–15]. Distributed-order fractional derivatives refer to fractional derivatives integrated over a continuum of derivative orders within a specified range [6, 16]. Since analytical solutions to many fractional differential problems are often unavailable, considerable research has been devoted to developing efficient numerical and analytical methods [1, 8, 10, 11, 17–19]. Numerous researchers have developed numerical methods for solving fractional integro-differential equations (FIDEs), which combine the complexities of both fractional derivatives and integral operators [20–24]. In cases where exact analytical solutions are unattainable, attention has been directed toward accurate approximate solutions using various computational techniques [7, 25–27]. For instance, Mingxu et al. [1] employed the Legendre wavelet approach to investigate numerical solutions of FIDEs with weakly singular kernels, transforming the original equations into an algebraic system for efficient computation. More recently, several wavelet-based methods have been proposed, including Haar wavelets [7], Bell wavelets [28], and modified hat functions [29].

The challenge of handling weakly singular kernels in FIDEs has attracted significant attention due to their prevalence in modelling real-world phenomena [30–32]. These kernels, typically of the form $(t-s)^{-\beta}$ where $0<\beta<1$, introduce computational difficulties requiring specialized numerical treatments [33, 34]. In this research, we develop a numerical method for solving linear and nonlinear FIDEs with a weakly singular kernel as described by Equations (1) and (2), respectively, subject to appropriate initial conditions. The method applies to both linear and nonlinear problems.

$$D^{\alpha} f(t)=\lambda_1\int_0^t \frac{f(x)}{(t-x)^{\gamma}}dx+\lambda_2\int_0^1 u(t,x)f(x)dx+g(t) \tag{1}$$

and

$$D^{\alpha} f(t)=\lambda_1\int_0^t \frac{f(x)^p}{(t-x)^{\gamma}}dx+\lambda_2\int_0^1 u(t,x)f(x)^q dx+g(t) \tag{2}$$

2. Materials and Methods

2.1 Fractional Integral and Derivative

In this section, we present the fundamental definitions, notations, and theoretical concepts related to fractional integrals and derivatives used throughout this study.

Definition 1 (Riemann–Liouville Fractional Integral). The integral operator defined by Equation (3) is called the Riemann–Liouville fractional integral operator of order α [5].

$$I^{\alpha} f(t)=\begin{cases}\dfrac{1}{\Gamma(\alpha)}\displaystyle\int_0^t \frac{f(x)}{(t-x)^{1-\alpha}}dx, & \alpha>0\\ f(t) & \alpha=0.\end{cases} \tag{3}$$

For any constants λ and μ, the operator is linear, as expressed in Equation (4).

$$I^{\alpha}\left(\lambda f(t)\pm\mu g(t)\right)=\lambda I^{\alpha} f(t)\pm\mu I^{\alpha} g(t) \tag{4}$$

Definition 2 (Caputo Fractional Derivative). The derivative defined by Equation (5) is called the Caputo fractional derivative of order α, where n is the smallest integer such that $n-1<\alpha<n$ [2–4].

$$\left(D^{\alpha} f\right)(t)=\frac{1}{\Gamma(n-\alpha)}\int_0^t \frac{f^{(n)}(x)}{(t-x)^{\alpha+1-n}}\,ds, \qquad n-1<\alpha<n,\ n\in\mathbb{N}, \tag{5}$$

For any constants, the Caputo derivative is a linear operation, as shown in Equation (6). From Definitions 1 and 2, the composition property is given by Equation (7), and additional key properties are provided as Equations (8) and (9).

$$D^{\alpha}\left(\lambda\, f(t)\pm \mu\, g(t)\right)=\lambda D^{\alpha} f(t)\pm \mu D^{\alpha} g(t)\ . \tag{6}$$

$$I^{\alpha}\left(D^{\alpha} h(t)\right)=h(t)-\sum_{k=0}^{n-1} h^{(k)}(0)\frac{t^k}{k!} \tag{7}$$

For any real number α such that $n-1<\alpha\le n$ and $n\in\mathbb{N}$, we have

$$I^{n-\alpha}D^{n}h(t) = \frac{1}{\Gamma(n-\alpha)}\int_0^t \frac{D^{n}(h(x))}{(t-x)^{1-(n-\alpha)}}\,dx$$

$$= \frac{1}{\Gamma(n-\alpha)}\int_0^t \frac{D^{n}(h(x))}{(t-x)^{\alpha+1-n}}\,dx$$

$$= D^{\alpha}h(t)$$

$$I^{n-\alpha}D^{n}h(t)=D^{\alpha}h(t) \tag{8}$$

$$D^{\beta}\overline{B}(t,\alpha)=D^{\beta}I^{\beta}I^{\alpha-\beta}B(t)=\overline{B}(t,\alpha-\beta)\,. \tag{9}$$

2.2 Hybrid of Block-Pulse Functions and Taylor Polynomials

2.2.1 Definition of Hybrid Functions

The hybrid functions denoted by $b_{nm}(t)$ are defined by Equation (10), where n is the order of block-pulse functions such that $T_m(t)=t^m$, $n=1,2,...,N$ and $m=0,1,...,M-1$, defined on the interval $[0,t_f)$. The hybrid of block-pulse functions and Taylor polynomial functions constitutes a semi-orthogonal set on the interval $[0,t_f)$.

$$b_{nm}(t)=\begin{cases} T_m\left(Nt-(n-1)t_f\right) & ,t\in\left[\dfrac{n-1}{N}t_f,\dfrac{n}{N}t_f\right), \\ 0 & ,\textit{otherwise.}\end{cases} \tag{10}$$

For the four elements $(N=2,M=2)$, the basis functions are explicitly expressed.

2.2.2 Function Approximation

A function $f(t)$ defined over $[0,t_f)$ may be expanded as a series in hybrid functions as Equation (11). Truncating this expansion yields the approximation given in Equation (12).

$$f(t)\cong\sum_{n=1}^{\infty}\sum_{m=0}^{\infty}c_{nm}b_{nm}(t)\,, \tag{11}$$

where $C^{T}=\left[c_{10},c_{20},...,c_{N0},c_{11},c_{21},...,c_{N1},...,c_{1M-1},c_{2M-1},...,c_{NM-1}\right]$,

and $$B^T(t)=\left[b_{10}(t),b_{20}(t),\ldots b_{N0}(t),b_{11}(t),b_{21}(t),\ldots,b_{N1}(t),\ldots,b_{1M-1}(t),b_{2M-1}(t),\ldots,b_{NM-1}(t)\right]. \quad (12)$$

2.3 Riemann–Liouville Fractional Integral Operator for Hybrid Functions

The operational matrix for the Riemann–Liouville fractional integral of hybrid functions is introduced in Equation (13) and obtained via the Laplace transform applied to each basis function, as shown in Equation (14).

$$I^{\alpha}B(t)=\overline{B}(t,\alpha), \quad (13)$$

$$b_{nm}(t)=\mu_{\frac{n-1}{N}t_f}(t)T_m\left(Nt-(n-1)t_f\right)-\mu_{\frac{n}{N}t_f}(t)T_m\left(Nt-(n-1)t_f\right), \quad (14)$$

2.4 Numerical Scheme

Without loss of generality, assume the initial condition $\beta\geq\alpha$. Expanding $D^{\beta}f(t)$ in hybrid functions as Equation (15) and applying Equations (7) and (13) yields the fractional derivative approximation Equation (16).

$$D^{\beta}f(t)=C^T B(t). \quad (15)$$

$$f(t)=C^T\overline{B}(t,\beta)+\sum_{k=0}^{\beta-1}\frac{f^{(k)}(0)t^k}{k!}. \quad (16)$$

Substituting into Equation (1) and collocating at Newton–Cotes nodes t_i as defined by Equation (18) converts the integral equation into an algebraic system (Equation 17), from which the coefficient vector C, and hence the numerical solution $f(t)$, is obtained.

$$C^T\overline{B}(t,\beta-\alpha)+\sum_{k=0}^{\beta-1}D^{\alpha}\left(t^k\right)\frac{f^{(k)}(0)}{k!}=\lambda_1\int_0^1\frac{C^T\overline{B}(x,\beta)+\sum_{k=0}^{\beta-1}\frac{f^{(k)}(0)x^k}{k!}}{(t-x)^{\beta}}+\lambda_2\int_0^1u(t,x)C^T\overline{B}(t,\beta)$$

$$+\sum_{k=0}^{\beta-1}\frac{f^{(k)}(0)t^k}{k!}dx+g(t). \quad (17)$$

$$t_i=\frac{2i+1}{2N(M+1)},\quad i=0,1,\ldots,N(M+1)-1. \quad (18)$$

3. Results and Discussion

To assess the performance and efficiency of the proposed method, three illustrative examples are presented: two linear FIDEs and one nonlinear FIDE with weakly singular kernels. Results are compared with the Legendre wavelet method (LWM) [1] and exact solutions.

3.1 Example 1 – Linear FIDE (N = 1, M = 3)

Consider the linear fractional integro-differential equation given by Equation (19), subject to initial conditions $f(0)=0$ and Equation (20). The equation has a unique exact solution $u(t)=t^2+t^3$.

$$D^{0.25}f(t)=\frac{1}{2}\int_0^t\frac{f(x)}{(t-x)^{\frac{1}{2}}}dx+\frac{1}{3}\int_0^1(t-x)f(x)dx+g(t) \quad (19)$$

$$g(t)=\frac{\Gamma(3)}{\Gamma(2.75)}t^{1.75}+\frac{\Gamma(4)}{\Gamma(3.75)}t^{2.75}-\frac{\sqrt{\pi}t^{\frac{5}{2}}\Gamma(3)}{2\Gamma\left(\frac{7}{2}\right)}-\frac{\sqrt{\pi}t^{\frac{7}{2}}\Gamma(4)}{2\Gamma\left(\frac{9}{2}\right)}-\frac{7t}{36}+\frac{3}{20}. \tag{20}$$

Applying the hybrid scheme with $N=1$ and $M=3$, the coefficient vector C is obtained by collocating Equation (21) at Newton–Cotes nodes $t_0=\frac{1}{8},t_1=\frac{3}{8},t_2=\frac{5}{8}$ and $t_3=\frac{7}{8}$, we obtain

$c_{10}=-2.4978\times10^{-17}, c_{11}=2$ and $c_{12}=3$. The numerical solution is then reconstructed via Equation (22).

$$C^T\overline{B}(t,0.75)=\frac{1}{2}\int_0^t\frac{C^T\overline{B}(x,1)}{(t-x)^{\frac{1}{2}}}dx+\frac{1}{3}\int_0^1(t-x)C^T\overline{B}(x,1)dx+g(t) \quad . \tag{21}$$

$$f(t)=C^T\overline{B}(t,1)=t^2+t^3, \tag{22}$$

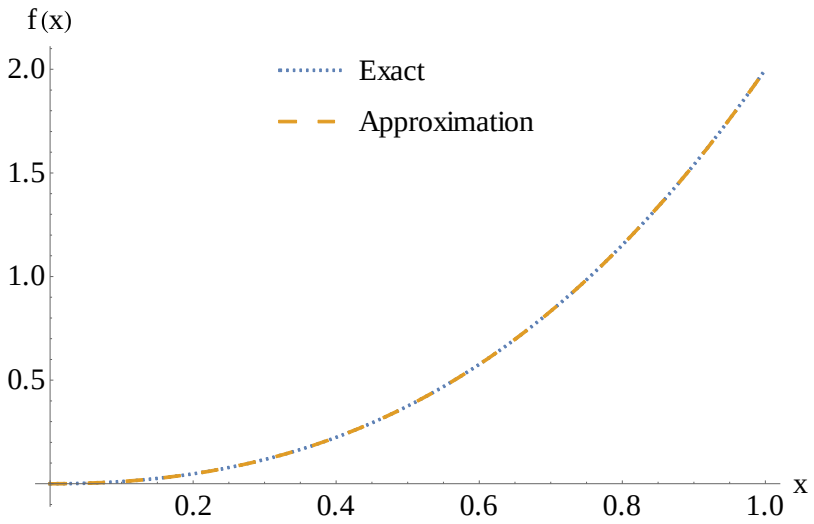


Figure 1. Comparison of exact solution and approximate solution with $N = 1$ and $M = 3$ (Example 1).

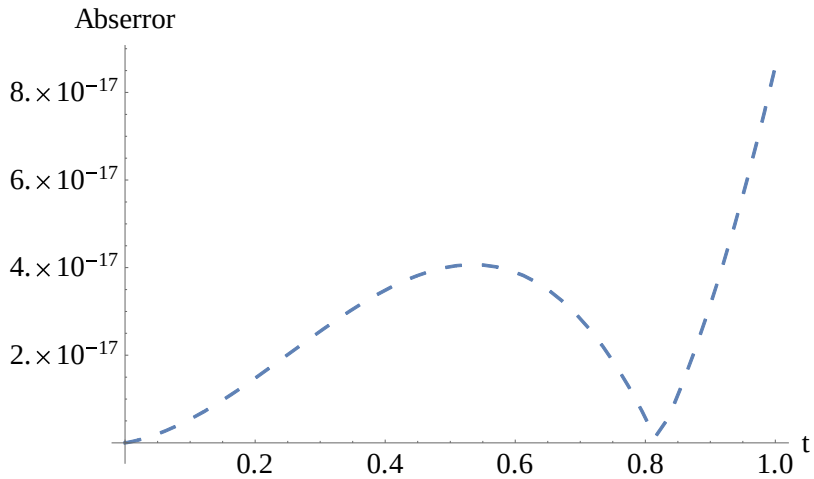


Figure 2. Absolute errors with $N=1$ and $M=3$ (Example 1).

3.2 Example 2 – Linear FIDE (N = 1, M = 2)

Consider the linear fractional integro-differential equation given by Equation (23), subject to conditions in Equation (24). The unique exact solution is $u(t) = -t + t^2$. Applying the hybrid scheme with $N = 1$ and $M = 2$ and collocating at Newton–Cotes nodes $t_0 = \frac{1}{6}, t_1 = \frac{3}{6}$ and $t_2 = \frac{5}{6}$, we obtain $c_{10} = -1, c_{11} = 2$. Table 1 presents numerical results at selected collocation points for $N = 1$ and $M = 2$ in Example 2.

$$D^{0.15} f(t) = \frac{1}{4}\int_0^t \frac{f(x)}{(t-x)^{\frac{1}{2}}} dx + \frac{1}{7}\int_0^1 e^{t+x} f(x) dx + g(t) \tag{23}$$

$$g(t) = \frac{\Gamma(3)}{\Gamma(2.85)} t^{1.85} + \frac{\Gamma(2)}{\Gamma(1.85)} t^{0.85} - \frac{\sqrt{\pi} t^{\frac{5}{2}} \Gamma(3)}{4\Gamma\left(\frac{7}{2}\right)} + \frac{\sqrt{\pi} t^{\frac{3}{2}} \Gamma(2)}{4\Gamma\left(\frac{5}{2}\right)} - \frac{e^{t+1} - 3e^t}{7} \tag{24}$$

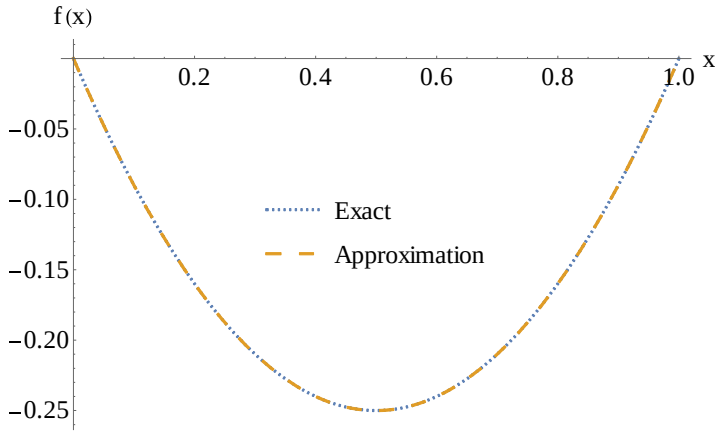


Figure 3. Comparison of exact solution and approximate solution with $N = 1$ and $M = 2$ (Example 2).

Table 1. Approximate solution at selected points for $N = 1$ and $M = 2$ (Example 2).

t	LWM	Present Method	Exact Solution
0	0.0000	0.0000	0.0000
1/8	-0.1090	-0.1094	-0.1094
2/8	-0.1869	-0.1875	-0.1875
3/8	-0.2338	-0.2344	-0.2344
4/8	-0.2498	-0.2500	0.2500
5/8	-0.2337	-0.2344	-0.2344
6/8	-0.1869	-0.1875	-0.1875
7/8	-0.1084	-0.1094	-0.1084

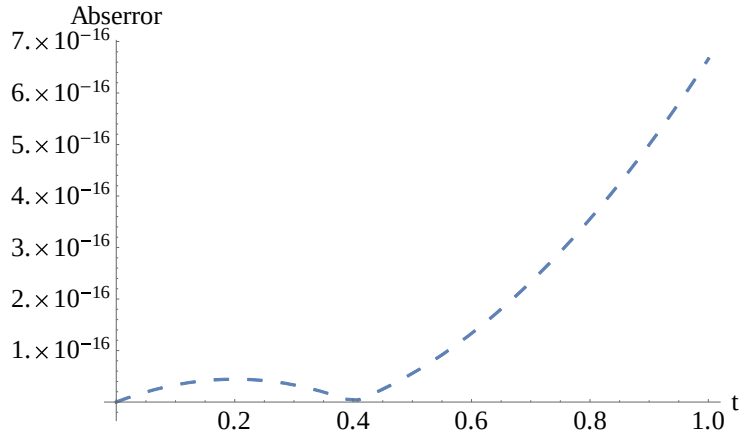


Figure 4. Absolute errors with $N=1$ and $M=2$ (Example 2).

3.3 Example 3 – Nonlinear FIDE (N = 2, M = 2)

Consider the nonlinear fractional integro-differential equation given by Equation (25), subject to conditions in Equation (26). The unique exact solution is $u(t)=t^2$. Applying the hybrid scheme with $N=2$ and $M=2$ and collocating at Newton–Cotes nodes produces the following numerical solution.

$$D^{0.5} f(t) = \int_0^x \frac{\left[f(x) \right]^2}{(t-x)^{\frac{1}{2}}} dx + \int_0^1 (t+\sin x)\left[f(x) \right]^3 dx + g(t) \tag{25}$$

$$g(t) = \frac{\Gamma(3)}{\Gamma(2.5)} t^{1.5} - \frac{\sqrt{\pi} t^{\frac{9}{2}} \Gamma(5)}{\Gamma\left(\frac{11}{2}\right)} - \frac{t}{7} - 389\cos 1 - 606\sin 1 + 720. \tag{26}$$

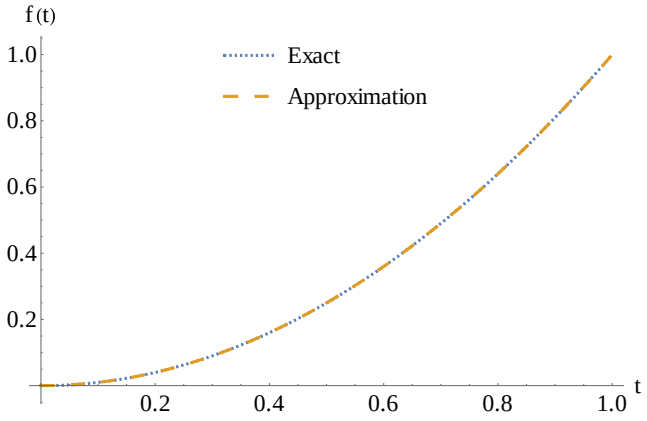


Figure 5. Comparison of exact solution and approximate solution with $N=2$ and $M=2$ (Example 3, nonlinear).

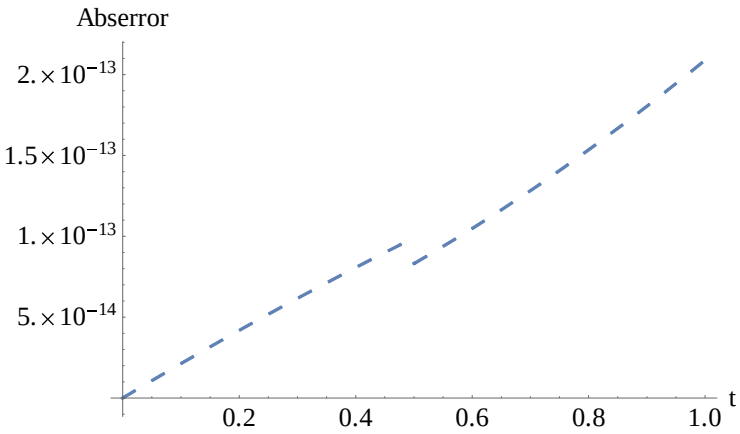


Figure 6. Comparison of absolute errors between the proposed method and exact solution with $N = 2$ and $M = 2$ (Example 3, nonlinear).

4. Conclusions

In this study, a numerical method based on a hybrid combination of block-pulse functions and Taylor polynomials was proposed for solving linear and nonlinear fractional integro-differential equations (FIDEs) with weakly singular kernels, formulated within the Caputo fractional derivative framework. By transforming the fractional problem into an equivalent algebraic system via the Riemann–Liouville operational matrix and Newton–Cotes collocation, three illustrative examples were examined. The results demonstrate that the proposed technique yields solutions in excellent agreement with the exact solutions while achieving lower absolute errors than the Legendre wavelet method (LWM).

5. Acknowledgments

The author would like to express sincere gratitude to the Faculty of Science and Technology, Nakhon Si Thammarat Rajabhat University, for their valuable support and encouragement in conducting this research. Their continuous support has significantly contributed to the successful completion of this study.

Author Contributions: Conceptualization, N.K. and W.T.; methodology, N.K. and W.T.; software, O.R. and W.I.; formal analysis, N.K., O.R., W.I., and R.R.; investigation, all authors; writing — original draft preparation, N.K. and W.T.; writing — review and editing, N.K.; visualization, O.R.; supervision, N.K. All authors have read and agreed to the published version of the manuscript.

Funding: This research did not receive any specific grant from funding agencies in the public, commercial, or not-for-profit sectors.

Conflicts of Interest: The authors declare no conflict of interest.

References

[1] Mingxu, Y.; Lifeng, W.; Jun, H. Legendre Wavelets Method for the Numerical Solution of Fractional Integro-Differential Equations with Weakly Singular Kernel. *Appl. Math. Modell.* **2016**, *40*, 3422–3437. https://doi.org/10.1016/j.apm.2015.10.055

[2] Garrappa, R. Numerical Solution of Fractional Differential Equations: A Survey and a Software Tutorial. *Mathematics* **2018**, *6*(2), 16. https://doi.org/10.3390/math6020016

[3] Yumei, Z.; Guoping, H. On the Uniqueness of Solutions for a Class of Fractional Differential Equations. *Appl. Math. Lett.* **2017**, *74*, 68–73. https://doi.org/10.1016/j.aml.2017.05.002

[4] Chen, Y.-M.; Wang, Y.-Q.; Liu, D.-Y.; Yang, H. Numerical Solution for a Class of Nonlinear Variable-Order Fractional Differential Equations with Legendre Wavelets. *Appl. Math. Lett.* **2015**, *46*, 83–88. https://doi.org/10.1016/j.aml.2015.01.012

[5] Sun, H.; Chen, A.; Zhang, Y.; Chen, W. A Review on Variable-Order Fractional Differential Equations: Mathematical Foundations, Physical Models, Numerical Methods and Applications. *Fract. Calc. Appl. Anal.* **2019**, *22*(1), 27–59. https://doi.org/10.1515/fca-2019-0003

[6] Nintanavongsa, J.; Boonklurb, Y.; Razzaghi, M. An Efficient Method for Numerical Solutions of Distributed-Order Fractional Differential Equations. *J. Comput. Nonlinear Dyn.* **2018**, *13*(11), 111001. https://doi.org/10.1115/1.4040495

[7] Amin, R.; Shah, K.; Asif, M.; Khan, I.; Ullah, F. An Efficient Algorithm for Numerical Solution of Fractional Integro-Differential Equations via Haar Wavelet. *J. Comput. Appl. Math.* **2021**, *381*, 113028. https://doi.org/10.1016/j.cam.2020.113028

[8] Ravichandran, C.; Logeswari, K.; Jarad, F. New Results on Existence in the Framework of Atangana–Baleanu Derivative for Fractional Integro-Differential Equations. *Chaos Solitons Fractals* **2019**, *125*, 194–200. https://doi.org/10.1016/j.chaos.2019.05.029

[9] Aghajani, A.; Jalilian, Y.; Trujillo, J. J. On the Existence of Solutions of Fractional Integro-Differential Equations. *Fract. Calc. Appl. Anal.* **2012**, *15* (1), 44–69. https://doi.org/10.2478/s13540-012-0004-8

[10] Ma, X.; Huang, C. Numerical Solution of Fractional Integro-Differential Equations by a Hybrid Collocation Method. *Appl. Math. Comput.* **2013**, *219*(12), 6750–6760. https://doi.org/10.1016/j.amc.2013.01.016

[11] Eslahchi, M. R.; Dehghan, M.; Parvizi, M. Application of the Collocation Method for Solving Nonlinear Fractional Integro-Differential Equations. *J. Comput. Appl. Math.* **2014**, *257*, 105–128. https://doi.org/10.1016/j.cam.2013.08.021

[12] Sene, N. Fundamental Results about the Fractional Integro-Differential Equation Described with Caputo Derivative. *J. Funct. Spaces* **2022**, *2022*, 9174488. https://doi.org/10.1155/2022/9174488

[13] Sun, H.; Zhang, Y.; Baleanu, D.; Chen, W.; Chen, Y. A New Collection of Real-World Applications of Fractional Calculus in Science and Engineering. *Commun. Nonlinear Sci. Numer. Simul.* **2018**, *64*, 213–231. https://doi.org/10.1016/j.cnsns.2018.04.010

[14] Diethelm, K. *The Analysis of Fractional Differential Equations: An Application-Oriented Exposition Using Differential Operators of Caputo Type*; Springer: Berlin, Germany, 2010. https://doi.org/10.1007/978-3-642-14574-2

[15] Baleanu, D.; Diethelm, K.; Scalas, E.; Trujillo, J. J. *Fractional Calculus: Models and Numerical Methods*; World Scientific: Singapore, 2012. https://doi.org/10.1142/8180

[16] Patnaik, S.; Hollkamp, J. P.; Semperlotti, F. Applications of Variable-Order Fractional Operators: A Review. *Proc. R. Soc. A* **2020**, *476*(2234), 20190498. https://doi.org/10.1098/rspa.2019.0498

[17] Li, C.; Zeng, F. *Numerical Methods for Fractional Calculus*; CRC Press: Boca Raton, FL, 2015. https://doi.org/10.1201/b18588

[18] Garrappa, R. Numerical Solution of Fractional Differential Equations: A Survey and a Software Tutorial. *Mathematics* **2018**, *6*(2), 16. https://doi.org/10.3390/math6020016

[19] Stynes, M.; O'Riordan, E.; Gracia, J. L. Error Analysis of a Finite Difference Method on Graded Meshes for a Time-Fractional Diffusion Equation. *SIAM J. Numer. Anal.* **2017**, *55*(2), 1057–1079. https://doi.org/10.1137/16M1082329

[20] Wang, Y.; Zhou, X. An Efficient Numerical Method Based on Bell Wavelets for Solving the Fractional Integro-Differential Equations with Weakly Singular Kernels. *Fractal Fract.* **2024**, *8*(2), 74. https://doi.org/10.3390/fractalfract8020074

[21] Behera, S.; Saha Ray, S. Euler Wavelets Method for Solving Fractional-Order Linear Volterra–Fredholm Integro-Differential Equations with Weakly Singular Kernels. *Comput. Appl. Math.* **2021**, *40*, 192. https://doi.org/10.1007/s40314-021-01530-5

[22] Keshavarz, E.; Ordokhani, Y.; Razzaghi, M. A Fast Numerical Algorithm Based on the Taylor Wavelets for Solving the Fractional Integro-Differential Equations with Weakly Singular Kernels. *Math. Methods Appl. Sci.* **2019**, *42*(13), 4427–4443. https://doi.org/10.1002/mma.5647

[23] Nemati, S.; Lima, P. M. Numerical Solution of Nonlinear Fractional Integro-Differential Equations with Weakly Singular Kernels via a Modification of Hat Functions. *Appl. Math. Comput.* **2018**, *327*, 79–92. https://doi.org/10.1016/j.amc.2017.12.003

[24] Yi, M.; Huang, J. CAS Wavelet Method for Solving the Fractional Integro-Differential Equation with a Weakly Singular Kernel. *Int. J. Comput. Math.* **2015**, *92*(8), 1715–1728. https://doi.org/10.1080/00207160.2014.982674

[25] Zhu, L.; Wang, Y. SCW Method for Solving the Fractional Integro-Differential Equations with a Weakly Singular Kernel. *Appl. Math. Comput.* **2016**, *275*, 72–80. https://doi.org/10.1016/j.amc.2015.11.090

[26] Mohammed, J. K.; Khudair, A. R.; Pandian, N. R. Numerical Solution of Fractional Integro-Differential Equations via Fourth-Degree Hat Functions. *Iraqi J. Comput. Sci. Math.* **2023**, *4*(2), 10–30. https://doi.org/10.52866/ijcsm.2023.4.2.2

[27] Mahdy, A. M. S.; Nagdy, A. S.; Mohamed, D. S. H. Solution of Fractional Integro-Differential Equations Using Least Squares and Shifted Legendre Methods. *J. Appl. Math. Comput. Mech.* **2024**, *23* (1), 59–70. https://doi.org/10.17512/jamcm.2024.1.06

[28] Wang, Y.; Zhou, X. An Efficient Numerical Method Based on Bell Wavelets for Solving the Fractional Integro-Differential Equations with Weakly Singular Kernels. *Fractal Fract.* **2024**, *8*(2), 74. https://doi.org/10.3390/fractalfract8020074

[29] Nemati, S.; Lima, P. M.; Ordokhani, Y. Numerical Solution of a Class of Two-Dimensional Nonlinear Volterra Integral Equations Using Legendre Polynomials. *J. Comput. Appl. Math.* **2013**, *242*, 53–69. https://doi.org/10.1016/j.cam.2012.10.028

[30] Brunner, H. *Volterra Integral Equations: An Introduction to Theory and Applications*; Cambridge University Press: Cambridge, U.K., 2017. https://doi.org/10.1017/9781108235802

[31] Chen, Y.; Tang, T. Convergence Analysis of the Jacobi Spectral-Collocation Methods for Volterra Integral Equations with a Weakly Singular Kernel. *Math. Comput.* **2010**, *79*(269), 147–167. https://doi.org/10.1090/S0025-5718-09-02267-2

[32] Alkan, S.; Hatipoglu, V. F. Approximate Solutions of Volterra–Fredholm Integro-Differential Equations of Fractional Order. *Tbilisi Math. J.* **2017**, *10*(2), 1–13. https://doi.org/10.1515/tmj-2017-0001

[33] Shu, X. B.; Wang, Q. The Existence and Uniqueness of Mild Solutions for Fractional Differential Equations with Nonlocal Conditions of Order $1 < \alpha < 2$. *Comput. Math. Appl.* **2012**, *64*(6), 2100–2110. https://doi.org/10.1016/j.camwa.2012.02.018

[34] Taghipour, M.; Aminikhah, H. A Fast Collocation Method for Solving the Weakly Singular Fractional Integro-Differential Equation. *Comput. Appl. Math.* **2022**, *41*, 142. https://doi.org/10.1007/s40314-022-01834-3

ASEAN
Journal of Scientific and Technological Reports
Online ISSN:2773-8752

Research article

Facial Emotion Recognition – A Comprehensive Review of Deep Learning and Traditional Learning Approaches with Emerging Challenges

Sushilkumar Salve[1*], Shubham Kumar[1], Irfan Shaikh[1], Pranay Gawade[1], Sujit Ramesh Borey[2], and Puja Padiya[3]

[1] Department of Electronics and Telecommunication Engineering, Sinhgad Institute of Technology, Lonavala, Maharashtra, India
[2] Department of Electronics and Communication Engineering Visvesvaraya National Institute of Technology (VNIT), Nagpur, Maharashtra, India
[3] Xavier Institute of Engineering, Mumbai, Maharashtra, India
* Correspondence: sushil.472@gmail.com

Citation:
Salve, S.; Kumar, S.; Shaikh, I.; Gawade, P.; Borey R.S.; Padiya, P. Facial emotion recognition – A comprehensive review of deep learning and traditional learning approaches with emerging challenges. *ASEAN J. Sci. Tech. Report.* **2026**, *29*(7), e262457. https://doi.org/10.55164/ajstr.v29i7.262457

Article history:
Received: October 30, 2025
Revised: April 11, 2026
Accepted: April 12, 2026
Available online: June 15, 2026

Publisher's Note:
This article is published and distributed under the terms of the Thaksin University.

Abstract: In the domains of computer vision and artificial intelligence, facial expression-based emotion recognition (FER) has emerged as a key research area and industrial challenge. Its growing importance is evident in applications such as intelligent surveillance, healthcare monitoring, interactive systems, and mental health assessment. This review systematically examines 95 research papers published between 2014 and 2024, focusing exclusively on studies employing facial imagery for FER. The reviewed works encompass traditional machine learning, deep learning, and hybrid approaches, and analyze their methodologies for preprocessing, data augmentation, and temporal feature extraction. Traditional machine learning methods such as SVM, KNN, and Random Forest achieved average accuracies ranging from 85% to 93%, with the best reaching 99% on the CK+ dataset. Deep learning architectures, including VGG16, ResNet-50, MobileNetV2, and DenseNet-161, reported accuracy improvements of up to 99.5% across benchmark datasets such as FER2013 (35,887 images), CK+, JAFFE, KDEF, and RAF-DB (≈40,000 images). Hybrid models combining CNN feature extraction with classifiers such as SVM and GMM achieved 3–6% improvements in recognition accuracy over standalone CNN or SVM systems, reaching 99.69% on CK+ and 99.53% on JAFFE. By comparing benchmark datasets, algorithms, and performance metrics, this study highlights the significant evolution from handcrafted feature-based systems to fully automated deep learning pipelines. The findings provide a quantitative synthesis of the current state of FER research, offering both newcomers and advanced researchers a comprehensive understanding of the field's progress, challenges, and future opportunities.

Keywords: Facial expression recognition (FER); deep learning; hybrid models; temporal feature extraction; motion classification.

1. Introduction

A study shows that approximately 67% of human communication is nonverbal, leaving only 33% for spoken language [1, 2]. Facial expressions are the primary means of nonverbal communication, enabling people to interpret their emotions and intentions. Along with vocal tone, these expressions help identify states such as happiness, sadness, or anger. Because facial expressions

carry strong emotional meaning, their study has expanded rapidly in recent decades, with applications ranging from perceptual science and affective computing to computer animation and cognitive research. Furthermore, facial expression analysis has gained significance in mental health, psychology, and psychiatry [3]. The starting point of any Facial Emotion Recognition (FER) system is face detection, which isolates the face or its features from single images or video streams. Since images often contain complex backgrounds, preprocessing becomes essential [4]. While humans effortlessly identify faces and expressions even in such conditions, machines without proper training face challenges [5,6]. The primary goal of face detection is to distinguish useful facial regions from irrelevant elements. Its applications include surveillance video systems, gesture-based interactive recognition, automated photography, gender detection, tagging, and teleconferencing [7,8]. Many current methods operate primarily on grayscale inputs, though a limited number can process color images as well. Pixel-based approaches often fail to distinguish faces from similar regions such as hands, whereas window-based methods are restricted in analyzing multi-view characteristics [9,10]. For this reason, model matching remains the most prevalent technique for face detection in FER pipelines.

The main objective of FER is to build relationships between facial expressions and the internal feelings they represent [11]. Conventionally, FER systems involve two fundamental processes: emotion detection and feature extraction. Image preprocessing, including normalization, scaling, cropping, and face localization, is a critical step for ensuring accuracy [12]. Removing irrelevant background elements narrows the focus to facial regions. Feature extraction then follows, with common methods such as Discrete Wavelet Transform (DWT) and Linear Discriminant Analysis (LDA) being widely used [13]. Once features are obtained, Neural Networks (NN) and other machine learning models are typically employed for classification. This stage also benefits from preprocessing steps such as alignment and rotation correction [14]. Cascade classifiers, particularly those based on AdaBoost, are highly reliable for face detection [15]. FER often combines geometric and appearance-based approaches. Geometric techniques, for instance, map facial landmarks into vectors containing positional attributes such as coordinates, angles, and distances [16]. To better capture facial variations, spatial analysis of external features has also been employed [17]. Motion characteristics play a significant role in recognizing dynamic expressions, with classifiers designed to handle a diverse set of emotions [18].

In recent years, attention has shifted towards deep learning architectures for FER [19]. Convolutional Neural Networks (CNNs), in particular, have demonstrated better accuracy than classical methods such as Recurrent Neural Networks (RNNs) and Support Vector Machines (SVMs), though they are resource-intensive [20]. Large, well-annotated datasets are vital for improving training performance. FER research has also expanded to related tasks, such as predicting age and gender from facial cues [21,22]. Smart healthcare applications showcase the practical advantages of FER, in which intelligent cameras continuously capture patients' facial data and send it to cloud platforms for monitoring [23]. In addition, lightweight architectures designed for embedded devices, such as the Jetson Nano, have potential applications in law enforcement, particularly for suspect identification [24]. Among all the approaches, CNN-based systems are considered the most advanced, with specialized architectures created for emotion recognition in static images [25]. To further improve recognition rates, researchers suggest networks containing multiple convolutional and hidden layers [26]. Preprocessing remains vital for removing noise and extracting key features during pretraining [27]. Recent work has also examined how factors such as gender, activity, and occupation influence emotional expression in interactive settings, such as robotics labs and classrooms.

Figure 1 presents a pictorial view of the growing research interest in emotion recognition over 15 years, from 2010 to 2025. This is a plot of a distinct, strong, increasing trend, showing an exponential rise in publication numbers. This is an indication of the field's growing significance and the rapid development of computational models and applications that have attracted increasing interest from the scientific community. Figure. 2 provides a conceptual delineation of the major uses of emotion recognition technology in the principal sectors of healthcare and teaching. As the data shows, healthcare usage, including patient monitoring and therapeutic assistants, is a principal field of application. In the teaching arena, technology is used through applications such as monitoring student participation and enabling personalized learning. This illustration highlights the real-world application and societal contribution of FER systems. In summary, the growing integration of emotion-aware systems into intelligent environments reflects a broader trend toward human-

centered artificial intelligence. As FER continues to advance through deep learning and hybrid models, its potential extends across smart healthcare, adaptive education, and intelligent surveillance systems. However, real-world deployment still faces challenges related to data privacy, cultural variability, and interpretability. Thus, this review aims to consolidate current findings, compare methodologies, and identify emerging opportunities and challenges to guide future research in developing reliable and ethically responsible FER systems.

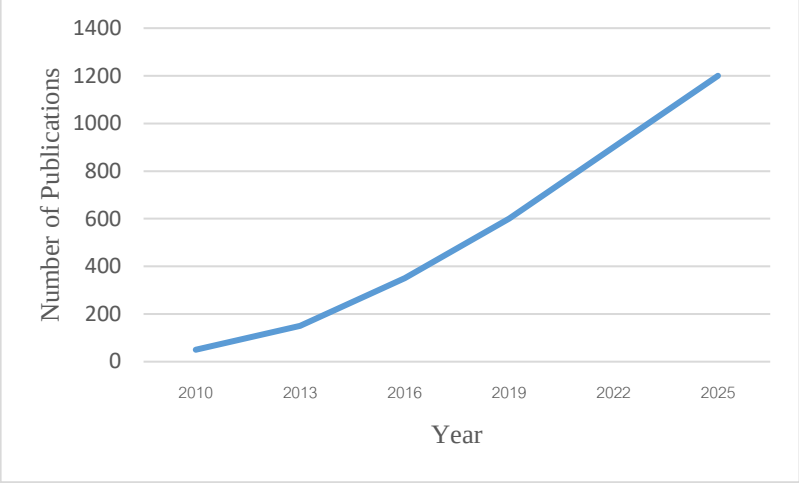


Figure 1. Growth of publications in emotion recognition [4,19,30].

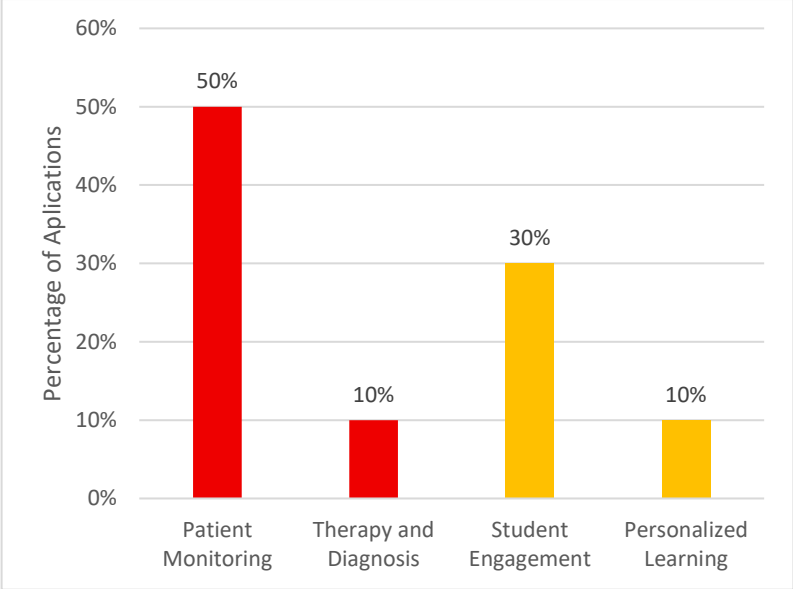


Figure 2. Global applications of emotion recognition in education/healthcare.[3, 23, 28]

2. Method of Review

The methodology adopted for this review follows a systematic literature review (SLR) framework designed to synthesize and critically evaluate recent advances in Facial Emotion Recognition (FER) across machine learning, deep learning, and hybrid paradigms. The study focuses on applications of FER in healthcare monitoring, intelligent surveillance, behavioral analytics, education, and adaptive user interfaces. The review process was conducted in accordance with established SLR guidelines and comprises three key stages: literature search, screening and selection, and analysis and synthesis.

2.1 Literature Search Strategy

Relevant publications were systematically retrieved from five major scientific databases**:** IEEE Xplore**,** ScienceDirect**,** SpringerLink**,** Wiley Online Library**,** and Google Scholar**.** To ensure comprehensive coverage, the following Boolean keyword combinations were used during the search:
("Facial Emotion Recognition" OR "Facial Expression Recognition") AND ("Machine Learning" OR "Deep Learning" OR "Hybrid Models" OR "Affective Computing") AND ("Datasets" OR "Feature Extraction" OR "Preprocessing").

The search covered 10 years (2014–2024) and captured both foundational and state-of-the-art studies. Additional manual searches were conducted in conference proceedings such as *IEEE ICMEAS* and *CVPR* to include the most recent advancements.

2.2 Inclusion and Exclusion Criteria

The retrieved articles were filtered using the following criteria:
Inclusion Criteria:

- Studies focused explicitly on facial emotion or facial expression recognition using machine learning, deep learning, or hybrid techniques.
- Peer-reviewed journal or conference papers published between 2014 and 2024.
- Articles that included quantifiable performance metrics (accuracy, precision, recall, or F1-score).
- Studies employing publicly available datasets such as FER2013, CK+, JAFFE, RAF-DB, MMI, and KDEF.

Exclusion Criteria:

- Non-English publications, theses, and unpublished manuscripts.
- Studies that focused solely on speech or gesture emotion recognition without facial analysis.
- Duplicate or overlapping studies were retrieved from multiple databases.

2.3 Screening and Filtration Process

An initial pool of approximately 230 publications was identified. After title and abstract screening, 120 studies were shortlisted for full-text evaluation. After applying the inclusion and exclusion criteria, 95 papers were selected for detailed analysis. Each paper was examined in terms of:

1. Dataset characteristics and preprocessing strategies.
2. Feature extraction and augmentation techniques.
3. Model architecture (traditional, deep, or hybrid).
4. Performance metrics and benchmarking protocols.

2.4 Analysis and Synthesis

The selected studies were categorized into three methodological groups—traditional machine learning, deep learning, and hybrid approaches—to enable structured comparison. Quantitative data, such as accuracy and dataset size, were tabulated for benchmarking, while qualitative aspects, such as robustness, computational cost, and ethical challenges, were synthesized thematically. Statistical trends and performance comparisons were then consolidated to provide a holistic overview of the evolution and current state of FER research.

2.5 Keywords and search strategy

Literature searching was supplemented with a combination of prespecified keywords and Boolean operators to achieve a relevant, focused retrieval of studies. The following key search terms were used:

2.2.1 "Facial Expression Recognition (FER)" AND "Internet of Things (IoT)".

2.2.2 "Deep Learning".

2.2.3 " Hybrid Models" AND "Affective Computing".

2.2.4 "Temporal Feature Extraction".

2.2.5 "Emotion Classification" AND "Benchmark Datasets."

The searches were performed across all fields (keyword, title, abstract, and full text, where available). Truncation and wildcard characters were used to capture variation in keywords (e.g., sensor, sensing, sensors).

3. Machine Learning Approaches

One common challenge is that while the main existing systems perform effectively on images from a regulated image environment, the model's performance may decline on difficult datasets due to increased image variation and partially visible facial regions. To address the concern, one approach uses the Histogram of Oriented Gradients (HOG) descriptor. The approach starts with the initial processing of the input image to identify the reference region for extracting the critical content, followed by the development of a face emotion classifier using the RF algorithm. This method's effectiveness and accuracy were demonstrated through analysis on the Japanese Female Facial Emotions (JAFFE) Database [32].

3.1 Introduction to different machine learning approaches

Within the domain of facial emotion recognition, several machine learning algorithms have been extensively explored by researchers. Among these, Support Vector Machine (SVM), K-Nearest Neighbors (KNN), and Random Forest (RF) are the most frequently used due to their simplicity, robustness, and effective classification performance on small and medium-sized datasets. For instance, one study applied facial expression recognition to classify consumer gratification with products and services. Their architecture involved three primary stages: data collection (including user satisfaction, age, gender, and facial expressions), classification using machine learning algorithms, and a final model assessment to confirm accuracy [33].

X, Liu et al. proposed a method for sentiment analysis of subjects by employing two new geometry-based attributes: the landmark curve and the vectorized landmark, extracted from multiple facial regions related to facial muscle activity [34]. N. Iromini et al. implemented an innovative geometric extraction technique that uses six different distance measurements to compute facial features that optimally reflect one emotion, followed by the application of a decision tree to the JAFFE dataset. This system could distinguish between seven discrete emotions and achieved an identification rate of 89.20% on the JAFFE database, whereas the COHEN database achieved an identification rate of 90.61% [36]. For face detection, investigators have applied Principal Component Analysis (PCA) to identify faces using a reduced set of attributes and have utilized the KNN algorithm to derive features from the JAFFE dataset, achieving 85.71% accuracy after image preprocessing [37].

Other studies have focused on rigorous validation and direct classifier comparisons. H. I. et al. applied one-way analysis of variance and fivefold cross-validation ($p < 0.01$) to confirm the precision of the derived features, ultimately training KNN and Decision Tree (DT) classifiers to identify multiple categories of facial emotional states. KNN recorded a mean accuracy of 98.03%, whereas DT averaged 97.21% rate [38]. A comprehensive examination of a separate experiment revealed that the approach performed best when an SVM classifier was used. The accuracy declined to 79.98% with KNN and rose to 82.96% when Multilayer Perceptron (MLP) was employed [39]. To enhance performance, Linear Discriminant Analysis (LDA) has been used to improve SVM classification, achieving 99% accuracy and a 98% F1-score. Similarly, B. Tamer Ghareeb et al. integrated SVM, Random Forest, KNN, and Naive Bayes algorithms, which exhibited varying degrees of accuracy [40].

Another enhancement technique proposed by B. Tamer et al. involves using Principal Component Analysis (PCA) approach on effective Haar Face features to reduce dimensionality, allowing the resulting Eigenvectors to be used with an SVM classifier to detect fundamental human emotions [41]. SVM methods and Active learning have also been adopted to recognize human facial emotions by categorizing facial action units into classifications [42]. A study used the Yale Face dataset, which includes 11 human facial states, such as normal, happy, sad, sleepy, and surprised. Using sensitivity, precision, F-measure, G-mean, and accuracy as performance evaluation metrics, the proposed BGA-RF method achieved a maximum precision of 96.03%. The experimental outcomes confirmed the method’s efficacy, highlighting its enhanced accuracy compared to similar methods [43].

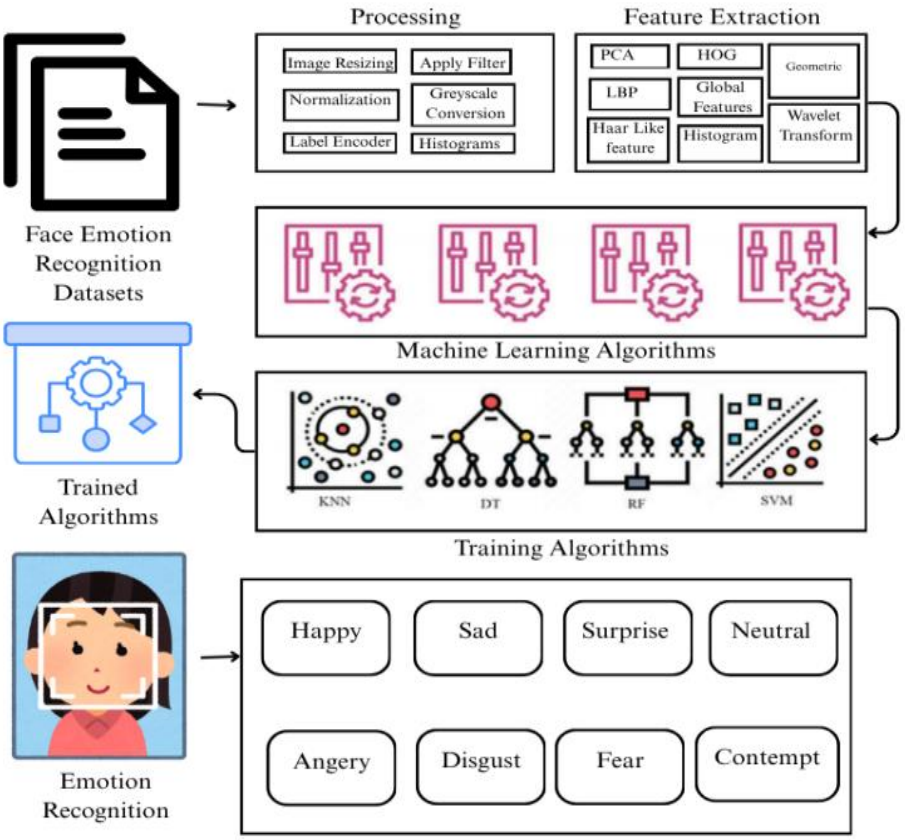


Figure 3. Computational Approaches to FER using Machine Learning.

Figure 3 shows a typical pipeline of an FER system with machine learning. This pipeline is activated by a labeled image dataset, which is prepared (e.g., resizing, normalization) to bring the images into a standard format. Then, discriminative face features are extracted through methods such as HOG, LBP, or PCA. These extracted face features are now passed to a Machine Learning Algorithm for training, e.g., SVM, KNN, or a Random Forest. This trained algorithm can now accept a new face image and return its class, indicating the emotion it belongs to, such as happy, sad, or angry.

Table 1. Comprehensive evaluation of machine learning for FER system.

Reference	Databases	Techniques	Properties	Emotion
[31]	FECR	SVM	LDA, PCA	6
[32]	JAFFE	RF	Histograms of oriented gradient (HOG)	7
[33]	Private	SVM	No	7
[34]	CK+, MUG	SVM	Geometric	8
[35]	CK+, JAFFE	CART	Geometric and global features	7
[36]	JAFFE	KNN	PCA	7
[37]	Private	KNN	Haar-like features	6
[38]	CK+	SVM	LBP, Gabor filter, PCA	7
[39]	CK+	SVM	PCA	7
[40]	AffectNet	SVM	Grid search	8
[41]	FER 13	LR	No	5
[42]	CK+	SVM	PCA and LBP	7
[43]	Yale faces	RF	Histograms of oriented gradient (HOG)	11

Table 1 provides a comparative overview of machine learning techniques used for facial emotion recognition (FER) across multiple benchmark datasets. The studies used algorithms such as SVM, KNN, RF, CART, and LR, often combined with feature extraction methods such as PCA, LBP, Gabor filters, and geometric features**.** The number of recognized emotions ranged from 5 to 11, depending on the dataset and feature type. Notably, SVM emerged as the most widely used classifier due to its strong generalization across datasets such as CK+, JAFFE, and AffectNet**.** Overall, this comparison highlights how the choice of features and classifiers significantly influences FER system performance. Note: The "Emotion" column indicates the number of discrete emotional classes recognized in each study (e.g., six basic emotions — happiness, sadness, anger, fear, surprise, and disgust — or extended sets including neutral and contempt)

4. Deep Learning Approaches

Deep learning has witnessed remarkable progress in Facial Emotion Recognition (FER), with researchers achieving high accuracy using various pre-trained models and novel architectures. For instance, one methodology that used pre-configured models found that DenseNet-161 achieved the highest accuracy on both the JAFFE and Karolinska Directed Emotional Faces (KDEF) test sets, reaching 99.52% and 96.51%, respectively, using a 10-fold cross-validation method [44]. Z. Y. Huang et al. have developed a high-performing model, the Facial Emotion Recognition using Convolutional Neural Networks (FERC) model, which uses an Expressional Vector (EV) and a two-level CNN to identify five distinct facial gestures, attaining an accuracy rate of 96% on a database of 10,000 images [45]. In a comprehensive evaluation across 25 cutting-edge techniques on 5 standard datasets (including JAFFE and CK+), one proposed methodology was found to perform better than all other advanced methods on every dataset [46]. For specific real-time applications, deep learning models have been rigorously compared. A study proposed by S. Gupta et al. focused on measuring online learners' engagement by analyzing facial expressions compared to Inception-V3 (89.11% accuracy), VGG19 (90.14%), and ResNet-50. The results showed that ResNet-50 surpassed the other models, achieving 92.32% accuracy in real-time facial emotion categorization on widely used benchmark datasets, namely the Real-world Affective Faces Database (RAF-DB), CK+, and FER-2013 [47].

4.1 Different methodologies in deep learning

A major focus in FER research is creating efficient, lightweight networks that do not sacrifice accuracy. MobileNetV2, a CNN model known for its speed, produces quick and accurate real-time output when integrated with supervised transfer learning, an island loss, and a joint supervision strategy, surpassing other approaches on the CK+, JAFFE, and FER2013 datasets [48]. Building on this, a lightweight model called A-MobileNet integrates an attention module into MobileNetV1 to enhance local feature extraction. By combining softmax loss and center loss to tune the model's parameters, this strategy improves accuracy while maintaining the original MobileNet series' model size, demonstrating superior efficiency on the FERPlus and RAF-DB datasets [49].

Beyond lightweight models, researchers have improved existing architectures. C. Dong et al. proposed modifications to the VGG16 network by replacing its three dense layers with one dense layer and two convolutional layers, and switching to local-based adaptive pooling before training on the Static Facial Expressions in the Wild (SFEW) and RAF-DB datasets [51]. Innovations in residual networks include a residual masking network, which merges a deep residual network with a U-Net-like design to retain high accuracy on the Versatile Elastic Multi-modal (VEMO) and FER2013 datasets [52]. B. Li et al.'s method offers a way to extract attributes from ResNet-50 that exhibit superior performance in experimental simulations compared to the most popular existing models [53]. Furthermore, a deep learning approach leveraging attentional convolutional networks has been shown to surpass previous models by precisely identifying and focusing on important facial attributes across datasets such as CK+, FER-2013, JAFFE, and FERG [54].

A key challenge is that existing models are often inadequate for real-world situations involving inconsistent lighting conditions, partially hidden faces, and random noise in images. To solve this, L. Xiong et al. have proposed integrating a Context Transformer (CoT) module with CNN and Vision Transformer (ViT) architectures [55]. This improves the model's resilience to illumination and its capability to uncover intricate dependencies among local characteristics in intricate situations [56]. Advanced techniques proposed by

Z. Gao et al. and M. Verma et al. include a hierarchical attention architecture incorporating a progressive feature fusion methodology, a selective kernel network, and an innovative feature descriptor called the Cross-Centroid Ripple Pattern (CRIP) [57,58]. For specialized conditions, researchers have developed a method for detecting faces using drones to improve identification in poor lighting or aerial scenarios [59]. A method for identifying emotion from masked facial images using CNN feature analysis and low-light image augmentation [60].

Many projects have focused on building deep learning frameworks for specific tasks. E. Pranav et al. in their study have aimed to build a Deep Convolutional Neural Network (DCNN) that can recognize a set number of distinct emotions, often using manually compiled photo collections for training and verification [61]. A real-time face emotion classification and recognition using a deep learning model study demonstrated this by training a CNN framework on the JAFFE and FER-2013 datasets, achieving 98.64% and 70.01% accuracy, respectively [62]. Real-time recognition systems have applications in security, healthcare, and safety assessments, with some systems using a sequential approach that combines Haar cascade detection for facial identification with a Keras CNN model for emotion analysis. These deep learning approaches are attracting considerable attention from the research community and are becoming crucial for classification, enabling innovative biomedical applications and even systems that detect individuals with autism instantaneously [63]. Even with extensive research, facial expressions remain intricate and dynamic, hindering accurate identification. Based on both laboratory and real-world findings, it is evident that deep learning holds significant potential for the future of facial emotion recognition. The field is constantly advancing, with researchers now refining models that build on ConvNeXt and Vision Transformer, using improved hyperparameters on new datasets [64].

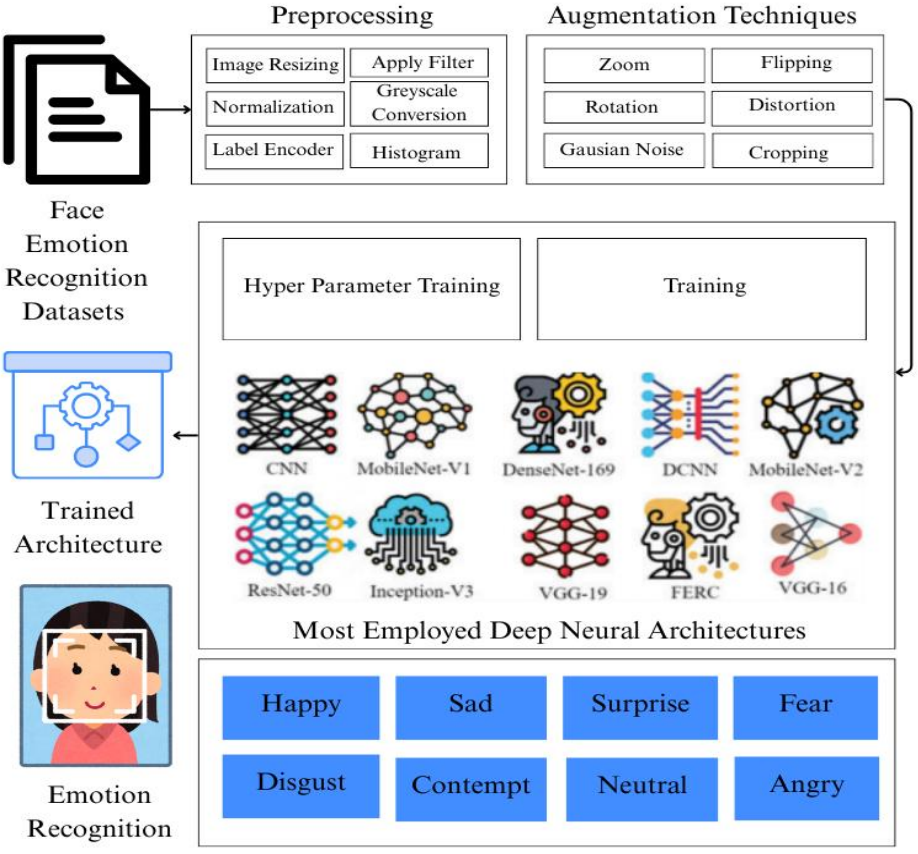


Figure 4. Computational Approaches to FER using Deep Learning

Figure 4 illustrates an end-to-end, complete pipeline of an FER system that is deep learning-based. A large image Dataset is first made ready by preprocessing (e.g., normalization, resizing) and augmentation (e.g., rotation, flipping) to make it robust. Such prepared images are then fed directly to a deep neural network, e.g., a CNN, ResNet, or even MobileNet, to train and perform hyperparameter tuning. Finally, the trained

architecture is ready to classify emotions from new facial images. Note: The "Emotion" column indicates the number of discrete emotional classes recognized in each study (e.g., six basic emotions — happiness, sadness, anger, fear, surprise, and disgust — or extended sets including neutral and contempt)

Table 2. Comprehensive evaluation of deep learning for FER system

Reference	Datasets	Methods	Emotions
[44]	NIST, CMU, and Caltech face	FERC	7
[46]	FERPlus and RAF-DB	MobileNet	7
[47]	FER2013 and CK+	VGG16	7
[49]	JAFFE,CK+ and FER2013	MobileNet V2	7
[51]	Random dataset, FER-2013	MobileNet-V1	7
[52]	CK	ResNet-50	7
[53]	KDEF	VGG16	6
[54]	KDEF and JAFFE	DenseNet-161	7

Table 2 summarizes the performance of various deep learning models for facial emotion recognition (FER) across different datasets. The studies primarily focused **on** CNN-based architectures such as VGG16, ResNet-50, MobileNet (V1 and V2), DenseNet-161, and FERC**,** across well-known datasets including FER2013, CK+, JAFFE, KDEF, RAF-DB, and NIST. Most approaches focused on recognizing six to seven basic emotions, demonstrating the robustness of convolutional neural networks in learning spatial and hierarchical facial features. Among these, lightweight models such as MobileNet variants offered efficient performance suitable for real-time FER applications, while deeper architectures such as VGG16 and DenseNet-161 achieved higher accuracy on more complex datasets.

5. Hybrid Approaches

Hybrid learning in FER often involves integrating the powerful feature extraction of deep networks with the effectiveness of traditional classifiers. For instance, the Hybrid facial emotion recognition using CNN-based features study used a Deep Belief Network (DBN) to create a comprehensive video feature representation by averaging segment-level features, and then leveraged a Support Vector Machine (SVM) for classification. The approach was particularly useful for complex scenarios, such as interpreting emotions from concealed faces [65]. It's known that concealing the mouth complicates emotion recognition, and to address this, H. M. Shahzad et al. used prominent deep learning models such as VGG-16 and AlexNet for feature extraction, followed by multiple classifiers to improve predictive accuracy [66]. Another method employed facial recognition software to derive extract Network Difference Features (NDF) by analyzing connections between adjacent locations, before using a random forest classifier to sort expressions into seven groups [67].

5.1 Different methodologies in deep learning

More intricate integrations involve combining various kinds of neural networks. To capture the geometric interactions among facial landmarks, one approach integrates Attention Long Short-Term Memory (ALSTM) networks with Spatial Attention Convolutional Neural Networks (SACNNs) to develop robust integrated features for expression identification [68]. The concept of Deep Hybrid Learning (DHL) involves combining deep learning and transfer learning methods, and one study compared models such as CNN, LSTM, Inception, and ResNet to categorize facial emotions as happy or angry [69]. Another successful strategy is the fusion of shallow and deep features. Cross-database studies have demonstrated the immense potential of this approach, yielding promising results compared with other cutting-edge models [70]. A specific example of this is a combined method that uses the energy-entropy-based Dual-Tree M-Band Wavelet Transform (DTMBWT) for high-precision feature extraction, which is then classified using a Gaussian mixture model (GMM) [71].

Several advanced hybrid systems have been developed for unique applications. One state-of-the-art system sorts facial motion flows by combining CNN-based classification of facial geometry motion and SVM-based classification of facial motion, achieving much higher performance than individual classifiers [72].

Another model introduces a deep learning approach that uses one CNN to assess a primary emotion (such as neutral or angry) and a subsequent CNN to determine the subordinate emotion [73]. To achieve results comparable to human assessors, a Gaussian Mixture Model (GMM) and a Deep Neural Network (DNN) were tested in .in under both low- and high-noise conditions [74]. Furthermore, in scenarios where facial expressions may be fundamentally misleading, a multimodal emotion recognition paradigm is highly effective at accurately determining emotions, with performance that surpasses or compares favorably with that reported in the existing literature [75]. A comprehensive investigation of the efficacy of Hybrid learning for the FER system is presented in Table 3.

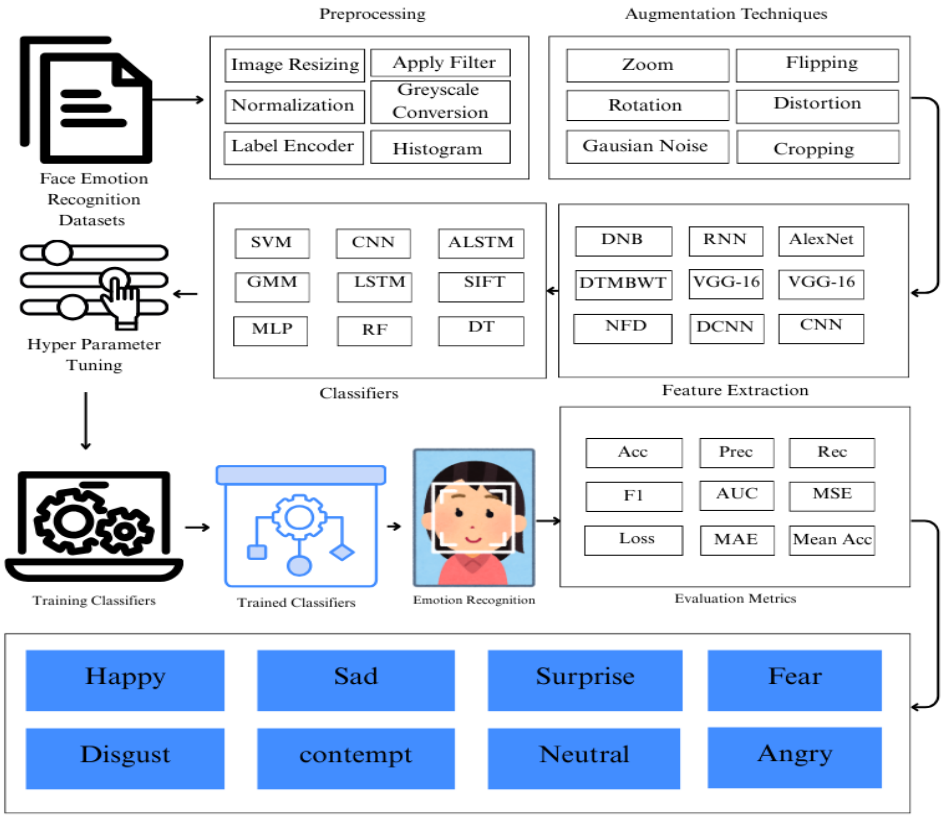


Figure 5. Computational Approaches to FER using Hybrid Learning

Figure 5 illustrates a hybrid FER pipeline that divides feature extraction from classification. Following initial Preprocessing and Augmentation of a prepared Dataset, a deep network (e.g., a CNN or VGG-16) serves as a Feature Extractor. These higher-level features are passed through a distinct, sometimes traditional, Classifier (e.g., SVM, Random Forest) to produce an emotion prediction. The model is optimized through training and confirmed using evaluation metrics.

Table 3. Comprehensive evaluation of hybrid learning for FER system.

Reference	Datasets	Feature extraction	Segmentation	Emotions
[65]	BAUM-1s, RML, and MMI	Deep belief network (DBN)	SVM	6
[66]	M-LFW-FER	AlexNet and VGG-16, CNN	SVM	7
[67]	SFEW, RAF	Neighborhood difference features NFD	RF	7
[68]	FER2013, CK+, and JAFFE	Spatial attention convolutional neural network (SACNN)	Long short-term memory networks with attention mechanism (ALSTMs)	7
[69]	Multisource	CNN	LSTM	6
[70]	CK+	CNN	-	7
[71]	JAFFE	Dual-tree M-band Wavelet Transform (DTMBWT)	Gaussian Mixture Model (GMM)	7
[72]	CK+, BU4D	CNN	SVM	7
[73]	JAFFE, FER2013	CNN	CNN	7
[74]	ESD	Gaussian Mixture Model and Deep Neural Network (GMM-DNN)	SVMs and MLP	6
[75]	LUMED-2, DEAP	CNN	DT	3

Table 4. Benchmarking Datasets for Facial Emotion Recognition Systems.

Dataset	Description
MUG [76]	The database contains details of 86 Caucasian individuals aged 20-35 years. Among them, 35 are women, and 51 are men, with some participants being clean-shaven. Apart from seven entries found in the latter portion of the dataset, no subjects were related to sports. The few irregularities observed were stray facial hairs. In some images in the second part, a hand was partially covering the face.
RAF-DB [77]	The Real-world Affective Faces Database (RAF-DB) is designed for facial emotion analysis. It contains 39,672 images annotated by 40 independent evaluators, covering both basic and compound emotional expressions. The dataset includes individuals of varying ages, genders, and ethnicities, as well as a wide range of lighting conditions. It also accounts for different types of obstructions, such as glasses, self-obstruction, or facial hair, and incorporates subsequent processing steps, such as filters and special effects.
MMI [78]	This dataset contains more than 2,900 videos and high-definition static images of 75 individuals. Event coding tracks the presence of Action Units (AUs) in video sequences, while incomplete-frame encoding indicates whether an AU is at the onset, peak, offset, or neutral stage within a given frame. In addition, limited annotations are provided for multimodal entertainment purposes. The researchers can freely access the database.
FER2013 [79]	The FER+ dataset classifies images into neutral, surprised, angry, disgusted, sad, contemptuous, and fearful categories. It serves an enhanced version of the initial FER dataset. In addition to the standard FER labels, FER+ includes supplementary annotations. These annotations are generated by averaging responses from 10 independent crowdsourced evaluators, resulting in more reliable ground-truth labels for emotions in static images than in the original FER dataset. Using multiple annotators per image also allows researchers to derive a probabilistic model of each face's emotions.
KDEF [80]	The dataset consists of colour facial images without visible hairlines, taken from the Karolinska Directed Emotional Faces (KDEF) database. It includes 490 photographs representing 70 individuals, evenly divided into 35 males and 35 females. As reported by Lundqvist et al. (1998), the facial configurations captured cover a range of intensities, from neutral to a full emotional display, including disgust, happiness, surprise, fear, and sadness. All images are presented in a frontal view.

A comparative examination of learning techniques uncovers the most important trade-off between hand and algorithmic methods. Classical machine learning involves handcrafted feature engineering, so it is efficient for smaller datasets, where domain knowledge can guide simpler algorithms with lower computational expense. Conversely, deep learning learns features automatically using complex neural networks that perform better on enormous datasets but require substantial computational power and large amounts of data to learn well. Hybrid learning addresses the gap between these two paradigms by combining techniques from both in synergistic models, solving complex problems more accurately. Among the above approaches, data augmentation is an essential technique that artificially enlarges training data to enhance model generalization, avoid overfitting, and improve overall robustness. Therefore, the comparative study of various learning approaches is shown in Table 5.

Table 5. Comparative study of various learning approaches.

Reference	Datasets	Classification	Performance (%)	Comments
[33]	Private	SVM-SMOTE	86.01	The results were confirmed in subsequent presentations, and the initial experiment validated the method for collecting the machine learning dataset. The study demonstrated the technique's ability to determine user satisfaction accurately.
[34]	JAFFE and CK+	CART	89.21	Facial distance was calculated using Minkowski, Manhattan, or Euclidean metrics. A decision tree was then used to analyze these three distance measurements. On the JAFFE dataset, the Minkowski distance yielded the best results.
[36]	JAFFE	KNN	85.71	The algorithm's effectiveness was assessed using MATLAB scripts, with accuracy and the number of correct versus incorrect classifications used to evaluate performance. The final results showed that 60 images were correctly classified and 10 were not, yielding an overall accuracy of 85.71%.
[37]	Private	KNN	98.02	This study used the Lucas-Kanade optical flow method to monitor marker placements continuously. The significance of distance-based features extracted from six different emotions was then examined using a single-factor analysis of variance.
[38]	CK+	SVM	93.53	This work presents an algorithm for identifying eight archetypal facial emotions. Principal Component Analysis (PCA) was applied to reduce the feature space. These authors trained

Table 5. Comparative study of various learning approaches. (continue)

Reference	Datasets	Classification	Performance (%)	Comments
[38]	CK+	SVM	93.53	and evaluated three different classifiers for categorization employing a 10-fold cross-validation approach.
[39]	CK+	SVM	91.5	The outcomes clearly confirmed the effectiveness of the recommended technique for reliably extracting facial expressions from video.
[46]	FERPlus and RAF-DB	MobileNet	88.11	According to experimental findings, the enhanced model outperforms other advanced techniques, including the lightweight MobileNet series. The model achieved 88.11% accuracy on FERPlus and 84.5% on the RAF-DB dataset.
[47]	FER2013 dataset and CK+	VGG16	57.34	The authors modified the pre-trained VGG16 model by substituting two entirely connected layers with convolutional layers. This was done to minimize network parameters and alter the pooling strategy.
[51]	FER-2013, Random dataset	MobileNet-V1	97.9	A key contribution of this research is the accurate and effective retrieval of seven distinct behaviors. The method successfully created a seven-class emotion recognition system using photographic inputs.
[53]	KDEF	VGG16	88	The CNN model, validated using performance metrics, achieved 88% accuracy. The results demonstrate that this network design significantly surpasses previous approaches.
[63]	FER-2013, CK+ and RAF-DB	ResNet-50	92.32	The proposed method was evaluated in an online learning scenario involving twenty students. The system successfully used automated facial expression recognition to differentiate between “engaged” and “disengaged” states.
[65]	BAUM-1s, RML, and MMI	SVM	55.85, 73.73, 71.43	The authors first trained a VGG16 model on ImageNet, then separately modified the temporal and spatial CNN networks using video data. A deep DBN was used to study multiple spatio-temporal CNN

Table 5. Comparative study of various learning approaches. (continue)

Reference	Datasets	Classification	Performance (%)	Comments
[65]	BAUM-1s, RML, and MMI	SVM	55.85, 73.73, 71.43	characteristics for effective integration jointly.
[66]	M-LFW-FER	SVM	65.5	The presence of a mask reduces realism by obscuring key facial features. A mask can also alter facial characteristics, making detection more difficult for an algorithm. Furthermore, a machine's accuracy may be limited by its inability to understand the complexity of human emotions fully.
[67]	RAF, SFEW	RF	57.7, 59	Previous approaches often required significant computational power due to their reliance on deep models and were limited to specific emotions. In contrast, the suggested technology is adaptable and can recognize complex expressions, with performance depending on the training.
[69]	Multisource	LSTM	81.42	Experimental results showed that VGG19 had the lowest and most consistent accuracy during training. Among the transfer learning methods tested, the InceptionResNet Model achieved the peak precision.
[70]	CK+	Scale-invariant feature transform (SIFT)	94.82	This work demonstrated a method for extracting features from individual image frames to recognize various facial expressions. By integrating SIFT with features from a deep learning CNN model, composite characteristics are created. An SVM is then used for expression analysis, considering all attributes simultaneously.
[71]	JAFFE	Gaussian mixture model (GMM)	99.53	This study introduces a method to enhance the accuracy of high-performance FER. To achieve the desired performance level, a hybrid approach is recommended, using the DTMBWT algorithm, which relies on the Gray-level Co-occurrence Matrix (GLCM) and energy.

Table 5. Comparative study of various learning approaches. (continue)

Reference	Datasets	Classification	Performance (%)	Comments
[72]	CK+, BU4D	SVM	99.69, 94.69	While the outlined techniques are useful for large datasets, they tend to generate an excessive number of interest points. A current limitation is the system's reliance on Western databases; the final goal is to incorporate an Eastern dataset.
[73]	JAFFE, FER2013	CNN	94.12, 97.07	This research employs a CNN for identifying the main emotion in an image (joyful or angry) and for estimating a subsequent emotion. When optimized on the JAFFE and FER2013 datasets, the model demonstrated greater effectiveness than traditional methods.
[74]	ESD	MLP and SVMs	83.97	A key limitation was the use of a synthetic Emirati speech sample that lacked naturalness, reflecting the general difficulty of capturing genuine emotions on video. Most available databases of this type operate similarly.
[75]	LUMED-2, DEAP	DT	74.2, 53.8	The EEG modality has low subject-independent accuracy because of its non-stationary nature, but this can be beneficial when there are few output classes. The system only classified two states—high/low valence and arousal—to determine emotional state.

6. Discussion

While many existing reviews have emphasized facial emotion recognition (FER) in various contexts, they often miss certain innovative approaches and fail to cover the full range of classification models available. The primary objective of the study is to analyze deep learning models capable of accurately detecting diverse facial emotions. Model training, testing, and validation were carried out using a manually designed image collection protocol. A referenced study highlighted the evolution of a CNN-based deep learning data-driven structure that successfully classified emotions from images with high precision. This work offers a thorough overview of deep learning, machine learning, and hybrid fuzzy systems applied to FER. It also explores a wide array of applications and the challenges associated with FER systems. The research aims to conduct a detailed literature review of recent publications and identify the most widely used architectures for emotional state detection in facial expression datasets, along with their preprocessing methods. The study initially examines classical machine learning techniques, including Random Forests (RF), Support Vector Machines (SVM), Decision Trees (DT), and K-Nearest Neighbors (KNN). The results varied depending on the datasets and the hyperparameter tuning. For example, RF achieved 99.59% accuracy that utilized the CK+ dataset for both training and validation, while SVM reached 57.10% accuracy on the RAF dataset. This study also summarizes several convolutional neural network (CNN) architectures, with a particular emphasis on deep learning models such as CNN, MobileNet, ResNet, and VGG-16. Both lightweight and intricate network designs were

evaluated in the FER context. A key challenge in comparing model performance was the use of different datasets—some containing image sequences and others containing single frames —limiting the consistency of training and testing.

Hybrid models outperform conventional CNN architectures primarily because they **combine** deep feature extraction with robust statistical classification. While CNNs automatically learn hierarchical spatial features, their softmax classifiers often struggle with small or imbalanced datasets. Integrating traditional classifiers such as SVMs, RFs, or GMMs enhances decision boundary precision and reduces overfitting, particularly when training data is limited. Moreover, hybrid systems leverage handcrafted features to capture subtle geometric and textural variations that CNNs miss. However, hybrid methods are not without limitations. They often involve higher computational complexity due to multi-stage training, and performance depends heavily on the feature fusion strategy. Additionally, their deployment in real-time applications remains challenging because of increased processing time and memory requirements. Future work should focus on optimizing lightweight hybrid architectures that maintain accuracy without compromising computational efficiency.

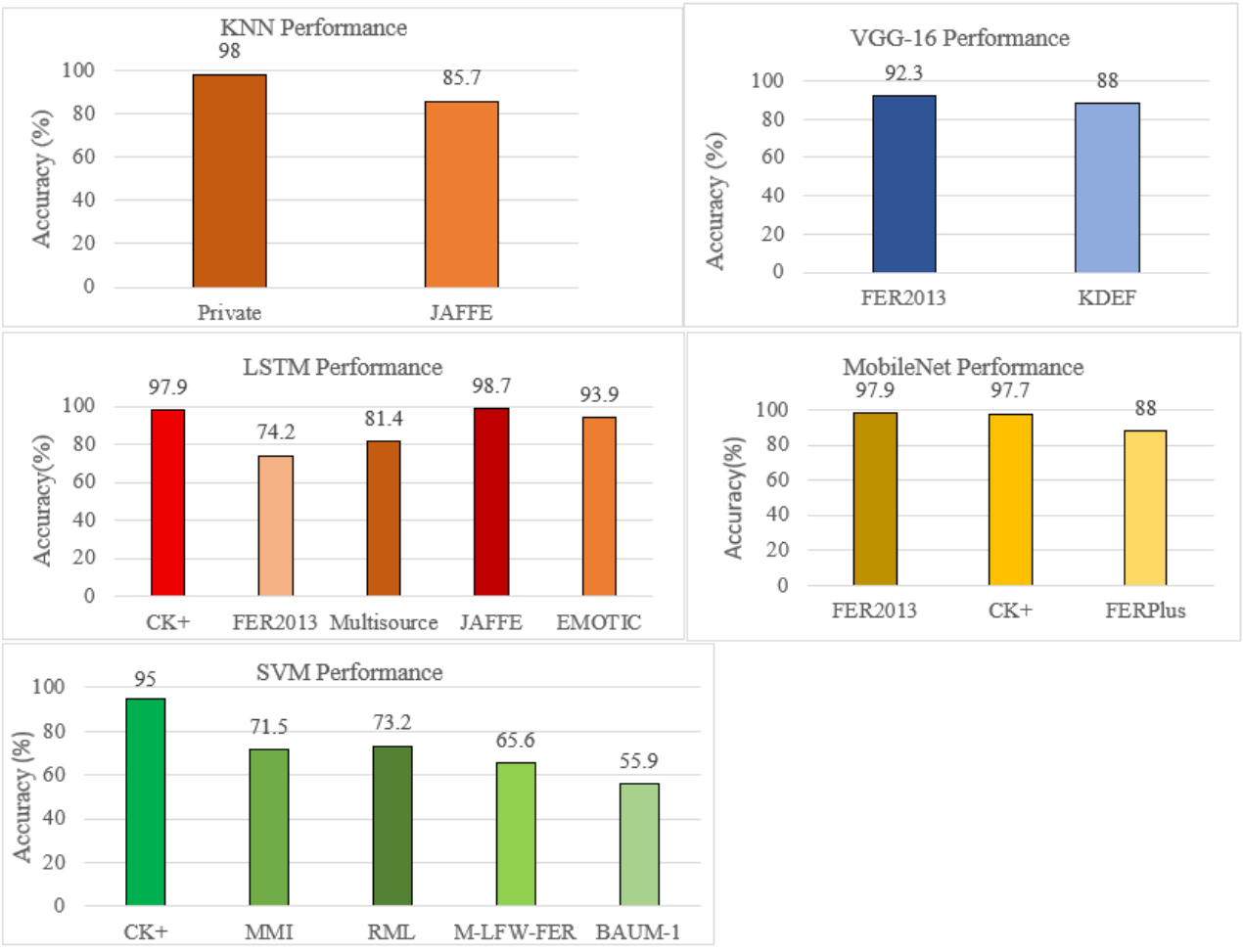


Figure 6. Employed approaches and their effectiveness using various FER datasets

Figure 6: Practical assessment has shown that deep learning- and hybrid-learning-based FER methods achieve very high accuracy. However, several challenges remain and require further research. As the complexity of these frameworks grows, data preparation requires large-scale datasets and significant computational resources. Running experiments and tests demands considerable memory, extended processing time, and a large collection of human-curated, labeled samples. The computational capability

required by the model for these approaches—especially those that rely on deep learning—is quite extensive. In addition, many of these approaches are designed to recognize only a fixed set of emotions, which limits their ability to detect other emotional states. Hence, designing a revised framework that is generally relevant and capable of encompassing the full spectrum of emotional states would be extremely valuable and could conceivably be extended to recognize more intricate and nuanced facial expressions.

6.1 Quantitative Performance and Computational Efficiency Analysis

A quantitative analysis of FER techniques indicates trade-offs between accuracy and computational cost. Conventional machine learning algorithms, such as Support Vector Machine (SVM), Random Forest (RF), and K-Nearest Neighbors (KNN), have relatively low computational costs because they rely on handcrafted features. However, the performance of these algorithms deteriorates on large-scale, complex data sets.

On the other hand, the performance of deep learning algorithms such as VGG16, ResNet-50, DenseNet-161, and MobileNet in the FER system is relatively higher because these algorithms learn hierarchical features directly from raw facial images. The performance of these algorithms in the FER system has been observed to be above 95% for the CK+ and JAFFE data sets. However, these algorithms have relatively higher computational costs because they depend on the training process and the availability of GPUs and large-scale training datasets. Hybrid models are also used to achieve a balance between the trade-offs by using a combination of deep features and traditional classifiers such as SVM and GMM. Hybrid models have been known to improve classification accuracy by 3 to 6 percent compared to traditional models. However, it is important to note that the improvement comes at a price: the system becomes more complex as it undergoes a series of processes. Future facial emotion recognition (FER) systems should be designed to be lean and simple, achieving a balance between high accuracy and real-time performance.

7. Challenges and Constraints

There are still several limitations that affect the accuracy and real-world performance. Even though deep learning models like CNNs and ViTs can effectively recognize emotions from facial features, they are quite sensitive to environmental and contextual factors. Some of them are listed below:

1. Partial Face Occlusion: The accuracy of FER systems decreases significantly when hands, accessories, or other objects block parts of the face. In real-world scenarios, it is not always possible to capture the entire face clearly, which limits recognition performance.
2. Head Pose Variations: Variations in head posture—for instance, tilting, turning sideways, or looking away create strain on facial muscles and distort visible expressions, making recognition more difficult. Most FER systems perform optimally when the subject is facing forward in a stable position.
3. Lighting Conditions: Fluctuations in illumination can reduce the accuracy of facial detection and tracking. Both low light and excessive brightness can hide critical facial features or introduce noise, thereby affecting model performance.
4. Cultural Variability: Emotional expressions often differ across cultures, leading to diverse ways of perceiving and expressing emotions. This cultural variability makes it challenging for FER systems trained on a specific population to generalize well across global users.

Deployment Challenges: Although both manual and automated FER approaches can achieve good results, implementing them is not always straightforward. In dynamic or unstructured environments, they may produce inconsistent results depending on the dataset, features, or context.

8. Future Directions

Subsequent research in FER should have a primary focus on key points such as existing complications, reducing algorithmic bias, and enhancing system usability in real-world environments. A key priority is creating larger, more representative datasets that capture a broad spectrum of facial expressions across diverse regions, cultural contexts, and demographic groups. Additionally, incorporating multimodal techniques—combining facial features with speech tone, gestures, and body movements—can significantly improve recognition accuracy. For practical deployment, developing dynamic FER systems that are optimized for speed, storage efficiency, and operation in disorganized or dynamic settings will be essential. Tackling

population bias requires systematic strategies to ensure fair performance across diverse groups, resulting in more equitable, unbiased outcomes. The interpretability and trustworthiness of FER models can be enhanced by explainable AI (XAI) methods, which are especially valuable in low-resource and high-stakes applications. Further, advancing temporal modeling with architectures such as Transformers or enhanced LSTM networks will enable a better understanding of emotion sequences over time. Finally, emerging research highlights the potential of unsupervised and self-supervised learning techniques to decrease the necessity for extensive amounts of labeled training data, making FER systems more scalable and adaptable to new domains.

9. Conclusions

This review provided a comprehensive synthesis of Facial Emotion Recognition (FER) techniques based on machine learning, deep learning, and hybrid models, analyzing nearly a decade of research (2014–2024). Traditional approaches such as SVM, KNN, and Random Forests achieved competitive accuracy on small, controlled datasets such as JAFFE and CK+, typically ranging from **85–93%**. Deep learning methods, particularly CNN-based architectures including VGG16, ResNet-50, and DenseNet-161, significantly enhanced performance, attaining up to 99.5% accuracy on large-scale datasets such as FER2013 and RAF-DB. Hybrid methods that integrate deep feature extraction with classical classifiers, such as SVMs or GMMs, demonstrated additional improvements of 3–6% over standalone models. While deep learning has redefined FER accuracy and robustness, challenges remain concerning data diversity, real-world generalization, and computational cost. Future work should emphasize the development of cross-cultural datasets, bias mitigation, and lightweight FER models suitable for real-time and edge deployment. Overall, this study consolidates key advancements, comparative performance, and open challenges to guide researchers and practitioners toward more inclusive, efficient, and interpretable FER systems.

Acknowledgement

I extend my profound thanks to my **team members** for their cooperation, commitment, and teamwork. Your collective effort and support have been invaluable in achieving our common goal.

Author Contributions: The authors confirm their contribution to the paper as follows:

Study conception and design: Sushilkumar Salve, Shubham Kumar, Irfan Shaikh.

Literature review and data collection: Pranay Gawade, Irfan Shaikh, **Sushilkumar Salve**

Analysis and interpretation of findings: Shubham Kumar, Pranay Gawade, Sushilkumar Salve.

Draft manuscript preparation and editing: Irfan Shaikh, Shubham Kumar, **Sushilkumar Salve**

Critical review of the manuscript and validation of content: Sushilkumar Salve, Sujit Ramesh Borey, Puja All authors discussed the results, contributed to the writing, and approved the final version of the manuscript.

Funding Statement: "The author(s) received no specific funding for this study".

Conflicts of Interest: "The authors declare that they have no conflicts of interest to report regarding the present study".

References

[1] Chu, W.-S.; De la Torre, F.; Cohn, J. F. Selective Transfer Machine for personalized facial expression analysis. *IEEE Trans. Pattern Anal. Mach. Intell.* **2017**, *39*, 529–545. https://doi.org/10.1109/TPAMI.2016.2547397

[2] AlBdairi, A. J. A.; Qasim, M. A.; Nsaif, A. K.; Al Bdairi, S. J. A.; Al-Obaidy, M. T.; Hassan, M. A.; Ali, A. R. Face recognition based on deep learning and FPGA for ethnicity identification. *Appl. Sci.* **2022**, *12*, 2605. https://doi.org/10.3390/app12052605

[3] Simcock, G.; Reavley, N. J.; Vitis, L.; O'Sullivan, J. S.; Murray, A. L. Associations between facial emotion recognition and mental health in early adolescence. *Int. J. Environ. Res. Public Health* **2020**, *17*, 330. https://doi.org/10.3390/ijerph17010330

[4] Yang, H.; Ciftci, U.; Yin, L. Facial expression recognition by DE-expression residue learning. In *2018 IEEE/CVF Conf. Comput. Vis. Pattern Recognit.*; IEEE: Salt Lake City, UT, USA. 2018. https://doi.org/10.1109/CVPR.2018.00231

[5] Majumder, A.; Behera, L.; Subramanian, V. K. Automatic facial expression recognition system using deep network-based data fusion. *IEEE Trans. Cybern.* **2018**, *48*, 103–114. https://doi.org/10.1109/TCYB.2016.2625419

[6] Deshmukh, S.; Patwardhan, M.; Mahajan, A. Survey on real-time facial expression recognition techniques. *IET Biom.* **2016**, *5*, 155–163. https://doi.org/10.1049/iet-bmt.2014.0104

[7] Ekweariri, A. N.; Yurtkan, K. Facial expression recognition using enhanced local binary patterns. In *2017 9th Int. Conf. Comput. Intell. Commun. Netw. (CICN)*; IEEE: Girne, Northern Cyprus. 2017, pp. 43–47. https://doi.org/10.1109/CICN.2017.8319353

[8] Yasmin, S.; Pathan, R. K.; Biswas, M.; Khandaker, M. U.; Faruque, M. R. I. Development of a robust multi-scale featured local binary pattern for improved facial expression recognition. *Sensors* **2020**, *20*, 5391. https://doi.org/10.3390/s20185391

[9] Yu, Z.; Dong, Y.; Cheng, J.; Sun, M.; Su, F. Research on face recognition classification based on improved GoogLeNet. *Secur. Commun. Netw.* **2022**, 1–6. https://doi.org/10.1155/2022/7192306

[10] Cheng, E. J.; Fan, S. C.; Chen, Y. C.; Chen, G. Y.; Su, C. H.; Wang, C. Y.; Chu, Y. H. Deep sparse representation classifier for facial recognition and detection system. *Pattern Recognit. Lett.* **2019**, *125*, 71–77. https://doi.org/10.1016/j.patrec.2019.03.006

[11] Li, L.; Mu, X.; Li, S.; Peng, H. A review of face recognition technology. *IEEE Access* **2020**, *8*, 139110–139120. https://doi.org/10.1109/ACCESS.2020.3011028

[12] Mliki, H.; Fourati, N.; Smaoui, S.; Hammami, M. Automatic facial expression recognition system. In *2013 ACS Int. Conf. Comput. Syst. Appl. (AICCSA)*; IEEE: Ifrane, Morocco. 2013. https://doi.org/10.1109/AICCSA.2013.6616505

[13] Bendjillali, R. I.; Beladgham, M.; Merit, K.; Taleb-Ahmed, A. Improved facial expression recognition based on DWT feature for deep CNN. *Electronics* **2019**, *8*, 324. https://doi.org/10.3390/electronics8030324

[14] Shan, K.; Guo, J.; You, W.; Lu, D.; Bie, R. Automatic facial expression recognition based on a deep convolutional-neural-network structure. In *2017 IEEE 15th Int. Conf. Softw. Eng. Res., Manag. Appl. (SERA)*; IEEE: London, UK. 2017. https://doi.org/10.1109/SERA.2017.7965717

[15] Owusu, E.; Zhan, Y.; Mao, Q. R. A neural-AdaBoost based facial expression recognition system. *Expert Syst. Appl.* **2014**, *41*, 3383–3390. https://doi.org/10.1016/j.eswa.2013.11.041

[16] Durmusoglu, A.; Kahraman, Y. Facial expression recognition using geometric features. In *2016 Int. Conf. Syst., Signals Image Process. (IWSSIP)*; IEEE: Bratislava, Slovakia. 2016. https://doi.org/10.1109/IWSSIP.2016.7502700

[17] Yu, Z.; Dong, Y.; Cheng, J.; Sun, M.; Su, F. Research on face recognition classification based on improved GoogLeNet. *Secur. Commun. Netw.* **2022**, 1–6. https://doi.org/10.1155/2022/7192306

[18] Kumar, S.; Sagar, V.; Punetha, D. A comparative study on facial expression recognition using local binary patterns, convolutional neural network and frequency neural network. *Multimed. Tools Appl.* **2023**, *82*, 24369–24385. https://doi.org/10.1007/s11042-023-14753-y

[19] Baffour, P. A.; Nunoo-Mensah, H.; Keelson, E.; Kommey, B. A survey on deep learning algorithms in facial emotion detection and recognition. *Inform: Jurnal Ilmiah Bidang Teknologi Informasi dan Komunikasi* **2022**, *7*, 24–32. https://doi.org/10.25139/inform.v7i1.4282

[20] Ge, H.; Zhu, Z.; Dai, Y.; Wang, B.; Wu, X. Facial expression recognition based on deep learning. *Comput. Methods Programs Biomed.* **2022**, *215*, Art. no. 106621. https://doi.org/10.1016/j.cmpb.2022.106621

[21] Singh, S. K.; Thakur, R. K.; Kumar, S.; Anand, R. Deep learning and machine learning based facial emotion detection using CNN. In *2022 9th Int. Conf. Comput. Sustain. Glob. Dev. (INDIACom)*; IEEE: New Delhi, India. 2022. https://doi.org/10.23919/INDIACom54597.2022.9763165

[22] Khattak, A.; Asghar, M. Z.; Ali, M.; Batool, U. An efficient deep learning technique for facial emotion recognition. *Multimed. Tools Appl.* **2022**, *81*, 1649–1683. https://doi.org/10.1007/s11042-021-11298-w

[23] Bisogni, C.; Castiglione, A.; Hossain, S.; Narducci, F.; Umer, S. Impact of deep learning approaches on facial expression recognition in healthcare industries. *IEEE Trans. Ind. Inform.* **2022**, *18*, 5619–5627. https://doi.org/10.1109/TII.2022.3141400

[24] Alsharekh, M. F. Facial emotion recognition in verbal communication based on deep learning. *Sensors* **2022**, *22*, 6105. https://doi.org/10.3390/s22166105

[25] Borgalli, M. R. A.; Surve, S. Deep learning for facial emotion recognition using custom CNN architecture. *J. Phys. Conf. Ser.* **2022**, *2236*, 012004.

[26] Saad, A. A.; Shah, M.; Ehsan, M. R. K.; Amirzada, A.; Mahmood, T. Automated facial expression recognition framework using deep learning. *J. Healthc. Eng.* **2022**, *2022*, 1–11. https://doi.org/10.1155/2022/5707930

[27] Arora, T. K.; Garg, M.; Kaushik, B.; Kaushik, R.; Gupta, V.; Gulati, M. Optimal facial feature based emotional recognition using deep learning algorithm. *Comput. Intell. Neurosci.* **2022**, Art. no. 8379202.

[28] Dukic, D.; Sovic Krzic, A. Real-time facial expression recognition using deep learning with application in the active classroom environment. *Electronics* **2022**, *11*, 1240. https://doi.org/10.3390/electronics11081240

[29] Zhao, X.; Zhu, J.; Luo, B.; Gao, Y. Survey on facial expression recognition: History, applications, and challenges. *IEEE Multimed.* **2021**, *28*, 38–44. https://doi.org/10.1109/MMUL.2021.3107862

[30] Al-Modwahi, A. A. M.; Sebetela, O.; Batleng, L. N.; Parhizkar, B.; Lashkari, A. H. Facial expression recognition intelligent security system for real time surveillance. In *World Congr. Comput. Sci., Comput. Eng., Appl. Comput. (WORLDCOMP'12)*; CSREA Press: Las Vegas, NV, USA. 2012.

[31] Varma, S.; Shinde, M.; Chavan, S. S. Analysis of PCA and LDA features for facial expression recognition using SVM and HMM classifiers. In *Techno-Societal 2018*; Springer: Cham, Switzerland. 2020, pp. 109–119. https://doi.org/10.1007/978-3-030-16848-3_11

[32] Saeed, V. A. A framework for recognition of facial expression using HOG features. *Int. J. Math.* **2024**, *2*, 1–8. https://doi.org/10.59543/ijmscs.v2i.7815

[33] Koonsanit, K.; Nishiuchi, N. Classification of user satisfaction using facial expression recognition and machine learning. In *2020 IEEE Region 10 Conf. (TENCON)*; IEEE: Osaka, Japan. 2020, pp. 561–566. https://doi.org/10.1109/TENCON50793.2020.9293912

[34] Liu, X.; Cheng, X.; Lee, K. GA-SVM-based facial emotion recognition using facial geometric features. *IEEE Sens. J.* **2021**, *21*, 11532–11542. https://doi.org/10.1109/JSEN.2020.3028075

[35] Salmam, F. Z.; Madani, A.; Kissi, M. Facial expression recognition using decision trees. In *2016 13th Int. Conf. Comput. Graph., Imag. Visualizat. (CGiV)*; IEEE: Beni Mellal, Morocco. 2016, pp. 125–130. https://doi.org/10.1109/CGiV.2016.33

[36] Iromini, N.; Asi, B. T.; Okuwa, C. O.; Gbadamosi, K. Facial expression recognition system using KNN. *Int. J. Sci. Eng. Environ. Technol.* **2021**, *6*, 31–38.

[37] Murugappan, M.; Alshehri, A. A. M.; Ahamed, S. R.; Ananth, C.; P. S.; Kumar, M. M. S. Facial expression classification using KNN and decision tree classifiers. In *4th Int. Conf. Comput., Commun. Signal Process. (ICCCSP)*; IEEE: Chennai, India. 2020, pp. 1–6. https://doi.org/10.1109/ICCCSP49186.2020.9315234

[38] Dino, H. I.; Abdulrazzaq, M. B. Facial expression classification based on SVM, KNN and MLP classifiers. In *2019 Int. Conf. Adv. Sci. Eng. (ICOASE)*; IEEE: Zakho-Duhok, Iraq. 2019, pp. 70–75. https://doi.org/10.1109/ICOASE.2019.8723728

[39] Priya, M.; Ranjani, B.; Rajammal, K.; Murali, N.; Tamilselvi, M.; Kavitha, M. Automatic emotion detection using SVM-based optimal kernel function. In *2024 11th Int. Conf. Comput. Sustain. Global Develop. (INDIACom)*; IEEE: New Delhi, India. 2024, pp. 1607–1611. https://doi.org/10.23919/INDIACom61295.2024.10498982

[40] Alhussan, A. A.; Ghoneim, S. S. M.; Kamal, E. K. M.; Abdelkhalek, O. O. O. Facial expression recognition model depending on optimized SVM. *Comput., Mater. Contin.* **2023**, *76*, 499–515. https://doi.org/10.32604/cmc.2023.039368

[41] Tamer Ghareeb, B.; Tarek, F.; Said, H. FER_ML: Facial emotion recognition using machine learning. *J. Comput. Commun.* **2023**, *2*, 40–49. https://doi.org/10.21608/jocc.2023.282094

[42] Yao, L.; Wan, Y.; Ni, H.; Xu, B. Action unit classification for facial expression recognition using active learning and SVM. *Multimed. Tools Appl.* **2021**, *80*, 24287–24301. https://doi.org/10.1007/s11042-021-10836-w

[43] Alzawali, M. I. H.; Abed, S. A.; Ghayyib, K. K.; Risan, M. R. Facial emotion images recognition based on binarized genetic algorithm-random forest. *Baghdad Sci. J.* **2024**, *21*, Art. no. 0780. https://doi.org/10.21123/bsj.2024.9698

[44] Akhand, M. A. H.; Roy, S.; Siddique, N.; Kamal, M. A. S.; Shimamura, T. Facial emotion recognition using Transfer Learning in the Deep CNN. *Electronics* **2021**, *10*, 1036. https://doi.org/10.3390/electronics10091036

[45] Huang, Z.-Y.; Liang, J.-K.; Luo, C.-F.; Liu, M.-Y.; Lin, S.-H.; Chang, C.-Y.; Wang, D.-Y.; Hsu, S.-M.; Chen, R.-C. A study on computer vision for facial emotion recognition. *Sci. Rep.* **2023**, *13*, 8425. https://doi.org/10.1038/s41598-023-35446-4

[46] Prajapat, G. K.; Sharma, B. P.; Agrawal, A.; Soni, R.; Saini, S. K. Universal model for facial expression detection using convolutional neural network. *AIP Conf. Proc.* **2024**, *3111*, 030022. https://doi.org/10.1063/5.0221449

[47] Gupta, S.; Kumar, P.; Tekchandani, R. K. Facial emotion recognition based on real-time learner engagement detection system in online learning context using deep learning models. *Multimed. Tools Appl.* **2023**, *82*, 11365–11394. https://doi.org/10.1007/s11042-022-13558-9

[48] Hu, L.; Ge, Q. Automatic facial expression recognition based on MobileNetV2 in Real-time. *J. Phys. Conf. Ser.* **2020**, *1549*, 022136. https://doi.org/10.1088/1742-6596/1549/2/022136

[49] Nan, Y.; Ju, J.; Hua, Q.; Zhang, H.; Wang, B. A-MobileNet: An approach of facial expression recognition. *Alex. Eng. J.* **2022**, *61*, 4435–4444. https://doi.org/10.1016/j.aej.2021.09.066

[50] Ngwe, J. L.; Lim, K. M.; Lee, C. P.; Ong, T. S.; Alqahtani, A. PAtt-Lite: Lightweight patch and attention MobileNet for challenging facial expression recognition. *IEEE Access* **2024**, *12*, 79327–79341. https://doi.org/10.1109/ACCESS.2024.3407108

[51] Dong, C.; Wang, R.; Hang, Y. Facial expression recognition based on improved VGG convolutional neural network. *J. Phys. Conf. Ser.* **2021**, *2083*, 032030. https://doi.org/10.1088/1742-6596/2083/3/032030

[52] Pham, L.; Huynh Vu, T.; Tran, T. A. Facial expression recognition using residual masking network. In *2020 25th Int. Conf. Pattern Recognit. (ICPR)*; IEEE: Milan, Italy. 2021. https://doi.org/10.1109/ICPR48806.2021.9411919

[53] Li, B.; Lima, D. Facial expression recognition via ResNet-50. *Int. J. Cognit. Comput. Eng.* **2021**, *2*, 57–64. https://doi.org/10.1016/j.ijcce.2021.02.002

[54] Minaee, S.; Minaei, M.; Abdolrashidi, A. Deep-emotion: Facial expression recognition using attentional convolutional network. *Sensors* **2021**, *21*, 3046. https://doi.org/10.3390/s21093046

[55] Xiong, L.; Zhang, J.; Zheng, X.; Wang, Y. Context transformer and adaptive method with visual transformer for robust facial expression recognition. *Appl. Sci.* **2024**, *14*, 1535. https://doi.org/10.3390/app14041535

[56] Tao, H.; Duan, Q. Hierarchical attention network with progressive feature fusion for facial expression recognition. *Neural Netw.* **2024**, *170*, 337–348. https://doi.org/10.1016/j.neunet.2023.11.033

[57] Gao, Z.; Gao, H.; Xiang, Y. Facial emotion recognition based on selective kernel network. *J. Flow Vis. Image Process* **2024**, *31*, 33–52. https://doi.org/10.1615/JFlowVisImageProc.2023048881

[58] Verma, M.; Vipparthi, S. K. Cross-centroid ripple pattern for facial expression recognition. *Multimed. Tools Appl.* **2024**, *48*, 384. https://doi.org/10.1007/s11042-024-19364-9

[59] Rostami, M.; Farajollahi, A.; Parvin, H. Deep learning-based face detection and recognition on drones. *J. Ambient Intell. Humaniz. Comput.* **2024**, *15*, 373–387. https://doi.org/10.1007/s12652-022-03897-8

[60] Mukhiddinov, M.; Djuraev, O.; Akhmedov, F.; Mukhamadiyev, A.; Cho, J. Masked face emotion recognition based on facial landmarks and deep learning approaches for visually impaired people. *Sensors* **2023**, *23*, 1080. https://doi.org/10.3390/s23031080

[61] Pranav, E.; Kamal, S.; Chandran, C. S.; Supriya, M. H. Facial emotion recognition using deep convolutional neural network. In *2020 6th Int. Conf. Adv. Comput. Commun. Syst. (ICACCS)*; IEEE: Coimbatore, India. 2020. https://doi.org/10.1109/ICACCS48705.2020.9074302

[62] Jaiswal, A.; Krishnama Raju, A.; Deb, S. Facial emotion detection using deep learning. In *2020 Int. Conf. Emerg. Technol. (INCET)*; IEEE: Belgaum, India. 2020.

[63] Hussain, S. A.; Al Balushi, A. S. A. A real time face emotion classification and recognition using deep learning model. *J. Phys. Conf. Ser.* **2020**, *1432*, 012087. https://doi.org/10.1088/1742-6596/1432/1/012087

[64] Akeh, L. J.; Kusuma, G. P. Mixed emotion recognition through facial expression using transformer based model. *Stat., Optim. Inf. Comput.* **2024**. https://doi.org/10.19139/soic-2310-5070-2103

[65] Zhang, S.; Pan, X.; Cui, Y.; Zhao, X.; Liu, L. Learning affective video features for facial expression recognition via hybrid deep learning. *IEEE Access* **2019**, *7*, 32297–32304. https://doi.org/10.1109/ACCESS.2019.2901521

[66] Shahzad, H. M.; Bhatti, S. M.; Jaffar, A.; Akram, S.; Alhajlah, M.; Mahmood, A. Hybrid facial emotion recognition using CNN-based features. *Appl. Sci.* **2023**, *13*, 5572. https://doi.org/10.3390/app13095572

[67] Alreshidi, A.; Ullah, M. Facial emotion recognition using hybrid features. *Informatics* **2020**, *7*, 6. https://doi.org/10.3390/informatics7010006

[68] Liu, C.; Hirota, K.; Ma, J.; Jia, Z.; Dai, Y. Facial expression recognition using hybrid features of pixel and geometry. *IEEE Access* **2021**, *9*, 18876–18889. https://doi.org/10.1109/ACCESS.2021.3054332

[69] Mishra, R. K.; Urolagin, S.; ArulJothi, J. A.; Gaur, P. Deep hybrid learning for facial expression binary classifications and predictions. *Image Vis. Comput.* **2022**, *128*, 104573. https://doi.org/10.1016/j.imavis.2022.104573

[70] Sun, X.; Lv, M. Facial expression recognition based on a hybrid model combining deep and shallow features. *Cognit. Comput.* **2019**, *11*, 587–597. https://doi.org/10.1007/s12559-019-09654-y

[71] Kommineni, J.; Mandala, S.; Sunar, M. S.; Chakravarthy, P. M. Accurate computing official expression recognition using a hybrid feature extraction technique. *J. Supercomput.* **2021**, *77*, 5019–5044. https://doi.org/10.1007/s11227-020-03468-8

[72] Kim, J. C.; Kim, M.-H.; Suh, H.-E.; Naseem, M. T.; Lee, C.-S. Hybrid approach for facial expression recognition using convolutional neural networks and SVM. *Appl. Sci.* **2022**, *12*, 5493. https://doi.org/10.3390/app12115493

[73] Verma, G.; Verma, H. Hybrid-deep learning model for emotion recognition using facial expressions. *Rev. Socionetwork Strat.* **2020**, *14*, 171–180. https://doi.org/10.1007/s12626-020-00061-6

[74] Shahin, I.; Nassif, A. B.; Hamsa, S. Emotion recognition using hybrid Gaussian mixture model and deep neural network. *IEEE Access* **2019**, *7*, 26777–26787. https://doi.org/10.1109/ACCESS.2019.2901352

[75] Cimtay, Y.; Ekmekcioglu, E.; Caglar-Ozhan, S. Cross-subject multimodal emotion recognition based on hybrid fusion. *IEEE Access* **2020**, *8*, 168865–168878. https://doi.org/10.1109/ACCESS.2020.3023871

[76] Aifanti, N.; Papachristou, C.; Delopoulos, A. The MUG facial expression database. In *11th Int. Workshop Image Anal. Multimed. Interact. Serv. (WIAMIS 10)*; IEEE: Desenzano del Garda, Italy. 2010, pp. 1–4.

[77] Li, S.; Deng, W.; Du, J. Reliable crowdsourcing and deep locality-preserving learning for expression recognition in the wild. In *Proc. IEEE Conf. Comput. Vis. Pattern Recognit.*; IEEE: Honolulu, HI, USA. 2017, pp. 2852–2861. https://doi.org/10.1109/CVPR.2017.277

[78] Pantic, M.; Valstar, M.; Rademaker, R.; Maat, L. Web-based database for facial expression analysis. In *2005 IEEE Int. Conf. Multimed. Expo.*; IEEE: Amsterdam, The Netherlands. 2005. https://doi.org/10.1109/ICME.2005.1521424

[79] Sambare, M. FER-2013: Facial expression recognition dataset; Kaggle, 2013. https://www.kaggle.com/datasets/msambare/fer2013

[80] Lundqvist, D.; Flykt, A.; Öhman, A. Karolinska directed emotional faces; APA PsycTests, 2015. https://doi.org/10.1037/t27732-000

ASEAN
Journal of Scientific and Technological Reports
Online ISSN:2773-8752

Research article

Baseline Assessment of Dairy Cow Welfare Using Animal and Resource-based Indicators in Camarines Sur, Philippines

Angelo Francis F. Atole[1*]

[1] Department of Animal Science, Central Bicol State University of Agriculture, San Jose, Pili, Camarines Sur, 4418, Philippines
[*] Correspondence: angelofrancis.atole@cbsua.edu.ph

Citation:
Atole, A.F.F. Baseline assessment of dairy cow welfare using animal and resource-based indicators in Camarines Sur, Philippines. *ASEAN J. Sci. Tech. Report.* **2026**, *29*(7), e260555. https://doi.org/10.55164/ajstr.v29i7.260555

Article history:
Received: July 28, 2025
Revised: March 24, 2026
Accepted: April 11, 2026
Available online: June 15, 2026

Publisher's Note:
This article is published and distributed under the terms of the Thaksin University.

Abstract: The increasing interest in dairy cattle production raises animal welfare issues that need to be assessed and addressed on the farm. No prior studies have assessed the welfare status of dairy cows in small-hold dairy systems in Camarines Sur, Philippines; hence, this study. On-farm animal- and resource-based indicators were applied using the Welfare Quality® Assessment Protocol for dairy cattle to assess herd-level welfare, with binary data reported as percentages of farms. The welfare criteria for animal-based indicators were assessed by observing the dairy cows on the farm. Sixteen dairy farms were assessed, with a total dairy cow population of 125 (mean: 7.8, median: 7.5, mode: 8). The welfare criteria for resource-based indicators were assessed by evaluating the farm resources. The majority of the dairy farms visited have well-fed dairy cows (87%), with low injury rates (13-20%) and disease rates (0-13%). Additionally, they were provided with a comfortable (76-93%) and sufficient (67-100%) resting area, thereby avoiding agonistic behavior (0%). Some dairy farmers need education on the benefits of clean and accessible water and facilities (73-100%) to improve dairy cow welfare. The majority of dairy farmers considered the importance of comfort, protection from adverse weather (67-87%), and spatial requirements (67-100%). However, grooming facilities were absent, compromising dairy cow welfare. The animal-based indicators on the farm reflected better dairy cow welfare; however, some dairy farmers should improve the resource-based indicators to provide their cows with better welfare.

Keywords: Animal-based indicators; animal welfare; dairy cows; resource-based indicators

1. Introduction

Bicol (Region 5) is a large region in the Philippines, covering 17,366 km^2 (5.67% of the country's land area), and includes the Province of Camarines Sur [1, 2]. Camarines Sur is the largest province (5,327 km^2), comprising 31% of the Bicol region, and experiences year-round rainfall [2]. This implies that dairy farmers can cultivate forages in Bicol year-round to feed dairy cattle. Furthermore, the vast agricultural land enables a year-round forage supply. The abundance of forages contributes to high milk production at a low cost. However, feeding forages does not always guarantee that a cow will produce more milk. Some dairy farmers are unaware of the natural needs of dairy cows for well-being [3]. For example, dairy cows require daily access to pasture and exposure to sunlight (i.e., freedom to express normal behavior), protection from inclement weather (i.e., freedom from discomfort), and protection against diseases (i.e., freedom from pain, injury, or disease). These situations may be

exacerbated when the frequency and duration of the region's rainy and dry seasons are imbalanced. During the extended rainy season, dairy cows have reduced access to the outdoors, thereby limiting grazing behavior. Moreover, excessive rainfall can cause muddy, slippery floors, which may lead to foot rot and leg injuries. During the extended dry season, the supply of high-quality fresh forage is scarce, leading to low-quality forage and hunger. In extreme heat, dairy cows may experience dehydration and, in severe cases, heat stroke. Inadequate knowledge among dairy farmers about the geographic impacts on dairy farming may put dairy cows' welfare at stake. This implies that improving dairy cows' welfare will enhance performance [4, 5].

Providing better welfare (e.g., good housing, freedom, health, social interaction) for dairy cows may lead to higher milk production. However, many dairy farmers are unaware of the welfare issues dairy cows face, despite high production levels. Examples of welfare issues in dairy cows are lameness [6], mastitis [7], unsanitary practices (e.g., dirty hands at milking), spatial limitation (e.g., crowded barn), improper handling (e.g., hitting), and restriction from expression of natural behaviors [e.g., grazing, social interaction; 8]. Thus, poor welfare can negatively affect milk production and, in turn, the economic aspects of dairy farming [9]. Several studies have reported that dairy cows with better welfare exhibit improved production performance [10]. For example, allowing cows to be nursed before and after milk collection yields more saleable milk than milked cows alone [10]. Furthermore, nursed cows have better udder health than milked cows [11]. Compared with other methods, allowing dairy cows to graze is associated with a lower incidence of lameness [6] and mastitis [7]. Mastitis can likely be reduced by maintaining a clean environment [12]. Dairy cows that are handled humanely on the farm produce more milk and have better affective states. Dairy cows that are accustomed to socializing with conspecifics exhibit more positive affective states and freely express their social behavior. In summary, healthy, comfortable, and well-managed dairy cows have better longevity and, thus, have better welfare. To achieve these, dairy farmers must be aware of their cows' welfare. However, this is sometimes neglected in the countryside as dairy farmers focus more on reducing production costs, thereby impairing the dairy cows' welfare. Therefore, this study was conducted to obtain baseline data and assess the welfare status of dairy cows using animal- and resource-based indicators in small-hold dairy systems in Camarines Sur, Philippines. Since this study is pioneering in Region 5, Philippines, the findings will serve as benchmark data for future studies, policy formulation, and educating dairy farmers on improving the welfare and productivity of their dairy cows.

2. Materials and Methods

2. 1 Indicators of Dairy Cow Welfare

Dairy cow welfare was assessed using on-farm welfare indicators developed by [13]. The on-farm welfare indicators used were animal- and resource-based, following the Welfare Quality Protocol® for dairy cattle. For the animal-based indicators, the following criteria were assessed: absence of prolonged hunger, absence of injuries, absence of disease, comfort during rest, and expression of behaviors. For the resource-based indicators, the following criteria were assessed: ease of movement and absence of prolonged thirst. Some criteria measures were added, excluded, or modified based on the dairy farm setting in Camarines Sur. For the animal-based indicators, additional forage and supplements were offered [14]. The following measures for comfort during resting, such as the time needed to lie down, animals colliding with housing equipment during lying down, and animals lying partly or completely outside the lying area, have been excluded from the Welfare Quality Protocol® for dairy cattle. Measures of disease absence, such as milk somatic cell count, mortality, dystocia, and downer cows, were excluded. Lastly, for the expression of social behaviors, avoidance distance and qualitative behavior assessment were excluded from the assessment. For the resource-based indicators, cows tied in stalls were added under the criterion of ease of movement [15]. Additionally, measures for comfort and protection against adverse weather (e.g., provision of housing, roofs, partitions, concrete floors, and bedding materials) were added [16, 17]. The measure for the functioning of water points was modified to include dairy cows having access to water. These changes were tailored to fit the existing resources on the farm and dairy farmers' practices in Camarines Sur [18].

2.2 Farm Selection and Location

The dairy farms visited were randomly selected based on dairy farmers' willingness to participate, the presence of dairy cows on the farm, and the area accessibility. Thus, from 21 dairy farms listed, 16 participated and were assessed from Naga City (4) and municipalities of Goa (2), Ocampo (2), Pili (1), Tigaon (3), and Sagñay (4), Camarines Sur, Philippines (Fig. 1). Dairy farmers raised crosses between Holstein-Friesian and Sahiwal, and between Holstein-Friesian and Jersey for milk production and environmental adaptability. They have several years of experience, regardless of the number of cows they raise; therefore, they have developed skills in dairy farming.

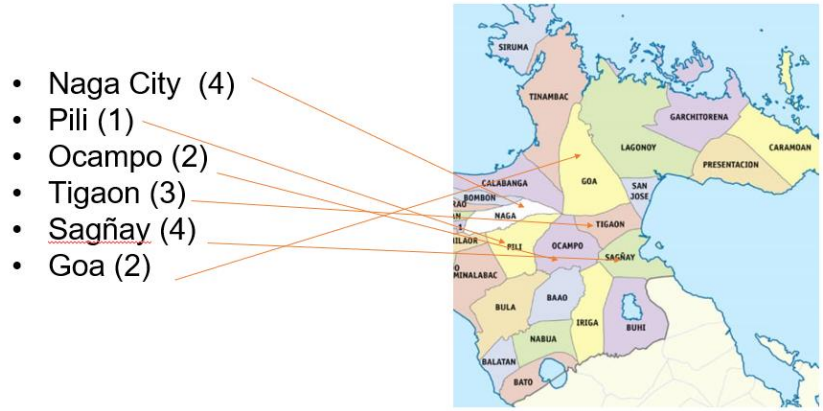


Figure 1. Location of the dairy farms visited in Camarines Sur, Philippines

2.3 Assessment of Animal- and Resource-based Indicators

Dairy farmers were informed of the objectives and purpose of this study, and their consent was obtained before participation. The data were gathered through on-farm visits and assessments from January to February, 2021. Assessment was performed when the dairy cattle were fed to ensure they were active. During the assessment, animals were approached only in the presence and with the consent of the dairy farmers. The animal-based indicators were assessed by observing dairy cows at a distance, undisturbed. Each welfare criterion (e.g., absence of injuries) has measures assessed (e.g., % of farms with lame cows) on the farm. The total population of dairy cows was 125 (average/farm: 7.8, median: 7.5, mode: 8). For dairy farms with fewer dairy cows (e.g., ≤10), the total enumeration approach was employed. For dairy farms with more dairy cows (e.g., ≥10), 50-75% of the population was assessed. This was employed because sub-sampling for small herds is not statistically appropriate due to the risk of sampling error and reduced representativeness. This was consistent with the recommendations of the Welfare Quality® Assessment Protocol to assess all animals in small herds [13]. The resource-based indicators were assessed through visual inspection of the housing systems and other on-farm resources. Since the data were binary (Yes/No) at the herd level, welfare measures were expressed as percentages [13]. Since the dairy cow population varies and the objective of this study was to benchmark dairy cows' welfare in Camarines Sur, a herd-level assessment was conducted. This was implemented to minimize stress during individual dairy cow assessments and to prevent interruptions by dairy farmers that could result in incomplete data collection [18]. Also, the herd-level assessment was performed to save time and resources in data collection and to minimize disturbance to dairy farmers' routines [19]. Additionally, the welfare status of dairy cows reflects the management practices employed by dairy farmers, thereby providing an assessment of herd-level housing, feeding, and hygiene systems [18]. A single observer assessed the animal- and resource-based indicators in the farms visited. The number of dairy farms visited and assessed daily varies (1-3) depending on inter-farm distance, accessibility, and dairy farmers' availability upon confirmation.

2.4 Institutional Animal Care and Use Committee Application

This study obtained approval from the Institutional Animal Care and Use Committee (IACUC) at the Central Bicol State University and Agriculture, San Jose, Pili, Camarines Sur, Philippines, which was granted exemption due to the non-invasive nature of the procedures, which included (1) visual observation of lesions; and (2) minimal handling of dairy cattle. Additionally, no dairy cattle or humans were harmed during the conduct of this study.

3. Results and Discussion

3.1 Absence of Prolonged Hunger

The measures for the animal-based indicators were presented in Table 1. All dairy farmers provide extra forage and concentrate to their dairy cows in addition to the basal feed. Although not measured (i.e., variable in amounts and frequency), the vast and available local vegetation [e.g., mixed grasses and legumes (*sakati*), corn stover] on the farm provides a sufficient source for cocktail forage supply. For concentrate supplements, complete feeds, and rice bran, supplementation was variable when available in variable amounts. Because dairy cows produce milk, they require increased nutrient intake to meet higher metabolic demands. Supplemental feeding prevents mobilization of body reserves, which can lead to emaciation, reduced lactation period, and delayed reproductive performance. This has resulted in the majority of farms visited having dairy cows with regular body condition. Additional forage provision supplies neutral detergent fiber, enhancing rumen function by cud chewing (20). Consequently, saliva production increases, serving as a rumen pH buffer, reducing the risk of acidosis (20, 21). Increased forage intake by dairy cows enhances cellulolytic microbial diversity and fiber digestion efficiency (21). Thereby, improving nutrient availability and contributing to better body condition in dairy cows as observed in this study. In Tanzania, Uganda, and Ethiopia, smallholder dairy farmers reported improved milk production and farm sustainability when additional feed was provided to dairy cows [14, 22, 23]. Therefore, the dietary requirements of dairy cows must be satisfied to prevent hunger, sustain a healthy rumen environment, and for optimum body conformation and milk yield.

Table 1. Animal-based indicator of dairy cow welfare in Camarines Sur.

Welfare Criteria	Yes	No
Absence of Prolonged Hunger		
% of farms offer extra forage and supplements to dairy cows	100	0
% of farms with cows having a regular body condition	87	13
Absence of Injuries		
% of farms with lame cows	13	87
% of farms with cows having integument alterations	20	80
Absence of Disease		
% of farms with cows coughing	7	93
% of farms with cows having nasal discharge	0	100
% of farms with cows having ocular discharge	0	100
% of farms with cows having vulval discharge	0	100
% of farms with cows having hampered breathing	7	93
% of farms with cows having diarrhea	7	93
% of farms with mastitis prevalence	13	87
Comfort Around Resting		
% of farms with cows having clean udders	73	27
% of farms with cows having clean flanks/upper legs	93	7
% of farms with cows having clean lower legs	73	27
Expression of Social Behavior		
% of farms with dairy cows show agonistic behavior	0	100

3.2 Absence of Injuries

The majority of the dairy farms visited (87%) had no dairy cows with lameness, while 13% had dairy cows that were partially lame. No dairy cows with severe lameness were observed during the visit. The low incidence of lameness can be attributed to the benefits provided by loafing and pasture areas (see Table 2). Additionally, providing bedding materials can reduce leg pressure, making lying and standing easier and more comfortable. Exercise may enhance hoof health and leg integrity, thereby improving dairy cows' welfare [24]. Lameness due to leg pain and injury causes discomfort in many dairy cows and is a major animal welfare concern. When dairy cows are lamed, the expression of animal behavior, such as lying down, feeding, cud chewing, reproduction, and interaction with conspecifics, is interfered with [25]. Discomfort can also negatively affect rumination and estrus, thereby lowering social and reproductive behaviors in dairy cows [26]. In Thailand, a researcher observed that lame dairy cows have poor reproductive performance (e.g., ovarian function), reduced time at feeding and feed intake, and reduced milk synthesis [26-28]. Several studies reported that lameness can reduce milk yield (approx. 0.5 -1.5 kg/day), consequently impacting the economics of dairying [6, 28]. Additionally, 80% of the dairy farms visited have dairy cows with no integumentary alterations, whereas only 20% have on-body parts, which cause pain and discomfort [29]. Providing sufficient space (e.g., loafing and pasture areas) for dairy cows enables them to exercise and avoid collisions with sharp edges, which may lead to skin bruises or abrasions. In developing countries, integumentary alterations in dairy cows are associated with poor husbandry practices and biological environmental stressors (e.g., infectious diseases), particularly in resource-limited operations [30]. Therefore, dairy farmers should improve management practices (e.g., by providing spatial allowance) to prevent lameness and integumentary alterations despite economic constraints.

3.3 Absence of Disease

The majority of the dairy farms visited had dairy cows that were free of nasal, ocular, or vulval (pus) discharges. Some dairy farms have dairy cows that were coughing, had hampered breathing, and diarrhea (7%), while 13% have mastitis. Cough, nasal and ocular discharges, and hampered breathing are commonly associated symptoms of respiratory disease in dairy cows [31]. The well-ventilated and spacious housing systems of the dairy farms visited have contributed to the low incidence of respiratory infections observed. In contrast, poor housing systems, dusty environments, and limited veterinary access due to financial constraints exacerbate respiratory infections in dairy cows in smallholder systems in developing countries [32, 33]. Consequently, coughing, nasal or ocular discharge, and impaired breathing impair normal respiration, feeding, and physiological functions and thus require urgent treatment. Dairy cows exhibiting these symptoms suffer from distress and potential respiratory infections [e.g., bovine respiratory disease; 34].

Although diarrhea is less common in dairy cows, moderate to severe cases can reduce appetite and milk production. The low diarrheal incidence can be attributed to the hygienic water management employed by dairy farmers in this study. In contrast, diarrheal prevalence in dairy cows on some farms visited may be attributed to the poorly maintained water sources. In many smallholder dairy systems in Africa and Southeast Asia, low population density, scattered housing, and frequent grazing (i.e., limited confinement) can reduce diarrheal incidence by reducing fecal-oral transmission [35]. Diarrhea can result in dehydration and electrolyte imbalance in the body due to body fluid losses from frequent watery defecation. The fluid losses include essential salts such as potassium and chloride, leading to dehydration, weakness, and depression [36]. Consequently, feed intake will decrease due to reduced appetite, thereby reducing milk production. To minimize the spread of diarrhea in the herd, dairy farmers must be knowledgeable about detecting its early signs and report immediately to the authorities for medication.

The low incidence of mastitis observed can be attributed to the cleaning of dairy cows' udders, flanks/upper legs, and lower legs, particularly at milking (see 3.4). Additionally, the provision of bedding materials by dairy farmers in this study improves body hygiene by absorbing excess moisture and reducing pathogen exposure [e.g., 37,38]. Mastitis can reduce dairy cows' mobility and appetite due to the pain in their udders [39]. The cows experience pain and discomfort, resulting in reduced milk yield and quality, long-term udder damage, and reduced fertility [40]. Poor housing conditions and unhygienic milking practices predispose cows to mastitis, leading to an increased incidence rate of 25-45% [39, 40]. Early detection by

periodic milk evaluation (e.g., California Mastitis Test) and treatment can minimize the risk of cow-to-cow transmission at the herd level. Therefore, it is important to keep dairy cows' udders healthy by maintaining a hygienic environment and by carefully handling them during milk collection.

3.4 Comfort Around Resting

The majority of the dairy farms visited have dairy cows with clean udders and (upper and lower) legs. The use of dry bedding, such as straw, absorbs excess moisture, while proper housing ventilation reduces humidity that harbors dirt [37, 38, 41]. In contrast, some dairy farms have dairy cows with dirty udders and legs, which could have contributed to the mastitis incidence reported in this study. Cows with dirty legs and flanks were the source of dirt adhering to the udders [42]. The absence of concrete flooring and adequate bedding materials in some of the dairy farms visited substantially contributed to the accumulation of dirt, thus forming unsanitary, muddy housing conditions. Factors such as poor hygiene (e.g., dirty floors and bedding), improper cleaning of the lying area, and infrequent manure removal can result in dirty flanks, legs, and udders. The accumulation of dirt in the lower limbs is associated with an increased prevalence of skin lesions and infections, predisposing dairy cows to integumentary alterations [43]. A loose housing system contributes to a higher proportion of dairy cows with clean legs, flanks, and udders [44], which have been observed on some of the dairy farms visited, particularly those with roofs, concrete flooring, and bedding materials (see Table 2). These resources keep floors dry, particularly during the rainy season or when drinking water spills. Therefore, despite the positive effects of a loose housing system on the freedom of movement and expression of the emotional state of dairy cows [44], the cleanliness of body parts must be given more weight for a healthy udder and mastitis-free herd.

3.5 Expression of Agonistic Behavior

No dairy cows were observed exhibiting agonistic behavior during the visit. The provision of additional spaces, such as loafing and pasture areas, as observed in this study, has reduced the competition for resources. A pasture area is an expansive space for dairy cows under a grazing system, limiting frequent contact and avoiding aggressive encounters [5, 45, 46]. Evidence indicates that a loafing area (e.g., 3-6 m^2/cow) provides modest space, reducing restlessness associated with aggressive encounters [5]. Agonistic behavior, such as aggression, causes submissive cows to displace or flee, especially during feeding or drinking. In times of spatial conflict, dominant cows bully submissive cows for wider or preferred spatial needs. Dairy cows that are less competitive tend to receive more agonistic interactions, which limit their access to resources (e.g., feed, water, space), hence impairing their welfare [47]. At feeding and drinking time, subordinate cows are displaced, reducing their intake and leading to nutritional stress and dehydration [48]. Continued agonistic behavior in the herd increases stress levels, a negative emotional state (e.g., fear, anxiety), poorer health conditions, and reduced milk production [47]. Therefore, dairy farmers should observe and correct agonistic behaviors by providing sufficient resources (e.g., space, partitions) to reduce aggression and improve productivity.

3.6 Ease of Movement

The measures for the resource-based indicators were presented in Table 2. All dairy farmers provide loafing and pasture areas for dairy cows. Many of the dairy farmers in this study have fewer dairy cows, thus have less competition for space. Providing a loafing area allows the cows to display a wider range of natural behaviors, such as grazing, grooming, and social interaction, and supports their physical (e.g., running, flight response, outdoor exposure) and psychological well-being (e.g., feeling of freedom) [5, 49, 50]. Additionally, loafing areas help dairy cows regulate body temperature by exposing them to sunlight or allowing them to cool down, depending on barn conditions [5, 49]. Dairy farmers practice integrated farming systems, allowing fallow and spacious lands to be utilized for grazing. These benefits are enhanced when dairy cows are allowed to run in the pasture. For instance, grazing encourages cows to walk, lie down, stand, and socialize, reducing boredom and aggression [51]. Access to pasture also lowers the risk of lameness, mastitis, hoof issues, hock lesions, uterine diseases, and death compared to confinement alone [50]. Moreover, cows feel more comfortable and relaxed with longer, synchronized lying periods, increased activity, and improved longevity [5]. Therefore, providing additional space for physical activities is essential for dairy cows' welfare.

In contrast, 33% of dairy farms use the tie-stall system, thereby limiting their dairy cows' access to outdoor space, which can lead to various welfare issues. Although the benefits of the tie-stall system were identified (e.g., saving space, preventing chasing), the primary negative impact on dairy cows' welfare is restriction of freedom of movement and the expression of natural behavior on the loose [52, 53]. Dairy cows in tie stalls cannot groom freely, choose a resting place with conspecifics, or explore their habitat [16]. Consequently, stereotypical (i.e., abnormal) behaviors such as tongue rolling, rubbing against equipment or facilities, or bar biting may be expressed, particularly when restricted (or denied) from outdoor access [15]. The risk of collision with partitions, walls, and the like is higher and can result in skin alterations/bruises, as observed in other dairy cows assessed (see Table 1). In extreme cases, the risk of lameness, injuries (e.g., foot rot, hock lesions, tail injuries), infections, mastitis, and mental welfare (e.g., frustration) increases [16]. Dairy farmers using tie-stall systems need to be informed of the welfare limitations of these systems and encouraged to promote natural behavioral expression in dairy cows. Therefore, the disadvantages of the tie-stall system outweigh its advantages, as it denies dairy cows the freedom to express their natural behavior, thereby impairing their welfare.

Table 2. Resource-based indicator of dairy cow welfare in Camarines Sur.

Welfare Criteria	Yes	No
Ease of Movement		
% of farms with loafing area	100	0
% of farms with pasture area	100	0
% of farms with cows tied in stalls	33	67
Absence of Prolonged Thirst		
% of farms provide potable water	100	0
% of farms with clean water points	73	27
% of farms with cows having access to water	100	0
Comfort and Protection from Adverse Weather		
% of farms with housing provision	67	33
% of farms providing roofs to dairy cows	73	27
% of farms providing partitions to dairy cows	67	33
% of farms providing concrete floors to dairy cows	67	33
% of farms providing bedding to dairy cows	87	13
% of farms providing grooming facilities to dairy cows	0	100

3.7 Absence of Prolonged Thirst

All the dairy farmers provide potable water accessible to dairy cows. The provision of clean, potable water by dairy farmers in this study results in higher dairy cow incidence rates without diarrhea. Milk is primarily composed of water (approximately 85-87%) and thus requires a sufficient supply for normal physiological functions. Free access to potable water hydrates dairy cows, especially during diarrhea, summer, hay feeding, or body exhaustion [54]. A study comparing herds of dairy cows with restricted and free access to drinking water showed that herds with free access to drinking water produce 1.7 L more milk/cow/day than herds of cows with restricted access to drinking water [55]. In contrast, 27% of the dairy farms have dirty water points. Consequently, dirty water points harbor pathogens that may predispose dairy cows to waterborne diseases, thereby increasing veterinary costs and shortening productivity [56]. Contaminated water points exacerbate water scarcity, which is associated with competition for water access, impairing dairy cows' feed intake, milk production, and health [57, 58]. In contrast, clean water facilities increase water intake because of the absence of unpleasant odors, tastes, and appearances. Therefore, dairy farmers should keep water points clean to ensure adequate water intake in line with their physiological needs.

3.8 Comfort and Protection from Adverse Weather

The majority of the dairy farms visited have housing with roofs and concrete flooring, with partitions and beddings provided. These dairy farmers who provide these facilities value their dairy cows more in

adverse weather, thereby protecting their welfare. Housing is one of the most important investments to protect dairy cows from adverse weather. An ideal housing system should not restrict cows from expressing their normal behaviors, as it will impair their welfare [59]. Partitions in dairy cows' housing are essential because they provide each cow with a comfortable resting place, helping reduce conflict and aggression [60]. Since dairy cows rest for 12-14 hours daily, they need clean, dry, and comfortable lying areas [61]. Indicators of optimal welfare in partitions include cows resting in a comfortable position, no collisions, rising effortlessly, and exhibiting grooming behavior [62]. Moreover, sufficient space (min. 10 m2/cow) and suitable bedding materials are crucial for preventing injuries and lameness [63]. Conversely, no dairy farmers have provided grooming facilities to dairy cows. This may be attributed to economic constraints, infrastructural limitations, cultural practices, or knowledge gaps about the benefits of grooming on dairy cow welfare [64-66]. Financially constrained dairy farmers prioritize essential needs, such as feed and veterinary services, over grooming facilities for dairy cows [64, 65]. The absence of grooming facilities on the dairy farms visited reflects traditional management practices passed down through generations, in which such facilities were deemed unnecessary. Consequently, the dairy farmers involved in this study were unaware of the benefits of adopting improved care and management practices, such as installing grooming facilities. By grooming, dirt, debris, and external parasites are eliminated, thereby decreasing skin irritation and infection [4]. Furthermore, grooming has a calming effect, thereby lowering stress levels and improving immune function, feed intake, milk production, and expression of natural behaviors [4, 67]. Conversely, the absence of grooming facilities can impair dairy cows' welfare because they are unable to express natural behaviors, such as scratching and grooming [68]. Consequently, stress levels, health problems, and discomfort increase, which can later reduce milk production and shorten the dairy cows' longevity [4, 31, 67]. Although providing grooming facilities entails an additional cost for the dairy farmer, the benefits outweigh the costs, improving dairy cows' welfare.

4. Conclusions

The majority of the dairy cows assessed on the dairy farms visited have good welfare, as indicated by animal-based indicators. This is supported by a low percentage of dairy farms with ill or ill dairy cows (e.g., respiratory infection, mastitis) among the assessed dairy cows. Although the majority of dairy farmers practice sanitary measures, some should improve resource-based indicators (e.g., installing grooming facilities, providing housing, and implementing a tied-in stalls system) to enhance dairy cows' welfare. The long-term benefits of grooming facilities (e.g., removal of external parasites, calming effect) to the dairy cow welfare can outweigh the cost of investment. Similarly, providing housing can protect dairy cows from inclement weather, which may weaken their immune systems. The reported negative effects of the tie stall system compromise dairy cows' freedom to express behavior and require an effective solution (e.g., tethering, practicing a loose-housing system, policy development). For future studies, assessing the impacts of improving dairy cows' welfare on milk production and quality, their income would educate dairy farmers about its economic benefits. Given that management-based indicators can affect dairy cows' welfare, their assessment is essential to achieve a more comprehensive understanding. Since they produce dairy calves, their welfare needs to be assessed.

5. Acknowledgments

The author acknowledges the efforts and participation of Dr. Guia L. Hermoso, Mr. Neil V. Cordenete, the Bicol Federation of Dairy Cooperatives, the dairy farmers of Camarines Sur and their cooperatives, and the Central Bicol State University of Agriculture (CBSUA) during the research.

Author Contributions: The author performed the activities of conceptualizing the research proposal, coordinating with stakeholders, consolidating and analyzing data, and writing the manuscript.

Funding: This research was made possible by the financial support of the Research Division of CBSUA.

Conflict of Interest: The author declares that there are no conflicts of interest in the conduct of this study.

References

[1] Department of Trade and Industry (DTI). *Profile of Region 5*; Department of Trade and Industry: Makati City, Philippines, 2024.

[2] National Economic and Development Authority (NEDA). *Bicol Regional Development Plan 2023–2025*; National Economic and Development Authority Region V: Legazpi City, Philippines, 2023.

[3] Donaldson, S. L.; Albright, J.; Black, W. Primary social relationships and cattle behavior. In *Proceedings of the Indiana Academy of Science*; 1971; pp 345–351.

[4] Goncu, S.; Yesil, M. I.; Yilmaz, N. The cattle grooming behavior and some problems with technological grooming instruments for cow welfare. *J. Environ. Sci. Eng.* **2019**, *8*, 190–196. https://doi.org/10.17265/2162-5263/2019.05.005

[5] Crump, A.; Jenkins, K.; Bethell, E. J.; Ferris, C. P.; Arnott, G. Pasture access affects behavioral indicators of wellbeing in dairy cows. *Animals* **2019**, *9* (11), 902. https://doi.org/10.3390/ani9110902

[6] Warnick, L.; Janssen, D.; Guard, C.; Gröhn, Y. The effect of lameness on milk production in dairy cows. *J. Dairy Sci.* **2001**, *84*(9), 1988–1997. https://doi.org/10.3168/jds.S0022-0302(01)74642-5

[7] Barkema, H.; Schukken, Y.; Lam, T.; Beiboer, M.; Wilmink, H.; Benedictus, G.; Brand, A. Incidence of clinical mastitis in dairy herds grouped in three categories by bulk milk somatic cell counts. *J. Dairy Sci.* **1998**, *81*(2), 411–419. https://doi.org/10.3168/jds.S0022-0302(98)75591-2

[8] Dechow, C. D.; Smith, E.; Goodling, R. The effect of management system on mortality and other welfare indicators in Pennsylvania dairy herds. *Anim. Welfare* **2011**, *20*(2), 145–158. https://doi.org/10.1017/S0962728600002633

[9] Hogeveen, H.; Huijps, K.; Lam, T. Economic aspects of mastitis: New developments. *N. Z. Vet. J.* **2011**, *59*(1), 16–23. https://doi.org/10.1080/00480169.2011.547165

[10] Margerison, J.; Preston, T.; Phillips, C. Restricted suckling of tropical dairy cows by their own calf or other cows' calves. *J. Anim. Sci.* **2002**, *80* (6), 1663–1670. https://doi.org/10.2527/2002.8061663x

[11] Fröberg, S.; Aspegren-Güldorff, A.; Olsson, I.; Marin, B.; Berg, C.; Hernández, C.; Galina, C.; Lidfors, L.; Svennersten-Sjaunja, K. Effect of restricted suckling on milk yield, milk composition and udder health in cows and behaviour and weight gain in calves in dual-purpose cattle in the tropics. *Trop. Anim. Health Prod.* **2007**, *39*(1), 71–81. https://doi.org/10.1007/s11250-006-4418-0

[12] Schreiner, D.; Ruegg, P. Relationship between udder and leg hygiene scores and subclinical mastitis. *J. Dairy Sci.* **2003**, *86*(11), 3460–3465. https://doi.org/10.3168/jds.S0022-0302(03)73950-2

[13] Winckler, C.; Algers, B.; Van Reenen, K.; Leruste, H.; Veissier, I.; Keeling, L. *Welfare Quality® Assessment Protocol for Cattle (Fattening Cattle, Dairy Cows, Veal Calves)*; Welfare Quality® Consortium, 2009.

[14] Nyawira, S. S.; Mwendia, S. W.; Mwema, E.; Gonzalez-Quintero, R.; Nzogela, B.; Sila, A.; Mwilawa, A.; Kizima, J.; Paul, B. K.; Notenbaert, A. Forage crops boost the productivity and environmental sustainability of dairy farmers in southern Tanzania. *Agric. Ecosyst. Environ.* **2025**, *389*, 109649. https://doi.org/10.1016/j.agee.2025.109649

[15] Popescu, S.; Borda, C.; Diugan, E. A.; Spinu, M.; Groza, I. S.; Sandru, C. D. Dairy cows welfare quality in tie-stall housing system with or without access to exercise. *Acta Vet. Scand.* **2013**, *55*(1), 43. https://doi.org/10.1186/1751-0147-55-43

[16] EFSA Panel on Animal Health and Welfare; Nielsen, S. S.; Alvarez, J.; Bicout, D. J.; Calistri, P.; Canali, E.; Drewe, J. A.; Garin-Bastuji, B.; Gonzales Rojas, J. L.; Gortázar Schmidt, C.; et al. Welfare of dairy cows. *EFSA J.* **2023**, *21*(5), e07993. https://doi.org/10.2903/j.efsa.2023.7993

[17] Rushen, J. *Housing and the Welfare of Dairy Cattle*; Burleigh Dodds Science Publishing: Cambridge, U.K., 2017.

[18] de Vries, M.; Bokkers, E.; Van Schaik, G.; Botreau, R.; Engel, B.; Dijkstra, T.; De Boer, I. Evaluating results of the Welfare Quality multi-criteria evaluation model for classification of dairy cattle welfare at the herd level. *J. Dairy Sci.* **2013**, *96* (10), 6264–6273. https://doi.org/10.3168/jds.2012-6129

[19] Linstädt, J.; Thöne-Reineke, C.; Merle, R. Animal-based welfare indicators for dairy cows and their validity and practicality: A systematic review of the existing literature. *Front. Vet. Sci.* **2024**, *11*, 1429097. https://doi.org/10.3389/fvets.2024.1429097

[20] Van Saun, R. Nutritional Requirements of Dairy Cattle. In *MSD Veterinary Manual*; MSD Animal Health: Rahway, NJ, USA, 2024.

[21] Ramos, S. C.; Jeong, C. D.; Mamuad, L. L.; Kim, S. H.; Kang, S. H.; Kim, E. T.; Cho, Y. I.; Lee, S. S.; Lee, S. S. Diet transition from high-forage to high-concentrate alters rumen bacterial community composition, epithelial transcriptomes and ruminal fermentation parameters in dairy cows. *Animals* **2021**, *11*(3), 838. https://doi.org/10.3390/ani11030838

[22] Bezabih, M.; Adie, A. *Cultivated Forages Boost Production and Income for Dairy Farmers in Bishoftu District, Ethiopia*; 2024.

[23] Herforth, N.; Tirivanhu, P.; Ewell, H.; Miethbauer, T.; Nawrotzki, R. Appetite for forages? The adoption and multidimensional impacts of improved forage grasses in Uganda. *Front. Sustain. Food Syst.* **2025**, *9*, 1585410. https://doi.org/10.3389/fsufs.2025.1585410

[24] Black, R.; Van Amstel, S.; Krawczel, P. Effect of prepartum exercise, pasture turnout, or total confinement on hoof health. *J. Dairy Sci.* **2017**, *100*(10), 8338–8346. https://doi.org/10.3168/jds.2016-12082

[25] Cook, N.; Hess, J.; Foy, M.; Bennett, T.; Brotzman, R. Management characteristics, lameness, and body injuries of dairy cattle housed in high-performance dairy herds in Wisconsin. *J. Dairy Sci.* **2016**, *99*(7), 5879–5891. https://doi.org/10.3168/jds.2016-10956

[26] Whay, H. R.; Shearer, J. K. The impact of lameness on welfare of the dairy cow. *Vet. Clin. North Am. Food Anim. Pract.* **2017**, *33*(2), 153–164. https://doi.org/10.1016/j.cvfa.2017.02.008

[27] Tsousis, G.; Boscos, C.; Praxitelous, A. The negative impact of lameness on dairy cow reproduction. *Reprod. Domest. Anim.* **2022**, *57* (Suppl. 5), 33–39. https://doi.org/10.1111/rda.14210

[28] Prasomsri, P. Effect of lameness on daily milk yield in dairy cow. *Thai J. Vet. Med.* **2022**, *52*(4), 679–687. https://doi.org/10.56808/2985-1130.3263

[29] Alrhmoun, M.; Zanon, T.; Poulopoulou, I.; Katzenberger, K.; Gauly, M. Associated risk factors for skin alterations in dairy cattle kept on small-scale mountain farms. *PLoS One* **2023**, *18*(8), e0285394. https://doi.org/10.1371/journal.pone.0285394

[30] Davies, F. G. Lumpy skin disease of cattle: A growing problem in Africa and the Near East. *World Anim. Rev.* **1991**, *68*(3), 37–42.

[31] World Organisation for Animal Health (WOAH). *Terrestrial Animal Health Code*; WOAH: Paris, France, 2018.

[32] Gorden, P. J.; Plummer, P. Control, management, and prevention of bovine respiratory disease in dairy calves and cows. *Vet. Clin. North Am. Food Anim. Pract.* **2010**, *26*(2), 243–259. https://doi.org/10.1016/j.cvfa.2010.03.004

[33] Massi, R. P.; Lunardi, M.; Alfieri, A. F.; Alfieri, A. A. Neglected bacterial infections associated with bovine respiratory disease in lactating cows from high-yielding dairy cattle herds. *Braz. J. Microbiol.* **2023**, *54*(4), 3275–3281. https://doi.org/10.1007/s42770-023-01165-1

[34] Molina, F. M.; Marín, C. C. P.; Moreno, L. M.; Buendía, E. I. A.; Marín, D. C. P. Welfare Quality® for dairy cows: Towards a sensor-based assessment. *J. Dairy Res.* **2020**, *87*(S1), 28–33. https://doi.org/10.1017/S002202992000045X

[35] Zirra-Shallangwa, B.; González Gordon, L.; Hernandez-Castro, L. E.; Cook, E. A. J.; Bronsvoort, B. M. de C.; Kelly, R. F. The epidemiology of bovine viral diarrhea virus in low- and middle-income countries: A systematic review and meta-analysis. *Front. Vet. Sci.* **2022**, *9*, 947515. https://doi.org/10.3389/fvets.2022.947515

[36] MSD Veterinary Manual. *Intestinal Diseases in Cattle*; Merck & Co., Inc.: Rahway, NJ, USA, 2025.

[37] Food and Agriculture Organization of the United Nations (FAO); International Dairy Federation (IDF). *Guide to Good Dairy Farming Practice*; Animal Production and Health Guidelines No. 8; FAO: Rome, Italy, 2011.

[38] Smith, K.; Hogan, J. Bedding's contribution to mastitis in dairy cows. In *Dairy Housing and Equipment Systems: Managing and Planning for Profitability*; Natural Resource, Agriculture, and Engineering Service: Ithaca, NY, 2000; pp 265–270.

[39] Mainau, E.; Temple, D.; Manteca, X. Welfare issues related to mastitis in dairy cows. *Farm Anim. Welfare Educ. Cent.* **2014**, *10*(2).

[40] Cheng, W. N.; Han, S. G. Bovine mastitis: Risk factors, therapeutic strategies, and alternative treatments—A review. *Asian-Australas. J. Anim. Sci.* **2020**, *33*(11), 1699–1713. https://doi.org/10.5713/ajas.20.0156

[41] Wolfe, T.; Vasseur, E.; DeVries, T.; Bergeron, R. Effects of alternative deep bedding options on dairy cow preference, lying behavior, cleanliness, and teat end contamination. *J. Dairy Sci.* **2018**, *101*(1), 530–536. https://doi.org/10.3168/jds.2016-12358

[42] Neja, W.; Bogucki, M.; Jankowska, M.; Sawa, A. Effect of cow cleanliness in different housing systems on somatic cell count in milk. *Acta Vet. Brno* **2016**, *85*(1), 55–61. https://doi.org/10.2754/avb201685010055

[43] Schenkenfelder, J.; Winckler, C. To meet or not to meet welfare outcome thresholds: A case-control study in dairy cow herds. *Animal* **2022**, *16*(3), 100461. https://doi.org/10.1016/j.animal.2022.100461

[44] Ostojić Andrić, D.; Hristov, S.; Zlatanović, Z.; Nikšić, D.; Pajić, M.; Petrović Caro, V.; Stanojković, A. Dairy cows' welfare quality in relation to housing system. *Large Anim. Rev.* **2022**, *28*, 265–272.

[45] Crump, A.; Jenkins, K.; Bethell, E. J.; Ferris, C. P.; Kabboush, H.; Weller, J.; Arnott, G. Optimism and pasture access in dairy cows. *Sci. Rep.* **2021**, *11*(1), 4882. https://doi.org/10.1038/s41598-021-84371-x

[46] Smid, A.-M. C.; Weary, D. M.; von Keyserlingk, M. A. The influence of different types of outdoor access on dairy cattle behavior. *Front. Vet. Sci.* **2020**, *7*, 257. https://doi.org/10.3389/fvets.2020.00257

[47] Krahn, J.; Foris, B.; Sheng, K.; Weary, D. M.; von Keyserlingk, M. A. Effects of group size on agonistic interactions in dairy cows: A descriptive study. *Animal* **2024**, *18*(3), 101083. https://doi.org/10.1016/j.animal.2024.101083

[48] Foris, B.; Thompson, A.; von Keyserlingk, M. A.; Melzer, N.; Weary, D. M. Automatic detection of feeding- and drinking-related agonistic behavior and dominance in dairy cows. *J. Dairy Sci.* **2019**, *102*(10), 9176–9186. https://doi.org/10.3168/jds.2019-16697

[49] Haskell, M. J.; Masłowska, K.; Bell, D. J.; Roberts, D. J.; Langford, F. M. The effect of a view to the surroundings and microclimate variables on use of a loafing area in housed dairy cattle. *Appl. Anim. Behav. Sci.* **2013**, *147*(1–2), 28–33. https://doi.org/10.1016/j.applanim.2013.04.016

[50] Pasture for Life Association (PFLA). *The Animal Welfare and Environmental Benefits of Pasture for Life Farming*; Pasture for Life Association: U.K., 2018.

[51] Langford, F. M.; Bell, D. J.; Nevison, I. M.; Tolkamp, B. J.; Roberts, D. J.; Haskell, M. J. What type of loafing areas do housed dairy cattle prefer? *Appl. Anim. Behav. Sci.* **2021**, *245*, 105511. https://doi.org/10.1016/j.applanim.2021.105511

[52] Beaver, A.; Weary, D. M.; von Keyserlingk, M. A. Invited review: The welfare of dairy cattle housed in tie-stalls compared to less-restrictive housing types: A systematic review. *J. Dairy Sci.* **2021**, *104*(9), 9383–9417. https://doi.org/10.3168/jds.2020-19609

[53] Robbins, J. A.; Roberts, C.; Weary, D. M.; Franks, B.; von Keyserlingk, M. A. Factors influencing public support for dairy tie-stall housing in the United States. *PLoS One* **2019**, *14*(5), e0216544. https://doi.org/10.1371/journal.pone.0216544

[54] Golher, D.; Patel, B.; Bhoite, S.; Syed, M.; Panchbhai, G.; Thirumurugan, P. Factors influencing water intake in dairy cows: A review. *Int. J. Biometeorol.* **2021**, *65*, 617–625. https://doi.org/10.1007/s00484-020-02038-0

[55] Daros, R. R.; Bran, J. A.; Hötzel, M. J.; von Keyserlingk, M. A. Readily available water access is associated with greater milk production in grazing dairy herds. *Animals* **2019**, *9*(2), 48. https://doi.org/10.3390/ani9020048

[56] Crossley, R.; Bokkers, E.; Browne, N.; Sugrue, K.; Kennedy, E.; Conneely, M. Risk factors associated with indicators of dairy cow welfare during the housing period in Irish spring-calving hybrid pasture-based systems. *Prev. Vet. Med.* **2022**, *208*, 105760. https://doi.org/10.1016/j.prevetmed.2022.105760

[57] Robertson, J. Water: The good, the bad, and the ugly. *Vet. Ireland J.* **2019**, *9*(12).

[58] Popescu, S.; Borda, C.; Diugan, E. A.; Niculae, M.; Stefan, R.; Sandru, C. D. The effect of the housing system on the welfare quality of dairy cows. *Ital. J. Anim. Sci.* **2014**, *13*(1), 2940. https://doi.org/10.4081/ijas.2014.2940

[59] Phillips, C.; Beerda, B.; Knierim, U.; Waiblinger, S.; Lidfors, L.; Krohn, C.; Canali, E.; Valk, H.; Veissier, I.; Hopster, H. A review of the impact of housing on dairy cow behaviour, health and welfare. In

Livestock Housing; Wageningen Academic Publishers: Wageningen, The Netherlands, 2013; pp 37–54. https://doi.org/10.3920/978-90-8686-771-4_02

[60] Gaworski, M. How do we recognize the effects of dairy cattle activity in the lying area? A case study in free-stall barns. *Animals* **2025**, *15*(6), 880. https://doi.org/10.3390/ani15060880

[61] Macrae, A. Housing in dairy cattle farms. In *Encyclopedia of Livestock Medicine for Large Animals and Poultry Production*; Simões, J., Ed.; Springer: Cham, Switzerland, 2024; pp 1–10. https://doi.org/10.1007/978-3-031-52133-1

[62] Gieseke, D.; Lambertz, C.; Gauly, M. Effects of cubicle characteristics on animal welfare indicators in dairy cattle. *Animal* **2020**, *14*, 1934–1942. https://doi.org/10.1017/S1751731120000609

[63] Witkowska, D.; Ponieważ, A. The effect of housing system on disease prevalence and productive lifespan of dairy herds—A case study. *Animals* **2022**, *12*(13), 1610. https://doi.org/10.3390/ani12131610

[64] Loura, M.; Ghalawat, S.; Malik, J.; Mehla, S.; Yadav, E.; Kumar, M. Constraints faced by dairy farmers in Haryana. *Constraints* **2021**, *51*(3).

[65] Buchan, M. S.; Lhermie, G.; Mijar, S.; Pajor, E.; Orsel, K. Individual drivers and barriers to adoption of disease control and welfare practices in dairy and beef cattle production: A scoping review. *Front. Vet. Sci.* **2023**, *10*, 1104754. https://doi.org/10.3389/fvets.2023.1104754

[66] Fita, L.; Trivedi, M.; Galmessa, U. Constraints of farmers in adopting improved dairy husbandry practices: The case of Ada'a District, Oromiya State, Ethiopia. *J. Sci. Sustain. Dev.* **2013**, *1*(1), 63–70.

[67] Li, H.; Zhang, R.; Li, H.; Yuan, H.; Zhang, R.; Ren, H.; Xiao, J.; Li, Z.; Wang, A.; Jin, Y. Effects of using mechanical brushes on the productive performance of dairy cows. *Vet. Sci.* **2024**, *11*(10), 481. https://doi.org/10.3390/vetsci11100481

[68] Dickson, E. J.; Monk, J. E.; Lee, C.; McDonald, P. G.; Narayan, E.; Campbell, D. L. Loss of a grooming enrichment impacts physical, behavioural, and physiological measures of welfare in grazing beef cattle. *Animal* **2024**, *18*(3), 101091. https://doi.org/10.1016/j.animal.2024.101091

ASEAN
Journal of Scientific and Technological Reports
Online ISSN:2773-8752

Research article

Study of Surface Water Quality Using Biological Indicators Inside the Ruean Thai Pond Area, Nakhon Si Thammarat Rajabhat University

Wilasinee Nongnueang[1], and Wattananarong Markphan[1*]

[1] Faculty of Science and Technology, Nakhon Si Thammarat Rajabhat University, Nakhon Si Thammarat, 80280, Thailand
* Correspondence: wattanarong_mak@nstru.ac.th

Citation:
Nongnueang, W.; Markphan, W. Study of surface water quality using biological indicators inside the ruean Thai pond area, Nakhon Si Thammararat Rajabhat University. *ASEAN J. Sci. Tech. Report.* **2026**, *29*(7), e264369. https://doi.org/10.55164/ajstr.v29i7.264369

Article history:
Received: March 16, 2026
Revised: April 16, 2026
Accepted: April 25, 2026
Available online: June 16,2026

Publisher's Note:
This article is published and distributed under the terms of the Thaksin University.

Abstract: Biological monitoring using macroinvertebrate bioindicators provides an ecologically integrative approach to water quality assessment, capturing cumulative pollution effects that physicochemical measurements alone cannot reflect. This study assessed the surface water quality of the Ruean Thai Pond, a natural spring-fed water body within Nakhon Si Thammarat Rajabhat University, using aquatic macroinvertebrate assemblages. Five sampling stations were established along the pond. Sampling was conducted four times over two months (September–October 2021), totaling 20 station-sampling events. Aquatic insect larvae and associated bioindicator organisms were collected using brick substrates and colander nets, then identified to family level and classified into water quality categories according to the Stream Detective Manual (Green World Foundation, 2018). A total of 13 bioindicator types (morphotypes) representing 5 orders and 9 families were recorded. Ephemeroptera was the most diverse order with 3 families (*Leptophlebiidae*, *Potamanthidae*, *Baetidae*), followed by *Gastropoda* and *Trichoptera* (2 families each), and *Caridea*, *Odonata*, and *Hemiptera* (1 family each). "Very clean water" bioindicators — branched-gill and feathered-gill mayfly larvae (*Leptophlebiidae*, *Potamanthidae*) and cased and uncased caddisfly larvae (*Odontoceridae*, *Hydropsychidae*) — dominated Stations 2–5, accounting for 54–78% of total bioindicator counts. Station 1 (pond entrance station) was the only station classified as "fair–clean," where fair-category organisms (n = 30) outnumbered very-clean-category organisms (n = 0). Four of five stations (80%) were consistently classified as "very clean water" across all sampling rounds, yielding an overall classification of "very clean" for the Ruean Thai Pond. These findings provide a preliminary wet-season biological assessment for university water resource management and for downstream community water-use planning.

Keywords: Water quality; macroinvertebrates; bioindicators; ephemeroptera; Thailand

1. Introduction

Water is an essential resource for all living organisms. Despite covering approximately 70% of the Earth's surface, only about 1% of the total global water volume is conveniently accessible for human consumption or agriculture [1]. Surface waters, including rivers, ponds, and lakes, account for only 0.6% of global freshwater and are particularly vulnerable to pollution from agricultural, industrial, and domestic sources [2]. Thailand has faced persistent water-resource challenges over recent decades, including severe drought, degraded water sources, and heavy flooding, exacerbated by a growing population, climate change, and inadequate water-management strategies [3-5]. Maintaining water quality in natural surface water bodies

located within educational institutions is particularly important, as these systems serve local communities and support aquatic biodiversity.

Conventional water quality assessment relies on physicochemical and bacteriological parameters [6]. However, biological monitoring using macroinvertebrates, especially aquatic insect larvae, provides an integrative measure of ecological health by reflecting cumulative exposure to environmental stressors over time [6]. Benthic macroinvertebrates are widely used as bioindicators because different taxa exhibit distinct tolerances to dissolved oxygen and organic pollution [7, 8]. Clean water sources support sensitive groups such as mayfly larvae (Ephemeroptera) and stonefly larvae (Plecoptera), whereas polluted waters are dominated by tubificid worms and red midge larvae [9]. Nakhon Si Thammarat Rajabhat University contains a natural surface water body known as the "Kha Mahachai Stream," which flows through the campus and into surrounding communities. The Ruean Thai Pond within this stream network serves as an important habitat for diverse aquatic organisms. Despite its ecological significance, systematic biological water quality monitoring has not previously been conducted at this site [10]. This study aimed to (1) survey the diversity of aquatic insect larvae and other bioindicator organisms in the surface water of the Ruean Thai Pond, and (2) assess water quality at five sampling stations using the Stream Detective Manual (Green World Foundation, 2018) as the classification standard.

2. Materials and Methods

2.1 Study Area

The study was conducted at the Ruean Thai Pond located within Nakhon Si Thammarat Rajabhat University (approximately 8°25′N, 99°58′E), Nakhon Si Thammarat Province, southern Thailand. The pond is a section of the Kha Mahachai Stream, a natural, spring-fed waterway that flows through the campus. Five sampling stations were established across the pond area (Fig. 1).

Station 1: Ruean Thai entrance area (pond entrance station — spatial starting point of transect)

Station 2: Bridge behind Building 28 (Cultural Center)

Station 3: Ruean Thai, adjacent to the Demonstration School

Station 4: Area behind Building 53

Station 5: Bridge behind Building 8 (Arts and Culture College)

2.2 Sampling Procedure and Schedule

Sampling was conducted four times over two months (September–October 2021), with collections on 1 September, 15 September, 1 October, and 15 October 2021, between 09:00 and 12:00 h at each station. Aquatic insect larvae and associated bioindicator organisms were collected using a standard colander-net by sweeping bank margins, leaf litter, and submerged substrates. Brick substrates (approximately 20 × 10 × 5 cm) were placed at each station for organism attachment and retrieved during each collection event [11]. Collected organisms were transferred to a white tray for sorting. Identification was performed under a hand lens against pictorial identification cards of the Stream Detective Kit (Green World Foundation, 2018), and organisms were assigned to bioindicator categories: very clean water, clean water, fair water, dirty water, or non-indicator [12].

2.3 Equipment

Standard equipment used in this study included the Stream Detective Kit (Green World Foundation, 2018), basins, colander nets, spoons, and cups for sorting, hand lenses (×10), brick substrates, nylon rope, field notebooks, and digital cameras.

2.4 Data Analysis

Water quality at each station and sampling event was determined by the dominant bioindicator group recorded, following the scoring criteria of the Stream Detective Manual. Overall water quality per station was assessed across all four sampling rounds and summarized in comparative tables and bar graphs.

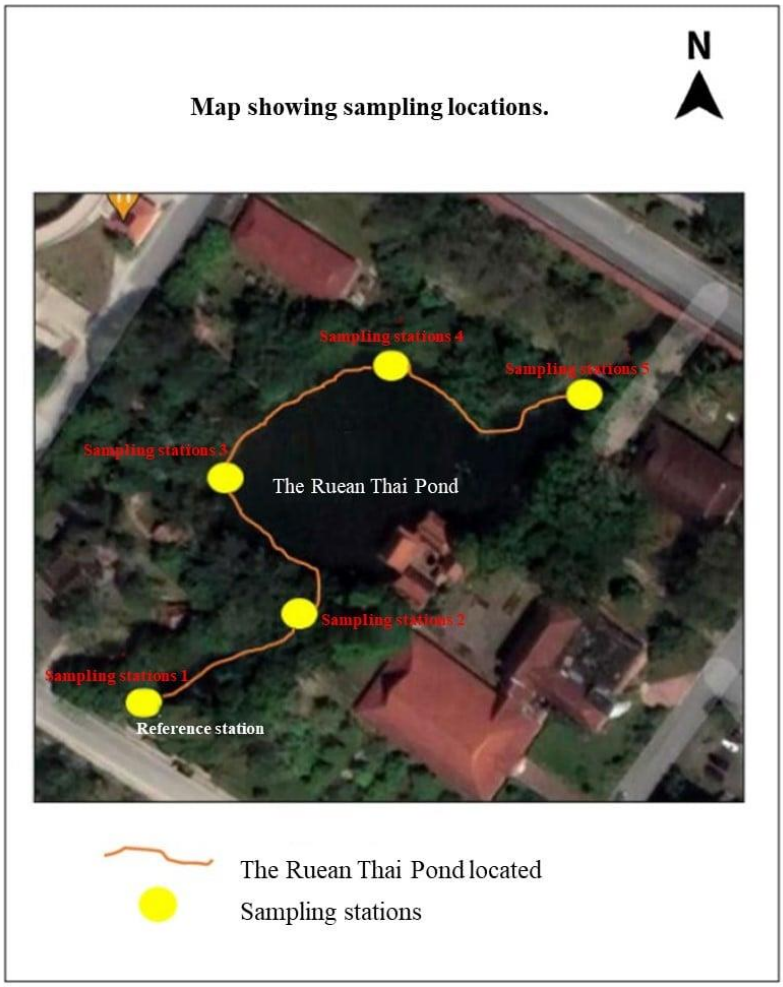


Figure 1. Map of the Ruean Thai Pond within Nakhon Si Thammarat Rajabhat University showing the five surface water sampling stations: Station 1 (pond entrance), Station 2 (bridge behind Building 28, Cultural Centre), Station 3 (Ruean Thai area adjacent to the Demonstration School), Station 4 (behind Building 53), and Station 5 (bridge behind Building 8, Arts and Culture College). Sampling was conducted four times over two months (September–October 2021).

3. Results and Discussion

3.1 Diversity of Bioindicator Organisms

A total of 6 orders and 9 families of aquatic insects and associated organisms were recorded across all five stations and four sampling events (Table 1). The order *Ephemeroptera* (mayflies) was the most species-rich, represented by 3 families (*Leptophlebiidae*, *Potamanthidae*, and *Baetidae*). Gastropoda and Trichoptera each contributed 2 families, while Caridea and Hemiptera each contributed 1 family (Table 2). The diversity of bioindicator taxa recorded in this study is consistent with findings from comparable university pond surveys in Thailand. Phrommi et al. [13] reported similar Ephemeroptera-dominated communities in freshwater ponds at Kasetsart University, while Rungnapa and Thattaporn [14] documented EPT assemblages (Ephemeroptera, Plecoptera, Trichoptera) as characteristic of good-quality streams in northern Thailand.

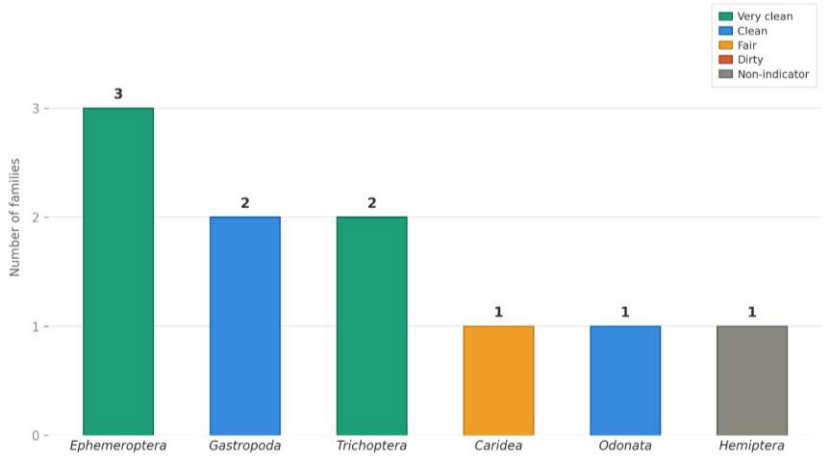
Table 1. Summary of bioindicator taxa recorded in the Ruean Thai Pond (September–October 2021).

Bioindicator Organism	Family	Order	Water Quality Category
Branched-gill mayfly larva	*Leptophlebiidae*	*Ephemeroptera*	Very clean
Feathered-gill mayfly larva	*Potamanthidae*	*Ephemeroptera*	Very clean
Cased caddisfly larva	*Odontoceridae*	*Trichoptera*	Very clean
Uncased caddisfly larva	*Hydropsychidae*	*Trichoptera*	Very clean
Tower snail	*Thiaridae*	*Gastropoda*	Clean
Short dragonfly larva	—	*Odonata*	Clean
Waterfall shrimp	*Palaemonidae*	*Caridea*	Clean
Freshwater shrimp (Goby shrimp)	*Palaemonidae*	*Caridea*	Fair
Single-valve snail	*Viviparidae*	*Gastropoda*	Fair
Swimming mayfly larva	*Baetidae*	*Ephemeroptera*	Fair
Red midge larva	*Chironomidae*	—	Dirty
Sewage worm	*Tubificidae*	—	Dirty
Water strider	*Gerridae*	*Hemiptera*	Non-indicator

A total of 5 orders (plus infraorder Caridea within Decapoda) and 9 families of aquatic insects and associated organisms were recorded across all five sampling stations (Fig. 2). The order Ephemeroptera (mayflies) was the most taxonomically diverse, represented by 3 families: *Leptophlebiidae* (branched-gill mayfly larvae), Potamanthidae (feathered-gill mayfly larvae), and Baetidae (swimming mayfly larvae). Gastropoda and Trichoptera each contributed 2 families, while Caridea, Odonata, and Hemiptera each contributed 1 family (Figure 2; Table 1). In terms of water quality indication, organisms classified as "very clean water" bioindicators dominated the recorded assemblage, including larvae of Leptophlebiidae, Potamanthidae, Hydropsychidae, and Odontoceridae — all taxa sensitive to dissolved oxygen depletion. Organisms tolerant of moderate oxygen reduction ("fair water" category), such as Palaemonidae shrimp and Viviparidae snails, were also present at several stations, particularly Station 1. Two taxa associated with "dirty water" conditions (*Chironomidae* red midge larvae and *Tubificidae* sewage worms) were recorded at low abundance at Stations 3 and 4, while Gerridae (water striders, order Hemiptera) were classified as non-indicators due to their ability to inhabit any water condition.

3.2 Water Quality Assessment by Station

The total counts of bioindicator organisms recorded at each station across all four sampling rounds are summarized in Figure 3. Marked differences in assemblage composition were observed between Station 1 and Stations 2–5. At Station 1 (pond entrance), organisms indicating "fair" water quality were most abundant, with Palaemonidae shrimp and Viviparidae snails collectively accounting for 30 individuals, followed by "clean" water indicators (Thiaridae snails, n = 21). No "very clean" bioindicators were recorded at this station (Fig. 3). Overall water quality classification: fair–clean. At Station 2, "very clean" bioindicators dominated the assemblage (n = 26), comprising primarily caddisfly larvae (Hydropsychidae, Odontoceridae) and mayfly larvae (Leptophlebiidae, Potamanthidae), alongside a subset of "fair" indicators (n = 15). Overall classification: very clean. At Station 3, "very clean" bioindicators were overwhelmingly dominant (n = 32), represented mainly by branched-gill mayfly larvae (Leptophlebiidae) and feathered-gill mayfly larvae (Potamanthidae). A small number of "dirty" water indicators (n = 2) were recorded but did not alter the overall classification (Figure 3).



Order	Families (n)	Families recorded	Water quality category
Ephemeroptera	3	Leptophlebiidae, Potamanthidae, Baetidae	Very clean / Fair
Gastropoda	2	Thiaridae, Viviparidae	Clean / Fair
Trichoptera	2	Hydropsychidae, Odontoceridae	Very clean
Caridea	1	Palaemonidae	Clean / Fair
Odonata	1	—	Clean
Hemiptera	1	Gerridae	Non-indicator

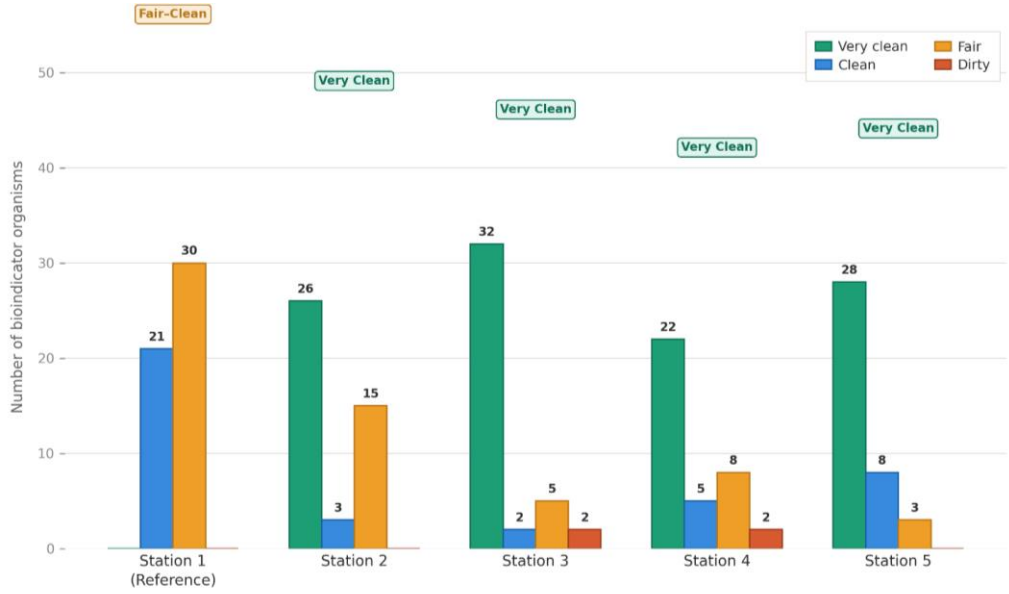
Figure 2. Number of families recorded per aquatic insect order in the Ruean Thai Pond surface water, classified by water quality indication category according to the Stream Detective Manual (Green World Foundation, 2018). A total of 9 families across 6 orders were recorded. Ephemeroptera was the most taxonomically diverse order with 3 families, followed by Gastropoda and Trichoptera (2 families each).

Overall classification: very clean. At Station 4, "very clean" bioindicators remained dominant across all four sampling rounds (n = 22), with "fair" indicators present at lower abundance (n = 8) and a minor occurrence of "dirty" water organisms (n = 2). Overall classification: very clean. At Station 5, the highest proportion of "clean" water indicators among Stations 2–5 was recorded (n = 8), while "very clean" bioindicators continued to dominate (n = 28). No "dirty" organisms were detected (Fig. 3). Overall classification: very clean. Across all five stations, Stations 2–5 consistently yielded a "very clean" classification, whereas Station 1 was classified as "fair–clean" (Fig. 3). The lower water quality at Station 1 likely reflects the accumulation of allochthonous organic material at the pond entrance. This pattern may reflect the accumulation of allochthonous organic material (leaf litter, surface runoff) at the pond entrance. However, as the Ruean Thai Pond is a lentic (not lotic) system, applying a riverine longitudinal gradient model is imprecise; a dedicated physicochemical investigation at Station 1 is recommended to identify specific stressors [12, 15].

3.3 Overall Water Quality

Considering all five stations collectively, the Ruean Thai Pond is classified as "very clean water," as organisms in the very clean category—particularly branched-gill mayfly larvae (Leptophlebiidae), feathered-gill mayfly larvae (Potamanthidae), cased caddisfly larvae (*Odontoceridae*), and uncased caddisfly larvae (Hydropsychidae)—dominated the bioindicator community across most stations and sampling events. The continuous flow of water through the system maintains adequate dissolved oxygen concentrations, supporting these oxygen-sensitive groups. The co-occurrence of "dirty water" bioindicators (red midge larvae, sewage worms) and "very clean" bioindicators at certain stations is consistent with the behavioral adaptability

of some taxa and local substrate heterogeneity, rather than indicating a deterioration in overall water quality. Similar co-occurrence patterns have been noted by Issara et al. [15] in streams with heterogeneous habitat patches.



Station	Very clean	Clean	Fair	Dirty	Total	Overall quality
St.1 (Reference)	0	21	30	0	51	Fair-Clean
St.2	26	3	15	0	44	Very Clean
St.3	32	2	5	2	41	Very Clean
St.4	22	5	8	2	37	Very Clean
St.5	28	8	3	0	39	Very Clean

Figure 3. Total counts of bioindicator organisms by water quality category recorded at five sampling stations in the Ruean Thai Pond surface water (September–October 2021, 4 sampling rounds combined). Badges above each group indicate the overall water quality classification for each station, based on the dominant bioindicator category, as defined in the Stream Detective Manual (Green World Foundation, 2018).

Table 2. Comparative summary of bioindicator counts across all five stations (total counts, all four sampling events).

Station	Very Clean	Clean	Fair	Dirty	Overall Quality
1 (Reference)	0	21	30	0	Fair–Clean
2	26	3	15	0	Very Clean
3	32	2	5	2	Very Clean
4	22	5	8	2	Very Clean
5	28	8	3	0	Very Clean

4. Conclusions

This survey of the Ruean Thai Pond at Nakhon Si Thammarat Rajabhat University recorded 5 orders (plus infraorder Caridea within Decapoda) and 9 families of aquatic insects and associated organisms. Using biological indicators in accordance with the Stream Detective Manual criteria, the pond's overall water quality was assessed as "very clean," primarily supported by the dominance of Ephemeroptera and Trichoptera larvae, which require high dissolved oxygen. These findings provide a preliminary wet-season biological assessment

for water resource management within the university [17, 18] and can serve as a reference for communities downstream of the campus. Continuous biological monitoring across multiple seasons is recommended to track temporal trends in water quality and to establish a year-round ecological baseline. Future studies should incorporate physicochemical measurements (dissolved oxygen, temperature) and standardized quantitative sampling to strengthen the bioassessment framework for this important campus water body [16, 17, 18].

5. Acknowledgments

The authors gratefully acknowledge Assoc. Prof. Dr. Wattananarong Markphan for guidance and corrections throughout the study, all faculty members of the Environmental Science Program for advice, and Ms. Kanlayarat Sakchanampan for assistance during field sampling. Support from the Faculty of Science and Technology at Nakhon Si Thammarat Rajabhat University is also acknowledged.

Author Contributions: Conceptualization, W.N. and W.M.; methodology, W.N.; formal analysis, W.N.; investigation, W.N.; resources, W.M.; data curation, W.N.; writing—original draft preparation, W.N.; writing—review and editing, W.M.; supervision, W.M.; project administration, W.M. All authors have read and agreed to the published version of the manuscript.

Funding: This research received no external funding.

Conflicts of Interest: The authors declare no conflict of interest.

References

[1] Weerawattananon, W. *Environmental Science*; Odeon Store Publishing: Bangkok, Thailand, 2017.
[2] Thartong, S. *Water Management in Thailand*; Rajabhat Institute Press: Nakhon Ratchasima, Thailand, 2017.
[3] Butsuk, B. *Water Resource Challenges in Thailand*; Kasetsart University Press: Bangkok, Thailand, 2017.
[4] Al-Jawahery, H. F.; Naji, N. S.; Al-Azawey, A. S. N. Physicochemical and Microbiological Evaluation of Reverse Osmosis Drinking Water Quality in Babylon Province, Iraq. *ASEAN J. Sci. Technol. Rep.* **2024**, *29*, e260629. https://doi.org/10.55164/ajstr.v29i1.260629
[5] Alburo, R. P.; Villegas, L. M. G. Ecological Risk Assessment of Heavy Metal Pollution in Surface Water and Sediment of Lahug River, Cebu, Philippines. *ASEAN J. Sci. Technol. Rep.* **2024**, *28*, e257492. https://doi.org/10.55164/ajstr.v28i3.257492
[6] Pattarasini, P. *Nature Studies*; V-Print: Bangkok, Thailand, 2017.
[7] Soontornprasit, K.; Valunpion, S.; Pithakpol, S. Biodiversity of Aquatic Insects in Ing River. *Khon Kaen Agric. J.* **2013**, *41* (Suppl. 1), 142–148.
[8] Soontornprasit, K. Use of Aquatic Insects as Bioindicators of Water Quality in Kwan Phayao, Phayao Province. *J. Community Dev. Res.* **2012**, *5*(1), 15–24.
[9] Tagun, R.; Kunpradid, T. The Relationship between Diversity and Distribution of Aquatic Insects with Water Quality of Mae Chaem Headwater Streams, Kanlayaniwattana District, Chiang Mai Province. *Srinakharinwirot Sci. J.* **2017**, *33*(1), 117–133.
[10] Tangmangmee, H. *Environmental Survey of Mahachai Stream*; Internal Report; Nakhon Si Thammarat Rajabhat University: Nakhon Si Thammarat, Thailand, 2015.
[11] Issarawanrong, T. *Using Benthic Macroinvertebrates for Biological Monitoring*; Department of Biology, Mahasarakham University: Maha Sarakham, Thailand, 2017.
[12] Kanjanavanit, S. *Field Guide to Freshwater Invertebrates*, 2nd ed.; Green World Foundation: Bangkok, Thailand, 2018.
[13] Vitheepradit, A.; Mitpuangchon, N.; Prommi, T.-O. *Biodiversity and Community Structure of Aquatic Insects in Freshwater Ponds*; Faculty of Liberal Arts and Science, Kasetsart University, Kamphaeng Saen Campus: Nakhon Pathom, Thailand, 2016.
[14] Thiptaban, R.; Kanjanatheeraphong, T. *Distribution of Aquatic Insects (EPT) and Water Quality in Mae Chaem Headwater Streams*; Chiang Mai Rajabhat University: Chiang Mai, Thailand, 2017.

[15] Issarawanrong, T. *Benthic Macroinvertebrate-Based Biomonitoring*; Department of Biology, Mahasarakham University: Maha Sarakham, Thailand, 2017.

[16] Thepnarong, K.; Chiayvareesajja, S.; Kantachote, D.; Sangnoi, Y. Effects of Selected Probiotics on Water Quality and Growth Performance of Nile Tilapia Cultured in a Recirculating Water System. *ASEAN J. Sci. Technol. Rep.* **2024**, *28*, e255832. https://doi.org/10.55164/ajstr.v28i2.255832

[17] Ruangrak, E.; Salaemae, N.; Sornnok, S.; Sin Htwe, N. M. P. Effect of Pre-Harvest Periods by Replacing Nutrient Solution with Tap Water on Nitrate and Quality in Hydroponic Lettuce. *ASEAN J. Sci. Technol. Rep.* **2023**, *26*(1), 76–83. https://doi.org/10.55164/ajstr.v26i1.247666

[18] Matondang, P. A. S.; Taparhudee, W.; Yoonpundh, R.; Jongjaraunsuk, R. Water Quality Management Guidelines to Reduce Mortality Rate of Red Tilapia (*Oreochromis niloticus* × *Oreochromis mossambicus*) Fingerlings Raised in Outdoor Earthen Ponds with a Recirculating Aquaculture System Using Machine Learning Techniques. *ASEAN J. Sci. Technol. Rep.* **2022**, *25*(4), 30–41. https://doi.org/10.55164/ajstr.v25i4.247049

ASEAN
Journal of Scientific and Technological Reports
Online ISSN:2773-8752

Research article

Participatory Extension Approaches for Good Manufacturing Practices (GMP) Adoption in Rural Fish Processing: Evidence from Southern Thailand

Amonrat Thanonkaew[1]*, Pornpimon Mayachiew[1], Thanidchaya Luanunkarb[2], Pimchana Hoktha[3], Suphada Kiriratnikom[2], and Vilailak Klompong[1]

[1] Faculty of Agro- and Bio-Industry, Thaksin University, Phatthalung, 93210, Thailand
[2] Faculty of Agriculture, Thaksin University, Phatthalung, 93210, Thailand
[3] Faculty of Science and Digital Innovation, Thaksin University, Phatthalung, 93210, Thailand
* Correspondence: tamonrat@tsu.ac.th

Citation:
Thanonkaew, A.; Mayachiew, P.; Luanunkarb, T.; Hoktha, P.; Kiriratnikom, S.; Klompong, V. Participatory extension approaches for good manufacturing practices (GMP) adoption in rural fish processing: evidence from southern Thailand. *ASEAN J. Sci. Tech. Report.* **2026**, *29*(7), e262437. https://doi.org/10.55164/ajstr.v29i7.262437

Article history:
Received: November 20, 2025
Revised: May 23, 2026
Accepted: May 26, 2026
Available online: June 16, 2026

Publisher's Note:
This article is published and distributed under the terms of the Thaksin University.

Abstract: Dry-fermented catfish (pla-duk-ra) is a potential value-added product in Southern Thailand; however, it faces food safety hazards because small-scale backyard operations dominate and lack supporting regulations. This study evaluated a participatory extension approach to promote Good Manufacturing Practices (GMP) within the Banphabontam Agricultural Innovation Community Enterprise (BAICE). The original GMP evaluation involved the design of facilities, control of equipment, process operations, cleanliness and sanitation, maintenance, and personnel practices. None of the six domains achieved a score of 60%, indicating that all areas remained below the minimum acceptable level. Participatory extension led to the implementation of various improvements, such as facility redesign, workflow zoning, hygiene training, and basic sanitation systems. Following the upgrade, BAICE achieved GMP certification and formal recognition as a licensed food producer. The refined layout separated wet and dry zones, improved drainage and pest control, and established distinct storage and preparation spaces. These interventions increased workers' hygiene awareness and responsibility without altering the sensory characteristics or cultural identity of pla-duk-ra. This initiative exemplifies community-driven food safety enhancement through participatory extension. It demonstrates how scientific principles and traditional knowledge can align to improve product quality, regulatory compliance, and market potential. Findings from the BAICE case provide practical, context-specific evidence that may inform GMP implementation and rural food system improvement in similar community-based food enterprises. The results align with national agendas to support the development of sustainable food and highlight that extension work plays a crucial role in making traditional foods safe, competitive, and sustainable products.

Keywords: Participatory extension; GMP; rural fish processing; technology transfer, food safety

1. Introduction

Aquaculture is very important for agricultural diversification and food security in Southeast Asia. Among the freshwater species in Thai aquaculture, hybrid catfish (pla-duk-big-oui) is the second-most successful species being

raised in central and southern Thailand. Thailand has become a regional model for coupling sustainable fish culture with value-added processing to improve marketability and create economic gains. In 2024, Thailand produced approximately 91,095 metric tons of catfish, which accounted for around 20% of the country's overall freshwater aquaculture production. This has derived an annual income of around 121 million USD [1].

Pla-duk-ra is a processed fish product with a strong cultural heritage and significant economic importance to the southern Thai population. As one of the most popular value-added catfish products, it is a good example of maximizing available natural resources and enhancing local people's livelihoods. The amount of pla-duk-ra produced is a good example of combining the tradition of fish farming with indigenous knowledge over the generations. The preparation process begins with selecting fresh catfish of appropriate size, followed by removing the head, internal organs, and excess fat. The cleaned fish are then washed thoroughly before being mixed with salt and sugar for fermentation. Fermentation typically lasts 1 to 2 days, after which the fish are dried in the sun or under a controlled heat source. This process results in a distinct salty-sweet flavor and a mild fermented aroma, which differentiate pla-duk-ra from other forms of salted fish [2]. According to a recent market report by our research team, pla-duk-ra had a potential estimated annual market value of approximately USD 5.4–8.1 million in 2024. This indicates that it represents a major component of the regional fish-processing industry. In Phatthalung province, community-based businesses that combined catfish farming and the processing of pla-duk-ra recorded the highest profit increase. The monthly income of this family increased from about USD 620 to USD 2,600, and net profit increased by 346% as a result of adding value production methods based on the fry pla-duk-ra paste product form (chili paste, sweet fish sauce, and rice seasoning powder) that were practiced in the process line [3].

The Banphabontam Agricultural Innovation Community Enterprise (BAICE) is one example of such a local innovation ecosystem in Phatthalung province. Traditional techniques are what the company has staked its name on. In 2023, the business earned only 1,860 USD in sales and netted just 744 USD in profits, with average monthly production at a very low level of about 200 kg. However, it struggled to scale up production, comply with regulations, and develop marketable derivatives. These questions illuminate the general problem of reconciling traditional food processing methods with modern requirements for food safety, a pressing issue in much of the developing world's community-based agricultural production. Small-scale community-processed food manufacturers must meet the Good Manufacturing Practices (GMP) prescribed by the Thai FDA. For these producers, this is a key step forward. Basic food safety regulations include the following: cleanliness in production spaces and equipment, proper personal hygiene, safe product preparation, clear boundaries between clean and dirty areas, and good organization of storage and transportation [4]. For a community enterprise like BAICE, achieving GMP certification offers easier entry into new markets, an added layer of customer trust, and the ability to register with the FDA. To ensure food safety and quality in the aquaculture and fish processing sectors, GMPs are essential. In agricultural extension terms, GMP constitutes both a technical intervention and a participatory-action process that builds on the capacity of community-based enterprise, elicits change in producer behavior, and triggers development in the rural economy.

The GMP provides guidelines for small-scale producers on sanitation, process control, and equipment management. This enables them to maintain an amazing practice in fish processing, on the one hand, observe formal food safety standards, maintain a competitive edge over competitors, and increase consumers' confidence, on the other. The empirical experience across Southeast Asia has demonstrated that GMP can have a transformative effect on the safety and market value of aquatic products. For instance, the adoption of GMP in the production of pla-duk-ra in Phatthalung province (Thailand) has made the microbiological process safer, more efficient, and more cost-effective. Their monthly profits from local manufacturers were more than 300% higher after adding the ready-to-eat and by-product lines [5]. Analogous actions were applied to Indonesian small-scale fish production, resulting in reduced contamination and spoilage and making the certification process more applicable [6]. In terms of extension systems, the GMP training and certification cycles indicate that the transfer of agricultural technology can increase productivity and sustainability while preserving cultural knowledge. Participatory GMP (hygienic) upgrading (including sanitation, process flow design, and environmental management) is an instance of a science-and-practice-driven integrated rural

development model [3]. By shifting the focus of agricultural extension work from productivity-driven interventions to public health- and environmental-sustainability-oriented initiatives, GMP drives important systems-level changes that improve local business capabilities and foster more inclusive food value chains. The implementation of GMP to improve the quality of traditional beverages also aligns with the Thai government's National Strategic Framework (2018–2037) for enhancing competitiveness. This structure advocates for security and safe, sustainable agriculture to increase farmers' Gross Domestic Product [7]. Strategically, this linkage underscores the relevance of GMP-related interventions to other overriding national development objectives and to the convergence of extension policy.

This research examined technical interventions in community-based catfish processing establishments regarding the extent of GMP compliance. It also examined the role of GMP in disseminating innovation, facilitating knowledge transfer, and promoting sustainable rural development. It investigates BAICE's work in Phatthalung Province and adds to a growing body of evidence on extension strategies that successfully combine traditional knowledge systems with contemporary food safety standards. This integration enriched cultural identity and strengthened the economic viability of community-based agro-enterprises.

2. Materials and Methods

This study hypothesizes that a participatory extension approach can significantly elevate traditional pla-duk-ra production to GMP-compliant standards, yielding safer and more uniform products, broader consumer acceptance, and sustainable community income. To test this hypothesis, the study draws on Participatory Action Research (PAR), agricultural extension theory, and food-safety management principles, conceptualizing Good Manufacturing Practices (GMP) adoption not as one-way technology transfer but as an iterative, multi-stakeholder learning process in which scientific knowledge and indigenous wisdom are jointly mobilized. The framework comprises four interconnected components (Figure 1). Contextual inputs capture the pre-intervention state of the Banphabontam Agricultural Innovation Community Enterprise (BAICE): indigenous fermentation know-how, baseline GMP compliance below 60 %, limited food-safety infrastructure, absence of regulatory registration, and restricted market access. The participatory intervention process engages three stakeholder groups - university researchers, BAICE processors, and public health consultants - through a 30-month PAR cycle of diagnosis, co-design, trial, and reflection spanning four functional domains: facility redesign, hygiene control, packaging design, and regulatory documentation. Measurable outputs are evaluated across regulatory compliance, product safety, product quality, and economic performance, while outcomes and wider impact unfold at enterprise, community, and systems levels, aligning with Thailand's National Strategic Framework and the Sustainable Development Goals. Participatory extension thus serves as the bridge between traditional wisdom and modern regulation, allowing cultural identity and regulatory compliance to advance together through bidirectional knowledge flows.

2.1 Study area, research design, and general approach

The study was conducted at the Banphabontam Agricultural Innovation Community Enterprise (BAICE), located in Phabon District, Phatthalung Province, Thailand, over 30 months from March of 2023 to August of 2025. It employed a mixed-methods design, using (i) Participatory Action Research (PAR), (ii) laboratory assessment of product quality, and (iii) questionnaire-based evaluation. We chose PAR as the study design because addressing our research question required a cycle of action (a trial production run with modified procedures) followed by critical reflection and revision with stakeholders before moving on to the next round of interventions between researchers and community processors.

2.2 Participants & Sampling Strategy

This study comprised three stakeholder groups: (1) Research team, five researchers and research assistants from Thaksin University who facilitated the study, conducted laboratory work, and prepared documentation; (2) BAICE processors, five members, selected through purposive complete enumeration, as they represented the entire active workforce involved in pla-duk-ra processing at the time of the study. The inclusion criteria were: (i) at least two years of experience in processing pla-duk-ra; (ii) a primary role in at least one step of production, including preparation, salting, drying, or packaging; and (iii) agreement to

participate throughout the duration of the project. Because the sample size was small (n = 5), this group was considered a census of the target enterprise rather than a randomly drawn sample from a larger population. This structural feature and limitation of single-enterprise PAR studies are elaborated on in Section 2.3; and (3) Regulatory consultants—two food-safety officers from the Phatthalung Provincial Public Health Office, who provided regulatory advice and assisted with the FDA submission.

2.3 Participatory process and intervention/treatment timeline

The participatory process lasted 30 months, during which 30 site visits to BAICE were conducted. Engagement activities included: (1) 10 group meetings-situational analysis, joint planning, and post-cycle reflection meetings (approximately 2–3 h each); (2) five hands-on training workshops outlining GMP principles, hygienic processing, packaging, labelling, and microbiology (one day each); (3) five semi-structured in-depth interviews with BAICE members, using an interview guide addressing processing history, perceived problems, willingness to change, and post-intervention experiences; and (4) 10 on-site demonstrations of revised processing procedures performed jointly by researchers and BAICE member(s).

The different roles within the PAR cycles were clearly defined. (1) BAICE members selected locally relevant production challenges, designed changes to processing, carried out trials following modified protocols, and reported sensory and operational observations at the end of each experimental round. (2) Researchers and research assistants conducted workshops and facilitated reflection sessions, while all laboratory analyses, preparation of regulatory documents, and quantitative and qualitative data analyses were completed by the research team. (3) Public health consultants provided recommendations on good manufacturing practices and Thai FDA-compliant facility upgrades, as well as investigations of labeling and registration submissions.

2.4 Stage 1 Refined production of pla-duk-ra aligned with GMP

All production processes, equipment, tools, and storage practices at BAICE were evaluated and modified according to the Manual for Inspection of Food Production Facilities Based on Legally Mandated Good Manufacturing Practice Criteria 420 [8], issued under the Ministry of Public Health Notification No. 420, B.E. 2563 (2020), hereinafter referred to as "GMP 420." Non-conformities identified during the baseline audit were considered jointly with BAICE members and public health consultants, followed by the co-design of corrective actions that were implemented before the next production cycle.

2.5 Stage 2 Laboratory and sensory quality assessment of pla-duk-ra

Pla-duk-ra samples were collected from BAICE both before the GMP intervention (baseline) and after implementation (post-intervention), allowing the same enterprise to serve as its own control. A total of three subsamples were randomly selected from at least a 1 kg production batch and analyzed in triplicate within 7 days of production at the Food Science and Technology Laboratory, Thaksin University.

Chemical and microbiological analyses included: (1) water activity (aw), measured using an AQUA LAB Model 050796243 water-activity meter, calibrated against saturated salt standards on each day of use; and (2) enumeration of yeasts and molds, *Escherichia coli*, and *Staphylococcus aureus*, conducted according to the Bacteriological Analytical Manual (BAM, 2001) [9].

The Community Product Standards (TCPS, 2005) were followed for sensory evaluation [10]. Sensory evaluation of general appearance, color, flavor, and texture was performed according to the indicated testing protocol. At least five assessors trained in the evaluation of pla-duk-ra were assigned to the sensory evaluation panel. The samples were reviewed and scored independently by each assessor. The general appearance and color of the pla-duk-ra samples were visually assessed by placing them on white ceramic plates. The samples were fried under suitable temperature and time conditions, after which flavor and texture were assessed organoleptically. The scoring criteria were applied with sufficient evaluative instructions [10].

2.6 Stage 3 Packaging design and Thai FDA certification

The packaging and labeling of pla-duk-ra products were developed in accordance with the Ministry of Public Health Notification No. 367, B.E. 2557 (2014). Six products were submitted for Thai FDA certification in cooperation with the Phatthalung Provincial Public Health Office: (1) dry-fermented catfish, (2) ready-to-

eat fried pla-duk-ra, (3) sweet fish sauce, (4) khao yam sauce, (5) rice seasoning, and (6) dry-fermented catfish chili paste. The products were categorized by regulatory food category, including processed foods requiring labels, ready-to-cook foods, and ready-to-eat foods.

Thai FDA certification involved both the issuance of a food production facility license and the assignment of individual product registration numbers for each product and manufacturer via Form SB applications. The Thai FDA e-submission system then assessed the ingredient composition and permitted use levels. [8] The Phatthalung Provincial Public Health Office issued final certification.

2.7 Stage 4 Economic analysis

Upon completion of the intervention, a systematic cost–benefit analysis was conducted using project data through August 2025. Three financial indicators were calculated for each of the six FDA-certified products: (i) monthly income, (ii) cost of production, and (iii) net profit. Cost components included raw materials, packaging, labor, utilities, equipment depreciation, and certification fees, allocated to each product based on the selected allocation method.

2.8 Statistical analysis

All data were analyzed using IBM SPSS Statistics (version 26.0; IBM Corp., USA). Continuous variables are expressed as mean ± standard deviation of triplicate measurements. As BAICE served as its own control, paired comparisons between baseline and post-intervention values were performed. Water activity and sensory scores (general appearance, color, flavor, and texture) were compared using the paired-samples t-test, while $\log_{10}$-transformed microbial counts (yeasts, molds, *E. coli*, and *S. aureus*) were compared using the Wilcoxon signed-rank test. Differences were considered statistically significant at $p < 0.05$. GMP compliance percentages, Thai FDA registration outcomes, and economic indicators are reported descriptively.

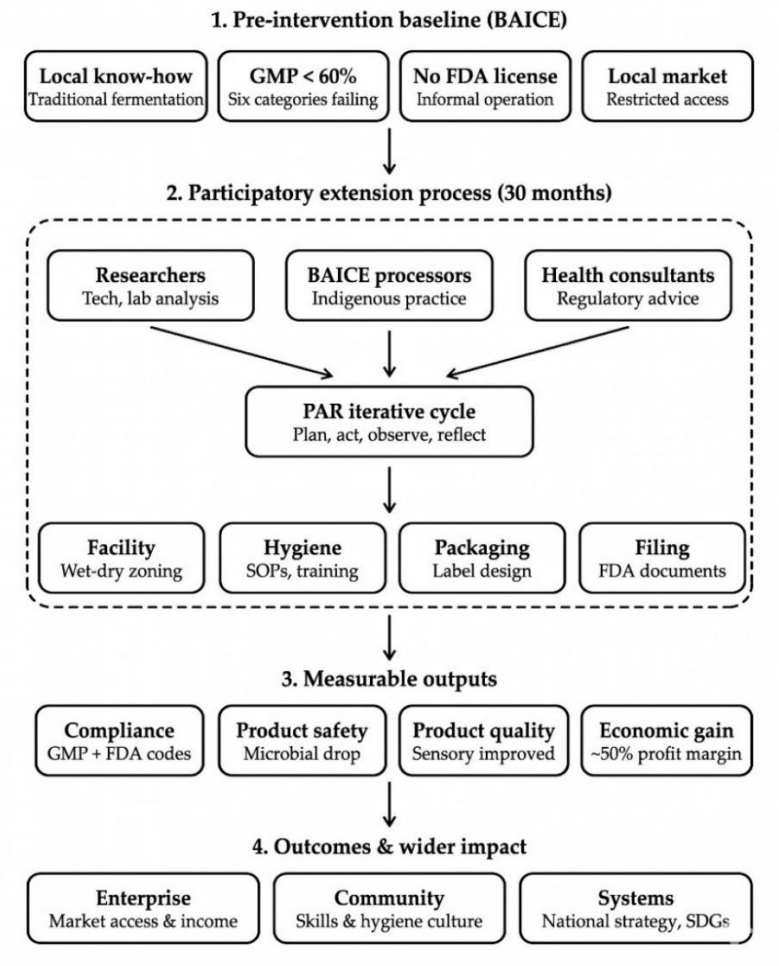


Figure 1. Conceptual framwork

3. Results and Discussion

3.1. Development of pla-duk-ra products to GMP

BAICE was ready to go on facilities, as it already had a production site that could be improved to meet GMP standards. It also had a strong community with members who could keep the business running. A detailed study was conducted to inspect the production method using the food production facility inspection and evaluation form, according to the Ministry of Public Health Notification for BAICE, before and after improvements to meet GMP standard production systems. The GMP assessment of BAICE revealed that the pla-duk-ra production system faced food safety vulnerabilities at the pre-intervention stage. There were six aspects to be concerned about: 1) Locations and production buildings, 2) Production equipment and utensils, 3) Process control, 4) Sanitation, 5) Maintenance and cleaning, and 6) Personnel. The BAICE factory was not a factory under statistical classification, as it had less than 20 HP from aggregate machinery and/or fewer than 7 workers. Form SB. 1 was applied to matters that did not originate from a factory. However, the facility had to adhere to the Ministry of Public Health Notification (No. 342) B.E. 2555 (2012), which pertains to how food is prepared, which equipment and utensils should be used, and how processed food in containers offered for retail sale is stored. To pass the inspection evaluation, the total score for each topic and the overall total score must be at least 60%, and there must not be any significant problems.

Quantitative evaluation showed that overall compliance across six GMP categories was below 60%, indicating substantial non-conformities and a high level of risk requiring corrective action (Table 1). The lowest score was attributed to maintenance and cleaning (30.10%), with sanitization next (30.71%). Personnel were rated with the highest average percent (41.91%), but still below the acceptance level for GMP certification. These initial results are consistent with longstanding weaknesses in rural and small-scale food processing businesses, which often operate with little technical support. The small and medium-sized processors often struggle to meet the key quality and safety requirements due to limited or no formal hygiene specifications, poor infrastructure, and insufficient staff training [11]. The results, therefore, highlight the critical need for structured technology transfer through extension programs to facilitate improvements in compliance. The GMP assessment of BAICE at the case level highlights persistent structural deficiencies in sanitation and maintenance within small community-based food enterprises, aligning with broader sectoral findings. These shortcomings reflect systemic issues rather than isolated cases. The analysis, framed by theories such as prerequisite-program theory and innovation-diffusion, underscores the necessity and theoretical basis for targeted interventions. The baseline scores serve as diagnostic tools to guide theory-driven improvements in the pla-duk-ra production system rather than as final measures of organizational effectiveness.

3.1.1 GMP assessment by categories

The facility faced major structural issues, including poor zoning, unsealed ceilings, pest infestations, and uneven flooring, which increased the risk of contamination (Figure 3). These inadequacies are consistent with emerging evidence from studies of small- and medium-scale enterprise (SME) food processors in Southeast Asia, where inadequate infrastructure and site layout were identified as critical factors in contamination and pest infestation within facilities [12]. Before the renovation, the production building was an open, common space without any separation, where the supply of processed products and packages was made at the same location for drying (Figure 3). The remodeling of the pla-duk-ra processing layout balances modernization with traditional rural culture, promoting hygienic and safe production. This reflects the broader challenge in Southeast Asia of integrating Good Manufacturing Practices (GMP) with longstanding methods. Small community-based producers often face constraints in equipment hygiene and operational efficiency. Suggested improvements, such as better tools, hygienic zoning, and clear Standard Operating Procedures (SOPs), aim to enhance safety and efficiency without compromising cultural values. Major process issues, such as reckless water use, poor storage of raw materials, and inadequate procedures, pose contamination risks in rural fermentation [13]. Planned improvements to water filtration and record-keeping enhance safety and traceability. Research in Thailand confirms that capacity-building in rural enterprises reduces contamination and boosts compliance [14].

The facility faced major non-compliance issues, including pest control, open containers, and poor hand-washing facilities, threatening pla-duk-ra hygiene. Traditional open-air processing highlights the

challenge of balancing cultural norms with modern safety measures to prevent contamination. Similar challenges in fish processing show that GMP integration improves quality and safety [15]. Key weaknesses included a lack of sanitation protocols and improper storage of chemicals. Recommended improvements focus on cleaning schedules, secure chemical storage, and ongoing staff training to sustain a strong food safety culture.

The six GMP non-compliance categories at BAICE reveal a rural food enterprise that is structurally underdeveloped yet culturally rich and behaviorally unique. Each issue aligns with established food safety literature on sanitation, knowledge transfer, and microbial hazard control [16]. This assessment offers a theory-based framework for targeted improvements, demonstrating that traditional production can be systematically enhanced under GMP without losing its cultural identity, making the approach especially effective for pla-duk-ra.



Figure 2. The BAICE production facility that produced pla-duk-ra before the improvement project. Front area (a), Inner area (b)

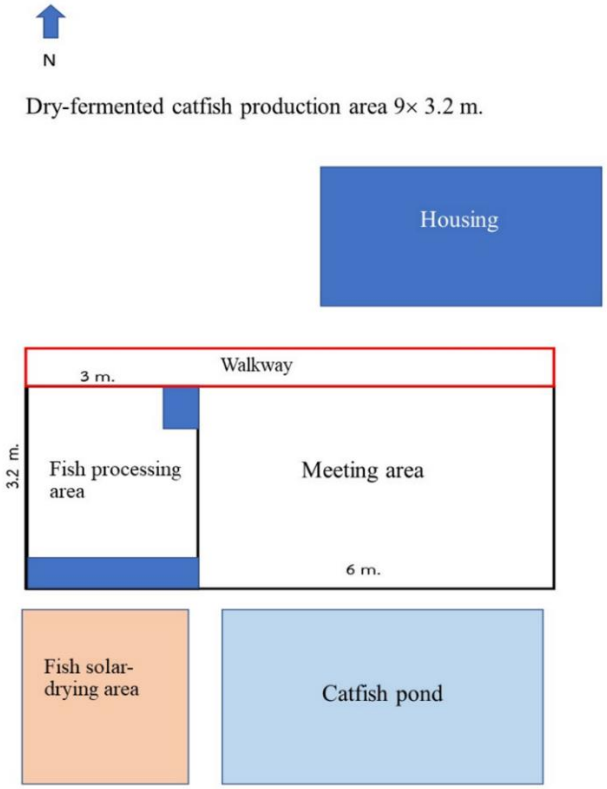


Figure 3. Diagram of the pla-duk-ra product processing facility before the Primary GMP audit and improvement

Table 1. Assessment of food production processes of Pla-duk-ra

Aspects	Score (%)	Issues detected	Recommendations
1. Locations and production buildings	31.58	-Unused items or items that weren't related to production are in the production area. -Failure to proportionally separate production areas. -Some areas do not have insect screens to prevent contamination, especially at doors and windows. -The arrangement of the production area does not follow the production line sequence. -The division of the production area is not proportional. -The lack of standard drainage pipes. -The rough building floors with corners collecting dust and pathogens. -The absence of a ceiling. -The lack of light bulb covers in some places.	-Clear the production area of unused items. -Divide work and packaging space with separate rooms. -Add more insect screens in places with no protection. -Make sure the ceiling is installed correctly in the packaging area. -Maximize production line sequence. -Independent packing spaces prevent cross-contamination.-Upgrading the drainage pipes to meet standards. -Making the floors of the building smooth and free of dust and germs. -Putting covers on all the light bulbs. -Making additional improvements as appropriate.
2. Production equipment and utensils	31.55	-Not enough tools and equipment. -Not enough space for storing items. -Cabinets used for tool storage that were not in the right place. -No instructions for how to use tools.	-Changing the layout of machinery and equipment to make cleaning easier. -Getting more equipment that is needed for the production process. -Getting shelves and cabinets to store different types of equipment. -Making signs and documents that explain how to use tools.
3. Process control	35.00	-Not having enough space to store raw materials. -Moving raw materials, ingredients, and packaging containers during production in a way that could contaminate them. -Water systems coming into contact with food during production that didn't meet standards and didn't have quality analysis inspections.	-To build shelves and change the way raw materials are stored. -To build a whole new production line system. -To install water filtration systems used in production to meet standards. -To make quality analysis inspection data files. -To keep written records for at least two years.

Table 1. Assessment of food production processes of Pla-duk-ra (continue)

Aspects	Score (%)	Issues detected	Recommendations
4. Sanitation	30.71	-Not enough covered trash cans in the right places. -Not enough toilets for workers. -Not enough soap or disinfectant and hand-drying equipment at all positions. -No measures to keep bugs away and get rid of them in the GMP production area.	-Changing open trash cans to covered ones. -Setting up hand-washing stations. -Getting enough soap for hand-washing at those stations.
5. Maintenance and cleaning	30.10	-No set procedures for cleaning tools and machines. -No clear place to store cleaning supplies. -No labels showing names and safe storage of cleaning chemicals or other chemicals used for sanitation maintenance. -No regular cleaning methods and measures for tools, machines, and production equipment.	-To wash tools and equipment before and after use. -Store cleaning chemicals in the right amounts. -Make clear signs showing where to store chemicals for cleaning. -Make plans for cleaning tools, machines, and equipment.
6. Personnel	41.91	-No health screening of employees. -Absence of rules on the handling of shoes used in production areas. -Staff allowed to wear jewelry, such as rings, necklaces, and bracelets. -Absence of protocols for washing hands and disinfection before starting work. -Employees not adhering to the cap and hairnet rule. -Lack of training for employees regarding employee hygiene, with some employees not understanding procedures.	-Holding meetings with employees to talk about sanitation.

3.1.2 Participatory extension–driven transformation

Participatory extension redefined BAICE and enabled public health officers, extension specialists, and communities to collaboratively examine GMP issues and development strategies. The community gained hands-on experience, a better understanding of regulation, and shared responsibility for compliance-the ingredients needed to make long-term rural food safety sustainable ultimately. This is through an intervention that simultaneously addresses the technical, organizational, and cultural dimensions by reframing extension as co-production rather than a top-down transfer; enabling an institution-wide helix arrangement; and embedding learning in a social context. The results confirm that how capacity is built can be as significant as what is taught.



Figure 4. On-site inspection and assessment of pla-duk-ra product production facilities by the public health officers in Phatthalung province

3.1.3 Layout improvement and compliance achievement

Following the GMP assessment, BAICE redesigned its production layout to support a hygienic workflow (Figure 5), with distinct rooms for changing, raw material handling, processing, and packaging/storage (Figure 6). These improvements enhanced hazard control, met Primary GMP standards, and preserved pla-duk-ra's traditional character. BAICE earned SB.1 registration from the Ministry of Public Health, demonstrating its effective capacity-building. This case exemplifies how culturally grounded, participatory modernization can transform rural food enterprises into safe, competitive businesses without sacrificing cultural identity.

3.1.4 Apply for food production facility licensing

After the GMP assessment, BAICE reorganized its production facility to meet food safety standards, creating distinct areas including a changing room, a wet zone for raw material reception and cleaning, a dry processing zone with shelves and preparation tables, and a packaging and finished product storage area. This layout met the requirements for a food production facility license. In Thailand, small-scale facilities with fewer than 50 employees and machinery under 50 horsepower apply via Form SB.1, while larger factories use Form O.1. With seven workers and machinery below 20 horsepower, BAICE qualified under Group 1 (non-factory) and applied accordingly. The application to the Provincial Consumer Protection Unit included verification documents, business registrations, premises evidence, and technical materials such as layout maps, flowcharts, machinery lists, sanitation, and water quality plans. Although not classified as a factory, BAICE complied with Ministry of Public Health Notification No. 342 (B.E. 2555/2012). After review and inspection, BAICE obtained an eight-digit food production registration number, enabling legal operation and market

distribution. This success reflects the integration of facility design, food safety science, regulatory compliance, and small enterprise development, demonstrating that GMP adherence can drive microenterprise upgrading and competitive positioning rather than serve as a regulatory burden.

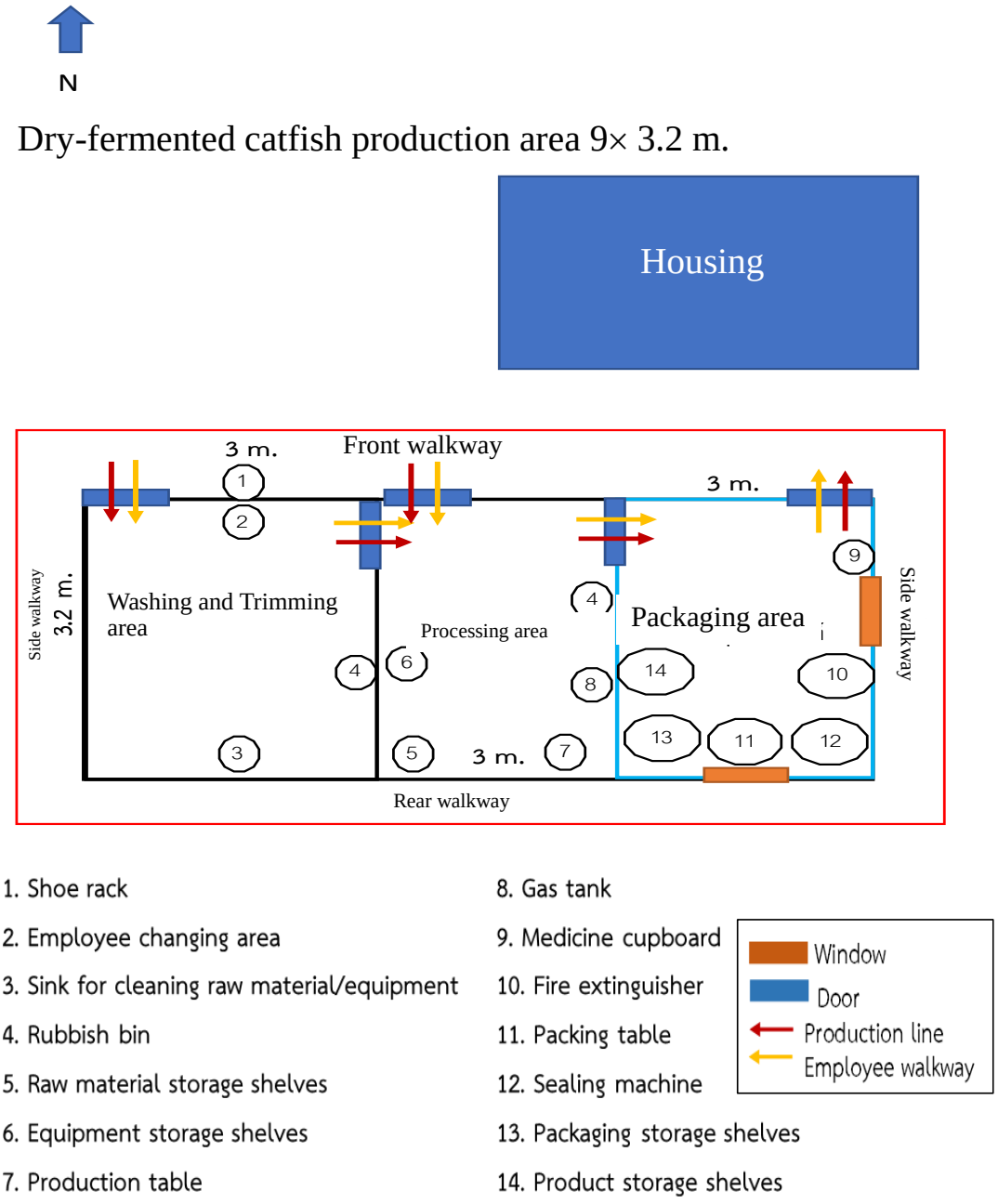


Figure 5. Diagram of the pla-duk-ra product processing facility after Primary GMP audit and improvement



Figure 6. The BAICE production facility that produced pla-duk-ra after the improvement project. Front area (a), Side area (b), Employee changing area (c), Raw material washing and preparation area (d), Mixing area (e), Packing area (f)

3.2. Quality evaluation of pla-duk-ra products

The chemical and biological properties of pla-duk-ra products are presented in Table 2. Quality parameters were compared before and after GMP implementation using the Thai Community Product Standards as the reference criteria. The results showed that water activity (a_w) decreased significantly after GMP implementation ($p<0.05$), from 0.85 before implementation to 0.71 after implementation. The post-intervention value was below the Thai Community Product Standard limit of 0.80 [10]. This reduction is important for product safety and shelf-life extension, as lower water activity can inhibit the growth of pathogenic and spoilage microorganisms. The improvement may be associated with better control of fermentation and drying practices following GMP-based training and process standardization. This finding is consistent with previous studies on fermented fish products, which have emphasized the importance of controlling water activity in producing safer intermediate-moisture foods with extended shelf life [2]. A substantial reduction in yeast contamination was also observed, with counts decreasing from 1.2×10^4 CFU/g before implementation to 1.0×10^2 CFU/g after implementation. The post-intervention value was well below the Thai standard limit of 1.0×10^4 CFU/g. This approximately two-log reduction indicates improved sanitation,

handling practices, and process control. Similar improvements have been reported in fish products when strict hygiene practices, clean water, and controlled drying conditions were applied [15].

Lower yeast counts may also reflect better environmental control, improved equipment cleaning, and more hygienic handling during production [16]. Mold counts were low both before and after GMP implementation, at 13 and 10 CFU/g, respectively, well below the Thai standard limit of 500 CFU/g. The low mold counts may be partly related to the natural antimicrobial effects of salt and fermentation. The slight reduction after implementation may also be associated with improved facility conditions, better ventilation, reduced environmental contamination, and improved humidity control. Appropriate facility design and good airflow are important factors in reducing mold growth in fermented fish products. The most critical safety concern was observed in the pathogenic bacterial indicators. Before GMP implementation, *E. coli* was detected at 30 MPN/g, exceeding the Thai standard limit of 10 MPN/g. After GMP implementation, *E. coli* decreased to less than 3.0 MPN/g, meeting the standard requirement. This reduction indicates improved hygiene control, especially in raw material handling, water quality, equipment sanitation, and the prevention of fecal contamination. Similarly, *S. aureus* decreased from 150 MPN/g before implementation to less than 3.0 MPN/g after implementation. Importantly, the pre-intervention value of 150 MPN/g exceeded the Thai standard limit of 100 MPN/g, indicating a genuine public health concern before the intervention. The presence of *S. aureus* above the standard may reflect inadequate personal hygiene, improper handling, insufficient sanitation of equipment and production areas, or lack of systematic health and hygiene practices among workers. Since *S. aureus* is commonly associated with human handling and can produce heat-stable enterotoxins under favorable conditions, its detection above the regulatory limit highlights the need for strict hygiene management in traditional fermented fish processing. After GMP implementation, the reduction of *S. aureus* to less than 3.0 MPN/g suggests that improved management practices were effective in reducing contamination risks. These practices included worker hygiene training, hand-washing procedures, use of protective clothing, improved sanitation of production areas, better cleaning of equipment and utensils, and stronger process control.

Therefore, the microbiological results demonstrate not only product quality improvement but also a meaningful reduction in public health risk. Fundamentally, controlling intrinsic parameters such as water activity, in conjunction with minimizing initial contamination through hygienic practices, is the primary mechanism for inhibiting specific spoilage organisms and extending the shelf life of fish products [17]. Overall, the reductions in water activity, yeasts, *E. coli*, and *S. aureus* indicate that GMP-based upgrading contributed to improved safety and quality of pla-duk-ra. These findings support the participatory action research approach used in this study, which combined community participation and expert guidance to achieve measurable improvements in production practices. Although the post-intervention results met the relevant Thai Community Product Standards, continued monitoring is still necessary to ensure that product safety and quality are consistently maintained over time.

Table 2. Chemical and biological properties of pla-duk-ra product from BAICE

Chemical and biological properties	Before the project implementation	After the project implementation	Thai Community Product Standards
Water activity (aw)	0.85±0.02	0.71±0.04	0.80±0.06
Yeasts (CFU/ g sample)	1.2×10^4	1.0×10^2	$1x10^4$
Molds (CFU/g sample)	13	10	500
E. coli (MPN/g sample)	30	<3.0	10
S. aureus (MPN/g sample)	150	<3.0	100

Note: Values of water activity are expressed as mean ± standard deviation. Microbiological values are reported as CFU/g or MPN/g sample, as appropriate.

Sensory evaluation was conducted before and after project implementation by the same five trained assessors who had experience in evaluating pla-duk-ra (Table 3). Employing a trained sensory panel is critical for minimizing individual psychological biases and obtaining objective, reproducible analytical data on

specific product attributes [18]. The study concludes that GMP implementation improves all sensory attributes, indicating that this type of quality improvement is not only related to food safety and legal aspects but also to sensory attributes important for consumer appeal and market value. The appearance stringency was increased by 18.1%, and the appearance scores were expectedly elevated from an average of 3.20 to 3.78, verifying that a standardized manufacturing process protocol, performed in compliance with GMP, can indeed be successfully established. This improvement is probably due to better selection of raw materials, consistent processing procedures, and superior quality assurance practices. Sensory parameters indicate that the size is uniform, the skin is intact, and the product is not over-dried. Further, the higher post-implementation scores indicate that the GMP training and SOPs were successful in training workers to consistently produce products that are appealing.

The color scores fared the best, with a 5.9% gain from 3.70 to 3.92, very close to "excellent". Quality standards demand that commodities have a natural color of pla-duk-ra. The relatively high initial product suggests that the traditional recipe already provided good color development, and the GMP modification improved stability more fundamentally, even though this property changed significantly. Fermented fish product color development is mediated by a number of complex biochemical mechanisms, including Maillard reactions, lipid oxidation, and enzymatic browning, which are better regulated under GMP conditions.

The flavor had the largest improvement, increasing by 26.8% from 3.10 to 3.93. This development is particularly noteworthy because flavor perception extends beyond mere physical taste; it is a profound psychological determinant that significantly influences consumer food choice, overall acceptance, and eventual repurchase behavior [19]. According to quality standards, fermented catfish should have a natural taste without off-flavors such as mustiness, rancidity, or bitterness. The large decrease was associated with a significant reduction in microbial load, especially *E. coli* and *S. aureus*. Since the survival and proliferation of these pathogens during fermentation pose significant safety risks and can lead to the production of metabolites that alter characteristic flavor profiles, controlling them through systematic hygiene is crucial [20]. Furthermore, GMP for cleaning food-grade materials and equipment prevents chemical contamination that might alter taste.

Texture scores for pla-duk-ra rose by 18.8%, from 3.20 to 3.80, meeting quality standards of softness and tenderness without undesirable sensations. This improvement resulted from better control of the fermentation-drying cycle using standardized methods, which lowered water activity from 0.85 to 0.71, limiting microbial growth and enhancing product stability. All sensory attributes showed statistically significant improvements ($p<0.05$) post-GMP implementation, with ratings near or above the "excellent" category (≥3.80). This demonstrates that GMP enhances both safety and consumer-relevant quality, aligning with Codex guidelines on hygiene supporting safe, suitable food production [21]. Unlike conventional methods, BAICE maintained original sensory characteristics while improving quality, addressing concerns about authenticity loss through standardization. These sensory gains have important business implications, as product quality influences consumer satisfaction, repeat purchases, and willingness to pay premium prices. Sensory evaluation is crucial to understanding consumer perceptions and acceptance. The improved appearance and taste reinforce pla-duk-ra's status as a Southern Thai specialty, supporting efforts to promote traditional foods that enhance nutritional value and commercial potential while preserving cultural identity.

In this study, the objective of the sensory evaluation was therefore not to quantify direct consumer preference or purchase behavior, but rather to evaluate the quality attributes of pla-duk-ra in line with established product-specific criteria with intermediate moisture foods [22]. Therefore, the sensory score increases seen in the present study should be interpreted as increased product quality from a trained sensory panel perspective rather than consumer acceptance [23]. Enhancements are likely due to improved control of raw catfish, salting, drying, sanitation, and overall process management under GMP. However, further consumer-focused sensory studies, including acceptance and purchase intent, are needed to confirm if these quality improvements meaningfully influence consumer preferences and purchasing behavior in the market.

Table 3. Sensory property of pla-duk-ra from BAICE

Sensory property	Before the project implementation	After the project implementation
Appearance	3.20 ± 0.43	3.78 ± 0.32
Color	3.70 ± 0.23	3.92 ± 0.44
Flavor	3.10 ± 0.33	3.93 ± 0.39
Texture	3.20 ± 0.38	3.80 ± 0.39

Note: Values are expressed as mean ± standard deviation. Different letters within the same row (horizontally) indicate statistically significant differences ($p < 0.05$).

Sensory/quality criteria

General appearance: Must be fairly dry; units within the same container should be similar in size; skin must be intact (no tears).

Color: Should exhibit a good, natural color characteristic of fermented catfish (pla duk ra).

Aroma & taste: Should have a good, natural aroma and taste characteristic of fermented catfish; free from undesirable off-odors/off-flavors such as musty, rancid, or bitter notes.

Texture: Should be soft; neither mushy nor overly hard/tough.

Scale: 4 = Excellent; 3 = Good; 2 = Fair (acceptable); 1 = Needs improvement.

3.3 Packaging and Thai FDA certification

To enhance pla-duk-ra's market competitiveness, continued focus on packaging and label design is essential. Good packaging not only improves product appeal and security but also preserves quality and extends shelf life, facilitating market expansion. According to the Ministry of Public Health Notification B.E. 2557 (2014), retail packaging must comply with specified volume limits and include clear labels detailing product name, ingredients, nutrition facts, usage instructions, and necessary warnings to meet regulatory requirements and consumer expectations. Good packaging helps protect food products, maintain quality and safety, and extend shelf life during storage and distribution [24]. For retail packaging, the declared net quantity should comply with the Ministry of Commerce regulation on prepackaged goods. Labeling of pla-duk-ra products should follow the Ministry of Public Health Notification No. 450 B.E. 2567 on labeling of prepackaged foods, which replaced earlier labeling notifications, including Notification No. 367 B.E. 2557 [25]. Product labels for pla-duk-ra must be clear, readable, and easy for consumers to understand. Labels should include production or expiry dates, proper storage instructions, and a detailed list of main ingredients. This aligns with Ministry of Public Health Notification No. 450 B.E. 2567 (2024), which mandates that prepackaged food labels be legible, accurate, and informative, including food name, net quantity, allergen information, date marking, warnings, and usage instructions. The notification also clarifies expiration and consume-before dates based on food quality and storage conditions, emphasizing the importance of clear date marking and storage guidance [25].

Packaging and labels for BAICE products are presented in Figures 7 and 8. Packaging and labels influence consumer decisions by conveying quality, safety, and product identity. Appropriate packaging for pla-duk-ra adds value and sustainability by protecting food quality, controlling environmental contact, reducing waste, and extending shelf life when matched to preservation needs. Good packaging can also help slow quality deterioration by reducing exposure to factors that may cause oxidation, mold growth, microbial contamination, and other changes that affect product safety and shelf life [26]. Clear and well-designed label graphics can help build consumer confidence when the label is easy to read and contains complete, accurate, and non-misleading information. According to the Thai FDA labeling requirements, label text must be prominent, readable, and presented with appropriate contrast between the text and background [25]. Sustainable packaging preserves food quality, reduces waste, and offers economic and environmental benefits through eco-friendly materials and technologies [27].

The process of obtaining food registration numbers in Thailand demonstrates BAICE's success in securing Thai FDA certification for six traditional fermented fish products. This achievement is significant because traditional fermented foods must be rigorously controlled as they are developed from household or community-based production into standardized commercial products. Steinkraus [28] emphasized that the

industrialization of indigenous fermented foods should preserve traditional characteristics while improving hygiene, process control, consistency, and safety. In this context, BAICE's certification represents an important step toward transforming fermented fish products into regulated, market-ready foods. Food registration in Thailand requires submission of Form SB.7 through the Thai FDA E-submission system, which evaluates product formulations and ingredient compositions. BAICE's six FDA registration numbers indicate progress in quality standardization, Primary GMP implementation, and compliance with food safety regulations. This is especially important for fish-based products, which are vulnerable to quality deterioration and microbial contamination if raw materials, processing, drying, packaging, storage, and distribution are not properly controlled. Huss et al. [29] noted that seafood safety management must address hazards throughout the production chain. The dry-fermented catfish product, FDA No. 93-2-00567-6-0002, is classified as a general food under animal products and requires microbiological safety evaluation for pathogens such as *S. aureus*, *Salmonella* spp., and *Clostridium* spp. Overall, BAICE's certification reflects the integration of traditional fermentation knowledge with modern food safety standards [28], [29].



Figure 7. Labels of products from the PLA-duk-ra production process. Ready to eat fried pla-duk-ra (a), Khao-yum sauce (b), Sweet fish sauce (c), Rice seasoning (d), Dry-fermented catfish chili paste (e).

Most registered BAICE products are classified as ready-to-eat or ready-to-cook foods, including FDA Nos. 93-2-00567-6-0003, 93-2-00567-6-0004, 93-2-00567-6-0006, and 93-2-00567-6-0007. This classification shows how processing innovation can enhance the value chain of traditional fermented fish products by converting them into convenient forms that meet modern consumer needs. This development aligns with the Thailand 4.0 approach, which emphasizes innovation, product development, knowledge application, and quality management to improve the competitiveness of community enterprises [30]. The Khao-yum sauce product, FDA No. 93-2-00567-6-0005, also reflects product diversification by transforming traditional fermented fish knowledge into a value-added condiment. This helps preserve regional culinary identity while expanding market opportunities. Fermented fish products are culturally important in Asia, and their characteristics are influenced by raw materials, traditional processing, and microbial activity, as shown in studies of *ngari*, *hentak*, and *tungtap* [31]. Globally, fermented foods demonstrate how traditional knowledge can be developed into diverse products while maintaining cultural and sensory qualities [32]. Overall, BAICE's FDA certification reflects effective quality control, product standardization, and technical support. This achievement enhances market access, consumer confidence, product value, and sustainable rural livelihoods.



Figure 8. Packaging of pla-duk-ra product (a) and ready-to-eat products (b) from pla-duk-ra production process of BAICE

Table 4. Thai FDA certification for food products in the form of food registration numbers of BAICE

No.	FDA Registration code	Name of product	Type of product
1	93-2-00567-6-0002	Dry-fermented catfish	General foods, including animals and animal products that have passed evaluation and inspection
2	93-2-00567-6-0003	Ready to eat fried Pla-duk-ra	Ready-to-cook foods and ready-to-eat foods, including ready-to-eat food products
3	93-2-00567-6-0004	Sweet fish sauce	Ready-to-cook foods and ready-to-eat foods, including ready-to-eat food products
4	93-2-00567-6-0005	Khao-yum sauce	General foods, including seasonings that have passed evaluation and inspection
5	93-2-00567-6-0006	Rice seasoning	Ready-to-cook foods and ready-to-eat foods, including ready-to-eat food products
6	93-2-00567-6-0007	Dry-fermented catfish chili paste	Ready-to-cook foods and ready-to-eat foods, including ready-to-eat food products

3.4 The economic analysis

This economic investigation of BAICE after GMP implementation and Thai FDA approval demonstrates the financial feasibility of upgrading traditional fermented fish products. Based on August 2025 data, six FDA-approved products generated total monthly revenue of USD 2,821, with production costs of USD 1,383 and net income of USD 1,438. The overall profit margin was 51.0%, indicating that quality improvement, food safety certification, and product standardization can increase product value and strengthen market competitiveness. BAICE's performance is consistent with consumer behavior studies showing that consumers are willing to pay more for products perceived as safe, high quality, and produced under recognized standards. Thai FDA approval and GMP implementation may therefore enhance consumer confidence and support premium pricing for improved traditional fermented fish products [33]. Pla-duk-ra was the main revenue-generating product, contributing USD 2,480 (87.9% of total revenue) and USD 1,240 (86.2% of net income), with a 50.0% profit margin. This reflects strong market demand for traditional fermented fish. BAICE's success also underscores the importance of collective action in helping community enterprises improve quality, meet regulatory requirements, and access higher-value markets [34]. Overall, BAICE demonstrates how small-scale producers can adapt to changing agrifood markets through certification, quality management, and enterprise cooperation [35].

The five value-added derivative products contributed USD 341, or 12.1% of total monthly revenue, and USD 198, or 13.8% of total net income. These products showed profit margins ranging from 49.5% to 71.0%. The second-highest revenue was generated by ready-to-eat fried pla-duk-ra, with USD 155 in monthly revenue, USD 62 in production cost, USD 93 in net income, and a profit margin of 60.0%. Sweet fish sauce and Khao-yum sauce each generated USD 31 in monthly revenue, USD 9 in production cost, USD 22 in net income, and a profit margin of 71.0%. Rice seasoning generated USD 31 in monthly revenue, USD 16 in production cost, USD 15 in net income, and a profit margin of 48.4%. Dry-fermented catfish chili paste generated USD 93 in monthly revenue, USD 47 in production cost, USD 46 in net income, and a profit margin of 49.5%. These findings indicate that product diversification after GMP implementation and FDA certification helped BAICE generate additional income from value-added products. Such diversification may also strengthen market linkages by enabling producers to offer a broader product portfolio that responds to consumer demand and market opportunities. In addition, GMP implementation and FDA certification can enhance buyer confidence and trust in agribusiness supply chains, which are important factors supporting long-term market relationships and commercial sustainability.

Several factors explain BAICE's financial success after regulatory compliance. Certification and FDA registration strengthened the enterprise by improving access to formal retail markets, where certified products are often required and may command better prices [36], [37]. FDA approval also enhanced consumer trust, particularly among urban consumers who increasingly value food safety, health, and product quality [38], [39]. In addition, improved production management helped reduce losses from contamination, inconsistent quality, and batch failure. For fermented products, such control is especially important because quality depends on fermentation conditions and microbial activity [40]. BAICE's monthly net income of USD 1,438 is economically significant in rural Thailand, where household livelihoods are closely connected to local production and consumption systems. When distributed among community members, this income supports household welfare, food security, and local economic resilience. Product diversification also reduces dependence on a single product and reflects sound risk-management practice for smallholder food enterprises. The overall cost-to-revenue ratio of approximately 49.0% and profit margin of 51.0% indicate that quality improvement and regulatory compliance can be economically beneficial, not merely administrative obligations. BAICE demonstrates how traditional food wisdom can be integrated with modern quality standards to strengthen value-chain inclusion, support smallholders, and meet demand for safe products. This model may benefit other community enterprises and contribute to SDGs 1, 2, 8, and 12 [41].

Table 5. Cost analysis and returns of BAICE after the project implementation in August 2025

Product	Revenue (USD/Month)	Cost (USD /Month)	Net income (USD /Month)	Profit margin (%)
1. Dry-fermented catfish (pla-duk-ra)	2,480	1,240	1,240	50.0
2. Ready to eat fried Pla-duk-ra	155	62	93	60.0
3. Sweet fish sauce	31	9	22	71.0
4. Khao-yum sauce	31	9	22	71.0
5. Rice seasoning	31	16	15	48.4
6. Dry-fermented catfish chili paste	93	47	46	49.5
Total	**2,821**	**1,383**	**1,438**	**51.0**

Note: Calculation: Net income = Revenue – Cost, Profit margin (%) = (Net income ÷ Revenue) × 100

4. Conclusions

This study demonstrates that adopting GMP significantly improves food safety, product quality, and economic performance in community-based catfish production. Using an extension-by-participation approach, BAICE successfully reduced microbial contamination, improved sensory characteristics, and obtained Primary GMP and FDA validation, allowing it to enter the regulated marketplace. Economic analysis showed significant gains, with profit rates of 50%, reinforcing the possibility of improving ancient food systems. Results show that mid-tier rural enterprises can meet national standards through training and facility upgrades with a cultural foundation. This model provides a replicable platform to enhance sustainable rural food systems in Thailand.

5. Acknowledgments

This project was a collaboration between BAICE, the Provincial Public Health Office, and Thaksin University, Phatthalung Campus. We thank all staff and volunteers for the vital work in the field, technical assistance, and contribution to coordination.

Author Contributions: Conceptualization, A thanonkaew and S. Kiriratnikom and P Mayachiew methodology, A thanonkaew and S. Kiriratnikom.; validation, A thanonkaew, P Hoktha and T Luanunkarb formal analysis, A thanonkaew and S. Kiriratnikom and P Mayachiew investigation, A thanonkaew.; resources, A thanonkaew.; data curation, A thanonkaew and S. Kiriratnikom; writing—original draft preparation, A thanonkaew and S. Kiriratnikom.; writing—review and editing, A thanonkaew and P Hoktha; visualization, T Luanunkarb ; supervision, A thanonkaew ; project administration, A thanonkaew.; funding acquisition, A thanonkaew. All authors have read and agreed to the published version of the manuscript.

Funding: Please add: This research was financed by the National Science, Research, and Innovation Fund (NSRF) and PMU A. The contracts were A11F670135 (FY 2024) and A11F680114 (FY 2025).

Conflicts of Interest: The authors declare no conflict of interest.

References

[1] Swangdacharuk, P. Aquafeed Industry in Thailand: Current Status, Sustainability & Future Trends. *Int. Aquafeed Fish Farming Technol.* **2025**. Aquafeed Industry in Thailand: Current Status, Sustainability & Future Trends.

[2] Thanonkaew, A.; Jantachote, T.; Ruangrat, W.; Aksornniem, A. Quality Changes of Fermented Catfish (Pla-Duk-Ra) Products during Storage at Room Temperature. *J. Natl. Res. Counc. Thailand Sci. Sect.* **2009**, *41*(2), 27–41. (In Thai).

[3] Thanonkaew, A.; Klompong, V.; Mayachiew, P.; Luanunkarb, T.; Hoktha, P.; Intarat, N.; Phatcharasit, K.; Panomjan, N.; Kiriratnikom, S. Integrated Dry-Fermented Catfish Production to Promote Sustainable Livelihoods and Community-Based Economic Development: A Case Study of the Community Enterprise Group in Koh Tao Subdistrict, Pa Phayom District, Phatthalung Province, Thailand. *Area Based Dev. Res. J.* **2025**, *17*(3), 175–194. https://doi.org/10.48048/abcj.2025.175 (In Thai).

[4] Danudol, A.; Weerawatanakorn, M. Good Manufacturing Practice (GMP 420): The Easiest Practice for Food Safety. *J. Nutr. Assoc. Thailand* **2022**, *57*(2), 43–62. (In Thai).

[5] Klompong, V.; Klomklao, S.; Mayachiew, P.; Luanunkarb, T.; Hoktha, P.; Thanonkaew, A. Quality Improvement and By-Product Utilization in Dry-Fermented Catfish Processing: A Case Study of Ban Chumphon Community Enterprise, Phatthalung Province, Thailand. *Area Based Dev. Res. J.* **2025**, *17*(1), 35–54. https://doi.org/10.48048/abcj.2025.035 (In Thai).

[6] Febri; Apriani, A.; Lugeri, L.; Siskawanti, F.; Kurniasari, M. Implementation of Good Manufacturing Practices (GMP) in the Small-Scale Fish Ball Food Industry. *J. Fish. Mar. Appl. Sci.* **2024**, *2*(3), 123–135. https://doi.org/10.58184/jfmas.v2i3.376

[7] National Strategy Secretariat Office. *National Strategic Framework of Thailand 2018–2037*; Office of the National Economic and Social Development Board: Thailand, 2018. National Strategic Framework of Thailand 2018–2037.

[8] Food and Drug Administration. *Inspection Manual of Food Production Facility According to Good Manufacturing Practice in Production That Is Enforced by Law (GMP 420)*; FDA: Thailand, 2020. (In Thai). Inspection Manual of Food Production Facility According to GMP 420.

[9] U.S. Food and Drug Administration. *Bacteriological Analytical Manual (BAM): Microbiological Detection Methods*; FDA: Silver Spring, MD, 2001. Bacteriological Analytical Manual (BAM).

[10] Office of Industrial Product Standards. *Community Product Standards No. 1029/2005*; Office of Industrial Product Standards: Thailand, 2005. Community Product Standards No. 1029/2005.

[11] Purwantiningrum, I.; Widyhastuty, W.; Christian, J.; Sari, N. Assessment of Good Manufacturing Practice for Small-Scale Food Industry in Malang Region, East Java, Indonesia. *IOP Conf. Ser.: Earth Environ. Sci.* **2018**, *131*, 012028. https://doi.org/10.1088/1755-1315/131/1/012028

[12] Anal, A. K.; Perpetuini, G.; Petchkongkaew, A.; Tan, R. P.; Avallone, S.; Tofalo, R.; Nguyen, H. V.; Chu-Ky, S.; Ho, P. H.; Phan, T. T.; Waché, Y. Food Safety Risks in Traditional Fermented Food from South-East Asia. *Food Control* **2020**, *109*, 106922. https://doi.org/10.1016/j.foodcont.2019.106922

[13] Rodmanee, S.; Huang, W.-C. Hygiene and Manufacturing Practices, Interagency Collaboration, and a Proposal for Improvement: A Case Study of Community Food Enterprise in Thailand. *Int. J. Soc. Sci. Humanit.* **2013**, *3*(3), 284–289. https://doi.org/10.7763/IJSSH.2013.V3.232

[14] Rujijanakul, P.; Suwannaporn, P.; Kulthamrongsri, N. Development of Pickled Fish (Pla Som) Facilities in Khon Kaen Province to Safety Standards According to GMP through Community Participation. *J. Food Saf. Health* **2023**, *9*(1), 78–92. (In Thai).

[15] Geraldo, V.; Ampofo-Asiama, J.; Adinortey, C.A.; Okyere, I.; Tulashie, S.K.; Nuer, A.T.K.; Nkansah, S.B.; Omega, S.; Seidu-Larry, S.; Kizzie-Hayford, N. Implementation of Good Manufacturing Practices (GMP) to Improve the Quality of Smoked Fish (*Scomber colias*). *Heliyon* **2024**, *10*, e27401. https://doi.org/10.1016/j.heliyon.2024.e27401

[16] Frazier, W. C.; Westhoff, D. C. *Food Microbiology*, 5th ed.; McGraw Hill Education: India, 2022.

[17] Gram, L.; Huss, H. H. Microbiological Spoilage of Fish and Fish Products. *Int. J. Food Microbiol.* **1996**, *33*(1), 121–137. https://doi.org/10.1016/0168-1605(96)01134-8

[18] Lawless, H. T.; Heymann, H. *Sensory Evaluation of Food: Principles and Practices*, 2nd ed.; Springer: New York, 2010. https://doi.org/10.1007/978-1-4419-6488-5

[19] Köster, E. P. Diversity in the Determinants of Food Choice: A Psychological Perspective. *Food Qual. Prefer.* **2009**, *20*(2), 70–82. https://doi.org/10.1016/j.foodqual.2007.11.002

[20] Adams, M. R.; Mitchell, R. Fermentation and Pathogen Control: A Risk Assessment Approach. *Int. J. Food Microbiol.* **2002**, *79*(1–2), 75–83. https://doi.org/10.1016/S0168-1605(02)00181-2

[21] Codex Alimentarius Commission. *General Principles of Food Hygiene: CXC 1-1969*; Food and Agriculture Organization of the United Nations/World Health Organization: Rome, Italy, 2023. General Principles of Food Hygiene: CXC 1-1969.

[22] U.S. Food and Drug Administration. *Water Activity (aw) in Foods*; U.S. Food and Drug Administration: Silver Spring, MD, 2024. Water Activity (aw) in Foods.

[23] Meilgaard, M. C.; Civille, G. V.; Carr, B. T. *Sensory Evaluation Techniques*, 5th ed.; CRC Press: Boca Raton, FL, 2016. https://doi.org/10.1201/b19493

[24] Kohli, D.; Loushigam, G.; Richa, R.; Bajad, R. Recent Advances in Food Packaging for Shelf Life of Food. In *Food Production, Diversity, and Safety under Climate Change*; Springer, 2024; pp 273–284. https://doi.org/10.1007/978-3-031-51647-4_23

[25] Food and Drug Administration, Ministry of Public Health. *Notification of the Ministry of Public Health (No. 450) B.E. 2567 (2024), Issued by Virtue of the Food Act B.E. 2522: Labeling of Prepackaged Foods*; FDA: Thailand, 2024. (In Thai). Notification of the Ministry of Public Health No. 450 (2024).

[26] Fadiji, T.; Rashvand, M.; Daramola, M. O.; Iwarere, S. A. A Review on Antimicrobial Packaging for Extending the Shelf Life of Food. *Processes* **2023**, *11*(2), 590. https://doi.org/10.3390/pr11020590

[27] Guillard, V.; Gaucel, S.; Fornaciari, C.; Angellier-Coussy, H.; Buche, P.; Gontard, N. The Next Generation of Sustainable Food Packaging to Preserve Our Environment in a Circular Economy Context. *Front. Nutr.* **2018**, *5*, 121. https://doi.org/10.3389/fnut.2018.00121

[28] Steinkraus, K. H. *Industrialization of Indigenous Fermented Foods*, 2nd ed.; Marcel Dekker: New York, 2004. https://doi.org/10.1201/9780203022047

[29] Huss, H. H.; Ababouch, L.; Gram, L. *Assessment and Management of Seafood Safety and Quality*; FAO Fisheries Technical Paper No. 444; FAO: Rome, Italy, 2000.

[30] Mettathamrong, J.; Promket, C.; Vichasilp, K. How Community Enterprises of Thailand Managed to Become Thailand 4.0. *Int. J. Oper. Quant. Manag.* **2022**, *28*(1), 121–133. https://doi.org/10.46970/2022.28.1.7

[31] Thapa, N.; Pal, J.; Tamang, J. P. Microbial Diversity in Ngari, Hentak and Tungtap, Fermented Fish Products of North-East India. *World J. Microbiol. Biotechnol.* **2004**, *20*, 599–607. https://doi.org/10.1023/B:WIBI.0000043171.91027.7E

[32] Tamang, J. P.; Kailasapathy, K., Eds. *Fermented Foods and Beverages of the World*; CRC Press: Boca Raton, FL, 2010. https://doi.org/10.1201/EBK1420094954

[33] Boccaletti, S.; Nardella, M. Consumer Willingness to Pay for Pesticide-Free Fresh Fruit and Vegetables in Italy. *Int. Food Agribus. Manag. Rev.* **2000**, *3*(3), 297–310. https://doi.org/10.1016/S1096-7508(01)00049-0

[34] Markelova, H.; Meinzen-Dick, R.; Hellin, J.; Dohrn, S. Collective Action for Smallholder Market Access. *Food Policy* **2009**, *34*(1), 1–7. https://doi.org/10.1016/j.foodpol.2008.10.001

[35] Reardon, T.; Barrett, C. B.; Berdegué, J. A.; Swinnen, J. F. M. Agrifood Industry Transformation and Small Farmers in Developing Countries. *World Dev.* **2009**, *37*(11), 1717–1727. https://doi.org/10.1016/j.worlddev.2008.08.023

[36] Henson, S.; Caswell, J. The Economic Implications of Using HACCP as a Food Safety Regulatory Standard. *Food Policy* **1999**, *24*, 625–635. https://doi.org/10.1016/S0306-9192(99)00074-3

[37] Unnevehr, L.; Jensen, H. H. The Economic Implications of Food Safety Regulations for Food Processors. *Food Policy* **1999**, *24*, 667–683.

[38] Grunert, K. G. Food Quality and Safety: Consumer Perception and Demand. *Eur. Rev. Agric. Econ.* **2005**, *32*, 369–391. https://doi.org/10.1093/eurrag/jbi011

[39] Reardon, T.; Timmer, C. P. The Economics of the Food System Revolution. *Annu. Rev. Resour. Econ.* **2012**, *4*, 225–264. https://doi.org/10.1146/annurev.resource.050708.144147

[40] Udomsil, N.; Rodtong, S.; Tanasupawat, S.; Yongsawatdigul, J. Proteinase-Producing Halophilic Lactic Acid Bacteria Isolated from Fish Sauce Fermentation. *Int. J. Food Microbiol.* **2011**, *141*(3), 186–194. https://doi.org/10.1016/j.ijfoodmicro.2010.05.016

[41] United Nations. *Sustainable Development Goals 2025: Progress and Recommendations*; United Nations: New York, 2025.

ASEAN
Journal of Scientific and Technological Reports
Online ISSN:2773-8752

Research article

Analysis of Electromagnetic Shielding Effectiveness of Multilayer to Protect Against Lightning Strike Effect on Aerospace Applications

Siva Chakra Avinash Bikkina[1*], G. Suneetha[2], and Kakarla Gopi Sri Koushiki[3]

[1] Department of Electronics and Communication Engineering, Aditya University,Surampalem, Andhra Pradesh, 533437, India
[2] Department of Electronics and Communication Engineering, Ramachandra College of Engineering, Eluru, Andhra Pradesh, 534007, India
[3] P.G Scholar, Ramachandra College of Engineering, Eluru, Andhra Pradesh, 534007, India
[*] Correspondence: bscavinash1997@gmail.com

Citation:
Bikkina, S.C.A.; Suneetha, G.; Koushiki, K.G.S. Analysis of electromagnetic shielding effectiveness of multilayer to protect against lightning strike effect on aerospace applications. *ASEAN J. Sci. Tech. Report.* **2026**, *29*(7), e260760. https://doi.org/10.55164/ajstr.v29i7.260760

Article history:
Received: August 8, 2025
Revised: February 18, 2026
Accepted: March 8, 2026
Available online: June 18, 2026

Publisher's Note:
This article is published and distributed under the terms of the Thaksin University.

Abstract: When lightning strikes in aerospace applications, the structural integrity and electrical systems of aircraft are put at great risk. Lightning creates very powerful electromagnetic pulses that conventional aluminium structurescan't handle. This work examines how well mesh topologies protect multilayer metal matrix composites (MMCs) that include conductive and ceramic reinforcements, such as Al_2O_3, SiC, and fly ash, within an Al6061 matrix. The composite structure has layers of metallic mesh coated with nickel to improve electromagnetic shielding and heat dissipation further. This investigation presents a theoretical and computational analysis of the efficacy of electromagnetic shielding, utilising Schelkunoff's theory in conjunction with a transmission-line model to evaluate multilayer MMC mesh structures. The suggested multilayer Al6061-based metal matrix composite (MMC) structures reinforced with SiC, Al_2O_3, and fly ash exhibit improved electromagnetic shielding effectiveness in the X-band frequency range (8-12 GHz). The shielding performance is around 96.12dB better than that of regular aluminium structures due to improved absorption and impedance mismatch. This work demonstrates a useful way to build sophisticated aeronautical structures utilising lightweight, highly effective shielding materials.

Keywords: Lightning strike protection; shielding effectiveness (SE); transmission line model; fly ash reinforcement.

1. Introduction

The electronic parts and communication systems used in today's aeroplanes make them vulnerable to electromagnetic interference. There are three primary locations where electromagnetic interference may affect aircraft. Lightning is one thing that may trigger them. a) Emissions from radio waves, radar, and other electromagnetic sources; b) Items on board the aircraft that cause circuit spark discharges; and c) External parts [1]. Aeroplanes and passenger safety are jeopardised by electromagnetic interference (EMI), which can cause communication problems and major equipment failures. Electromagnetic shielding technologies are urgently required to lessen the negative effects of electromagnetic interference. Lightning EMPS and other pulsed intense electromagnetic radiations are non-nuclear EMPS that may

disrupt electronic devices. This issue gravely threatens the normal functioning of the concerned devices. The costs associated with these threats may be reduced by implementing electromagnetic protection measures [2].

Meshes and plates made of MMCs are used extensively as primary shielding structures in electromagnetic protection engineering. MMC's mesh structures have become more common in place of plate structures due to their many advantages in areas such as ventilation, illumination, weight, and cost [3-5]. The requirement for electromagnetic shielding is another factor that cannot be ignored. Metal meshes with only one layer cannot provide electromagnetic shielding. The research provides an overview of the practical use of double- and multilayer MMC mesh systems in electromagnetic protection. A few scientific models were introduced to assess the viability of single-layer metal cross sections for providing security. Casey (1988) [5] presented a technique for deciding the typical impedance of a metal lattice with square openings. This strategy uses the typical field hypothesis. The estimation approach assumes that the rate frequency and the metal lattice size are much larger than the width of the metal wire [6-8]. Hyun et al. (2016) conducted a review in which they made numerical changes to the Casey model. The motivation behind these changes was to explicitly upgrade the exactness of calculation results for denser metal lattices. It is critical to note that these changes were made while keeping the recurrence consistent [9].

Precisely determining the shielding efficacy of double-layer metal meshes using analytical methods poses significant challenges. The insightful model created by Losito et al. in 2010 [10] was utilised to appraise the protective adequacy of single-layer metal froths. The Casey model evaluated the viability of twofold-layer metal lattices as a safeguard across various frequencies. In any case, it didn't give an exact evaluation of their viability. In 2019, Wang et al. conducted an investigation into the protective performance of double-layer metal lattices. They used the same transmission line approach [11-13] for their investigation. The development of the insightful model was obtained from Casey's work. The scientists encountered difficulties performing precise computations across an extensive range of frequencies, as in the model referenced in [14]. In many examinations investigating the adequacy of multi-facet metal cross sections for safeguarding, mathematical models are typically preferred over analytical models [15]. The test of achieving quick outcomes across different designs and sizes arises from the sluggish performance of reenactments and the extensive resource use. Previous research has suggested that accurately assessing the shielding effectiveness of single- and double-layer metal meshes using the Casey model [5] poses a significant challenge. Determining the shielding efficacy of multilayer meshes is a challenging and intricate undertaking. This study presents an analytical model that expands on the Hyun model [9]. This model aims to assess the efficiency of double- and multilayer metal meshes in providing effective shielding. The initial presentation highlights an MMC's single-layer mesh model, which exhibits a plane impedance. The extension of shielding theory to multilayer metal plates has been applied to a technique involving multilayer meshes. Now, let's analyse the factors that affect the precision of the calculations used to evaluate the efficacy of double- and multilayer metal meshes as protective shields.

The study examines improvements in electromagnetic shielding coatings for aircraft applications, emphasizing materials such as ZrB_2 and composites. These coatings enhance longevity and efficiency, ensuring the reliability and safety of aviation equipment for both crew and passengers [16-17]. Electromagnetic environmental shielding is essential in aerospace to safeguard equipment and personnel from space radiation, including solar particle events, cosmic rays, and proton-electron radiation. Recent advancements in materials aim to improve reliability for upcoming space missions [18].To improve system reliability and minimise errors caused by external electromagnetic sources, this paper investigates the optimisation of electromagnetic shielding techniques for aerospace systems. It focuses on a dual-layer shielding approach that uses aluminium foil to augment protection against high-frequency EMC [19]. For some aerospace applications, you need electromagnetic interference (EMI) shielding materials that can suit your particular functional needs while also efficiently reducing EMI. The article delves into composite EMI shielding materials optimized for aircraft applications through careful consideration of structural design and raw material selection [20]. Investigating how various infinite sheet metals can attain varying shielding effectiveness (SE) to fulfil the rigorous 40 dB SE criterion for electromagnetic compatibility, the study highlights the critical role of electromagnetic interference (EMI) shielding in aerospace, especially for space vehicles [21]. This paper presents a braided sheath for electromagnetically shielded cables suitable for aerospace applications. The sheath is composed of a

polytetrafluoroethylene film, aluminum, and copper shielding layers, all of which contribute to the cable's excellent mechanical properties, insulation, and shielding effectiveness, ensuring stable signal transmission even in electromagnetic environments [22]. The electromagnetic environment and onboard equipment may cause interference with aerospace applications, electromagnetic shielding is necessary. Optimizing protection while reducing weight, advanced materials, especially nanomaterials, increase shielding efficiency over a frequency range from Hz to THz [23].

Even though materials for electromagnetic shielding have advanced, accurately analysing multilayer metal-mesh-based metal-matrix composites (MMCs) remains challenging due to the complexity of impedance interactions and frequency-dependent behaviour. Most current investigations are either on single-layer shielding setups or numerical simulations. There aren't many analytical methods that can effectively anticipate how multilayer systems would behave across a wide range of frequencies [24-25]. The main purpose of this research is to create and evaluate multilayer Al6061-based MMC mesh structures fortified with SiC, Al_2O_3, and fly ash, to improve electromagnetic shielding efficacy for aerospace applications. This study uses Schelkunoff's theory of electromagnetic shielding and a transmission-line modelling approach to look at the theoretical and computational aspects of shielding mechanisms. It focuses on reflection and absorption losses in the X-band frequency range (8–12 GHz). The research seeks to assess the impact of reinforcement composition and multilayer architecture on shielding efficacy, and to propose lightweight composite solutions suitable for aeronautical electromagnetic conditions.

2. Materials and Methods

When designing sophisticated multilayer metal-matrix composites (MMCs) that can withstand lightning strikes in aerospace applications, it is crucial to use the right materials. This research uses a hybrid material system to find a balance between mechanical performance, thermal stability, electrical conductivity, and light weight. The suggested system comprises an Al6061 alloy matrix strengthened with a blend of fly ash particles, silicon carbide (SiC), and aluminium oxide (Al_2O_3). Also, conductive nickel-coated mesh layers are placed between the MMC layers to enhance electromagnetic shielding effectiveness (SE). Al6061 was selected as the base matrix material. It is a common aluminium alloy utilised in aerospace applications. Al6061 is known for being very strong for its weight, highly corrosion-resistant, and having a high thermal conductivity. It can absorb lightning-induced currents due to its relatively high electrical conductivity (approximately 40% IACS) [26]. It also works very well with ceramic reinforcements and is suitable for casting and extrusion, both of which are important for making multilayer composite structures. Adding ceramic reinforcements such as Al_2O_3 and SiC makes the composite stronger and better at withstanding heat. Al_2O_3 (10 wt%) was selected because it is very strong, resistant to wear and tear, and very stable at high temperatures. These properties help it withstand erosion and deterioration after a lightning strike. Silicon carbide (5 wt%) is added to improve heat conduction and mechanical strength while maintaining the material's excellent oxidation resistance. The ceramic particles act as thermal barriers, making the composite better able to withstand the very high temperatures associated with lightning strikes [27–28]. Fly ash is a cheap and light filler made from industrial waste that is high in alumino-silicate compounds. It is utilised at a concentration of 10 wt%. Adding this element lowers the composite's overall density while improving its ability to insulate against heat and resist deformation at high temperatures. In addition, using fly ash to make aeroplane parts from trash helps develop sustainable materials [29]. To meet the demand for improved electromagnetic shielding, layers of nickel-coated stainless steel mesh are inserted between the composite layers. The mesh structures have several uses: they allow electrical current to flow through them with little resistance, reflect incoming electromagnetic radiation, and improve energy absorption by reflecting it multiple times. Nickel plating makes the surface more conductive and corrosion-resistant, both of which are important for long-lasting performance in aviation applications [30]. Nickel-coated stainless-steel meshes (200 mesh per inch, ~150 μm wire thickness) with a nickel coating thickness of approximately 3–5 μm were employed as conductive interlayers to enhance electromagnetic shielding performance. The multilayer architecture features MMC layers and nickel-mesh interfaces that alternate. This setup improves performance by improving reflection and absorption processes and fixing impedance mismatches between layers. This makes high-frequency electromagnetic waves less

powerful. The concept combines mechanical performance with electromagnetic shielding, making it suitable for aircraft skin, unmanned aerial vehicles (UAVs), and other aerospace components that are struck by high-energy lightning [31].

2.1 Fabrication Process

Utilising the stir-casting method, we fabricated multilayer Al6061-based metal-matrix composite (MMC) structures reinforced with ceramic and industrial byproduct particles. Stir casting is an economical and scalable technique for manufacturing aluminium matrix composites in their molten form. This technique offers exceptional control over particle dispersion and is optimal for generating a large number of particles [32]. The selection of commercial-grade Al6061 alloy as the matrix material was based on its superior casting characteristics, moderate strength, corrosion resistance, and appropriateness for aerospace applications. Aluminium oxide (Al_2O_3) and silicon carbide (SiC) were used as ceramic particles, while fly ash was employed as a low-density industrial waste filler. All reinforcements were filtered to guarantee that the particles were fewer than 50 μm in size. The materials were further heated to 300°C for 2 hours to remove moisture, improve wettability, and prevent hydrogen gas from being trapped during casting [24]. Nickel-coated stainless steel mesh (200 mesh per inch, approximately 150 μm thick) was used as the conductive substrate between the layers. Before casting, the meshes were ultrasonically cleaned in acetone and then dried to enhance their adhesion to the matrix during layer integration. A resistance furnace with a graphite crucible was used for the stir casting process. The Al6061 alloy was melted at a processing temperature between 700 and 750 °C, which is sufficiently above its liquidus temperature to ensure complete melting and effective reinforcement incorporation. A little proportion (1 wt%) of magnesium (Mg) was integrated into the melt to improve the adherence of the molten matrix to the ceramic and fly ash particles [25]. Upon achieving stability in the mixture, the heated reinforcements (10% Al_2O_3, 10% SiC, and 5% fly ash) were meticulously incorporated into the molten aluminium, which was agitated at 450 rpm for 10 minutes using a graphite-coated impeller. An argon gas purge was maintained while stirring to prevent oxidation of the mixture and to remove dissolved gases. This guaranteed homogeneous particle distribution and minimised voids in the final casting [33].

Table 1. Percentage combination of materials

Material	Name of Specimen
AL6061+5%Al2O3+5%SiC+5%FA	MMCs-10
AL606+7.5%Al2O3+7.5%SiC+5%FA	MMCs-11
AL606+10%Al2O3+10%SiC+5%FA	MMCs-12

2.2 Analysis of Multilayer MMC Meshes

The calculation of shielding efficiency for multilayer MMC meshes. To accomplish this, we modify the plane impedance model originally developed for a single-layer MMC mesh to apply it to shielding theory for multilayer conductors.

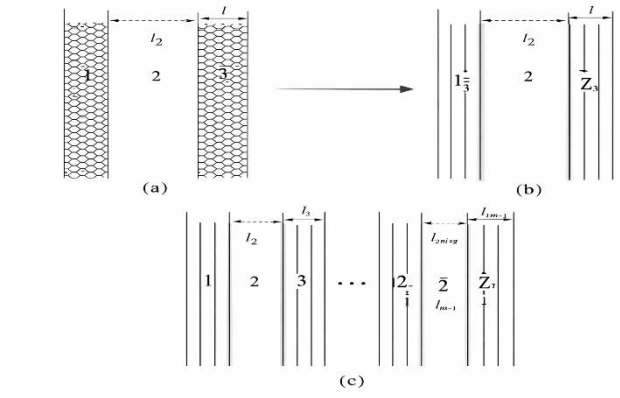


Figure 1. Electromagnetic Shielding model of a multilayer sheet and mesh

The initial step of this process involves examining an MMC's plate, which consists of only one layer. Figure 1: Electromagnetic Shielding model of a multilayer sheet and mesh. The formula provided can be used to calculate the shielding efficiency of a single plate [34].

$$SE = A + R + M \tag{1}$$

$$\text{SE}=\underbrace{20\,log_{10}\,e^{l/\delta}}_{\text{A}} + \underbrace{20\,log_{10}\left|\frac{(\eta_0+\eta)^2}{4\eta_0\eta}\right|}_{\text{R}} + \underbrace{20\,log_{10}\left|1-\left(\frac{(\eta_0-\eta}{(\eta_0+\eta}\right)^2 e^{-2\gamma l}\right|}_{\text{M}} \tag{2}$$

In the given context, absorption loss is represented by the symbol "A," reflection loss by "R," and multiple reflection loss by "M." The effectiveness of using a single-layer MMC plate as a conveyor is often attributed to its inherent impedance (η), which is lower than the impedance of free space (η_0). Additionally, it is important to acknowledge that the thickness (l) of the MMC's plate generally exceeds the skin depth.

$$\delta = \frac{1}{\sqrt{\pi f \mu \sigma}} \tag{3}$$

$$\gamma = \sqrt{j\omega\mu(\sigma + j\omega\varepsilon)} \tag{4}$$

The equation includes variables that represent different properties of the MMC's plate. γ represents the propagation constant, which describes how waves propagate through the plate. ε, μ, and σ represent the plate's permittivity, permeability, and conductivity, respectively. The variable "f" represents the frequency of the incident wave. The M worth is far less critical than the benefits of the first two boundaries (A and R). Thus, the safeguarding viability of a solitary MMC's plate can be communicated as follows.

$$SE_{single\ plate} = A + R \tag{5}$$

Figure 1(a) shows the game plan of twofold-layer MMC plates, with each plate having thickness and material properties similar to those of a solitary-layer plate. The client has determined the interlayer between the metal plates as "l_2." To thoroughly examine the safeguarding viability of the twofold-layer plate structure, the design has been partitioned into three distinct regions, designated as locales 1, 2, and 3, as shown in Figure 1(a). To discover the composite design's general protective adequacy, it is essential to process the combined safeguarding viability values for these three individual locales

$$SE_{Double\ plate} = SE_1 + SE_2 + SE_3 \tag{6}$$

The MMC's plates in this arrangement have similar safeguarding adequacy because of their reliable mathematical and electromagnetic properties, addressed as $SE_1 = SE_3$. It's essential to note that the safeguarding adequacy (SE) of the air interlayer doesn't adhere to the two suspicions applied to the MMC's plates. The methodology for registering misfortunes due to various reflections within the air interlayer (district 2) can be outlined as follows. The image λ_0 It is utilized to address the frequency in free space.

$$M_2=20\,log_{10}\left|1-\left(\frac{z_0-z_s}{z_0+z_s}\right)^2 e^{-2\gamma_2 l_2}\right| \tag{7}$$

$$M_2=20\,log_{10}\left|1-\left(\frac{z_0-z_s}{z_0+z_s}\right)^2\left(cos4\pi\frac{l_2}{\lambda_0}-jsin4\pi\frac{l_2}{\lambda_0}\right)\right| \tag{8}$$

In Figure 1(b), a twofold-layer structure is delineated, where the MMC plates in locales 1 and 3 are subbed with networks made of the same material and having the same thickness. The thickness of an MMC's plate (l) rises to the thickness of an MMC's cross-section. Ultimately, the configuration of multilayer metal meshes, as illustrated in Fig. 1(c), can be achieved by extending horizontally the configuration of a dual-layer mesh is illustrated in Fig. 1(b). Since the porosity of the lattice is higher than that of the MMC's plate, its

assimilation misfortune is unimportant. The strategy for registering the protective adequacy of the twofold layer MMC's lattice is framed as follows:

SE Double Mesh = Reflection loss for first layer +Reflection loss for second layer + Multiple Reflection loss for second layer (9)

$$A_{first\ layer} = \exp\left(\frac{t_m}{\sqrt{2}}\sqrt{k_0\sigma_m\mu_m}\right) \tag{10}$$

$$R_{first\ layer} = 20\log_{10}\left|\frac{(z_0+z_s)^2}{4z_0z_s}\right| \tag{11}$$

$$M_2 = 20\log_{10}\left|1-\left(\frac{z_0-z_s}{z_0+z_s}\right)^2 e^{-2\gamma_2 l_2}\right| \tag{12}$$

$$z_{s1} = z'_w a_s + j\omega L_S \tag{13}$$

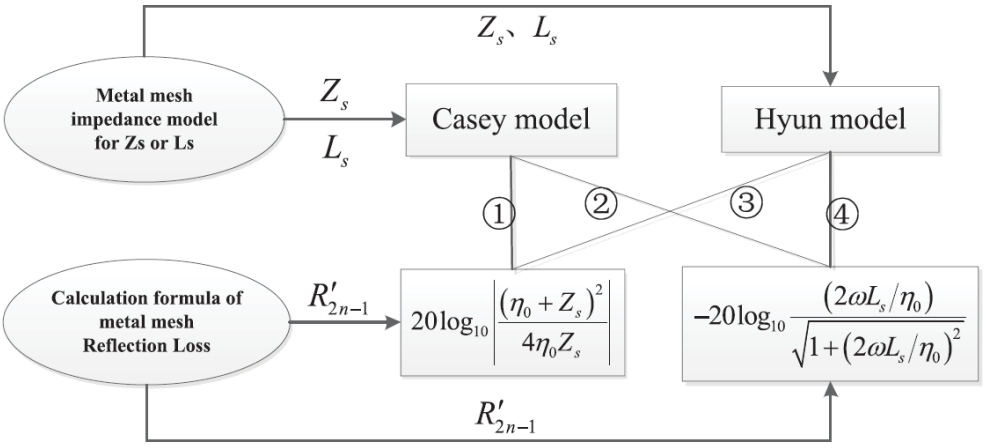


Figure 2. Overview of the various calculation methods used to determine the reflection loss [31].

The k_0 is used to address the free-space wave number. z'_wrepresents the normalised wave impedance of the multilayer structure relative to that of open space.a_s The attenuation coefficient (Np/m) shows how the field weakens within a conductive medium.

The impedance model for a metal mesh is depicted in Figure 2, providing a succinct representation. Additionally, the approach used to compute the metal-mesh reflection losses is outlined. To ensure high accuracy in shielding effectiveness calculations, it is crucial to implement stringent measures and methodologies. The user emphasises the importance of using precise and reliable mathematical models, advanced simulation techniques, and accurate input parameters and data. In addition, it is important to emphasise the need for comprehensive validation and verification procedures to ensure the accuracy and reliability of the calculations. The accuracy of the shielding effectiveness calculations can be improved by implementing these analytical approaches. An examination is underway to assess the use of multilayer meshes across a wide range of frequencies. Analysing data is crucial for making well-informed decisions. The figure depicts the visibility of both Casey and Hyun. The use of models is a common practice in computing the impedance Zs or Ls of a system. A single-layer metal mesh is a material composed of interwoven metal wires or threads arranged in a single layer. Furthermore, it is important to acknowledge that there are two separate schemes for calculating the reflection loss of a metal mesh, which is essential for determining its shielding effectiveness.

3. Results and Discussion

Figure 3 portrays the protective viability of a miniature absorbing material supported by an Al6061 composite at 1 mm for the ordinary frequency of electromagnetic waves in the X-band. Nickel was the most engrossing material, with the most extreme shielding of 51 dB and the least shielding of 39.9 dB at 8 GHz and 12 GHz, respectively. Figure 4 illustrates the effectiveness of a Miniature retaining material supported by an 85% Al6061 + 5% Sic + 5% Al_2O_3 + 5% FA composite at a thickness of 1 mm for typical electromagnetic wave occurrences in the X-band. The chosen retaining material is nickel, which provides a maximum shielding of 79.3 dB and a minimum shielding of 40.2 dB at frequencies of 8 GHz and 12 GHz, respectively.

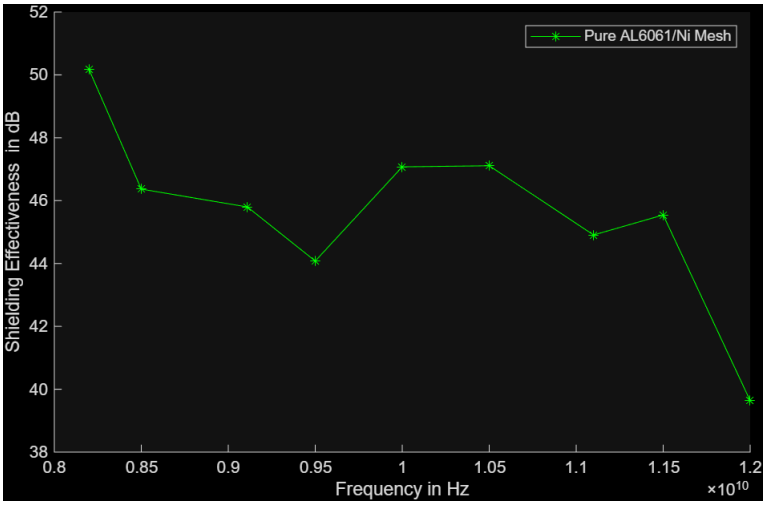


Figure 3. Shielding Effectiveness of Multilayer Pure Al6061/ Ni Mesh

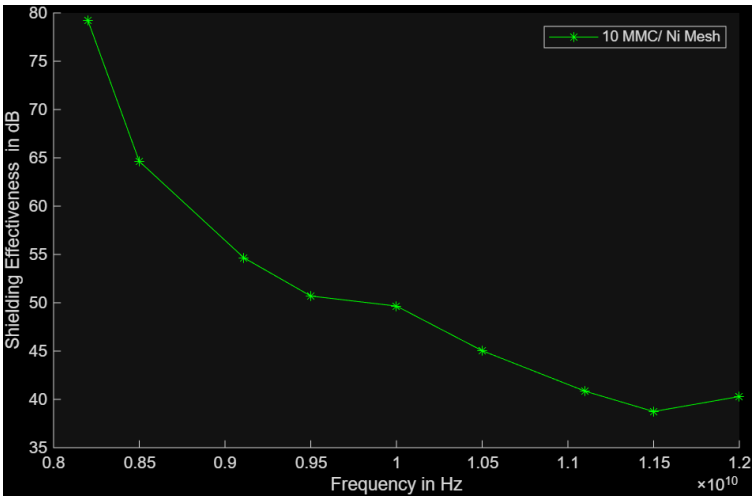


Figure 4. Shielding Effectiveness of Multilayer MMC-10/ Ni Mesh

Figure 5 illustrates the effectiveness of a Miniature absorbing material, which is reinforced by an 80% Al6061, 7.5% Sic, 7.5% Al_2O_3, and 5% FA composite. The material's ability to protect against X-band electromagnetic waves is evaluated at a thickness of 1 mm. The choice of nickel as the engrossing material was based on its maximum shielding of 83.33 dB and minimum shielding of 42.2 dB at frequencies of 8 GHz and 12 GHz, respectively. Figure 6 illustrates the effectiveness of a Miniature absorbing material, which is reinforced by a composite consisting of 75% Al6061, 10% Sic, 10% Al_2O_3, and 5% FA. The material's ability to protect against X-band electromagnetic waves is evaluated at a thickness of 1 mm. The chosen material for

engrossing purposes is nickel, which exhibits a maximum shielding effectiveness of 95.20 dB and a minimum of 42.2 dB at 8 GHz and 12 GHz, respectively.

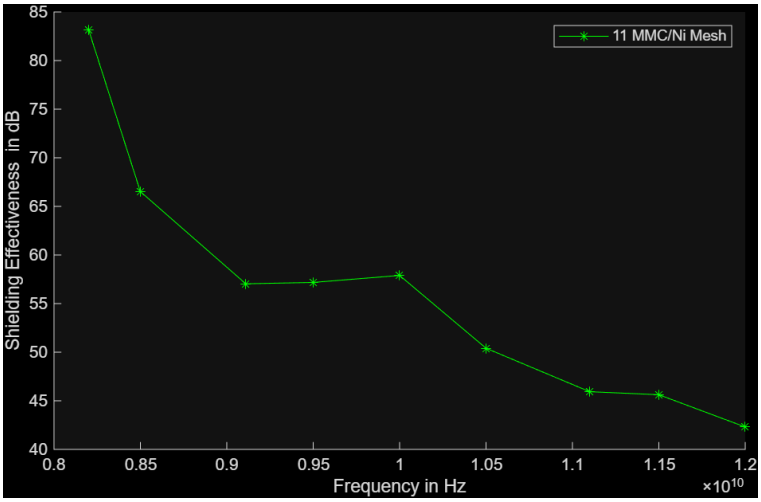


Figure 5. Shielding Effectiveness of Multilayer MMC-11/ Ni Mesh

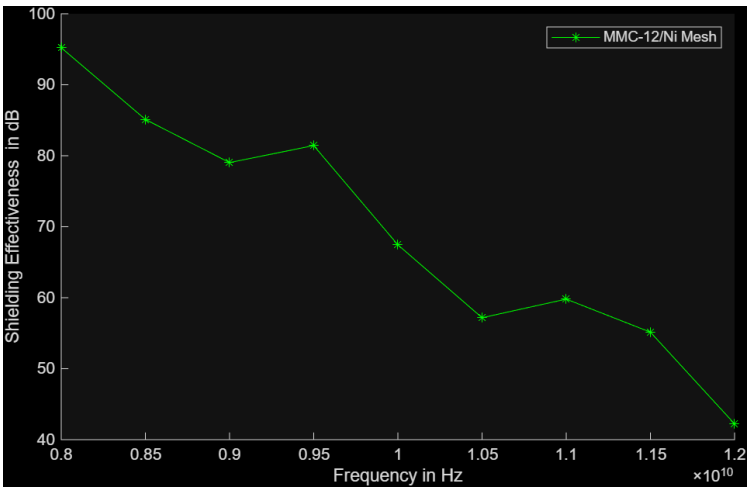


Figure 6. Shielding Effectiveness of Multilayer MMC-10/ Ni Mesh

A clear trend is observed in Figure 7, wherein the shielding effectiveness improves with increasing reinforcement concentration. The ceramics (SiC and Al_2O_3) enhance the dielectric properties and interfacial area, contributing to both absorption and reflection losses. The presence of fly ash, with its lightweight, porous nature, may help impede EM wave propagation through internal scattering and impedance mismatch.

Table 2. Comparison of MMC with Ni mesh

References	Frequency range	Existing work
35	8-12 GHz	59.4dB
36	8-12 GHz	89.23dB
37	1-9 GHz	38.9
Proposed	8-12 GHz	95.20

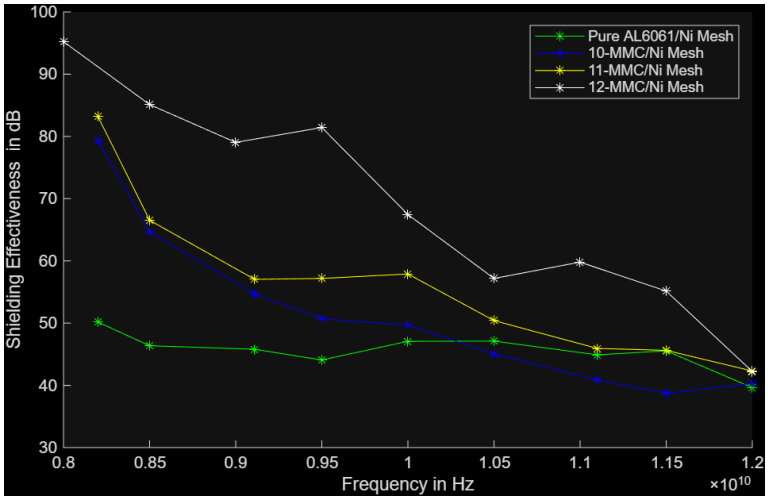


Figure 7. Comparison of Shielding Effectiveness of different materials.

4. Conclusions

This study examined the electromagnetic shielding capabilities of multilayer Al6061-based metal matrix composites (MMCs) enhanced with different ratios of SiC, Al_2O_3, and fly ash, incorporating nickel as a surface-absorbing layer. The analysis of shielding effectiveness (SE) was conducted across the X-band frequency range (8–12 GHz) with a uniform composite thickness of 1 mm, focusing on conditions pertinent to lightning strike protection in aerospace settings. The findings indicate a clear correlation between the type and proportion of reinforcements and the material's shielding behaviour. In the study, pure Al6061 and low-reinforcement configurations reached moderate SE values of approximately 51 dB at 8 GHz. However, with increased reinforcement levels, particularly the composition of 75% Al6061, 10% SiC, 10% Al_2O_3, and 5% FA, a significant improvement in shielding was observed, resulting in a maximum SE of 96.21 dB at 8 GHz. The enhancement can be linked to heightened interfacial polarisation, dielectric loss, and various internal scattering facilitated by the ceramic and fly ash components. The study's findings indicate that the strategic design of multilayer MMCs can greatly enhance electromagnetic shielding while maintaining both weight and structural performance. The refined formulation offers a robust approach for cutting-edge aerospace uses, particularly in addressing the challenges posed by high-intensity electromagnetic pulses and lightning strikes.

5. Acknowledgments

The authors express their gratitude to the Electronics and Communication Engineering, Ramachandra College of Education, for their assistance and for creating a conducive scientific atmosphere that enabled us to complete this work.

Author Contributions: Conceptualization, Siva Chakra Avinash Bikkina; methodology, Siva Chakra Avinash Bikkina; software, Kakarla Gopi Sri Koushiki ; validation, Kakarla Gopi Sri Koushiki; formal analysis, G.Suneetha ; investigation, Kakarla Gopi Sri Koushiki ; resources, Siva Chakra Avinash Bikkina.; data curation, Kakarla Gopi Sri Koushiki; writing—original draft preparation, Kakarla Gopi Sri Koushiki; writing—review and editing G.Suneetha .; visualization, G.Suneetha .; supervision, Siva Chakra Avinash Bikkina; project administration, Siva Chakra Avinash Bikkina; . The author has read and agreed to the published version of the manuscript.

Funding: Not applicable

Conflicts of Interest: The authors declare no conflict of interest.

References

[1] Bijulin Greety, D. J.; Jims John Wessley, G. A Study on EMI Shielding in Aircraft: Introduction, Methods and Significance of Using Electrospun Nanocomposites. *J. Space Saf. Eng.* **2024**, *11*(1), 150–160. https://doi.org/10.1016/j.jsse.2023.09.012

[2] Hoole, P.; Hoole, S. Introduction to Lightning and Lightning Protection. In *Lightning Engineering: Physics, Computer-Based Test-Bed, Protection of Ground and Airborne Systems*; Springer International Publishing: Cham, 2022; pp 1–50. https://doi.org/10.1007/978-3-030-93277-2_1

[3] Miyano, I.; Komuro, O.; Takahashi, M.; Fujita, M. Electromagnetic Field Shielding Plate, Method for Manufacturing Same, Electromagnetic Field Shielding Structure, and Semiconductor Manufacturing Environment. U.S. Patent 10,527,217, 2020.

[4] Banker, K.; Dhruv, A. B. Recent Development in Aluminium MMCs: Materials, Methods and Applications. In *Futuristic Trends in Mechanical Engineering*; Dhruv, A. B., Ed.; IIP Series; Elsevier, 2024; Vol. 3, pp 82–92. https://doi.org/10.1016/j.matpr.2018.01.090

[5] Casey, K. F. Electromagnetic Shielding Behavior of Wire-Mesh Screens. *IEEE Trans. Electromagn. Compat.* **1988**, *30*(3), 298–306. https://doi.org/10.1109/15.1956

[6] Young, J. L.; Wait, J. R. Shielding Properties of an Ensemble of Thin, Infinitely Long, Parallel Wires over a Lossy Half Space. *IEEE Trans. Electromagn. Compat.* **1989**, *31*(3), 238–244. https://doi.org/10.1109/15.30877

[7] Wilson, P. A Comparison of Various Measured and Calculated Shielding Effectiveness Data for a Wire Cage. *IEEE Trans. Electromagn. Compat.* **1995**, *37*(1), 126–131. https://doi.org/10.1109/15.372926

[8] Hyun, S. Y.; Jung, I.; Hong, I. P.; Jung, C.; Kim, E. J.; Yook, J. G. Modified Sheet Inductance of Wire Mesh Using Effective Wire Spacing. *IEEE Trans. Electromagn. Compat.* **2016**, *58*(3), 911–914. https://doi.org/10.1109/TEMC.2016.2530742

[9] Qian, W. X.; Liu, H. B.; Xiao, B.; Wang, D.; Bi, L. P.; He, R.; Xu, K. Q. Analytical Study of Electromagnetic Shielding Characteristics of a Wire Mesh. In *Proceedings of the 11th Asia Pacific Power and Energy Engineering Conference (APPEEC 2019)*; CRC Press: Boca Raton, FL, 2019; p 375. https://doi.org/10.1201/9780429295300

[10] Cristina, S. An Equivalent Transmission Line Model for Electromagnetic Penetration through Reinforced Concrete Walls. *IEICE Trans. Commun.* **1995**, *78*(2), 218–229.

[11] Sarto, M. S. A New Model for the FDTD Analysis of the Shielding Performances of Thin Composite Structures. *IEEE Trans. Electromagn. Compat.* **1999**, *41*(4), 298–306. https://doi.org/10.1109/15.805438

[12] Hyun, S. Y.; Lee, K. W.; Yook, J. G. Modeling of Shielding Effectiveness of Reinforced Concrete Walls for Electromagnetic Pulse. In *Proceedings of the 42nd European Microwave Conference (EuMC 2012)*; Amsterdam, The Netherlands, 2012; pp 453–456. https://doi.org/10.23919/EuMC.2012.6459266

[13] Losito, O.; Barletta, D.; Dimiccoli, V. A Wide-Frequency Model of Metal Foam for Shielding Applications. *IEEE Trans. Electromagn. Compat.* **2010**, *52*(1), 75–81. https://doi.org/10.1109/TEMC.2009.2034476

[14] [14] Hyun, S. Y.; Du, J. K.; Lee, H. J.; Lee, K. W.; Lee, J. H.; Jung, C.; Yook, J. G. Analysis of Shielding Effectiveness of Reinforced Concrete against High-Altitude Electromagnetic Pulse. *IEEE Trans. Electromagn. Compat.* **2014**, *56*(6), 1488–1496. https://doi.org/10.1109/TEMC.2014.2329291

[15] Sun, X.; Wei, B.; Li, Y.; Yang, J. A New Model for Analysis of the Shielding Effectiveness of Multilayer Infinite Metal Meshes in a Wide Frequency Range. *IEEE Trans. Electromagn. Compat.* **2021**, *64*(1), 102–110. https://doi.org/10.1109/TEMC.2021.3053265

[16] Bharti, R.; Mursaleen, M.; Dey, A. Advancements in Electromagnetic Shielding Coatings for Aerospace Applications: A Comprehensive Review. *Surf. Innov.* **2024**, in press, 1–11. https://doi.org/10.1680/jsuin.24.00045

[17] Vargas-Bernal, R. Advances in Electromagnetic Environmental Shielding for Aeronautics and Space Applications. In *Electromagnetic Compatibility for Device Design and System Integration*; IGI Global: Hershey, PA, 2021; pp 80–96. https://doi.org/10.4018/978-1-7998-4879-0.CH003

[18] Mahalle, P. N.; Hemelatha, S.; Mishra, M.; Kalanandhini, G.; Samrat, B.; Ramachandran, T. Optimizing Shielding Techniques for High-Frequency EMC Applications in Aerospace Systems. In *Proceedings of*

the 15th International Conference on Computing, Communication and Networking Technologies (ICCCNT 2024); IEEE, 2024; pp 1–6. https://doi.org/10.1109/ICCCNT61001.2024.10726064

[19] Zheng, X.-Y.; Wang, Y.; Liu, Z.; Zhao, Q.; Liu, Y.; Li, H.; Qiu, J. Functional Composite Electromagnetic Shielding Materials for Aerospace, Electronics and Wearable Fields. *Mater. Today Commun.* **2022**, *33*, 104498. https://doi.org/10.1016/j.mtcomm.2022.104498

[20] Evaluating the Shielding Effectiveness (SE) in the Electric Field and Magnetic Field and Plane Wave for Infinite Sheet Metals. *Front. Res. Phys. Sci.* **2023**, *5*, 1–15. https://doi.org/10.9734/bpi/fraps/v5/5351c

[21] Zhang, X.; She, C.; Xu, H.; Xu, G. Electromagnetism-Resistant Cable Shielding Braided Sheath Used for Aerospace as Well as Preparation Method Thereof. Chinese Patent CN110227118A, September 6, 2019.

[22] Vargas-Bernal, R.; Bermúdez-Reyes, B.; Tecpoyotl-Torres, M. Progress in Advanced Materials Used in Electromagnetic Interference Shielding for Space Applications. In *Electromagnetic Compatibility for Device Design and System Integration*; IGI Global: Hershey, PA, 2021; pp 97–118. https://doi.org/10.4018/978-1-7998-4879-0.ch004

[23] Surappa, M. K. Aluminum Matrix Composites: Challenges and Opportunities. *Sādhanā* **2003**, *28*(1–2), 319–334. https://doi.org/10.1007/BF02717141

[24] Collin, R. E. *Foundations for Microwave Engineering*; IEEE Press, 2001. https://doi.org/10.1109/9780470544662

[25] Schelkunoff, S. A. Electromagnetic Theory of Shielding. *Bell Syst. Tech. J.* **1934**, *13*, 532–579.

[26] Rana, R. S.; Purohit, R.; Das, S. Review on Effect of Reinforcement Particles on Mechanical Behavior of Aluminum Metal Matrix Composites. *Mater. Today Proc.* **2015**, *2*(4–5), 3032–3041. https://doi.org/10.1016/j.matpr.2015.07.284

[27] Ray, S. Synthesis of Cast Metal Matrix Particulate Composites. *J. Mater. Sci.* **1993**, *28*, 5397–5413. https://doi.org/10.1007/BF00367809

[28] Ravindran, P.; Manisekar, K.; Narayanasamy, P. Characterization of Al6061 Hybrid Composite Reinforced with SiC and Fly Ash Particles. *J. Mech. Sci. Technol.* **2012**, *26*(12), 3865–3870. https://doi.org/10.1007/s12206-012-0841-7

[29] Liu, M.; Li, W.; Deng, C.; Yang, D. Multilayer Conductive Mesh Structures for High-Performance EMI Shielding. *Compos., Part B: Eng.* **2019**, *163*, 150–158. https://doi.org/10.1016/j.compositesb.2018.11.058

[30] Schelkunoff, S. A. The Electromagnetic Theory of Coaxial Transmission Lines and Cylindrical Shields. *Bell Syst. Tech. J.* **1934**, *13*, 532–579. https://doi.org/10.1002/j.1538-7305.1934.tb00443.x

[31] Umanath, K.; Selvamani, S.; Kumar, V. S. S. Analysis of Dry Sliding Wear Behaviour of Al6061/SiC/Fly Ash Metal Matrix Composites. *Compos., Part B: Eng.* **2013**, *53*, 159–168. https://doi.org/10.1016/j.compositesb.2013.04.064

[32] Mazahery, A.; Shabani, M. O. Characterization of Cast A356 Alloy Reinforced with Nano SiC Composites. *Trans. Nonferrous Met. Soc. China* **2012**, *22*(2), 275–280. https://doi.org/10.1016/S1003-6326(11)61174-0

[33] Kuttan, A. A.; Rajesh, R.; Anand, M. Microstructural and Mechanical Characterization of Al6061 Alloy Reinforced with Varying Titanium Carbide Content via Stir Casting. *J. Mater. Eng. Perform.* **2026**, 1–16. https://doi.org/10.1007/s11665-026-13946-4

[34] Pushpa, T. A. J. M.; Selvam, J. D. R.; Dinaharan, I.; Peter, E. Electromagnetic Interference Shielding Effectiveness of *in situ*-Synthesized Ultrafine SiC- and Al_2O_3-Reinforced AA6061 Aluminum Matrix Composites. *J. Mater. Sci.: Mater. Electron.* **2022**, *33*(7), 3774–3785. https://doi.org/10.1007/s10854-021-07569-9

[35] Wu, J.; Gao, Y. High-Performance Electromagnetic Shielding Composite Materials Based on Carbon Nanotubes and Sandwich Laminate Structures. *Polym. Compos.* **2024**, *45*(15), 13639–13649. https://doi.org/10.1002/pc.28724

[36] Morales, M. A.; Henry, T. C.; Salamanca-Riba, L. G. Model of Electromagnetic Interference Shielding Effectiveness for a Multifunctional Composite Containing Carbon-Fiber-Reinforced Polymer and Copper Mesh Layers. *Carbon* **2023**, *212*, 118179. https://doi.org/10.1016/j.carbon.2023.118179



ASEAN
Journal of Scientific and Technological Reports
Online ISSN:2773-8752

ASEAN
Journal of Scientific and Technological Reports
Online ISSN: 2773-8752

Article type

Type of the Paper (Article, Review, Communication, etc.) *about 8,000 words maximum*

Title (Palatino Linotype 18 pt, bold)

Firstname Lastname[1], Firstname Lastname[2] and Firstname Lastname[2*]

[1] Affiliation 1; e-mail@e-mail.com
[2] Affiliation 2; e-mail@e-mail.com
* Correspondence: e-mail@e-mail.com; (one corresponding authors, add author initials)

Citation:
Lastname, F.; Lastname, F.; Lastname, F. Title. *ASEAN J. Sci. Tech. Report.* **2023**, *26*(X), xx-xx. https://doi.org/10.55164/ajstr.vxxix.xxxxxx

Article history:
Received: date
Revised: date
Accepted: date
Available online: date

Publisher's Note:
This article is published and distributed under the terms of the Thaksin University.

Abstract: A single paragraph of about 400 words maximum. Self-contained and concisely describe the reason for the work, methodology, results, and conclusions. Uncommon abbreviations should be spelled out at first use. We strongly encourage authors to use the following style of structured abstracts, but without headings: (1) Background: Place the question addressed in a broad context and highlight the purpose of the study; (2) Methods: briefly describe the main methods or treatments applied; (3) Results: summarize the article's main findings; (4) Conclusions: indicate the main conclusions or interpretations.

Keywords: keyword 1; keyword 2; keyword 3 (List three to ten pertinent keywords specific to the article yet reasonably common within the subject discipline.)

1. Introduction

The introduction should briefly place the study in a broad context and highlight why it is crucial. It should define the purpose of the work and its significance. The current state of the research field should be carefully reviewed and critical publications cited. Please highlight controversial and diverging hypotheses when necessary. Finally, briefly mention the main aim of the work. References should be numbered in order of appearance and indicated by a numeral or numerals in square brackets—e.g., [1] or [2, 3], or [4–6]. See the end of the document for further details on references.

2. Materials and Methods

The materials and methods should be described with sufficient details to allow others to replicate and build on the published results. Please note that your manuscript's publication implicates that you must make all materials, data, computer code, and protocols associated with the publication available to readers. Please disclose at the submission stage any restrictions on the availability of materials or information. New methods and protocols should be described in detail, while well-established methods can be briefly described and appropriately cited.

Interventional studies involving animals or humans, and other studies that require ethical approval, must list the authority that provided approval and the corresponding ethical approval code.

2.1 Subsection

2.1.1. Subsubsection

3. Results and Discussion

This section may be divided by subheadings. It should provide a concise and precise description of the experimental results, their interpretation, as well as the experimental conclusions that can be drawn.Authors should discuss the results and how they can be interpreted from previous studies and the working hypotheses. The findings and their implications should be discussed in the broadest context possible. Future research directions may also be highlighted.

3.1. Subsection

3.1.1. Subsubsection

3.2. Figures, Tables, and Schemes

All figures and tables should be cited in the main text as Figure 1, Table 1, etc.



Figure 1. This is a figure. Schemes follow the same formatting.

Table 1. This is a table. Tables should be placed in the main text near the first time they are cited.

Title 1	Title 2	Title 3
entry 1	data	data
entry 2	data	data [1]

[1] Table may have a footer.

3.3. Formatting of Mathematical Components

This is example 1 of an equation:

$$a = 1, \tag{1}$$

The text following an equation need not be a new paragraph. Please punctuate equations as regular text. This is example 2 of an equation:

$$a = b + c + d + e + f + g + h + i + j + k + l + m + n + o + p + q + r + s + t + u \tag{2}$$

The text following an equation need not be a new paragraph. Please punctuate equations as regular text. The text continues here.

4. Conclusions

Concisely restate the hypothesis and most important findings. Summarize the significant findings, contributions to existing knowledge, and limitations. What are the future directions? Conclusions MUST be well stated, linked to original research question & limited to supporting results.

5. Acknowledgements

Should not be used to acknowledge funders – funding will be entered as a separate. As a matter of courtesy, we suggest you inform anyone whom you acknowledge.

Author Contributions: For research articles with several authors, a short paragraph specifying their individual contributions must be provided. The following statements should be used "Conceptualization, X.X. and Y.Y.; methodology, X.X.; software, X.X.; validation, X.X., Y.Y. and Z.Z.; formal analysis, X.X.; investigation, X.X.; resources, X.X.; data curation, X.X.; writing—original draft preparation, X.X.; writing—review and editing, X.X.; visualization, X.X.; supervision, X.X.; project administration, X.X.; funding acquisition, Y.Y. All authors have read and agreed to the published version of the manuscript." Please turn to the CRediT taxonomy for the term explanation. Authorship must be limited to those who have contributed substantially to the work reported.

Funding: Please add: "This research received no external funding" or "This research was funded by NAME OF FUNDER, grant number XXX" and "The APC was funded by XXX". Check carefully that the details given are accurate and use the standard spelling of funding agency names at https://search.crossref.org/funding. Any errors may affect your future funding.

Conflicts of Interest: Declare conflicts of interest or state "The authors declare no conflict of interest." Authors must identify and declare any personal circumstances or interest that may be perceived as inappropriately influencing the representation or interpretation of reported research results. Any role of the funders in the design of the study; in the collection, analyses or interpretation of data; in the writing of the manuscript, or in the decision to publish the results must be declared in this section. If there is no role, please state "The funders had no role in the design of the study; in the collection, analyses, or interpretation of data; in the writing of the manuscript, or in the decision to publish the results".

References

References must be numbered in order of appearance in the text (including citations in tables and legends) and listed individually at the end of the manuscript. We recommend preparing the references with a bibliography software package, such as EndNote, ReferenceManager to avoid typing mistakes and duplicated references. Include the digital object identifier (DOI) for all references where available.

Citations and references in the Supplementary Materials are permitted provided that they also appear in the reference list here.

In the text, reference numbers should be placed in square brackets [ ] and placed before the punctuation; for example [1], [1–3] or [1, 3]. For embedded citations in the text with pagination, use both parentheses and brackets to indicate the reference number and page numbers; for example [5] (p. 100), or [6] (pp. 101–105).

Using the American Chemical Society (ACS) referencing style

[1] Author 1, A.B.; Author 2, C.D. Title of the article. *Abbreviated Journal Name* Year, *Volume*, page range.

[2] Author 1, A.; Author 2, B. Title of the chapter. In *Book Title*, 2nd ed.; Editor 1, A., Editor 2, B., Eds.; Publisher: Publisher Location, Country. **2007**, Volume 3, pp. 154–196.

[3] Author 1, A.; Author 2, B. *Book Title*, 3rd ed.; Publisher: Publisher Location, Country, **2008**, pp. 154–196.
[4] Author 1, A.B.; Author 2, C. Title of Unpublished Work. *Abbreviated Journal Name* stage of publication (under review; accepted; in press).
[5] Author 1, A.B. (University, City, State, Country); Author 2, C. (Institute, City, State, Country). Personal communication, 2012.
[6] Author 1, A.B.; Author 2, C.D.; Author 3, E.F. Title of Presentation. In Title of the Collected Work (if available), Proceedings of the Name of the Conference, Location of Conference, Country, Date of Conference; Editor 1, Editor 2, Eds. (if available); Publisher: City, Country, Year (if available); Abstract Number (optional), Pagination (optional).
[7] Author 1, A.B. Title of Thesis. Level of Thesis, Degree-Granting University, Location of University, Date of Completion.
[8] Title of Site. Available online: URL (accessed on Day Month Year).

Reviewers sugestion

1. Name, Address, e-mail
2. Name, Address, e-mail
3. Name, Address, e-mail
4. Name, Address, e-mail

URL link:

Notes for Authors >>
https://drive.google.com/file/d/1r0zegnIVeQqe4iLQyT1xDEIinNggINPD/view?usp=sharing
https://drive.google.com/file/d/1r0zegnIVeQqe4iLQyT1xDEIinNggINPD/view?usp=sharing

Online Submissions >> https://ph02.tci-thaijo.org/index.php/tsujournal/user/register

Current Issue >> https://ph02.tci-thaijo.org/index.php/tsujournal/issue/view/16516

AJSTR Publication Ethics and Malpractice >> https://ph02.tci-thaijo.org/index.php/tsujournal/ethics

Journal Title Abbreviations >> http://library.caltech.edu/reference/abbreviations



ASEAN
Journal of Scientific and Technological Reports
Online ISSN:2773-8752



ASEAN
Journal of Scientific and Technological Reports
Online ISSN:2773-8752

ASEAN Journal of Scientific and Technological Reports (AJSTR)
Institute of Research and Innovation, Thaksin University, Phatthalung Campus
222 Moo. 2, Baan Prao Sub-District, Papayom District, Phatthalung, 93210, Thailand
Tel. +668 1540 7304